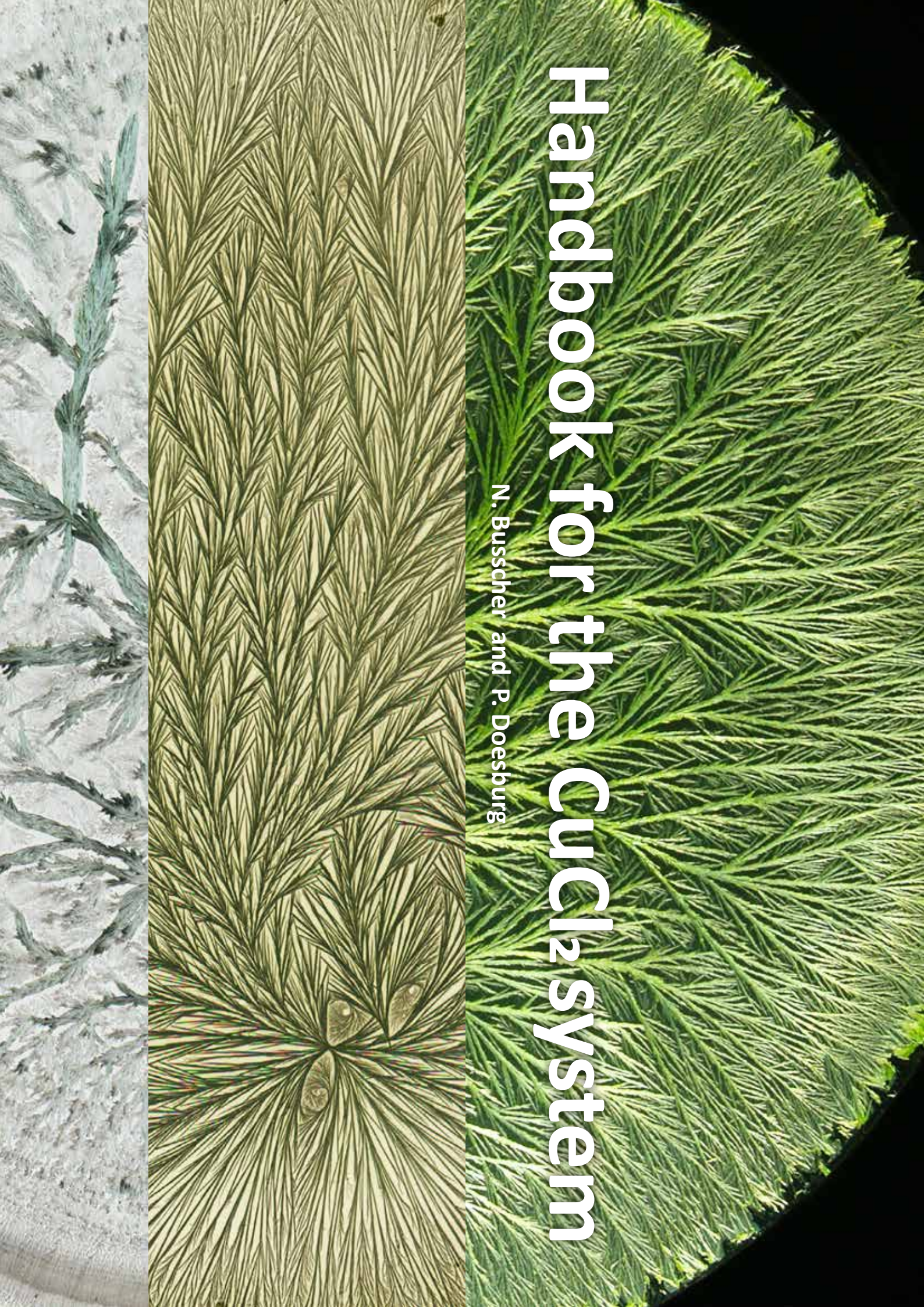
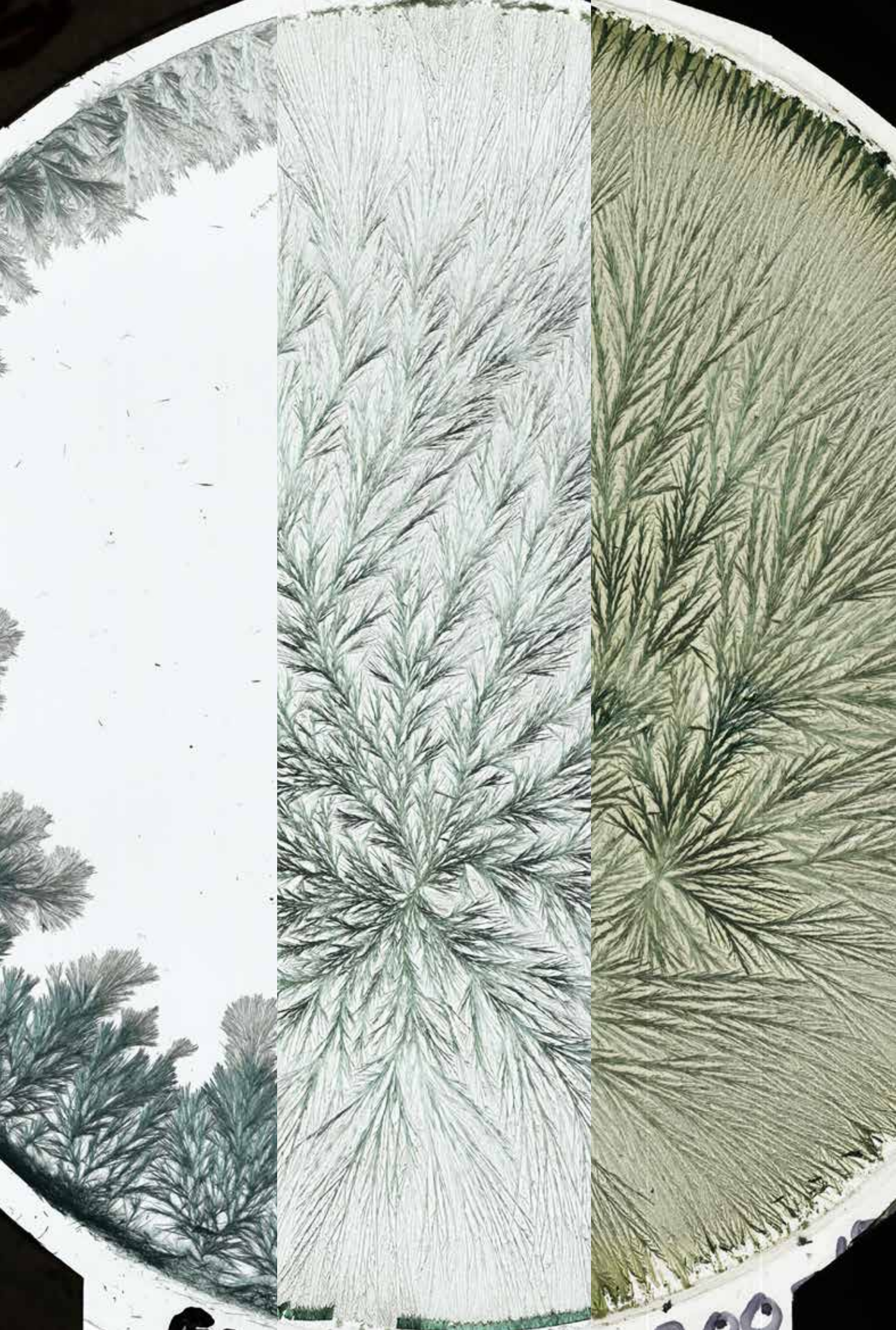


Handbook for the CuCl₂ system

N. Busscher and P. Doesburg





Handbook for the CuCl₂ system

N. Busscher and P. Doesburg

Colofon

Dr. Nicolaas Busscher
mail: nicolaas.busscher@posteo.de

Paul Doesburg
mail: p.doesburg@protonmail.com

Copyright:

Verein zur Förderung der Qualitätsforschung Bildschaffende Methoden e.v.
Sebastian-Kneipp-Strasse 44
37217 Witzenhausen, Germany

The pdf of the book will be sent on request by the authors.

This book is a result of an intensive feedback process. This was done by
Claudia Scherr, Greta Guglielmetti, Johanna Zeise, Uwe Geier,
and in the beginnig also by Miriam Athmann, Jürgen Fritz and Roya Bornhütter.

The production of this book was financed by
Software AG Stiftung, Darmstadt, Germany
(Project nr P 10 986)

Graphic credits:

Photo Johannes Kahl by Nicole Karnebogen
1.13.1 Uwe Geier, Forschungsring Darmstadt
1.13.2, 1.13.3, 1.13.4 Klostermann Verlag Frankfurt
1.13.5 Elsevier (ccc)
2.14.2, 2.14.3 Elsevier (NH)
2.6.1, 2.6.3, 2.6.4, 2.7.3 Jens-Otto Andersen
2.11.12 Libreight (ccc)
2.11.3 Wiley (ccc)
2.2.2 Beatrix Waldburger
2.14.2 ureview@bell.net
2.17.1 Gaby Mergardt
3.5.5 Andreas Degert
2.4.1, 2.4.2, 2.4.3, 2.4.4, 2.13.5 Naturwissenschaftliche Sektion am Goetheanum
2.11.20 Martin Thoma (wikimedia)
3.1.1 Roya Bornhütter
3.2.1 Jürgen Fritz
1.8.8 BenRG (Public domain)

All other photos or graphs are from the authors or from the authors' publications
and are referenced there.

Graphic Design | Gerda Peters, www.fingerprint.nl

Print | De Toekomst, Hilversum, The Netherlands

Content

Preface	7
Introduction	9
1 Practical considerations	17
1.0 Which parameters are important to handle?	18
1.1 Crystallization starting time	21
1.2 Water transport	28
1.3 Crystallization start and starting humidity	38
1.4 Surface tension, cleaning, ring height.....	41
1.5 Meniscus breakdown.....	56
1.6 Sensitive area.....	59
1.7 Evaporation issues	64
1.8 Concentration Matrix.....	78
1.9 Optimal Amounts.....	90
1.10 Transition between crystal types	103
1.11 Wetting up phase.....	108
1.12 Multiple Centers	110
1.13 Picture Zones	113
1.14 Chamber reset	128
2 Theoretical considerations.....	135
2.0 Steps to understanding the DCC picture building process	136
2.1 State of the art.....	137
2.2 Arrangement.....	140
2.3 Crystal growth and Branching	153
2.4 Concentration gradient in the dish	160
2.5 Warmth of process	166
2.6 Molecular weight and branching	174
2.7 Substance spirals, banding, spherulite	190
2.8 Dewetting by crystallization.....	196
2.9 Additive built into $\text{CuCl}_2 \cdot 2\text{H}_2\text{O}$?.....	198
2.10 Evaporation prefiguration (Vorbild)	202
2.11 Nucleation	203
2.12 Light polarization effect	236
2.13 Evaporation model.....	240
2.14 Self-organisation and $\text{CuCl}_2 \cdot 2\text{H}_2\text{O}$	255
2.15 Formation integrated pattern	261
2.16 Complex physical versus simple biological	271
2.17 Lowering disturbances.....	278
2.18 What is special for $\text{CuCl}_2 \cdot 2\text{H}_2\text{O}$?	286
2.19 How to name the $\text{CuCl}_2 \cdot 2\text{H}_2\text{O}$ system, especially in publications.....	288
3 Evaluation and documentation tools	293
3.0 Tools to document the DCC system, Image analysis, Image features evaluation	294
3.1 Chamber Systems	296
3.2 LabDoc tool.....	307
3.3 CrystEval tool	313
3.4 Image analysis tool	317
3.5 Additional tools.....	321
Glossary	327



This book is dedicated to Johannes Kahl (02.10.1968 – 12.11.2020)

Preface

The text on this page is in German, all other pages are in English.

*Willst du immer weiter schweifen?
Sieh, das Gute liegt so nah.
Lerne nur das Glück ergreifen
denn das Glück ist immer da.*

J. W. von Goethe

Mein Glück war und ist es, das ich vor rund 25 Jahren zur rechten Zeit das richtige Thema, die richtigen Menschen und die räumliche und finanzielle Unterstützung gefunden habe um meine Arbeit machen zu können. Während dieser Zeit wurden in den Projekten viele Gesichtspunkte sichtbar, für die damals keine Zeit war sie weiter auszuarbeiten oder aufzuschreiben. Es wurde mir vergönnt, dies als noch zum Teil aufschreiben zu dürfen.

*Weite Welt und breites Leben,
Lange Jahre redlich Streben...
Ältestes bewahrt mit Treue,
Freundlich aufgefasstes Neue,
Heitern Sinn und reine Zwecke:
Nun, man kommt wohl eine Strecke.*

J. W. von Goethe

I would like to thank the people in the following list for talking, ideas, hints, listening, patience and possibilities. The order of the list is according to the order I met the people.

Carla van Dijk, Ferdie Amons, Machteld Huber, Ate Koopmans, Jens-Otto Andersen, Jürgen Fritz, Ursula Graf, Johannes Kahl, Angelika Ploeger, Gaby Mergardt, Uwe Geier, Paul Doesburg, Aneta Zalecka, Maria Kokornaczyk, Aumaporn Meelursarn, Haijo Knijpenga, Jean-Georges Barth, Christine Ballivet, Roya Bornhütter, Francois Schweizer, Günther Reiter, Claudia Scherr, Beatrix Waldburger, Miriam Athmann, Stephan Baumgartner, Wintfried Kurth, Greta Guglielmetti, Johanna Zeise, Nicolas Herzer, Elsa Rommerskirchen und Christina Benny.

Witzenhausen, Juni 2024,
Nicolaas Busscher

Introduction

The reader of this handbook should have had an empirical encounter with the $\text{CuCl}_2 \cdot 2\text{H}_2\text{O}$ (Dihydrate Cupric Chloride, further abbreviated [DCC](#)) crystallization pictures. This comprises at least one complete experiment from sample to DCC crystallization pictures in the lab. For a beginner it is necessary to have at least joined a lab and observed and asked the person who is doing the work. This gives a realistic access to the names and the concepts which are used in this handbook.

The so called DCC crystallization pictures appear in the following way: a watery sample, from chemical compounds or an extract or juice from an agricultural product, is mixed with a watery DCC solution in a Petri-dish. Under defined (e.g. climatic) conditions the water and the volatiles of the mixture evaporate. After 12 to 16 hours the crystallization starts, resulting in tree-like patterns, usually starting from one nucleation location.

The hypothesis is: *“The sample and the process which defines the sample shows up in the picture and can be recognized and characterized by trained humans or computer image analysis”.*

The entire process will be referred to in this document as “DCC crystallization with additives” or the DCC method (for further reading on the naming issue, see the chapter [2.19 Name \$\text{CuCl}_2 \cdot 2\text{H}_2\text{O}\$ system](#)).

This is not a monolithic, hierarchical teaching book. We avoided this, because the status of the knowledge is not far enough for this and because most factors are connected to each other. It is more like building a network, where everything is strongly or weakly connected to each other, rather than a pyramid. Nevertheless, some questions could be solved, but the questions that arose from the answers or the remaining open questions point to a lack in our understanding and toward the future. Therefore, this book leaves some questions unanswered, such as why the relative humidity in the Triangle chambers is always below 67%, yet we had simulation results that indicated a dynamic effect and not a partial pressure effect.

The goal of this handbook is to describe the actual knowledge and the future research paths for the research question: *“How can I gain a better understanding of the DCC picture building process?”*. The understanding of the human Gestalt evaluation of the DCC pictures is not the focus of this handbook.

The handbook is divided in the following four chapters

- 1: Practical considerations
- 2: Theoretical considerations
- 3: Evaluation and documentation tools
- 4: Glossary

The sub chapters in chapter 1 and chapter 2 are usually structured in the following way:

- Abstract
- Introduction
- Historical overview
- Authors Measurements
- Resume
- Additional Research

The basic idea behind this structure is to list what has been done on a topic (as far as we know) in the Historical Overview. The Authors Measurements (if any) were added as a foundation, and based on these two chapters, the Additional Research described what the next step of the research could be. The Additional Research is a list of keyword phrases, including thoughts that came to mind when we had an overview of all the results on a topic so far. Each subchapter has the references listed at the end of the subchapter. In you wish to work on the topic of a subchapter and need the pdf of a reference, please contact us and we can see if we can send it to you. In chapter 3 the tools we are using for Evaluation and documentation are shortly described. Chapter 4 is the Glossary. It describes all the terms and abbreviations used in the text and, if available, provides a link to a chapter in the text for more details.

The following is an introduction to a more detailed presentation of the DCC phenomenon and the hypotheses and concludes this introductory chapter with a historical overview of the DCC method and the people who have been involved in the development and use of the DCC method.

DCC picture phenomenon and hypothesis

Fig. I.1 shows the process starting with a sample, defined by a treatment, up to the judgment using the DCC phenomenon. In the laboratory in Fig. I.1, the sample is transformed into a watery solution (a juice or an extract) and added to the DCC solution. The solution is pipetted into a Petri-dish in a chamber and starts crystallizing into a DCC pattern after 12 to 16 hours of evaporation.

The images of different samples associated with different treatments, e.g untreated and treated carrots, are evaluated by a human based Gestalt evaluation [1] [2] or by a computer image analysis [3] [4]. Based on the comparison a judgment is formulated.

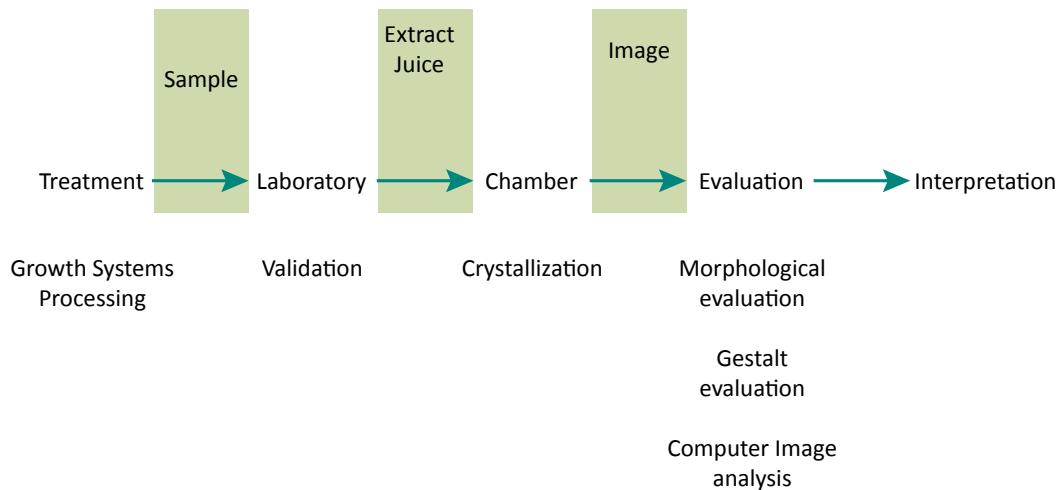


Fig. I.1 Process description of the path from a treatment (sample) to a judgment using the DCC phenomenon.

The simplest example of comparing two pictures is between a DCC image without and with an additive. For the usual DCC amount of 100 to 200 mg per plate, pictures with and without carrot juice as additive are shown in Fig. I.2 below.



Fig. I.2 DCC pictures with 110 mg DCC per plate. Left without additive, right with freeze dried carrot, 11.5 mg per plate. Data from Busscher 2014 [5]. Pictures were scanned in light transmission mode.

In Fig. I.2 left, without additive, the DCC accumulates at the rim of the Petri-dish. In Fig. I.2 right, with freeze dried carrot juice as additive, the DCC covers the entire plate. This is discussed in [6] and [7]. As a simple example of a process comparison, the DCC images of fresh and aged carrot juice are shown in Fig. I.3 below. When comparing the pictures, people usually arrive at a description (or judgment) that is close to the concepts (*Begriff*) of fresh (for the left picture) and aged / old (for the right picture).

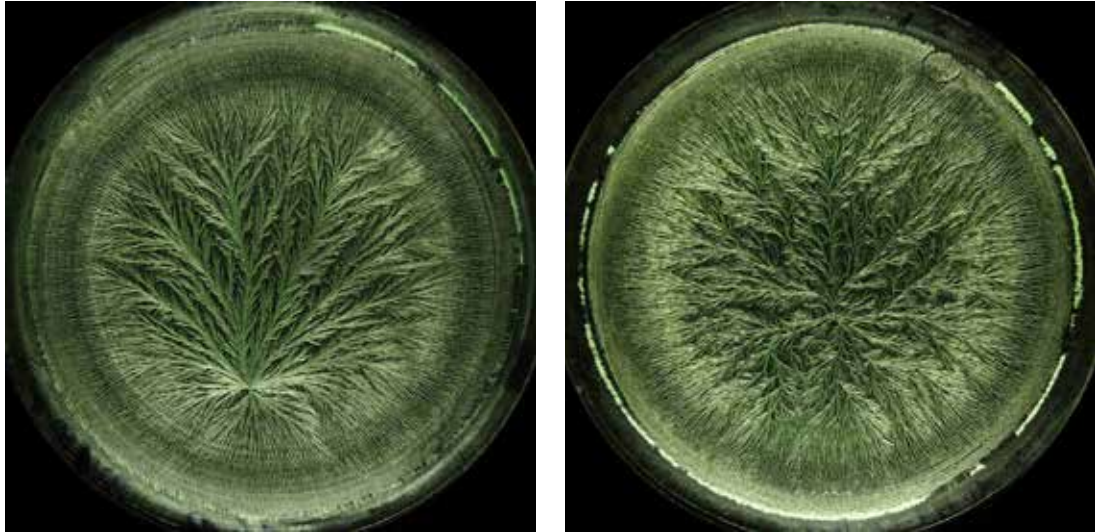


Fig. I.3 DCC pictures of carrot juice. Left: fresh juice, right: juice aged for 7 days at 4 °C. Pictures from LabDoc Series, AC (fresh) and AE (aged juice) chamber C University of Kassel (D). Pictures were photographed in dark field mode.

This observation allows us to formulate the hypothesis for the DCC phenomenon:

When comparing DCC images of samples from different treatments, humans and computer image analysis can recognize the sample and the treatment.

This is expressed in Fig. I.4, by the arrow between the judgment and the treatment. A simple explanation for the images in Fig. I.3, but not for the judgment, is by relating the aging of the solution to a decrease in mean molecular weight of the additive [5], [8].

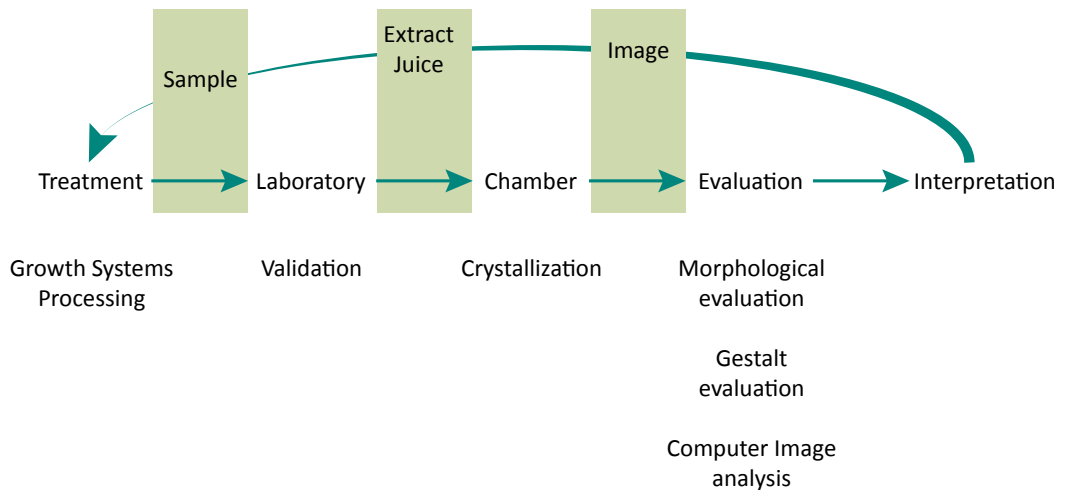


Fig. I.4 Process description of the path from a treatment (sample) to a judgment using the DCC phenomenon, showing the hypothesis (by the arrow), that the judgment is connected to the treatment.

The same procedure can be used for different growing systems such as bio-dynamic / organic / mineral for the same seeds. The differences are not as easily visible and explainable as in Fig. I.3 above and require more training for the judgment [1] [2] [9] and a higher number of replications for the image analysis [10].

Historical overview

The “DCC crystallization with additives” was invented by Pfeiffer in 1924 [11] [12] [13] [14]. He called it “*Empfindliche Kristallisation*”. He first applied it to human blood and received an honorary degree of Doctor of Medicine from Hahnemann Medical College and Hospital in Philadelphia in 1939 on how the health status of a cancer person showed up in the DCC crystallization pictures (see biography of A. Selawry p. 61, 62 and biography Pfeiffer [15], p. 118 ff.). He was followed by several successors who extended the application and the research questions to other samples like those of agricultural origin. The following is a description of those people with whom we had contact or could understand their work, and their contributions to the development of the DCC method.

When Pfeiffer moved to the USA, his work was continued by Bessenich and Selawry. Bessenich continued the work on the blood crystallization [16] and the principle questions of the building process [17]. A. Selawry worked in collaboration with her brother O. Selawry on a method description for human blood application [18]. A. Selawry additionally worked on germination and growth of seeds [19] and the influence of potentized preparations on the growth process.

In Dornach the work continued with Koopmans on blood crystallization [20] [21] [22] [23] [24], Knijpenga worked on additives like blood, milk [25] [26] [27] [28] and the DCC principle [29] [30]. Ballivet worked on the DCC principle and the crystallization chamber development [31] [27] and Barth researched the blood of mine workers, and worked on the principle of the method and chamber development [32] [33] [34] [35] [36] [37] [38]. Waldburger worked on the principle of the method [39] [40] [41] [42] [43]. Heinze [44] [45] worked together with Pfeiffer. Krüger worked at Weleda with the DCC method [46]. Von Hahn created a new and smaller chamber in 1962 and used smaller dishes. He called his approach *Thesigraphie* [47].

Engquist learned the method from Selawry and applied it on food questions (1975) in Järna (S) [48] [49] [50] [51]. In parallel Petterson [52] [53] [54] [55] [56] used it for discriminating samples from growth systems (Nordic experiments). Both Engquist and Petterson also worked on the question of the principles behind the phenomenon.

Amons [57] began crystallizing blood at the Louis Bolk Institute. Huber and van der Bie joined Amons in blood crystallization research [58] and simultaneously focused on the standardization of the visual evaluation [1]. Huber continued by researching food quality. Doesburg joined the Louis Bolk Institute and later started his own Company (Crystal Lab) to continue on food quality questions. He worked on structure image analysis, the basis of the Gestalt evaluation [4] [2] [59] and on basic homeopathic research questions [60] [61]. Abel [62] worked on the question of thermal and non thermal treatments of milk.

Graf [63] [64] [65] [66] integrated three picture forming methods to discriminate farming systems. Fritz and Geier learned the method from Graf. Fritz focused on farming systems and the evaluation of the pictures [67] [68] [69] [9] [70]. Athmann did her doctorate on growing conditions of rocket lettuce [71]. Geier worked on the question of plant organs (root, leave, flower) [72] [73] and later on farming systems and food production systems [74].

Andersen in Copenhagen contacted Engquist and Petterson and through a master’s [75] and a PhD [76] thesis, began to develop a chamber. He worked with PVP [77], stimulated by the work of Hummel [8]. Later moved to Hertha (BRAD) and researched the potency question together with Baumgartner and Doesburg [60] [61]. Kokornaczyk worked on the wheat quality question and wrote a PhD about it [78].

In Kassel University, in the research group of Ploeger, a group for food quality research was founded with Mergardt, Kahl and Busscher in 2001. The Triangle Consortium was founded in 2002 with the Louis Bolk Institute (NL) with Huber and Doesburg and with BRAD (DK) with Andersen and Paulsen and the group in Kassel. The focus of the Triangle consortium was the validation of the DCC crystallization [79] [80] for research questions like growth systems, food processing for different samples like carrot [81] [82] [83] [84], wheat [81] [85] [10] [86], milk [87] [88] [89] and apples [81] [90] and the understanding of the DCC building process [6] [7] [5] [91].

References

- [1] Huber M, Andersen J-O, Kahl J, Busscher N, Doesburg P, Mergardt G et al. Standardization and Validation of the Visual Evaluation of Biocrystallizations. *Biological Agriculture and Horticulture* 2010; 27: 25–40.
- [2] Doesburg P, Huber M, Andersen J-O, Athmann M, van der Bie G, Fritz J et al. Standardization and performance of a visual Gestalt evaluation of biocrystallization patterns reflecting ripening and decomposition processes in food samples. *Biological Agriculture & Horticulture* 2014; 31: 128-145.
- [3] Andersen JO, Henriksen CB, Laursen J, Nielsen AA. Computerised image analysis of biocrystallograms originating from agricultural products. *Computers and Electronics in Agriculture* 1999; 22: 51-69 [https://doi.org/doi:10.1016/S0168-1699\(98\)00043-X](https://doi.org/doi:10.1016/S0168-1699(98)00043-X).

- [4] Doesburg P, Nierop AF. Development of a structure analysis algorithm on structures from CuCl₂·2H₂O crystallization with agricultural products. *Computers and Electronics in Agriculture* 2013; 90: 63-67 <https://doi.org/doi:10.1016/j.compag.2012.11.003>.
- [5] Busscher N, Kahl J, Ploeger A. From needles to pattern in food quality determination. *Journal of the Science of Food and Agriculture* 2014; 94: 2578-2581 <https://doi.org/doi:10.1002/jsfa.6498>.
- [6] Busscher N, Kahl J, Doesburg P, Mergardt G, Ploeger A. Evaporation influences on the crystallization of an aqueous dihydrate cupric chloride solution with additives. *Journal of Colloid and Interface Science* 2010; 344: 556–562 <https://doi.org/doi:10.1016/j.jcis.2009.12.045>.
- [7] Busscher N, Doesburg P, Mergardt G, Sokol A, Kahl J, Ploeger A. Influence of dewetting on the crystallization behavior of CuCl₂ in the presence of BSA during evaporation in a Petri dish. *Heliyon* 2019; 5: e01102 <https://doi.org/10.1016/j.heliyon.2018.e01102>.
- [8] Hummel RE. Liefert die Kupferchlorid-Kristallisations-Methode einen Nachweis für die Gestaltkräfte des Lebendigen?. *Elemente der Naturwissenschaft* 1992; 57: 112-121 <https://doi.org/10.18756/edn.57.112>.
- [9] Fritz J, Athmann M, Andersen J-O, Doesburg P, Geier U, Mergardt G. Advanced panel training on visual Gestalt evaluation of biocrystallization images: ranking wheat samples from different extract decomposition stages and different production systems. *Biological Agriculture & Horticulture* 2018; 35: 1-12 <https://doi.org/doi:10.1080/01448765.2018.1492457>.
- [10] Kahl J, Busscher N, Mergardt G, Maeder P, Torp T, Ploeger A. Differentiation of organic and non-organic winter wheat cultivars from a controlled field trial by crystallization patterns. *J. Sci. Food Agric.* 2014; 95: 53-58 <https://doi.org/doi:10.1002/jsfa.6818>.
- [11] Pfeiffer E. *Kristalle* (Orient Occident Verlag, 1930).
- [12] Pfeiffer E. *Studium von Formkräften an Kristallisationen* (Naturwissenschaftliche Sektion am Goetheanum, 1931).
- [13] Pfeiffer E. *Empfindliche Kristallisationsvorgänge als Nachweis von Formkräften im Blut* (Emil Weises Buchhandlung Dresden, 1935).
- [14] Pfeiffer E. *Sensitive Crystallization Processes: A Demonstration of Formative Forces in the Blood* (Anthroposophic Press, 1975).
- [15] Meyer T. *Ein Leben für den Geist : Ehrenfried Pfeiffer (1899-1916)* (Perseus Verlag, 2000).
- [16] Bessenich F. *Zur Methode der empfindlichen Kristallisation* (Naturwissenschaftliche Sektion am Goetheanum Dornach, 1960).
- [17] Bessenich F. *Beiträge zur Erforschung der Bildkräfte durch empfindliche Kristallisation* (Goetheanum (Dornach), 1951).
- [18] Selawry A and Selawry O. *Die Kupferchlorid-Kristallisation in Naturwissenschaft und Medizin* (Gustav-Fischer-Verlag, 1957).
- [19] Selawry A. *Samenkeimung und Metallpotenzen im Kristallisationstest* (Forschungsring für biologisch-dynamische Wirtschaftsweise, 1975).
- [20] Koopmans A. Zeitabhängigkeiten bei empfindlichen Kristallisationen. *Elemente der Naturwissenschaft* 1965; 2: 1-7 <https://doi.org/10.18756/edn.2.1>.
- [21] Koopmans A. Die Frage der Lokalisation im Kupferchlorid-Kristallisationsbild. *Elemente der Naturwissenschaft* 1971; 14: 19-30 <https://doi.org/10.18756/edn.14.19>.
- [22] Koopmans A. Jahreszeitliche Veränderungen im Kristallisationsbild von Visum Alba. *Elemente der Naturwissenschaft* 1972; 16: 43-52.
- [23] Koopmans A. Pfeiffersche Blutkristallisation und Malignom-Bereitschaft. Ein Arbeitsbericht. *Elemente der Naturwissenschaft* 1990; 52: 28-35.
- [24] Koopmans A. Zum Begriff der Malignomdisposition im Hinblick auf die Blutkristallisations—Methode. *Elemente der Naturwissenschaft* 1990; 52: 36-41 <https://doi.org/10.18756/edn.52.36>.
- [25] Knijpenga H. Zur Frage der Interpretation von Blutkristallisationsbildern. *Elemente der Naturwissenschaft* 1995; 62.
- [26] Knijpenga H. Kristallisationsbilder und vergleichende Methode. *Elemente der Naturwissenschaft* 1993; 58: 83-84.
- [27] Ballivet C, Knijpenga H, Barth J-G, Clad R. Zur Empfindlichkeit der Methode der Kupferchloridkristallisation. *Elemente der Naturwissenschaft* 1999; 70: 1-32 <https://doi.org/10.18756/edn.70.1>.
- [28] Knijpenga H. Einflüsse unterschiedlicher Behandlungen auf die biologische Wertigkeit von Kuhmilch. Untersuchungen mit der Methode der Empfindlichen Kristallisation. *Elemente der Naturwissenschaft* 2001; 75: 48-60 <https://doi.org/10.18756/edn.75.48>.
- [29] Knijpenga H. Wie können die Einflüsse der Laborprozesse von den Pflanzenqualitäten im Bild unterschieden werden?. *Elemente der Naturwissenschaft* 2002; 77: 114-118 <https://doi.org/10.18756/edn.77.114>.
- [30] Knijpenga H. Stoff und Bild bei der Methode der Empfindlichen Kristallisation. *Elemente der Naturwissenschaft* 2023; 118: 5-23 <https://doi.org/10.18756/edn.118.5>.
- [31] Ballivet C. Empfindliche Kristalle zwischen unorganischer und organische Natur. *Elemente der Naturwissenschaft*

- 1993; 58: 76-82.
- [32] Barth JG. Image de cristallisation du chlorure cuivrique et structure chimique de l'additif. *Elemente der Naturwissenschaft* 1997; 66: 16-42.
- [33] Barth JG. Empfindliche Kristallation. Krebs und Praeakanzerose. *Elemente der Naturwissenschaft* 1990; 52: 42-50.
- [34] Barth J-G. Cristallisation avec additif, cas particulier du chlorure cuivrique et de ses applications*. *Phytothérapie* 2004; 2: 183-190.
- [35] Barth J-G, Roussaux J, Wilkens A, Jacobi M. Techniques for washing the supports used for copper chloride crystallization with additive. *Elemente der Naturwissenschaft* 2013; 98: 5-19 <https://doi.org/DOI: 10.18756/edn.98.5>.
- [36] Reiter G, Barth J-G. Some general remarks on crystallization in the presence of additives. *Elemente der Naturwissenschaft* 2010; 92: 39-61 <https://doi.org/10.18756/edn.92.39>.
- [37] Barth J-G. Cupric chloride crystallisation with additives and its applications. *Elemente der Naturwissenschaft* 2004; 81: 23-39 <https://doi.org/10.18756/edn.81.23>.
- [38] Barth J-G. Eléments de physique et expérience de laboratoire en matière de cristallisation du chlorure cuivrique en présence d'additif. *Elemente der Naturwissenschaft* 2002; 77: 121-124 <https://doi.org/10.18756/edn.77.121>.
- [39] Waldburger B. Über die Bedeutung von Lautsinn und Begriffssinn bei der Beurteilung von Kristallisationsbildern. *Elemente der Naturwissenschaft* 2007; 87: 68-75.
- [40] Waldburger B. Morphologie und Empathie- Studien zur Auswertung von Kristallisationsbildern. *Elemente der Naturwissenschaft* 2009; 90: 80-91.
- [41] Waldburger, B. Die Methode der Empfindlichen Kristallisation, 2003 .
- [42] Waldburger B. Begriff und Kontext in der Methode der Empfindlichen Kristallisation. *Elemente der Naturwissenschaft* 2005; 83: 79-89 <https://doi.org/10.18756/edn.83.79>.
- [43] Waldburger B. Die Blutkristallisation als Schulungsmethode. *Merkurstab* 2013; 5: 402-414.
- [44] Heinze H. Vom Entstehen der "Methode der empfindlichen Kristallation" im Dornacher Labor Ehrenfried Pfeiffers. *Lebendige Erde* 1959; 1: 3-18.
- [45] Heinze H. Aus der Entwicklung der Qualitätsforschung im Institut für biologisch-dynamische Forschung. Fortsetzung aus "Lebendige Erde" 3/78. Methode der empfindlichen Kristallisationen nach E. Pfeiffer. *Lebendige Erde* 1978; 4: 139-143.
- [46] Krüger H. Kupferchlorid-kristallisationen. Ein Reagenz auf die Bildkräfte des Lebendigen. *Weleda Schriftenreihe* 1950; 1: 1-29.
- [47] Von Hahn F-V Thesigraphie. (Franz Steiner Verlag, 1962).
- [48] Engquist M. Structural changes in the crystallization pictures of plant substances due to aging and fertilizing. *Bio-dynamics* 1962; 63.
- [49] Engquist M. Die Gestaltkräfte des Lebendigen (Vittorio Klostermann, 1970).
- [50] Engquist M. Physische und lebensbildende Kräfte in der Pflanze (Vitorio Klostermann, 1975).
- [51] Engquist M. Qualitätsprüfung an Gemüse durch die Kupferchlorid-Kristallisationsmethode (Järna Tryckeri AB, Schweden, 1989).
- [52] Pettersson BD, Engquist M. Versuche mit den Präparaten "Hornmist" und "Hornkiesel". *Lebendige Erde* 1963; 1: 1-25.
- [53] Pettersson B. D. und Engquist M. Die Auswirkungen der Düngung auf die Qualitätseigenschaften von Kartoffeln. *Lebendige Erde* 1964; 5: 199-219.
- [54] Pettersson BD. Beiträge zur Entwicklung der CuCl₂ Methode nach Pfeiffer. *Elemente der Naturwissenschaft* 1966; 5: 29-39.
- [55] Pettersson BD. Beiträge zur Entwicklung der Kristallisationsmethode mit Kupferchlorid nach Pfeiffer IV. Wie verschiedene Kristallbilder bei der Pflanzenkristallisation entstehen. *Lebendige Erde* 1969; 3: 112-126.
- [56] Pettersson BD. Die Einwirkung von Standort, Düngung und wachstumbeeinflussenden Stoffen auf die Qualitätseigenschaften von Speisekartoffeln. *Lebendige Erde* 1970; 3: 78-87.
- [57] Amons F. De goetheanistische fenomenologie en haar toepassing op de zogenaamde koperchloride-kristallisatietest. *Nederlands Tijdschrift voor Integrale Geneeskunde* 1988; 4: 331-337.
- [58] Amons F, van der Bie G, Huber M. Eindrapport: Grondslagenonderzoek Proefpersoon-Bloedkristallisatie. Kwalitatieve oordelen in de beelddiagnostiek gekwantificeerd. Technical Report, Louis Bolk Instituut. 1999.
- [59] Doesburg P, Fritz J, Athmann M, Bornhütter R, Busscher N, Geier U et al. Kinesthetic engagement in Gestalt evaluation outcores analytical 'atomic feature' evaluation in perceiving aging in crystallization images of agricultural products. *PLOS* 2021; 16 <https://doi.org/https://doi.org/10.1371/journal.pone.0248124>.
- [60] Baumgartner S, Doesburg P, Scherr C, Andersen J-O. Development of a Biocrystallisation Assay for Examining Effects of Homeopathic Preparations Using Cress Seedlings. *Evidence-Based Complementary and Alternative Medicine* 2012; 2012: 14 <https://doi.org/10.1155/2012/125945>.
- [61] Doesburg P, Andersen J-O, Scherr C, Baumgartner S. Empirical investigation of preparations produced according

- to the European Pharmacopoeia monograph 1038. *European Journal of Pharmaceutical Sciences* 2019; 137: 104987 <https://doi.org/https://doi.org/10.1016/j.ejps.2019.104987>.
- [62] Abel, D. Evaluation of picture forming methods compared to standard analytical methods for detection of structural changes caused by different thermal and non-thermal treatments of raw bovine milk, 2013.
- [63] Balzer-Graf U, Balzer F. Milchqualität im Spiegel bildschaffender Methoden. *Lebendige Erde* 1991; 5: 236-255.
- [64] Balzer-Graf U. Vitalqualität von Weizen aus unterschiedlichem Anbau. *Beiträge zur Förderung der biologisch-dynamischen Landwirtschaft 11. SH Forschung* 1996; 44: 440-450.
- [65] Balzer-Graf U, Hoppe HSM. Äpfel – organisch und biologischdynamisch. Erntemenge und Vitalqualität im Vergleich. *Lebendige Erde* 1998; 5: 387-395.
- [66] Balzer-Graf, U. and Gallmann, P. U. Analytische und bildschaffende Methoden in der Untersuchung von Milchprodukten (Vitalqualitätsuntersuchung Joghurt), 2000.
- [67] Fritz JGM, M Athmann UK. Untersuchung von Traubensaft mit den drei Bildschaffenden Methoden. *Wiss Tagung Zürich 2009* 2009.
- [68] Fritz J, Athmann M, Kautz T, Köpke U. Grouping and classification of wheat from organic and conventional production systems by combining three image forming methods. *Biological Agriculture & Horticulture* 2011; 27: 320-336.
- [69] Fritz J, Athmann M, Meissner G, Kauer R, Köpke U. Quality characterisation via image forming methods differentiates grape juice produced from integrated, organic or biodynamic vineyards in the first year after conversion. *Biological Agriculture & Horticulture* 2017; 33: 1-19.
- [70] Fritz J, Athmann M, Meissner G, Kauer R, Geier U, Bornhütter R et al. Quality assessment of grape juice from integrated, organic and biodynamic viticulture using image forming methods. *OENO One* 2020; 54 <https://doi.org/10.20870/oenone.2020.54.2.2548>.
- [71] Athmann M. Produktqualität von Salatrauke (*Eruca sativa* L.) und Weizen (*Triticum aestivum* L.): Einfluss von Einstrahlungsintensität, Stickstoffangebot, Düngungsart und Hornkieselapplikation auf Wachstum und Differenzierung. PhD Thesis, University of Bonn. 2011.
- [72] Geier U. Pflanzenorganbildtypen in Kupfer-chloridkristallisation und Steigbild. *Lebendige Erde* 2005; 5: 42-45.
- [73] Geier U. Grundlagen der Bildauswertung in den Bildschaffenden Methoden Kupferchloridkristallisation, Steigbild und Rundfilterchromatogramm. Technical Report, Forschungsinstitut am Goetheanum. 2005.
- [74] Geier U. Untersuchung der Auswirkungen verschiedener Leuchtmittel unterschiedlicher Herkunft auf Lebensmittel (Möhre, Apfel, Honig). Technical Report, Forschungsring Darmstadt. 2016.
- [75] Andersen J-O. Kobberklorid—krystallisationsmetoden kvalitativt og kvantitativt. MSc Thesis, University of Copenhagen. 1992.
- [76] Andersen J-O. Development and application of the biocrystallization method. PhD Thesis, Department of Agricultural Sciences/Organic Farming Unit The Royal Veterinary and Agricultural University Copenhagen. 2001.
- [77] Andersen JO, Laursen J, Koelster P. A Refined Biocrystallization Method applied in a Pictomorphological Investigation of a Polymer. *Elemente der Naturwissenschaft* 1998; 68: 1-20 <https://doi.org/DOI: 10.18756/edn.68.1>.
- [78] Kokornaczyk M. Quality comparison of organic and conventional wheat by use of common and holistic methods of analysis. PhD Thesis, The University of Pisa. 2008.
- [79] Kahl J. Entwicklung, in-house Validierung und Anwendung des ganzheitlichen Verfahrens Biokristallisation für die Unterscheidung von Weizen-, Möhren- und Apfelproben aus unterschiedlichem Anbau und Verarbeitungsschritten. Habil Thesis, University of Kassel. 2007.
- [80] Kahl J, Busscher N, Ploeger A. Validation of holistic methods testing organic food quality. *Biological Agriculture and Horticulture* 2010; 27: 81-94.
- [81] Kahl J, Busscher N, Meier-Ploeger. A. Differenzierung und Klassifizierung von Öko-Produkten mittels validierter analytischer und ganzheitlicher Methoden, Abschlussbericht zum Projekt Nr. 02OE170/F2. Technical Report, Bundesprogramm Ökologischer Landbau. 2007.
- [82] Busscher N, Kahl J, Andersen J-O, Huber M, Mergardt G, Doesburg P et al. Standardization of the Biocrystallization Method for Carrot Samples. *Biological Agriculture and Horticulture* 2010; 27: 1-23 <https://doi.org/10.1080/01448765.2010.10510427>.
- [83] Paoletti F, Raffo A, Kristensen H, Thorup-Kristensen K, Seljåsen R, Torp T et al. Multi-method comparison of carrot quality from a conventional and three organic cropping systems with increasing levels of nutrient recycling. *J Sci Food Agric* 2012; 92: 2855-2869 <https://doi.org/DOI:10.1002/jsfa.5819>.
- [84] Seidel K, Kahl J, Paoletti F, Birlouez I, Busscher N, Kretzschmar U et al. Quality assessment of baby food made of different pre-processed organic raw materials under industrial processing conditions. *Food Sci Technol* 2013; : 1-10 <https://doi.org/DOI 10.1007/s13197-013-1109-5>.
- [85] Szulc M, Kahl J, Busscher N, Mergardt G, Doesburg P, Ploeger A. Discrimination between organically and conventionally grown winter wheat farm pair samples using the copper chloride crystallisation method in combination with computerised image analysis. *Computers and Electronics in Agriculture* 2010; 74: 218-222

<https://doi.org/doi:10.1016/j.compag.2010.08.001>.

- [86] Kahl J, Busscher N, Mergardt G, Ploeger A. Standardization and performance test of crystallization with additives applied to wheat samples. *Food Analytical Methods* 2014; 8: 2533-2543 <https://doi.org/doi:10.1007/s12161-015-0142-6>.
- [87] Kahl J, Busscher N, Doesburg P, Mergardt G, Huber M, Ploeger A. First tests of standardized biocrystallization on milk and milk products. *European Food Research and Technology* 2009; 229: 175-178 <https://doi.org/doi:10.1007/s00217-009-1039-7>.
- [88] Kahl J, Busscher N, Hoffmann W, Mergardt G, Clawin-Raedecker I, Kiesner C et al. Development and Performance of Crystallization with Additives Applied on Different Milk Samples. *Food Analytical Methods* 2013; : 1-8 <https://doi.org/doi:10.1007/s12161-013-9759-5>.
- [89] Kahl J, Busscher N, Hoffmann W, Mergardt G, Clawin-Raedecker I, Ploeger A. A novel approach for differentiation of milk fractions and polyvinylpyrrolidone with different molecular weight by patterns derived from cupric chloride crystallization with additives. *Anal. Methods* 2014; 6: 3173-3176 <https://doi.org/doi:10.1039/C3AY41568F>.
- [90] Kahl J, Busscher N, Doesburg P, Mergardt G, Will F, Schulzova V et al. Application of Crystallization with Additives to Cloudy and Clear Apple Juice. *Food Analytical Methods* 2016; 10: 1-9 <https://doi.org/doi:10.1007/s12161-016-0575-6>.
- [91] Busscher N, Doesburg P, Mergardt G, Sokol A, Kahl J, Ploeger A. Crystallization patterns of an aqueous dihydrate cupric chloride solution in the presence of different amounts of Bovine Serum Albumin. *Journal of Crystal Growth* 2019; <https://doi.org/doi:10.1016/j.jcrysgro.2019.125272>.

CHAPTER 1

PRACTICAL CONSIDERATIONS

Which parameters are important to handle?

1.0 Which parameters are important to handle?

In the following, the parameters which have to be taken into account when dealing with a $\text{CuCl}_2 \cdot 2\text{H}_2\text{O}$ (cupric chloride di-hydrate, further called DCC) system, are described. The links to the chapters for a deeper understanding are added in the text. This chapter gives the reader a condensed overview of the important parameters and serves as a link table to the chapters for a deeper understanding of a topic for the daily work.

Crystallization Starting Time

From the beginning of the method the crystallization starting time was, besides Good Laboratory Practice (See also the habilitation of Kahl [1]) the decisive parameter (Pfeiffer, p. 84 in Bessenich [2], Selawry [3], Koopmans [4], Kahl [5], Barth [6]). The crystallization starting time is an important parameter for most samples and experiments (see chapter [1.1 Crystallization starting time](#)). It has a strong influence on the picture properties. For the Triangle system, when the environmental climate conditions are kept at defined values, the crystallization starting times is usually between 12 and 14 hours. So far, the known factors for the variation of the crystallization starting time are the location in the (inner) evaporation chamber and the nucleation process. The nucleation process depends on the evaporation of the water from the dish and the transport (see chapter [1.2 Water transport](#)) of the evaporated water out of the chamber. The mean crystallization starting time depends on the humidity in the chamber, when the solutions are pipetted into the dish (called the starting humidity) (see chapter [1.3 Crystallization start and starting humidity](#)) and the water transport of the evaporated water out of the inner chamber (see chapter [1.2 Water transport](#)). Maintaining the starting humidity at a defined value (see chapter [1.14 Chamber reset](#)) prior to each experiment is not simple and requires attention.

Through the evaporation each dish interacts with the other dishes. When different samples or different combinations of additive/DCC are being used in the chamber, the overall evaporation behavior, and thus the crystallization starting times, may be different from the experience with one sample and one additive/DCC combination.

The height of the (acrylic) ring of the Petri-dish (see chapter [1.4 Surface tension, cleaning, ring height](#)) has an influence on the evaporation - of mostly the water - from the dish. The ring height depends on the used chamber-system. The cleaning of the plates (see chapter [1.4 Surface tension, cleaning, ring height](#)) can also have an influence on the evaporation, because the surface tension of the solution depends on the cleaning.

It is important to take care of the meniscus after pipetting the solution, e.g. closing the meniscus with the tip of the pipette (see also chapter [1.5 Mensicus breakdown](#)). The meniscus influence on the "sensitive area" (see chapter [1.6 Sensitive area](#)) during crystallization is important.

Another reason why it is important to keep the evaporation rate constant (and therefore the crystallization starting time) is to maintain the chemical composition of the solution in the Petri-dish. The interaction of the DCC with the sample depends on the dynamic of the change of the pH over time. (see chapter [1.7 Evaporation issues](#)). As the pH of the solution changes from pH = 6 at the start of evaporation to pH = 0.5 at the start of the crystallization phase (see chapter [1.7 Evaporation issues](#)), variations in the evaporation time to a longer or a shorter time can affect the chemical composition in the dish.

Differences between winter and summer seasons

There are observations that the crystallization starting time has a yearly variation. Maybe this is a regulator problem (Triangle Systems). See "Other Effects" in chapter [1.1 Crystallization starting time](#).

Define Additive and DCC amounts for a sample

When the chamber environmental conditions are stable, the (3-5) amount(s) of the sample in question and the DCC amount (usually 150 mg DCC per plate) have to be chosen. The finding of the amounts is historically driven from experience by a balance between the additive influence and the DCC influence (Selawry [3], Engquist [7], Andersen [8], Waldburger [9]). The simplest way to define the optimal concentration is to ensure that the picture shows neither too much nor too little influence of the additive. From a study of concentration-matrix effects for different samples (see chapter [1.8 Concentration matrix](#)) we defined a procedure to find the optimal additive/DCC amounts in a matrix (see chapter [1.9 Optimal amounts](#)) for a sample. It boils down to finding the additive range where only one-centered pictures appear. At the lower end of the range, the crystallization type is usually split-

growth. At the upper end of the range the crystallization types dendritic or substance spirals appear (see [chapter 2.7 Substance spirals](#)). The beginning of the substance spiral range (or an increase in the number of centers) defines the upper end of the range. 3-5 amounts in the above defined range can be used. The optimal amount and choice of additional concentrations is usually in this range and depends on the research question, the samples, and the experience of the researcher. For more details see [chapter 1.9 Concentration matrix](#) and also [chapter 1.10 Transition between crystal types](#).

Influence of vibrations

Some chamber types (see [chapter 3.1 Chamber systems](#)) have taken precautions to prevent the influence of vibrations on the crystallization.

Wetting-up after an experimental free period

After a period of inactivity, on a routine base a wetting-up phase with water or DCC evaporation is performed. See [chapter 1.11 Wetting up phase](#).

Storage/Visual Light effects

During scanning, photographing and the visual evaluation on the light box the DCC pictures need to be kept in a dry air atmosphere where the relative humidity is below 70 %. Otherwise the humidity will damage the DCC picture and the pictures will dissolve.

On the light box, and in some cases on photos taken from the photo box, the pictures show a 4-quadrant effect. Two quadrants are connected by the shape of an hourglass. One hourglass is brighter, the other is darker: when the image is rotated the bright/dark hourglasses maintain their position. This can be seen as a light polarization effect or a local light effect (in the case the photo or light box contains only two TL bulbs and not a circular light source). The photos of the DCC pictures are taken with a so called photo box (see master of Daniel Funda 2012 [10]).

The scanning of the DCC pictures (see [chapter 3.2 LabDoc tool](#)) is done (usually two days after the pictures were made) with a so called IT8 reference slide (see [chapter 3.2 LabDoc tool > IT8-reference-dia](#)). The IT8 reference slide, which is scanned with the pictures, is used for two reasons. On the one hand, the IT8 slide is used to check whether the scanner is stable in the color measurements of the picture, on the other hand, it is used in the image analysis to convert the R(ed) G(reen) B(blue) values into the L(uminiscence) C(hroma) h(ue) color system.

Multiple Centers and picture zones

When looking at the pictures, it is usually only for higher amounts of additive that multiple centers (see [chapter 1.12 Multiple centers](#)) can appear. Unexpected multiple centers may indicate a problem during the process from sample to picture.

The zone in the picture (see [chapter 1.13 Picture zones](#)) where the highest differentiation between different samples is expected, is the so called middle zone. This area is also called the sensitive area (see [chapter 1.6 Sensitive area](#)) with the highest differentiation.

References

- [1] Kahl J. Entwicklung, in-house Validierung und Anwendung des ganzheitlichen Verfahrens Biokristallisation für die Unterscheidung von Weizen-, Möhren- und Apfelproben aus unterschiedlichem Anbau und Verarbeitungsschritten. Habil Thesis, University of Kassel. 2007.
- [2] Bessenich F. Zur Methode der empfindlichen Kristallisation (Naturwissenschaftliche Sektion am Goetheanum Dornach, 1960).
- [3] Selawry A and Selawry O. Die Kupferchlorid-Kristallisation in Naturwissenschaft und Medizin (Gustav-Fischer-Verlag, 1957).
- [4] Koopmans A. Zeitabhängigkeiten bei empfindlichen Kristallisationen. *Elemente der Naturwissenschaft* 1965; 2: 1-7 <https://doi.org/10.18756/edn.2.1>.
- [5] Kahl Johannes NBGMJ-OAMH, Meier-Ploeger A. Bestimmung der Zeitabhängigkeit der Kristallisationsvorgänge bei der Kupferchloridkristallisation als eine Voraussetzung zur Validierung der Methode. *Elemente der Naturwissenschaft* 2004; 80: 90-100.

- [6] Barth J-G, Roussau J, Suppan K, dos Santo SR. Crystallisation of a film of copper chloride in the presence of additives. *Elemente der Naturwissenschaft* 2011; 94: 69-99 <https://doi.org/DOI: 10.18756/edn.94.69>.
- [7] Engquist M. Die Gestaltkräfte des Lebendigen (Vittorio Klostermann, 1970).
- [8] Andersen JO, Huber M, Kahl J, Busscher N, MeierPloeger A. A concentration matrix procedure for determining optimal combinations of concentrations in biocrystallization.. *Elemente der Naturwissenschaft* 2003; 79: 97-114.
- [9] Waldburger B. Begriff und Kontext in der Methode der Empfindlichen Kristallisation. *Elemente der Naturwissenschaft* 2005; 83: 79-89 <https://doi.org/10.18756/edn.83.79>.
- [10] Funda, D. Konstruktion und Aufbau einer Fotobox für Streulichtphotographie von $\text{CuCl}_2 \cdot 2\text{H}_2\text{O}$ Bildern, 2012.

1.1 Crystallization starting time

How can we determine / define / constitute the crystallization starting time?

Abstract

The crystallization starting time (in short [tcrStart](#)) is besides the additive and the $\text{CuCl}_2 \cdot 2\text{H}_2\text{O}$ (cupric chloride di-hydrate, further called [DCC](#)) amount one of the important factors of influence for the [picture properties](#) of a DCC crystallization. To define the [tcrStart](#), the factors of influence like the starting humidity (short and long term), the gradient between the inner and outer chamber, the temperature in the chamber, but also the DCC amount should be considered. This chapter describes and discusses how to deal with these factors based on the example of a so called Triangle chamber. The short term starting humidity depends on the water reservoir in the inner chamber, the recovery of the climatic conditions after a previous experiment (see chapter [1.14 Chamber reset](#)), and on the breathing intensity of the pipetting person. The long term starting humidity depends on the gradient between the inner and outer chamber and on maintaining constant conditions in the inner and outer chamber. These conditions are set by regulating 1) the relative humidity and the temperature in the outer chamber, 2) the temperature in the inner chamber, and 3) the humidity in the inner chamber, as defined by the coverage of the reservoir with plastic balls in the inner chamber. Finally, nucleation, as the cause of the [tcrStart](#), is considered a statistical effect.

Introduction

When a mixture of an additive and $\text{CuCl}_2 \cdot 2\text{H}_2\text{O}$ (cupric chloride di-hydrate, further called [DCC](#)) is pipetted into a Petri-dish, the evaporation starts and, after some time, the crystallization begins. The [tcrStart](#) is defined as the time difference between the moment the solution is pipetted into the Petri-dish and the moment of first appearance of a crystal in the Petri-dish. As the crystallization is not induced by seeding a crystal into the solution in the Petri-dish, the images in most cases have different [tcrStart](#) values. Besides the additive and the DCC amount of the solution, [tcrStart](#) is an important factor for the [picture properties](#) of a DCC picture. The value of [tcrStart](#) depends on the following factors:

- 1.1 starting humidity and temperature in the inner chamber.
- 1.2 humidity and temperature in the outer chamber.
- 1.3 the permeability of the wall between inner and outer chamber.
2. the airflowing around the Petri-dish (position on the evaporation apparatus).
3. the chamber solution volume pipetted into the Petri-dish.
4. the sample in question (additive, evaporation rate).
5. the DCC and the additive amount.
6. the statistical nucleation effect.

In the following, these factors will be described and ways to deal with them are discussed.

Historical overview

From the very beginning of the work with DCC pictures Pfeiffer (1935 [1], p. 59) already described the importance of a “waiting” or “preparation period” of 14 - 16 hours before the crystallization starts, in order to obtain expressive and one-centered pictures (see also chapter [1.12 Multiple centers](#)). He claimed that the starting time was dependent on the location in the chamber and had to be chosen based on empirical data, determining which location had which starting time (Pfeiffer 1935 [1], p. 60). Later, Selawry emphasized that the [tcrStart](#) should be below 18 hours and preferably around 7 - 8 hours (1957 [2], p. 26, Fig. 13). Von Hahn also emphasized the importance of the so called “*preparation period*” (1962 [3], p. 12). Lastly, Koopmans (1965 [4]) tested the influence of the starting time on blood samples between 8 and 26 hours and found the highest differentiation at 13 hours. He observed significant changes in a picture at a time difference of as little as 15 minutes. Notice, this is not the so called “latency” or “hold-on” phase that occurs when the evaporation stops, around the solubility border of DCC in the Petri dish.

The general difference between pictures with different [tcrStart](#) values is that the early pictures are more rigid or skeletonized and the late pictures are more chaotically shaped and richer in finer details. Selawry (1957 [2], p. 25) connected the forms of the late pictures for blood crystallization to the degradation of the proteins due to prolonged exposure to high DCC concentrations. During the evaporation the pH of the solution decreases and reaches 0.5 at the [solubility border](#) of DCC. This can affect the sample quite strongly, and the longer the sample remains under these conditions the greater the chance is to observe this effect (see also chapter [1.7 Evaporation issues](#)). See for examples of early and late pictures [Appendix 1.1.1 Carrot and wheat](#) and [Appendix 1.1.2 Cress](#).

Andersen designed a type of evaporation apparatus (1998 [5], Fig. 4 and Fig. 5), to minimize the influence of the position of the Petri-dishes on the tcrStart. To increase the stability of the starting humidity and the permeability of the chamber walls, Andersen added a water reservoir to the inner chamber (1998 [5], Fig. 5). The resulting humidity in the chamber depended on the coverage of the reservoir with plastic balls, the temperature in the chamber, the conditions of the permeability of the walls between the inner and outer chamber and the humidity and temperature in the outer chamber. The resulting humidity is stable when the difference between the humidity leaving the reservoir and the humidity leaving the inner chamber is zero (see also chapter [1.2 Water transport](#)). This also maintains the stability of the permeability of the wooden chamber walls.

Authors Research

The tcrStart can be seen as the result of two interconnected phases. The first is the evaporation phase, with duration t_{evap} from the time the solution is pipetted in the Petri-dishes until the DCC concentration reaches the solubility border, and the second is the nucleation phase in which the DCC concentration increases above the DCC solubility border until the start of crystallization. During the second phase the DCC concentration is above the solubility border and has a positive [supersaturation](#), which means that nucleation can occur, therefore the supersaturation is called t_{nuc} (see also chapter [2.11 Nucleation](#)).

$$t_{\text{crStart}} = t_{\text{evap}} + t_{\text{nuc}}$$

If we divide the influencing factors according to their contribution to the two phases, we obtain the following table:

Table 1.1.1 Factors influencing the tcrStart, divided according to their contribution to the evaporation phase (t_{evap}) or the nucleation phase (t_{nuc}).

factor	t_{evap}	t_{nuc}
1.1 starting humidity and temperature in the inner chamber	X	
1.2 humidity and temperature in the outer chamber	X	
1.3 the permeability of the wall between inner and outer chamber	X	
2. the airflow passing the Petri-dish (position on the evaporation apparatus)	X	
3. the volume which is pipetted into the Petri-dish	X	
4. the sample in question (additive)	X	X
5. the DCC and the additive amount	X	X
6. statistical nucleation effect		X

The first three items in Table 1.1.1 (1.1, 1.2 and 1.3) are interconnected. Kahl (2004 [6]) checked for the dependency of the mean tcrStart on the [starting humidity](#) (the humidity in the chamber before the pipetting of the solution). He found an increase in tcrStart of approximately one hour for 1 % increase in relative humidity (starting from 50 % rel. humidity). The dependency of tcrStart on the starting humidity is described in detail in the chapter [1.3 Crystallization start and starting humidity](#). In summary: the volume of the chamber can hold only a part of the humidity evaporating from the Petri-dish. The humidity has to leave the chamber during the evaporation process or the evaporation rate will firstly decrease and eventually stop.

The long term starting humidity can be set by adapting the climate in the outer chamber. The humidity flow from the inner to the outer chamber depends on the difference of the absolute humidity between the inner and outer chamber. The absolute humidity in g / m^3 is calculated from the temperature and the relative humidity (see Appendix in chapter [1.2 Water transport](#)). In a project in 2012 the need to reduce the tcrStart by 1 hour arose. In order to do so, the absolute humidity was reduced for a year (from February 2012 to February 2013, chamber B and C, Witzhausen) by a reduction of the temperature of the outer chamber from 26 °C to 25 °C. Changing the relative humidity would have taken 2 - 3 months for the wooden walls to adapt, see Busscher 2009 ([7], p. 82 ff.). As a result, there was a greater flow of humidity from the inner to the outer chamber which resulted in a lower starting humidity in the inner chamber. The heat flow from the inner to the outer chamber also increased which resulted in increased heating of the crystallization apparatus, which led to a higher airflow around the dishes. Both effects, the humidity flow and the heat flow resulted in a decrease of the tcrStart of roughly one hour.

The short-term starting humidity, shortly before or during the pipetting of the solution into the Petri-dishes, depends on the residual humidity of the preceding experiment, the so called reset of the chamber, the amount of respiration during pipetting and the humidity losses caused by opening the chamber door when entering

and leaving the chamber. This is discussed in detail in the chapter [1.14 Chamber reset](#). In summary, with specific management the starting humidity can be maintained on a constant value. The breathing influence is around and below 1 % relative humidity (data from CO₂ measurements). How much it is compensated by the opening of the door during entering and leaving the chamber is not clear.

The permeability of the chamber wall can be controlled in a static way by monitoring the amount of water to refill the reservoir and maintaining the absolute humidity in the chamber. The dynamic control can be done with a so called “[Step response](#)” test, where the temperature and / or the humidity in the outer chamber is stepwise changed and the time response is evaluated (see Busscher 2009 [7], p. 36 ff.).

The influence of factors 2. (airflow per dish) and 6. (statistical nucleation effect) from Table 1.1.1, can be visualized by plotting the $t_{crStart}$ values for two years against the position of the Petri-dishes in the chamber. The plot in Fig.1.1.1 shows the combination and separation of these two phases (evaporation due to airflow and nucleation):

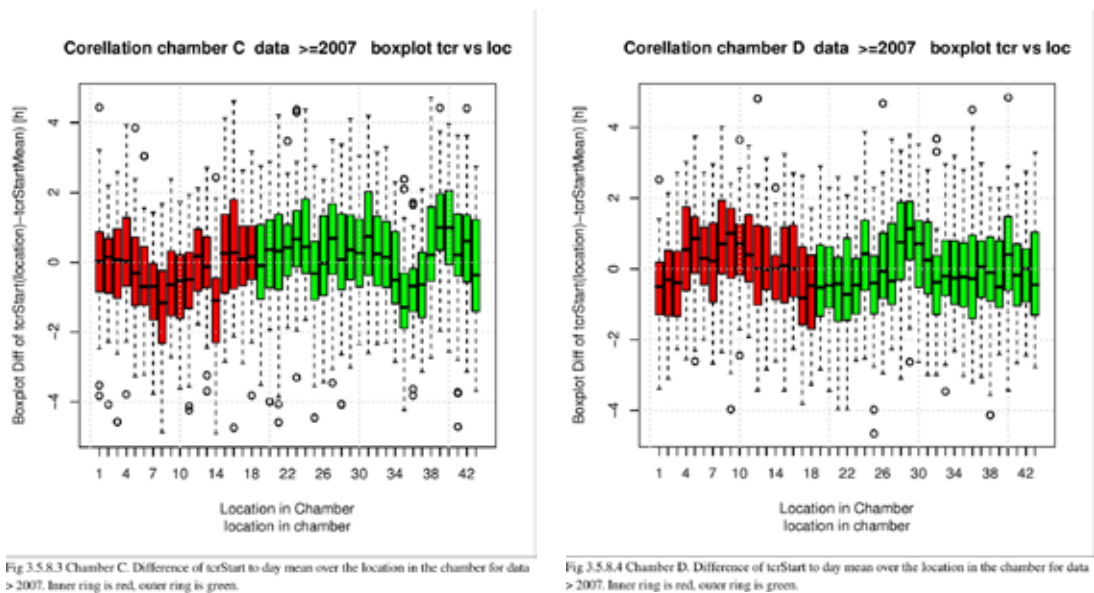


Fig.3.5.8.3 Chamber C. Difference of $t_{crStart}$ to day mean over the location in the chamber for data > 2007. Inner ring is red, outer ring is green.

Fig.3.5.8.4 Chamber D. Difference of $t_{crStart}$ to day mean over the location in the chamber for data > 2007. Inner ring is red, outer ring is green.

Fig.1.1.1 Boxplots of the crystallization starting times versus the location in the Triangle type chamber (43 Petri-dishes) for two chambers; in Kassel Witzenhausen C (left) and Louis Bolk Institute NL (right). Data are plotted from all combined experiments for the years 2007 and 2008, regardless of DCC and additive amounts and samples. Red boxes represent the 18 inner ring locations, green boxes represent the 25 outer ring locations. Data from Busscher 2009 [7].

In Fig.1.1.1 the influence of the two phases (evaporation due to airflow and nucleation) can be visualized. The t_{evap} influence is visible through the dependency on the position in the chamber, because each position has a slightly different airflow passing the Petri-dish. The variation per position is comparable for each dish and shows the t_{nuc} effect. See for the statistical distribution of the $t_{crStart}$ in chapter [2.11 Nucleation](#). Consequently, pictures with the same $t_{crStart}$ can have a different t_{evap} and t_{nuc} . It was observed, that when the pictures from the same sample and the same DCC and additive amounts were sorted according to $t_{crStart}$ a trend in the patterns from early to late pictures became apparent. One out of 5 to 10 pictures does not fit this trend. We hypothesized that this could be because t_{evap} and t_{nuc} resulted in the same $t_{crStart}$ but that the balance between t_{evap} and t_{nuc} differed from the other pictures (see Additional Research).

The influence of Table 1.1.1 item 5. (DCC and additive amount) on the $t_{crStart}$ is that when the amount of additive is increased, the $t_{crStart}$ value also increases in the cases that have been observed so far. This is consistent with the idea that an increase in additive inhibits the nucleation process and therefore increases supersaturation, ergo a longer evaporation time is needed before the nucleation can start.

As the DCC amount is increased (usually 150 mg per plate is used), the $t_{crStart}$ will also increase to a maximum DCC amount of 2000 mg per plate. The $t_{crStart}$ will then decrease to zero as the DCC amount is increased towards the solubility border of ~ 5600 mg DCC per plate. The increase of the $t_{crStart}$ to 2000 mg DCC per plate is counter intuitive, because the amount of water to evaporate decreases as the DCC amount increases. This is a consequence of the effect of the partial pressure above a salt solution, which decreases as the salt amount

increases, thus decreasing the evaporation rate. For details see chapter [1.2 Water transport](#) and chapter [2.13 Evaporation model](#).

Other effects

In Kassel Witzhausen a variation of $t_{crStart}$ with the seasons was observed. In the summer the $t_{crStart}$ was slightly higher than in the winter. The hypothesis was that due to the heating in winter an increase in PM2.5 and PM10 sized dust particles occurred, resulting in an earlier nucleation. Another hypothesis is that the floor of the chamber, which is located in the cellar, cools down in winter, which leads to an increased heat compensation of the heating system and consequently an increase of the airflow passing the dish, resulting in an earlier $t_{crStart}$. Additionally, due to the regulation principle, the humidity regulation in the outer chamber is slightly higher in the summer and slightly lower in the winter, which results in a later $t_{crStart}$ in the summer and an earlier in the winter.

In general, in all chambers, it is a routine practice that after a prolonged period of experimental inactivity, the first experiment should be a water-only experiment, as the pictures from the first experiment generally do not match the usual pictures. This is discussed in the chapter [1.11 Wetting up phase](#).

Resume

The $t_{crStart}$ is, along with the DCC and additive amount, an important factor determining the [picture properties](#). The dependence of the mean $t_{crStart}$ per experiment on the starting humidity requires special handling to restore the humidity to a defined value after an experiment. The summands of the evaporation and nucleation contributing to the $t_{crStart}$ have not been easy to separate. In particular, this caused problems when two pictures have the same $t_{crStart}$ and one has a shorter evaporation time and a longer nucleation time while the other has a longer evaporation time and a shorter nucleation time. During the nucleation time the pH is at its lowest and the sample is degraded the most, as Selawry (1957 [2]) already mentioned, which is not accurately reflected in the $t_{crStart}$ value.

Additional research

$t_{crStart}$ versus additive amount

The influence of a higher $t_{crStart}$ on the picture properties has some effects which resemble those of higher additive amounts (J. Kahl, private communications). If a higher $t_{crStart}$ value degrades the sample, as Selawry proposed, then a higher additive amount, which causes a higher $t_{crStart}$, could cause a higher degradation of the sample too. Perhaps an increase of the $t_{crStart}$ could be a possibility to research this hypothesis.

The degradation of a sample could be measured by viscosity measurements of the additive at different DCC amounts, e.g. the type of viscosity could change (Lombrana 1985 [8]). So far lower DCC amounts seem to conserve the sample (observation Mergardt 2023). Higher DCC amounts possibly degrade the sample, depending on the duration of exposure. The measurements of Mergardt (2012 [9]) did not take this question into account. The DCC was increased by adding DCC to the solution, while the additive remained in the solution.

Quality control chamber

The variation of the $t_{crStart}$ versus the location in the chamber should be constant, if nothing is changed in the setup of the chamber system (e.g. repositioning of the heating, humidifier, dehumidifier in the outer chamber).

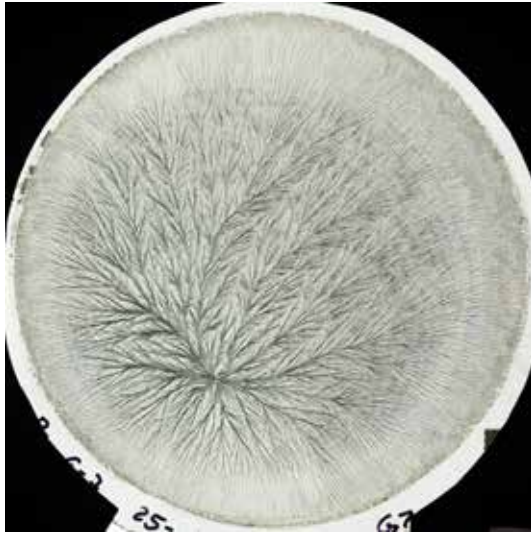
$t_{crStart}$ and t_{evap} and t_{nuc}

To study the summands t_{evap} and t_{nuc} of $t_{crStart}$, a pH indicator as additive should be used. By calibrating the color of the pH indicator with the DCC concentration (e.g. with a [one dish test bench](#)), the concentration can be determined for a defined length of time and from this the evaporation rate and t_{evap} can be determined for each location in the chamber. From t_{evap} and $t_{crStart}$, t_{nuc} can be determined. This also provides an opportunity to study the evaporation stability at each position.

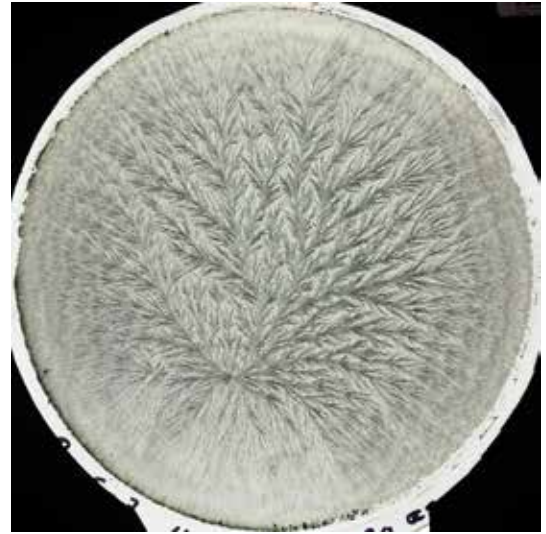
Summer winter influence

The observation of the seasonal effect needs to be made more explicit. If the effect is significant, the heating information and the amount of particles in the air (from own direct measurements or from nearby state monitoring stations) can be compared. In this context the influence of the outer chamber regulator needs to be taken into account.

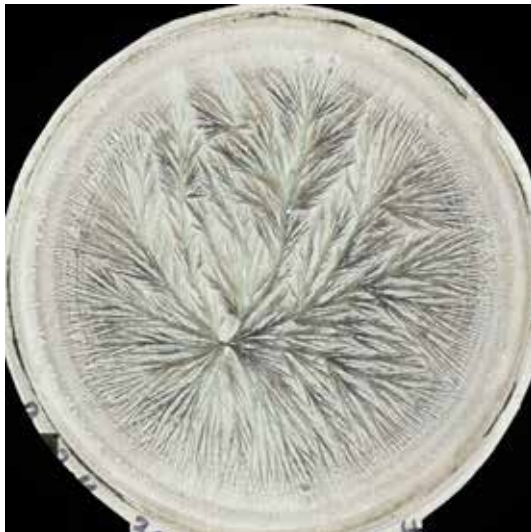
Appendix 1.1.1 Carrot and wheat



G-J 25, tcrStart = 11:30 h



G-J 11 tcrStart = 15:50 h



J-M 30, tcrStart = 10:51 h



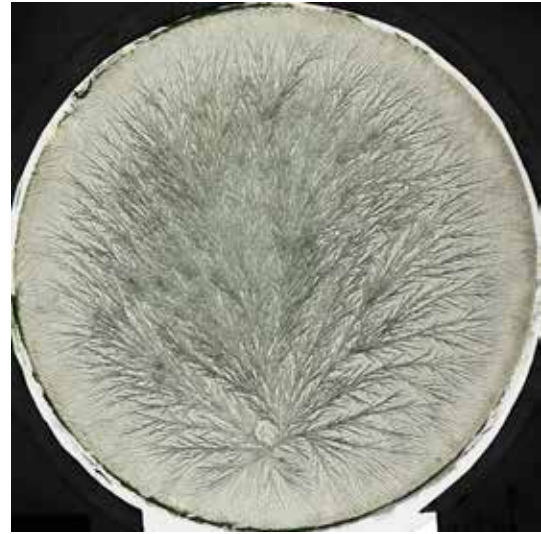
J-M 18, tcrStart = 16:11 h

Fig. 1.1.2 Difference between picture properties for early and late DCC pictures. Upper row DCC pictures from carrot. DCC amount = 90 mg per plate, carrot = 115 mg per plate, LabDoc series = B.2004.10.14.G-J from chamber B University of Kassel (D). Lower row DCC pictures from wheat. Left column low tcrStart values, right column high tcrStart values. DCC amount = 90 mg per plate, additive amount = 70 mg per plate, LabDoc series = B.2006.02.14.J-M from chamber B University of Kassel (D).

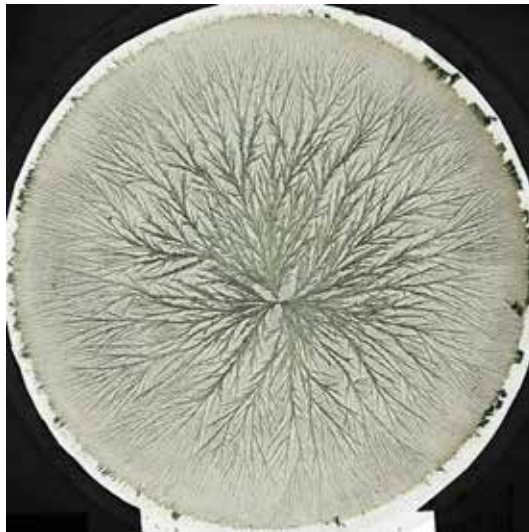
Appendix 1.1.2 Cress



CY 39 tcrStart = 12:50 h



CY 29 tcrStart = 16:10 h



CY 02 tcrStart = 13:00 h



CY 34 tcrStart = 16:10 h

Fig. 1.1.3 Difference between picture properties for early and late DCC pictures. All DCC pictures from cress. Left column low tcrStart values , right column high tcrStart values. DCC amount = 150 mg per plate, cress = 300 mg per plate. LabDoc series P.2015.08.03.CY from chamber P (NL).

References

- [1] Pfeiffer E. Empfindliche Kristallisationsvorgänge als Nachweis von Formkräften im Blut (Emil Weises Buchhandlung Dresden, 1935).
- [2] Selawry A and Selawry O. Die Kupferchlorid-Kristallisation in Naturwissenschaft und Medizin (Gustav-Fischer-Verlag, 1957).
- [3] Von Hahn F-V Thesigraphie. (Franz Steiner Verlag, 1962).
- [4] Koopmans A. Zeitabhängigkeiten bei empfindlichen Kristallisationen. *Elemente der Naturwissenschaft* 1965; 2: 1-7 <https://doi.org/10.18756/edn.2.1>.
- [5] Andersen JO, Laursen J, Koelster P. A Refined Biocrystallization Method applied in a Pictomorphological Investigation of a Polymer. *Elemente der Naturwissenschaft* 1998; 68: 1-20 <https://doi.org/DOI: 10.18756/edn.68.1>.
- [6] Kahl Johannes NBGMJ-OAMH, Meier-Ploeger A. Bestimmung der Zeitabhängigkeit der Kristallisationsvorgänge bei der Kupferchloridkristallisation als eine Voraussetzung zur Validierung der Methode. *Elemente der Naturwissenschaft* 2004; 80: 90-100.
- [7] Busscher N. Checking Influences: Untersuchung der Einflussgrößen bei der Biokristallisation als Voraussetzung für die Übertragbarkeit der Kammern und Prozeduren in andere Laboratorien und zur Reduzierung der Variationen durch die Kammer und die Orte. Technical Report, University of Kassel. 2009.
- [8] Lombraña J, Días J. Rheological and Chemical Changes in Stored Carrot Juice. *Can. Inst. Food Sel. Technol. J.* 1985; [https://doi.org/doi:10.1016/S0315-5463\(85\)71918-9](https://doi.org/doi:10.1016/S0315-5463(85)71918-9).
- [9] Mergardt G. Simulation des Entstehungsvorganges von Kristallbildern zur Messung der physikalischen Parameter pH-Wert, Dichte und Viskosität am Beispiel von PVP, Glykogen und Bovine Serum Albumin. Technical Report, University of Kassel. 2012.

1.2 Water transport

How is the water transport from the dish to the inner chamber, outer chamber and outer world.

Abstract

The transport of the evaporated water from the dish depends on different factors. The evaporated water is transported from the dish into the chamber volume by the airflow around the dish. The amount of water vapor in the chamber volume therefore increases by this amount. Some of the water vapor leaves the chamber volume. Either into the walls or through the walls of the inner chamber ([Triangle type](#)) to the humidity controlled outer chamber (see [Appendix 1.2.2 Chamber](#)). Other types of chambers have some kind of a regulation of the relative humidity (the so called Topf type [1]) or temperature and relative humidity (Bonn type, used at the University of Bonn and chamber Jean-George Barth) of the airflow. The evaporation rate, the amount of water leaving the solution in the Petri-dish, is more complicated for the $\text{CuCl}_2 \cdot 2\text{H}_2\text{O}$ (cupric chloride di-hydrate, further named [DCC](#)) only case than for the water only case. For both cases (water with and without DCC), the humidity in the chamber increases during the evaporation which decreases the evaporation rate from the dish. For the case with DCC, the evaporation rate of the DCC solution also decreases as the concentration of DCC increases, which decreases the partial pressure or the humidity above the solution. This is reflected in the formula of Stefan, see Suehrcke (1995 [2]) for an introduction. If and how the evaporation process is affected by an additive is not clear until now.

Introduction

The appearance of the $\text{CuCl}_2 \cdot 2\text{H}_2\text{O}$ (cupric chloride di-hydrate, further named [DCC](#)) picture is influenced by the start of the crystallization (tcrStart). The tcrStart primarily depends on the time needed for the solution to reach the solubility border concentration of [DCC](#). The required time depends on the rate of the evaporation of the water from the dish, which depends on the velocity and humidity of the airflow passing the Petri-dish. The evaporation rate also depends on the design (e.g. the direction of the airflow relative to the Petri-dish) and the parameters of the evaporation system (e.g. the height of the rim of the Petri-dish, the type of humidity control) including the chamber walls. The evaporation rate of the solution can be subdivided into three different cases: water only, DCC without additive and DCC with additives. In the following, the factors of influence and how they interact with each other are described in more detail.

Historical Overview

The evaporation from a Petri-dish with DCC was first researched by Holleman [3], as a special case of the problem of Stefan [4]. The measurements were repeated and confirmed by Busscher in 2010 [5]. The work from other authors is mentioned in the context of the section "Authors Measurements", and is therefore not mentioned here.

Authors Measurements

Transport rate and evaporation rate

The transport of the water (and other volatile compounds) from the dish depends on the height of the ring (shielding) and the condition of the air and the velocity of the air passing the dish. This can be summarized as the transport rate of the air passing the dish. The condition of the air refers to the ability of the air to absorb water proportional to the difference between the actual relative humidity and the maximum relative humidity of 100 %. During the evaporation, the chamber volume is "filled" by the evaporating water, increasing the actual relative humidity, which reduces the difference between actual and maximum humidity, and with that the transport rate.

The evaporation rate is the amount of water leaving the solution in the dish. This depends on the so called saturation humidity directly (≤ 1 mm) above the solution in the dish. For water this saturation humidity is 100 %. When adding DCC this value decreases with the DCC amount according to Lilich 1956 [6] and 1963 [7] (see [Appendix 1.2.3 PartialPressure](#) for the graphs). For a saturated DCC solution the saturation humidity is 67 % (Rockland [8]) and is almost temperature independent between 25 °C to 40 °C. How the additive in question influences this evaporation rate is not clear (additional research needed).

When we look at a DCC-only solution during evaporation, the transport rate and thus the evaporation rate decreases over time. The relative humidity in the chamber does not exceed 67 %. When the relative humidity in the chamber reaches the saturation value of the relative humidity above the solution, evaporation stops. This is

reflected in the formula of Stefan (1873 [9]), see Suehrcke (1995 [2]) for an introduction. Whether the maximum of 67 % is due to the saturation value of DCC or a dynamic feature of the system was investigated in the chapter [2.13 Evaporation model](#). A precise theoretical approach with measurements is given by Misyura [10], who worked on the evaporation of water solutions of CaCl₂, BaCl and LiCl in a Petri-dish.

Influence of chamber volume

Koopmans (1970) [1] expected that the volume of the chamber could hold all the humidity. For the Triangle chamber with 10 m³ volume and with 43 dishes with 6 mL each, we can calculate the amount of water leaving the dish. Around 5.86 mL per dish needs to evaporate for the usual used DCC amounts (see [Appendix 1.2.4 Water](#)) to start crystallization. In total 5.86 * 43 = 252 mL water must evaporate. The maximum amount of water vapor per m³ that can be absorbed in air at 30 °C is around 30.32 mg [11]. That means that at 100 % relative humidity 1 m³ of air contains 30.32 mg water vapor. The starting humidity is around 50 % which means that only half of the 30.32 mg / m³ is left for the water vapor from the Petri-dishes. To raise the relative humidity from 50 to 100 %, 15.16 mg per m³ is required. In 10 m³ this means that there is a maximum “space” for 150 mg water vapor. The 215 mL from the 43 dishes would not fit into this. When we take into account that the maximum humidity is below 67 % because of the saturated DCC solution (see also Fig. 1.2.1) then the available space for the water vapor to fill is limited to the difference between the initial chamber humidity (50 %) and the saturation humidity (67 %) which amounts to 17 % (67 % - 50 %) instead of 50 = 100 - 50 %. This gives a real water vapor “space” of 150 * (17 / 50) = 51 mg.

Resume

The conclusion is that most of the water evaporating from the dishes has to leave the inner chamber, either through the walls to the outer chamber or by absorption of the wooden inner wall of the chamber (Triangle chambers) or be transported away by the airflow (Topf type, Bonn type, see chapter [3.1 Chamber systems](#)), otherwise the evaporation would stop, inhibiting the crystallization start.

Humidity measurements

Fig. 1.2.1 shows the humidity measurements for the Triangle system according to Andersen [12], during a crystallization process. This is a typical result (see [Appendix 1.2.2 Chamber](#) for more info).

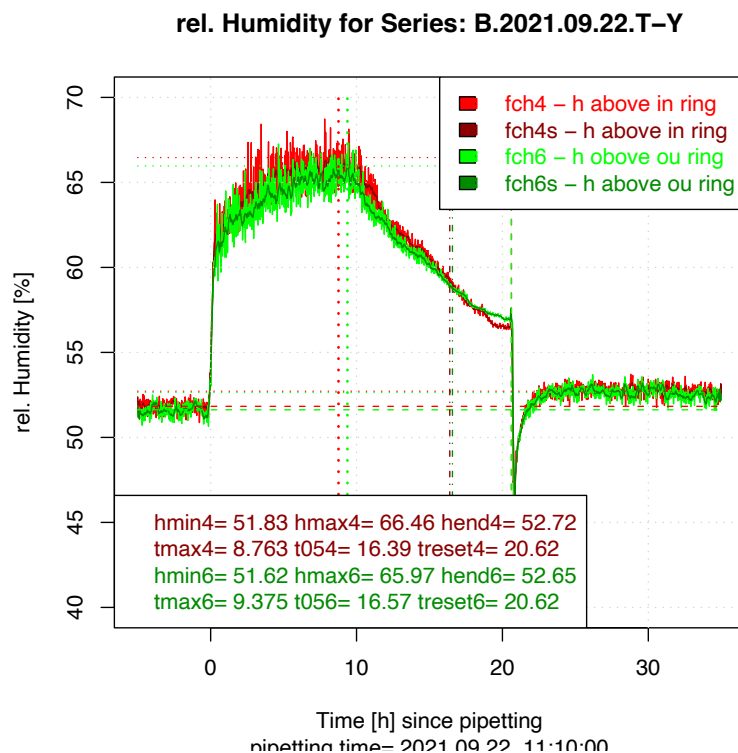


Fig. 1.2.1 Relative humidity (Y-axis in %, red and green curves) above two Petri-dishes versus evaporation time (X-axis in hours) since pipetting (at t = 0) for a Triangle type of chamber. The sample is reference wheat, amounts DCC = 90 mg per plate, additive = 90 mg per plate, in a total volume of 6.0 mL with a 3.5 cm high rim mounted onto the glass plate. Location is University of Kassel (D), Witzenhausen chamber C.

In Fig. 1.2.1 [Relative humidity](#) measurements are shown. The solution is pipetted at t = 0. The relative humidity (red curve: sensor above the dish on the so called inner ring, green curve: sensor above the dish on the

outer ring) first increases very strongly, then at > 60 % the increase is significantly slowed down. Between 8.76 to 9.37 hours the maximum relative humidity is reached (< 67 %, dotted red and green vertical lines) and the humidity decreases. After 20 hours (t-reset, green dashed vertical line, which is partly hidden by the measurement data of the reset) the chamber door is opened and the relative humidity drops due to the contact with the outer chamber air, which is lower and cooler.

Transport into or through the outer chamber wall

Based on the previous discussion on the effect of the volume of the chamber, it was concluded that most of the water vapor must leave the chamber. The first hypothesis would be that the driving force for the water transport should be the difference in absolute humidity (in g / m^3) inside the chamber between the dishes and the inner wall and over the chamber wall (inner wall – outer wall).

For the evaporation curve as shown in Fig. 1.2.1 (but for another experiment and the additive cheese) the absolute humidity (fabs) is displayed in Fig. 1.2.2 (see for details [Appendix 1.2.1 Absolute Humid](#)). Also shown are the fabs values from a sensor at the inner chamber wall (magenta) and the difference between the fabs values above the dish and at the wall (red-yellow and green-blue; units according to the right Y-axis). The black line represents the cumulative number of started crystallizations, with the 14th, 28th and 40th marked.

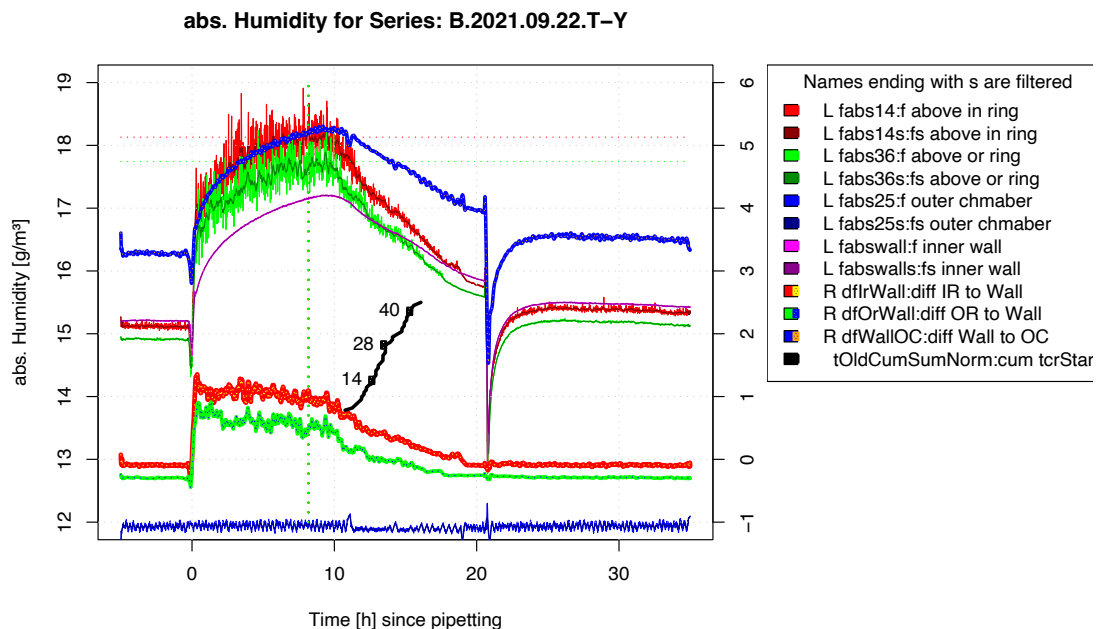


Fig. 1.2.2 Absolute humidity fabs (left Y-axis in mg / m^3) versus evaporation time (X-axis in hours) since pipetting at $t = 0$ for a Triangle chamber type. In red, fabs over the inner ring, in green, over the outer ring; in magenta, for the inner wall; and in blue, for the outer wall. The right Y-axis shows the differences in fabs (in mg / m^3) between: in red-yellow the inner ring and inner wall, in green-blue between the outer ring and inner wall. Data from the [Triangle type chamber](#) from the University of Kassel, Witzenhausen Chamber C.

In Fig. 1.2.2 the X-axis represents the time since pipetting in hours. Left from $x = 0$ the values for the red, green (above the dishes) and the magenta curves (at the inner wall) should be the same (deviations are due to aging of the sensors), because the distribution of the water vapor in the chamber is uniform when there is no evaporation from the dishes (only from the reservoir). Due to the location of the inner chamber heating below the dishes, the temperature above the dishes is higher than the inner wall sensor temperature. But if there is no evaporation the fabs should be nearly constant throughout the chamber. After pipetting, the fabs above the dishes (red and green curves) rises rapidly as already shown in Fig. 1.2.1. The inner wall fabs (magenta) slowly follows. After reaching a maximum (green perpendicular dotted line at $x = \sim 9$ hours) the humidity decreases and ~ 1 hour later the first crystallization starts (begin of the black line). The cumulative number of started crystallizations follows the black curve and roughly after 5 hours all solutions have started crystallizing.

To visualize the water flow from the dishes to the wall, the difference between the fabs above the dishes and the fabs at the wall (magenta) is plotted as the red-yellow and green-blue lines (values indicated on the right Y-axis). Between the start at $x = 0$ (pipetting) and the maximum at $x = \sim 9$ hour (green perpendicular dotted line) the difference of the fabs between the dishes and the wall is roughly constant. Between the maximum fabs value and the first crystallization (at $x = \sim 10$ hours) the difference decreases, which points to a decrease in the

evaporation, probably due to the influence of the DCC concentration in the Petri-dish. This question is handled in the chapter [2.13 Evaporation model](#).

Influence of the chamber reservoir

The Triangle type chambers contain a water reservoir in the inner chamber. The purpose of the reservoir in the chamber (see Andersen [12], p. 8, Fig. 5) is to keep the inner (starting) humidity at a defined level and the wood of the inner chamber in a defined condition. There is a constant flow of vapor from the water reservoir in the inner chamber through the chamber walls to the outer chamber. The water “consumption” of the reservoir is around 1.4 L per week, which means roughly 200 mL per day, which is of the same magnitude as the 215 mg evaporating from the dishes during an experiment. The water flow from the reservoir is $200 \text{ mL} / 24 \text{ h} = 8.33 \text{ mL} / \text{h}$. Assuming that 50 % of the water from the dishes evaporates in 9 hours (until the maximum fabs level is reached), then the mean evaporation rate from the dishes is $0.50 * 252 \text{ mg} / 9:00 \text{ h} = 14 \text{ mL} / \text{h}$.

The difference in fabs - as a driving force, like a concentration gradient - between the inner and outer chamber, when no experiment is running, is around $(15 - 12) = 3 \text{ g} / \text{m}^3$ (see Fig. 1.2.2, $t = -5 \text{ h}$). The maximum fabs difference across the chamber walls during an experiment is, based on the magenta and blue curves in Fig. 1.2.2 $(18 - 12) = 6 \text{ g} / \text{m}^3$. If there is a linear relationship between the water flow through the chamber wall and the difference in fabs across the chamber wall, then based on the reservoir data ($8.33 \text{ mL} / \text{h}$ for a difference of $3 \text{ g} / \text{m}^3$) we would expect $16.66 \text{ mL} / \text{h}$ of water flow through the chamber wall at $6 \text{ g} / \text{m}^3$ fabs difference across the chamber wall. 14 and $16.6 \text{ mL} / \text{h}$ are not that different and would support the hypothesis that all the water from the dishes goes directly through the walls into the outer chamber. The precise conditions, and if some of the vapor is adsorbed and stored in the chamber wall, needs to be simulated (see Additional Research).

Influence on crystallization starting time

Fig. 1.2.3 shows the dependency of the $t_{crStart}$ on different amounts of DCC for different additives. So far, we have seen this behavior for all additives tested. The $t_{crStart}$ was expected to decrease approximately linearly with the DCC amount (see simulation in Fig. 1.2.3 right). The amount of water in a total volume of 6 mL solution decreases as the DCC in the solution increases. The increasing density of the solution has to be taken into account (see Appendix 1.2.4 Water for details). Instead, we measured first an increase in the $t_{crStart}$ followed by a maximum and finally a decrease to a value close to zero for a saturated solution (5110 mg DCC per plate).

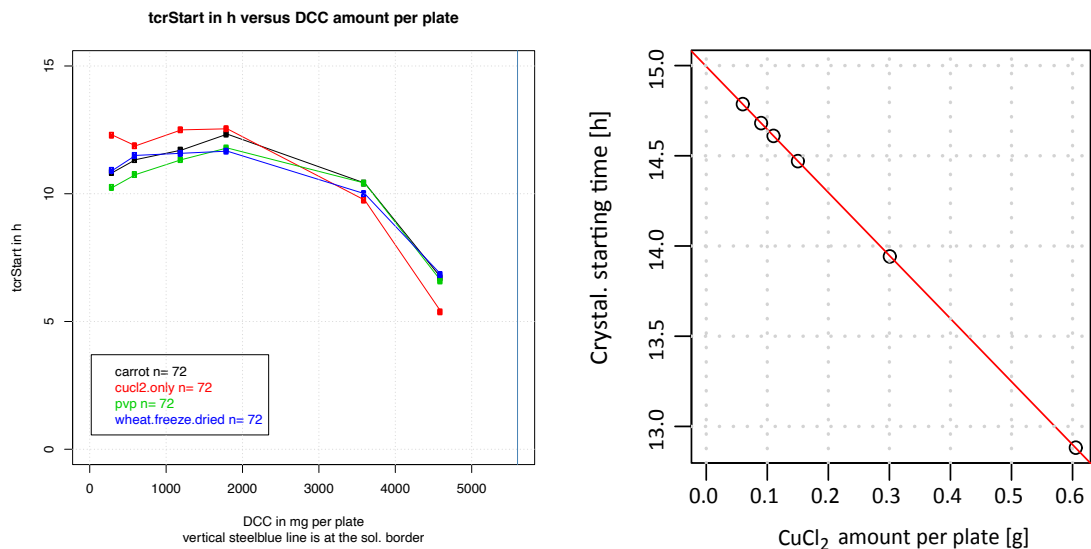


Fig. 1.2.3 Left plot: median crystallization starting time in hours (Y-axis) for different amounts of DCC (X-axis) in mg per plate in 6 mL solution with different additives as parameter. Additive colors: black, carrot samples; red, pure DCC; green, PVP K90 and blue, freeze dried wheat. Number of pictures for the median of an additive are noted in the legend as cnt. Right plot: simulation of the dependency of the crystallization starting time on the DCC amount, assuming that the evaporation rate does not depend on the DCC amount (from Busscher 2010 [5], Fig. 12).

The hypothesis for the behavior in Fig. 1.2.3 left is, that the partial pressure above the solution in the dish decreases with the increasing DCC amount (see [Appendix 1.2.3 Partial Pressure](#), data from Lilich [7] [6]), which results in a reduction of the transport rate of the vapor from the solution into the airflow passing the dishes. This

happens when the humidity of the air in the chamber increases and the partial pressure (the maximal humidity above the solution) decreases and the difference becomes too small to transport the vapor from the dish. This would fit to the behavior shown in Fig. 1.2.2 at the maximum fabs (green dotted perpendicular line at $x \sim 9$ hours). This means that (in the Triangle type chambers) the evaporation would slow down, 1 hour before the crystallization starts, as was indeed seen in Fig. 1.2.2.

Resume humidity and tcrStart measurements

Both the humidity and the tcrStart measurements showed that before crystallization started, the evaporation slowed down or halted, having a “latency moment” (see Additional Research with additional sensor). The question of whether the spreading of the DCC concentration gradient in the Petri-dish from the geometric center to the rim or the transport of water vapor from the Petri-dish to the chamber is the limiting factor cannot yet be decided.

Additional Research

“Latency moment”: An additional sensor is placed below the dishes in Crystal Lab and Witzenhausen. This make it possible to check whether the evaporation has stopped by calculating the difference of the absolute humidity below and above the dish.

Saturation humidity: Plot the starting humidity versus the maximum humidity during evaporation, to see if it is always below 67 % (evaluation of all measurements).

Diffusion case?: Check the humidity over time for experiments from different ring heights (see in chapter [1.4 Surface tension, cleaning, ring height](#)) to determine the evaporation rate.

Evaporation rate: Check the evaporation rate of water from the dishes (use different volumes 6, 7, 8, 9, 10 mL with small amounts of BSA to prevent dewetting) [so far only Petri-dishes with water were used, and dewetting occurred].

DCC: starting a complete chamber with 600, 2800 (max tcrStart) and 4500 mg DCC / plate, see the evaporation rate balancing the transport through the wall. Repeat experiment with BSA, PVP, FDW as additive.

To separate the tcrStart dependency on the evaporation rate and on the supersaturation, the evaporation should be measured on a balance in a one dish Prüfstand.

Transport through the wall: Hypothesis: does the water flow through the wall only depend on fabs differences, or is there also a temperature influence?

Do the so called “[Step response](#) Measurements”.

The evaporation with a higher amount of volume, with the same DCC amount, should give access to the limitation of the transport through the wall. (or do we see evaporation stopping?)

Chamber startup: What is the influence of the chloride gas evaporating from the dish on the wood?

Restart of the chamber after a phase of inactivity (see chapter [1.11 Wetting up phase](#)).

Supersaturation sigma:

Extrapolating the tcrStart data in Fig. 1.2.3 for increasing DCC amounts to the value of tcrStart = 0, should give the DCC amount at which the crystallization starts immediately. The difference with 56 w / w % (or 5100 mg per plate) would give access to the supersaturation. More measurements close to 5100 mg per plate would be necessary. Would the addition of an additive give a higher supersaturation?

Appendix 1.2.1 Absolute Humidity

In Fig. 1.2.4 below, the calculated values of the water vapor in g / m^3 are shown, with which the difference between relative and absolute humidity can be explained.

The maximum amount of water vapor, that can be absorbed by the air depends on the temperature. The amount increases with the temperature, just as you can dissolve more sugar in hot tea than in a cold tea. Like sugar in tea there is a maximum amount of water vapor that can be absorbed for a given temperature. The saturation values for water in air double roughly every twelve degrees. This is represented by the steel blue line in Fig. 1.2.4. It has different values for different temperatures. This line represents the 100 % relative humidity value. The 100 % value does not change with the temperature. If we consider a constant amount of water vapor in the air, like $10 \text{ g} / \text{m}^3$, then this represents 100 % relative humidity at 12°C (where the blue horizontal line begins). The relative humidity decreases as the temperature increases, like 25 % at 35°C , where the blue horizontal line meets the magenta line in Fig. 1.2.4.

The relative humidity gives an indication how relative dry or wet the air is at a certain temperature. Your body reacts to the relative humidity level, for example, at 30°C you feel more strained at higher relative humidity levels than at lower values.

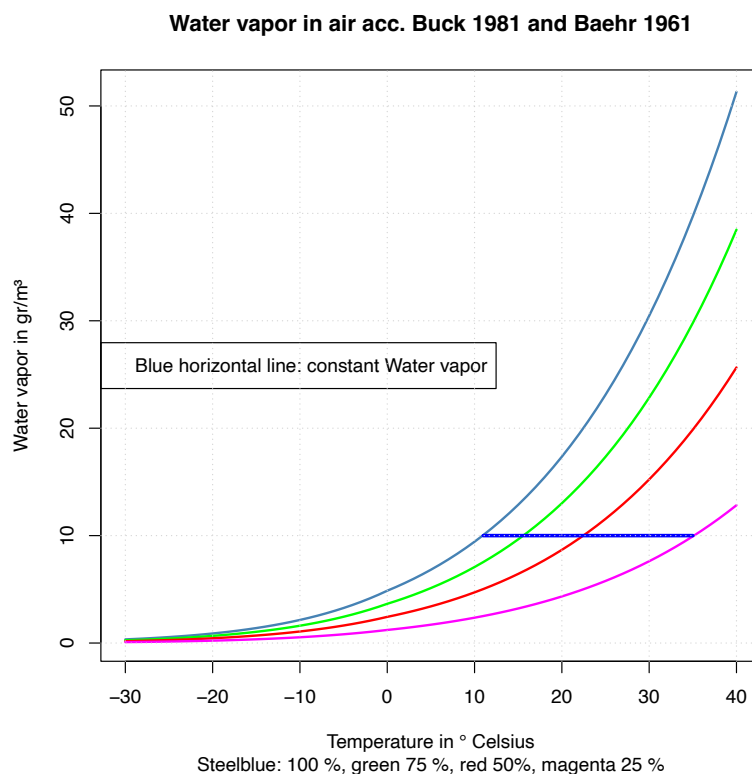


Fig. 1.2.4 Calculated Water vapor in g / m^3 (Y-axis) versus temperature in $^\circ\text{C}$ (X-axis) according to Buck 1981 [13] and Baehr 1960 [11]. The colored curved lines represent different relative humidity values: steel blue 100 %, green 75 %, red 50 %, magenta 25 %.

The values for the vapor amount in air are calculated with formula 10 from Baehr 1961 [11] from the calculated partial pressure values according to Buck 1981 [13]. The further improvement from Buck 1996 [14] was recognized but not applied. Obviously the absolute humidity value is not completely independent from the temperature, because the density of the air changes with the temperature and the energy content changes with the temperature. For precise values we have to work with the Mollier Diagram (Baehr 1961 [11]).

Appendix 1.2.2 Chamber

As an example for the different areas around the Petri-dish, the chamber at the University of Kassel (D) in Witzenhausen is taken. This description follows the path from the outside to the Petri-dish. The so called outer world is the world outside the building with the usual climate variations. Inside the building is a room, the so called [outer chamber](#), located in Fig. 1.2.5 within the square. This outer chamber is acclimatized, the temperature and the humidity in this room are kept constant. This is to minimize the climatic influences of the weather and the seasons. Inside this outer chamber is the so called [inner chamber](#), which is drawn in Fig. 1.2.5 as an octagon. Inside the inner chamber (the octagon) is the evaporation apparatus, represented by the two circles. The Petri-dishes are positioned on these circles. The inner chamber octagon shields the Petri-dishes from the air movements in the outer chamber. The evaporation apparatus and the acrylic rings of the Petri-dishes have the same purpose with respect to the air movements in the inner chamber. This system was designed by Anderen 1998 [12].

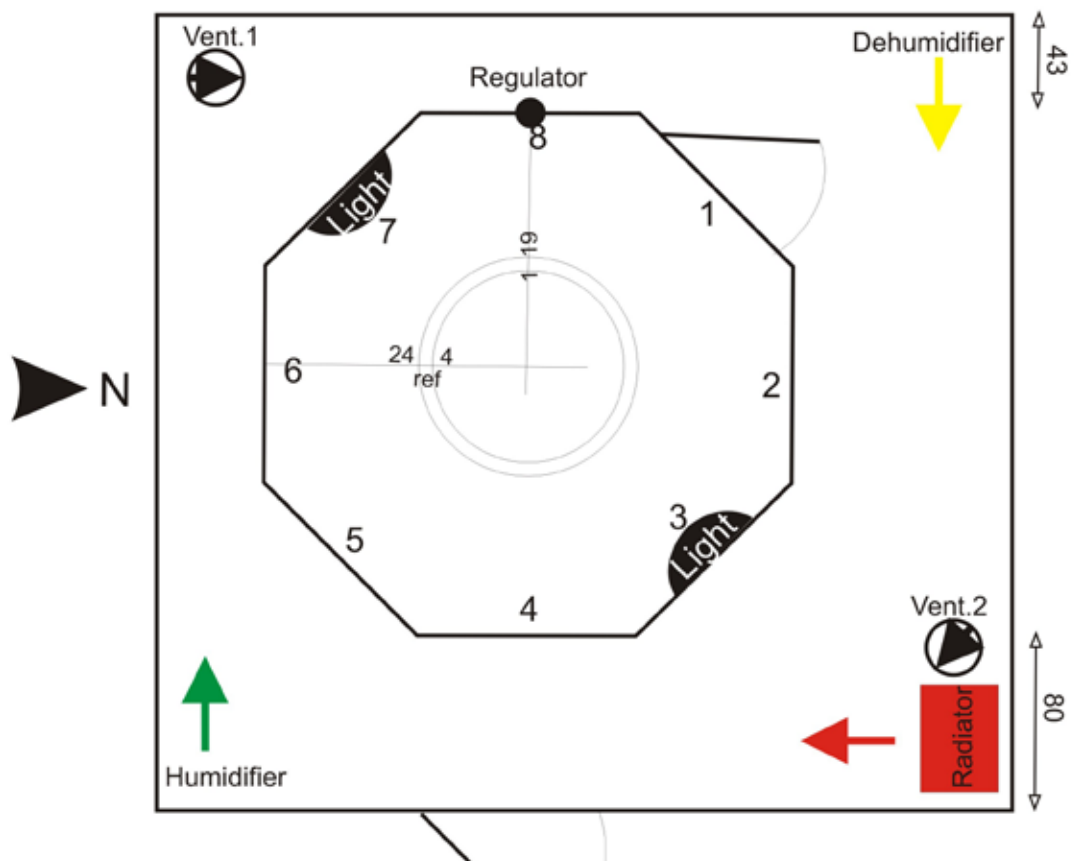


Fig. 1.2.5 View of the DCC system at the University of Kassel (D) in Witzenhausen. Rectangle: room in the building called outer chamber. Octagon: evaporation chamber, called inner chamber. Circles: evaporation apparatus on which the Petri-dishes are placed.

Appendix 1.2.3 Partial Pressure

The partial pressure data measured by Lilich 1956 [6] and 1963 [7] are plotted in Fig. 1.2.6.

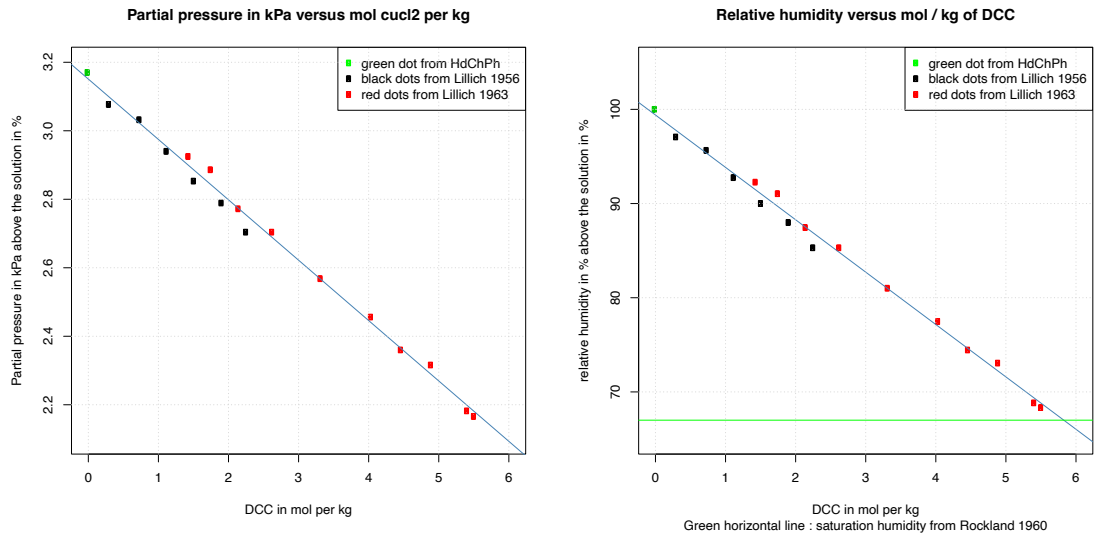


Fig. 1.2.6 Left plot: partial pressure (Y-axis in kPa, data from Lilich [6] [7]) of water vapor above a solution at 298 K (24.85 °C), versus the concentration of DCC (X-axis in mol DCC per kg). Right plot: the relative humidity (Y-axis in %) versus the concentration of DCC (X-axis in mol DCC per kg). Relative humidity data are calculated from the partial pressure data based on the value for the solubility border (5.5 mol / kg, indicated by the horizontal green line) as 67 % (Rockland [8]).

The linear relation of the partial pressure with the mol amount of DCC in water shows that we have an ideal gas above the Petri-dish with DCC (see Raoult's law e.g. at Wikipedia [Wikipedia: Raoult's Law](https://en.wikipedia.org/wiki/Raoult's_Law)). The values in the right plot are calculated to show the intermediate values of the relative humidity for different DCC concentrations above the solution in the Petri-dish.

Appendix 1.2.4 Water

With increasing amounts of DCC, the amount of water in a 6 mL volume of a DCC / water mixture decreases in a non-linear manner. This is due to the increasing density of the DCC / water solution (reflected by the red line in Fig. 1.2.7). The green line reflects the amount of water remaining in the volume when the DCC solubility border is reached after evaporation. The evaporation starts at $x = 0$. In the absence of DCC, the 6 mL volume contains only water. All the water has to evaporate and the solubility border will never be reached. At 0.01 g DCC some water will remain when the solubility border is reached by evaporation. The more DCC in the initial volume, the more water is left at the solubility border. At around 5 g of DCC the DCC value approaches the solubility border at the start of evaporation, where the red and green line coincide. The blue line reflects the difference between the red and the green line and gives the amount of water to evaporate to reach the solubility border. For the commonly used amounts of DCC of 0.15 g per plate (see the steel blue vertical line in Fig. 1.2.7), 5.8 mL of water has to evaporate.

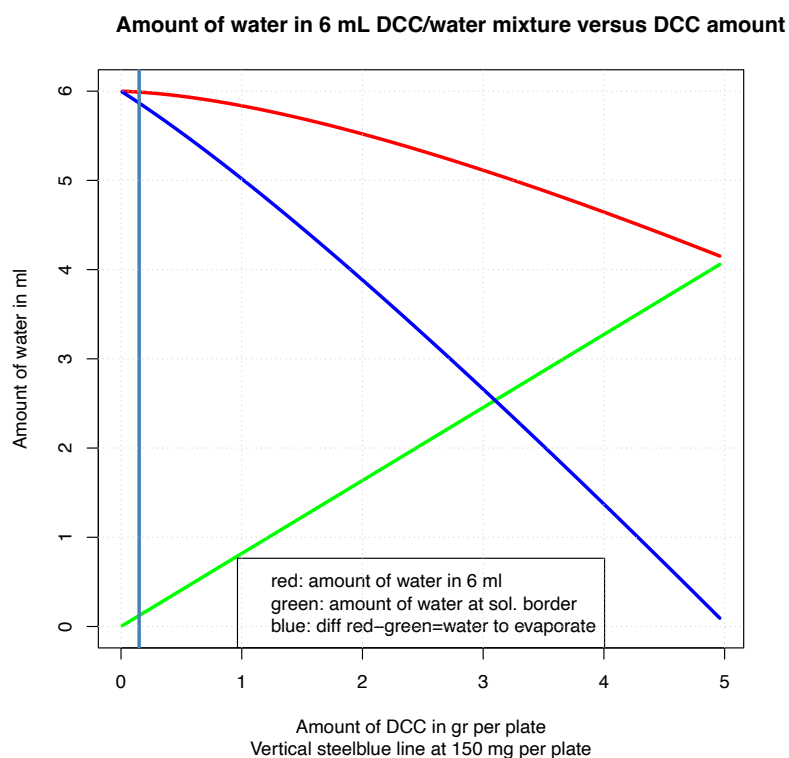


Fig. 1.2.7 Water amount (Y-axis in mL) of water / DCC mixtures in 6 mL. Versus the DCC amount (X-axis) in g per plate.

References

- [1] Koopmans A. Die Frage der Lokalisation im Kupferchlorid-Kristallisationsbild. *Elemente der Naturwissenschaft* 1971; 14: 19-30 <https://doi.org/10.18756/edn.14.19>.
- [2] Suehrcke H and Harris JA Enhancement of water evaporation from a cylindrical container due to concentration induced free convection (Twelfth Australasian Fluid Mechanics Conference, 1995).
- [3] Holleman LWJ. Ein Beitrag zum Verständnis der empfindlichen Kristallisation. *Elemente der Naturwissenschaft* 1966; 4: 24-33 <https://doi.org/10.18756/edn.4.24>.
- [4] Stefan J. Ueber die Beziehung zwischen den Theorien der Capillarität und der Verdampfung. *Annalen der Physik* 1886; 265: 0655 - 0665.
- [5] Busscher N, Kahl J, Doesburg P, Mergardt G, Ploeger A. Evaporation influences on the crystallization of an aqueous dihydrate cupric chloride solution with additives. *Journal of Colloid and Interface Science* 2010; 344: 556–562 <https://doi.org/doi:10.1016/j.jcis.2009.12.045>.
- [6] Lilich LS, Sapozhnikova OV. Dampfdruck in den Systemen $\text{CuCl}_2 - \text{HCl} - \text{H}_2\text{O}$ und $\text{Cu}(\text{ClO}_4)_2 - \text{HClO}_4 - \text{H}_2\text{O}$. *Izv. Vyssh.Uchebn.Zaved.Khim.Khim.Tekhnol.* 1963; 6: 572-577.
- [7] Lilich LS, Timofeev VI. Dampfdruck in den Systemen: $\text{MeCl}_2 - \text{HCl} - \text{H}_2\text{O}$ ($\text{ZnCl}_2 - \text{HCl} - \text{H}_2\text{O}$ und $\text{CuCl}_2 - \text{HCl} - \text{H}_2\text{O}$).

- H₂O). *Vestn.Leningr.Univ.Fiz.Khim* 1956; 10: 68-74.
- [8] Rockland LB. Saturated Salt Solutions for Static Control of Relative Humidity between 5 and 40 C. *Analytical Chemistry* 1960; 32: 1375-1376.
- [9] Stefan J. Versuche über die Verdampfung. *Sitzungsberichte / Akademie der Wissenschaften in Wien, Philosophisch-Historische Klasse* 1873; 2: 385-423.
- [10] Misyura S. Evaporation and heat transfer of aqueous salt solutions during crystallization. *Applied Thermal Engineering* 2018; 139: 203 - 212 <https://doi.org/https://doi.org/10.1016/j.applthermaleng.2018.04.068>.
- [11] Baehr HD Mollier-i, x-Diagramme für feuchte Luft: in den Einheiten des Internationalen Einheitensystems (German Edition) (Springer, 1961).
- [12] Andersen JO, Laursen J, Koelster P. A Refined Biocrystallization Method applied in a Pictomorphological Investigation of a Polymer. *Elemente der Naturwissenschaft* 1998; 68: 1-20 <https://doi.org/DOI: 10.18756/edn.68.1>.
- [13] Buck A. New equations for computing vapor pressure and enhancement factor. *J. Appl. Meterol.* 1981; 20: 1527-1532.
- [14] Buck A. Hygrometer CR-A1 Operating Manual. 1996.

1.3 Crystallization start and starting humidity

How sensitive is the crystallization starting time to the starting humidity in the inner chamber?

Abstract

The [crystallization starting time](#) (the time between the pipetting of the solution into the Petri-dish and the first appearance of a crystal, also abbreviated as tcrStart) is besides the $\text{CuCl}_2 \cdot 2\text{H}_2\text{O}$ amount (cupric chloride di-hydrate, further called [DCC](#)) and the additive amount, an important factor for the picture properties of a DCC picture. The tcrStart depends in a surprisingly sensitive way on the so called starting humidity (the relative humidity in the chamber when the solution is pipetted into the Petri-dish); a 1 % change in the starting humidity causes a 1 hour change in tcrStart. To understand this sensitivity, measurement results are shown and the results of a model simulation are discussed.

Introduction

The picture properties of a $\text{CuCl}_2 \cdot 2\text{H}_2\text{O}$ (cupric chloride di-hydrate, further called [DCC](#)) picture depend, in addition to the DCC and additive amount, on the [crystallization starting time](#) (tcrStart). The tcrStart itself is a function of the so called starting humidity. This can be intuitively understood, because laundry will dry faster in dry weather conditions. The surprising effect is, that the correlation is quite sensitive, with an increase of tcrStart of roughly 0.5 to 1 hour for an increase of 1 % relative humidity (at around 50 % relative humidity). The effect was first quantified by Kahl (2004, [1]) and confirmed in the Checking Influences project by Busscher (2009, [2]). The understanding was based on a simulation of the whole process, including the Petri-dish and the evaporation chamber. In the following, first the historical information regarding this question is given, then the authors' measurements are shown, and the chapter concludes with a resume and a list of additional research ideas. The effect on the increase in relative humidity in the chamber due to the breathing of the person pipetting the solutions into the Petri-dishes is not discussed here, but in chapter [1.14 Chamber reset](#).

Historical overview

The first to describe the influence of the humidity on the tcrStart was Koopmans (1965, [3]). He used it to create DCC pictures with blood as additive, with different crystallization starting times, to find the optimal range of tcrStart. The height of the tcrStart of DCC with blood as additive at different temperatures in a Trockenschrank (evaporation chamber) was measured by Nickel (1968 [4], p. 95, Fig. 14). Using the final humidity in Nickel's Fig. 14 as the starting humidity and neglecting the effect of the temperature (from 30 °C to 50 °C), he arrived at a change in tcrStart of about 0.5 hours per 1 % relative humidity change. Kahl (2004, [1]) published results for the [Triangle chambers](#) showing a correlation between tcrStart and the relative humidity in the evaporation chamber, with tcrStart increasing roughly 1 hour in response to a 1 % increase in relative humidity. This was confirmed by Busscher (2009, [2]) in the Checking Influences project, where he found a change in tcrStart of 0.8 h for a 1 % change in relative humidity. Barth (2011 [5], 2013 [6] and 2019 [7]) was concerned with reducing the variation of the tcrStart values between plate replicates. He designed a chamber where the airflow was precisely steered and an equal temperature below the dishes was controlled by a metal ring [5] on which the Petri-dishes were placed. Optimal conditions were found for a mean tcrStart around 24 h. He achieved an sd of 23 min (2013 [6]), which is quite low for the high tcrStart value. An sd value of 1.45 h was achieved for the Triangle Chamber at a mean tcrStart of 13.2 h (see crystallization starting time in chapter [2.11 Nucleation](#)).

In a project in 2012 at the University of Kassel (D) the need arose to reduce the tcrStart by 1 hour. For this the absolute humidity was reduced for a year (from 02.2012 to 02.2013) by a reduction of the temperature of the outer chamber from 26 °C to 25 °C (changing the relative humidity would have taken 2 - 3 months for the wooden walls to adapt; see Checking Influences project 2009 [2], p. 82 ff.). As a result, there was a greater flow of humidity from the inner to the outer chamber which resulted in a lower starting humidity in the inner chamber. The heat flow from the inner to the outer chamber also increased, which resulting in increased heating in the crystallization apparatus, which led to a higher airflow around the dishes. Both effects, the humidity flow and the heat flow resulted in a shorter tcrStart of roughly one hour.

Authors measurements

The results from the Checking Influences project (2009 [2], p. 61) showed a correlation of tcrStart with the starting relative humidity between 0.5 and 0.8 hour per 1 % relative humidity, depending on the chamber (see for the other chambers located in DK, D, NL in the Checking Influences report 2009 [8], p. 61). The [r_{adj square}](#) was

around 0.32, so roughly 70 % of the variation is not explained by the starting humidity. In Fig. 1.3.1 (right) the results for the Triangle chamber C University of Kassel (D), are shown. The evaporation process, combining the Petri-dish and the evaporation chamber, was simulated with a simple model. For details see chapter [2.13 Evaporation model](#). The results of the simulation for the dependence of the tcrStart on the starting humidity are shown in Fig. 1.3.1 left.

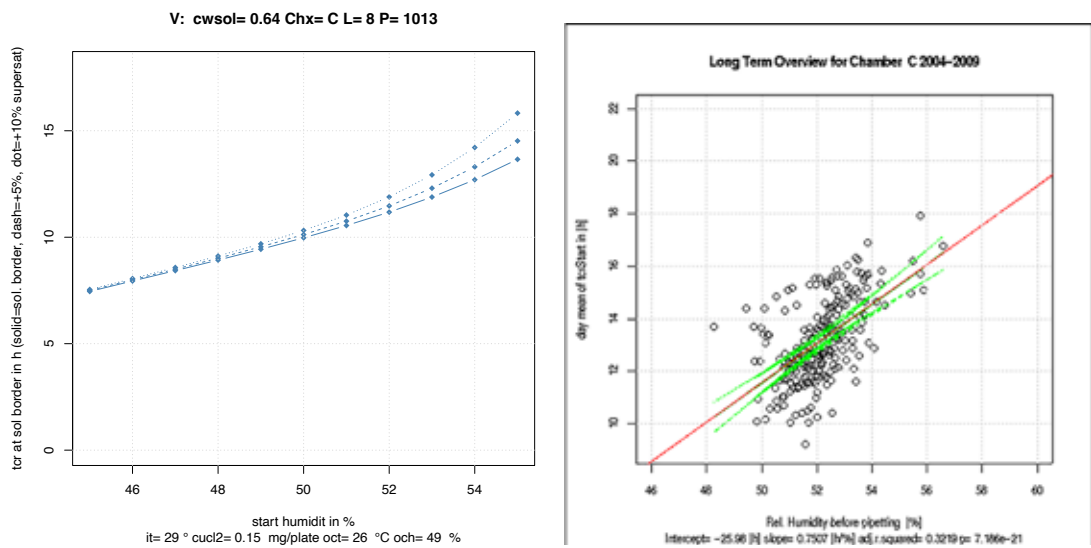


Fig. 1.3.1 Dependence of tcrStart (Y-axis) on the (relative) starting humidity (X-axis) in %. Left: results of the simulation, right measurement data. Left: Points on the continuous line represent the evaporation time until the DCC concentration reaches the solubility border. Points on the dashed line represent the evaporation time until the DCC concentration reaches 5 % supersaturation, points on the dotted line represent the evaporation time until the DCC concentration reaches 10 % supersaturation. Right: Measurements from the Checking Influences project 2009 [2], p. 61. In red the regression line with a slope of 0.75 hour / %. Data from University of Kassel, Witzenhausen (D) from 2004 to 2009 for chamber C.

To understand the sensitivity of the tcrStart to the relative starting humidity, the evaporation process was simulated. See for details chapter [2.13 Evaporation model](#). The simulation showed that the model for the Triangle system has to include the evaporation of the DCC / additive solution in the Petri-dish as well as the volume of the evaporation chamber.

Two limiting factors of the evaporation are responsible for the sensitive correlation between tcrStart and the relative starting humidity. The first is the volume of the evaporation chamber (10 m³ for a Triangle system), which is filled by the evaporating humidity from the Petri-dishes, thereby increasing the humidity in the chamber and reducing the evaporation rate from the dish. See for more details chapter [1.2 Water transport](#). The higher the starting humidity is, the earlier this reduction of the evaporation takes place. The second is the decrease in evaporation rate due to the increasing DCC concentration in the Petri-dish. As the DCC concentration in the Petri-dish increases (see chapter [1.7 Evaporation issues](#) for details), the water is increasingly prevented from leaving the solution. This is described as the decrease of the partial pressure or the relative humidity just above the surface (1mm) of the solution. This effect is used to calibrate humidity sensors, because a dish with a saturated salt solution will absorb the humidity from the surrounding air until the humidity in the air is at equilibrium with the humidity directly surrounding the salt solution. For DCC the equilibrium value for the humidity above a saturated solution is 67 % [9]. Due to the evaporation, the relative humidity in the chamber increases from 50 % to a maximum of 67 %. Due to the increase of the concentration of the DCC in the solution the relative humidity above the DCC solution decreases from 100 % (for no DCC) down to 67 % for a saturated solution. The difference between the increasing humidity in the chamber and the decreasing humidity above the solution in the Petri-dish is the driving force for the transport of the humidity from the dish surface to the chamber (problem of Stefan 1886 [10]). This difference approaches zero, which more or less stops the evaporation needed to cross the solubility border to start the crystallization. The volume of the chamber and the reduction in partial pressure due to the increasing concentration of the DCC is the reason for the sensitive correlation between tcrStart and the starting relative humidity. Keeping the tcrStart stable thus depends to a considerable extent on maintaining a consistent starting humidity in the chamber (see chapter [1.14 Chamber reset](#)).

Resume

The measurements of the sensitive correlation between tcrStart and the relative starting humidity gave a value between 0.5 and 1 hour per 1 % relative humidity. This could be confirmed and understood by simulating a model of the evaporation, consisting of the Petri-dish and the evaporation chamber.

Additional research

Evaluate the correlation between tcrStart and the starting humidity for the years after 2009. Add the sample and the amounts (additive and DCC) as well as the humidity / temperature in the outer chamber as parameter into the statistical evaluation.

For the period when a reference sample was present in the experiments (from 2004 to ~ 2012), limit the evaluation to the usually 7 reference pictures per chamber.

Conduct an annual evaluation to see the development of the chamber as a quality check.

References

- [1] Kahl Johannes NBGMJ-OAMH, Meier-Ploeger A. Bestimmung der Zeitabhängigkeit der Kristallisationsvorgänge bei der Kupferchloridkristallisation als eine Voraussetzung zur Validierung der Methode. *Elemente der Naturwissenschaft* 2004; 80: 90-100.
- [2] Busscher N. Checking Influences: Untersuchung der Einflussgrößen bei der Biokristallisation als Voraussetzung für die Übertragbarkeit der Kammern und Prozeduren in andere Laboratorien und zur Reduzierung der Variationen durch die Kammer und die Orte. Technical Report, University of Kassel. 2009.
- [3] Koopmans A. Zeitabhängigkeiten bei empfindlichen Kristallisationen. *Elemente der Naturwissenschaft* 1965; 2: 1-7 <https://doi.org/10.18756/edn.2.1>.
- [4] Nickel E. Die Reproduzierbarkeit der sogenannten empfindlichen Kupferchloridkristallisation. PhD Thesis, Universitätsverlag, Freiburg (Schweiz). 1968.
- [5] Barth J-G, Roussau J, Suppan K, dos Santo SR. Crystallisation of a film of copper chloride in the presence of additives. *Elemente der Naturwissenschaft* 2011; 94: 69-99 <https://doi.org/DOI: 10.18756/edn.94.69>.
- [6] Barth J-G, Roussaux J, Wilkens A, Jacobi M. Techniques for washing the supports used for copper chloride crystallization with additive. *Elemente der Naturwissenschaft* 2013; 98: 5-19 <https://doi.org/DOI: 10.18756/edn.98.5>.
- [7] Barth J-G. Cupric Chloride Crystallisation in the Presence of Additive: Experimental Conditions and Developmental Perspectives. *Elemente der Naturwissenschaft* 2019; 111: 46-55 <https://doi.org/10.18756/edn.111.46>.
- [8] Busscher, N.; Kahl, J.; Doesburg, P. and Andersen, J.-O. Untersuchung der Einflussgrößen bei der Biokristallisation als Voraussetzung für die Übertragbarkeit der Kammern und Prozeduren in andere Laboratorien und zur Reduzierung der Variationen durch die Kammer und die Orte, 2009.
- [9] Rockland LB. Saturated Salt Solutions for Static Control of Relative Humidity between 5 and 40 C. *Analytical Chemistry* 1960; 32: 1375-1376.
- [10] Stefan J. Ueber die Beziehung zwischen den Theorien der Capillarität und der Verdampfung. *Annalen der Physik* 1886; 265: 0655 - 0665.

1.4 Surface tension, cleaning, ring height

How does the glass plate cleaning and the ring height influence the picture?

Abstract

The influence of the cleaning procedure of the glass plate was researched by Doesburg (ProPar Project 2017 [1]) with three different cleaning procedures. After the usual laboratory dishwasher (Miele Desinfektor G7735) procedure, the final step was modified. Final step procedure 1: rinsing with Ethanol (EtOH, alcohol), procedure 2: submerging in a 15 % (w / w) $\text{CuCl}_2 \cdot 2\text{H}_2\text{O}$ (cupric chloride di-hydrate, further called DCC) solution, and 3: rinsing with MEK (methyl ethyl ketone or denaturated / *vergällter* alcohol, which is considerably cheaper than pure EtOH). Criteria were 1: homogeneity of the plate coverage and 2: surface tension of the plates. EtOH gave the best results (see [Appendix 1.4.1 Cleaning](#)). When 2.68 mg Bovine Serum Albumin (BSA) per plate was applied (theoretically 316 monolayers), no differences in the coverage of the plates could be measured. The BSA covered the glass plates and changed the surface properties irrespective of the last cleaning step. When 0.085 mg BSA per plate was applied (theoretically 10 monolayers), the results were unclear.

Ring height experiments with heights of 10, 20, 35, 55 and 70 mm were made relative to the default ring height of 35 mm by Doesburg (ProPar Project 2017 [1]). The coverage of the plate changed according to the hypothesis that the radius of the coverage depends on the location of the concentration and temperature gradient in the dish. A higher shielding (from 10 to 20 to 35 mm ring height) resulted in a lower coverage of the dish. For 35, 55 and 70 mm ring height the coverage was more or less constant.

Introduction

The cleaning of the glass plates, which are used to create the DCC pictures with additives, has been an important topic ever since the beginning of the method in 1924 when Pfeiffer started making DCC pictures ([2], p. 11). Usually the glass plates were cleaned in three steps. First, they were bathed in a soap solution to release the grease on the glass plates. This was followed by an acid bath to remove the alkaline properties of the soap, followed by a water phase, to remove the acid. The ring height was seldom a topic. Only Andersen put some work into it. In order to realize a minimal temperature variation at the surface of the solution [3] he increased the ring height to 35 mm.

Historical overview

For the cleaning procedures different soaps and different acids were used. From chrome-sulfuric acid (Selawry [4]) to nitric acid (Andersen [5]). Also, only DCC (Knijpenga, Geier and Bornhütter, private communication 2019) was used. Von Hahn [6] used the petroleum naphtha product "white gas" (*Reinigungs-Benzin*). Gallinet [7] described the influence of the cleaning procedure (boiling in water at 100 °C) to achieve a hydrophilic surface as a possibility to avoid dewetting during evaporation. Recently Barth 2013 [8] presented an overview of the influence of different cleaning procedures.

The evaporation from a Petri-dish is known as the Stefan problem [9] (see also chapter [2.13 Evaporation model](#)). The rim height of the Petri-dish has a strong influence on the evaporation profile above the solution in the Petri-dish. This was simply visualized by Engquist (1970 [10], p. 12, 13). Concentration measurements in the dish were made by Holleman 1966 [11] and Busscher 2010 [12] (for details see chapter [2.4 Concentration gradient](#)). The height of the ring was also varied by Ballivet 1999 [13] and the influences discussed.

Authors Measurements

In the context of the ProPar Project in 2017 [1] experiments were performed with BSA as additive with different ring heights, cleaning procedures and DCC amounts in Crystal Lab (NL). See also chapter [3.1 Chamber systems](#). In contrast to the structure of the Abstract and Introduction sections, in this section the results of the ring height experiments will be discussed first, since the outcome parameters are defined in this topic.

Ring Height experiments

The experimental parameters were:

Ring Heights: 10, 20, 35, 55 and 70 mm,

DCC: 17.78, 100.0 and 177.8 mg per plate,

BSA: 2.68 mg per plate (316 calculated monolayers).

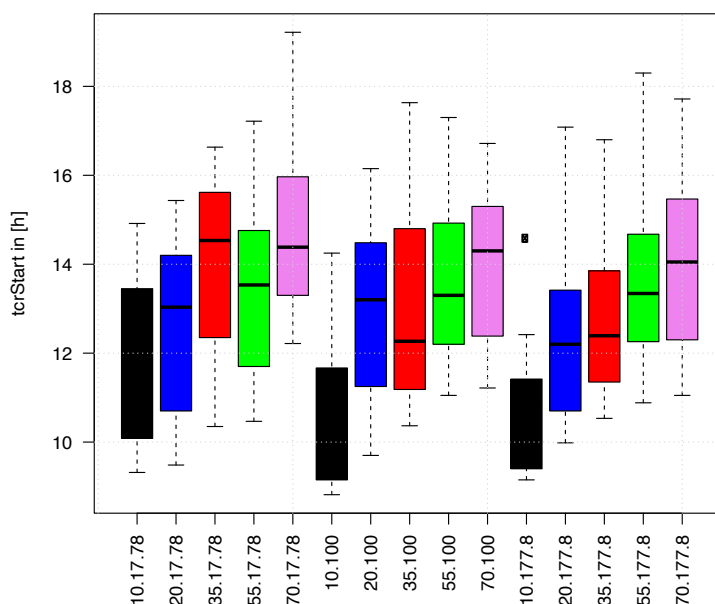


Fig. 1.4.1 TcrStart in hours (Y-axis) versus the combination of DCC and ring height (X-axis). Ring heights: black boxes = 10 mm, blue = 20 mm, red = 35 mm (default Triangle ring height), green = 55 mm, violet = 70 mm. The three repetitions of the 5 colored boxes represent the 3 DCC concentrations. From left to right: first repetition 17.7 mg, second repetition 100 mg, third repetition 177.8 mg DCC per plate. BSA is 2.68 mg per plate for all conditions. Each box represents 12 - 25 data points.

The crystallization starting time (tcrStart, Y-axis) in Fig. 1.4.1 increased with the increasing height of the ring from black to violet. The effect hardly depended on the DCC amount. Linear regression (see [Appendix 1.4.4 Statistics](#)) estimated the effect of the increasing ring height (10 – 70 mm) at + 2.5 h, and - 0.48 h for the increase in DCC amount (17.7 - 177 mg DCC per plate). For the DCC effect a positive correlation was expected.

Evaluation of the DCC Coverage of the plate

The coverage of the plate is measured by the radius of a circle drawn around the covered area. See for details and examples in [Appendix 1.4.2 Radius](#).

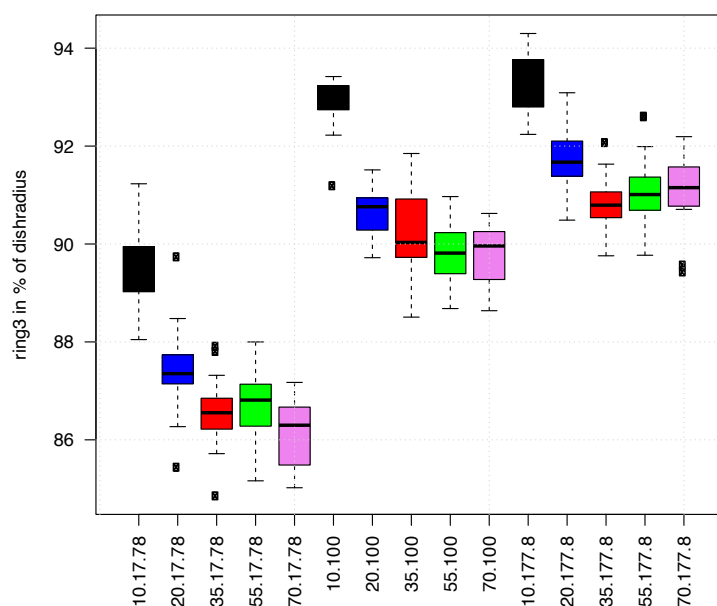


Fig. 1.4.2 Surface coverage radius (ring3, Y-axis) dependency on the combination of DCC and ring height (X-axis). Ring heights: black boxes = 10 mm, blue = 20 mm, red = 35 mm (default Triangle ring height), green = 55 mm, violet = 70 mm. The three repetitions of the 5 colored boxes represent the different DCC amounts. From left to right: first repetition 17.7 mg, second repetition 100 mg, third repetition 177.8 mg DCC per plate. BSA is 2.68 mg per plate for all conditions.

Fig. 1.4.2 demonstrated that lower ring heights (black and blue) generate higher coverage values. These findings fit with the hypothesis from Busscher 2019 [14] that the location of the gradient defines the coverage of the plate. If the ring height is lower, then the gradient is closer to the rim, because a smaller part of the area is shielded by the ring. The surface coverage for 35, 55 or 70 mm ring heights (red, green and violet boxes) are more or less similar, which would agree with the result from Andersen 1992 [3] that a 35 mm ring height resulted in no (detectable) variation of the temperature signal measured directly above the glass plate.

The dependency of the plate coverage on the DCC amount is strong between 17.7 and 100 mg DCC per plate. A possible reason could be that at 17.78 mg DCC and 2.68 mg BSA per plate there is no DCC left at the rim, whereas at 100 and 177.8 mg DCC per plate there still is (see Fig. 1.4.3 below).

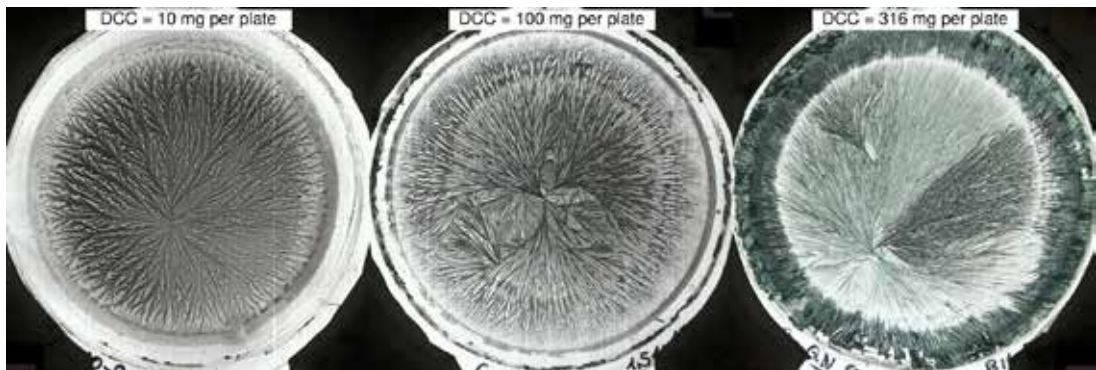


Fig. 1.4.3 Coverage of the plate for different amounts of DCC per plate. Left: 10 mg DCC per plate, middle 100 mg DCC per plate, right 316 mg DCC per plate. BSA additive amount was kept constant at 1.51 mg per plate (177.6 calculated monolayers). From Busscher 2019 [14], Fig. 4.

Dependency of the radius of the first center

The radius is the distance between the geometric center of the Petri-dish and the location of the first crystallization center. It is in percentage of the dish radius (see also in the glossary [radiusCenter](#)).

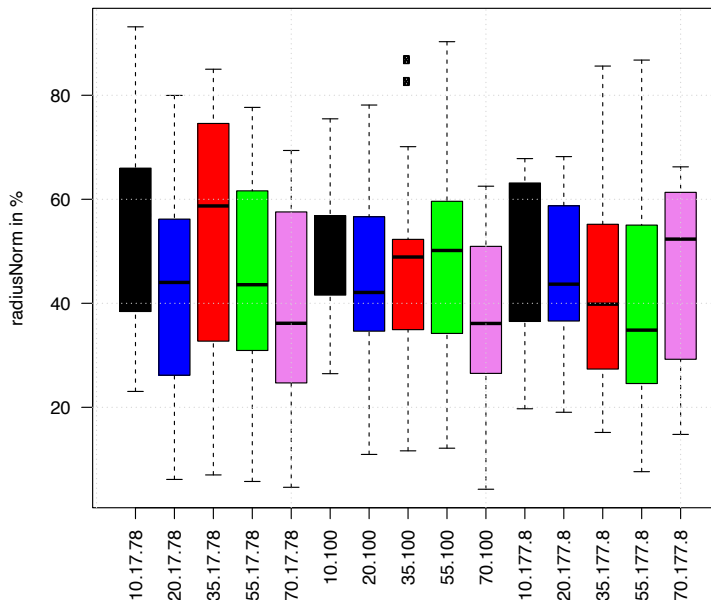


Fig. 1.4.4 [Radius](#) dependency (Y-axis) on DCC and ring height (X-axis). Ring heights: black box = 10 mm, blue = 20 mm, red = 35 mm (default Triangle ring height), green = 55 mm, violet = 70 mm. The three repetitions of the 5 colored boxes represent the different DCC amounts. From left to right: first repetition 17.7 mg, second repetition 100 mg, third repetition 177.8 mg DCC per plate. BSA is 2.68 mg per plate for all conditions.

The radius dependency is not simple to understand. There is no clear signal. The dependency on the ring height is just significant ($p = 0.056$), the dependency on the DCC amount not ($p = 0.2$). Linear regression estimated the effect of the increasing ring height at a - 6 % decrease in radius (from black to violet, most visible in the middle repetition), but this needs further research.

The expectations for the ring height experiments presented above were based on Hollemans findings ([11], Fig. 4, see also chapter [2.4 Concentration gradient](#)) which suggested that the depth of the airflow into the dish should be the same for all ring heights. The concentration and temperature gradient should be flatter for higher ring heights. The ring3 (Fig. 1.4.2) reacts in the expected way (a broader DCC coverage at smaller ring heights). The radius shows the same tendency. Maybe the study and the comparison of the statistical distributions of the radius (see chapter [2.11 Nucleation](#)) give more insights.

Resume ring height experiments

The increase of tcrStart with the increase of the ring height was expected. The dependency of the coverage of the plate (ring3) on the ring height could be understood as the location of the DCC and temperature gradient is closer to the rim as the ring height decreases. The low dependency of the radius (distance between the primary crystallization center and the geometric center of the Petri-dish) on the ring height is not understood.

Glass plate cleaning procedures

After the usual laboratory dishwasher procedure (Miele Desinfektor G7735) the final step in the cleaning of the glass plates was modified. The following final steps were tested:

- procedure 1 (default Triangle procedure): rinsing the plates with EtOH 95 % w /w.
- procedure 2: submerging the plates in a DCC solution (15 % w / w).
- procedure 3: rinsing the plates with MEK (methyl ethyl ketone or denaturated / *vergällter* alcohol, which is considerably cheaper than pure EtOH).

See for details and the characterization of the cleaning procedures in Appendix 1.4.1 Cleaning.

Further experimental parameters were:

- Two DCC amounts: 17.78 mg and 100 mg per plate.
- Two ring heights: 10 mm and 35 mm (35 mm is the default Triangle ring height).
- BSA (2.68 mg per plate, 316 theoretical monolayers).

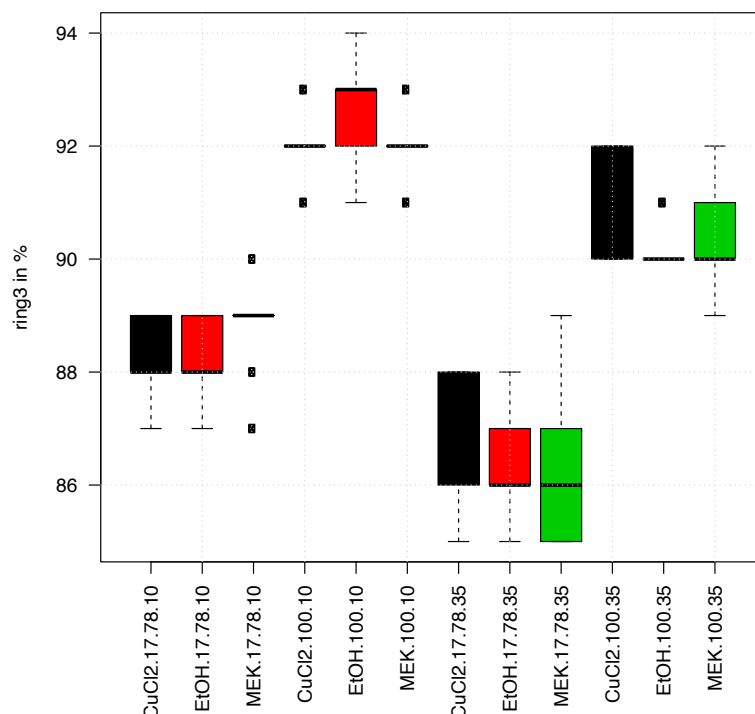


Fig. 1.4.5 Coverage of the plate (ring3, Y-axis) versus combinations of 2 DCC amounts (17.78 mg and 100 mg per plate), 2 ring-heights (10 mm, the two left repetitions of the 3 colored boxes and 35 mm, the two right repetitions), and 3 cleaning procedures: DCC (black), EtOH (red), MEK (green). BSA amount for all conditions was set to 2.68 mg per plate. Each box represents a number of 9 measurements.

The coverage of the glass plate with DCC and 2.86 mg BSA (316 calculated monolayers) as additive is independent of the cleaning procedure, otherwise there would have been a difference in the three colored boxes. BSA is known for covering glassware with an amount around one to three monolayers (Norden 2012 [15]), depending on the pH of the solution and the surface conditions of the target.

For the DCC system (pH = 0.5 at the DCC solubility border) we saw (Busscher 2019 [16]) that dewetting is inhibited upon the addition of 1 to 3 calculated monolayers BSA. The above behavior is as expected, because the solution had a surplus of BSA with a concentration equivalence of 316 calculated monolayers. The glass plate was covered so efficiently, that the cleaning procedure did not show up as a factor in the coverage of the plate. The different cleaning procedures could be quite easily detected at the pipetting time of the solution. The flow of the pipetted solution was considerably easier with the DCC rinsed plates and considerably harder with the MEK rinsed plates, as was to be expected from the surface tension properties of the glass plates according to the cleaning procedures.

The coverage of the plates depended on the height of the ring as seen earlier in Fig. 1.4.2, with lower coverage for higher ring heights. Additionally, the increase of plate coverage with the increase in DCC amount from 17.7 mg per plate to 100 mg per plate is strong.

In order to check if the coverage of the plate depends on the excess amount of BSA in the solution, thus potentially nullifying the effect of the cleaning of the glass plates, (following the work of Svensson 2010 [17]) experiments with 10 calculated monolayers of BSA were performed. However, they could not be evaluated in the same way, because the ring3 parameter was difficult to evaluate due to an overgrowth with DCC from the rim for the 100 mg DCC (see Fig. 1.4.7), which was unexpected based on previous results from Uni Kassel (Witzenhausen, D).

Experiment with BSA amounts equivalent to 10 calculated monolayers.

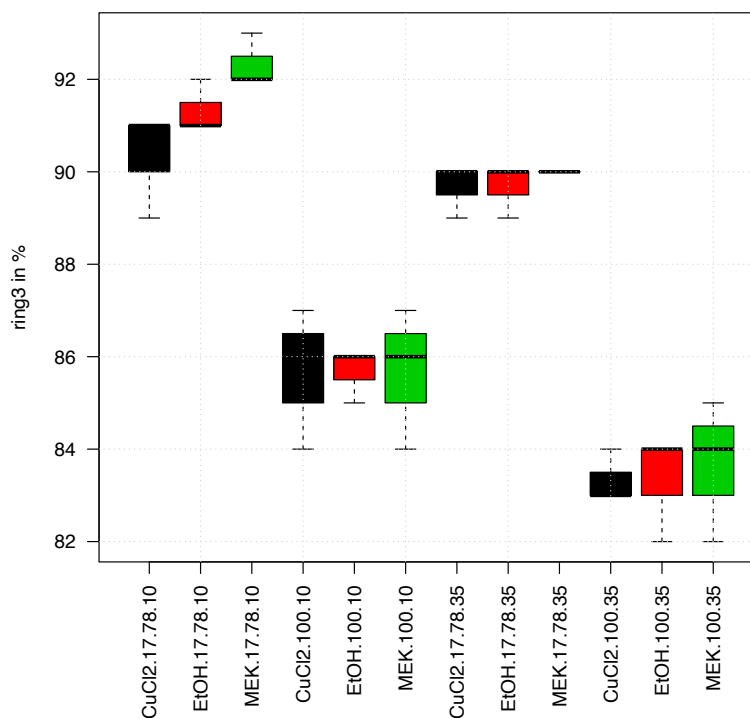


Fig. 1.4.6 Coverage of the plate (ring3, Y-axis) versus combinations of 2 DCC amounts (17.78 mg and 100 mg per plate), 2 ring-heights (10 mm, the two left repetitions of the 3 colored boxes and 35 mm, the two right repetitions), and 3 cleaning procedures: DCC (black), EtOH (red), MEK (green). BSA amount for all conditions was set at 0.085 mg per plate (10 calculated monolayers).

The expected results were that the radius would increase with an increasing DCC amount, according to Fig. 1.4.5 and (Busscher 2019 [14], Fig. 5). The result in Fig. 1.4.6 showed however the opposite. The evaluation was repeated, but the same result was found. The results for 17.78 mg DCC per plate and 10 mm ring height show a difference in plate coverage with the cleaning procedure (most left repetition of the three boxes), but not for the 35 mm ring height.

No conclusion could be drawn from this. Maybe 10 monolayers is still enough to cover the glass plate and quench the effects of the different cleaning procedures so only noise is registered at the 10 mm ring height.

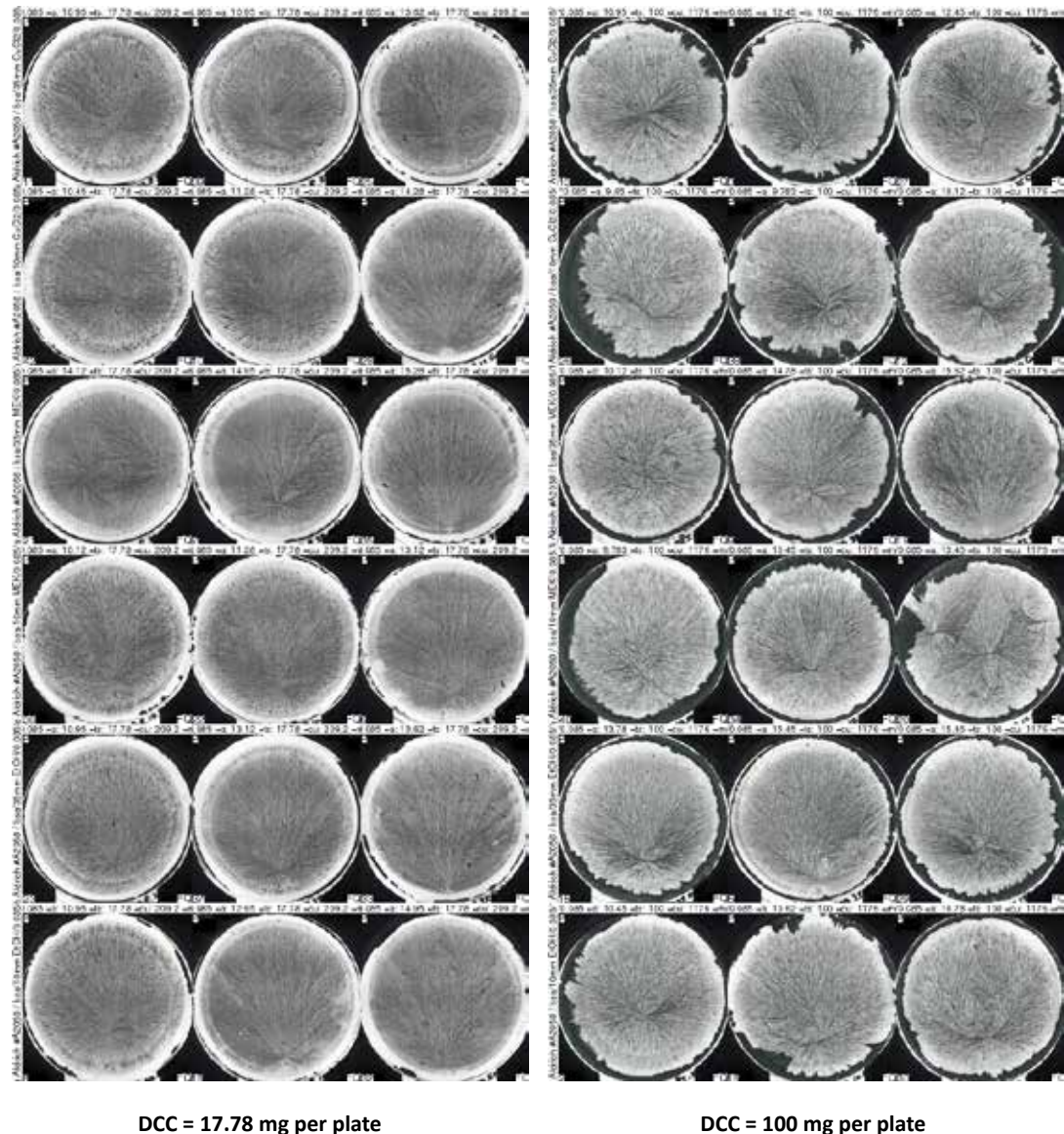


Fig. 1.4.7 Pictures from series FQ chamber P (NL). Comparison of the cumulative effect of plate cleaning procedures and ring heights for the additive BSA with 0.085 mg per plate (10 calculated monolayers). On the Y-axis: from top to bottom: 1st row DCC rinsing, 35 mm ring height, 2nd row DCC rinsing, 10 mm ring height, 3rd row MEK rinsing, 35 mm ring height, 4th row MEK rinsing, 10 mm ring height, 5th row EtOH rinsing, 35 mm ring height, 6th row EtOH rinsing, 10 mm ring height. The plate replicates are sorted according to the tcrStart, lowest on the left, highest on the right.

Experiments with freeze dried wheat

To investigate the cumulative effect of ring height and cleaning procedure on freeze dried wheat (FDW) as additive, an experiment was conducted with the three cleaning procedures and ring heights at mixing ratios near the dewetting border of FDW (series 2018.11.14.FU, chamber P, Roepaen NL). The evaluation is pending because the simple ring3 evaluation did not fit the irregular structures that appeared in the covering of the plate (see Fig. 1.4.8). The fact that the first two rows (plates rinsed with DCC) had less irregular structures is understandable because of the lower surface tension (see Appendix 1.4.1 Cleaning). That the MEK rinsed plates in rows 3 and 4 (higher surface tension than EtOH) had less irregular structures than EtOH rinsed plates (rows 5 and 6) was not expected.

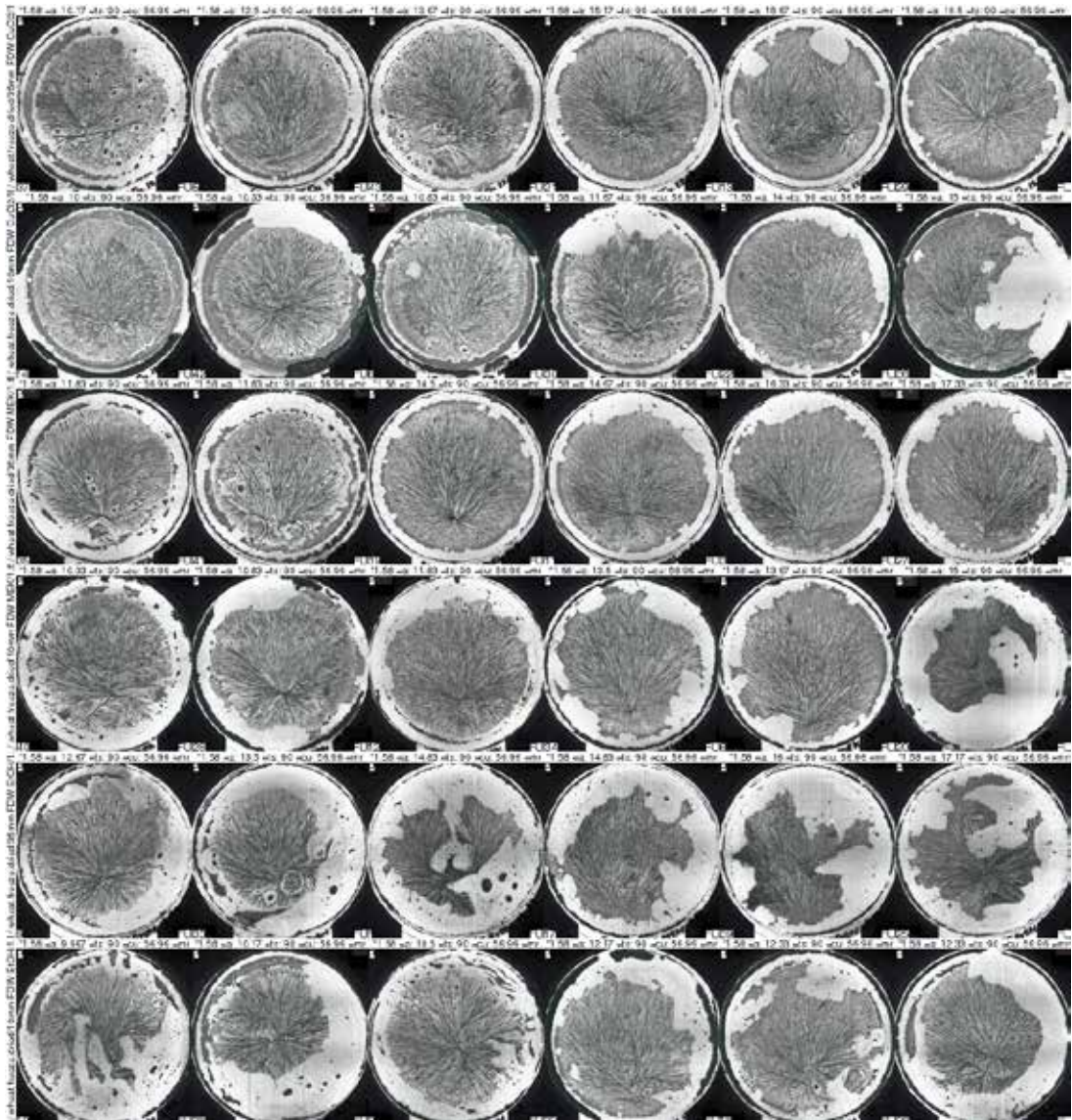


Fig. 1.4.8 Comparison of cumulative effect of plate cleaning procedures and ring heights for the additive FDW. On the X-axis the replicates are sorted per row according to the tcrStart. Lowest on the left, highest on the right. On the Y-axis from top to bottom: 1st row DCC submersion, 35 mm ring height, 2nd row DCC submersion, 10 mm ring height, 3rd row MEK rinsing, 35 mm ring height, 4th row MEK rinsing, 10 mm ring height, 5th row EtOH rinsing, 35 mm ring height, 6th row EtOH rinsing, 10 mm ring height.

Resume

For 2.68 mg BSA per plate (316 calculated monolayers) the cleaning procedures DCC, EtOH and MEK, performed after the default machine washing procedure of the glass plates, were not reflected in the coverage of the plate. Albeit that during pipetting of the chamber solutions a clear effect was perceivable. For 0.085 mg BSA per plate (10 calculated monolayers) the results were not clear, maybe a dependency does exist. The data for FDW await evaluation.

The coverage of the plate showed the expected dependency on the increasing ring height. This can be understood from the location of the concentration and temperature gradient in the dish [14]. The lower the height of the ring, the closer the gradient will be to the rim because the ring will shield less of the rim. The sharp increase in plate coverage from 17.7 mg DCC per plate to 100 mg DCC per plate is not yet understood. Maybe it has something to do with the behavior of the meniscus during the evaporation (see also chapter [1.5 Breakdown meniscus](#)).

Additional research

- Evaluate existing data:
 - According to Stefan [18] and Suehrcke [19] the median $t_{crStart} \sim$ ring-height. How does this fit in Fig. 1.4.1?
- Perform measurements with lower BSA amounts and lower FDW amounts.
 - Evaluate whether the plate coverage is different for different cleaning procedures at lower additive amounts (as with BSA at 10 monlayers per plate)?
- Perform measurements with “higher” amounts of FDW.
 - Do we also see no impact of cleaning as at 2.68 mg BSA per plate?
- Perform measurements on both sides of the glass plates.
 - One side has a Zn coverage (visible with UV light).
 - How does this show up in the coverage of the plate?
 - Can the glass plate on this side be reused (when washing the DCC off on the other side)?
- Compare pictures from Witzenhausen with those from Crystal Lab for 100 mg DCC per plate. Are there differences in the coverage of the plate (ring3)?
- Discuss the work from Ballivet [13] about different ring heights in more detail.
- Discuss the work from Barth [8] about the cleaning in more detail.
- Measure the temperature and rel. humidity dependency in the dish (first with 70 mm ring height) from the ring top. Especially check whether the variation decreases. Can it be connected to the airflow “bending in” from Hollemann [11] Fig. 4, see also chapter [2.4 Concentration gradient](#).

Appendix 1.4.1 Cleaning

Measurement procedure and results from Doesburg in the ProPar Projekt 2017, p. 28, 29.

- Adjust Olympus white balance so the white background on which the glass plates will be positioned on is seen as 100% white (One.touch.WB).
- After washing machine and consecutive rinsing steps, glass plates are left to dry for 30' under the fume hood.
- 8 x 25 μ L. 100 mg DCC / 6 mL is pipetted on a glass plate in the outer room and left standing for 1' upon which a photo is taken. Thereby ensuring that mm-paper partially underlying the glass plate (omitting the droplet area) is within the photographed area.
- Photos are evaluated with ImageJ.
 - First the straight-line-tool is used to draw a straight line over the mm paper. This line is used for subsequent scaling via Analyze-Set.scale (set known.distance to the actual cm, then set unit. of.length to cm which should give approx. 290 pix / cm at present Olympus height).
 - Images are then transformed to 8-bit B-W images via Image-Type-8.bit, and subsequently thresholded via Image-Adjust-Threshold. Adjust the minimum and maximum displayed pixel values (the two numbers under the plot) until the droplets are visible as enclosed circles and all other noise is minimized (do not Apply).
 - Then analyze the area via Analyze-Analyze.Particles (set Size from 0.4 - infinity; Circularity from 0.1 - 1.0 to minimize noise, set Show to Masks).
 - Usually noise is further reduced by selection of a rectangular area around the droplets in which the particles have to be recognized.
 - If Analyze.Particles doesn't work then apply a circle or freehand form as accurately as possible around the droplet boundary and do Analyze-Measure to get the Area in cm.

Outcome experiment 27.11.2017

Table 1.4.1 Droplet area measurements to determine the extent of hydrophobicity and homogeneity of the outcome (StDev) after different rinsing procedures. Treatment refers to the last cleaning step after the washing machine procedure, being either: no treatment (Untreated), EtOH rinsing, MEK rinsing, DCC submersion, or submerging in boiling demineralised water. Area 1 - 8 is the measured area (in cm²) of the 8 droplets.

Treatment	Area.1	Area.2	Area.3	Area.4	Area.5	Area.6	Area.7	Area.8	Mean area	SD
Untreated	1.15	1.23	1.21	1.31	1.22	1.21	1.18	1.18	1.21	0.05
Untreated	1.2	1.17	1.27	1.37	1.18	1.23	1.24	1.26	1.24	0.06
1xEtOH	1.05	1.08	1.09	1.04	1.03	1.09	1.07	0.98	1.05	0.01
1xEtOH	1.21	1.15	1.13	1.15	1.07	1.08	1.12	1.07	1.12	0.02
MEK	0.61	0.61	0.61	0.6	0.61	0.6	0.6	0.61	0.61	0.01
MEK	0.62	0.61	0.58	0.61	0.61	0.63	0.62	0.63	0.61	0.02
DCC	1.66	1.84	1.96	1.84	1.59	1.9	2.01	1.27	1.76	0.24
DCC	1.64	1.51	1.5	1.49	1.65	1.6	1.6	1.5	1.56	0.07
Boiling	0.84	0.9	0.68	0.81	0.88	0.78	0.79	0.84	0.82	0.07
Boiling	1.01	0.87	0.5	0.42	1.05	0.8	0.97	0.99	0.83	0.24

In a second experiment the effect of prolonged drying in the fume hood was examined for the none-EtOH and MEK procedures, as in these procedures water hasn't been displaced by EtOH, consequently these plates dry slower.

Outcome experiment 29.11.2017

Table 1.4.2 Droplet area measurements to determine the extent of hydrophobicity and homogeneity of the outcome (StDev) after different rinsing procedures. Treatment refers to the last cleaning step after the washing machine procedure, being either: no treatment (Untreated), EtOH rinsing, MEK rinsing, DCC submersion and subsequent 30' or 1 h of drying, submerging in boiling demineralized water and subsequent 30' or 1 h of drying. Area 1 - 8 is the measured area (in cm²) of the 8 droplets.

Treatment	Area.1	Area.2	Area.3	Area.4	Area.5	Area.6	Area.7	Area.8	Mean area	SD
Untreated + demi rinse	1.68	2.06	1.54	1.50	1.72	-	-	-	1.70	0.22
Untreated + demi rinse	1.86	2.31	1.99	1.61	2.13	2.50	2.21	1.88	2.06	0.28
1xEtOH	1.09	1.18	1.22	1.08	0.98	1.03	1.06	1.21	1.11	0.02
1xEtOH	1.09	1.15	1.09	0.82	1.07	1.00	1.19	1.07	1.06	0.02
MEK	0.65	0.64	0.63	0.63	0.66	0.65	0.60	0.61	0.63	0.02
MEK	0.63	0.63	0.60	0.65	0.64	0.64	0.60	0.65	0.63	0.02
DCC 30'drying	2.05	2.08	2.07	1.91	2.07	1.95	1.82	1.84	1.97	0.11
DCC 1h drying	1.95	1.65	2.12	1.76	1.88	1.90	1.80	-	1.87	0.15
Boiling 30 drying	0.75	0.94	0.95	0.97	0.74	0.75	0.82	0.80	0.84	0.10
Boiling 1h drying	1.42	1.46	1.51	1.52	1.47	1.43	1.77	-	1.51	0.12

The repeatability between the two experiments was best for the two EtOH-based rinsing procedures (*EtOH* mean 1.09 cm²; StDev 0.02 cm², *EtOH-MEK* mean 0.62 cm²; StDev 0.02 cm²), then for the *DCC* incubation (mean 1.79 cm²; StDev 0.22 cm²). The two water-only procedures (*untreated* and *boiling*) showed the highest variation in the measured droplet area: *untreated* mean 1.54 cm²; StDev 0.41 cm², *boiling* mean 0.98 cm²; StDev 0.32 cm². Although the *untreated* procedure differed slightly between the two experiments, in that in experiment 2 the plates were allowed to dry for 30' or 1 h after the rinsing procedure.

See for the calculation (data table) of the contact angle: dropvolume of 25 µL.

Summary

Area is largest (low hydrophobicity or a wettable surface) after submerging the plates in *DCC*. While treatment with EtOH-MEK gives the smallest surface coverage. The main criterion is the homogeneity of the plate which is highest for the two alcohols. Because EtOH rinsing also increases plate wettability, it is considered the best method for obtaining stable results.

Appendix 1.4.2 Radius

The determination of the coverage of the plate (ring3) is shown below. The red circle defines the coverage of the plate (ring3 is the radius of the read circle) parameter.



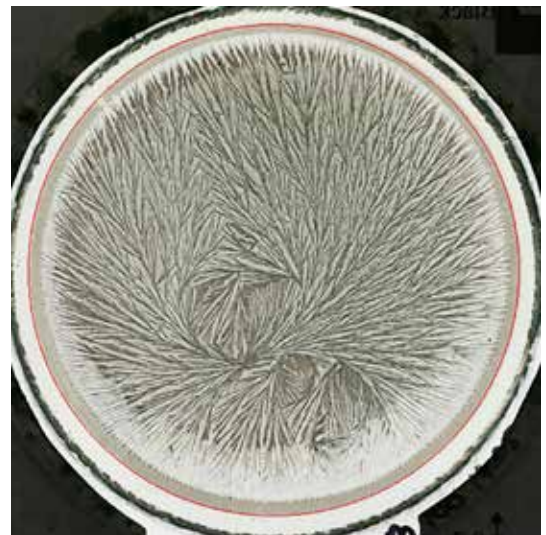
EP nr 16, 17.78 DCC, 10 mm ring



FL nr 17, 17.78 mg DCC, 70 mm ring



EP nr 12, 100 mg DCC, 10 mm ring



FL nr 11, 100 mg DCC, 70 mm ring

Fig. 1.4.9 Determination of the coverage of the plate (ring3 = radius of the red circle).

Appendix 1.4.3 Series

LabDoc Series names versus experimental parameters.

Table 1.4.3 LabDoc series (column names) versus ring height (row names). For each LabDoc series, the matrix shows the number of dishes used for each ring height.

	EK	EL	EM	EN	EO	EP	FJ	FL
BSA 10 mm	0	0	0	0	18	18	0	0
BSA 20 mm	22	18	0	0	18	18	0	0
BSA 35 mm	21	18	18	18	0	0	0	0
BSA 55 mm	0	0	18	18	0	0	18	18
BSA 70 mm	0	0	0	0	0	0	18	18

The list in Table 1.4.3 shows the overlap between two ring heights in the experiments. For example in series EM 35 and 55 mm ring heights are researched. This allows to check the day effect.

Table 1.4.2 DCC amount (column names) versus dish ring height (row names). The matrix indicates the number of dishes available for each combination.

	17.78 mg	100 mg	177.8 mg
BSA 10 mm	12	12	12
BSA 20 mm	25	25	25
BSA 35 mm	24	25	26
BSA 55 mm	24	24	24
BSA 70 mm	12	12	12

Table 1.4.3 LabDoc series names of experiments.

LabDoc Series names
P.2017.02.01.EK
P.2017.02.03.EL
P.2017.02.13.EM
P.2017.03.09.EN
P.2017.03.20.EO
P.2017.03.27.EP
P.2018.10.03.FJ
P.2018.10.10.FL

Appendix 1.4.4 Statistics

Dependency of tcrStarth from ring_height and DCC amount (Fig. 1.4.1).

Call:

```
lm(formula = ddy$tcrStarth ~ ddy$ring_height + ddy$cucl2_in_mg)
```

Residuals:

Min	1Q	Median	3Q	Max
-3.5772	-1.6465	-0.2243	1.4846	5.0715

Coefficients:

	Estimate	Std. Error	t value	Pr(> t)
(Intercept)	11.882590	0.289091	41.103	< 2e-16 ***
ddy\$ring_height	0.040535	0.005631	7.199	5.2e-12 ***
ddy\$cucl2_in_mg	-0.003833	0.001673	-2.291	0.0227 *

Signif. codes: 0 '***' 0.001 '**' 0.01 '*' 0.05 '.' 0.1 ' ' 1

Residual standard error: 1.874 on 291 degrees of freedom

Multiple R-squared: 0.164, Adjusted R-squared: 0.1583

F-statistic: 28.55 on 2 and 291 DF, p-value: 4.758e-12

Analysis of Variance Table

Response: ddy\$tcrStarth

	Df	Sum Sq	MeanSq	F value	Pr(>F)
ddy\$ring_height	1	182.05	182.047	51.8560	5.123e-12 ***
ddy\$cucl2_in_mg	1	18.43	18.431	5.2499	0.02266 *
Residuals	291	1021.59	3.511		

Signif. codes: 0 '***' 0.001 '**' 0.01 '*' 0.05 '.' 0.1 ' ' 1

Dependency of ring3_p from ring_height and DCC amount (Fig. 1.4.2)

Call:

```
lm(formula = ddy$ring3_p ~ ddy$ring_height + ddy$cucl2_in_mg)
```

Residuals:

Min	1Q	Median	3Q	Max
-2.73970	-0.79919	-0.05298	0.65328	2.74295

Coefficients:

	Estimate	Std. Error	t value	Pr(> t)
(Intercept)	88.3648413	0.1608135	549.49	<2e-16 ***
ddy\$ring_height	-0.0357071	0.0031322	-11.40	<2e-16 ***
ddy\$cucl2_in_mg	0.0269521	0.0009305	28.97	<2e-16 ***

Signif. codes: 0 '***' 0.001 '**' 0.01 '*' 0.05 '.' 0.1 ' ' 1

Residual standard error: 1.042 on 291 degrees of freedom

Multiple R-squared: 0.7692, Adjusted R-squared: 0.7676

F-statistic: 484.8 on 2 and 291 DF, p-value: < 2.2e-16

Analysis of Variance Table

Response: ddy\$ring3_p

	Df	Sum Sq	Mean Sq	F value	Pr(>F)
ddy\$ring_height	1	141.88	141.88	130.61	< 2.2e-16 ***
ddy\$cucl2_in_mg	1	911.44	911.44	839.01	< 2.2e-16 ***
Residuals	291	316.12	1.09		

Signif. Codes: 0 '***' 0.001 '**' 0.01 '*' 0.05 '.' 0.1 ' ' 1

Dependency of radiusNorm from ring_height and DCC amount (Fig. 1.4.4)

Call:

lm(formula = ddy\$radiusNorm ~ ddy\$ring_height + ddy\$cucl2_in_mg)

Residuals:

Min	1Q	Median	3Q	Max
-43.05	-12.99	-0.80	14.17	46.50

Coefficients:

	Estimate	Std. Error	t value	Pr(> t)
(Intercept)	51.68197	2.87751	17.961	<2e-16 ***
ddy\$ring_height	-0.10730	0.05605	-1.915	0.0565 .
ddy\$cucl2_in_mg	-0.01980	0.01665	-1.189	0.2354

Signif. codes: 0 '***' 0.001 '**' 0.01 '*' 0.05 '.' 0.1 ' ' 1

Residual standard error: 18.65 on 291 degrees of freedom

Multiple R-squared: 0.01714, Adjusted R-squared: 0.01038

F-statistic: 2.537 on 2 and 291 DF, p-value: 0.08083

Analysis of Variance Table

Response: ddy\$radiusNorm

	Df	Sum Sq	Mean Sq	F value	Pr(>F)
ddy\$ring_height	1	1273	1273.32	3.6609	0.05668 .
ddy\$cucl2_in_mg	1	492	491.66	1.4136	0.23544
Residuals	291	101214	347.82		

Signif. codes: 0 '***' 0.001 '**' 0.01 '*' 0.05 '.' 0.1 ' ' 1

References

- [1] Busscher N, Doesburg P. ProPar Project Report nr 5 2017. Technical Report, CuCl₂ Research. 2017.
- [2] Pfeiffer E. Kristalle (Orient Occident Verlag, 1930).
- [3] Andersen J-O. Kobberklorid—krystallisationsmetoden kvalitativt og kvantitativt. MSc Thesis, University of Copenhagen. 1992.
- [4] Selawry A and Selawry O. Die Kupferchlorid-Kristallisation in Naturwissenschaft und Medizin (Gustav-Fischer-Verlag, 1957).
- [5] Andersen JO, Laursen J, Koelster P. A Refined Biocrystallization Method applied in a Pictomorphological Investigation of a Polymer. *Elemente der Naturwissenschaft* 1998; 68: 1-20 <https://doi.org/DOI: 10.18756/edn.68.1>.
- [6] Von Hahn F-V. Thesigraphie. (Franz Steiner Verlag, 1962).
- [7] Gallinet JP, Gauthier-Manuel B. Wetting of a glass surface by protein adsorption induces the crystallization of an aqueous cupric chloride solution. *Journal of Colloid and Interface Science* 1992; 148: 155-159 [https://doi.org/doi:10.1016/0021-9797\(92\)90123-4](https://doi.org/doi:10.1016/0021-9797(92)90123-4).
- [8] Barth J-G, Roussaux J, Wilkens A, Jacobi M. Techniques for washing the supports used for copper chloride crystallization with additive. *Elemente der Naturwissenschaft* 2013; 98: 5-19 <https://doi.org/DOI: 10.18756/edn.98.5>.
- [9] Stefan J. Versuche über die Verdampfung. *Sitzungsberichte / Akademie der Wissenschaften in Wien, Philosophisch-Historische Klasse* 1873; 2: 385-423.
- [10] Engquist M. Die Gestaltkräfte des Lebendigen (Vittorio Klostermann, 1970).
- [11] Holleman LWJ. Ein Beitrag zum Verständnis der empfindlichen Kristallisation. *Elemente der Naturwissenschaft* 1966; 4: 24-33 <https://doi.org/10.18756/edn.4.24>.
- [12] Busscher N, Kahl J, Doesburg P, Mergardt G, Ploeger A. Evaporation influences on the crystallization of an aqueous dihydrate cupric chloride solution with additives. *Journal of Colloid and Interface Science* 2010; 344: 556–562 <https://doi.org/doi:10.1016/j.jcis.2009.12.045>.
- [13] Ballivet C, Knijpenga H, Barth J-G, Clad R. Zur Empfindlichkeit der Methode der Kupferchloridkristallisation. *Elemente der Naturwissenschaft* 1999; 70: 1-32 <https://doi.org/10.18756/edn.70.1>.
- [14] Busscher N, Doesburg P, Mergardt G, Sokol A, Kahl J, Ploeger A. Influence of dewetting on the crystallization behavior of CuCl₂ in the presence of BSA during evaporation in a Petri dish. *Heliyon* 2019; 5: e01102 <https://doi.org/10.1016/j.heliyon.2018.e01102>.
- [15] Norde W, Lyklema J. Interfacial behaviour of proteins, with special reference to immunoglobulins. A physicochemical study. *Advances in Colloid and Interface Science* 2012; 179-182: 5-13 <https://doi.org/http://dx.doi.org/10.1016/j.cis.2012.06.011>.
- [16] Busscher N, Doesburg P, Mergardt G, Sokol A, Kahl J, Ploeger A. Crystallization patterns of an aqueous dihydrate cupric chloride solution in the presence of different amounts of Bovine Serum Albumin. *Journal of Crystal Growth* 2019; <https://doi.org/doi:10.1016/j.jcrysgro.2019.125272>.
- [17] Svensson O, Arnebrant T. Adsorption of serum albumin on silica - The influence of surface cleaning procedures. *Journal of Colloid and Interface Science* 2010; 344: 44-47.
- [18] Stefan J. Ueber die Verdampfung aus einem kreisförmig oder elliptisch begrenzten Becken. *Annalen der Physik* 1882; 253: 550-560.
- [19] Suehrcke, H. and Harris, J. A. Enhancement of water evaporation from a cylindrical container due to concentration induced free convection. Proceedings of the Twelfth Australasian Fluid Mechanics Conference, The University of Sydney, Sydney, Australia, 1995.

1.5 Meniscus breakdown

Abstract

The observation that the $\text{CuCl}_2 \cdot 2\text{H}_2\text{O}$ (cupric chloride di-hydrate, further called DCC) amount at the rim decreases with the decreasing DCC amount was not understood in the publication of Busscher 2019 [1]. Doesburg's observations in the ProPar 2018 project [2] on the breakdown of the meniscus helped us to understand this phenomenon.

Introduction

One of the surprising results of the study of dewetting phenomena in the crystallization of mixtures of the salt $\text{CuCl}_2 \cdot 2\text{H}_2\text{O}$ (cupric chloride di-hydrate, further called DCC) and BSA, was that with decreasing DCC amounts, the DCC amount at the rim also decreased until it could no longer be observed any more (below 30 mg per plate in Busscher 2019 [1]), see Fig. 1.5.1).

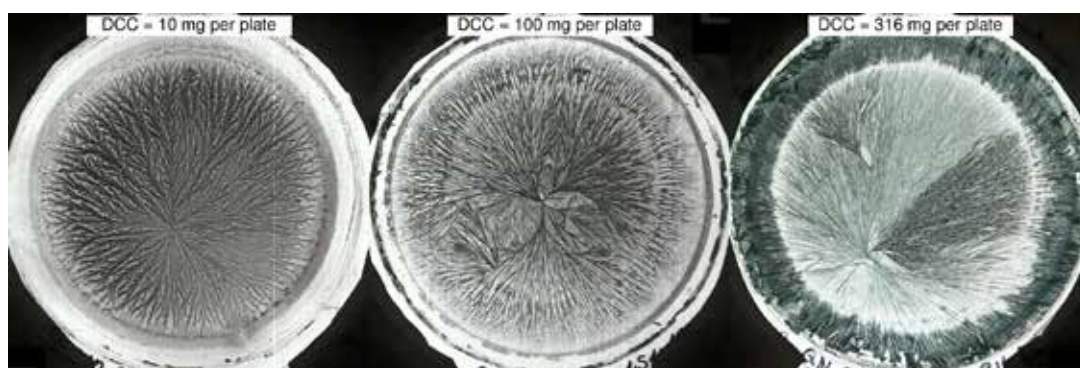


Fig. 1.5.1 Coverage of the plate for different amounts of DCC. Left: 10 mg DCC per plate, middle 100 mg DCC per plate, right 316 mg DCC per plate. BSA additive amount was kept constant at 1.51 mg per plate (177.6 calculated monolayers). From Busscher 2019 [1], Fig. 3.

In Fig. 1.5.1 the crystallization start is later for higher DCC amounts than for lower DCC amounts (see chapter 2.13 [Evaporation model](#)), although less water has to evaporate to reach the solubility border for higher DCC amounts. The coverage of the plate in Fig. 1.5.1 was quantified in Busscher 2019 [1] and presented in Fig. 1.5.2.

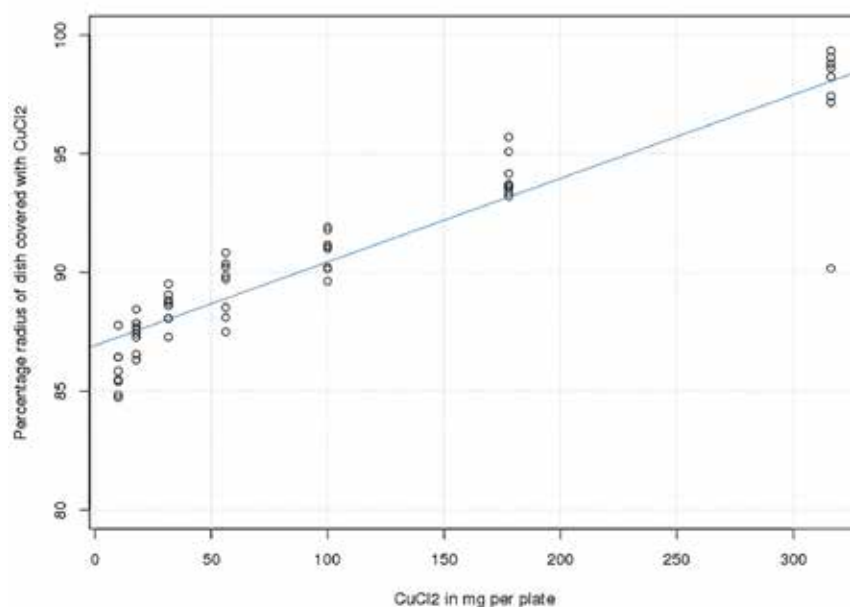


Fig. 1.5.2 Dependency of the radius of the DCC covered area in percentage of the Petri-dish radius (ring3, Y-axis) versus the DCC amount per plate (X-axis). BSA additive amount was kept constant at 1.51 mg per plate (177.6 calculated monolayers). From Busscher 2019 [1], Fig. 5.

From Fig. 1.5.1 and 1.5.2 it was concluded that dewetting after crystallization starts at a position closer to the rim (at a larger DCC covered area) for higher DCC amounts. For lower DCC amount this effect starts at a greater distance from the rim (i.e. at a smaller DCC covered area). This can be understood from the fact that the height of the solution decreases as the amount of DCC decreases. Consequently, dewetting after crystallization will occur at a greater distance from the rim. The understanding of the reduction of the DCC amount at the rim was not solved in Busscher 2019 [1]. Perhaps the following observation will provide a solution.

Authors Observations

During an experiment with DCC and BSA in 2018, Doesburg observed that the meniscus in the Petri-dish changed shape during evaporation.

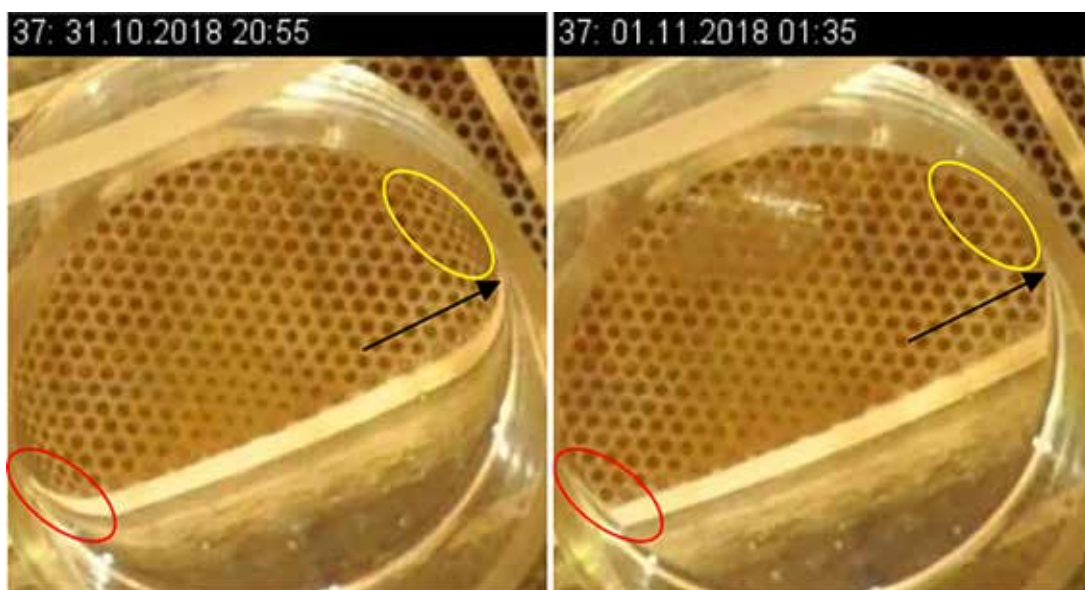


Fig. 1.5.3 Left situation ~ 8 hours after pipetting. Right: the situation at the start of crystallization after about ~ 13 hours after pipetting. Temporal lens effects at the rim of the dish. The lens effect is visible in the deformation of the perforations (yellow ellipse) and in the curved ends of the white line below the dishes (red ellipse). Both deformations decrease in time. The arrowhead indicates the position of the meniscus apex on the rim (from Pro-Par report 2018 [2], Fig. C4, Chamber P (Roepaen, NL) LabDoc series 2018.10.31 FQ, picture no. 37, DCC = 17.18 mg per plate, with 0.085 mg BSA per plate).

As can be seen in Fig. 1.5.3 the meniscus deforms during evaporation. The highest point of contact of the meniscus with the rim is in the same position on both the left and right image (indicated by the arrowhead). The angle θ at the apex of the meniscus, between the solution and the acrylic ring (as defined by Landau & Lifschitz 1959 [3] p. 235, Fig. 32 or Scott 2016 [4] p. 6, Fig. 2), decreases. The meniscus at the start of evaporation (Fig. 1.5.3 left) shows a smooth transition from the rim to the surface of the solution. Later (Fig. 1.5.3 right) this becomes increasingly steep. The resulting volume of the meniscus decreases accordingly, which would explain why there is hardly any DCC at the rim. The reason why the meniscus deforms could be due to the increasing concentration in the solution, which is higher than the concentration in the meniscus due to the shielding effect of the acrylic ring. Near to the solubility border of DCC, the thin solution film has a high viscosity, causing it to adhere to the glass plate and no longer behave as a solution. The shape of the meniscus in Fig. 1.5.3 right is now determined by the point at the rim and the adherent part on the glass plate.

Resume

The effect that the amount of DCC at the rim decreases for solutions with less than 30 mg of DCC per plate could be explained by Doesburg's observation that the volume of the meniscus decreases. The reason why the meniscus volume decreases is not clear.

Additional research

Meniscus development

Measure the shape of the meniscus during the evaporation with two or three points (the highest point at the acrylic ring and half the height between the highest point and the surface of the solution and – if it exists – the location of the “nick” in the solution surface with CrystEval (see chapter [3.3 CrystEval](#)). A different behavior for different DCC amounts is expected.

Preventing meniscus formation by making the acrylic ring hydrophobic (by means of a Vaseline layer).

Influence of tcrStart at the overgrowth border

The effects of DCC overgrowth from the rim should depend of the tcrStart, because the longer the evaporation can continue, the lower the height of the solution will be. Shorter tcrStart values will show overgrowth, while later tcrStart values will not. This could maybe explain the deviation in the results in chapter [1.4 Surface tension, cleaning, ring height](#) between the pictures from University Kassel (D) and Roepaen (NL).

References

- [1] Busscher N, Doesburg P, Mergardt G, Sokol A, Kahl J, Ploeger A. Influence of dewetting on the crystallization behavior of CuCl_2 in the presence of BSA during evaporation in a Petri dish. *Heliyon* 2019; 5: e01102 <https://doi.org/10.1016/j.heliyon.2018.e01102>.
- [2] Busscher N, Doesburg P. ProPar Project Report 2018. Technical Report, CuCl_2 Research. 2018.
- [3] Landau and Lifschitz Course of theoretical Physics Vol 6, Fluid dynamics (Pergamon Press, 1959).
- [4] Scott CF, Sander GC, Norbury J. Computation of capillary surfaces for the Laplace-Young equation. *The Quarterly Journal of Mechanics and Applied Mathematics* May 2005; 58: 201-212.

1.6 Sensitive area

Where is the (most) sensitive area with the highest differentiation in the picture?

Abstract

The results from the image analysis of $\text{CuCl}_2 \cdot 2\text{H}_2\text{O}$ (cupric chloride di-hydrate, further called DCC) pictures and Engquist's visual evaluation results indicate a concept of a sensitive area in the DCC picture. How can this sensitive area be understood, and how can it help to increase the discrimination between DCC pictures from different samples?

Introduction

In 1924, Pfeiffer called the pictures from $\text{CuCl}_2 \cdot 2\text{H}_2\text{O}$ (cupric chloride di-hydrate, further called DCC) with additive "sensitive crystallizations". This is due to the fact that crystallizations are quite sensitive to basic parameters such as the amount of additive and DCC, the climatic conditions and the cleaning of the glass plate, and on the other hand, if the parameters are chosen appropriately, the picture properties are quite sensitive to quality differences between samples such as from agricultural growth systems or processing techniques. The question is if the differences induced by the additive are evenly distributed across the picture or whether there are areas where the differences appear stronger. In case there are areas with higher discriminating sensitivity, the question arises whether human visual evaluation perceives the same location as computer based image analysis. This chapter builds on the knowledge of the following chapters: [1.13 Picture zones](#), [1.7 Evaporation issues](#), [2.11 Nucleation](#), [1.4 Surface tension, cleaning and ring height](#), [2.4 Concentration gradient](#), [2.8 Dewetting by crystallization](#).

Historical Overview

Engquist was the first (1970 [1]) who not only spoke about three different zones in a picture (see also chapter [1.13 Picture zones](#)) but also identified one zone, the middle zone, as the most discriminating one. The number of zones depends on the amount of additive. When the additive amount is too low, less than three zones are visible, when the additive amount is too high, additional centers appear. From computer image analysis it is known, that the highest differentiation of samples is not around the geometric center, and not at the rim of the Petri-dish, but in the middle, between these two. This can be found in the publications of Kahl (2007 Habilitation Thesis [2]), Kahl DOK samples (2014 [3]), Kahl apple juice (2016 [4]) and Baumgartner (2012 cress [5]). Andersen (1999 [6]) increased the discriminative power of DCC pictures of aged carrot juice by excluding pictures with a center radius (the distance between the geometric center and the crystallization center) that exceeded a threshold. Thereby reducing the pictures to more uniform, pictures, having roughly the same asymmetry.

In the chapter [1.13 Picture zones](#) the resume was:

1. A three zonal concept has been recognized and used by many authors.
2. The middle zone seems to be the most sensitive area (Engquist, and image analysis).
3. Future research will need to verify whether the areas identified by the crystallization / evaporation effects and the zones identified by visual and image analysis are the same.

Authors results

What is special for the crystallization / evaporation effect?

Crystallization / evaporation effects result in the emergence of a sensitive area, as discussed in chapter [2.8 Dewetting by crystallization](#). In this area, the surface tension forces due to the cleaning of the glass plate and the DCC concentration and temperature gradients, as well as the influence from the growing crystallization front sum up. In extreme situations, this will lead to dewetting, but if the solution in the Petri-dish is high enough, the weight of the solution can balance the surface tension forces. Nevertheless, the surface tension forces will still affect the growth of the crystals through this area. This requires additional research as defined in Additional research of chapter [2.8 Dewetting by crystallization](#).

How do different additives affect the sensitive area conditions?

The sensitive area conditions vary depending on the additive being used by influencing:

1. The evaporation rate, which influences the DCC concentration and temperature gradients.
 - 1.1 A lower evaporation rate will result in lower gradients.
2. The coverage of the glass plate by the additive, which affects the surface tension.

- 2.2 A lower coverage will result in a higher surface tension.
- 3. The crystallization starting time (actual supersaturation and height of the solution).
 - 3.1 The height of the solution decreases as the evaporation time increases.
 - 3.1.1 A lower surface height can compensate the surface tension effect less well.
 - 3.2 The supersaturation can define the crystal type and the growth velocity.
 - 3.2.1 The higher the growth velocity the higher the additional surface tension?
- 4. The location of the crystallization center, being either more in the middle or more towards the rim.
 - 4.1 How does this affect the surface tension? The growth front? This will result in a different geometry!
 - 4.2 The closer the location of the crystallization start is to the rim, the more asymmetrical the sensitive area will be.

How geometrically stable is the sensitive area?

From the above points we cannot expect that the location of the sensitive area in the Petri-dish (the geometry), to be the same for all additives. But how much does it vary? What is the impact of this variation on image analysis using the Regions of Interest (ROI) concept? The ROIs have a defined geometry while the sensitive area seemingly has a more “floating” geometry.

Improving the discrimination of pictures from different samples

Before we start looking for ways to improve discrimination, let's recall the basic structure in the Petri-dish. The basis for the concept of the sensitive area is a three zonal concept like that postulated by Engquist and Selawry. Crystallization starts in the 1st zone which is defined by the position of the crystallization center, in the 2nd zone the sensitive area appears, followed by the 3rd and final zone which includes the rim. Roughly speaking, the crystallization starting time (tcrStart) and the radius (the distance between the geometric center and the crystallization center) have a Gaussian distribution (see chapter [2.11 Nucleation](#)). The median value of the radius depends on the sample and lies between 30 % and 50 % for all samples measured so far (dish radius is 100 %). This means that most DCC pictures are asymmetrical. From a geometry perspective, the best way to match the sensitive areas of pictures from different samples would be to compare those pictures that are “close” to the median of the radius and tcrStart. This is what Andersen discovered in 1999 [6] for the comparison of DCC pictures from aging carrot juices. See chapter [2.11 Nucleation](#) for the distributions of the tcrStart and radius.

Because of the “floating” geometry of the sensitive area, we can't pinpoint the location from what we know about the evaporation process, but the geometry criteria can be deduced based on identifying the area of highest discrimination e.g. by computer image analysis. The question is whether these geometry criteria from the computer image analysis are also helpful for the visual evaluation of DCC pictures.

The visual evaluation criterion *durchstrahlung* (Huber 2010) or perradiation reflects the degree to which the crystal needle branches can span the three zones in a powerful, interconnected gesture, or stop rather abruptly at the transition from the 1st to the 2nd (sensitive) zone. Visually one looks at the perradiation spanning the three zones for each DCC picture, and then compares the perradiation between the different pictures. Image analysis determines an ROI where the calculated values differ most, based on geometrically defined ROIs, while the visual evaluator perceives the whole image and registers differences at different zones. Engquist's observation that she saw the greatest difference in the middle zone is therefore inevitably based on a dynamic zone concept, because zones will vary geometrically from dish to dish. The concept of ROI is a static, geometric concept, while the concept of zones is dynamically adapted to each DCC picture. It can be expected that the radii of the zones depend on the tcrStart, because the longer the evaporation the larger the first zone will be.

For image analysis, we expected that if we centered the circular ROIs around the crystallization center (as shown in the bottom row in Fig. 1.6.1) instead of around the geometric center (like in the upper row in Fig. 1.6.1), the discrimination would improve.

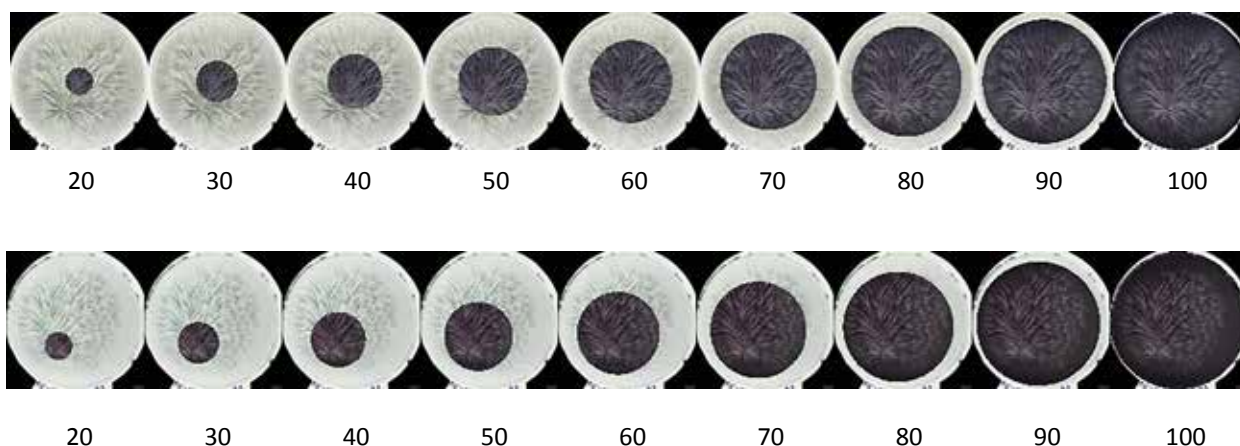


Fig. 1.6.1 The darkened area shows the geometric center based ROI (top row) or the crystallization start based ROI (bottom row). The radius of the circle is given as a percentage of the total dish radius. (From the Polar sampling report 2016 [7]).

However, this has not been the case so far. This can be used as an indication of where the sensitive area is formed during the evaporation / crystallization process. Crystallization starts in an supersaturated area in the Petri-dish, which has at its boundary the concentration of the solubility threshold (supersaturation = 0, see chapter [2.11 Nucleation](#)). This area is centered around the geometrical center, because it is defined by the evaporation geometry of the acrylic ring. If the crystal growth velocity exceeds the expansion rate of the supersaturated area, then the crystal front will extend to the solubility boundary and crystallization stops. The solution at the tip of the crystal continues to evaporate and the crystal growth will “follow” this. If the growth velocity is less than the expansion rate of the supersaturated area, then the crystal growth will be slow and steady. This could be explained by the bachelor work form Herzer (2022 [8]). He observed that the crystal growth velocity for DCC carrot pictures at lower amounts of additive had a steep start and a slow finish, while at higher additive amounts (where the crystal growth velocity is lower) a steady growth velocity was observed. For details see chapter [3.3 CrystEval tool](#). For BSA the reduction of the crystal growth velocity due to an increasing additive amount is at the border between the split-growth and the dendrite crystallization type (Busscher 2019 [9], Fig. 11, left). This fits with the findings in chapter [1.9 Optimal amounts](#).

Resume

The concepts of ROI and zones are shortly compared. ROI is a static geometrical concept, while the zonal concept is dynamically adapted to each picture. The geometry of the sensitive area could possibly be identified from the results of the computer image analysis, as having a circular slice shape with the center in the geometrical center rather than around the crystallization center. When the crystal growth velocity is below the expansion rate of the supersaturated area, a more steady crystal growth can be expected, which will still be affected by the sensitive area, but not as strong as when the growth velocity exceeds the expansion rate. Whether this is in agreement with the visual observed zones has to be researched.

Additional research

1. Check the radius of the crystallization center and the ROI with the highest discriminative ability.
 - 1.1 Is the radius of the center lower than the ROI radius?
2. Image analysis and difference between the zones.
 - 2.1 How to evaluate the building of a whole?
 - 2.2 Can we identify the different zones? When using the simple definition from chapter [1.13 Picture zones](#).
3. Is the image analysis homogeneous in the zones? See proposals for texture analysis in [Appendix 1.6.1 Homogeneous](#).
 - 3.1 Compare all image analysis results to check if there is an algorithm effect.
4. Compare the radius and the ROI of the highest discriminative ability for two pictures.

4.1 Does the ROI of the zone depend on the tcrStart?

5. When the zones are identified by CrystEval, is the discrimination with the computer image analysis greater when using these zones instead of fixed ROIs?

See also the Additional research in chapter [1.13 Picture zones](#), for the comparison of the results from the visual evaluation and the computer image analysis.

Appendix 1.6.1 Homogeneous

When we look at a DCC picture we can see zones with the same type of crystals. We perceive a homogeneity within this zone, despite small variations relative to the zone average. From this we expect that the image analysis should show the same homogeneity in the respective ROI. A small investigation was done for texture analysis and the variation within a zone does not look as homogeneous as expected.

Using a sliding box ROI approach (Hall Beyer 2000 [10]), the original picture could be transformed into a picture with the GLCM variable as a gray or color value. This would allow visualization of local variations, like for instance different zones, as opposed to the current fixed ROI approach, which provides an overall measure of pixel gray value relationships. It would also allow to investigate which variable shows a more homogeneous response to a crystal zone than others, and whether a combination of two or more variables can help to identify different crystal zones.

References

- [1] Engquist M Die Gestaltkräfte des Lebendigen (Vittorio Klostermann, 1970).
- [2] Kahl J. Entwicklung, in-house Validierung und Anwendung des ganzheitlichen Verfahrens Biokristallisation für die Unterscheidung von Weizen-, Möhren- und Apfelproben aus unterschiedlichem Anbau und Verarbeitungsschritten. Habil Thesis, University of Kassel. 2007.
- [3] Kahl J, Busscher N, Mergardt G, Maeder P, Torp T, Ploeger A. Differentiation of organic and non-organic winter wheat cultivars from a controlled field trial by crystallization patterns. *J. Sci. Food Agric.* 2014; 95: 53-58 <https://doi.org/doi:10.1002/jsfa.6818>.
- [4] Kahl J, Busscher N, Doesburg P, Mergardt G, Will F, Schulzova V et al. Application of Crystallization with Additives to Cloudy and Clear Apple Juice. *Food Analytical Methods* 2016; 10: 1-9 <https://doi.org/doi:10.1007/s12161-016-0575-6>.
- [5] Baumgartner S, Doesburg P, Scherr C, Andersen J-O. Development of a Biocrystallisation Assay for Examining Effects of Homeopathic Preparations Using Cress Seedlings. *Evidence-Based Complementary and Alternative Medicine* 2012; 2012: 14 <https://doi.org/10.1155/2012/125945>.
- [6] Andersen JO, Henriksen CB, Laursen J, Nielsen AA. Computerised image analysis of biocrystallograms originating from agricultural products. *Computers and Electronics in Agriculture* 1999; 22: 51-69 [https://doi.org/doi:10.1016/S0168-1699\(98\)00043-X](https://doi.org/doi:10.1016/S0168-1699(98)00043-X).
- [7] Busscher N, Doesburg P. Polar Sampling. Technical Report, CuCl₂ Research. 2016.
- [8] Herzer N. Bestimmung von Bildeigenschaften der Kupferchlorid-Bilder von Möhrensorten (EATMORE-Projekt) mittels computergestützter Auswertung. BSc Thesis, University of Kassel. 2022.
- [9] Busscher N, Doesburg P, Mergardt G, Sokol A, Kahl J, Ploeger A. Crystallization patterns of an aqueous dihydrate cupric chloride solution in the presence of different amounts of Bovine Serum Albumin. *Journal of Crystal Growth* 2019; <https://doi.org/doi:10.1016/j.jcrysro.2019.125272>.
- [10] Hall-Beyer M. Practical guidelines for choosing GLCM textures to use in landscape classification tasks over a range of moderate spatial scales. *International Journal of Remote Sensing* 2017; 38: 1312 - 1338.

1.7 Evaporation issues

What happens during evaporation as a result of an increase in salt concentration and a decrease in pH? What is the effect on the additive?

Abstract

During the evaporation phase of a $\text{CuCl}_2 \cdot 2\text{H}_2\text{O}$ (dihydrate cupric chloride, further DCC) / additive solution in a Petri-dish, the pH of the solution decreases from a starting point of around pH 4 down to a pH of 0.5 as the DCC concentration approaches the solubility border. Most proteins like BSA change their conformation as a consequence of low pH values. When the isoelectric point (the pH at which the protein has a neutral charge) of the main protein fraction of the sample is in the above range between pH 4 and 0.5, these proteins, or other parts of the additive will “drop out of the solution” and precipitate on the glass bottom of the Petri-dish. Other additives can (partly) disintegrate or start to coagulate. The pH value of 0.5, at which the crystallization can start, is in any case a stress factor for the additive in question.

The main question is whether there is a difference between the constituents making up the original additive when it is mixed with the DCC and pipetted into the dish at the start of evaporation and just prior to the onset of crystallization? This question is discussed for additives like [PVP](#), BSA and glycogen and an outline is given for other additives.

Introduction

An important question is, whether and how the additive changes during the evaporation, and what the conditions and the properties of the additive are when the crystallization starts. The mixture of additive and $\text{CuCl}_2 \cdot 2\text{H}_2\text{O}$ (dihydrate cupric chloride, further [DCC](#)) has defined properties when the solution is pipetted into the dish. During the evaporation, as water (and other volatile parts of the additive) evaporates from the solution, the concentrations of additive and DCC increase. This has different effects like an increase of the viscosity and the density of the solution and a decrease of the pH of the solution. For example, the decrease of the pH changes several properties of the additive. Additionally, complex formation of additive, DCC and nano-particles is possible [1] [2] [3]. One possibility to gain more insight into the changes occurring in the additive is to measure the density, the viscosity and the pH of the solution during evaporation.

Historical overview

The basis for the understanding of the changes during the evaporation process requires measurement data on the properties of the DCC solution during the evaporation process (when the concentration changes). Data for the density of DCC solutions can be found in the books of Gmelin [4] and Koglin [5]. The first measurements of the properties like viscosity, density and solubility of a DCC solution during evaporation were reported by Beckmann [6]. He measured the viscosity and solubility of DCC without and with 1% gelatin and 1% glycine (2-Amino acetic acid). From the viscosity curve of a 2.5 - 3 molar DCC solution without additives, he deduced ([6], p. 11) a structural change in the DCC (see also Fig. 1.7.6 below), which was supported by the color change from blue to green (see also Fig. 1.7.1 below). Adding 1 % glycine to the DCC solution gave a higher solubility of DCC, while adding 1% gelatin to the DCC solution decreased the solubility of DCC for temperatures below 37 °C. Selawry [7] documented the decrease in pH of a DCC solution with increasing DCC concentration. The first one who pointed to the evaporation phase as an important (pre-) phase for the DCC picture was versus von Hahn [8].

Authors Measurements (Mergardt 2012 [9])

In 2010 Mergardt measured the density, pH and viscosity of mixtures of different amounts of DCC and the additives [PVP](#) (molecular weights K30, K60, K90), glycogen and Bovine Serum Albumin (BSA) (Mergardt 2012 [9]; published in Busscher 2019 [10]). The DCC amount was increased from 0 to the solubility border of DCC. The amounts of the additives were chosen according to the usual amounts for a picture at the solubility border. This setting was chosen to simulate the evaporation process in the dish, although in this experiment only the DCC amount increases. The amounts of the additives were chosen as those at the end of the evaporation at the solubility border. This is for BSA 3.2 % w / w, glycogen 15 % w / w, PVP K90 2.88 % w / w).

Color of DCC concentrations



Fig. 1.7.1 Color of solutions with increasing DCC concentrations. From left to right 0 % w / w to 50 % w / w DCC. DCC amounts are 0 %, 1 %, 2 %, 3 %, 4 %, 5 %, 6 %, 7 %, 8 %, 9 %, 10 %, 15 %, 20 %, 25 %, 30 %, 35 %, 40 %, 45 %, and 50 % w / w. Data from Mergardt 2012 [9], Fig. 6.

The color of the DCC solution changes from clear (0 % w / w) to blue (20 % w / w) at higher concentrations, and to dark green (50 % w / w) near the solubility border (56 % w / w at 25 °C).

Density of mixtures

The simplest measurement to see interactions between DCC and an additive is to measure the density of the mixtures at increasing DCC amounts. This is shown in Fig. 1.7.2.

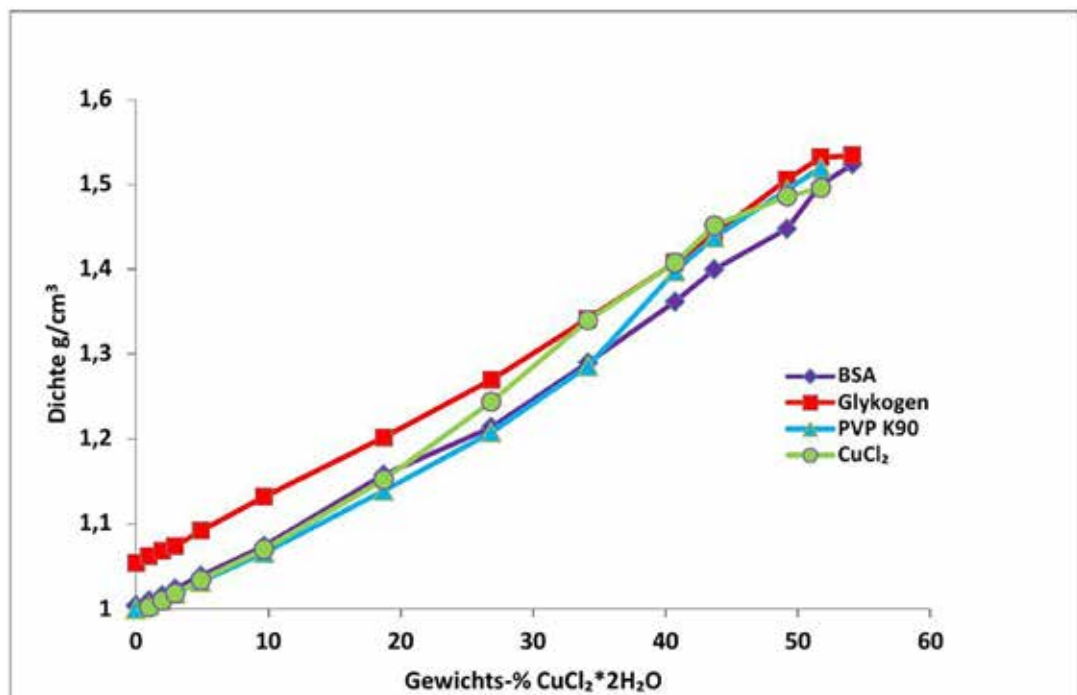


Fig. 1.7.2 Density of mixtures of different additives in g / cm³ (Y-axis) at increasing DCC amounts (X-axis) in % w / w. Additives used were: BSA 3.2 % w / w, glycogen 15 % w / w, PVP K90 2.88 % w / w. Mean density values are shown. Data from Mergardt 2012 [9], Fig. 12.

The glycogen curve (red) started at DCC = 0 % w / w with a density of 1.05 due to the used amount of 15 % w / w, compared to a density of ~ 1.0 for BSA (3.2 % w / w) and PVP K90 (2.88 % w / w). As the amount of DCC increased, the DCC only curve (green) appeared to have a steeper slope than the glycogen (red), with an anomaly at 20 % w / w DCC, while the BSA (violet) had a comparable slope to glycogen. The PVP K90 curve (cyan) showed an anomaly at 35 % w / w DCC. This seems to be a specific characteristic for PVP K90, as PVP K60 and PVP K30 did not show this change, as can be seen in Fig. 1.7.3.

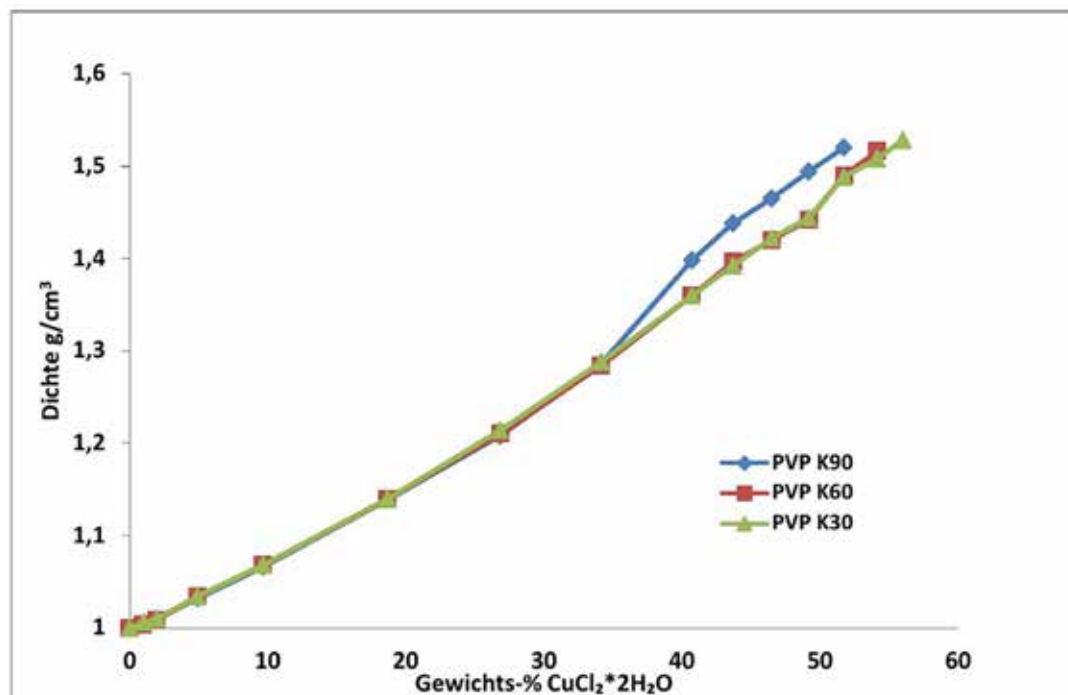


Fig. 1.7.3 Density of mixtures of different PVP additives in g/cm^3 (Y-axis) at increasing DCC amounts (X-axis) in weight %. Different PVP molecular weights (K30, K60, K90) were used as additives. Mean values are shown. (PVP amounts 2.88 % w / w). Data from Mergardt 2012 [9], Fig. 11.

In Fig. 1.7.3 the density for PVP K90 (blue) behaved differently than PVP K30 (green) or PVP K60 (red). So far no reason has been identified for this behavior. Mergardt observed that for PVP K90, The DCC / PVP solution became “slimy” and difficult to solubilize at about 40 % w / w DCC and higher (Mergardt 2012 [9], p. 17). For K60 and K30 these effects started around 55 % w / w DCC.

Resume density measurements

The density of a DCC solution increases with the % w / w DCC. In the case of glycogen a offset to the BSA and PVP K90 curves was observed, which can be explained by the higher amount of glycogen used. PVP K90 and DCC without additive show anomalies at 20 % w / w (DCC) and 35 % w / w (PVP K90). The deviation of DCC occurred in the range were the color changes from blue to green (20 - 30 % w / w, see Fig. 1.7.1). The DCC / PVP K90 becomes slimy at 35 % w / w.

pH measurements

Selawry [7] (p. 4, Fig. 4) reported a decrease of the pH of a DCC solution from pH 2.0 to pH 1.0 in response to an increase of the w / w % of the DCC solution from 10 - 20 % w / w. Mergardt 2012 [9] measured the pH of a DCC solution with different additives until the solubility border was reached and could reproduce the pH decrease as a consequence of the increasing DCC concentration as reported by Selawry, although the measured values were different, like pH 3 at 10 % w / w and pH 2.5 at 20 % w / w. The numerical differences cannot be explained so far.

The motivation for measuring the pH is that most of the additives, especially proteins, have a strong dependency on the pH value, with precipitation at the iso pH value and conformational changes due to the low pH. As can be seen in Fig. 1.7.4, the pH decreases (green curve for DCC only) to a value of about 0.5 at the DCC solubility border at 55 % w / w. The effect of an increasing DCC amount for different additives is shown in Fig. 1.7.4.

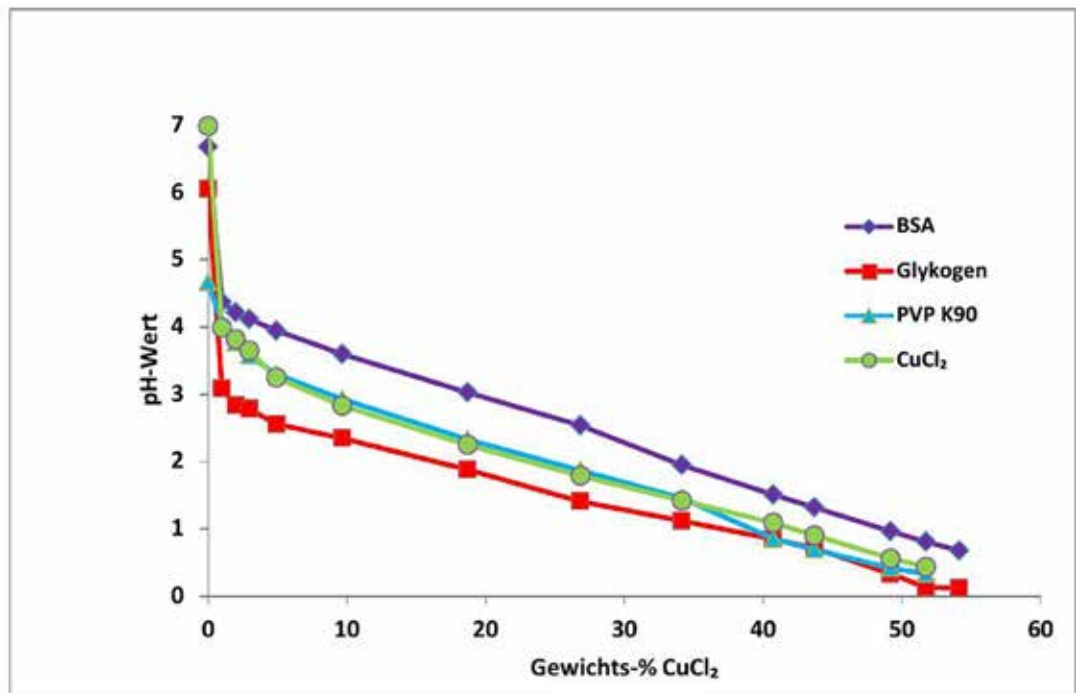


Fig. 1.7.4 Graph of pH (Y-axis) of mixtures of DCC with different additives at increasing DCC amounts (X-axis) in weight %. Additives used were: BSA 3.2 % w / w, glycogen 15 % w / w, PVP K90 2.88 % w / w. Data from Mergardt 2012 [9], Fig. 9.

The pH dependencies of mixtures of DCC and additives with increasing % w / w DCC in Fig. 1.7.4 are similar in that they start with a steep fall from pH 7 as DCC is added, and then continue to decrease linearly with the DCC increase. The pH values for BSA (violet) are higher and glycogen (red) are lower than the values for DCC only (green) and PVP K90 (cyan). For PVP K90 there is a change as observed in the density curve in Fig. 1.7.3 around 35 % w / w. This is also visible in comparison with PVP K60 and K30 in Fig. 1.7.5.

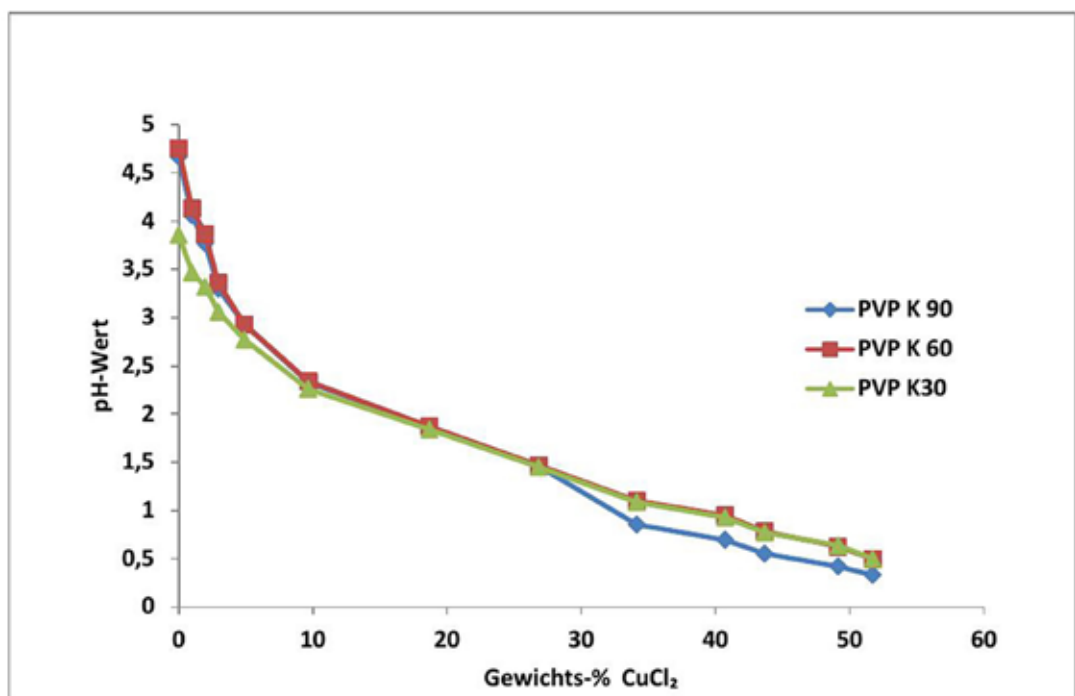


Fig. 1.7.5 Graph of pH (Y-axis) of mixtures of DCC with different PVP K-values (K30, K60, K90; at 2.88 % w / w) with increasing DCC amounts (X-axis in weight %). Data from Mergardt 2012 [9], Fig. 8.

Resume pH measurements

The pH is DCC concentration dependent from pH 7 (no DCC) to 0.5% (56% w / w DCC). The addition

of an additive has an effect on the pH values, the overall dependency is the same (towards lower pH values with increasing DCC amounts) for all researched additives. The pH affects the molecular structure of the additive. To check how the structure is affected, the next chapter focuses on the viscosity of mixtures DCC / additive during evaporation.

Viscosity measurements

The viscosity measurements point towards two aspects. One concerns the fluid characteristics of the additive solutions being tested, and the second is the degree to which varying amounts of DCC affect the fluid characteristics. A liquid's viscosity describes its resistance to flow and is related to the internal friction within the fluid. Many simple fluids are classified as so called Newtonian, meaning their viscosity is independent of the amount of force applied at a constant temperature. Examples would be water and simple hydrocarbon solutions. As fluid complexity increases, for example by the inclusion of bubbles, droplets, particles or polymers, fluids may take on more complex behavior and show a non-Newtonian response, where viscosity depends on the amount of applied force. This non-Newtonian characteristic is an invaluable aspect of paints, having a low resistance when the paint is smeared and a higher resistance when it is not smeared, keeping it adhered to the wall.

Varying amounts of DCC can influence the viscosity of the solutions in different ways by changing the molecular structure, e.g. conformational changes of proteins. Measurements were performed with PVP (K30, K60, K90), glycogen and BSA as additive. As illustrated below, after the DCC - only case (Fig. 1.7.1), the dependence of mixtures of PVP on the amount of DCC are shown first (Fig. 1.7.7), because PVP in water is specified by BASF as a Newtonian fluid [11]. Secondly, the glycogen measurements are shown (see Fig. 1.7.11 and 1.7.12), which show a strong deviation from the PVP measurements. And thirdly, in Fig. 1.7.13 the dependency of the viscosity of a BSA DCC mixture is shown at different DCC amounts.

Measurements from Beckmann (1957 [6])

Viscosity measurements of DCC only

The first results were reported by Beckmann [6]. His measurements were done with a Höppler (falling ball) equipment (See Fig. 1.7.6 below).

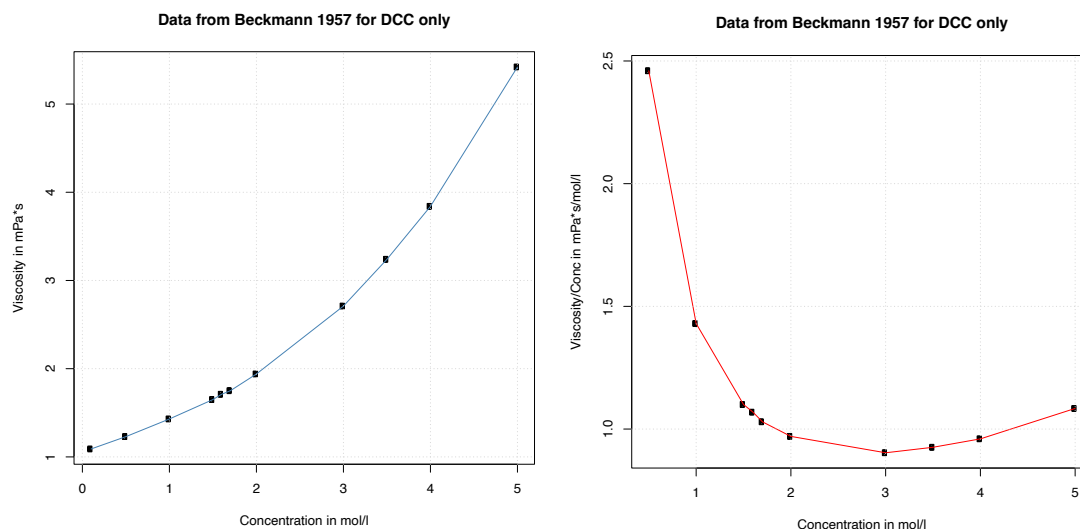


Fig. 1.7.6 Own plots with data from From Beckman [6] (p. 9) Left: Viscosity (Y-axis) in $\text{mPa} \cdot \text{s}$ versus the DCC concentration (X-axis) in mol / L . Right: Viscosity / DCC concentration (Y-axis) in $\text{mPa} \cdot \text{s} / \text{mol} / \text{L}$ versus the DCC concentration (X-axis) in mol / L .

In Fig. 1.7.6 left, the viscosity measurements from Beckmann [6] are shown. In Fig. 1.7.6 right the viscosity data for DCC - only were divided by the concentration, showing a minimum between 2.5 and 3 mol / L. From this behavior Beckmann deduced that the "structure" in the solution changed at a concentration between 2.5 to 3.0 mol / L DCC. This could be the same as was seen in the density measurements (see Fig. 1.7.2), where the density of DCC without additives changed between 20 % and 35 % w / w (the DCC solubility border is at 56 % w / w or 5 mol / L).

Measurements from Mergardt (2012 [9])

Viscosity measurements of DCC / PVP

A Brookfield L-V1 (61) teflon spindle was used in a concentric cylinder measuring system (see chapter 10 in Mezger 2020 [12]) when measuring the viscosity of DCC and additive mixtures because the expected low pH was thought to cause spindle problems. At the low viscosities measured (below 30 mPa * s), and the beaker diameter used (65 mm), turbulence effects could not be neglected. This became apparent because the rpm dependency of the reference oil viscosity (expected constant value of 30 mPa * s) was not constant for all rpm's (see [Appendix 1.7.1 Viscosity](#)), which is inconsistent with the expected true Newtonian behavior of the reference oil. The turbulence effect depends on the viscosity and the rpm. For lower viscosities, turbulence starts at lower rpm's ([12] chapter 10.2.2.4). The "real" value of the non-turbulent viscosity, as e.g. determined by ISO 3219-2 (see chapter 10.2.2 in [12]) cannot simply be extrapolated to 0 rpm, if the viscosity is approximately constant for rpm's below the rpm at which the turbulence began. In addition, the used viscometer is not accurate for low viscosity values (occurring at low rpm's). Therefore we decided to view the results qualitatively and compare the viscosities for several rpm's, to check for consistencies across all rpm's. In some cases we took rpm = 150, because at this rpm the reference oil showed the expected 30 mPa * s reference value (see [Appendix 1.7.1 Viscosity](#)).

PVP Measurements

Of the results for the different molecular weights of PVP, the highest one, K90, will be discussed first. The viscosity dependency on the shear rate in rpm is shown in Fig. 1.7.7. The linear increase of the viscosity with the applied shear rate in rpm is clearly visible, although it differs for the different weight % DCC added.

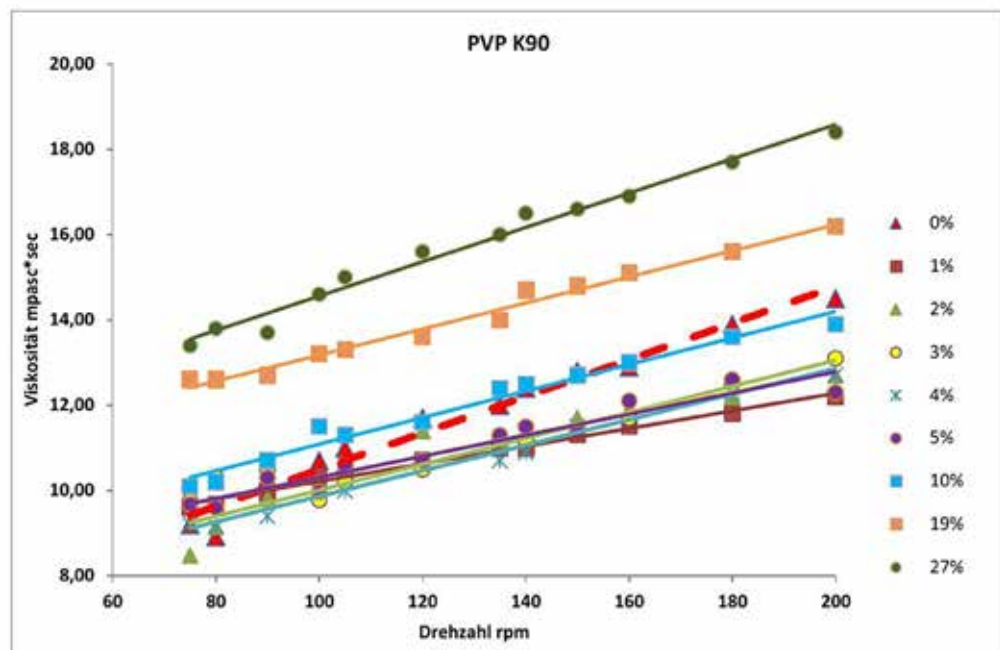


Fig. 1.7.7 Viscosity in mPa * S (Y-axis) versus the rpm (X-axis) with the DCC amount in % w / w as parameter (2.88 % w / w PVP K90 at DCC 0 % w / w). The red dashed line indicates PVP K90 without DCC. Data from Mergardt 2012 [9], Fig. 18.

Bolten [13] measured the viscosity of a watery solution of PVP K90 with the "falling ball method". At 25 °C and 25.01 g / dm³ for PVP K90 the viscosity value was 8.37 mPa * s (from Table 5 in Bolten [13]). The PVP Solution (2.88 % w / w at 0 % w / w DCC) in Fig. 1.7.7 (bold dashed red line) has a concentration of ~ 28.8 g / dm³ at 25 °C. The extrapolated viscosity value at 0 rpm is around 6 mPa * s. The expected value for the non-turbulent case should be higher than 6 mPa * s, i.e. closer to the value from Bolten for K90 (8.37 mPa * s).

The values in Fig. 1.7.7 for PVP K90 for different DCC amounts do not show parallel lines in all cases. To see the dependency of the viscosity values on the DCC amount, the data are plotted in Fig. 1.7.8 with rpm as parameter.

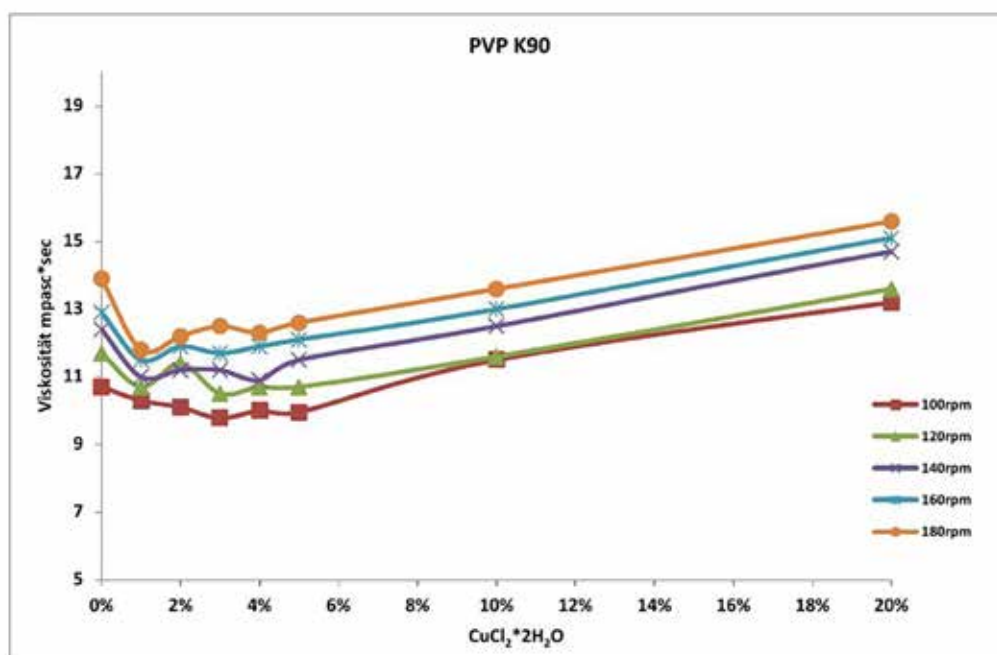


Fig. 1.7.8 Viscosity of a PVP K90 solution in mPa * s (Y-axis) versus the amount of added DCC in w / w %, with the shear rate in rpm as parameter. Concentration PVP K90 2.88 % w / w. Data from Mergardt 2012 [9], Fig. 19.

Fig. 1.7.8 shows that the addition of 0 to 3 % w / w DCC to the PVP K90 solution reduces the viscosity for all rpm's measured. This was also observed by Hao 2009 [14] for DCC with PVP (K90 Mw = 1.1 Mg / mol) in DMF (N,N-dimethyl formamide). This effect was compared with mixtures of PVP K90 and other metal chlorides (Li, Ca, Co) by Hao 2007 [15], which did not show this behavior. The argumentation was that Cu in particular builds complexes with PVP K90. They confirmed this with FTIR (Fourier Transform Infra Red spectroscopy) measurements. With TEM (Transmission electron microscopy) they observed micro phase separation of DCC (with solvent DMF). The conclusion was that this complex formation suppresses crystallization.

In a review about Cu and Cu-based nano particles [1] the emergence of Cu nano particles was described for different combinations of additive, stabilizer and solvent (also DCC was mentioned as solvent). Producing nano particles seems to be quite simple. Shikha [16] described how to do it with a DCC solution and Ascorbic acid. The viscosity measurements of Mergardt [9] for PVP K30 and K60 did not show the sudden decrease of the viscosity at 3 % w / w (see Fig. 1.7.10).

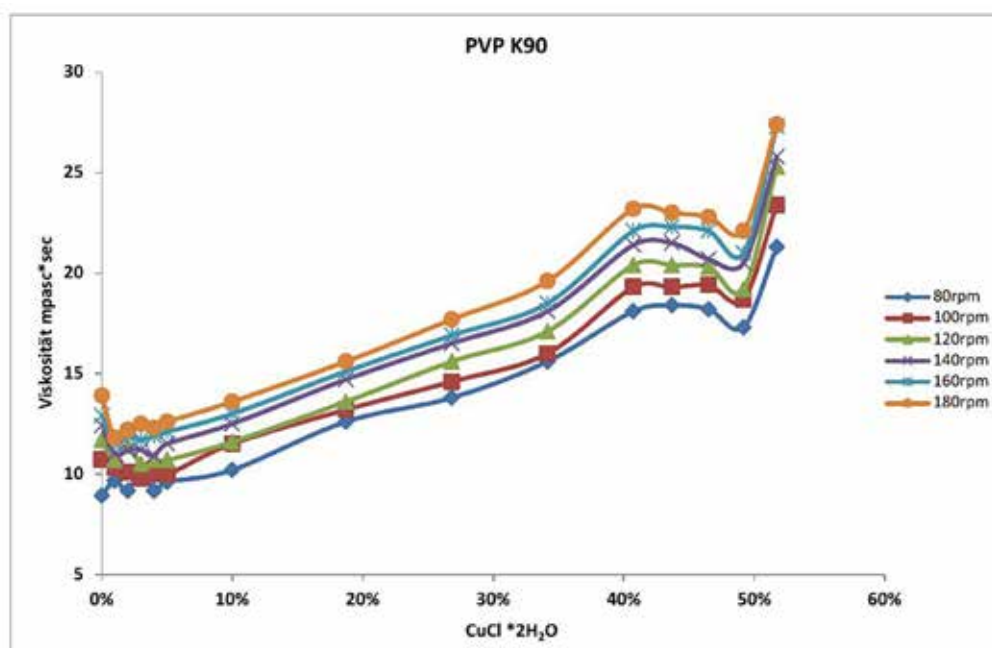


Fig. 1.7.9 Viscosity in mPa * s (Y-axis) versus the amount of DCC in weight %, with the shear rate in rpm as parameter. Concentration PVP K90 2.88 % w / w. Data from Mergardt 2012 [9], Fig. 20.

Following the decrease in viscosity of a PVP K90 solution at lower DCC amounts (2 - 3 % w / w in Fig. 1.7.8), a linear increase in viscosity with the DCC up to 40 % w / w was observed in Fig. 1.7.9. Between 40 % and 50 % w / w DCC, Mergardt ([9], p. 23) reported the formation of flocculations. The decrease in viscosity at 50 % w / w DCC coincides with the DCC saturation concentration. At higher DCC amounts, the solution began to stick to the viscometer spindle which resulted in an increase of the viscosity at 55 % w / w.

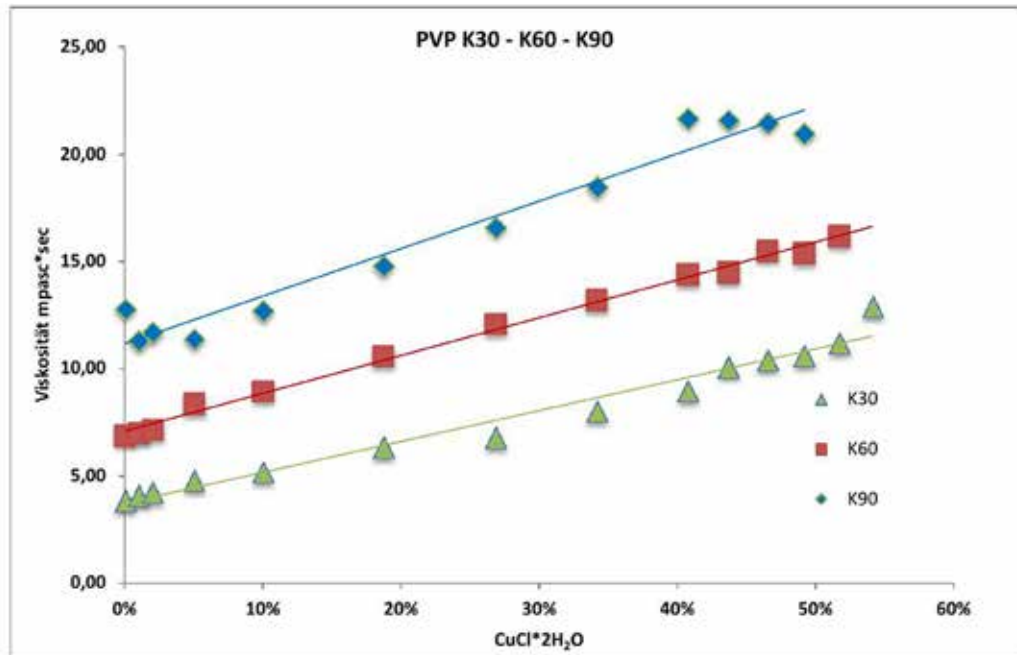


Fig. 1.7.10 Viscosity in mPa * s (Y-axis) of three PVP K values at a shear rate of 150 rpm versus the amount of DCC in weight %, with the K value as parameter. Concentration PVP 2.88 % w / w. Data from Mergardt 2012 [9], Fig. 21.

For the comparison of the PVP solutions at different K values, the viscosities were plotted for the shear rate of 150 rpm versus the added DCC amount. The viscosity increased by a factor 2 from K30 to K60 and from K60 to K90. PVP in water at 25 °C (see [17], Fig. 2 and Fig. 3) resulted in ~ 3 mPa * s for K30 and ~ 12 mPa * s for K90. This is roughly in the range, that could be inferred from the graphs in [17]. Viscosity increased by a factor of 2 over a range of 0 to 55 % w / w DCC added.

Glycogen measurements

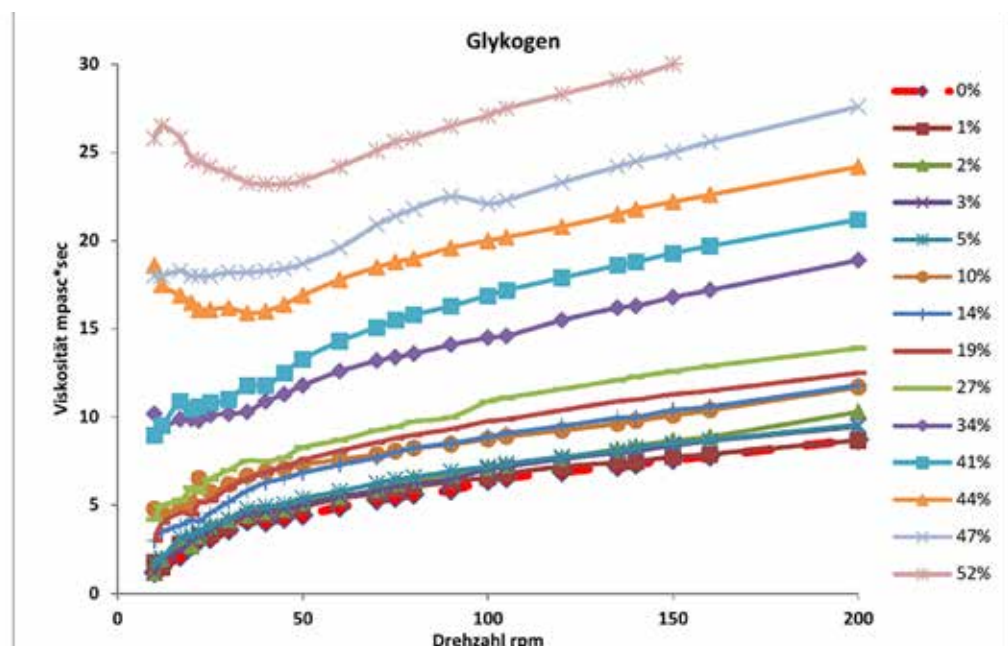


Fig. 1.7.11 Viscosity of glycogen in mPa * S (Y-axis) versus the shear rate in rpm (X-axis) with the DCC amount in weight % as parameter. Concentration glycogen 15 % w / w. Data from Mergardt 2012 [9], Fig. 22.

Glycogen behaved like a non-Newtonian fluid (Fig. 1.7.11). It changed its rpm dependency with the amount of DCC. For the DCC amounts from 0 to 41 % w / w the viscosity increased with the rpm, but tended towards a constant value. For DCC amounts higher than 41 % w / w the viscosity decreased with the rpm (like paint) from 0 till 50 rpm, and increased from 50 rpm onward.

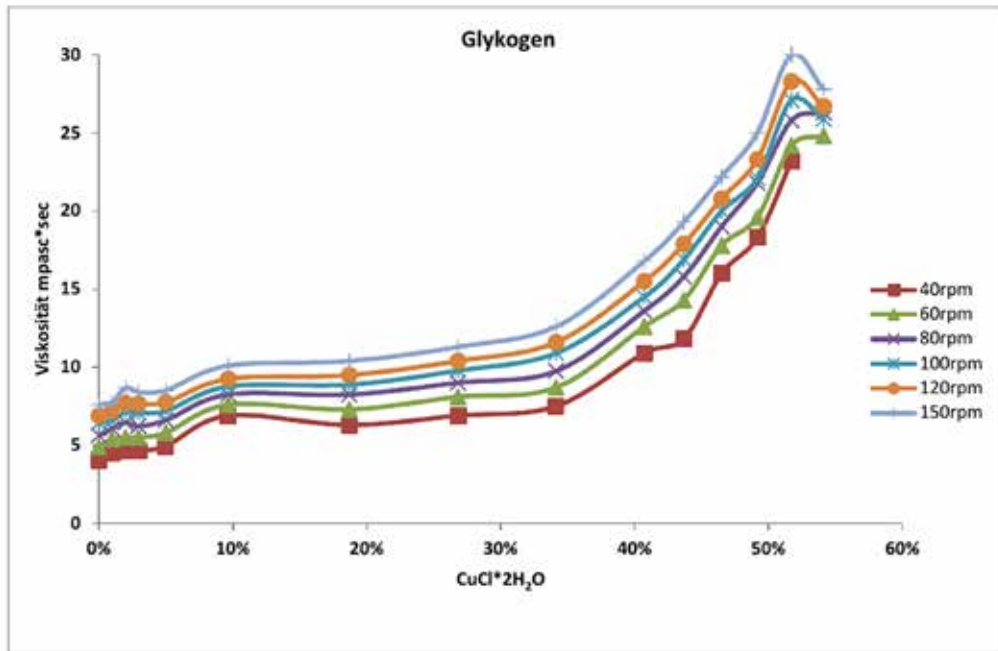


Fig. 1.7.12 Viscosity of glycogen in mPa * S (Y-axis) versus the amount of DCC in weight %, with the shear rate in rpm as parameter. Concentration glycogen 15 % w / w. Data from Mergardt 2012 [9], Fig. 24.

In Fig. 1.7.12. the viscosity of glycogen was approximately constant up to 35 % w / w. The increase from 35 % onward is not understood (hydrolysis?). The solubility of DCC in the 15 % glycogen solution was very good and not so time consuming as it was for PVP, where it took a longer time until the DCC was dissolved.

BSA Measurements

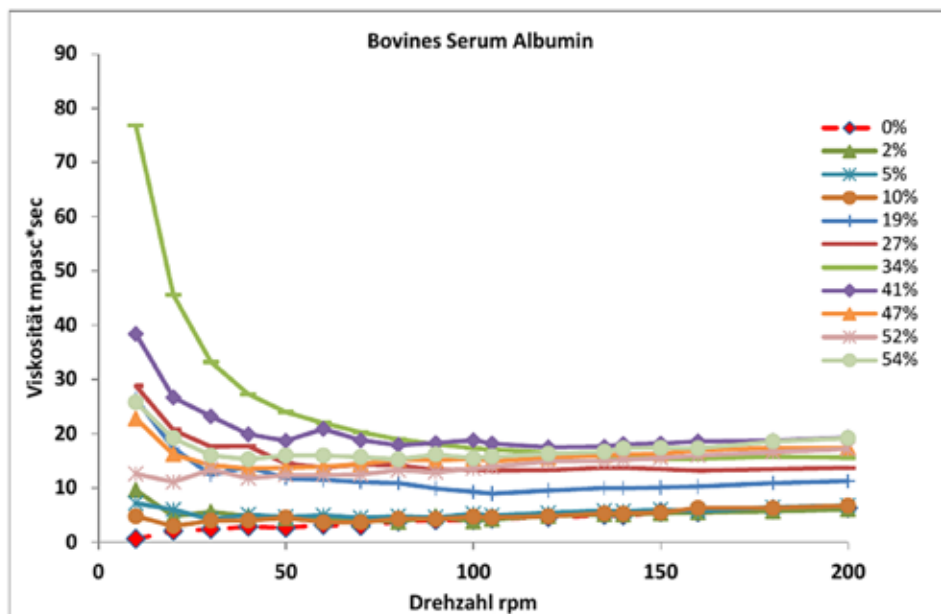


Fig. 1.7.13 Viscosity of BSA in mPa * S (Y-axis) versus the shear rate in rpm (X-axis) with the DCC amount in weight % as parameter. Concentration BSA was 3.2 % w / w. Data from Mergardt 2012 [9], Fig. 28.

In Fig. 1.7.13 the viscosity of DCC with BSA showed a different behavior than PVP or glycogen. The viscosity decreased with the shear rate (like paint) for all DCC amounts (except for 52 % w / w DCC). The effect was strongest for 34 % w / w DCC .

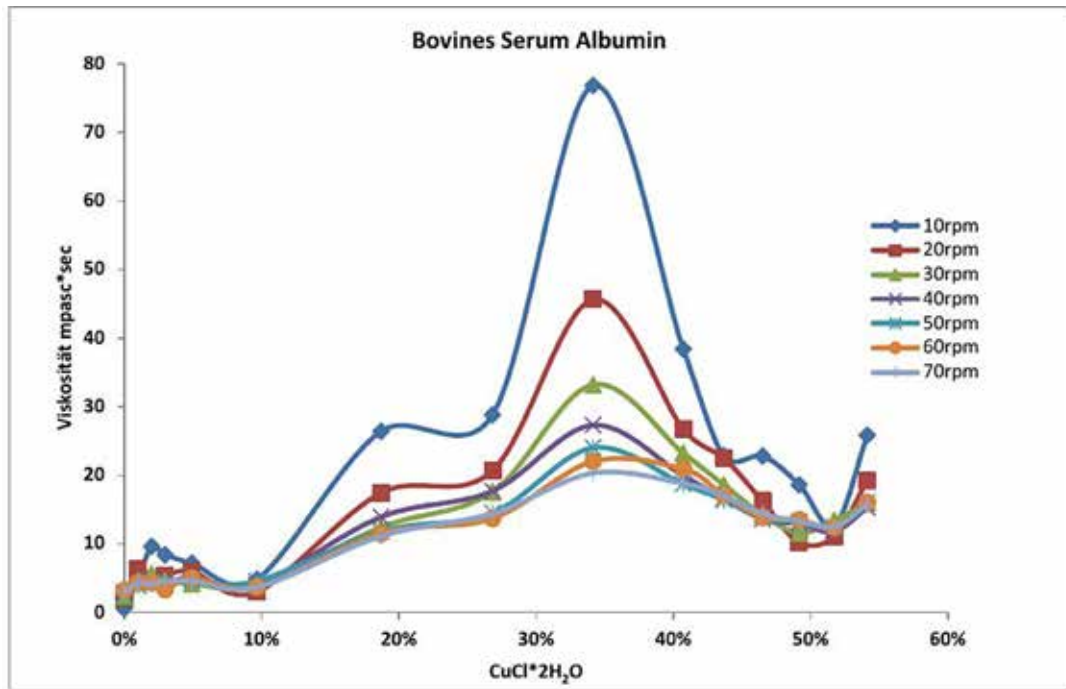


Fig. 1.7.14 Viscosity of BSA in mPa * s (Y-axis) versus the DCC amount (X-axis) in weight % with different shear rates in rpm as parameter. Concentration BSA was 3.2 % w / w. Data from Mergardt 2012 [9], Fig. 29.

In Fig. 1.7.14 the viscosity has a clear maximum at 34 % w / w DCC. The question was if this maximum showed the conformational changes of BSA with the pH as reported by Yang ([18], Fig. 4). To visually verify this, the DCC amount was replaced by the pH values from Fig. 1.7.4 as shown in Fig. 1.7.15.

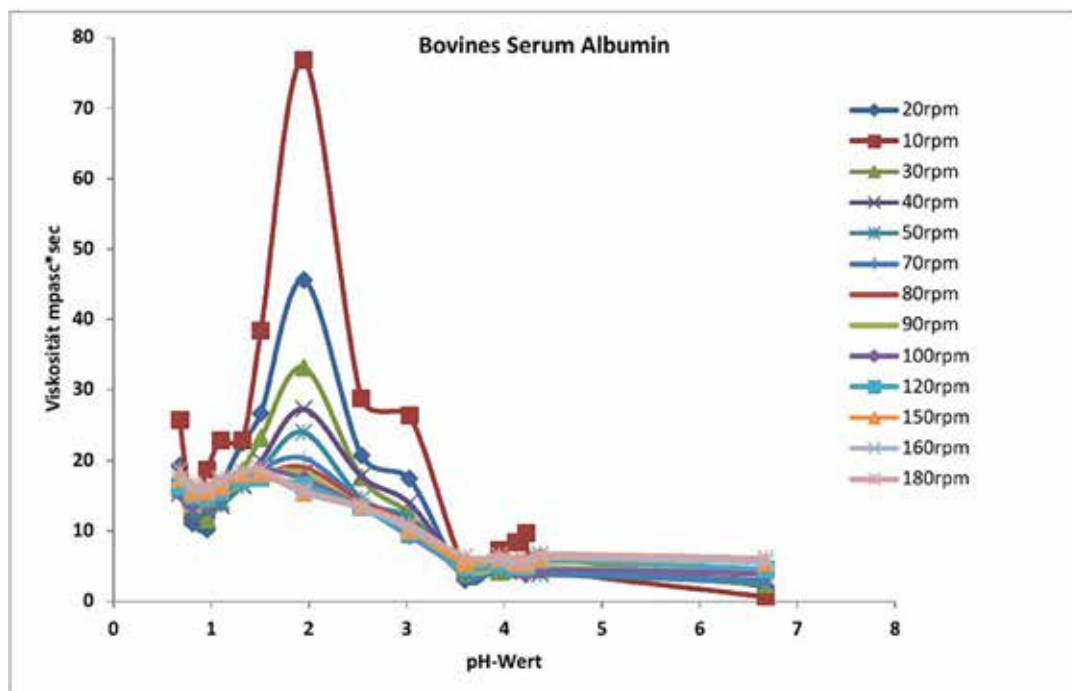


Fig. 1.7.15. BSA viscosity in mPa * S (Y-axis) versus pH value, using Fig. 1.7.4 to replace DCC from Fig. BSA.2 by pH values. Concentration BSA was 3.2 % w / w. Data from Mergardt 2012 [9], Fig. 30.

Fig. 4 from Yang [18] and Fig. 1.7.15 show a comparable dependency of the viscosity of BSA from the pH of the DCC solution.

Resume viscosity experiments with PVP, BSA and glycogen

The viscosity of DCC with additives is higher than the DCC only solutions. The simulations of the evaporation process by Mergardt [9] lack the stepwise increase of the concentration of the additive. Here the additive

concentration at the solubility border was taken. The change in viscosity is much stronger during evaporation, nevertheless it reached the same final value.

The samples react differently to the change in pH. PVP reacts with a linear increase in the viscosity with the DCC amount. BSA shows a conformational change of the structure. Glycogen reacts strongly. Maybe glycogen is undergoing a hydrolysis process. In general, it can be said that the samples undergo changes during evaporation. The sample at the start of the evaporation and the sample at the start of the crystallization are different. Close to the solubility border the DCC / sample mixtures become sticky. The question is how high the viscosity of the solution is when the crystallization starts.

Additional observations

Experiments with Milk

For Milk as additive it was observed that the opacity of the solution cleared (as a wave through the Petri-dish from center to periphery in approximately 30') ~ 1 hour before the crystallization start and remained so.

Experiments with BSA

Observations with BSA showed, that with higher amounts of BSA per plate the solution became turbid before the crystallization started (as a wave through the dish) and the meniscus "broke down" before the crystallization started. The release of the meniscus points to a change in the surface tension of the solution, which would be a quite dramatic effect. BSA already changed the surface properties of the solution at very low amounts [19], [10].

Other samples

In Fig. 1.7.4 it can be seen that the addition of 5 % w / w DCC decreased the pH of the solution to pH 4 for BSA, 3.2 for DCC only or PVP and 2.8 for glycogen (3.2 % w / w for BSA, 2.88 % w / w for PVP and 15 % w/w for glycogen). When the iso-pH of the sample is close to the pH of the solution then the decrease in pH due to the addition of DCC (or a further pH decrease due to evaporation) results in precipitation or flocculation of mainly the protein fraction of the sample. This could be observed by Mergardt [9] for BSA as the formation of turbidity prior to crystallization for 316 monolayers of BSA, or approximately 2.68 mg protein per dish.

When the pH is lower than the iso-pH, the net charge of the protein is reversed, the question remains whether and how the precipitated (protein) will dissolve again. This depends on the sample. In the case of a multi-component mixture, such as juices or extracts from agricultural samples, it may happen that a part of the mixture precipitates and is not in solution when the crystallization starts.

BSA is known for covering glass ware. This adhesion seemed to be stable during the entire evaporation process and affects the crystallization process (no dewetting from 3 calculated monolayers of BSA onwards [10]).

The DCC – milk chamber solution is opaque due to the casein in colloidal suspension. The opaqueness was lost prior to crystallization i.e. at a very low pH and high salt concentration. It is well known that a (acidic?) hydrolytic reaction will yield soluble, non-colloidal amino acids, hence the clearing of the milk solution. As BSA doesn't contain casein only a precipitation effect may be visible there. It can be imagined that this precipitation also occurs in milk but maybe is obscured due to the colloidal casein suspension [20].

For freeze dried wheat the amount required to prevent dewetting is much higher compared to BSA, but this [amount per plate](#) was calculated from the amount before solubilization, which does not reflect the amount of the surface active part on the plate, which can be much lower. Also the protein content in wheat is lower than in BSA.

For apple juice the iso-pH of pectin is around 3.5 [21]. Dewetting was observed for clear apple juice on glass plates with a higher surface tension than usual (see chapter [1.4 Cleaning, surface tension, ring height](#)), while this did not happen for turbid apple juice [22], p. 30. One of the main differences between turbid and clear apple juice is that turbid apple juice has an higher amount of pectin (697 mg / L) than clear apple juice (33 mg / L) [23].

Evaporation effects

Due to the cooling effect of evaporation, the area near the surface not only has a lower temperature than the bulk of the solution in the Petri-dish, but there is also a concentration gradient from the surface of the solution to the glass plate at the bottom of the Petri-dish. This gradient has its maximum at the surface. The conditions at the surface are therefore quite different from the bulk of the solution and can be a source of instabilities as reported by Style 2007 [24] [25].

Resume

Due to the low pH of 0.5 at the DCC solubility border, a strong effect on the sample can be expected. The samples behave differently under these conditions. The composition of the additive at the begin of the evaporation will undergo changes prior to the crystallization start. What remains in solution or precipitates on the Petri-dish will be different for each additive.

Additional research

Why does the viscosity of DCC without additives increase with the amount of DCC?

Start a literature study e.g. starting from Afzal [26].

Why does the viscosity of glycogen and PVP increase with DCC?

Start a Literature Study e.g. Hao [15] [14] and others [27] [28] [29].

Measure the viscosity of freeze dried wheat and freeze dried carrot with DCC.

Solubility border of mixtures (more DCC or less DCC possible)?

pH indicator as additive

comparison when the pH changes and the degree of homogeneity.

Study the photos and data for milk and BSA

Appearance of turbidity; When, where?

How does the type of viscosity influence the crystal growth?

Is the type still the same when the crystallization finally starts?

Or is the viscosity type more like glue?

For Pectin: study the viscosity, density and pH

How can the difference in dewetting be understood (DCC Matrix?)

Concentration gradient between surface of the solution in the Petri-dish and bottom of the Petri-dish.

Calculation of the effect following Style [25] [24].

When a molecule is affected by the low pH (e.g. hydrolysis) how would this show up in the viscosity measurement data? Can we use PVP as a model for this?

Hao [14] reported that micro phase separation of Cu ions was observed. Is this a general phenomenon for DCC/additive mixtures during evaporation? Observe mixtures in a beaker, placed in the evaporation chamber, with the usual camera.

Appendix 1.7.1 Viscosity

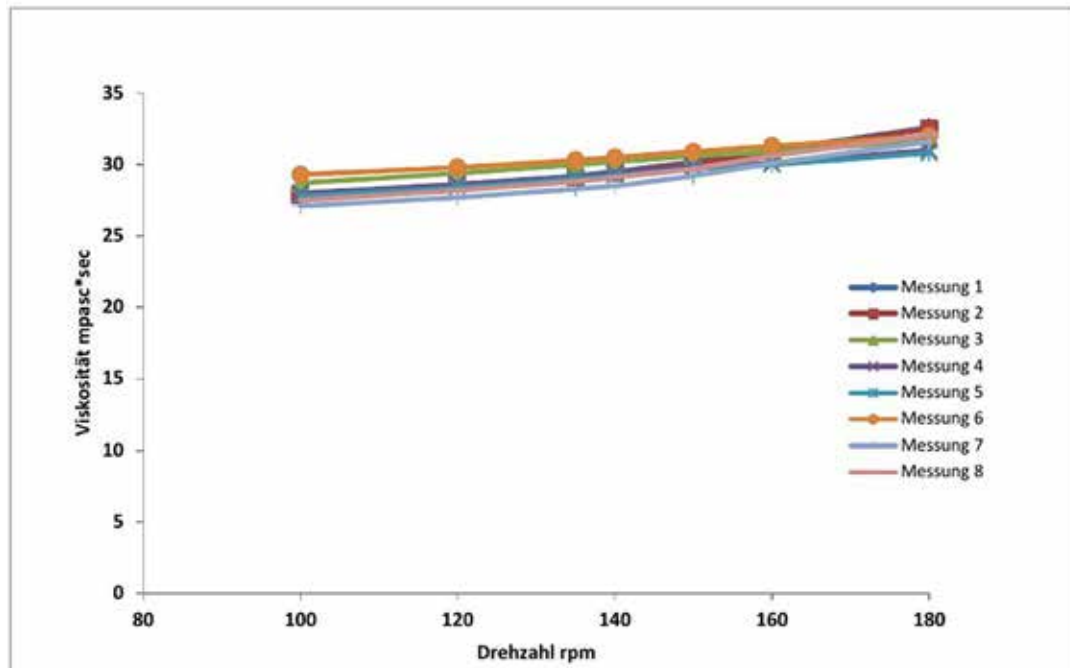


Fig. 1.7.16 Viscosity (Y-axis) versus the rotations per minute (X-axis) for the Brookfield calibration oil. Data from Mergardt 2012 [9], Fig. 13.

The oil is expected to exhibit true Newtonian behavior. The deviation from the constant behavior is due to the turbulence effect of the cylindrical setup caused by the specially made Teflon spindle. The measurement was repeated 8 times. The oil was expected to have a viscosity of 30.0 mPa · s.

References

- [1] Gawande MB, Goswami A, Felpin F-X, Asefa T, Huang X, Silva R et al. Cu and Cu-Based Nanoparticles: Synthesis and Applications in Catalysis. *Chem. Rev.* 2016; 116: 3722-3811 <https://doi.org/10.1021/acs.chemrev.5b00482>.
- [2] Bell JR, Tyvoll JL, Wertz DL. Solute structuring in aqueous copper(II) chloride solutions. *Journal of the American Chemical Society* 1973; 95: 1456-1459.
- [3] Fritz JJ. Chloride complexes of copper(I) chloride in aqueous solution. *The Journal of Physical Chemistry* 1980; 84: 2241-2246.
- [4] Gmelin Gmelin Handbuch der anorganischen Chemie (Gmelin-Institut, Frankfurt am Main, 1958).
- [5] Koglin W Koglin, W. editors. Kurzes Handbuch der Chemie (Koglin, W., 1952).
- [6] Beckmann H. Über Keimbildung, Einkristallwachstum und Auffächerungswachstum von $\text{CuCl}_2 \cdot 2\text{H}_2\text{O}$ in reinwässrigen und Eiweiß-haltigen Lösungen. PhD Thesis, Universität Bonn. 1959.
- [7] Selawry A and Selawry O Die Kupferchlorid-Kristallisation in Naturwissenschaft und Medizin (Gustav-Fischer-Verlag, 1957).
- [8] Von Hahn F-V Thesigraphie. (Franz Steiner Verlag, 1962).
- [9] Mergardt G. Simulation des Entstehungsvorganges von Kristallbildern zur Messung der physikalischen Parameter pH-Wert, Dichte und Viskosität am Beispiel von PVP, Glykogen und Bovine Serum Albumin. Technical Report, University of Kassel. 2012.
- [10] Busscher N, Doesburg P, Mergardt G, Sokol A, Kahl J, Ploeger A. Influence of dewetting on the crystallization behavior of CuCl_2 in the presence of BSA during evaporation in a Petri dish. *Heliyon* 2019; 5: e01102 <https://doi.org/10.1016/j.heliyon.2018.e01102>.
- [11] BASF. PVP viscosity, 2010.
- [12] Mezger T The Rheology Handbook: For users of rotational and oscillatory rheometers (Vincentz Network, 2020).
- [13] Bolten D, Türk M. Experimental Study on the Surface Tension, Density, and Viscosity of Aqueous Poly(vinylpyrrolidone) Solutions. *J. Chem. Eng. Data* 2011; 56: 582-588.
- [14] Hao C, Zhao Y, Dong X, Zhou Y, Xu Y, Wang D et al. Anomalous rheological behavior of poly(1-vinyl-2-pyrrolidone) and CuCl_2 in solution and their interactions in solid composites. *Polym. Int.* 2009; 58: 906-911.
- [15] Hao C, Zhao Y, Zhou Y, Zhou L, Xu Y, Wang D et al. Interactions between metal chlorides and poly(vinyl pyrrolidone) in concentrated solutions and solid-state films. *J. Polym. Sci. B Polym. Phys.* 2007; 45: 1589-1598.
- [16] Shikha Jain NN, Devra V. Synthesis and characterization of highly efficient copper nanoparticles and their catalytic application in oxidative kinetic study. *Advances in Applied Science Research* 2015; 6: 171-180.
- [17] Ashland. PVP Polyvinylpyrrolidone polymers, 2013.
- [18] Yang JT, Foster JF. Changes in the Intrinsic Viscosity and Optical Rotation of Bovine Plasma Albumin Associated with Acid Binding. *J. Am. Chem. Soc.* 1954; 76: 1588-1595 <https://doi.org/doi:10.1021/ja01635a038>.
- [19] Gallinet JP, Gauthier-Manuel B. Wetting of a glass surface by protein adsorption induces the crystallization of an aqueous cupric chloride solution. *Journal of Colloid and Interface Science* 1992; 148: 155-159 [https://doi.org/doi:10.1016/0021-9797\(92\)90123-4](https://doi.org/doi:10.1016/0021-9797(92)90123-4).
- [20] Dahal P. Casein Hydrolysis test. Technical Report. 2023.
- [21] Flutto, L. 2003. In: Caballero, B. editors, *Encyclopedia of Food Sciences and Nutrition (Second Edition)*, Academic Press.
- [22] Busscher N. Apple juice Project. Technical Report, University of Kassel. 2015.
- [23] Kahl J, Busscher N, Doesburg P, Mergardt G, Will F, Schulzova V et al. Application of Crystallization with Additives to Cloudy and Clear Apple Juice. *Food Analytical Methods* 2016; 10: 1-9 <https://doi.org/doi:10.1007/s12161-016-0575-6>.
- [24] Style RW, Wettlaufer JS. Evaporatively driven morphological instability. *Physical review. E, Statistical, nonlinear, and soft matter physics* 2007; 76: 1-6.
- [25] Style, R. The evaporation of a salty film. 2006 Program of Study: Ice, 2007, S. 204.
- [26] Afzal M, Saleem M, Mahmood MT. Temperature and concentration dependence of viscosity of aqueous electrolytes from 20.degree.C to 50.degree.C chlorides of (sodium(1+), potassium(1+), magnesium(2+), calcium(2+), barium(2+), strontium(2+), cobalt(2+), nickel(2+), copper(2+) and chromium(3+). *J. Chem. Eng. Data* 1989; 34: 339-346 <https://doi.org/10.1021/je00057a023>.
- [27] Lago AB, Carballo R, García-Martínez E, Vázquez-López EM. Metal to Ligand Interactions and Hydrogen Bonding in the Design of Metallosupramolecular Compounds: Effect of pH and Aprotic Solvents on the Nature of Materials Based on Bis(4-pyridylthio)methane and Copper(II) Chloride. *Crystal Growth & Design* 2011; 11: 59-68 <https://doi.org/10.1021/cg1004566>.
- [28] Jitka Eysseltová VZ, Jirsák J. Solubility in the CuCl_2 -NaCl-H₂O System and Hydration Analysis in the Case of Complexation. *Collect. Czech. Chem. Commun* 1999; 64: 1262-1268 <https://doi.org/https://doi.org/10.1135/cccc19991262>.
- [29] Annenkov VV, Danilovtseva EN, Saraev VV, Alsarsur IA, Lunionok OV. Reaction of the acrylic acid and 1-vinylimidazole copolymer with CuCl_2 in aqueous solution. *Russian Chemical Bulletin* 2001; 50: 1382-1389 <https://doi.org/DOI: 10.1023/A:1012724821247>.

1.8 Concentration Matrix

What is the influence of the $\text{CuCl}_2 \cdot 2\text{H}_2\text{O}$ and additive amounts on the picture in a matrix?

Abstract

The patterns of the $\text{CuCl}_2 \cdot 2\text{H}_2\text{O}$ (cupric chloride di-hydrate, further called DCC) pictures depend on the amount of DCC and additive. The extremes are, in the case of no additive, dewetting before crystallization [1], where all DCC is located at the rim of the Petri-dish, and, for a maximum of additive, inhibition of crystallization [2]. Without additive, dewetting before crystallization usually occurs for DCC amounts below 600 mg per plate.

With sufficient additive, dewetting can be avoided. In between the extremes of dewetting before crystallization and inhibition of crystallization, there are, depending on the additive amount, different areas of comparable pictures. For example, there is a range in which comparable pictures can be found for the same mixture ratio. For Bovine Serum Albumin (BSA) the areas for needle growth, split-growth and dendritic growth could be defined [2]. To see the variation of the pattern in the split-growth and dendrite area a logarithmic equidistant matrix is proposed, where all lines parallel to the major diagonal in the concentration matrix have the same mixture ratio.

Introduction

The pattern of the $\text{CuCl}_2 \cdot 2\text{H}_2\text{O}$ (cupric chloride di-hydrate, further called DCC) picture in the presence of an additive depends on the amounts of DCC and the additive. Usually a DCC amount between 100 and 200 mg per plate is used. The amount of additive is varied in so called concentration series to find the optimal concentration for the research question. More than one concentration or mixture ratio for a research question was used by Engquist 1970 [3], Athmann (2011 [4], p. 30), Fritz (2011 [5], p. 323, 2017 [6], p. 4 and p. 12, Fig. 6) and Kahl (2014 [7], p. 2). Studying the variation of both DCC and additive amounts helped to understand how the pattern depended on both.

Historical Overview

Selawry was the first to document her work on different amounts of DCC and blood [8] and later on germinating seeds [9]. She developed the routine to work on agricultural samples with 200 mg DCC per plate. Selawry used a Petri-dish with 8.4 cm inner diameter (Selawry 1957 [8], p. 8). With this amount of DCC, she sought the "optimal" amount of additive for the research question by testing the additive at increasing levels in concentration series.

In 1969, Petterson [10] also documented the effect of changes in both DCC and additive amount on the DCC pictures. This was done for a constant DCC amount, a constant additive amount, and a constant mixture ratio, see the [Appendix 1.8.3 Petterson](#) for details. Engquist [3] also worked with additive concentration series. Barth in 2002 [11] and in 2004 [12] pointed to the mixture ratio (like Pfeiffer did, quoted in versus von Hahn) as the important factor defining the pattern. Andersen [13] presented in 2003 a full concentration matrix (CMX) (see also [Appendix 1.8.2 Matrix](#) below). Walburger [14] 2005 also worked with the full matrix. Schweizer [15] showed that the angle between needle and stems for glycogen depends on the mixture ratio.

Work on finding the optimal concentration is documented in chapter [1.9 Optimal amounts](#). This chapter focuses on the concentration matrix and, in particular, the importance of the logarithmic equidistant matrix in which different mixture ratios can be compared. Allowing a systematic overview of the different mixture ratios.

Authors Measurements

To see the variation of the pattern and identify areas with comparable patterns a full matrix should be used. Andersen applied the approach of an equidistant spacing of the DCC and additive amounts, as can be seen in [Appendix 1.8.2 Matrix](#) below. The problem with an equidistant matrix is that most of the pictures have different mixture ratios, which complicates obtaining a systematic overview. If the pattern mainly depends on the mixture ratio as stated by Pfeiffer (quoted in von Hahn [16]) and supported by Selawry [8], Petterson [10] and Barth [11] [12], then matrices would be needed in which different mixture ratios could be compared. For this the logarithmic equidistant matrix is proposed, where all lines parallel to the major diagonal in the concentration matrix have the same mixture ratio (see for details [Appendix 1.8.4 Scale](#)).

The first complete matrix with logarithmic equidistant amounts was made for BSA [17] [2]. Based on this matrix a simple morphology map could be composed with areas with comparable patterns.

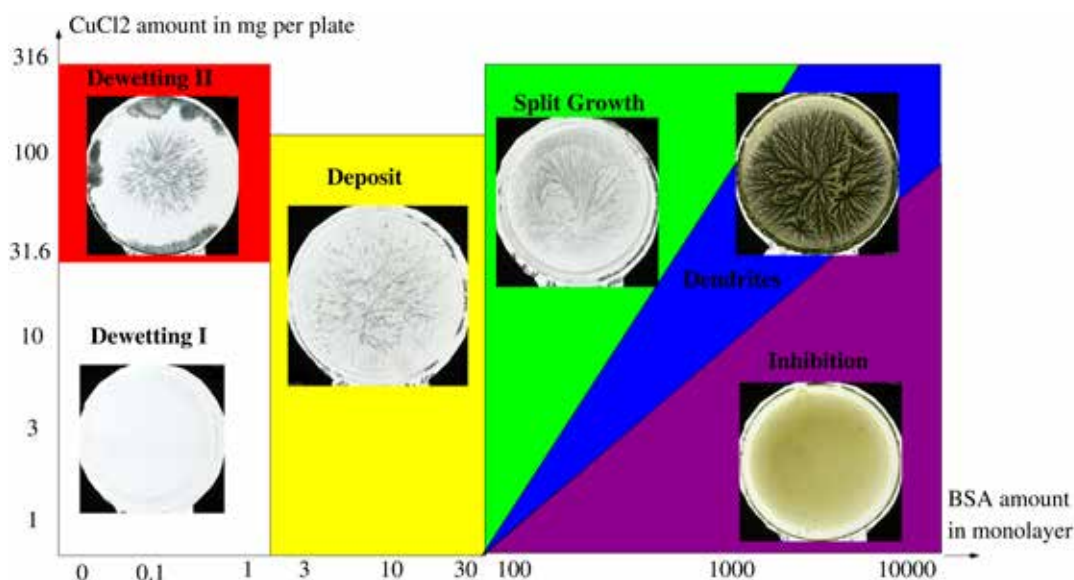


Fig. 1.8.1 Overview of the logarithmic equidistant DCC / BSA CMX with colored areas with comparable patterns and thumbnails of representative patterns. The DCC amount in mg per plate is plotted on the Y-axis. The X-axis represents the BSA amount in calculated monolayers per plate. The red area represents the dewetting II type, the yellow area the deposit type, the green area the split-growth type, the blue area the dendritic type, and the violet area the inhibition-like type. The plates in the white area, called dewetting I area have been discussed earlier [17].

The morphology map in Fig. 1.8.1 shows different crystallization types for BSA, relative to the DCC / additive ratio. The pictures for the different crystal types are shown in chapter [2.3 Crystal growth and branching](#) where the article [17] is described more extensively. In the area dewetting I, dewetting before crystallization occurs, as described in 2010 [1], in which all the DCC is deposited at the rim of the Petri-dish. In the area dewetting II, dewetting after crystallization occurs. The plate is covered with DCC, but there is a dewetted area between the crystal and the rim of the Petri-dish. This was published in 2019 [17], where the forces for the dewetting [18] were identified as the surface tension gradient caused by the concentration and temperature gradient (see more about this in chapter [2.4 Concentration gradient](#)). The next (yellow) area is called the deposit area. Here the pictures are covered with so called deposits. The border between the two dewetting areas and the deposit area is at around 3 calculated monolayers of BSA. This is the well known phenomena that BSA covers glass plates very efficiently, which was applied in DCC crystallization by Gallinet [19]. This boundary in the concentration matrix where dewetting stops is different for each sample. It defines how good the sample in question can cover the glass plate and can change the surface properties, avoiding dewetting. This became apparent in the application of DCC crystallization with apple juice as additive. A small change in the surface tension of the glass plate due to a different cleaning procedure resulted in dewetting of the DCC pictures of clear apple juice, whereas cloudy apple juice at the same mixture ratio resisted dewetting (report apple juice [20] p. 30).

At 30 to 100 calculated monolayers of BSA the area of split-growth appears. This area is characterized by the appearance of hole forms (*“hohlformen”*), because the angles between the crystal branches and needles are very small ($< 15^\circ$) and crystal growth is in the beginning restricted to only two directions. In this area most of the pictures are one-centered. This is a special topic which is described in detail in article [2] and in chapter [1.12 Multiple centers](#). The next area is the dendritic area. In the dendritic area the angle between the branches and the needles is larger than in the split-growth area. The border between the split-growth area and the dendritic area is along the concentration matrix diagonal with a mixture ratio of DCC / BSA of 7. Here a different phenomenon occurs in the CMX than before between the “deposit area” and the “split-growth” area, because the border is now not a perpendicular line but a line with a slope of 7. The border between the dendritic area and the inhibition area is also along a concentration matrix diagonal.

One other result from the dewetting article [17] is the dependency of the coverage of the plate from the DCC and additive amount.

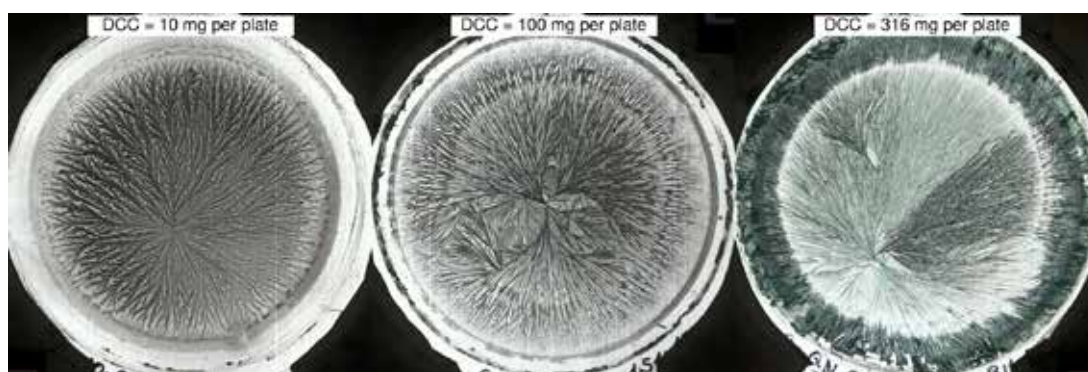


Fig. 1.8.2 Coverage of the plate for different amounts of DCC per plate. Left: 10 mg DCC per plate, middle 100 mg DCC per plate, right 316 mg DCC per plate. BSA additive amount was kept constant at 1.51 mg per plate (177.6 calculated monolayers). (Data from Busscher 2019 [17], Fig. 4).

As can be seen from Fig. 1.8.2, for a constant additive amount the coverage of the plate increases with the DCC amount. At 10 mg DCC, dewetting after crystallization occurs, visible in the crystal free area adjacent to the rim. For DCC amounts higher than 177 mg the crystals from the rim overgrow the crystal free area and the crystal covered area. This can be seen in the most right picture for 316 mg per plate DCC.

This increase of the coverage of the plate with the DCC amount is also reflected in Fig. 1.8.3 below. Interestingly the coverage of the plate hardly depends on the additive amount when more than 3 calculated monolayers BSA are applied (see Fig. 1.8.4).

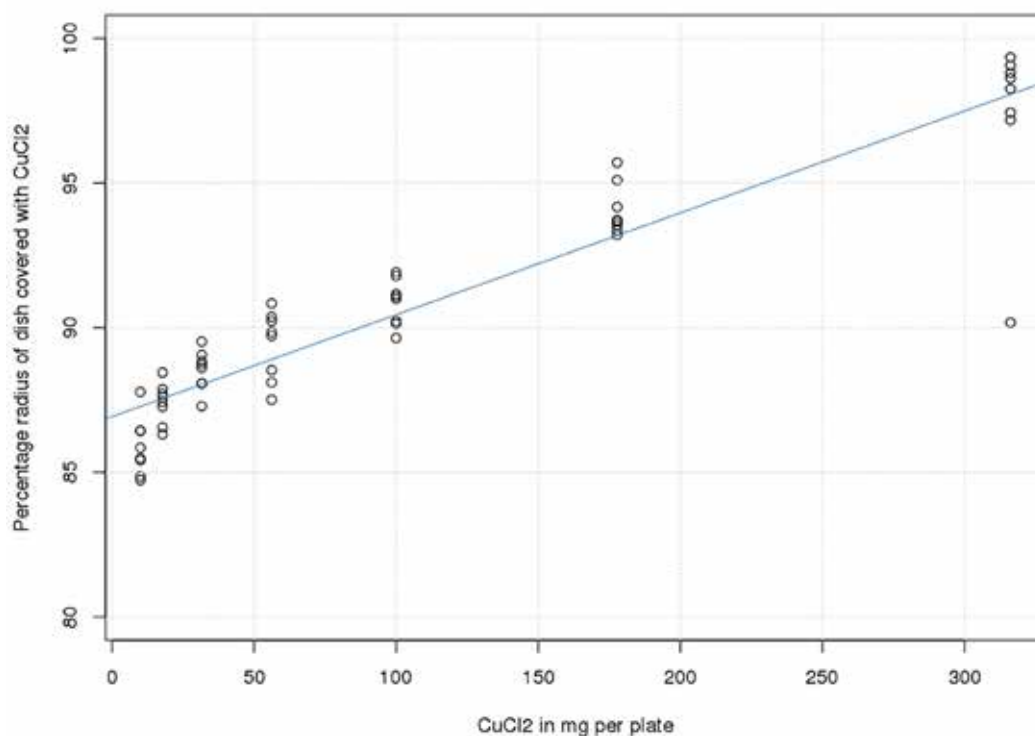


Fig. 1.8.3 Dependency of the radius of the DCC covered area in percentage of the Petri dish radius (ring3) (Y-axis) versus the DCC amount per plate (X-axis). BSA additive amount was kept constant at 1.51 mg per plate (177.6 calculated monolayers). Data from Busscher 2019 [17], Fig. 5.

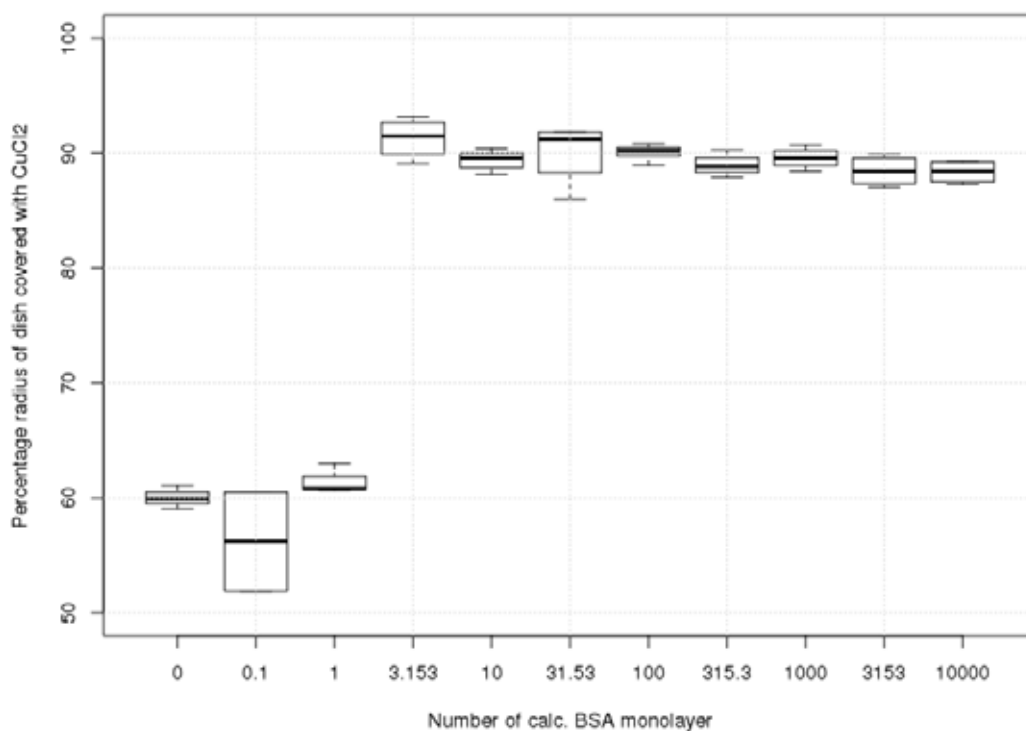


Fig. 1.8.4 Dependency of the radius of the DCC coverage of the plate, as percentage of the Petri-dish radius (ring3, Y-axis), versus the BSA Amount (X-axis) in calculated numbers of monolayers for a DCC amount of 100 mg per plate. Data from Busscher 2019 [17], Fig. 4.

Perhaps the DCC coverage data presented in Fig. 1.8.3 and Fig. 1.8.4 demonstrates the reason why most researchers work with the same DCC amount (150 - 200 mg / plate) (a review of the matrices of different samples will be included in the forthcoming article). If an amount is found that covers the plate well (see Fig. 1.8.3) and does not re-grow from the rim, then the coverage is hardly dependent on the amount of additive (Fig. 1.8.4). Hotho reported that (in Dornach) for a new sample, they usually first checked for good plate coverage with different DCC and additive amounts, and then performed concentration series to determine the most interesting additive amount.

For lower DCC amounts than 50 mg per plate it was observed that the meniscus (actually the DCC in the meniscus) could not be detected at the ring. This effect is discussed in chapter [1.5 Meniscus breakdown](#).

Resume BSA Matrix

BSA was researched over a 0.1 - 10.000 monolayer range and DCC over a 3.1 - 316 mg range. The resulting patterns could be divided into six distinct groups. These exhibit dewetting (type I and II), deposits, split-growth, dendrites and crystallization inhibition. Between split-growth and dendrites the light absorbance and growth velocity change (see article Busscher 2019 [2] supplement, Fig. S7). The dendrite and nucleation inhibition area are delimited by a fixed DCC / BSA ratio. This mixing ratio effect is important for the work with a concentration matrix and is discussed in more detail in the [Appendix 1.8.4 Scale](#).

The question is, does CMX Fig. 1.8.1 with BSA as additive represent a general scheme for the matrix of samples with DCC?

What can't be found in the BSA matrix is an area with substance spirals (see also chapter [2.7 Substance spirals](#)), which is present in wheat and carrot matrices (see Appendix 1.8.2 Matrix below). Currently research is being performed with freeze dried wheat to see how general the above areas in the BSA matrix are. After this matrix has been explored, the other existing (equidistant) matrices (see Appendix 1.8.1 List Matrices) will be re-evaluated to see whether they exhibit comparable characteristics.

Additional research

Freeze dried wheat matrix:

- Measure for additional amounts.
- Compare for common type of areas.
- Do we see the same dependency of the coverage of the plate with DCC additive as in Fig. 1.8.4 and Fig. 1.8.3?
- Compare for areas with one center (see also chapter [1.12 Multiple centers](#)).

Matrix comparison:

- Compare other matrices for similar types of areas.
- This is also done in chapter [1.10 Transition between crystal types](#).

Mensicus breakdown:

- Evaluate time still photos on the breakdown time of the meniscus.
- Compare breakdown time with the crystallization starting time for different DCC / additive amounts.
- What kind of scheme is showing up?

Extend the PVP matrix for lower and higher DCC and additive amounts.

- Does the cleaning have a strong influence on the amount of additive required to prevent dewetting?
- How is the dependency of the coverage of the plate from the ratio DCC / additive?
- Actual PVP matrix is shown in chapter [2.6 Molecular weight and branching](#).

Appendix 1.8.1 List Matrices

Table of existing matrices.

Table 1.8.1 Existing matrices for evaluation. The PVP matrix is shown in chapter [2.6 Molecular weight and branching](#).

Name	Research Question	Sample(s)	Status
BSA Matrix	Matrix	BSA [17]	Full matrix
Apple Juice processing	Turbid / clear apple juice	Apple Juice [20]	Partial matrix
Wheat Matrix (GEEL)	Differentiation farming system	Wheat [21]	Partial Matrix
Wheat Matrix (DOK)	Differentiation farming system	Wheat [22]	Partial Matrix
PVP	Molecular weight comparison	K15, K30, K60, K90	Small matrix

Appendix 1.8.2 Matrix

Here the matrices from Andersen, 2003 [13] for carrot and wheat are shown.

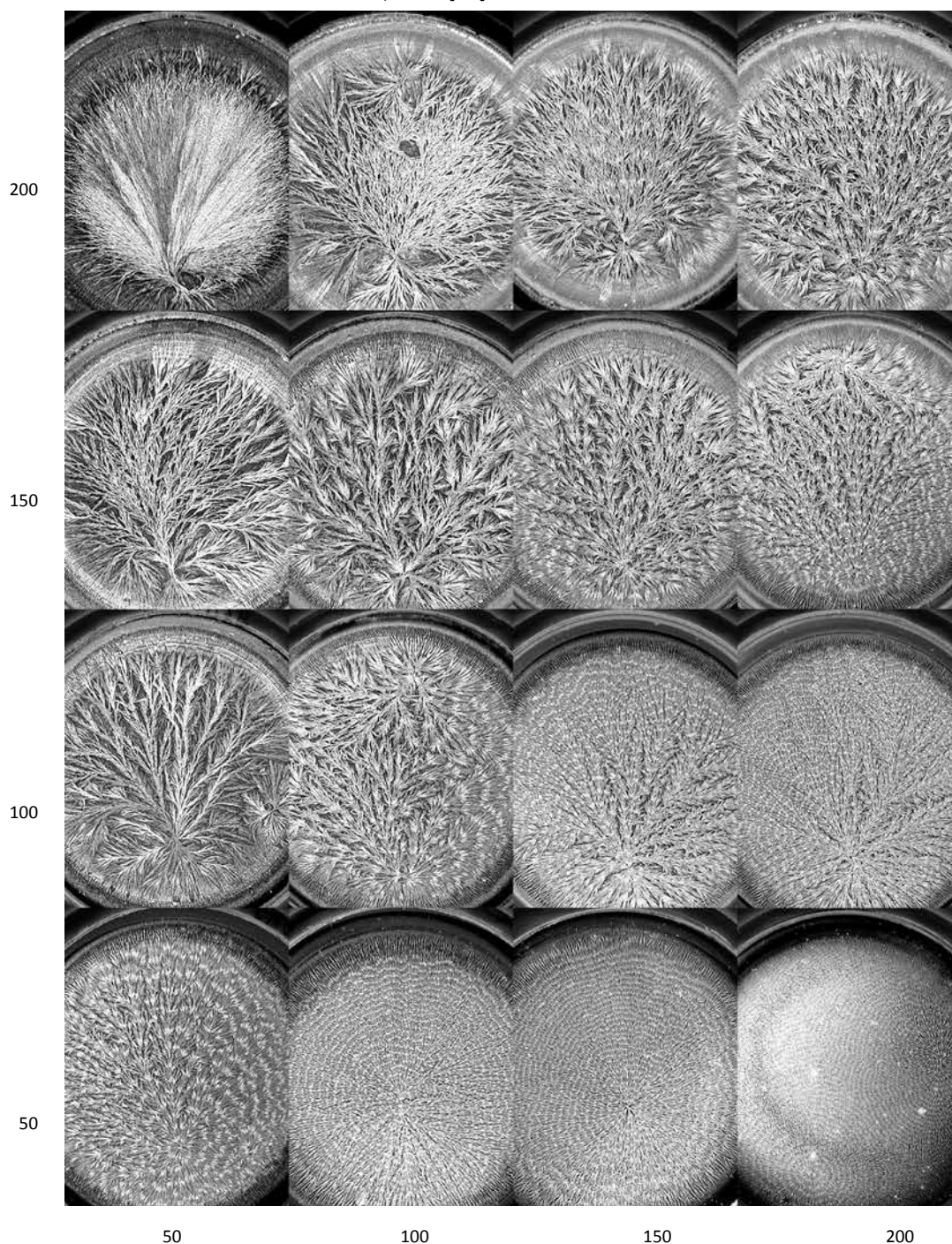


Fig. 1.8.5 Wheat matrix. Y-axis: DCC amount in mg per plate. X-axis: additive in mg per plate. Graph from Andersen 2003 [13], p. 11 - 14.

Table 1.8.2 Mixing ratios for the wheat matrix in Fig. 1.8.5. Y-axis: DCC amount in mg per plate. X-axis: additive in mg per plate. The matrix shows the different mixing ratios, whose randomness obscures a systemic view of the influence on the final crystal pattern.

200	4	2	1.33	1
150	3	1.5	1	0.75
100	2	1	0.67	0.5
50	1	0.5	0.33	0.25
DCC/additive	50	100	150	200

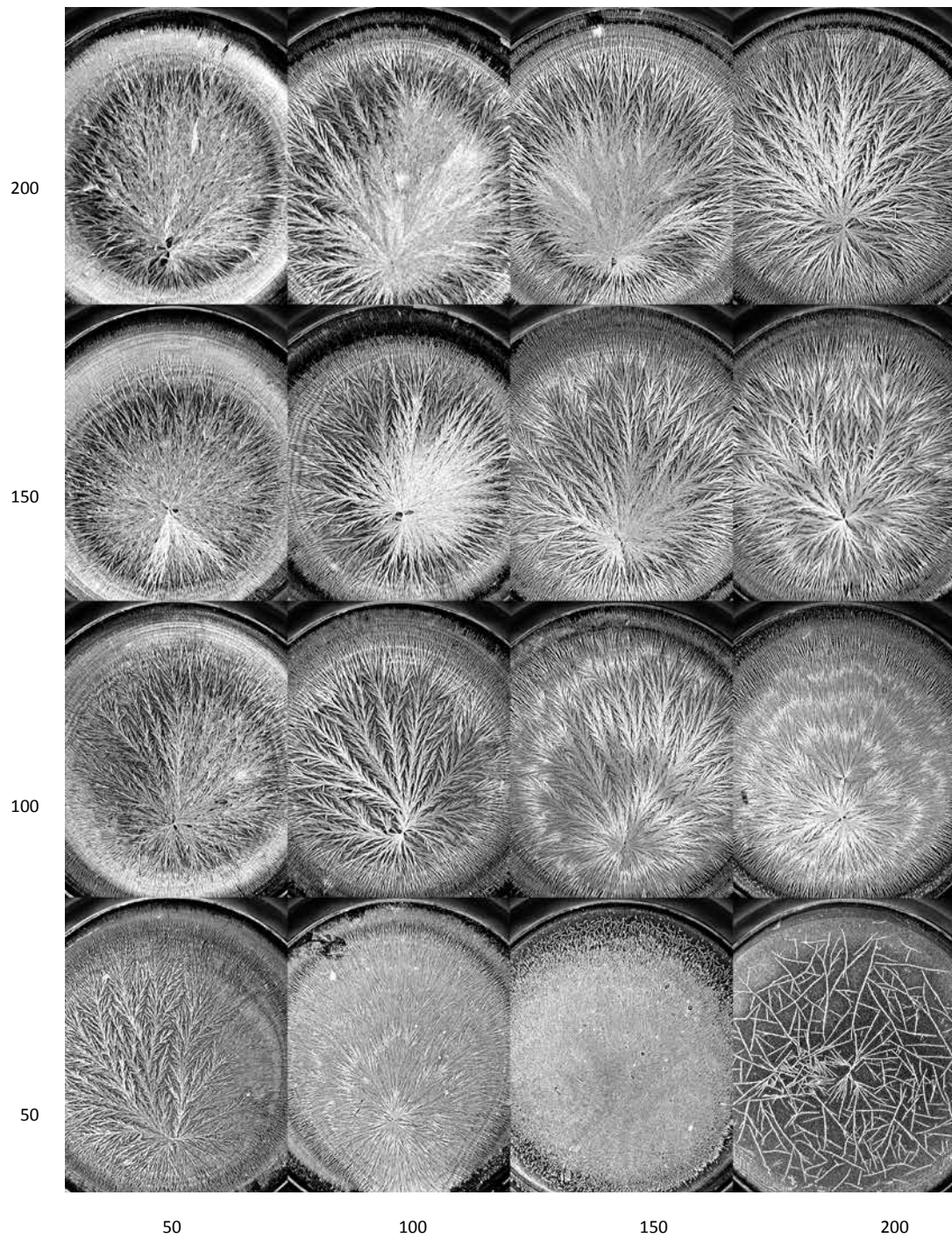


Fig. 1.8.6 Carrot matrix. Y-axis: DCC amount in mg per plate. X-axis: additive in mg per plate. Graph from Andersen 2003 [13], p. 15 - 18.

Appendix 1.8.3 Petterson

The matrix from Petterson's article in 1969 [10] about the variation of both DCC and additive amounts.

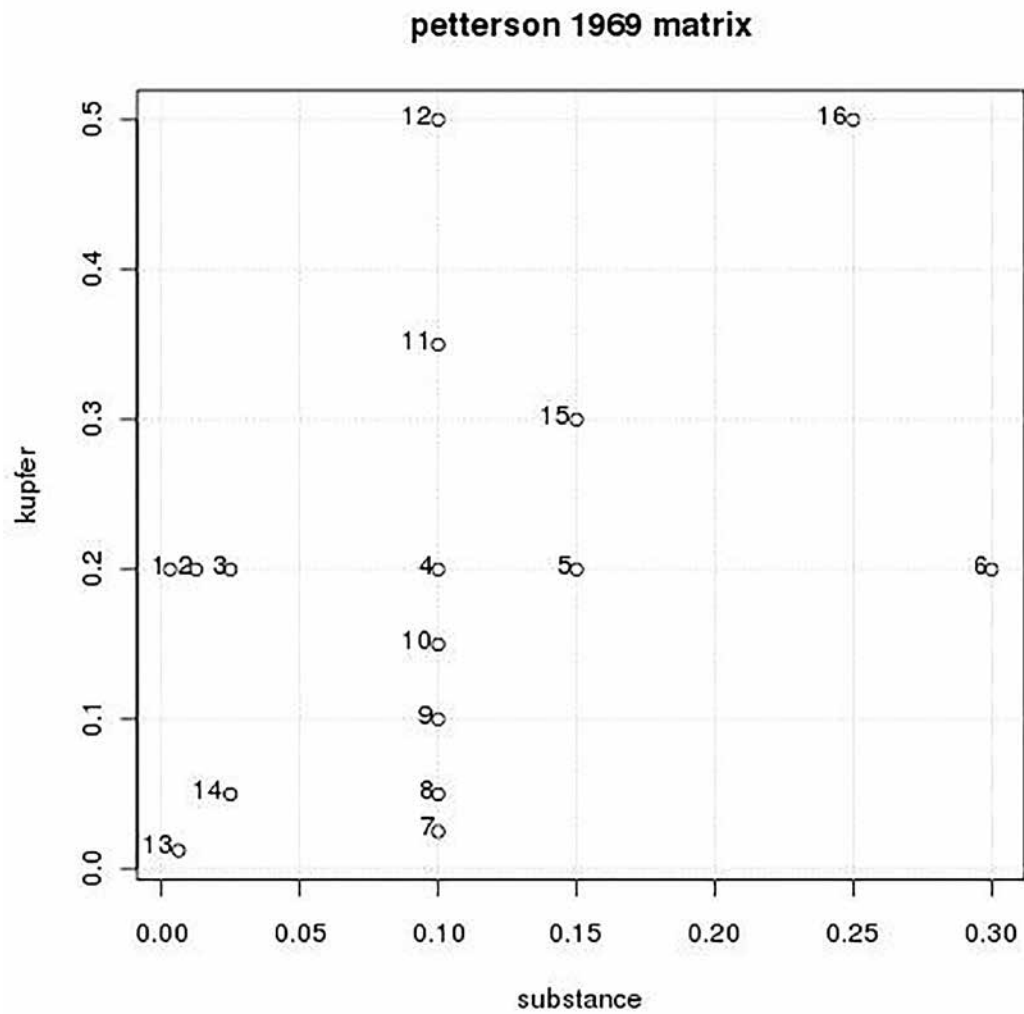


Fig. 1.8.7 DCC / additive matrix. On the Y-axis the DCC amount, on the X-axis the additive amount in mg per plate. Points indicate the used mixing ratios from Petterson 1969 [10] with the picture numbers from his article in the text.

Appendix 1.8.4 Scale

Taken from the supplementary data of Busscher 2019 [2].

DCC / additive mixing ratios are usually chosen so that the DCC pictures exhibit either split-growth, or dendrite crystal types. Interestingly, the crystal types appear to be preserved when the same mixing ratios are used, regardless of whether the DCC and additive amounts are changed. This was already documented by Selawry (1955) and Petterson (1969). Generating pictures for one mixture ratio is simple, but getting lines in a concentration matrix with different mixture ratios, where there are the same concentrations for each mixture ratio repeating on the Y-axis and X-axis, needs some planning. Finally one wants a matrix with defined values on the X- and the Y-axes and that the diagonals have the same mixture ratio. The solution is to use the same X and Y values where the logarithmic (values) are equidistant.

The logarithmic equidistant matrix

The simplest way to calculate amounts with a constant mixture ratio is to use 1, 10, 100, 1000, ... mg per plate. In Table 1.8.3 the matrix for these amounts is shown, with the calculated ratios salt to protein inside the table.

Table 1.8.3 Matrix with ratios of logarithmic equidistant numbers.

1000	1000	100	10	1
100	100	10	1	0.1
10	10	1	0.1	0.01
1	1	0.1	0.01	0.001
Y/X	1	10	100	1000

In Table 1.8.3 the minor diagonal has the ratio 1 (the slope 1). The other diagonals parallel to the minor diagonal also have a constant ratio (slope). This type of matrix has an identical range of values for X and Y, so the diagonal and the lines parallel to the diagonal have a constant ratio of Y / X.

Intermediate values in the matrix can be calculated by subsequently applying the square root. $\text{Sqrt}(10) = 3.162$, $\text{sqrt}(\text{sqrt}(10)) = 1.77$, $\text{sqrt}(\text{sqrt}(\text{sqrt}(10))) = 1.33$ and so on. To find the multiplying factor f_n for n points ($n = 1, 3, 5, 7, \dots$) between a and b simply calculate $f_n = (b / a)^{1 / (n + 1)}$. E.g. if $a = 1$ and $b = 10$, then $b / a = 10$. One point in between gives $f_1 = \text{sqrt}(10) = 3.16$. For 3 points between $a = 1$ and $b = 10$, $f_3 = \text{sqrt}(\text{sqrt}(10)) = 1.77$. This results in the values $1, 1.77, (1.77)^2 = 3.16, (1.77)^3 = 5.54, (1.77)^4 = 10$.

The BSA pictures in the matrix are shown again from the supplement of Busscher 2019 in Fig. 1.8.8.

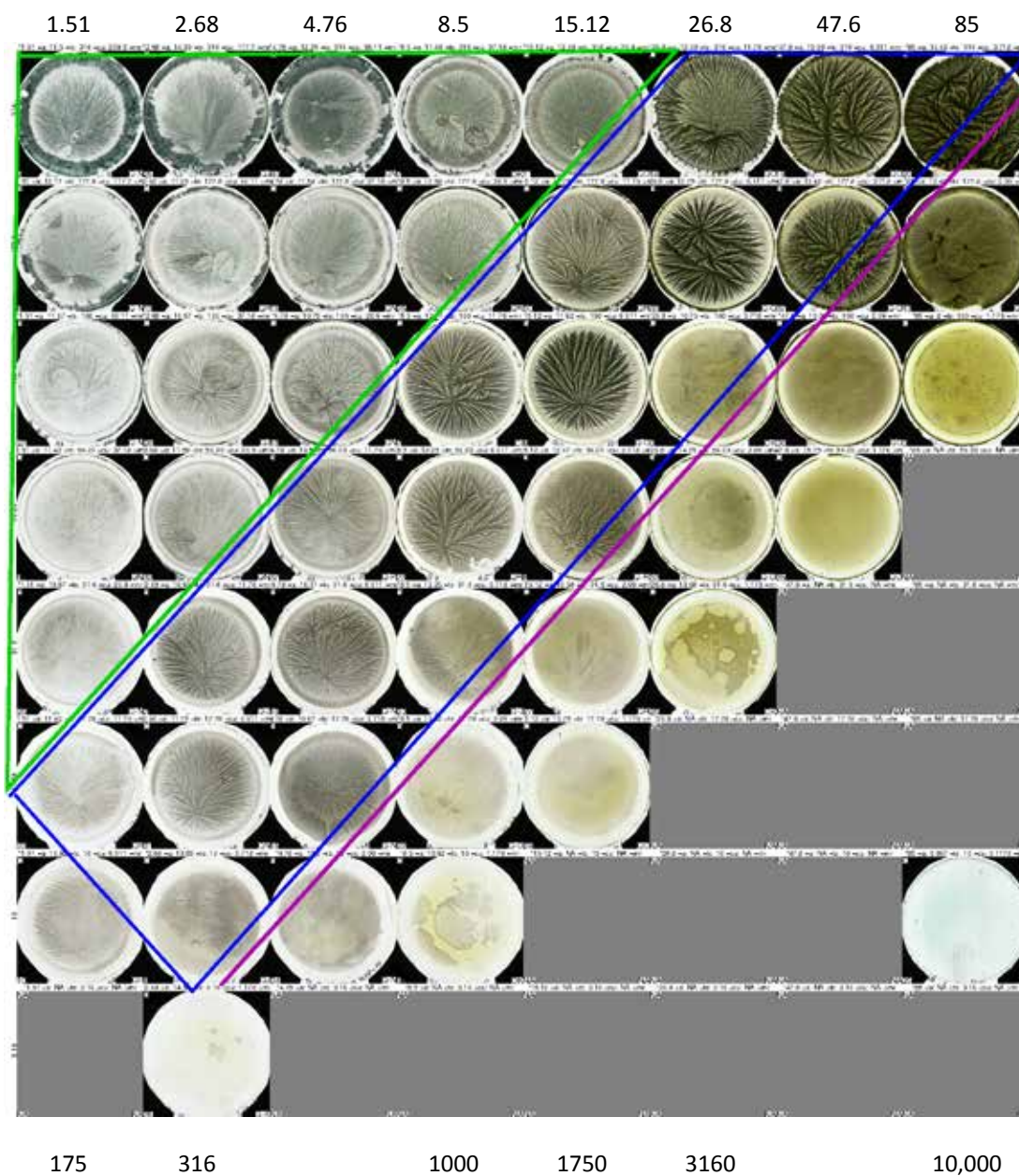


Fig. 1.8.8 Crystallization matrix of patterns from mixtures of BSA and DCC. Y-axis DCC amount in mg per plate, X-axis BSA amount. Lower horizontal axis in calculated monolayers BSA per plate, upper horizontal axis in mg BSA per plate. Green framed area: split-growth patterns, blue framed area: dendritic patterns, the violet diagonal line represents the inhibition border. The split-growth area is bordered by a DCC / BSA ratio of 20.9, the dendrite area is bordered between the DCC / BSA ratios 11.7 – 3.71. The inhibition area is bordered by a ratio of 2.1. Data from Busscher 2019, supplement, Fig. S.1.

References

- [1] Busscher N, Kahl J, Doesburg P, Mergardt G, Ploeger A. Evaporation influences on the crystallization of an aqueous dihydrate cupric chloride solution with additives. *Journal of Colloid and Interface Science* 2010; 344: 556–562 <https://doi.org/doi:10.1016/j.jcis.2009.12.045>.
- [2] Busscher N, Doesburg P, Mergardt G, Sokol A, Kahl J, Ploeger A. Crystallization patterns of an aqueous dihydrate cupric chloride solution in the presence of different amounts of Bovine Serum Albumin. *Journal of Crystal Growth* 2019; <https://doi.org/doi:10.1016/j.jcrysgro.2019.125272>.
- [3] Engquist M Die Gestaltkräfte des Lebendigen (Vittorio Klostermann, 1970).
- [4] Athmann M. Produktqualität von Salatrauke (*Eruca sativa* L.) und Weizen (*Triticum aestivum* L.): Einfluss von Einstrahlungsintensität, Stickstoffangebot, Düngungsart und Hornkieselapplikation auf Wachstum und Differenzierung. PhD Thesis, University of Bonn. 2011.
- [5] Fritz J, Athmann M, Kautz T, Köpke U. Grouping and classification of wheat from organic and conventional production systems by combining three image forming methods. *Biological Agriculture & Horticulture* 2011; 27: 320-336.
- [6] Fritz J, Athmann M, Meissner G, Kauer R, Köpke U. Quality characterisation via image forming methods differentiates grape juice produced from integrated, organic or biodynamic vineyards in the first year after conversion. *Biological Agriculture & Horticulture* 2017; 33: 1-19.
- [7] Kahl J, Busscher N, Mergardt G, Maeder P, Torp T, Ploeger A. Differentiation of organic and non-organic winter wheat cultivars from a controlled field trial by crystallization patterns. *J. Sci. Food Agric.* 2014; 95: 53-58 <https://doi.org/doi:10.1002/jsfa.6818>.
- [8] Selawry A and Selawry O Die Kupferchlorid-Kristallisation in Naturwissenschaft und Medizin (Gustav-Fischer-Verlag, 1957).
- [9] Selawry A Samenkeimung und Metallpotenzen im Kristallsationstest (Forschungsring für biologisch-dynamische Wirtschaftsweise, 1975).
- [10] Pettersson BD. Beiträge zur Entwicklung der Kristallisationsmethode mit Kupferchlorid nach Pfeiffer IV. Wie verschiedene Kristallbilder bei der Pflanzenkristallisation entstehen. *Lebendige Erde* 1969; 3: 112-126.
- [11] Barth J-G. Eléments de physique et expérience de laboratoire en matière de cristallisation du chlorure cuivrique en présence d'additif. *Elemente der Naturwissenschaft* 2002; 77: 121-124 <https://doi.org/10.18756/edn.77.121>.
- [12] Barth J-G. Cupric chloride crystallisation with additives and its applications. *Elemente der Naturwissenschaft* 2004; 81: 23-39 <https://doi.org/10.18756/edn.81.23>.
- [13] Andersen JO, Huber M, Kahl J, Busscher N, MeierPloeger A. A concentration matrix procedure for determining optimal combinations of concentrations in biocrystallization. *Elemente der Naturwissenschaft* 2003; 79: 97-114.
- [14] Waldburger B. Begriff und Kontext in der Methode der Empfindlichen Kristallisation. *Elemente der Naturwissenschaft* 2005; 83: 79-89 <https://doi.org/10.18756/edn.83.79>.
- [15] Schweizer F. Beobachtungen bei der Biokristallisation von Glykogen. *Elemente der Naturwissenschaft* 2007; 87: 76-89.
- [16] Von Hahn F-V Thesigraphie. (Franz Steiner Verlag, 1962).
- [17] Busscher N, Doesburg P, Mergardt G, Sokol A, Kahl J, Ploeger A. Influence of dewetting on the crystallization behavior of CuCl_2 in the presence of BSA during evaporation in a Petri dish. *Heliyon* 2019; 5: e01102 <https://doi.org/10.1016/j.heliyon.2018.e01102>.
- [18] Habibi M, Rahimzadeh A, Eslamian M. On dewetting of thin films due to crystallization (crystallization dewetting). *Eur. Phys. J. E* 2016; 39: 30 <https://doi.org/doi:10.1140/epje/i2016-16030-9>.
- [19] Gallinet JP, Gauthier-Manuel B. Wetting of a glass surface by protein adsorption induces the crystallization of an aqueous cupric chloride solution. *Journal of Colloid and Interface Science* 1992; 148: 155-159 [https://doi.org/doi:10.1016/0021-9797\(92\)90123-4](https://doi.org/doi:10.1016/0021-9797(92)90123-4).
- [20] Busscher N. Apple juice Project. Technical Report, University of Kassel. 2015.
- [21] Szulc M, Kahl J, Busscher N, Mergardt G, Doesburg P, Ploeger A. Discrimination between organically and conventionally grown winter wheat farm pair samples using the copper chloride crystallisation method in combination with computerised image analysis. *Computers and Electronics in Agriculture* 2010; 74: 218-222 <https://doi.org/doi:10.1016/j.compag.2010.08.001>.
- [22] Kahl J, Busscher N, Mergardt G, Ploeger A. Standardization and performance test of crystallization with additives applied to wheat samples. *Food Analytical Methods* 2014; 8: 2533-2543 <https://doi.org/doi:10.1007/s12161-015-0142-6>.

1.9 Optimal Amounts

How to find the optimal $\text{CuCl}_2 \cdot 2\text{H}_2\text{O}$ and additive amounts for a sample and research question?

Abstract

This is about the topic how to find the optimal amount of $\text{CuCl}_2 \cdot 2\text{H}_2\text{O}$ (cupric chloride di-hydrate, further named [DCC](#)) and [additive](#) for each [sample](#) and research question. For a new sample or a new research question the first step is to find those DCC and additive amounts where the DCC pictures are one-centered. In the second step the DCC amount can be found from the coverage of the plate with DCC, which hardly depends on the additive amount. In the third step the additive amount for simple molecules or for samples from agricultural samples can be found according to an optimization procedure. The use of more than one amount and the question of dry matter compensation is discussed.

Introduction

The amount of $\text{CuCl}_2 \cdot 2\text{H}_2\text{O}$ (cupric chloride di-hydrate, further named [DCC](#)) and the amount of additive per plate have a strong influence on the [picture properties](#) of a DCC picture. For the comparison of samples such as carrot juices which are processed in different ways, the optimal amount of DCC and the additive have to be defined for the research question. The question is how to obtain an adequate description of how to find these amounts. The chapter Historical Overview describes the existing approaches. In the Discussion chapter an attempt is made to find common ground between the different approaches. The reader is encouraged first to read the chapter [1.8 Concentration matrix](#), to get acquainted with the concept of a crystallization matrix. The differences in the picture properties due to differences in [crystallization starting time](#) ($t_{crStart}$) are not discussed in this chapter. The differences in picture properties are formulated as questions under the heading Additional Research at the end of this document.

Historical overview

The first to approach the amount question systematically was Selawry (1957 [1]), while referring to Krüger (1950 [2]). She studied a wide variety of samples and amounts. She distinguished 8 different crystallization types depending on the additive amount (1957 [1], p. 23). The types ranged from “no effect on the DCC” to “only additive effect”, for human blood as additive. She documented the optimal concentrations for texture and structure in 1957 [1] (p. 24, Table 3).

Later Selawry (1961 [3]) created a simpler approach with three levels; under-, optimal- and over-concentration (1975 [4], p. 56). The criteria for the over-concentration were multiple centers and coagulations from the additive. For the under-concentration the criterion was “lack of orientation”. For the texture and Gestalt evaluation of pictures from food samples she found that an amount of 200 mg DCC per plate (~ 8.4 cm inner diameter) worked best. She adapted the amount of the additive according to the sample and the research question. See for examples 1975 [4] (p. 8, 9). For an overview see Table 1 published in 1961 [3] (p. 37) or the corresponding table in 1975 [4] (p. 57, Table 4). Selawry (1957 [1], p. 22, 23) emphasized that the picture type was determined by the mixture ratio of additive to DCC, while the lowest DCC amount was around 100 mg per plate.

For the axes of the [concentration matrix](#) we decided to have the DCC amount on the Y-axis and the additive amount on the X-axis.

The additive concentration question was also studied by von Hahn (1962 [5], p. 23). He observed many centers for lower concentrations, and with increasing additive amount, the number was reduced to one center. This occurred only in a narrow concentration range. A further increase of the additive amount increased also the number of centers again.

Petterson (1966 [6]) studied the influence of increasing DCC amounts (100, 150, 200 and 250 mg per plate) on potatoes from different farming systems, keeping the additive amount constant at 100 mg per plate (8.5 cm inner diameter). He discussed his results according to Selawry [3] and found 150 mg DCC (1966 [6], p. 38) as the optimal amount for his research question. Petterson 1969 [7] was the first to document not only the results of different additive amounts (for potatoes) at constant DCC amounts, but also different DCC amounts at constant additive amounts. Additionally, he also documented the results of varying DCC and additive amounts at constant mixing ratios. See in chapter the [Appendix 1.8 Concentration matrix](#) for details. Petterson (1969 [7], p. 120) found that for DCC amounts of 200 mg per plate, the optimal picture was obtained with 75 to 100 mg of potato additive per plate. The criterion was “*zwei blättrige Hohlformen*” (two leaved [hole forms](#)). He found that for the same DCC / additive ratio, important image characteristics were maintained, but the image shapes became increasingly coarse

as the DCC amount increased (1969 [7], p. 124).

Engquist (1970 [8]) who had learned the DCC method from Selawry, worked with concentration series consisting of increasing additive amounts for a constant DCC amount. One of her criteria was the recognition of three zones. For the evaluation of pictures of increasing additive amounts, she defined three groups A, B, C, depending on the presence and number of zones: one zone (A), two zones (B) or three zones (C) (1970 [8], p. 16). The three zonal picture, type C, had the optimal concentration (1970 [8], p. 15). See for more information Chapter [1.13 Picture zones](#). Engquist (1970 [8], p. 14) worked with a DCC amount between 200 and 300 mg per plate (8.75 cm inner diameter, from Engquist 1970 [8], p. 51, Fig. 2). She worked with more than one additive concentration to deal with potential problems of differing dry matter contents for different sample qualities ([8], p. 15).

Andersen (2003, [9]) described how to find the balance between the polarities of DCC dominated pictures and additive dominated pictures (2003 [9] p. 100, Fig. 1, and in chapter the [Appendix 1.8 Concentration matrix](#)). In the upper left corner of the DCC / additive matrix (high DCC and low additive amount), DCC dominated - more radial - pictures appeared. Diagonal to the DCC polarity, in the lower right corner of the DCC / additive matrix (low DCC amount, high additive amount) the more circular structures of the so called substance spirals appeared, leading towards the inhibition of crystallization. In between these polarities the area was found - along the opposite diagonal - where a balance between these polarities appeared with clear stems and regular ramifications. In his PhD thesis Andersen (2001 [10], front page) used carrot crystallization pictures that were close to forming substance spirals. See for more details in chapter [2.7 Substance spirals](#).

Waldburger (2005 [11], p. 83, Fig. 2) called the area, which Andersen described, as the “*dendritic window*”. The limits of this window were defined for DCC as follows: too little DCC creates thin needles and too much DCC creates coarse structures. For the additive, the limits are: too little additive results in limited crystal forms, while too much additive results in too much precipitation and finally inhibition of crystallization. The optimal mixing ratio was defined by the highest form diversity and richness of the main stems, branches and fine structures. She also showed examples for the aging of extract over time in 2005 [11] (p. 86 and p. 87).

Geier (2006 [12]) described the application of the concept of over- and under-concentration to determine the picture optimum for the “horizontal capillary dynamolysis chromatography” (Chroma) method.

Schweizer (2007 [13]) showed that for glycogen as additive the branching angle of a needle depends on the mixing ratio of DCC / glycogen. At a mixing ratio of DCC / glycogen of 25, the variation of the branching angle was very small and the angle was in the range of 80 to 90 ° (2007 [13], p. 80, Fig. 2).

Busscher (2010 [14]) presented a DCC / additive concentration matrix for Bovine Serum Albumin (BSA). The main result was that for a defined DCC amount of 100 - 200 mg per plate, the needle type could be classified along the additive axis as deposit type, split-growth, dendrites and inhibition of crystallization. For the split-growth type (recognizable by the open spaces, as described by Petterson in (1969 [7]), on average one-centered pictures were found ([14], Fig. 10) as was previously found by von Hahn (1962 [5], p. 23). As described by Petterson in 1969 [7] (p. 124), and Selawry (1957 [1], p. 22, 23) pictures with the same mixing ratio looked comparable in the split-growth and dendrite area.

More than one additive concentration or mixing ratio for a research question was also used by Athmann (2011 [15], p. 30), Fritz (2011 [16], p. 323, 2017 [17], p. 4 and p. 12 Fig. 6) and Kahl (2014 [18], p. 2).

Resume historical overview

From the historical overview the terms: “*concentration series / matrix*”, “*polarity*”, “*optimal concentration*”, as well as the effect of the mixture ratio, the number of the centers, a minimum of centers and the use of more than one concentration, are introduced.

To sort and connect these terms, the effects of the same mixing ratio are used as a starting point. The pictures with the same mixing ratio are located in the concentration matrix on diagonals running from the lower left to the upper right corner. They have comparable picture properties in common. This means that pictures with the strongest polarity should be on a line perpendicular to these diagonals, which run from the upper left to the lower right corner of the matrix. The concentration series for constant DCC, which would be a horizontal line in the [concentration matrix](#), also contains the polarities.

In the historical overview the term “*optimal concentration*” is mentioned by several authors. The DCC amount seems not a problem to define, typically 150 - 250 mg per plate is mentioned. The challenge is to find the

amounts of the additive, because the picture properties change strongly with the additive amount. Most authors start with an additive amount that produces one-centered pictures. The appearance of more centers is considered a sign that the concentration is too high. Engquist used more than one concentration, also to overcome the problem of differing dry matter contents for different sample qualities.

Discussion

How to define a simple procedure?

The discussion is based on a comparison of the following two research questions. One is the differentiation of different additive amounts, which can be discussed within e.g. the BSA matrix. The other is the differentiation of food samples that are e.g. grown in different farming systems or processed in different ways, like clear and turbid apple juice (Kahl 2016 [19]). There is a fundamental difference between these two samples. BSA consists of one type of molecule with one molar weight, while an additive from an agricultural product consists of different chemical structures, while also each molecule can have a distribution, e.g. pectin has a molar weight distribution (Zhu 2020 [20], Fig. 1). In between these two is [PVP](#), which, like BSA, consists of one type of molecule but has a molar weight distribution. Also, the approach for BSA is more of a quantitative evaluation of crystal types, while the process of finding the optimum concentration of more complex additives is based on a Gestalt evaluation as described by Huber 2010 [21], Doesburg 2014 [22], Fritz 2018 [23], Doesburg 2021 [24].

For the DCC amount most authors agreed on an amount between 150 and 250 mg per plate for additives of samples from agricultural and chemical origin. From the perspective of a concentration matrix, what remains is a concentration series with increasing additive amounts, which is called an [additive vector](#). The additive vector has two extremes: Starting with zero amount of additive results in dewetting before crystallization and all DCC accumulates at the rim of the Petri-dish. As the amounts of additive are increased, there is a point at which the dewetting before crystallization changes to dewetting after crystallization (Busscher 2019 [25]). This is where the covering properties of the sample on the glass plate become visible. The dewetting after crystallization effect depends on the surface tension between glass surface and solution. For BSA this transition from dewetting before to after crystallization is at an extreme low concentration. The other extreme of the additive vector is where the crystallization is inhibited, which is preceded by an increase in the number of centers and a decrease of the growth velocity (Busscher 2019 [14]). These two borders are sample specific and depend on the DCC amount. BSA has the lowest known limit at which dewetting after crystallization occurs, because it can cover the glass plate very efficiently as a monolayer (0.0085 mg BSA per plate data from Reynaud 1968 [26]). The value for other samples are therefore much higher. The inhibition amount for BSA at 177 mg DCC is 68 mg per plate (Busscher 2010 [14], supplementary data, Fig. S.1). BSA displays one-centered pictures in the concentration matrix for the split-growth area and partially for the dendrite area too. One would expect that the border between split-growth and dendrites is the most sensitive area to separate different BSA additive amounts, because there the crystallization type changes.

The search for the optimal concentration of other additives also takes place within the range resulting in one-centered pictures. While BSA shows a clear transition between split-growth, dendrites and inhibition, this not so clear for other samples. For agricultural samples, such as carrot and wheat, an additional phenomenon, called substance-spirals, is found between the dendrites and inhibition area (Andersen 2003 [9], Fig. 3 - 9 and Huber 2010 [21] Fig. 3). For more details see chapter [2.7 Substance spirals](#).

Optimal concentration: crystal types

A comparison of the optimal pictures from Petterson (1969 [7]) and Engquist (1970 [8]) with the types defined in the BSA matrix (Busscher 2109 [14]) would suggest that these optima are in fact split-growth crystallizations. Also Athmann (2011 [15], p. 122, Fig. 20) used the split-growth area for rocket lettuce samples (*Eruca sativa* L.). For apple juice (Kahl 2016 [19]), the split-growth pictures are not shown in the publication, but rather in the project report (2015 [27], p. 19, Fig. 4.8 and p. 26, Fig. GM.1). The optimal concentration, which was used for the evaluation, led to split-growth crystallizations, leaning towards dendrites. For the DOK wheat (see Maeder 2002 [28] and 2007 [29]) from Kahl (2014 [18]) the concentrations were 90 mg DCC and 70 and 90 mg additive per plate. These mixing ratios are located within the dendritic area, close to the substance spirals border (Kahl 2014 [30], Fig. 5), yet one-centered. The pictures from the DOK wheat from Fritz (2011 [16], Fig. 1) show characteristics of split-growth at the border of dendrites (small [hole forms](#)). For grape juice, the pictures from Fritz (2017 [17], p. 12, Fig. 6) also seem to be located at the border between split-growth and dendrites. The pictures from Graf (2000 [31], front page) for milk show clearly a split-growth crystallization type, while dendrites can exist for milk.

It seems that the split-growth type is the most frequently used crystallization type, which of course has to be quantified in detail (see Additional research). During the investigation of the use of the crystallization types of split-growth and dendrites in existing publications, the occurrence of Engquist's three zones (1970 [8]) at

the optimal concentration can be verified, as well as the observation from Schweizer (2007 [13]) that the variation of the branching angle has a minimum at the optimal concentration.

Using more than one concentration

The question of how to find the concentration to differentiate and rank samples from different agricultural growth systems or different types of food processing is related to whether more than one concentration will be used. In the case of using multiple concentrations, the best overview is obtained by generating a concentration matrix for each sample and comparing these matrices. As we saw before, the matrix can be reduced to a concentration vector (for a constant DCC amount). The problem with choosing concentrations is that the extracts or juices from an agricultural sample are not a defined molecule like BSA. As described above, the extract or juice is not only composed of different molecules, but each molecule may have a distribution of molecular weights, not taking into account all the possible interactions that the extracts and juices may have with the DCC and with each other during evaporation (for details see chapter [1.7 Evaporation issues](#)). The approach of using more than one concentration can be discussed using the results from the differentiation of clear / turbid apple juice (Kahl 2016 [19]). The differences between the pictures are very large, making the comparison of the pictures easy to discuss.

The apple juice experiment was based on research indicating a positive health effect from turbid apple juice versus a neutral or negative effect of clear apple juice on rats (Barth 2005 [32] and 2007 [33]), humans (Ravn-Haren 2013 [34]), and in a review on human intervention studies (Vallee Marcotte 2022 [35]). The two juices from the University of Geisenheim, Germany, were well defined by the measured components and had a large difference (factor 20) in the amount of pectin (Kahl [19], p. 5, Table 1). Pectin is a hetero polysaccharide, which implies a molecular weight distribution (Zhu 2020 [20], Fig. 1).

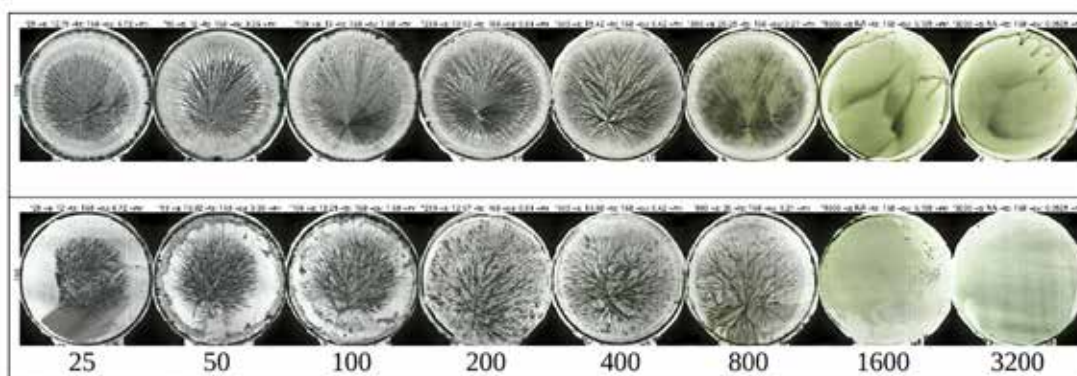


Fig. 1.9.1 Additive vector for two differently processed apple juices: turbid (upper row) and clear juice (lower row) versus the additive amount per plate (X-axis). Additive amounts in mg per plate were increased from picture to picture by a factor 2. DCC amount was 168 mg. Data from University of Kassel, Apple Juice project report (2016, p. Fig. 4).

In Fig. 1.9.1 the crystallization inhibition for higher additive amounts – 1600 and 3200 mg per plate on the right side - is clearly visible. For both juices, inhibition started between 800 and 1600 mg additive per plate, although the pictures at 800 mg were quite different from the higher additive concentrations (see [Appendix 1.9.2 Apple Juice at 951 – 1434 mg additive](#) for pictures for additive amounts between 800 mg and 1600 mg).

On the side of the lower amounts, the upper row (turbid apple juice) showed a regular picture already at 25 mg per plate, while in the lower row (clear apple juice) dewetting occurred with the appearance of a star-like formation in the center of the picture. Apparently, dewetting was overcome at lower additive levels for the turbid juice pictures (top row) compared to the clear juice pictures (bottom row), while the inhibition limit also starts at lower additive amounts for the turbid juice (see [Appendix 1.9.2 Apple Juice at 951 – 1434 mg additive](#)). The additive vector of the clear juice is shifted to higher additive amounts (to the right in Fig. 1.9.1) relative to the additive vector of the turbid juice.

The main difference was that the pictures from turbid apple juice (top row) showed split-growth at 200 to 400 mg per plate and dendrites from 400 to 800 mg per plate, while the clear juice (bottom row) showed split-growth from 400 to 800. Even at 800 mg, the clear juice pictures were still of the split-growth type or composed of individual needles (see [Appendix 1.9.3 Apple Juice at 566 - 800 mg additive](#) for the pictures for amounts between 400 and 800 mg), while the turbid apple juice pictures began to show inhibition of crystallization. Comparing the pictures of clear (bottom row) and turbid (top row) juices at 200, 400, or 800 mg of additive per plate, different crystallization types become apparent. In most experiments the differences are not so large, usually all samples

show all crystallization types and the extremes at the two boundaries are not so different. However, it is possible that the boundary between e.g. split-growth and dendrites occurs at slightly different concentrations for different samples. If more than one concentration is used, the difference in crystal types has a very high chance of showing up.

Comparing the differences between additives based on more than one concentration allows an additional characterization of the samples in relation to each other. It can be seen as an additional dimension for evaluation, which is especially valuable for Gestalt ranking.

It is also a matter of making the best use of the limited number of positions in the chamber. If you have 6 plates per additive, it makes more sense to spread the risk of finding the optimal amount for a sample with three concentrations of 2 pictures each than 6 pictures on one concentration.

When more than one concentration is used, it is necessary to extend the statistical method for the evaluation of the computer image analysis results, since the existing procedure is based on only one concentration (Meelursarn 2006 [36]).

Normalization of the concentration by the dry matter amount

The other question concerns the normalization of the concentration by the dry matter amount of a sample. At first glance, dry matter seems to be a possible solution to simplify the broad information of an additive originating from extracts or juices and make them comparable. Usually this approach is used when one compound out of the whole sample is related to the sample, e.g. nitrate related to dry matter or fresh matter. In our case the whole chemical profile is normalized by the mean weight of dry matter of the sample. The question is what the meaning of this relative normalized profile is. When we look at the concentration vector in Fig. 1.9.1 a normalization to the dry matter would shift the vector from the clear juice to the left. This would change the relative positions of the extreme boundaries, of which we do not precisely know what they depend on. As far as we know now, the lower boundary depends on the ability to cover the glass plate, to hinder the influence of the dewetting forces. The higher boundary depends on the ability to suppress the crystallization and lower the crystal growth velocity. When we look at the chemical profile and the molecular weight distribution, then it is not clear whether the sum of all molecular weights gives an independent value for these two borders, on the basis of which the vector could be transformed to a normalized additive vector. The most important portion of the dry matter would probably be the molecules with the higher molecular weights. They are with no doubt influencing the picture properties (Kahl 2014 [37], Busscher 2014 [38]) but they are not the only ones. When we compare e.g. pictures from carrot or apple juice with those from chemical pectin (pictures not shown), we can see a strong difference in the pictures. While pectin is in most cases the molecule with the highest molecular weight, it is not the only one that determines the form of the pictures. This needs more research.

If the additive vectors of two samples appear to be shifted with respect to each other, then the question arises as to whether a normalization (shifting of the lower and upper limits) will simply erase the signal that is, for example, due to different molecular weights.

One could also argue that we have a superposition of a quantitative and qualitative effect in the DCC pictures. The quantitative effect can be excluded by normalizing to the dry matter, while the qualitative effect becomes more apparent. This question should be researched on additive vectors for e.g. carrots with different dry matter and PVP with different molecular weights.

An important point of view in this context is that when we have two carrots and one (usually the organic one) has a higher dry matter, then this is an additional piece of information from the sample.

Resume how to establish a simple procedure

The first step is to find DCC / additive combinations where one-centered pictures appear. The DCC amount can then be found as a second step by optimizing the coverage of the plate. For the additive amount the concept of applying more than one concentration is very productive, but needs an extension of the statistical evaluation for the computer image analysis results. The crystal types found in the BSA matrix, extended with the substance spirals, seems to be a helpful concept also for extracts and juices from agricultural samples. A rough overview of the literature indicated that the split-growth crystal type is often used in research. The limits of the concentrations can be chosen in a range from the beginning of split-growth to the substance spirals (if present). Dry matter compensation is discussed, but not solved yet.

This description is not a shortcut for the determination of the optimum amounts by a Gestalt evaluation (described by Huber 2010 [21], Doesburg 2014 [22], Fritz 2018 [23], Doesburg 2021 [24]), it just demonstrates in another way that the practically found optimal amounts are located in the same crystal type range (split-growth type).

Additional research

Working with three or more concentrations:

- Evaluate the difference between qualities at different points in the matrix.
- Apply criteria from computer image analysis and Gestalt evaluation.
- Adapt the statistical evaluation to e.g. 2 pictures with 3 concentrations instead of 6 pictures with one concentration.
- Compare the variation of a picture caused by tcrStart variations to the difference caused by using two concentrations.

Re-evaluate the matrices in Table 1.9.1 from Appendix 1.9.1 Matrix.

- Do the crystal types split-growth and dendrites also occur in milk?
- Statistical model: coverage of the plate \sim DCC + additive (additive low correlation?)
- Check the zonal concept of Engquist. (mark the zones)
- Check the observation of a low variation in the branching angle from Schweizer.
- The tool would be CrystEval (see chapter [3.3 CrystEval](#)).
- Evaluate the pictures from Athmann / Fritz with the question of what type of crystal the different concentrations generate. Tool would be CrystEval (see chapter [3.3 CrystEval](#)).

Working on the split-growth type:

- How does the size of a hole (*Hohl*) form depend on the additive and DCC amount?
- Does the size of the hole form decrease with increasing additive amounts (keeping DCC constant)?
- What can the work of Adams / Wicher / Edwards tell us about the parameters of the hole form?
- How can we apply this on the DCC / additive matrix?

Experiments for the dry matter question:

- perform additive vectors for:
 - carrots with different dry matter contents.
 - PVP with different molecular weights (which DCC amount?).
 - Extract pectin from the carrots and compare the DCC pictures from carrot and the pectin from these carrots.

TcrStart and picture properties:

- This is handled in chapter [1.10 Transition between crystal types](#), Additional research.

Appendix 1.9.1 Matrix

The existing matrices are described in chapter [1.8 Concentration matrix](#). The following table provides an overview.

Table 1.9.1 Existing matrices.

Name	Research Question	Sample(s)	Status
BSA matrix	Crystal types in a matrix	BSA [25]	Full matrix
Apple Juice processing	Different matrices for Turbid/ Clear Apple Juice	Apple Juice [27]	Partial matrix
Wheat matrix (GEEL)	Differentiation Growth System	Wheat (Szulc 2010 [39])	Partial matrix
Wheat matrix (DOK)	Differentiation Growth System	Wheat (Kahl 2014 [30])	Partial matrix
PVP	Different matrices for different Molecular weights	K15, K30, K60, K90	Small matrix
Milk	Do dendrites occur in the matrix?	H-milk, raw milk	Small matrix

The matrices in Table 1.9.1 should/ can be reevaluated according to the coverage of the plate. Check to see if the plate coverage is less dependent on the amount of additive than on the amount of DCC.

Appendix 1.9.2 Apple Juice at 951 – 1434 mg additive

DCC pictures from clear apple juice

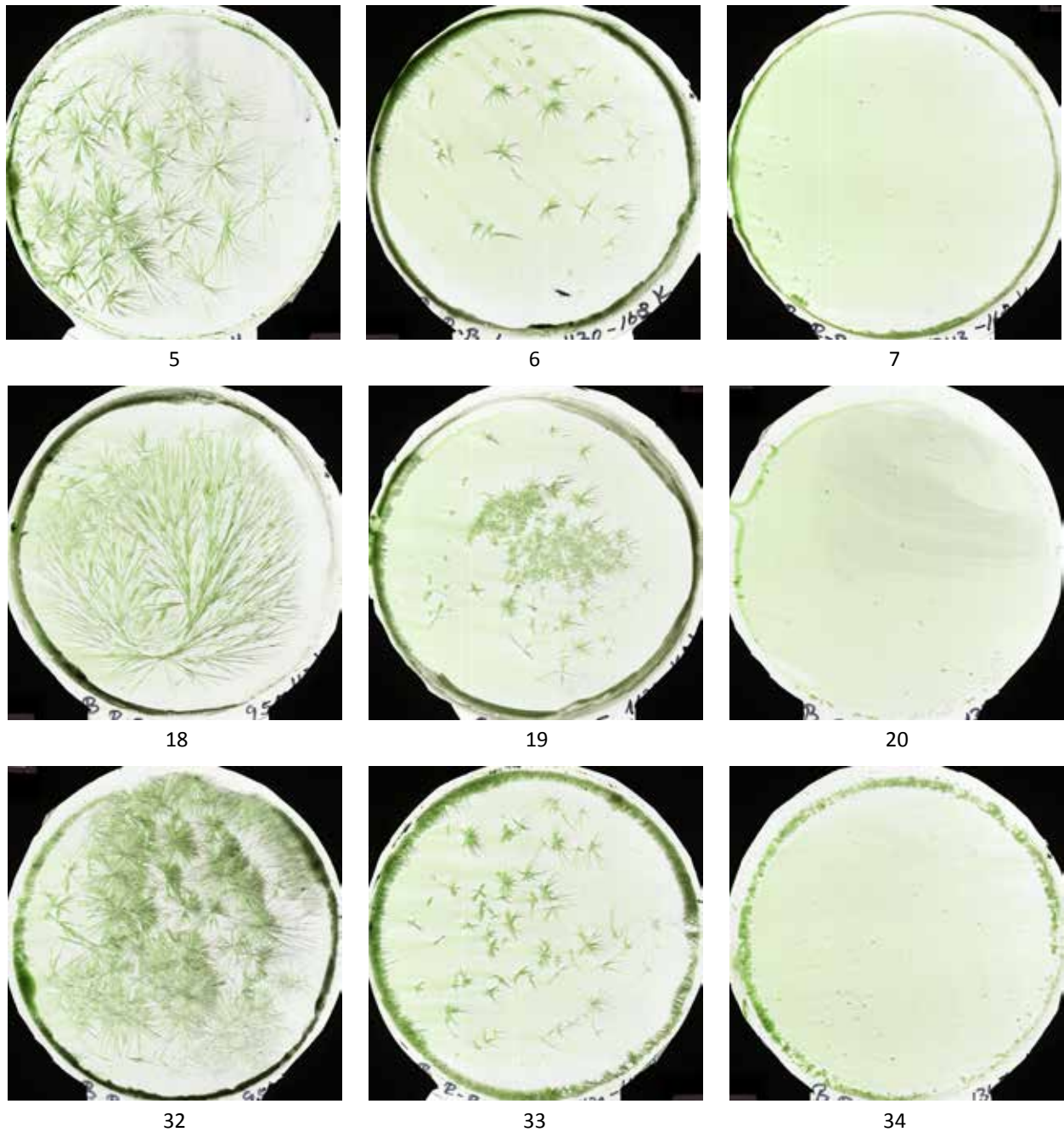


Fig. 1.9.2 Pictures from DCC with clear apple juice. Y-axis picture replicates. X-axis additive amount. Left column 951 mg per plate, middle column 1130 mg per plate, right column 1434 mg per plate, DCC amount = 168 mg per plate. Pictures from University of Kassel (D), LabDoc series B.2015.06.01.R-B.

DCC pictures from turbid apple juice

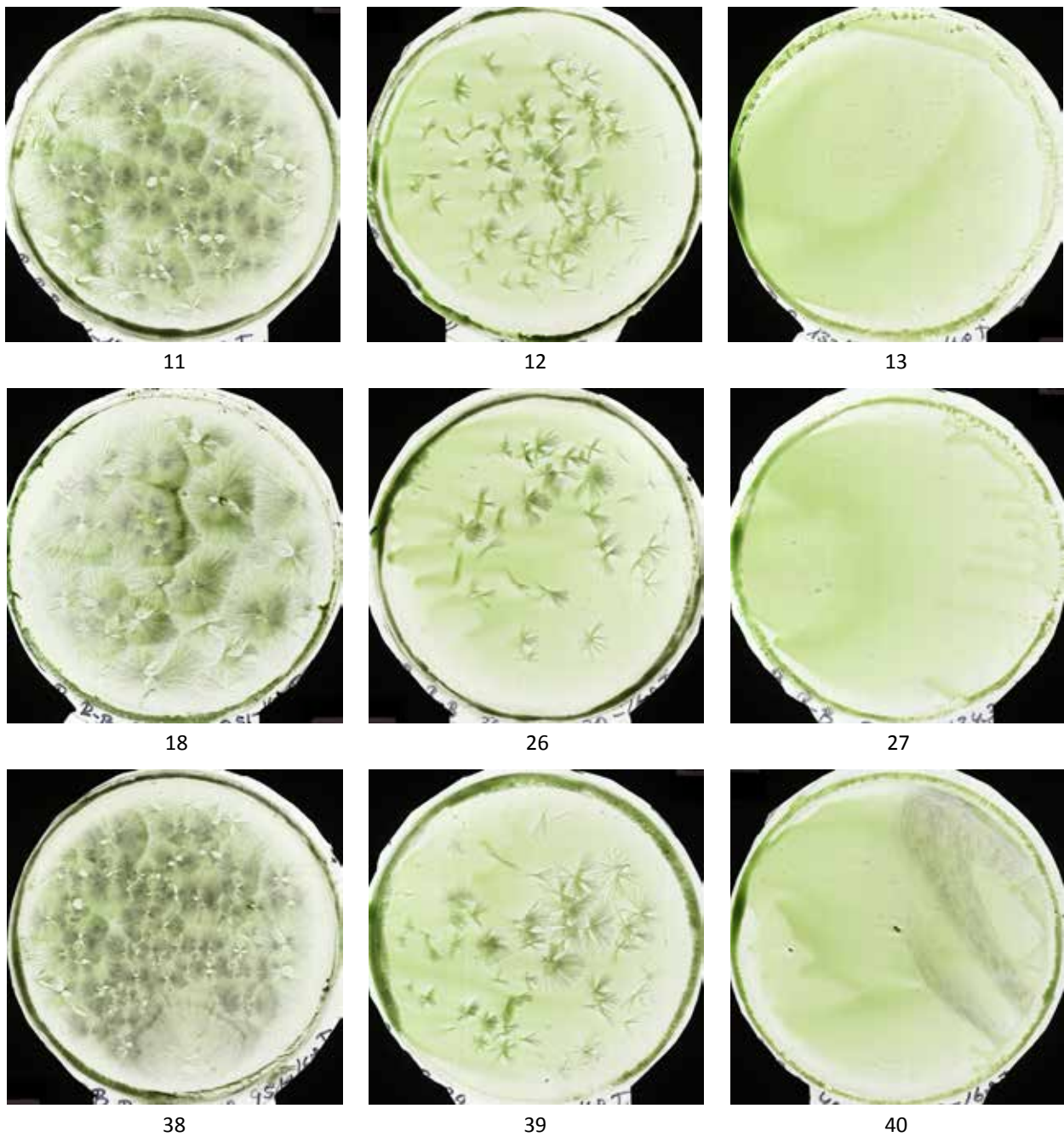


Fig. 1.9.3 Pictures from DCC with turbid apple juice. Y-axis picture replicates. X-axis additive amount. Left column 951 mg per plate, middle column 1130 mg per plate, right column 1434 mg per plate, DCC amount = 168 mg per plate. Pictures from University of Kassel (D), LabDoc series B.2015.06.01.R-B.

Appendix 1.9.3 Apple Juice at 566 – 800 mg additive

The DCC pictures from the clear apple juice (Fig. 1.9.4) are in the split-growth range, while the pictures from the turbid juice (Fig. 1.9.5) are in the dendrite range, with the first substance spirals, as heralds for the inhibition type of crystallization. The upper right picture in Fig. 1.9.4 is multi-centered due to a very late *tcrStart*, and not representative.

DCC pictures from clear apple juice

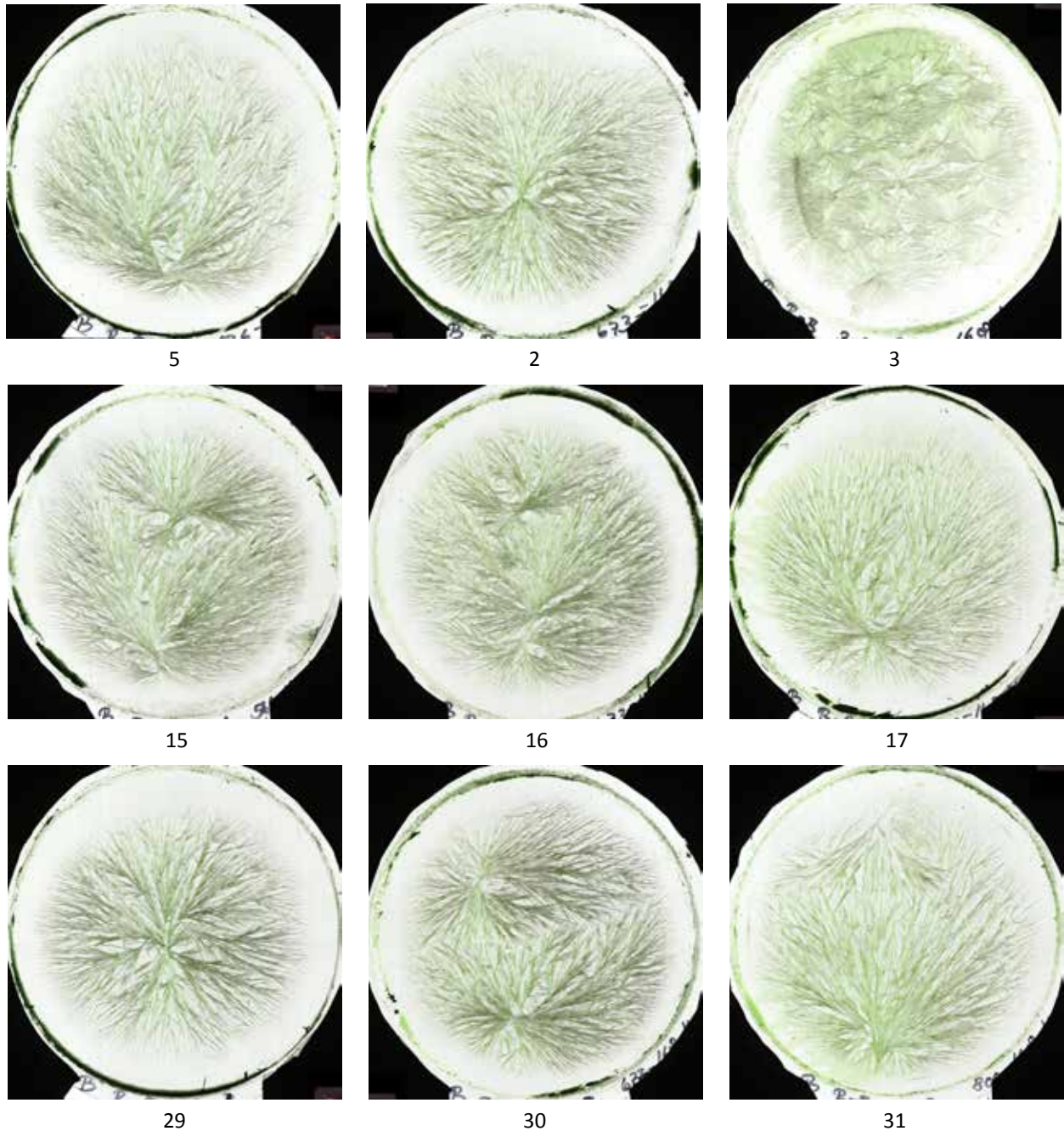


Fig. 1.9.4 Pictures from DCC with clear apple juice. Y-axis picture replicates. X-axis additive amount. Left column 566 mg per plate, middle column 673 mg per plate, right column 800 mg per plate, DCC amount = 168 mg per plate. Pictures from University of Kassel (D), LabDoc series B.2015.06.01.R-B.

DCC pictures from turbid apple juice

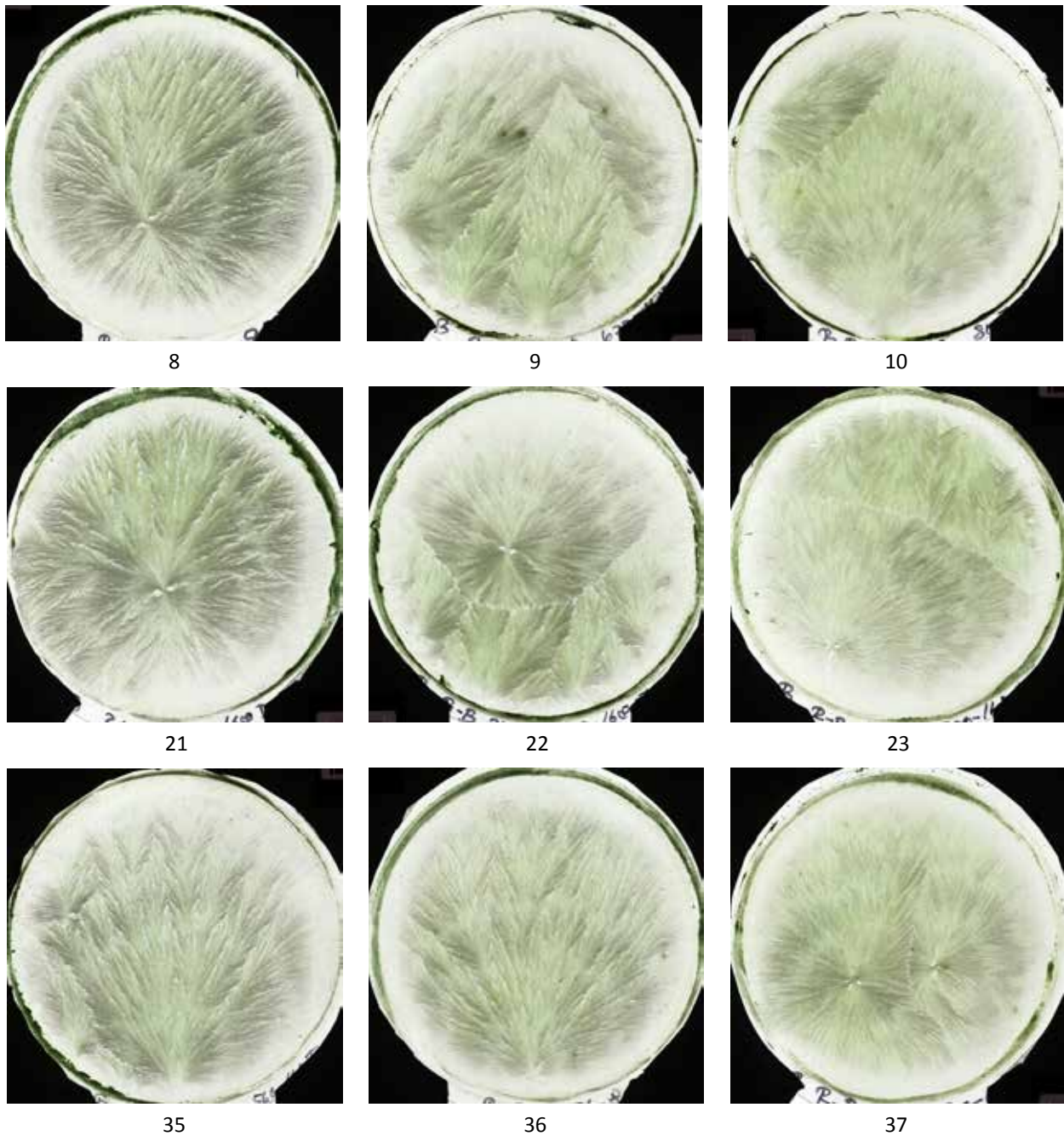


Fig. 1.9.5 Pictures from DCC with turbid apple juice. Y-axis picture replicates. X-axis additive amount. Left column 566 mg per plate, middle column 673 mg per plate, right column 800 mg per plate, DCC amount = 168 mg per plate. Pictures from University of Kassel (D), LabDoc series B.2015.06.01.R-B.

References

- [1] Selawry A and Selawry O Die Kupferchlorid-Kristallisation in Naturwissenschaft und Medizin (Gustav-Fischer-Verlag, 1957).
- [2] Krüger H. Kupferchlorid-kristallisationen. Ein Reagenz auf die Bildekräfte des Lebendigen. *Weleda Schriftenreihe* 1950; 1: 1-29.
- [3] Selawry A Neue Einblicke in die Samenkeimung (Naturwissenschaftliche Sektion am Goetheanum Dornach (CH), 1961).
- [4] Selawry A Samenkeimung und Metallpotenzen im Kristallsationstest (Forschungsring für biologisch-dynamische Wirtschaftsweise, 1975).
- [5] Von Hahn F-V Thesigraphie. (Franz Steiner Verlag, 1962).
- [6] Pettersson BD. Beiträge zur Entwicklung der CuCl₂ Methode nach Pfeiffer. *Elemente der Naturwissenschaft* 1966; 5: 29-39.
- [7] Pettersson BD. Beiträge zur Entwicklung der Kristallisationsmethode mit Kupferchlorid nach Pfeiffer IV. Wie verschiedene Kristallbilder bei der Pflanzenkristallisation entstehen. *Lebendige Erde* 1969; 3: 112-126.
- [8] Engquist M Die Gestaltkräfte des Lebendigen (Vittorio Klostermann, 1970).
- [9] Andersen JO, Huber M, Kahl J, Busscher N, MeierPloeger A. A concentration matrix procedure for determining optimal combinations of concentrations in biocrystallization. *Elemente der Naturwissenschaft* 2003; 79: 97-114.
- [10] Andersen J-O. Development and application of the biocrystallization method. PhD Thesis, Department of Agricultural Sciences/Organic Farming Unit The Royal Veterinary and Agricultural University Copenhagen. 2001.
- [11] Waldburger B. Begriff und Kontext in der Methode der Empfindlichen Kristallisation. *Elemente der Naturwissenschaft* 2005; 83: 79-89 <https://doi.org/10.18756/edn.83.79>.
- [12] Geier U, Seitz L. Bildoptimum und Bildtypen im Rundfilterchromatogramm (Chroma) bei der Untersuchung von Pflanzen. *Elemente der Naturwissenschaft* 2006; 85: 57-80 <https://doi.org/10.18756/edn.85.57>.
- [13] Schweizer F. Beobachtungen bei der Biokristallisation von Glykogen. *Elemente der Naturwissenschaft* 2007; 87: 76-89.
- [14] Busscher N, Doesburg P, Mergardt G, Sokol A, Kahl J, Ploeger A. Crystallization patterns of an aqueous dihydrate cupric chloride solution in the presence of different amounts of Bovine Serum Albumin. *Journal of Crystal Growth* 2019; <https://doi.org/doi:10.1016/j.jcrysgro.2019.125272>.
- [15] Athmann M. Produktqualität von Salatrauke (*Eruca sativa* L.) und Weizen (*Triticum aestivum* L.): Einfluss von Einstrahlungsintensität, Stickstoffangebot, Düngungsart und Hornkieselapplikation auf Wachstum und Differenzierung. PhD Thesis, University of Bonn. 2011.
- [16] Fritz J, Athmann M, Kautz T, Köpke U. Grouping and classification of wheat from organic and conventional production systems by combining three image forming methods. *Biological Agriculture & Horticulture* 2011; 27: 320-336.
- [17] Fritz J, Athmann M, Meissner G, Kauer R, Köpke U. Quality characterisation via image forming methods differentiates grape juice produced from integrated, organic or biodynamic vineyards in the first year after conversion. *Biological Agriculture & Horticulture* 2017; 33: 1-19.
- [18] Kahl J, Busscher N, Mergardt G, Maeder P, Torp T, Ploeger A. Differentiation of organic and non-organic winter wheat cultivars from a controlled field trial by crystallization patterns. *J. Sci. Food Agric.* 2014; 95: 53-58 <https://doi.org/doi:10.1002/jsfa.6818>.
- [19] Kahl J, Busscher N, Doesburg P, Mergardt G, Will F, Schulzova V et al. Application of Crystallization with Additives to Cloudy and Clear Apple Juice. *Food Analytical Methods* 2016; 10: 1-9 <https://doi.org/doi:10.1007/s12161-016-0575-6>.
- [20] Zhu D, Shen Y, Wei L, Xu L, Cao X, Liu H et al. Effect of particle size on the stability and flavor of cloudy apple juice. *Food Chemistry* 2020; 328: 126967 <https://doi.org/https://doi.org/10.1016/j.foodchem.2020.126967>.
- [21] Huber M, Andersen J-O, Kahl J, Busscher N, Doesburg P, Mergardt G et al. Standardization and Validation of the Visual Evaluation of Biocrystallizations. *Biological Agriculture and Horticulture* 2010; 27: 25-40.
- [22] Doesburg P, Huber M, Andersen J-O, Athmann M, van der Bie G, Fritz J et al. Standardization and performance of a visual Gestalt evaluation of biocrystallization patterns reflecting ripening and decomposition processes in food samples. *Biological Agriculture & Horticulture* 2014; 31: 128-145.
- [23] Fritz J, Athmann M, Andersen J-O, Doesburg P, Geier U, Mergardt G. Advanced panel training on visual Gestalt evaluation of biocrystallization images: ranking wheat samples from different extract decomposition stages and different production systems. *Biological Agriculture & Horticulture* 2018; 35: 1-12 <https://doi.org/doi:10.1080/01448765.2018.1492457>.
- [24] Doesburg P, Fritz J, Athmann M, Bornhütter R, Busscher N, Geier U et al. Kinesthetic engagement in Gestalt evaluation outscores analytical 'atomic feature' evaluation in perceiving aging in crystallization images of agricultural products. *PLOS* 2021; 16 <https://doi.org/https://doi.org/10.1371/journal.pone.0248124>.

- [25] Busscher N, Doesburg P, Mergardt G, Sokol A, Kahl J, Ploeger A. Influence of dewetting on the crystallization behavior of CuCl_2 in the presence of BSA during evaporation in a Petri dish. *Heliyon* 2019; 5: e01102 <https://doi.org/10.1016/j.heliyon.2018.e01102>.
- [26] Reynaud J, Tavernier I, Yu L, Cochet J. The adsorption of RNase A, BSA and cytochrome c at the graphite powder|liquid interface using in parallel the adsorption isotherm plot and linear sweep voltammetry on graphite paste electrode. *Bioelectrochemistry and Bioenergetics* 1986; 15: 103-112 [https://doi.org/doi:10.1016/0302-4598\(86\)80009-5](https://doi.org/doi:10.1016/0302-4598(86)80009-5).
- [27] Busscher N. Apple juice Project. Technical Report, University of Kassel. 2015.
- [28] Maeder P, Fliessbach A, Dubois D, Gunst L, Fried P, Niggli U. Soil Fertility and Biodiversity in Organic Farming. *Science* 2002; 296: 1694-1697 <https://doi.org/doi:10.1126/science.1071148>.
- [29] Maeder P, Hahn D, Dubois D, Gunst L, Alföldi T, Bergmann H et al. Wheat quality in organic and conventional farming: results of a 21 year field experiment. *Journal of the Science of Food and Agriculture* 2007; 87: 1826-1835.
- [30] Kahl J, Busscher N, Mergardt G, Ploeger A. Standardization and performance test of crystallization with additives applied to wheat samples. *Food Analytical Methods* 2014; 8: 2533-2543 <https://doi.org/doi:10.1007/s12161-015-0142-6>.
- [31] Balzer-Graf, U. and Gallmann, P. U.. Analytische und bildschaffende Methoden in der Untersuchung von Milchprodukten (Vitalqualitätsuntersuchung Joghurt), 2000.
- [32] Barth S, Fähndrich C, Bub A, Dietrich H, Watzl B, Will F et al. Cloudy apple juice decreases DNA damage, hyperproliferation and aberrant crypt foci development in the distal colon of DMH-initiated rats. *Carcinogenesis* 2005; 26: 1414-1421 <https://doi.org/10.1093/carcin/bgi082>.
- [33] Barth SW, Faehndrich C, Bub A, Watzl B, Will F, Dietrich H et al. Cloudy Apple Juice Is More Effective than Apple Polyphenols and an Apple Juice Derived Cloud Fraction in a Rat Model of Colon Carcinogenesis. *Journal of Agricultural and Food Chemistry* 2007; 55: 1181-1187.
- [34] Ravn-Haren G, Dragsted L, Buch-Andersen T, Jensen E, Jensen R, Nemeth-Balogh M et al. Intake of whole apples or clear apple juice has contrasting effects on plasma lipids in healthy volunteers. *European Journal of Nutrition* 2013; 52: 1875-1889.
- [35] Vallée Marcotte B, Verheyde M, Pomerleau S, Doyen A, Couillard C. Health Benefits of Apple Juice Consumption: A Review of Interventional Trials on Humans. *Nutrients* 2022; 14 <https://doi.org/10.3390/nu14040821>.
- [36] Meelursarn A. Effect of image parameters to differentiate samples from different farming systems. PhD Thesis, University of Kassel. 2007.
- [37] Kahl J, Busscher N, Hoffmann W, Mergardt G, Clawin-Raedecker I, Ploeger A. A novel approach for differentiation of milk fractions and polyvinylpyrrolidone with different molecular weight by patterns derived from cupric chloride crystallization with additives. *Anal. Methods* 2014; 6: 3173-3176 <https://doi.org/doi:10.1039/C3AY41568F>.
- [38] Busscher N, Kahl J, Ploeger A. From needles to pattern in food quality determination. *Journal of the Science of Food and Agriculture* 2014; 94: 2578-2581 <https://doi.org/doi:10.1002/jsfa.6498>.
- [39] Szulc M, Kahl J, Busscher N, Mergardt G, Doesburg P, Ploeger A. Discrimination between organically and conventionally grown winter wheat farm pair samples using the copper chloride crystallisation method in combination with computerised image analysis. *Computers and Electronics in Agriculture* 2010; 74: 218-222 <https://doi.org/doi:10.1016/j.compag.2010.08.001>.

1.10 Transition between crystal types

Abstract

The appearance of substance spirals exclusively in the area close to the rim of a $\text{CuCl}_2 \cdot 2\text{H}_2\text{O}$ (cupric chloride di-hydrate, further called DCC) picture is taken as a sign of the presence of an additive gradient in the Petri-dish. A hypothesis is put forth that a gradient in the ratio of the DCC / additive mixture is formed from the center to the periphery in all DCC pictures. The mixture ratio DCC / additive would be higher at the crystallization center and lower close to the rim of the Petri-dish.

Introduction

This chapter serves to condense the various chapters of the Handbook. To understand the following line of reasoning it is helpful to have read the chapters [1.8 Concentration matrix](#), [2.7 Substance spirals](#), [1.13 Picture zones](#) and chapter [1.7 Evaporation issues](#).

One topic of the 2021 / 2022 IFBC project [1] at the University of Kassel was the research of the number of substance spirals (see chapter [2.7 Substance spirals](#)) in the $\text{CuCl}_2 \cdot 2\text{H}_2\text{O}$ (cupric chloride di-hydrate, further called DCC) pictures with carrot juice as additive. For this research a DCC / carrot juice [concentration matrix](#) was made. During the comparison of the pictures exhibiting substance spirals, it was observed that, on occasion, only the outer part of the picture showed the substance spirals. This was especially evident in those pictures where DCC and additive amounts were near to the transition between dendrites and substance spirals. These pictures are shown in the middle column of Fig. 1.10.1 and 1.10.2. In addition, for lower crystallization starting times ($t_{crStart}$) (~ 12 hours) the substance spirals do not manifest, while for later $t_{crStart}$ values (~ 14 hours and above) this phenomenon was clearly visible.

If we assume that the appearance of substance spirals is indicative of a lower mixture ratio between DCC and additive, then this would imply that during the evaporation the mixture ratio DCC / additive decreases in the outer area close to the rim of the Petri-dish. The dependency of the appearance of substance spirals on the $t_{crStart}$ (the evaporation duration until the crystallization starts) could be interpreted as indicating that it takes time to reach this mixture ratio. The decrease of the mixture ratio can be attributed to an increase of the additive amount or a decrease of the DCC amount. Selawry 1957 [2] and Petterson 1969 [3] (see chapter [1.13 Picture zones](#)) both came to the conclusion that during evaporation the amount of additive increases towards the rim of the Petri-dish. When this occurs, it may be indicative of either the diffusion of the additive or the expulsion of the additive due to the crystallization process. During crystallization the DCC amount present in the solution will decrease, while the additive amount will increase due to expulsion. Selawry (1957 [2], p. 56) conducted an experiment in which a watery solution with protein as additive was evaporated. The results demonstrated that the protein concentration increased towards the rim, indicating a diffusion (or movement) phenomenon (see also [Appendix 1.10.1 Selawry](#)). This would fit to the time-dependent nature of the phenomenon, because more additive will have diffused to the rim, the later the crystallization starts. During the evaporation the concentration of DCC and additive will be higher in the area around the geometrical center (see chapter [1.7 Evaporation issues](#)). This will result in a flow of water from the rim to the center as well as a flow of DCC and additive towards the rim.

Hypothesis

Before the crystallization starts, during evaporation, there is a diffusion of additive and DCC from the geometric center of the Petri-dish to the rim, and simultaneously, a diffusion of water from the rim to the center (actually from the rim to the area with a constant evaporation). When the crystallization starts, the depletion of DCC in the solution leads to the reversal of the direction of DCC flow; from the rim to the crystallization center. Concurrently, the expulsion of the additive due to the crystallization strengthens the flow of the additive from the center to the rim.

This implies that in a DCC picture, a diverse range of mixture ratios is consistently appearing, rather than a single, fixed ratio. At the crystallization center, the mixture ratio of DCC to additive is higher, while towards the rim, the mixture ratio decreases. The question is whether the differences are sufficiently pronounced to be discernible. The gradient of the mixture ratios seems to be more pronounced for later crystallization starting times. Further research is required to determine the relationship between this phenomenon and the zonal concept of Engquist (1970 [4]) or the creation of substance spirals (see chapter [1.13 Picture zones](#) and chapter [2.7 Substance spirals](#)).

One crucial aspect to consider is the influence of the additive composition on the mixture ratio gradient. For example, consider the differences between solutions comprising a single molecule, such as Bovine Serum Albumin (BSA), and those containing a distribution of molecular weights, such as polyvinylpyrrolidone (PVP). Additionally, consider the varying chemical and molecular weight distributions present in juices. It may be of interest to investigate the potential role of pH indicators in such mixtures.

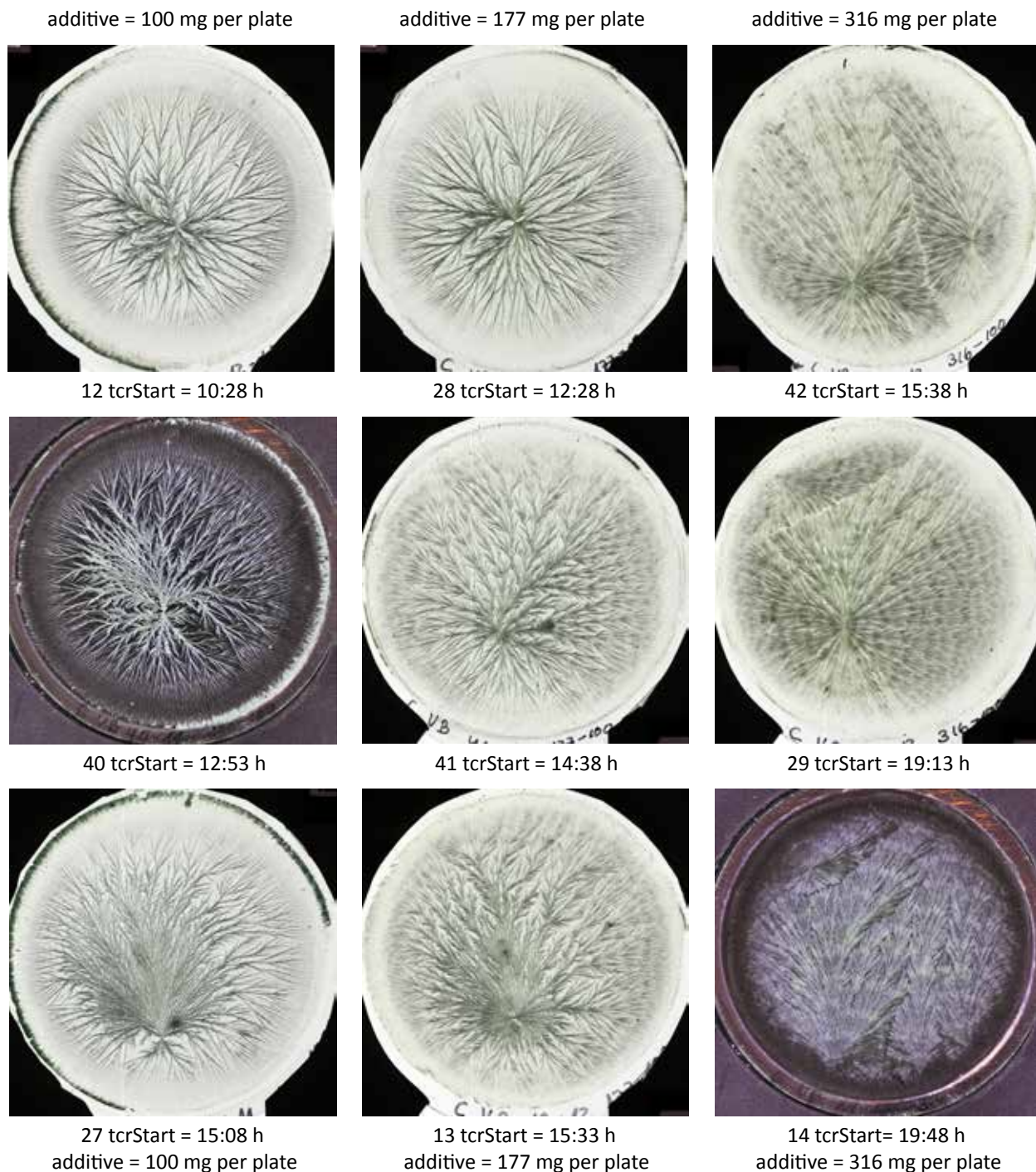


Fig. 1.10.1 X-axis: different additive amounts of carrot juice (from left to right 100, 177, 316 mg per plate) with 100 mg DCC per plate. Y-axis: replicates with the same additive amount per plate, sorted from top on increasing tcrStart (for pictures 14 and 40 no scans are available, only dark field illumination photos). Pictures from Uni-Kassel (D), LabDoc series C.2022.05.18.VB.

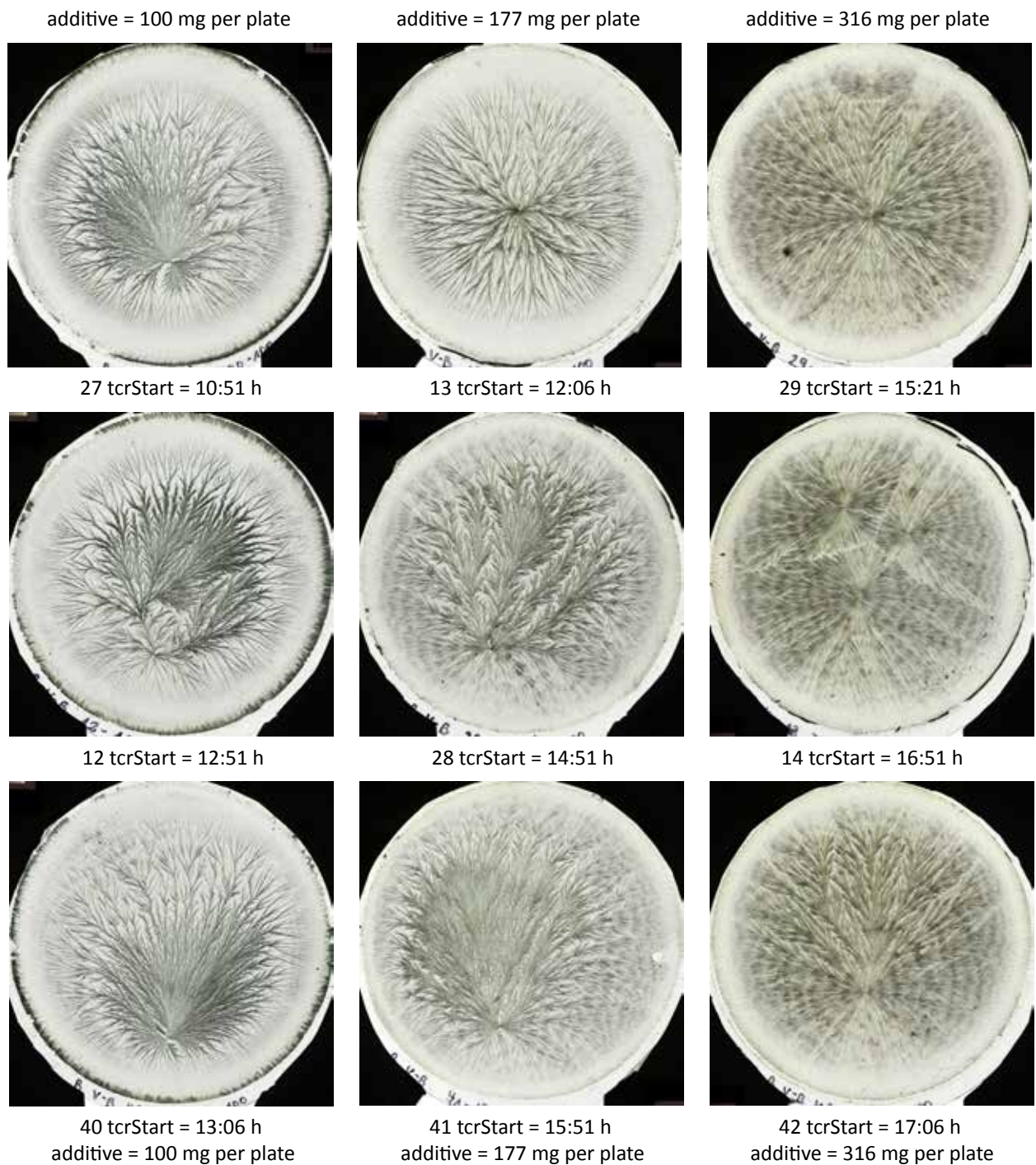


Fig. 1.10.2 X-axis: different additive amounts of carrot juice (from left to right 100, 177, 316 mg per plate) with 100 mg DCC per plate. Y-axis: replicates with the same additive amount per plate, sorted from top on increasing tcrStart. Pictures from Uni-Kassel (D), LabDoc series B.2022.05.18.V-B.

Resume

At the border between two crystallization types in the concentration matrix, the type with the higher additive amount appears to emerge first at the outer area, the rim, of the Petri-dish. The effect is pronounced for higher tcrStarts and negligible or absent for lower tcrStarts. The observation is interpreted as evidence of an additive gradient, with increasing amounts towards the rim, which result in a mixture ratio (DCC to additive) gradient from the crystallization center (high mixture ratio) to the rim of the Petri-dish (lower mixture ratio).

Additional research

- How discernible and verifiable is the statement:
- *“the same picture type for the same mixture ratio?”*
- How visible is the mixture ratio gradient in a Petri-dish (before and after crystallization)?
- How does it depend on the position in the concentration matrix?
- Impression of Kahl: “does a higher tcrStart appear like a higher additive amount”.
- Is the appearance of the zones correlated to the mixture ratio gradient? (zonal concept of M. Engquist, see chapter [1.13 Picture zones](#)).
- How strong does the ratio gradient depend on the additive composition (BSA, PVP, carrot juice)?
- Determine with [CrystEval](#) the size of the zones of the various types of crystals and the dependency on additive amount, DCC and tcrStart.

Additional research (Selawry / Gaubatz ideas)

Possible methods for detecting additive gradients: the RGB scan shows three colors which are reduced by the absorbance (and the reflection) of the sample. BSA and DCC should absorb RGB in a different relation (R to B to G). As an alternative simple protein staining dyes can be used. It should be enough to discriminate the samples from each other.

The possible experiments could be as follows:

- SG1.1 Evaporation of a solution containing BSA only in different amounts: does a distribution of BSA appear over the dish? -> does it increase towards the rim?
 - can the layer be removed e.g. by rinsing with water (Norde 2012 [5])?
- SG1.2 (Plate pretreatment) perform a DCC crystallization on the BSA covered plate from the experiment mentioned above. Does a BSA specific crystallization pattern emerge?
- SG1.3 Crystallize DCC only (different amounts of DCC) or use existing pictures and determine the DCC distribution.
- SG1.4 Crystallize mixtures of BSA and DCC (use existing matrices?)

How do the differences of the above proposed cases look like?:

- SG2.1 Can we differentiate (by RGB) only BSA and only DCC from SG1.1 and SG1.3?
- SG2.2. Is there a difference between SG1.2, and SG1.4 for areas with
 - BSA only,
 - DCC only
 - BSA with DCC
- SG2.3 Rewetting the finished picture. First crystallize DCC with BSA. Then add the amount of evaporated water (again), and let it crystallize again. Do we get the “same” pictures or do we see another crystallization type?

Appendix 1.10.1 Selawry

Selawry (1957 [2], p. 56, encouraged by E. Gaubatz) describes that a protein containing solution, when evaporated, exhibits an increase in protein concentration towards the rim of the Petri-dish. In addition Selawry describes the development of “protein layers” in experiments with tilted plates (1957 [2], p. 27, also encouraged by E. Gaubatz). She usually observed for DCC with blood as additive a consistent coloration in the center of the dish and concentric rings extending until the rim of the Petri-dish. This effect is disturbed when the plates deviate by more than 0.15° from horizontal balance. 0.15° is 2.618 mm on 1 meter ($\tan(0.15 / 90 * \pi / 4) * 1000$ mm). In his experiments, Jung (1952 [6]) describes the protein layers of a blood / DCC crystallization, when the DCC of a crystallization is washed away and replaced with a fresh DCC solution pipetted into the dish containing the protein layers. This process results in a new DCC picture. Norde (2012 [5]) provided an overview of the current knowledge regarding protein coverage and precoating.

Selawry mentions E. Gaubatz as the researcher connected to the experiments she describes. No publication was found about the E. Gaubatz work though.

References

- [1] Mansi Antil RJ, TanuYadav UA. Report: IFBC project 2022/2023. Technical Report, University of Kassel. 2023.
- [2] Selawry A and Selawry O Die Kupferchlorid-Kristallisation in Naturwissenschaft und Medizin (Gustav-Fischer-Verlag, 1957).
- [3] Pettersson BD. Beiträge zur Entwicklung der Kristallisationsmethode mit Kupferchlorid nach Pfeiffer IV. Wie verschiedene Kristallbilder bei der Pflanzenkristallisation entstehen. *Lebendige Erde* 1969; 3: 112-126.
- [4] Engquist M Die Gestaltkräfte des Lebendigen (Vittorio Klostermann, 1970).
- [5] Norde W, Lyklema J. Interfacial behaviour of proteins, with special reference to immunoglobulins. A physicochemical study. *Advances in Colloid and Interface Science* 2012; 179-182: 5-13 <https://doi.org/http://dx.doi.org/10.1016/j.cis.2012.06.011>.
- [6] Jung. Beiträge zur kristallographischen Blutuntersuchung. *Pharmazie* 1952; 7: 628-639.

1.11 Wetting up phase

Why do we need a wetting up phase when the chamber is not used for some time even though we have a reservoir? Will water suffice or do we need the chloride from the $\text{CuCl}_2 \cdot 2\text{H}_2\text{O}$?

Abstract

A routine for “re-wetting” the chamber after 2 - 4 weeks of inactivity has been developed from the daily work. Criteria to characterize the phenomenon requiring re-wetting are however lacking and need to be developed. There are indications that after a period of inactivity without re-wetting before the first experiment, a longer crystallization starting time (tcrStart) may occur.

Introduction

When the chamber has not been used for 2 - 4 weeks, then routinely, when an experiment is planned, a so called re-wetting run (experiment with only water in the Petri-dishes) is performed to “restart” the chamber. The basis for the re-wetting experiment is not easy to research. This re-wetting procedure was also reported for the so called Dornach Topf system (see chapter [3.1 Chamber systems](#)), which has no wooden walls (aluminum) to wet up. This suggests that the whole process, including the person handling the samples and dishes, may need a blank run to get acquainted with the work again. Because we have different labs with different people and different systems, we don't have a well-defined full factorial approach to separate the effects. The phenomena by which the need for a so called re-wetting phase is recognized are not clear. The procedure of the Forschungsring's DCC system in Darmstadt does not include a re-wetting phase. They are however working under complete different conditions, because their mean [crystallization starting time](#) is around 30 hours.

Historical

Bessenich describes (1960 [1], p. 14) that the optimal use of their wooden chambers (she called them “zellen”, which were 1.50 m deep, 1.50 m wide and 2 m high), was based on the fact that they were kept at a constant temperature of 30 °C and 50 % relative humidity. No information was found about a re-wetting phase.

Authors Thoughts

The first problem with this phenomenon is that we have no criteria to recognize the difference between DCC pictures without this re-wetting phase after a period of inactivity, and “normal” DCC pictures. From the simulation of the evaporation (see chapter [2.13 Evaporation model](#)) a humidity effect from the wooden inner wall in the chamber can be expected. The question is if without a re-wetting phase after a period of inactivity, conditions are created for e.g. an earlier or a later tcrStart , which affects the DCC pictures. This is a serious issue that is obvious to those who work with the DCC system on a daily basis, but until now there has been no description of the phenomena that allows for research. Once the above criteria are defined, the second question of whether the re-wetting phase should be done with DCC due to the possible effect of chloride can be answered.

Resume

This effect, born from the routine of daily working with the DCC system, should be taken as a serious problem. The criteria characterizing this phenomenon need to be elaborated, because they are missing.

Additional research

Is an effect in the inner chamber humidity visible when no experiments are performed for 2 - 4 weeks? Different periods are recorded in which no experiments were carried out.

Do a defined test with defined samples.

- Check the tcrStart , radius and the image analysis results.
- Look and describe visually the difference in the pictures.

Do 4-6 experiments with the same samples, starting after at least 6 weeks of non-activity.

References

- [1] Bessenich F. Zur Methode der empfindlichen Kristallisation (Naturwissenschaftliche Sektion am Goetheanum Dornach, 1960).

1.12 Multiple Centers

How can we understand the appearance of multiple centers? How is the dependency on the amounts of $\text{CuCl}_2 \cdot 2\text{H}_2\text{O}$ and additive?

Abstract

Usually the $\text{CuCl}_2 \cdot 2\text{H}_2\text{O}$ (cupric chloride di-hydrate, further named [DCC](#)) picture has only one location at which the crystallization starts, the so called center. However there are instances where multiple centers appear. From the literature it is known, that multi-centeredness appears at relatively high additive amounts. In the case of Bovine Serum Albumin (BSA), the number of centers is dependent on the amount of BSA used, which has been studied over a wide range of additive amounts [1]. This allowed us to understand why one-centered pictures appear at a specific range of the additive amounts, and why there are more above and below that range. The results are compared with literature results for other additives.

Introduction

Most people who are familiar with general crystallization phenomena are astonished that most of the [DCC](#) pictures have only one starting point (the center). See also chapter [2.11 Nucleation](#). However there are also cases where multiple centers appear. The multiple centers may appear “at the same” time in term of frequency of the photographs, or they may appear distinctly one after each other. The appearance of multiple centers depends on the additive amount and was studied for BSA over a wide range of additive amounts [1].

Historical overview

Selawry [2], p. 23, relates multi-centeredness to (too) high amounts. She bases this hypothesis on the evaluation of DCC pictures with increasing amounts of additives from a variety of sources (pure chemical additives and extracts from plant and animal tissues and blood). (See also chapter [1.13 Picture zones](#)). Petterson [3], p. 120, mentions the appearance of multi-centeredness in connection with high amounts of carrot extract. This was also observed and reported by Engquist [4] p. 15 for various plant extracts. Von Hahn [5] (p. 23, §40) mentions the appearance of multi-centeredness in connection with increasing additive amounts in the following way: “For lower amounts of additive there were many centers. As the amount of additive increased, the number of centers decreased to one. A further increase of the additive resulted in an increase in the number of centers. The area of one-centeredness is covering a defined range of additive amounts”. This was observed by von Hahn for a broad range of plant species extracts.

Authors Research

For BSA as additive, a [Concentration Matrix](#) was elaborated and documented in [1] and [6]. In this experiment, the number of centers was counted according to the following scale (see Fig. 1.12.1):

For the evaluation of multi-centeredness the following scale is defined in Fig. 1.12.1.

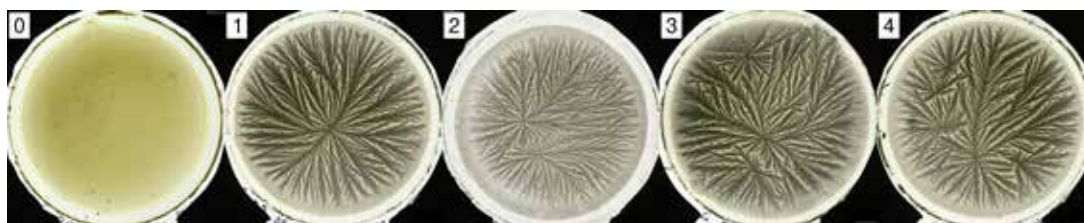


Fig. 1.12.1 Scaling the number of centers. From left to right. no. 0: no center, no. 1: one center, no. 2: two centers, no. 3: three centers, no. 4 : more than three centers = g3 (5 centers).

The results of the evaluation due to the scales in Fig. 1.12.1 are shown in Fig. 1.12.2 below.

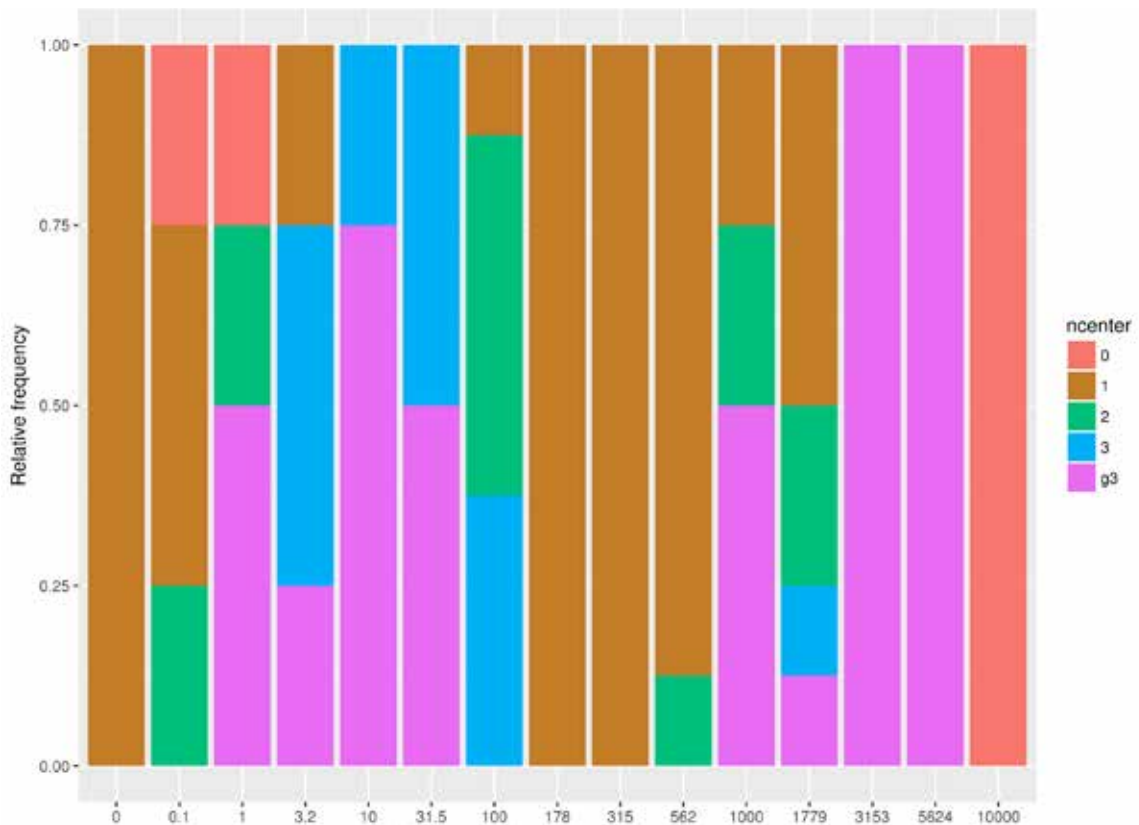


Fig. 1.12.2 Bar plots of the relative frequency of the no. of centers (Y-axis) versus the amount of BSA in calculated monolayers (X-axis). For 100 mg DCC per plate. Fig. 10 from [1].

In Fig. 1.12.2 the dark brown bars indicate the presence of one-centered pictures. This is observed for 0, 178 and 315 calculated monolayers of BSA (X-axis). This means that as the additive amount (X-axis) increases, the number of centers (Y-axis) increases too (green: 2 centers, blue: 3 centers, magenta: more than 3 centers), whereas between 178 and 315 calculated monolayers BSA the number of centers decreases to 1. Beyond 315 calculated monolayers BSA the number of centers increases again.

The results were consistent with von Hahn's observation [5] that the number of centers shows a minimum at a particular range of additive amounts for various plant species.

The area in the BSA matrix (see chapter [1.8 Concentration matrix](#) and [1]) where the number of centers is one coincides for BSA with the so called split-growth area. Possible reasons for the occurrence of a minimum number of centers are as follows:

For additive amounts below the one-center range, the additive contributes to heterogeneous nucleation sites. This would result in a high number of centers. As more additive is added the viscosity of the solution will outweigh the number of heterogeneous centers, and the nucleation probability is reduced to one. A further increase of the additive is associated with a decrease in the growth rate of the crystals.

At a higher growth rate, the crystal can cover the glass plate before the next nucleation can initiate an additional crystal growth. If the growth rate is lower, additional crystal formation can start before the whole plate is covered. Therefore the multi-centeredness reappears for higher additive amounts.

In the lower additive range the centers probably appear simultaneously (it was not possible to evaluate the time stills because the contrast was too low). In the higher additive range the centers appear mostly one after the other.

Resume

For BSA, the area in the [Concentration Matrix](#) with split-growth and hole forms produced one-centered pictures. Below and above this additive range, multiple centers appear. At higher additive levels they were due to a reduced crystal growth rate, and at lower levels they were due to an increase in the number of nucleation centers, which was not offset by the viscosity of the solution.

Additional research

- How to observe the pictures at “lower” levels of additive?
 - Are these centers appear sequentially?
- Do other samples have a comparable behavior as BSA? (as von Hahn observed)
 - Does the development of the number of centers coincide with the additive amount and the boundary between two crystal type regions in the crystallization matrix?
- Does the number of centers depend on the crystallization starting time?
 - E.g. in the BSA Crystallization Matrix?
 - or in the Crystallization Matrix for other samples?
- So far the influence of the additive amount on the number of centers is researched.
 - Sometimes all pictures of an experiment are multi-centered
 - Is there an influence of air pressure change or lightning?
 - Is the number of centers a quality signal e.g. for the influence of the processing on a sample?

References

- [1] Busscher N, Doesburg P, Mergardt G, Sokol A, Kahl J, Ploeger A. Crystallization patterns of an aqueous dihydrate cupric chloride solution in the presence of different amounts of Bovine Serum Albumin. *Journal of Crystal Growth* 2019; <https://doi.org/doi:10.1016/j.jcrysgro.2019.125272>.
- [2] Selawry A and Selawry O. Die Kupferchlorid-Kristallisation in Naturwissenschaft und Medizin (Gustav-Fischer-Verlag, 1957).
- [3] Pettersson BD. Beiträge zur Entwicklung der Kristallisationsmethode mit Kupferchlorid nach Pfeiffer IV. Wie verschiedene Kristallbilder bei der Pflanzenkristallisation entstehen. *Lebendige Erde* 1969; 3: 112-126.
- [4] Engquist M. Die Gestaltkräfte des Lebendigen (Vittorio Klostermann, 1970).
- [5] Von Hahn F-V. Thesigraphie (Franz Steiner Verlag, 1962).
- [6] Busscher N, Doesburg P, Mergardt G, Sokol A, Kahl J, Ploeger A. Influence of dewetting on the crystallization behavior of CuCl_2 in the presence of BSA during evaporation in a Petri dish. *Heliyon* 2019; 5: e01102 <https://doi.org/10.1016/j.heliyon.2018.e01102>.

1.13 Picture Zones

How can we understand the appearance of zones in the picture? How is the dependency on the amounts of $\text{CuCl}_2 \cdot 2\text{H}_2\text{O}$ and additive?

Abstract

The raw structure of a $\text{CuCl}_2 \cdot 2\text{H}_2\text{O}$ (cupric chloride di-hydrate, further called [DCC](#)) picture, both from readily available chemicals (e.g. with a CAS #) and from agricultural (food) products, can be visually divided into three circular concentric zones. They can be referred to as the “inner zone”, “middle zone” and “outer zone”. As in computer image analysis, a so called Region Of Interest (further abbreviated [ROI](#)) concept can be applied, that includes these three zones. At the same time from the crystallization growth observations three stages can be identified. The first stage (1) after the start of the crystallization comprises a fast covering of the Petri-dish by the crystals until the supersaturation border of the evaporation is reached. Then (2), a slower crystallization “follows” the evaporation, and finally (3) an interaction with the area close to the rim takes place. The possible correspondence of the stages with the zones needs more research. A simple description of how to recognize the three zones visually was elaborated. An example of image analysis is shown in which the ROI with the highest differentiation is determined for carrots. (FIBL Carrots 2003).

Introduction

From the beginning in 1924, different separate geometric areas, called zones, were recognized in the $\text{CuCl}_2 \cdot 2\text{H}_2\text{O}$ (cupric chloride di-hydrate, further called [DCC](#)) pictures. The zones have been used in varying ways by different evaluators (Pfeiffer 1935 [1], Selawry 1961 [2], Engquist 1970 [3]). Different explanations (Petterson 1969 [4], Engquist 1975 [5], Schweizer 2013 [6]) were given to understand the zones. The following is a list of the different views, by author, that are available. The computer image analysis (Carstensen 1992 [7], Andersen 1999 [8], Doesburg 2013 [9]) also uses a zonal concept which is called Region Of Interest (in short [ROI](#)).

Historical Overview

Blood Samples

Pfeiffer (1935) [1] (p. 24) described different zones for the evaluation of DCC pictures from blood samples. Selawry (1957) [2] (p. 65, Fig. 25) described a zonal scheme for the evaluation of DCC pictures for blood crystallization. Koopmans (1971) [10] discussed a localization phenomenon also in accordance with the work from Nickel [11]. The zonal scheme is not a simple geometry of concentric circles but it divides the DCC picture in to roughly three rows and perpendicular to this a left right symmetry (the center of the DCC crystallization picture is oriented downward). The differences in the used DCC and additive amounts between Pfeiffer (6 μL blood and 1.87 g DCC in 10 mL) and Selawry (1.8 μL Blood and 1.52 g DCC in 6 mL) resulted in different localization phenomena (data from Nickel [11] p. 102).

Food samples

For her work on plant seeds Selawry (1961) [12] described three concentric circular zones (in [12] p. 16, Fig. 5, like Fig. 1.13.1 below). Petterson (1969) [4] described the concept of zones in a picture, and he tried to understand the reason for these zones by exploring the system through a [concentration-matrix](#) approach. He associated the zones with different mixing ratios of DCC and sample in the Petri-dish, due to different strengths of diffusion movements of DCC and sample. He was followed by Engquist (1970) [3], who used a zonal concept in connection with different amounts of additives. In the following the details are shown and discussed. Schweizer (2013) [6] carried out experiments in which the crystallization environment was disturbed. He created a zonal structure in the DCC picture.

Selawry

In her book about *Samenkeimung* (Selawry 1975 [13], p. 11) Selawry describes three zones as can be seen in Fig.1.13.1 (from [13] p. 11).

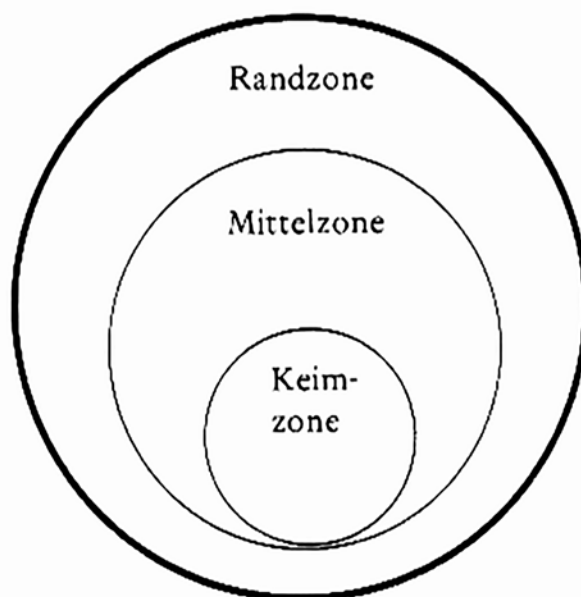


Fig. 1.13.1 Names of the zones in the DCC picture (from Selawry 1975 [13] p. 11).

In Fig.1.13.1, starting from the crystallization center, Selawry describes a “Keim zone” a “Mittel zone” and a “Randzone”. In an article published with Koepf [14], (p. 14) these are called “zone of start”, “middle zone” and “outer zone”.

Petterson

Petterson [4] (p. 121, 123) describes that throughout the Petri-dish the concentration of the additive and the DCC is not constant, resulting in different mixing ratios of DCC and additive, which should be the reason for the zones. Reasons for the varying mixing ratios could include (1), the diffusion of the DCC, (2), the depletion of DCC due to the crystallization, or (3) the additive-expelling effect due to the crystallization, i.e. increasing the amount of the additive outside the crystals like more and more snow in front of a snow plow.

Engquist

Engquist defines in (Engquist 1970 [3]) on p. 16 different types (A,B,C) of DCC pictures (see in Fig.1.13.2 below), depending on the number of visible zones. The type depends on the increasing amount of additive. For type C, most right in Fig.1.13.2, she describes three zones around the crystallization center. Starting at the crystallization center, the zones are called “Innere-zone”, followed by the “Mittel-zone” and finally at the rim of the Petri-dish the “Rand-zone”. The most typical needles for a sample she identified in the *Mittel zone* [3] (p. 16).

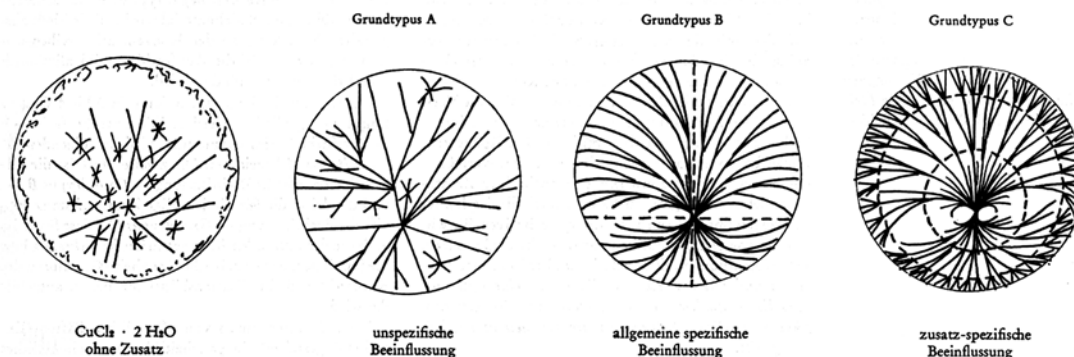


Fig. 1.13.2 Types of DCC pictures from Engquist [3] arranged according to an increasing additive amount on the plate (from left to right).

Also in [3] (p. 37) for the evaluation of different research questions, she describes an organization of the images in to zones or sectors. On p. 40 (in English on p. 42) she applies the three types (shown in Fig.1.13.2) to evaluate aging (in vivo and in vitro) and connecting it to different parts of milk, seeds and egg (see below in Fig.1.13.4).

Stage with three zones (Enlarged *Grundtypus C* from Fig.1.13.2).

In the following an approach how to recognize the zones is given:

To describe the three zones in a simple manner one can look from the rim for a zone with a common texture (the outer zone). Then from the crystallization center for a zone with a common texture (the inner zone). Then see if the remaining zone in between has common features or needs more subdivisions.

Common texture means the same type of needles.

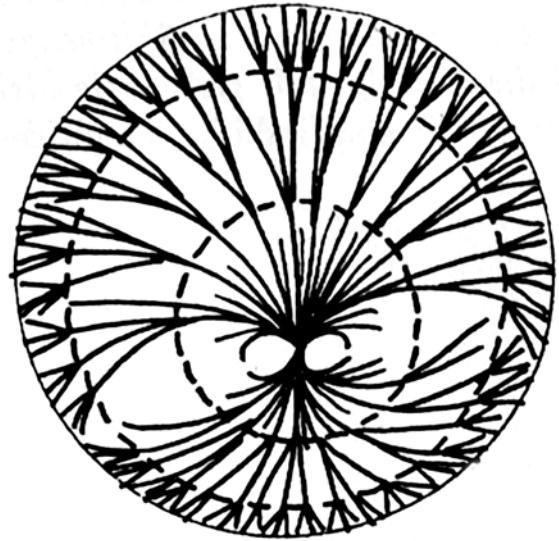





Fig. 1.13.3 Enlarged part of Fig. 1.13.2 *Grundtypus C* (most right).

Table 1.13.1 Types of DCC pictures from Engquist [3] (p. 42) according to different parts of a sample or aging processes.

	Basic Type A	Basic Type B	Basic Type C
Steps of the concentration series			
Ageing in vivo:	State III	State II	State I and 0
Ageing in vitro:	State III	State II	State I and 0
Pictures typical for:	Seed coats	Germ	Nutritive tissue of seed
Pictures typical for:	Starch Whey Eggshell Many refined organic substances	Gluten Skimmed milk Egg white Albumen	Whole flour Whole milk, cream yolk Fresh parts of plants

Engquist described, as shown in Table 1.13.1, a general feature of the DCC pictures, which sometimes shows up in terms of zones. In the concentration series, she recognized that the degradation of a sample (in vivo or in vitro) is reflected by as if there were less additive to structure the DCC.

Andersen

In 1999, Andersen [8] applied a texture analysis developed by Carstensen [7] to DCC pictures from aged carrot samples. For the evaluation, the ROI concept was used. See Fig. 1.13.5 below (from [8] p. 9, Fig. 5). The ROI concept includes circular concentric areas (a and b in Fig. 1.13.5), sectors (c in Fig. 1.13.5), and segments (d in Fig. 1.13.5).

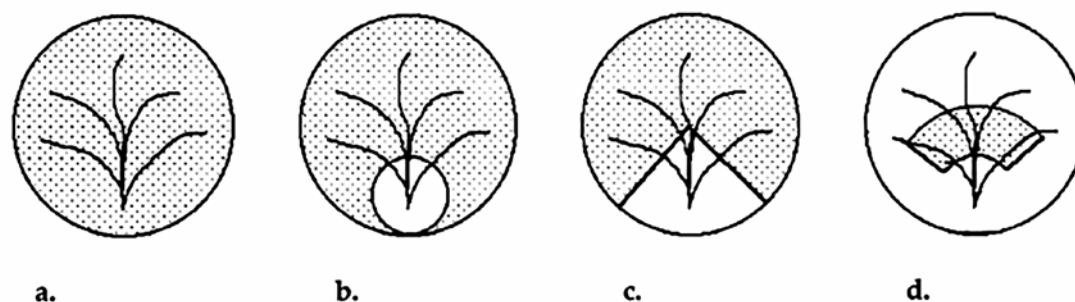


Fig. 1.13.5 ROI concept for the computer image analysis of DCC pictures (from Andersen [8], p. 9, Fig. 5). Diagrammatic depictions of the four main types of ROIs, from left to right: Circle; Circle - circle; Sector; and Segment. The dotted areas represent the ROIs.

Image Analysis results from carrot varieties (See for more details [Appendix 1.13.2 Image analysis.](#))

From Engquist's observation above, that the most typical needles were seen in the middle zone (Fig.1.13.3), it could be hypothesized that the highest differentiation between DCC pictures of different qualities should be found in this middle zone. The definition of the zones according to the ROIs used for the image analysis is shown below. Slices were used and the middle zone was expected to be located in the ROI range 30-50, 40-60 and 50-70 percent.

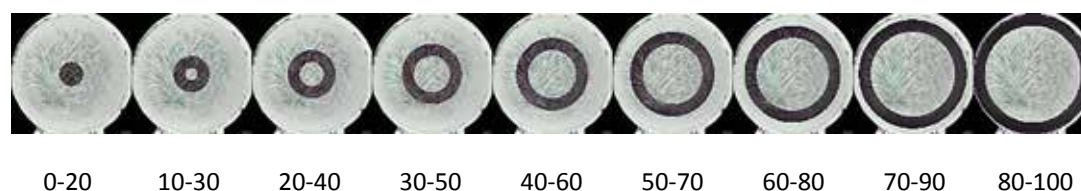


Fig. 1.13.6 From left to right. The darkened area shows the increasing slices oriented around the geometric-center. The inner and outer radius is in percentage of the total picture radius.

The used carrot experiment included 4 varieties (Tiptop, Bolero, Nipomo F1, Samson) grown at FIBL 2003. (documented in BLE report O2OE170-2003 [15] and by Arncken [16]). The experiment was done in two chambers and over two days. Image Analysis is described in chapter [3.4 Image analysis tool.](#)

Lmeplot of: BAH-Fibl-2003-DQDR: ROI=ExcenterRing 0.8-1/0-360

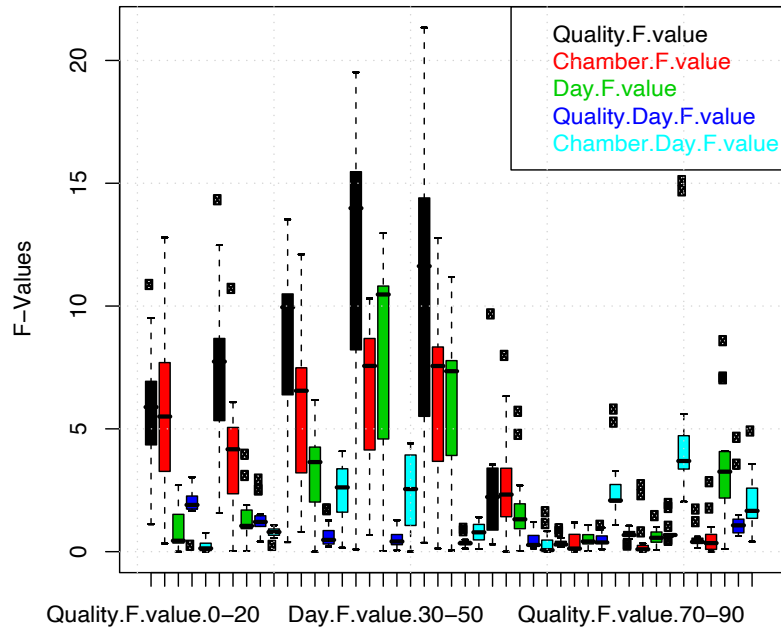


Fig. 1.13.7 Image analysis results for the differentiation of different carrot varieties (ANOVA F-Value). On the X-axis are the ROI values 0-20, 10-30, 20-40, 30-50, 40-60, 50-70, 60-80, 70-90, 80-100 from left to right. On the Y-axis are the ANOVA F-values of the difference between the four carrot samples for all texture samples. Meaning of colors are the influences of: black = quality, red = chamber, green = day, blue = interaction quality:day, cyan = interaction chamber:day.

Fig.1.13.7 shows that the quality difference (black bars) has its maximum at an ROI between 30-60 % of the Petri-dish radius. The F-values of the quality signal (black bars) are larger than those of the chamber variation (red bars) and the day repetition (green bars). This confirms the observations from Engquist, that the most typical needles were found in the middle zone (see Fig. 1.13.3).

Schweizer

Francois Schweizer [6] made experiments to find out what happens when the crystallization environment is disturbed. Usually the temperature and the humidity of the air above the evaporating dish is constant or slowly (within 20-30 minutes) changing. He realized that the crystallization creates a disturbed zone (with a high growth velocity, and many centers) when the environment changes rapidly (less than 1 minute). When the environmental conditions are turned back to the usual conditions, the crystallization continues to proceed as before. Does this point to disturbances as origin of a zonal structure?

Resume Historical Overview

When working with DCC pictures of agricultural products, several authors use a three zonal concept with an "inner zone", a "middle zone" and an "outer zone". Engquist's observation that the sample reveals itself most clearly in the middle zone was confirmed by the highest computer image analysis differentiation of carrot varieties in this zone. Engquist's zonal concept is developed based on concentration series characteristics.

Authors Measurements

Following Engquist's idea that the appearance of the zones depends on the additive amount, the question of the zones in the pictures should be studied over a wide range of possible combinations of DCC and additive amounts. This was done in the matrix experiments documented in chapter [1.8 Concentration matrix](#) (for BSA, PVP, apple juice).

From the BSA matrix, it was learned that in order to discuss the structure of the raw picture (the distribution of the DCC in the dish), the different phenomena in the final DCC crystallization picture should be ordered first. This was done by following the growth of the DCC crystallization pattern from the nucleation to the final coverage of the Petri-dish.

It was observed that there were pictures with:

- dewetting before crystallization (low amount of additive, DCC < 300 mg) (see Fig. 1.13.8 left),
- dewetting after crystallization (higher amount of additive, DCC < 300 mg) (see Fig. 1.13.8 right)
- and overgrowth of the picture from the rim of the Petri-dish (DCC > 300 mg).

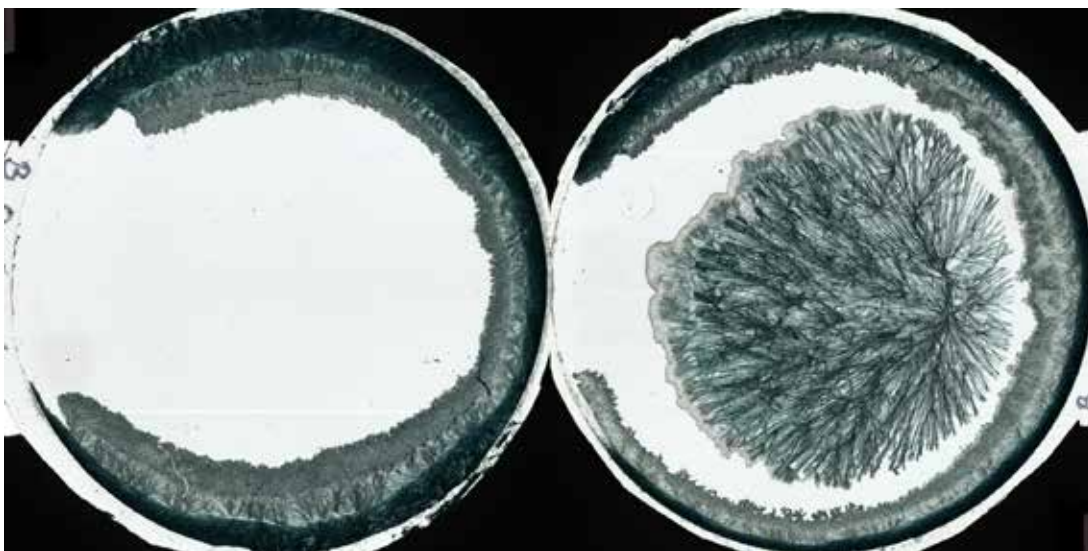


Fig. 1.13.8 Distribution of DCC in the dish. Left dewetting before crystallization, right dewetting after crystallization (from Busscher 2019 [17] Fig.1).

Examples for the time development of the three types can be seen in the supplementary information of the dewetting article Busscher 2019 [17].

Table 1.13.1 Development types and location in supplementary info file of the dewetting article, Busscher 2019 [17].

Type	Fig. in supplementary
Dewetting before crystallization	Fig. Si.1 in chapter 1.1
Dewetting after crystallization	Fig. Si.2 in chapter 1.3
Dewetting after crystallization and rewetting (overgrowth)	Fig. Si.3 in chapter 1.4

Case No Dewetting

First the case without dewetting is discussed. The case of dewetting, as described by Gallinet [18], Busscher 2010 [19] and Busscher 2019 [17] is discussed below. The main ideas are following the same line.

When the crystallization starts, the area where the DCC concentration is above the saturation concentration is filled by the growing crystals (see chapter 2.4 [Concentration gradient](#) Fig. 2.4.5 between the red and the blue line, indicated by the horizontal cyan arrow). The crystallization velocity, depending on the supersaturation, slows down [20], [21] when the area with a lower supersaturation is reached (the effect of the temperature, due to the crystallization heat, on the influence (reduction) of the supersaturation of the solution is not taken into account). In Fig. 2.4.5 the deceleration area is in the area between a [radius](#) of 40 % and 80 % where the gradient lies. The growth is slowing down until the crystallization follows the evaporation of the solution.

This would be the first area, defined by the evaporation and crystallization process. As evaporation continues, the crystallization “wave” now follows into the areas where the DCC concentration reaches the saturation concentration threshold. This is a much slower process than the one mentioned before. The DCC diffuses to the crystallization front where the crystal needles are built, which can result in a depletion of DCC in the solution. This area with possible depletion, which will be close to the rim of the Petri-dish, would define the third area the so called outer area.

From the physical point of view we can also hypothesize three areas:

- Inner area: high speed crystallization zone, starting from the crystallization center
- Middle area: low speed crystallization zone, following the evaporation

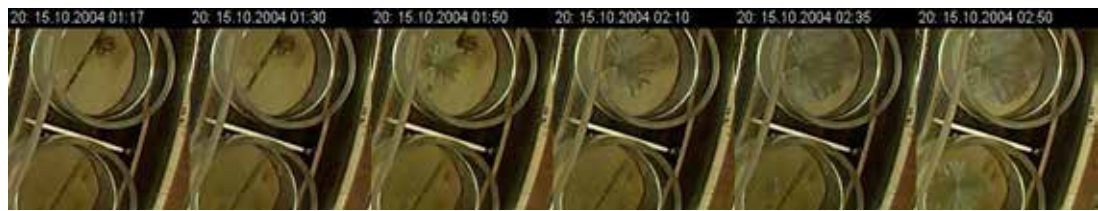
- Outer area: possible depletion and interaction with the rim.

The question is if the above defined areas are identical with the visually defined zones. In the next chapter, growth measurements are shown from which the identification would maybe be possible.

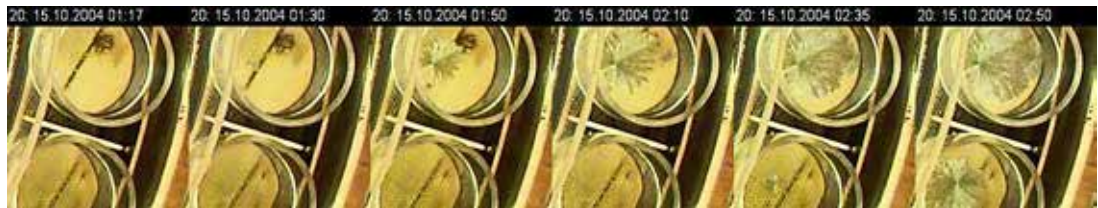
Observation of the growth

The growth of the crystallization was checked by following the crystallization coverage with a camera mounted on the ceiling of the crystallization chamber. Pictures were photographed every 10 minutes. In the beginning (around 2004), the camera system was not working stable, so the time differences between the pictures are more than 10 minutes. In the following, six photographs are shown. From left to right the time increases. The first picture on the left is the situation before the crystallization. The second picture includes the start of the crystallization ([tcrStart](#)), which is followed by the next four pictures.

After the end of the crystallization, the pictures were dried and scanned. For the scanning the crystallization center was oriented to 6 o'clock (downward). As a first comparison to the above assumption, we checked whether the DCC coverage looks circular over time.



Original Photos



Contrast increase pictures



Fig.1.13.9 Top: six successive time-lapse stills for series 2014.10.14.GJ, location no. 20, sample carrot H2. The stills were taken at 01:17, 01:30, 01:50, 02:10, 02:35, and 02:50. The crystallization starting time ([tcrStart](#)) is 1:30. The starting location is at 9 o'clock. The second center begins at 2:10 at the 2 o'clock position.

Bottom: scan of the final picture. Samples from University of Kassel (D), Witzenhausen, documented in BLE report O2OE170-2003 (Fleck Carrots 2004) [22].

And for a second picture



Original Photos



Contrast enhanced pictures



Fig. 1.13.10 Scanned crystallization picture for series 2004.10.14.GJ, location no. 16, sample carrot G1, tcr-Start after 13:10 h evaporation. Samples from University of Kassel (D), Witzenhausen, documented in BLE report O2OE170-2003 (Fleck Carrots 2004) [22].

As shown in Fig. 1.13.10 for the Fleck Carrot 2004 series, the assumption of a circular growth could be falsified. Not only one dimension has to be measured but at least two, the largest diameter and the smallest diameter. See [Appendix 1.13.1 Ring](#), *ipv.* Fig. 1.13.14 for an illustration of the visual determination of the images shown in Fig. 1.13.9 and 1.13.10.

For another series in 2005.09.06.GI (freeze dried carrot and freeze dried wheat) the dimensions of the crystal covered surface were quantified. Some pictures were observed that did not grow in a circular fashion, but in a different way. The development of the coverage of these pictures is shown in Fig. 1.13.11. The crystal covered area was determined by visual measurements. To overcome the asymmetric behavior, the minimum and maximum diameters were taken. This was done with a ruler (by A. Konzi) on the computer screen. The surface was calculated by the product of the minimum and the maximum values. The measure of a mean diameter of the crystal covered surface was calculated by the $\sqrt{\text{min} \cdot \text{max}}$, because the form is close to a circle. This mean diameter value as a percentage of the total dish diameter was plotted against evaporation time for each of the 43 positions in the chamber in Fig. 1.13.11.

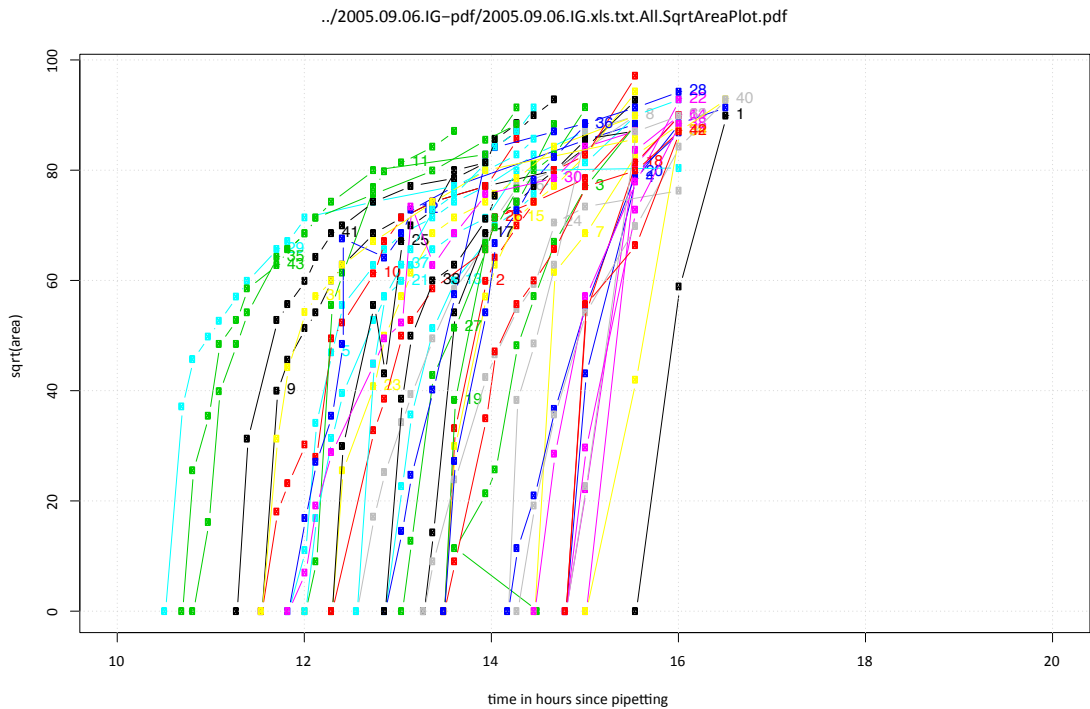


Fig.1.13.11 X-axis: mean diameter of crystal covered area (as a percentage of total dish area) versus time since pipetting (X-axis) for all 43 chamber positions. Different colors and numbers represent the different locations in the chamber. Crystallization starts at the point where the Y-axis is zero. Data are from University of Kassel (D), Witzenhausen, Series IG (freeze dried wheat and freeze dried carrot).

Starting from the leftmost cyan colored curve (dish no. 29), the start of the crystallization is where the value on the Y-axis is zero. This is for this curve around 10:45 hours after pipetting. Up to 40 % of the total dish area, the diameter of the area (Y-axis) grows very fast in relation to the slowdown when it reaches 70 % at 12:00 and 80 % after 14 hours. The other positions, where the crystallization starts later (more to the right on the X-axis) are showing a similar behavior, first growing very fast, then slowing down and entering into a asymptotic behavior, which is similar for all crystals regardless of crystallization starting time. This supports the above hypothesis that there is first a rapid growth within a supersaturated area, followed by a slower growth due to following a saturation border. The supersaturated area increases with time since pipetting.

Case Dewetting after crystallization

There are (surface tension) forces due to the concentration gradient which seem to be enlarged by the start of the crystallization [23]. This forces dewetting after crystallization [17], which is visible during the evaporation as a needle-free zone between the area covered by the crystal and the rim of the Petri-dish.

For BSA it was observed that at low DCC amounts (< 70 mg per plate), the solution disappears at the meniscus before dewetting begins [17]. For DCC amounts higher than 70 mg per plate there is still solution at the rim after the dewetting. For DCC amounts higher than 170 mg per plate, the final crystallization from the rim will overgrow the previously needle-free zone and the already existing crystal [17] (supplementary information). The zonal structure is then disturbed.

The DCC pictures from carrot juices are so far not showing this phenomenon. It is also known for PVP (Busscher 2010 [19] Fig. 6, and supplementary information Fig. 15 [see here Fig. 1.13.12]) and for wheat in some cases (Fritz2018 [24], Fig. 1). The BSA measurements suggest that this is a matrix effect related to the surface tension of the pipetted solution [19].

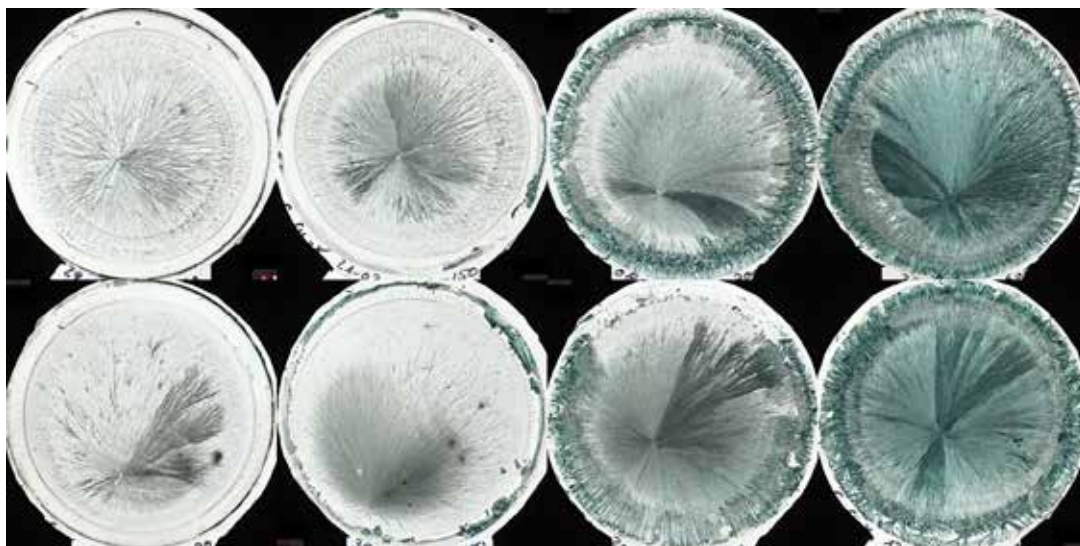


Fig. 1.13.12 Overgrowth after dewetting, Each column displays two plate replicates for the DCC concentrations, arranged from left to right: 90, 150, 300, and 600 mg DCC per plate with 0.2 mg PVP as additive. For the DCC amount of 300 and 600 mg the overgrowth after dewetting is visible. Data from Busscher 2010 [19] supplementary information, Fig.15.

In the case of no overgrowth, dewetting after crystallization disconnects the final crystallization picture from the interaction with the rim. If three zones are visible, the inner and middle zone may be comparable to the case of no dewetting, but in case of dewetting after crystallization the outer zone has completely different boundary conditions. This changes the evaporation conditions of the meniscus, in the case of dewetting after crystallization, to those of a sessile drop. See also chapter [1.5 Meniscus breakdown](#) and chapter [2.8 Dewetting by crystallization](#).

In the case of overgrowth, the final DCC image is not easy to evaluate because the percentage of overgrowth is not easy to determine.

Looking at the zones through Petterson's perspective, the DCC picture in Fig. 1.13.10 shows clear stems in the inner zone and substance spirals in the outer zone. This could be explained by the assumption that some of the additive is expelled outside the crystal area and moved to the outer zone, creating a higher additive concentration there. The appearance of the substance spirals can be seen in the matrix at higher additive levels. In the outer zone the effect of the increasing substance amount will show up first, which is supported by the fact that the substance spirals are first seen in the outer zone. See also chapter [1.10 Transition between different areas](#).

Resume

The zonal concept has been used by many authors. When sorting out the dewetting effects, the visually recognizable zones and the areas understandable from the evaporation and from the crystallization process seem to be in close proximity to each other. Further research will have to show whether they are identical. Petterson's idea that there is more additive in the outer zone is supported by visual evidence.

Additional research

The time resolution measurements of the coverage of the Petri-dish with DCC should be made for the time lap stills (photos) of the BSA pictures. Also for new pictures which are photographed with a higher resolution. Compare whether the transition from fast to slow crystal growth is identical to the boundary between the visually determined inner and the middle zones.

From a visual evaluation perspective, the border between the middle and the outer zone can be easier identified in Fig. 1.13.9 than in Fig. 1.13.10, but there is still no clear definition.

The border between the inner and the middle zone it not so simple to recognize and needs more work on the definition. With the CrystEval program (See chapter [3.3 Crysteval tool](#)), the technical evaluation of the scanned and photographed pictures is already prepared with the ring1, ring2 and ring3 options. See for an example in Appendix 1.13.1 Ring below.

To research the idea of Petterson, the distribution of the amounts of additive and DCC through the

Petri-dish could be measured by absorbance measurements. The relation between the RGB signal should be unique for DCC and the additive. The problem is the change in absorbance due to a change in the crystal type, e.g. found for the BSA pictures.

The other idea of Petterson is that in the outer zones the effect of the increasing substance amount will show up first. The substance spirals are e.g. first seen in the outer zones. This can be tested as a general hypothesis, that in the concentration matrix, when increasing the additive amount, at the border between two crystallization types, the new crystallization type will first appear in the outer zones. See also chapter [1.10 Transition between different area](#)).

Appendix 1.13.1 Ring

Fig. 1.13.13 below is taken from the ProPar report no. 1 (2015 [25]). It should indicate the option to measure the ring1 (border inner middle zone) and the ring2 (border between middle zone and outer zone). The criteria for the borders need more discussion.

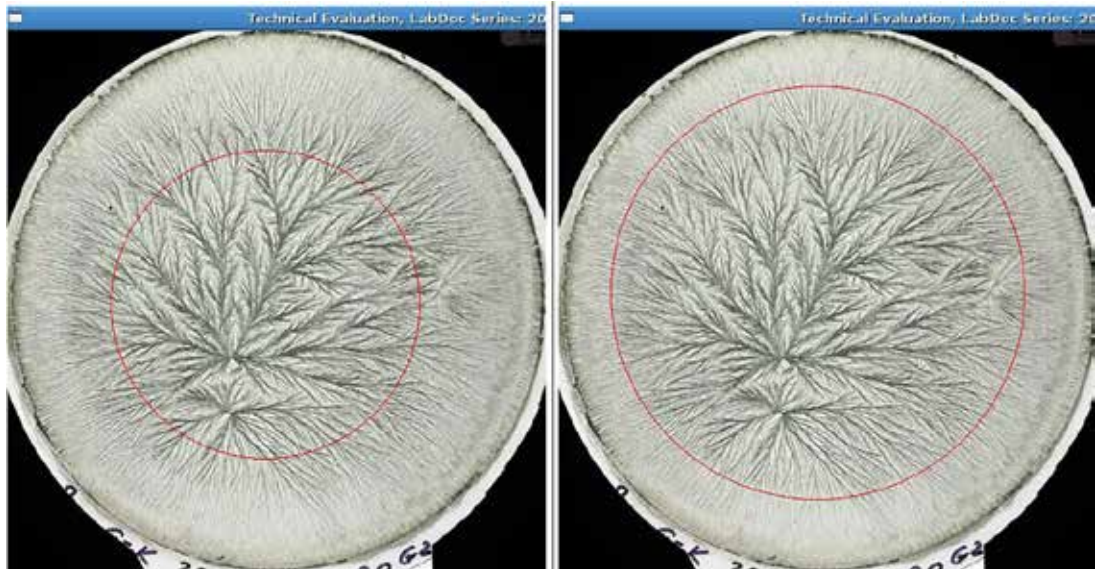


Fig. 1.13.13 Illustration of the inner and middle zone as marked in the LabDoc program (in future this will be done in the CrystEval program). Left : border between inner and middle zone (at $r = 57\%$) called ring1. Right: border between the middle and outer zone (at $r = 77\%$) called ring 2.

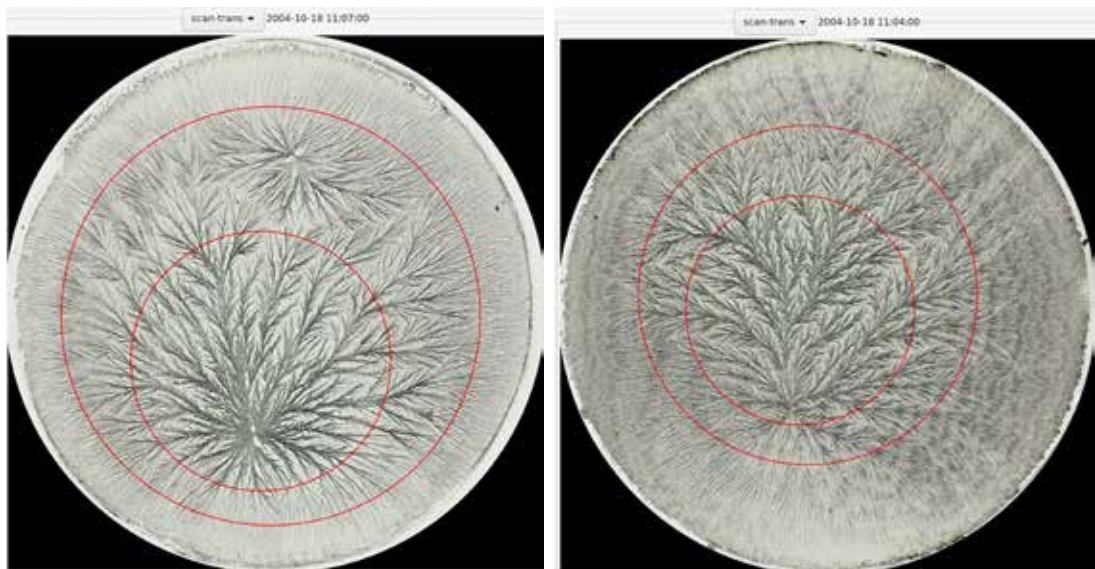


Fig. 1.13.14 Visually determined borders of inner and outer zone for pictures described in Fig. 1.13.9 (bottom) and 1.13.10 (bottom). Here circles are used. An elliptic approach would fit better for Fig. 1.13.10 (bottom).

Appendix 1.13.2 Image analysis

From ProPar report nr 2 (2016 [26]).
Evaluation of Slices ROI's.

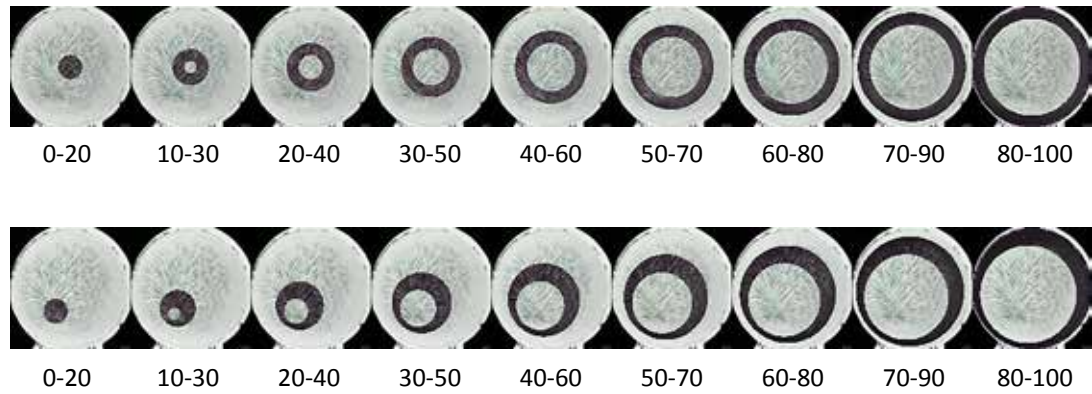


Fig. 1.13.15 From left to right. The darkened area is showing the increasing slices oriented around the geometric- (upper row, set 3) or crystallization-center (lower row, set 6). The inner and outer [radius](#) is in percentage of total picture radius.

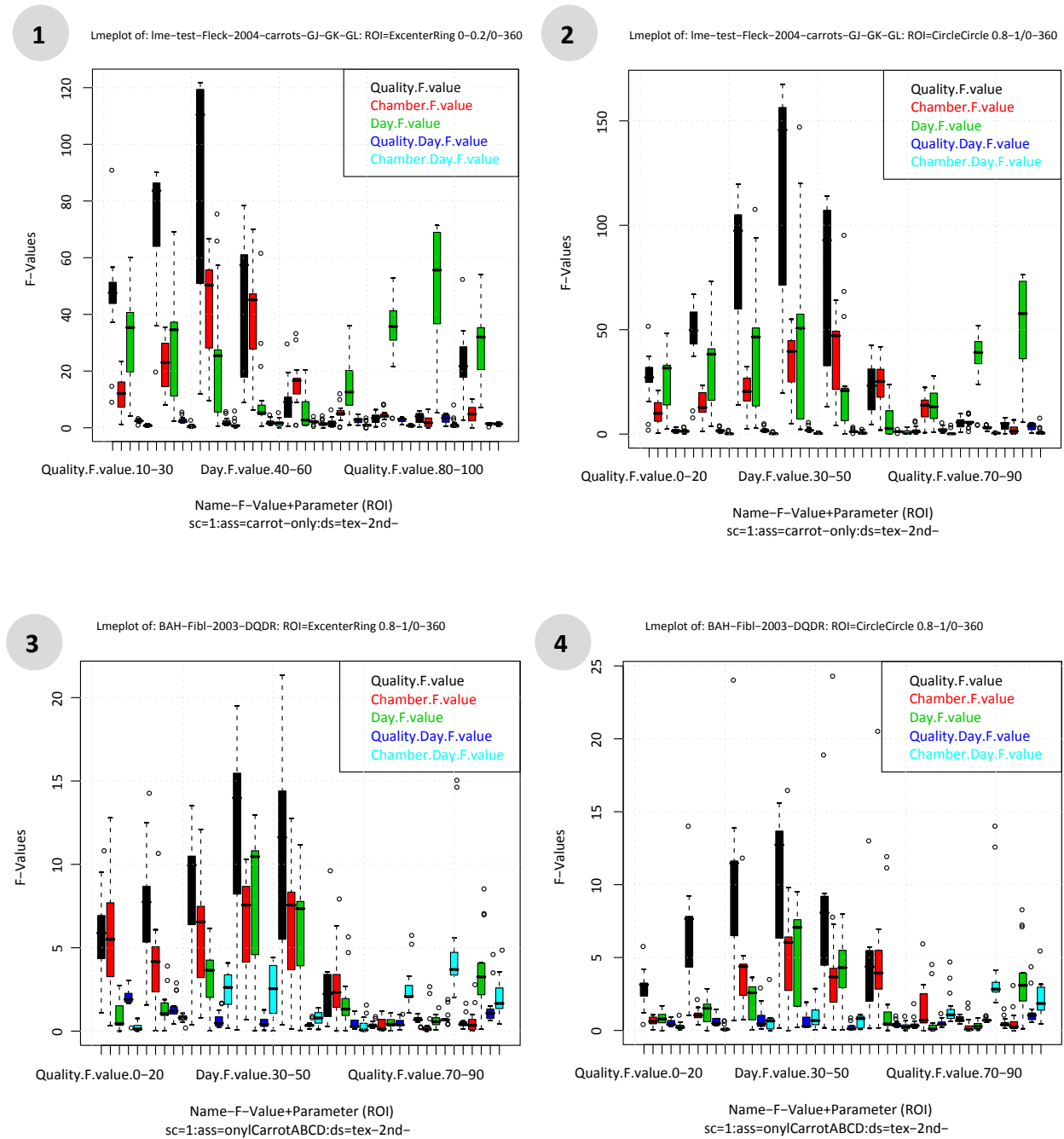


Fig. 1.13.16 Y-axis: Separated F values for Quality/Chamber/Days for all variables of the second order texture variables combined, versus the slice type ROI from 0-20%, 10-30, 20-40,... to 80-100% in steps of 10% (X-axis). Colors: Black: Quality, Red: Chamber, Green: Day effect. Figures 1 and 3 show F-values dependency on the ROI's oriented around the crystallization-start-center, figures 2 and 4 oriented around the geometric-center. Figures 1 and 2 data from Fleck 2004 carrots. Figures 3 and 4 same data from FIBL 2003 carrots.

The Quality factor (black) in Fig. 1.13.16 has a maximum at *radius* 30-50%. This is comparable to the Fleck 2004 carrots results. For the Fleck 2004 carrots (Fig. 1.13.16 -1, 2) for the *radius* > 60-80 the day effect (green) is dominating, which is not so strong for the FIBL 2003 carrots (Fig. 1.13.16-3, 4). The crystallization center oriented ROIs (Fig. 1.13.16-1,3) show for (3 FIBL2003) an increase in the chamber effect (red) for *radius* 0-20 to 40-60 and for (Fleck 2004) 30-50 and 40-60 in comparison to the geometric center orientation (2, 4). The maximum F-values at 30-50 are slightly higher for the crystallization-center orientation versus the geometric-center orientation for the FIBL carrots. More details can be found in the [ProPar](#) report no. 2 (2016 [26]).

References

- [1] Pfeiffer E. Empfindliche Kristallisationsvorgänge als Nachweis von Formkräften im Blut (Emil Weises Buchhandlung Dresden, 1935).
- [2] Selawry A and Selawry O. Die Kupferchlorid-Kristallisation in Naturwissenschaft und Medizin (Gustav-Fischer-Verlag, 1957).
- [3] Engquist M. Die Gestaltkräfte des Lebendigen (Vittorio Klostermann, 1970).
- [4] Pettersson BD. Beiträge zur Entwicklung der Kristallisationsmethode mit Kupferchlorid nach Pfeiffer IV. Wie verschiedene Kristallbilder bei der Pflanzenkristallisation entstehen. *Lebendige Erde* 1969; 3: 112-126.
- [5] Engquist M. Physische und lebensbildende Kräfte in der Pflanze (Vittorio Klostermann, 1975).
- [6] Schweizer F. Störungs- und Regenerationserscheinungen bei der Biokristallisation. *Elemente der Naturwissenschaft* 2013; 99: 5-20 <https://doi.org/10.18756/edn.99.5>.
- [7] Carstensen. JM. Description and Simulation of Visual Texture. PhD Thesis, Institute of Mathematical Statistics and Operations Research, Technical University of Denmark, Lyngby. 1992.
- [8] Andersen JO, Henriksen CB, Laursen J, Nielsen AA. Computerised image analysis of biocrystallograms originating from agricultural products. *Computers and Electronics in Agriculture* 1999; 22: 51-69 [https://doi.org/doi:10.1016/S0168-1699\(98\)00043-X](https://doi.org/doi:10.1016/S0168-1699(98)00043-X).
- [9] Doesburg P, Nierop AF. Development of a structure analysis algorithm on structures from $\text{CuCl}_2 \cdot 2\text{H}_2\text{O}$ crystallization with agricultural products. *Computers and Electronics in Agriculture* 2013; 90: 63-67 <https://doi.org/doi:10.1016/j.compag.2012.11.003>.
- [10] Koopmans A. Die Frage der Lokalisation im Kupferchlorid-Kristallisationsbild. *Elemente der Naturwissenschaft* 1971; 14: 19-30 <https://doi.org/10.18756/edn.14.19>.
- [11] Nickel E. Die Reproduzierbarkeit der sogenannten empfindlichen Kupferchloridkristallisation. PhD Thesis, Universitätsverlag, Freiburg (Schweiz). 1968.
- [12] Selawry A. Neue Einblicke in die Samenkeimung (Naturwissenschaftliche Sektion am Goetheanum Dornach (CH), 1961).
- [13] Selawry A. Samenkeimung und Metallpotenzen im Kristallisationstest (Forschungsring für biologisch-dynamische Wirtschaftsweise, 1975).
- [14] Koepf H, Selawry A. Application of the diagnostic-crystallization method for investigation of food and fodder. *Bio-dynamics* 1962; 64.
- [15] Kahl, J.; Busscher, N. and Meier-Ploeger, A. Ganzheitliche Untersuchungsmethoden zur Erfassung und Prüfung der Qualität ökologischer Lebensmittel: Stand der Entwicklung und Validierung, Abschlußbericht Projekt 02OE170, 2003 .
- [16] Arncken, C. Möhren: Populations- und Hybridsorten im Vergleich, Vortragstagung der Deutschen Gesellschaft für Qualitätsforschung (Pflanzliche Nahrungsmittel) DGQ e.V. – Qualität, Frische und Sicherheit pflanzlicher Lebensmittel aus ökologischer und traditioneller Produktion, Agroscope Changins-Wädenswil, 20.-21. März 2006.
- [17] Busscher N, Doesburg P, Mergardt G, Sokol A, Kahl J, Ploeger A. Influence of dewetting on the crystallization behavior of CuCl_2 in the presence of BSA during evaporation in a Petri dish. *Heliyon* 2019; 5: e01102 <https://doi.org/10.1016/j.heliyon.2018.e01102>.
- [18] Gallinet JP, Gauthier-Manuel B. Wetting of a glass surface by protein adsorption induces the crystallization of an aqueous cupric chloride solution. *Journal of Colloid and Interface Science* 1992; 148: 155-159 [https://doi.org/doi:10.1016/0021-9797\(92\)90123-4](https://doi.org/doi:10.1016/0021-9797(92)90123-4).
- [19] Busscher N, Kahl J, Doesburg P, Mergardt G, Ploeger A. Evaporation influences on the crystallization of an aqueous dihydrate cupric chloride solution with additives. *Journal of Colloid and Interface Science* 2010; 344: 556–562 <https://doi.org/doi:10.1016/j.jcis.2009.12.045>.
- [20] Beckmann H. Über Keimbildung, Einkristallwachstum und Auffächerungswachstum von $\text{CuCl}_2 \cdot 2\text{H}_2\text{O}$ in reinwässrigen und Eiweiß-haltigen Lösungen. PhD Thesis, Universität Bonn. 1959.
- [21] Leray JL. Growth kinetics of hydrated cupric chloride. *Journal of Crystal Growth* 1968; 3-4: 344-349 [https://doi.org/DOI:10.1016/0022-0248\(68\)90172-3](https://doi.org/DOI:10.1016/0022-0248(68)90172-3).
- [22] Kahl, J.; Busscher, N. and Meier-Ploeger, A. Differenzierung und Klassifizierung von Öko-Produkten mittels validierter analytischer und ganzheitlicher Methoden, Abschlussbericht zum Projekt Nr. 02OE170/F2, 2007.
- [23] Habibi M, Rahimzadeh A, Eslamian M. On dewetting of thin films due to crystallization (crystallization dewetting). *Eur. Phys. J. E* 2016; 39: 30 <https://doi.org/doi:10.1140/epje/i2016-16030-9>.
- [24] Fritz J, Athmann M, Andersen J-O, Doesburg P, Geier U, Mergardt G. Advanced panel training on visual Gestalt evaluation of biocrystallization images: ranking wheat samples from different extract decomposition stages and different production systems. *Biological Agriculture & Horticulture* 2018; 35: 1-12 <https://doi.org/doi:10.1080/01448765.2018.1492457>.
- [25] Busscher, N. and Doesburg, P. ProPar Project Report 2015.1, 2015.
- [26] Busscher, N. and Doesburg, P. ProPar Project Report 2016.1, 2016.

1.14 Chamber reset

Abstract

The conditions for an experiment should always be the same. The crystallization starting time ([tcrStart](#)) strongly depends on the climatic conditions in the inner chamber at the beginning of an experiment. The problem is how to reset the climate in the chamber after an experiment so that the following experiment is not affected by the previous one. Secondly, how to handle the influence of the person (breathing etc.) pipetting the solutions into the Petri-dishes inside the inner chamber. Several approaches to deal with this problem are described.

Introduction

The climatic conditions at the beginning of an experiment in the [inner chamber](#) should always be the same. In the following, first the conditions for a Triangle chamber are described, later this is extended to other chamber types.

The problems associated with starting an experiment can be divided into two parts. 1) the climatic conditions before and 2) after a person has entered the evaporation chamber, because a person must enter the chamber and pipette the solutions to start an experiment.

(1) The climatic conditions before a person enters the chamber for an experiment are in most cases dependent on how the climatic changes from a previous experiment are resolved. This not only includes the temperature and humidity inside the chamber (1.1), but also the condition of the chamber walls (1.2). The condition of the chamber walls defines the permeability for the humidity transfer from the inner to the outer chamber, and with this the dynamic of the evaporation system.

(2) The climatic conditions when a person enters the inner chamber to pipette the solutions into the Petri-dishes consists of three parts. First (2.1) the humidity and temperature in the chamber decrease due to the opening of the chamber door. Then (2.2) the humidity and the temperature increase because the person is breathing and sweating (in the closed inner chamber). Finally (2.3), the door is opened again, and humidity and temperature decrease once again. Different solutions were found to solve the two main problems. If possible the influences will be quantified and discussed. The results were used to look at other chamber systems.

Historical overview

Pfeiffer was already describing (1935 [1], p. 62) the importance of ventilation (*“gut lüften”*) between experiments. This was repeated by Selawry (1957 [2], p. 7) describing the use of air fans with a power of 30 m³/hour in the case of intensive use of the chambers.

Authors measurements

Table 1.14.1 summarizes the two problems described in the Introduction regarding the climatic conditions in the inner chamber (first two columns) and the sections in this chapter where possible solutions are proposed (3rd column).

Table 1.14.1 Solution of the Problems for case 1 and 2.

Case	What	Possible solutions
1. Restore conditions after an experiment	(1.1) temperature and humidity inside the chamber.	Climate reset after an experiment
	(1.2) condition of the chamber walls.	Climate reset after an experiment
2. Handle pipetting influences	2.1) humidity and temperature in the chamber decrease due to entering the chamber.	Covering positions with plates
	2.2) humidity and temperature increase due to respiration and sweating.	Defined door open time after pipetting
	2.3) humidity and temperature in the chamber decrease a 2 nd time due to exiting the chamber.	Dehumidifier in the chamber
		Defined pipetting time. Open door until humidity (e.g. above dishes) drops below threshold.

Climate reset after an experiment

In the Checking Influences project (2009 [3]) different reset times were tested. The experiments were done with water in the Petri-dishes in the Louis Bolk Institute (NL) Chamber D.

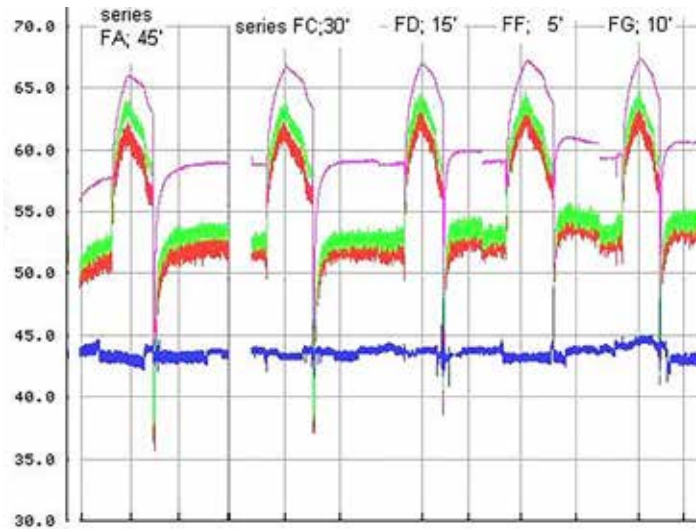


Fig. 1.14.1 Response of chamber humidity (Y-axis) to different lengths of time (X-axis) the chamber door is left open to recover the chamber humidity after an experiment. One step in the time grid corresponds to 20 hours. Results from 5 series are plotted. Reset times from left to right: 45 min, 30 min, 15 min, 5 min, 10 min. Colors: blue humidity in the outer chamber, red and green above the dishes, magenta at the inner wall. Data from the Louis Bolk Institute (NL) 2007/2008 chamber D.

In Fig. 1.14.1 concerning the recovery time, 45 min reset time resulted in a very slow recovery. For 5 minutes (2nd from the right) the recovery gave an over-swing. For 10 min (far right) the recovery to a constant value was rapid. 30 and 15 minutes also looked quite good. From the point of reaching the same value as before the 30 min looks the best.

Covering positions with plates

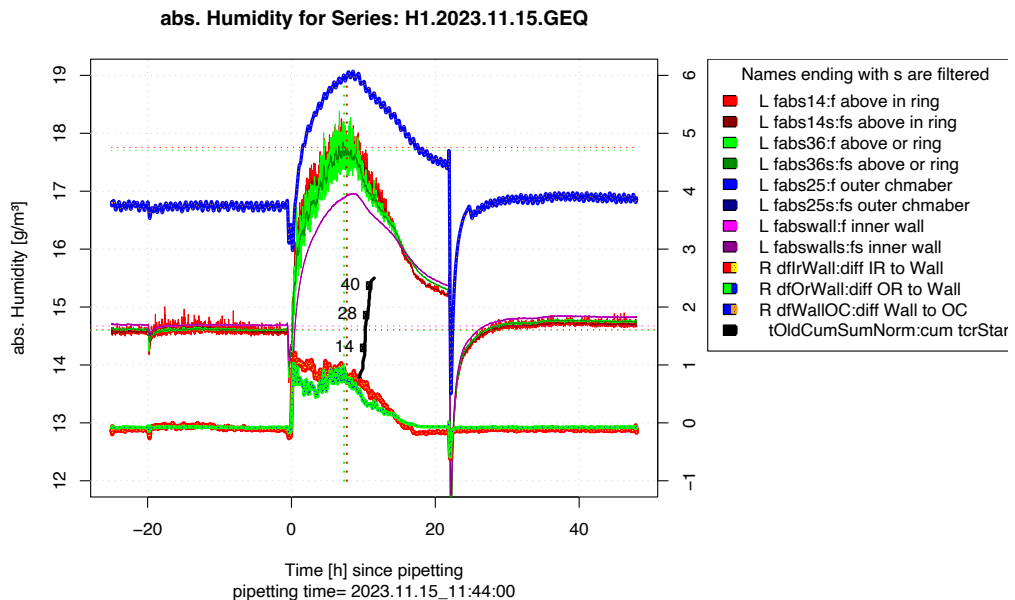


Fig. 1.14.2 Absolute humidity in g/m^3 (left Y-axis) versus the time in hours (X-axis). Pipetting at $t = 0$ h. Pipetting duration ~ 10 minutes. The humidity above the dishes is indicated by the green and red lines starting at $\sim 14.5 \text{ g}/\text{m}^3$ at $t = -25$ h, with a maximum at $t = 9$ h, and then decreasing. After pipetting the solutions, the chamber door is left open for 30". Reset (opening the chamber door) is at $t = 22$ h for 20 min. Green-blue and red-yellow (lower lines) and blue-orange lines are calculated differences (right Y-axis) and not discussed here. The black line is the cumulative number of crystallizations started.

Fig. 1.14.2 is an example of the absolute humidity development in a Triangle chamber, showing that the reset function is working quite well. The humidity after the reset (door open) is slightly higher than before the pipetting. This is achieved when a chamber reset of 20 min is commenced between 22 - 25 hours after pipetting. Additionally, the six positions below which the heating sensors of the inner and outer ring are located are covered with glass plates between experiments. This ensures that the sensors and the heating conditions are essentially the same whether an experiment is running or not.

Dehumidifier in the chamber

Experiments were performed with a dehumidifier in the chamber, to regulate the humidity until the pipetting was complete. This was done from 03.06.2015 onward in Roepaen (NL) chamber P. The tcrStart values were still showing a sample variation. There was no clear advantage or disadvantage visible. There were problems with heating due to the dehumidifier.

Defined door open time after pipetting

In [Appendix 1.14.1 Breathing](#) (breathing) and [Appendix 1.14.2 CO₂](#) (CO₂ measurements) some preliminary results were obtained estimating the change in the chamber due to respiration at or below 1 % relative humidity. In [Appendix 1.14.1 Breathing](#) the influence of different breathing frequencies on the humidity of the chamber is determined. In [Appendix 1.14.2 CO₂](#), based on the CO₂ measurements, the frequency of breathing was estimated to be 8 L / min or less. From [Appendix 1.14.1 Breathing](#), this results in an increase of roughly 1 % relative humidity due to breathing.

Earlier measurements made on 18.03.2011 in BRAD (DK) while working in the chamber without pipetting showed a maximum influence on the relative humidity of 0.5 % to 1 %. It seems that the chamber recovers quite quickly from the opening of the door, probably due to the presence of the water reservoir in the inner chamber.

A practical approach is to open the chamber door after pipetting, wait until a defined humidity level is reached, and then close the door. In doing so, one can say that the experiment always starts with the same conditions. The time that the door is opened (max 1 - 2 minutes) is not a lot in comparison to the overall time until the crystallization begins (10 hours). The problem is that opening the door not only removes the additional humidity from the breathing, but also the evaporated humidity from the dishes. So far the amount of removed humidity that would reduce the tcrStart cannot be estimated.

System in Forschungsring Darmstadt

The system in Forschungsring Darmstadt has a different approach. The chamber has no internal heating and no humidity reservoir. When no experiments are running, the door is open and the outer chamber heater and humidifier are turned off. Three days before an experiment the acclimatization is switched on. The chamber door is kept open. After the dishes are placed and the solutions are pipetted the door is closed until the crystallization is finished. The crystallization starting time is ~ 30 hours. See for more information about the systems in chapter [3.1 Chamber systems](#).

System in University of Bonn

Here the air, which passes through the room where the dishes are placed, has a defined temperature (30 °C) and humidity. This makes the system independent from the permeability of the chamber walls and the summer/winter climatic conditions. The system at the University of Bonn regulated the temperature and humidity by an active airflow through the inner chamber. The crystallization starting time was between 12 and 16 hours.

Both the systems at Forschungsring Darmstadt and University of Bonn open the chamber door after pipetting, wait until a defined humidity level is reached, and then close the door.

Dornach Topf System

Here the air, which passes through the space where the dishes are placed, has a defined humidity (dried air, through a silica-gel humidity exchange). Heating is from below, integrated in the Topf. This makes the system independent from the permeability of the chamber walls and the summer/winter climatic conditions. The Dornach Topf system is described in Koopmans (1971 [4], p. 6). The crystallization starting time is between 12 and 16 hours.

However, for most systems it is reported that after an experiment-free period (from 2 - 4 weeks onwards), the system needs at least one pre-run before working in the usual manner, as can be seen from the tcrStart. This question is discussed in chapter [1.11 Wetting up phase](#). See for more information about the systems in chapter [3.1 Chamber systems](#).

Resume

There is room for improvement in the handling of experimental conditions. The humidity influence of the previous experiment can be neutralized by resetting the chamber in a defined manner. The best strategy for dealing with the breathing humidity of the person pipetting the dishes is not clear. CO₂ measurements show that there is an effect on the humidity in the chamber. How this is balanced by the opening of the door, by entering and leaving the chamber, is not clear. It is not clear whether any specific action is required, such as opening the door after pipetting for a defined length of time to reduce additional humidity.

Additional research

- Calibrate the breathing and the CO₂ measurements per person in the chamber.
 - Place a simple measurement tool for CO₂ and atmospheric pressure / volatile organic compounds (VOC).
- Check to see if the reservoir can compensate for opening the chamber door.
- Test the reset effect with DCC solutions and different chamber door opening times
- Extend the existing model by adding a parameter to simulate the reset question.
 - What is the influence of the reservoir in connection with the opening of the door?
- Extend the existing model by adding a parameter to simulate the opening of the chamber door after pipetting.
 - How much humidity leaves the chamber?
- Extend the existing model with the effects from the temperature simulation.
- Use the CO₂ signal decay during an experiment to check for the “tightness” of the chamber.
- How large are the changes in tcrStart when in Darmstadt 43 instead of 52 pictures are used?
- How high is increase of the tcrStart when in the Triangle system 7, 8, 9, 10, 12, 14 mL instead of 6 mL is pipetted. Is the evaporation volume critical?

Appendix 1.14.1 Breathing

Calculate the amount of water exhaled in the inner chamber.

According to Kamke (1994 [5], p. 249) the exhaled air (*Ausatmungsluft*) has a defined water content. It depends on the partial pressure of water at 37 °C in the lungs. The partial pressure is 62.74 mbar with a density of 43.84 g/m³ (from Baehr 1961 [6], Table 2). The conditions of the inhaled air during pipetting are those of the chamber (30 °C and 50 % relative humidity). This gives a partial pressure of 42.42 mbar and a density of 30.32 g/m³ for 100 % rel. humidity (from Baehr 1961 [6], Table 2). At 50 % rel. humidity the density is 30.32 / 2 = 15.16 g/m³.

For the additional water the difference is calculated as:

$$43.84 - 15.16 = 28.68 \text{ g/m}^3$$

The breathing of a human being is according to Pleil (2021 [7], Table 1) between 6 L/min for a passive person, e.g. at rest, 16 L/min for normal activity and 40 L/min for moderate activity. The calculation of the additional amount of water exhaled by 15 min breathing is listed in Table 1.14.2 and calculated according to the formula:

$$\text{added water} = 28.68 / 1000 * \text{Breathing Rate} * 15 \text{ min} \quad (1000 \text{ L} \equiv 1 \text{ m}^3)$$

Table 1.14.2 Additional water amount from a pipetting person in the chamber at 30 °C and 50 % relative humidity at different breathing rates.

Activity	Breathing rate	Added water amount in 15 minutes
At rest	6 L/min	2.5 g
	8 L/min	3.4 g
Normal activity	16 L/min	6.8 g
Moderate activity	40 L/min	17.2 g

Working in the 30 °C chamber is considered normal to moderate activity. The amount of 6.8 g corresponds to the water evaporating from one dish (~ 5.5 gram to evaporate). 17.2 g corresponds roughly to three dishes extra in the chamber. To calculate the change in relative humidity in the chamber when 1, 2 or three additional dishes are added at 50 % relative humidity, the calculations of Baehr (Baehr 1961, Table 2) are used (the amount of humidity in a 10 m³ chamber at 50 % rel. humidity at 30 °C is 150 g).

$$\text{Rel. humidity} = (150 \text{ g} + \text{add amount}) / 150 * 50$$

Table 1.14.3 Change of the rel. humidity in the evaporation chamber, when different amounts of humidity are added due to respiration.

Added water due to respiration	rel. humidity
3.4 g	51.1 %
5.5 g	51.8 %
11 g	53.6 %
16.5 g	55.5 %

Appendix 1.14.2 CO₂

The following are preliminary results of CO₂ measurements. The instrument is under development.

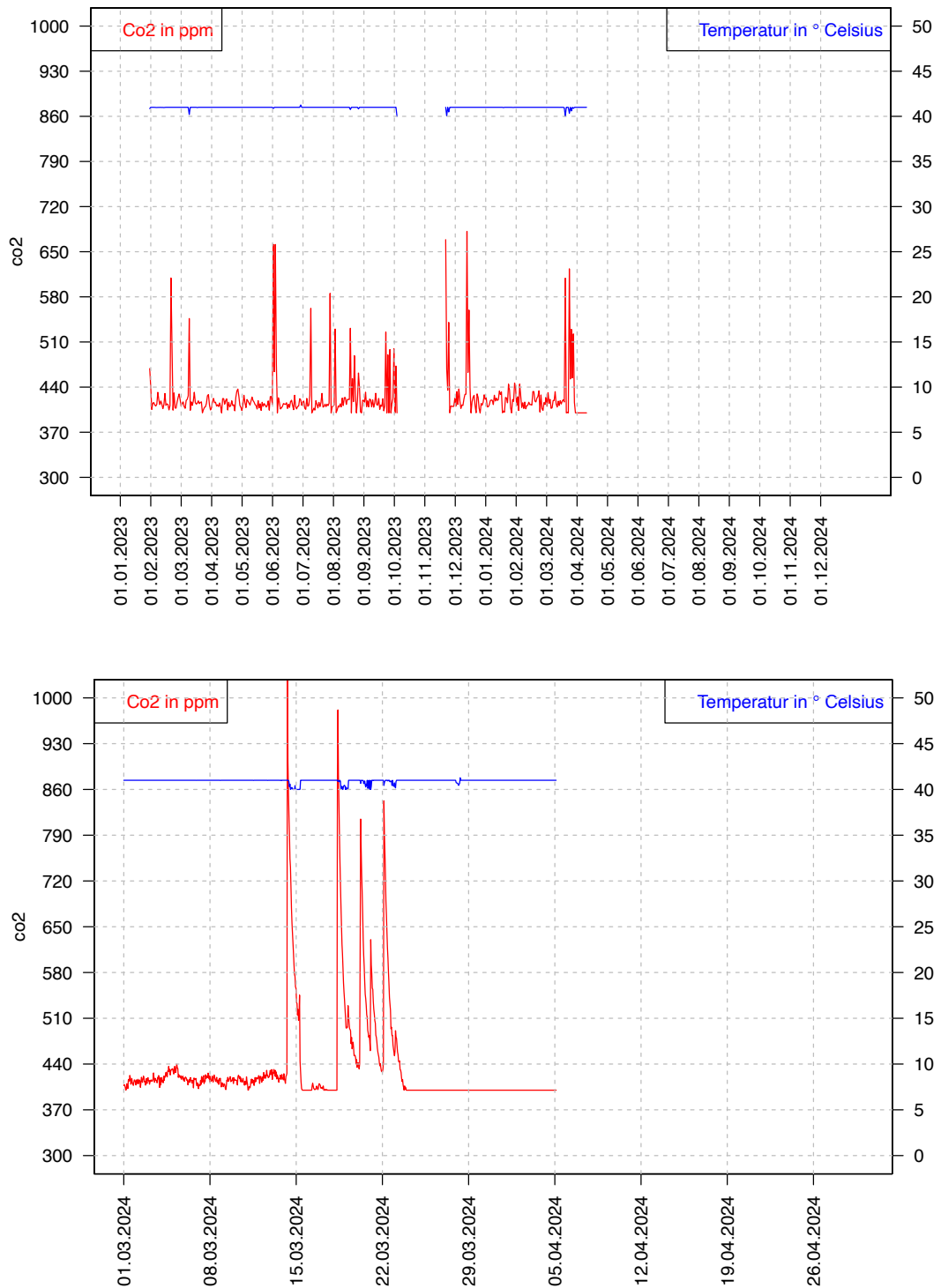


Fig. 1.14.3 Top: CO₂ (Y-axis) values in ppm versus the time (X-axis, 2 years). Bottom: CO₂ (Y-axis) values in ppm versus the time (X-axis, 2 months). Data from University of Kassel (D) chamber C from 2023 and 2024. Differences in peak heights are due to filtering. The upper plot is using 1-day averaged data. In the lower plot the data are averaged over 1 hour. Baseline is around 420 ppm.

In Fig. 1.14.3 upper it is obvious that the breathing of a person, when pipetting solutions in the chamber, is visible in the CO₂ measurement data. In Fig. 1.14.3 lower, the spikes are up to 1000 ppm CO₂, because the data filtering is per hour and not, as in the upper figure, per day. The amount of CO₂ added due to breathing is between (650 – 420 = 230 ppm) to (1000 – 420 = 580 ppm).

The amount of CO₂ expelled per breath is approximately 40 - 50 mL of CO₂ per 1 L of air (5 % according to Pleil [7], p. 7). The breathing rate (see Appendix 1.14.1 Breathing) is according to Pleil (2021 [7], p. 6 Table 1) between 6 to 40 L/min.

If the volume of the chamber is assumed to be 10 m³ = 10,000 L, then the amount of CO₂ for 15 min of breathing is given by the formula:

$$\text{additional CO}_2 = 40 \text{ mL/L} / 10000 \text{ L} * 15 \text{ min} * \text{breath rate}$$

Table 1.14.4 Exhaled CO₂ amount in ppm versus the breath rate of a person working in the chamber for 15 minutes.

Activity	Breath rate	Additional CO ₂ in 15 min.
At rest	4 L / min	240 ppm
	8 L /min	480 ppm
	11.3 L / min	680 ppm
Normal activity	16 L /min	960 ppm

The respiratory rate of a person at rest and during normal activity is approximately 8 L/min or less according to Table 1.14.4 and the data in Fig. 1.14.3 (230 to 680 ppm). This would give according to Table 1.14.3 a 1 % increase or less of the relative humidity due to breathing.

References

- [1] Pfeiffer E. Empfindliche Kristallisationsvorgänge als Nachweis von Formkräften im Blut (Emil Weises Buchhandlung Dresden, 1935).
- [2] Selawry A and Selawry O. Die Kupferchlorid-Kristallisation in Naturwissenschaft und Medizin (Gustav-Fischer-Verlag, 1957).
- [3] Busscher, N. Checking Influences: Untersuchung der Einflussgrößen bei der Biokristallisation als Voraussetzung für die Übertragbarkeit der Kammern und Prozeduren in andere Laboratorien und zur Reduzierung der Variationen durch die Kammer und die Orte, 2009.
- [4] Koopmans A. Die Frage der Lokalisation im Kupferchlorid-Kristallisationsbild. *Elemente der Naturwissenschaft* 1971; 14: 19-30 <https://doi.org/10.18756/edn.14.19>.
- [5] Kamke D and Walcher W. Physik für Mediziner (B. G. Teubner Stuttgart, 1994).
- [6] Baehr HD. Mollier-i, x-Diagramme für feuchte Luft: in den Einheiten des Internationalen Einheitensystems (German Edition) (Springer, 1961).
- [7] Pleil JD, Wallace MAG, Davis MD, Matty CM. The physics of human breathing: flow, timing, volume, and pressure parameters for normal, on-demand, and ventilator respiration. *Journal of Breath Research* 2021; 15: 042002 <https://doi.org/10.1088/1752-7163/ac2589>.

CHAPTER 2

THEORETICAL CONSIDERATIONS

Steps to understanding the DCC picture building process

2.0 Steps to understanding the DCC picture building process

The [2.1 State of the art](#) chapter summarizes the current knowledge of the $\text{CuCl}_2 \cdot 2\text{H}_2\text{O}$ (cupric chloride di-hydrate, further called DCC) picture as a result of the building process. Following Bessenich (1951 [1], p. 31), the building process is described by the name [arrangement](#) of the needles (see for more details in chapter [2.2 Arrangement](#)). The underlying basic process of branching is described in the chapter [2.3 Crystal growth and branching](#). Until now there are around 10 different hypotheses describing how the needles could be arranged in the picture facilitating the perception of a Gestalt. The hypotheses can be roughly divided into three groups related to the start of crystallization ([2.11 Nucleation](#)), namely before (b), during (n), or after (a).

The hypotheses (b), (n), (a) are considered in a broader context in the chapter [2.2 Arrangement](#).

Before nucleation:

- b.1. [Wachstumsfeld](#) ("growth field", see chapter [2.4 Concentration gradient](#) during evaporation and chapter [2.13 Evaporation model](#)).
- b.2. Maragoni forces: (surface tension due to concentration and temperature gradient during evaporation).
- b.3. Amount versus viscosity (influence of the viscosity on the building process).
- b.4. Chapter [2.10 Evaporation vorbild](#) (temperature structure on the surface during evaporation).
- b.5. Additive gradient (separation of the additive into different fractions).
- b.6. Protein *Vorbild* (nothing visible for juices).
- b.7. Phase separation (Entmischung) during evaporation?

During nucleation:

- n.1. Chapter [2.11 Nucleation](#) depending on "particles" (heterogeneous crystallization) or not (apple juice turbid/clear crystallization starting time).
- n.2. Chapter [2.6 Branching due to molweight](#) (see also chapter [2.3 Growth and branching](#)).
- n.3. Meso-crystals. DCC needles are built from smaller (nano) blocks.
- n.4. Chapter [2.9 Additive built into \$\text{CuCl}_2 \cdot 2\text{H}_2\text{O}\$?](#)

After nucleation:

- a.1. Chapter [2.5 Warmth of process](#) (warmth during crystallization used for the arrangement?).
- a.2. Entropy concept (ternary mixture water, DCC and additive).
- a.3. L+/L- enantiomer mixtures (malic acid, breakdown of crystallization).
- a.4. Dewetting by crystallization (see chapter [2.8 Dewetting by crystallization](#)).
- a.5. Chapter [2.12 Light polarization effect](#) (chiral effects ?)

General Concepts describing Complex Behavior

In the context of the building process, there are concepts in the natural sciences that describe complex behavior. One of the concepts is described in the chapter [2.14 Self organisation and \$\text{CuCl}_2\$](#) . The needles are built by a self-organizations process. However, the process underlying the arrangement of the needles is not known, so it cannot be decided whether the arrangement of the needles is a self-organization process.

From the human Gestalt evaluation of the DCC pictures, the question arises as to why the arranged needles are evaluated as representing a biological structure. This question is discussed in chapter [2.16 Complex physical versus simple biological](#) whether the DCC system is a simple biological system or a complex physico-chemical system. The question could not be answered, but there are different aspects that the DCC system with additives has in common with a biological system.

Related to the above is the question of how to understand the formation of an integrated pattern from the perceptual side. This is discussed in chapter [2.15 Formation integrated pattern](#). The question how to sort the variations of the DCC system into disturbances and degree of freedom is discussed in chapter [2.17 Lowering disturbances](#).

At the end in chapter [2.18 What is special for \$\text{CuCl}_2 \cdot 2\text{H}_2\text{O}\$](#) , the question is handled why the pictures appear especially with DCC and in the last how to choose a name in chapter [2.19 Name \$\text{CuCl}_2 \cdot 2\text{H}_2\text{O}\$ system](#).

References

- [1] Bessenich F. Beiträge zur Erforschung der Bildekräfte durch empfindliche Kristallisation (Goethenaum (Dornach), 1951).

2.1 State of the art

Abstract

The state of the art chapter is divided into three parts. The first part deals with the forces in the Petri-dish which influence the evaporation. The second part attends to the processes behind the nucleation and the growth of the needles and the third part consider the forces which arrange the needles in the Petri-dish.

For the first part most information is available. The second part is under research and more and more results are showing up. The third part, the most interesting, is the hardest to research and compared to the other two parts only sparse information is available.

Introduction

The state of the art should give a context, in which the published findings with references can be gathered and sorted. A compilation of the published results thereby forms the “state of the art”, which can be inserted into the introduction of forthcoming publications.

Historical overview

So far no history.

Authors research

The driving forces of the evaporation and crystallization of $\text{CuCl}_2 \cdot 2\text{H}_2\text{O}$ (cupric chloride di-hydrate, further named [DCC](#)) in the presence of additives in a Petri-dish can be structured into the following three parts:

1. The forces in the dish, which influence the evaporation and the growth of the needles.
2. The processes behind the nucleation and the growth of the needles
3. The forces which arrange the needles to a “whole” (image). (The arrangement)

To part 1: The forces in the dish, which influence the growth of the needles, depend on the DCC concentration gradient between the middle of the Petri-dish and the rim. The gradient is created by the shielding of the rim of the Petri-dish (Hollemann 1966 [1], Busscher 2010 [2]). This can induce strong surface forces (Habibi 2016 [3]), which can result in a dynamic start of dewetting after crystallization phenomenon. These forces are in an area between the geometrical center and the rim of the Petri-dish (Busscher 2019 [4]), roughly between 40 % to 70 % of the Petri-dish radius. The surface forces depend on the surface properties of the glass surface, the bottom of the Petri-dish. This was researched by Gallinet 1992 [5], who deduced that for BSA a monolayer changed the surface properties to a comparable situation of high hydrophilicity. This was verified by Busscher 2019 [4].

To part 2: The chosen working concentrations of DCC and additive are in a range where in most cases only one crystallization center appears (Busscher 2109 [6]). The nucleation is said by Reiter (2010 [7]) to be a heterogenic nucleation, due to the additives in the solution, which act as nucleation point. The needle elongates in most cases through split-growth (Neuhaus in Selawry1957 [8]) or dendritic growth Leray 1968 [9], Beckmann1959 [10]. For [BSA](#) as additive it was shown that for a DCC amount of 100 to 200 mg and a mixture ratio (DCC/BSA) between 20 and 11 the needles change from split-growth to dendritic growth (Busscher 2019 [6]). Dendritic growth is a well-researched topic for other materials than DCC (Haxhimali 2006 [11], Asta 2009 [12], Kurz 2001 [13]). The process behind the needles and branching is a so called self-organization process, which is modified by the additive (Busscher 2014 [14]). The frequency of branching of the needles increases in the presence of higher molecular weight additives (researched for PVP and ageing carrot juice), or higher additive amounts (Busscher 2019 [6], Busscher 2014 [14]).

To part 3: The forces that arrange the needles in the Petri-dish to a human perceivable “wholeness” have not been understood so far. We name this process “arrangement”, according to Bessenich (1951 [15], p. 31). The hypothesis, that they are connected to the entropy of the sample in question, could not be falsified due to missing data of the ternary system DCC, water and additive (Busscher 2014 [14]). Different hypotheses for parts of the arrangement were set up, but they could only give insights to parts of the process, without explaining the perceivable “wholeness”. We guess it will be a balance of top-down and bottom-up processes as described by Mukerjee 2015 [16] for soft thin films. Recently, in an article about the mass production of 3D microcomponents,

Blasco and Siegel (2024 [17]) stated that “...Top-down approaches can overcome the shortcomings of bottom-up techniques, providing pathways towards improved shape control...”

Resume

No resume so far

Additional Research

What are the next research steps?

Continue on the path of doing research with physically and chemically defined samples, which have e.g. a CAS No. The first defined sample was [BSA](#), clarifying the dewetting question and defining simple crystal types and the concentrations of additive and DCC at which they appear (Busscher 2019 [6]). With this as basis further samples can be compared to these results and the working concentration choices can be underpinned. The next step is to clarify the influence of the molecular weight. This can be done with [PVP](#), because for PVP different molecular weights exist, without changing the chemical composition, as it is e.g. for aging carrot juice. This makes it possible to study the influences of viscosity, molecular weight, the distribution of molecular weight (dispersity) and the amount of the sample on the DCC picture.

The three different parts are described in more detail in the chapters in Table 2.1.1 (below).

Table 2.1.1 Chapters connected to the three different parts.

Topic	Chapter
1. Forces in the dish	1.4 Surface tension, cleaning, ring height 2.4 Concentration gradient 1.7 Evaporation issues 1.6 Sensitive area 2.8 Dewetting by crystallization
2. Nucleation growth	2.11 Nucleation 2.3 Crystal growth and branching 2.6 Molecular weight and branching 2.14 Self-organization and CuCl₂ 2H₂O 2.9 Additive built into CuCl₂ 2H₂O?
3. Arrangement	2.2 Arrangement (the hypotheses) 2.18 What is special for CuCl₂ 2H₂O ?

References

- [1] Holleman LWJ. Ein Beitrag zum Verständnis der empfindlichen Kristallisation. *Elemente der Naturwissenschaft* 1966; 4: 24-33 <https://doi.org/10.18756/edn.4.24>.
- [2] Busscher N, Kahl J, Doesburg P, Mergardt G, Ploeger A. Evaporation influences on the crystallization of an aqueous dihydrate cupric chloride solution with additives. *Journal of Colloid and Interface Science* 2010; 344: 556–562 <https://doi.org/doi:10.1016/j.jcis.2009.12.045>.
- [3] Habibi M, Rahimzadeh A, Eslamian M. On dewetting of thin films due to crystallization (crystallization dewetting). *Eur. Phys. J. E* 2016; 39: 30 <https://doi.org/doi:10.1140/epje/i2016-16030-9>.
- [4] Busscher N, Doesburg P, Mergardt G, Sokol A, Kahl J, Ploeger A. Influence of dewetting on the crystallization behavior of CuCl₂ in the presence of BSA during evaporation in a Petri dish. *Heliyon* 2019; 5: e01102 <https://doi.org/10.1016/j.heliyon.2018.e01102>.
- [5] Gallinet JP, Gauthier-Manuel B. Wetting of a glass surface by protein adsorption induces the crystallization of an aqueous cupric chloride solution. *Journal of Colloid and Interface Science* 1992; 148: 155-159 [https://doi.org/doi:10.1016/0021-9797\(92\)90123-4](https://doi.org/doi:10.1016/0021-9797(92)90123-4).
- [6] Busscher N, Doesburg P, Mergardt G, Sokol A, Kahl J, Ploeger A. Crystallization patterns of an aqueous dihydrate cupric chloride solution in the presence of different amounts of Bovine Serum Albumin. *Journal of Crystal Growth* 2019; <https://doi.org/doi:10.1016/j.jcrysgro.2019.125272>.

- [7] Reiter G, Barth J-G. Some general remarks on crystallization in the presence of additives. *Elemente der Naturwissenschaft* 2010; 92: 39-61 <https://doi.org/10.18756/edn.92.39>.
- [8] Selawry A and Selawry O. Die Kupferchlorid-Kristallisation in Naturwissenschaft und Medizin (Gustav-Fischer-Verlag, 1957).
- [9] Leray JL. Growth kinetics of hydrated cupric chloride. *Journal of Crystal Growth* 1968; 3-4: 344-349 [https://doi.org/DOI: 10.1016/0022-0248\(68\)90172-3](https://doi.org/DOI:10.1016/0022-0248(68)90172-3).
- [10] Beckmann H. Über Keimbildung, Einkristallwachstum und Auffächerungswachstum von $\text{CuCl}_2 \cdot 2\text{H}_2\text{O}$ in reinwässrigen und Eiweiß-haltigen Lösungen. PhD Thesis, Universität Bonn. 1959.
- [11] Haxhimali T, Karma A, Gonzales F, Rappaz M. Orientation selection in dendritic evolution. *Nat Mater* 2006; 5: 660-664 <https://doi.org/doi:10.1038/nmat1693>.
- [12] Asta M, Beckermann C, Karma A, Kurz W, Napolitano R, Plapp M et al. Solidification microstructures and solid-state parallels: Recent developments, future directions. *Acta Materialia* 2009; 57: 941-971 <https://doi.org/10.1016/j.actamat.2008.10.020>.
- [13] Kurz W. Solidification Microstructure-Processing Maps: Theory and Application. *Advanced engineering materials* 2001; 3: 443-452 [https://doi.org/https://doi.org/10.1016/0956-7151\(94\)90044-2](https://doi.org/https://doi.org/10.1016/0956-7151(94)90044-2).
- [14] Busscher N, Kahl J, Ploeger A. From needles to pattern in food quality determination. *Journal of the Science of Food and Agriculture* 2014; 94: 2578-2581 <https://doi.org/doi:10.1002/jsfa.6498>.
- [15] Bessenich F. Beiträge zur Erforschung der Bildekräfte durch empfindliche Kristallisation (Goethenaum (Dornach), 1951).
- [16] Mukherjee R, Sharma A. Instability, self-organization and pattern formation in thin soft films. *Soft Matter* 2015; 11: 8717-8740 <https://doi.org/10.1039/C5SM01724F>.
- [17] Blasco CAS&E. Mass production of 3D microcomponents. *Nature* 2024; 627: 276-277.

2.2 Arrangement

Arrangement of the growth structures (needles and branched needles) of $\text{CuCl}_2 \cdot 2\text{H}_2\text{O}$ crystals in the Petri-dish.

Abstract

The perception of a Gestalt in the pictures of $\text{CuCl}_2 \cdot 2\text{H}_2\text{O}$ (cupric chloride di-hydrate, further called DCC) crystallization with additives is a special human ability (see chapter [2.15 Formation integrated pattern](#)). Understanding the organization of the needles into a Gestalt, is the unsolved question of DCC crystallization with additives. Different hypotheses are formulated to be tested in experiments. These hypotheses can be sorted into three levels of increasing complexity of interactions associated with the sample. These are: (1) the physical level, (2) the chemical level and (3) the biological level. At the physical level, the sample is not changed during evaporation, at the chemical level, the sample is chemically active and / or changed during evaporation, and at the biological level, the sample is biologically active during evaporation. Aspects related to the level of physical possibilities are: (1.1) the growth field (*Wachstumsfeld*) formed by the concentration gradient in the Petri-dish (Holleman [1], Nickel [2] Leray [3]). (1.2) The solution flows due to Marangoni forces [4] (Nitschmann) as a result of the concentration and temperature gradients. (1.3) The question, indirectly raised by Hummel [5], whether the DCC pattern is defined by the amount or the viscosity of the sample. (1.4) The possible evaporation structure [6]. (1.5) The thermal interactions in the Petri-dish [7]. (1.6) The effects of a nonuniform distribution of the additive in the Petri-dish (Pettersen [8]). (1.7) The protein prefiguration (called "*Vorbild*" by Pfeiffer in Bessenich [9]). (1.8) The meso-crystal formation ([10]). (1.9) The behavior of D+ / L- mixtures of malic acid [11] and (1.10) the entropy concept in general [12]. At the chemical level, there are several kinds of interactions between DCC and the sample due to the pH drop during evaporation (see [1.7 Evaporation issues](#)). At the biological level we are still at the beginning of formulating hypotheses. The possibilities identified so far for these three categories are listed below in a table with their corresponding hypotheses, in order to see how they can be verified or falsified.

Introduction

The arrangement of the crystal needles into human perceptible wholes (Gestalts) is the so far unsolved question of the $\text{CuCl}_2 \cdot 2\text{H}_2\text{O}$ (cupric chloride di-hydrate, further called DCC) crystallization with additives (see chapter [2.15 Formation integrated pattern](#) for an introduction to the concept of a Gestalt). One part of the question is how the arrangement can be recognized by a human being. The other is how to understand the arrangement of needles and branches into a Gestalt. To approach the latter, three levels of increasing complexity of sample interactions are defined. The levels are (1) the physical level, (2) the chemical level and (3) the biological level. The question is how these levels can be researched.

The simplest level, the physical level, is defined by the physical conditions in the Petri-dish, and assumes that the additive is not changed during the evaporation and crystallization process. This limits the influence on the arrangement to basic parameters of the Petri-dish processes, such as surface tension forces [13] [14], ring height, starting humidity, concentration matrix behavior etc.

The second level is the chemical level, where interactions of the sample during the evaporation and crystallization are assumed and discussed. Interactions of the Cu ion with different molecules are known. These phenomena are discussed in the paragraph "Complex building", and is covered in several publications [15] [16] [17] [18]. These complexes change the physical properties of the solution at the solubility border of DCC, e.g. the viscosity of the solution, as shown by Mergardt [19] for glycogen, which shows a constant viscosity at DCC levels between 10 and 30 % w/w and from 30 % w / w upwards an increasing viscosity. Also the amount of additive in the solution or the amount of DCC available for crystallization may change during evaporation. The decrease of the pH value to 0.5 (at the solubility border of DCC) changes the responsiveness of the additive to DCC. Especially additives from agricultural origin like juices or extracts have a broad range of potential interactions with the Cu ion.

The third level is the biological level. The reason why we included the biological level is the Gestalt that can be perceived in the DCC picture. A Gestalt is defined as "*a perceptual pattern or structure possessing qualities as a whole that cannot be described merely as a sum of its parts*" (Collins English Dictionary 2014 [20]). The concept of Gestalt implies reciprocal part-whole interactions as the whole depends on the parts to come forth, and simultaneously the parts depend on the coming forth of the whole to be assigned significant instead of superficial (Bortoft 1996 [21], Parnas 2012 [22], van der Bie 2012 [23], Galotti 2014 [24]). In the realm of Gestalt evaluation of DCC patterns, the parts refer to the characterizing morphological and gestural criteria. Weight and significance of the perceived criteria is assigned in the context of the recognized Gestalt (Doesburg 2014 [25]). The Gestalt of the

DCC picture, due to its tree- or plant-like needle structure, is best evaluated by humans using criteria taken from a biological context, like the plant world. The other reason why we included the biological level is that Pfeiffer in 1920 ([26], p. 118 - 122), when he “invented” the DCC method, envisioned what he called an “*aufbauende Technik*” (constructive technology) based on what he called “formative forces” in nature. This technology contrasts most existing technologies, which are based on decomposition processes for e.g. energy production. As mentioned above, the basic question is how to perform research at this level. As yet, we do not have a simple idea like the ones we formulated for the physical level or the more complicated ones for the chemical level. The first step towards addressing this question is the study of the physical basics of biological systems (e.g. entropy export) and concepts which deal with criteria to classify biological systems. We are aware of the contradiction that a mixture of a juice (from a living product) and the toxic DCC does not look like a biological system at first sight. The basic approach is worked out in more detail in chapter [2.16 Complex physical versus simple biological](#). This chapter Arrangement is intended to give an overview of the different hypotheses and, if available, a link to a chapter with a more detailed description.

In the following, the possibilities underlying the formation of the DCC arrangement are described for the different levels. The first level, the physical level, takes up most of the space in this chapter, because that is where most of our research efforts have been focused.

Historical overview

Von Hahn [27], p. 12, pointed to the evaporation phase as the stage in which the arrangement of the needles could take place. He called his work therefore *Thesigraphie* and not Copper Chloride Crystallization because he did not want to emphasize the indicator (copper chloride) nor the process (crystallization) but the arrangement of the needles. Schweizer made experiments on the effect of interruptions of the evaporation [28]. He observed that the crystals, after responding to the perturbation, returned to grow in the same way as before when the original evaporation conditions were restored. Vester [11] performed unperturbed experiments with DCC and mixtures of D + / L- mandelic acid. The overall crystallization structure disintegrated for the mixture ratios around the racemate (50 / 50) mixture. In the following the different influences on the arrangement as listed in the introduction are described in more detail.

Physical level

P1: *Wachstumsfeld* – growth field

Nickel [2] used, and perhaps created, the term *Wachstumsfeld* (“*growth field*”) for the concentration gradient that directs crystal growth like a magnetic field does for iron dust. The *Wachstumsfeld* is created by the influence of the rim of the Petri-dish on the evaporating DCC solution (see [chapter 1.4 Cleaning, surface tension, ring height](#)). He showed the influence with a simple experiment (see Fig. 2.2.1 on the next page).

In Fig. 2.2.1 the DCC solution with blood as additive, poured on a 25 cm * 25 cm glass plate, crystallizes in needles and hole forms. The centering of the picture and the progression of the needles to the periphery is an effect of the positioning of the glass rim. Waldburger repeated the experiment for milk as additive as shown in Fig. 2.2.2 on the next page. Prior to Nickel, the experiments of Holleman [1] showed the influence of the rim of the Petri-dish and the existence of a concentration gradient. The question is whether the *Wachstumsfeld* creates a surface deformation [29], as the temperature in the middle of the Petri-dish is lower than at the rim and the concentration of DCC and additive are highest in the geometrical center. Leray (1973 [3]) calculated by simulating the forces in the Petri-dish that the spatial profile of the solution should result in a [dewetting](#) at 50 - 70 % of the Petri-dish radius, which has indeed been observed in many cases [30] [13].

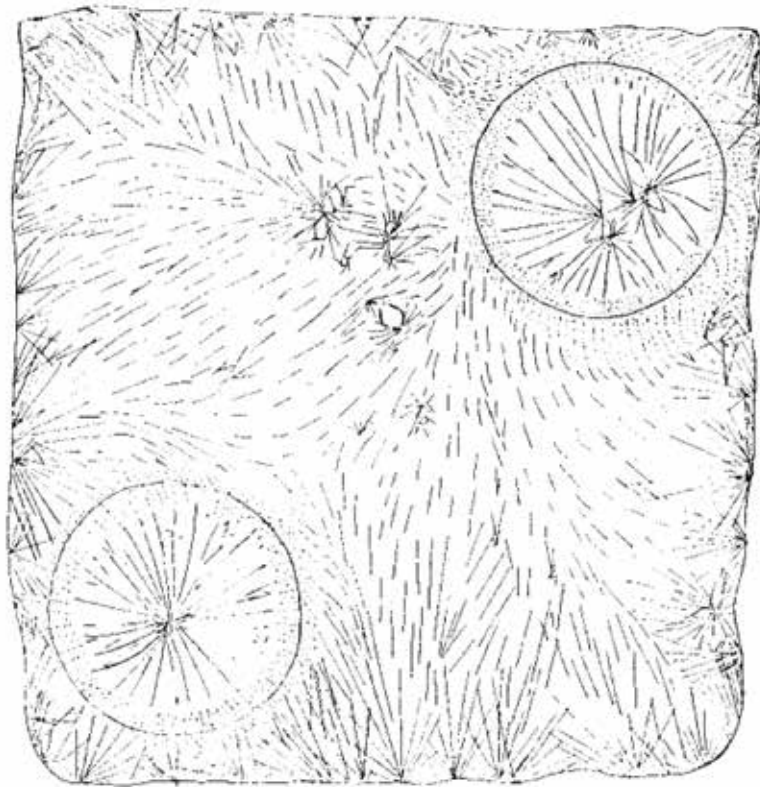


Fig. 2.2.1 Original translated caption text from Nickel: Two-dimensional growth field and centering. The solution required for a DCC picture with blood as additive was poured onto a polished glass plate delimited by a grease line - in the quantity calculated for the given surface (approx. 25 * 25 cm) - and brought to crystallization in a climatic chamber. Two glass rings (\varnothing 10 cm) were placed in two places on the plate immediately after pouring the solution. The drawing (based on a 1 : 1 photo) shows how crystallization within the glass rings leads to a centered structure; any other demarcation would produce a defined structure in the same way. In the dotted area (peripheral zone in the DCC picture) the crystallization is thin: however, the perradiation continues through all areas.



Fig. 2.2.2 From Waldburger. Same experimental setup as Nickel used in Fig. 2.2.1 but with milk as additive.

P2: Marangoni convection

Nitschmann [4] was the first to connect the DCC pictures to the concept of the Marangoni convection. These forces are caused by the concentration and temperature gradients in the Petri-dish [13]. This should cause a horizontal flow in the solution created by the surface forces. Pfeiffer in Bessenich [9] did not observe any movement with “white particles” (talcum powder) on the surface of the DCC solutions with blood as sample. A mathematical simulation of the solution in a Petri-dish showed a fluidic movement at the surface [31]. The conditions that determine whether Marangoni convection starts or stops, which depend on the viscosity, density, surface tension and height of the solution [29] [32] are calculated by Schatz [33].

A replication of Pfeiffer’s observation could be easily made by adding white powder or something more suitable to the surface of the solution and following the evaporation with the ceiling camera (see Additional research).

P3: amount versus viscosity

This is a fundamental question for the DCC system. Typically, the molecular weight (mean of the molecular weight profile) of a sample decreases during aging, as shown by Hummel (1992 [5] see also chapter [2.6 Molecular weight and branching](#)). The DCC picture of a fresh juice cannot be reproduced by a high concentration of aged juice, because when juice ages, several parameters change. The molecular profile changes to a lower average molecular weight and the viscosity can change. Consequently it is not easy to produce a higher concentration of aged juice without substantially changing the juice. Instead, if we use a high molecular weight PVP as a model for fresh juice and a low molecular weight PVP for aged juice, then different concentrations can be simply handled. The viscosity increases with increasing amounts of the additives. The viscosity influences the heat conductivity, which is responsible for the onset of the branching of the DCC crystals. A test could be done with different amounts and molecular weights of PVP. If possible the viscosity should be compared at the solubility border of DCC (see Additional research).

P4: evaporation structure

The DCC crystallization needle starts at the surface for blood as an additive (Nickel [2] p. 44). The temperature of the solution is lowest at the surface due to the cooling effect of evaporation, therefore it has the highest nucleation probability because the value of the solubility border of DCC increases exponentially with the temperature. If the surface of the solution has a temperature structure, the crystal growth would follow that structure. For the temperature structure see Zhang [32], Flack [34] and Saylor [6] who point to the dependence on a surfactant (additive), the velocity of the airflow (which in the articles is much higher than in our situation) and the energy export through the surface [35] (entropy export). Misyura [36] showed that when CaCl₂, LiCl, BaCl solutions evaporate in a Petri-dish, the onset of crystallization occurs at the surface of the solution and according to the radial distribution of the temperature. One possibility is that this could be caused by Marangoni cells. The other is that the buoyancy effect (overriding diffusion) creates the structures. The buoyancy effect is possible because the surface is cooler and the bottom of the Petri-dish is hotter.

Structures appear after heating from below and subsequent cooling [37]. This heating and cooling occurs in the inner chamber of a Triangle type chamber (two point regulator). A test could be to change the two point regulator to modulating thermoregulation, thereby drastically reducing the heating and cooling phases.

P5: warmth interaction

From the measurements in Busscher 2010 [13] (p. 560 Fig. 10) it is clear that, when the crystallization starts, the crystallization heat spreads quite fast through the dish. Results from the Checking Influences project [38] (p. 73 - 80) show that the chamber walls have different temperatures. The basic idea is that the heat from the walls influences the crystallization process. Kolwankar [7] [39] described an experiment in which the heating of a small absorber in a solution by laser light with a heating power of a few mW increased the rate of dendritic growth of BSA in phosphate buffer saline. The growth velocity of a crystal is “the” parameter defining the morphology of dendrites as shown by Kurz [40] in the so called morphology-map. Ergo, the temperature differences of the chamber walls could have an influence on the (a)symmetry of the distribution of DCC in the picture.

P5.1: a test could be conducted by means of a [one dish prüfstand](#) with defined temperature differences in the walls surrounding the dish.

P5.2: it should also be checked whether the asymmetry (amount of DCC on the plate as measured by the absorbance) correlates with the orientation of the chamber walls. This is necessary, because by default the pictures are reorientated during scanning so that the center faces downwards. This is possible with the [CrystEval](#) tool.

Previously, the degree of DCC asymmetry was evaluated from images of 4 series scanned in both the

way they were oriented in the chamber, and in the default way with the center facing down, but the results were inconsistent (see Absorbance Symmetry report [41]).

P5.3: when checking the correlation between the asymmetry of a picture and the orientation in the chamber, also check if the evaporation is homogeneous with the pH indicator from the [one dish prüfstand](#).

P6: distribution of the sample

The shielded evaporation in the dish will not only create a DCC gradient in the Petri-dish but also an additive concentration gradient. This concentration gradient may induce a separation of the different sub-fractions comprising the additive as Petterson [8] hypothesized. A sub-fraction could precipitate due to the pH decrease from the increasing salt concentration. If the distribution of the additive is not uniform throughout the Petri-dish, different patterns may appear along with the growing needles from the crystallization center to the Petri-dish rim.

Test: do different crystallization patterns occur in different regions (zones of the picture, see chapter [1.13 Picture zones](#)) when the mixture ratio is at the border between split- and dendritic-growth or near the substance spirals? Are the crystallization patterns more homogeneous when the mixture ratio is “far” from these borders? See also chapter [1.10 Transition between crystal types](#).

P7: protein Vorbild

The *vorbild* or preconfiguration question was first published by Pfeiffer in Bessenich for blood as additive. The question was studied by Schweizer for plant extracts as additive [42] but he could not find a protein *Vorbild* or preconfiguration. He found water insoluble DCC crystals, which remained on the glass plate after the water soluble part was washed away. Perhaps the protein *Vorbild* is only present for blood as additive (Pfeiffer in Bessenich [9]). So far this has not been a topic for non-blood samples. Gallinet [30] made an experiment with radioactive marked BSA as additive. At the concentrations used, after washing off the DCC, all radioactively labeled BSA remained on the glass-plate but showed no pattern.

P8: meso-crystals

The meso-crystal concept states that the growth of a crystal stops at various scales. DCC is known to build nano particles [43]. Further growth of a DCC crystal may be due to a combination of these meso-structures [44] [45] [10]. The meso-crystal approach, which denies a simple Lego-like step by step growth of a crystal by combining atoms, is supported by a nucleation observation of Zhou [46], in which the initial nucleation “crystals” differ from the later shape.

Test: the meso-character of the DCC needles could be checked by X-ray or electron diffraction [10] (p. 39).

P9: entropy concept

The interaction of the additive with the DCC results in at least a ternary system (3 components: 1: DCC, 2: H₂O, 3: additive) [12].

Hypothesis: the total entropy is reduced by the additive.

Can we use different aging stages of a sample, as they have different mean molecular weights?

The entropy export by evaporation of DCC in a Petri-dish system raised a lot of questions. A constant stream of heat flows through the Petri-dish [12]. One would expect that a higher entropy export of the system would enable more “complex” pictures to emerge. It is known from visual observations that optimal pictures occur between 12 and 16 hours after pipetting the solutions in the Petri-dishes (Pfeiffer 1935 [47], Koopmans 1965 [48]), which would contradict the expectation that shorter crystallization times due to a stronger warmth flow would produce more complex pictures and longer evaporation times would produce less complex pictures. The results from Baumgartner [49] showed that later crystallization starting times (*t_{crStart}*) are not a limiting factor for the differentiation of cress seedlings, grown in different ultra high diluted potencies.

P9.1: test samples with different entropies. How to handle the ternary question? Missing data for a components mixture.

P9.2: test higher evaporation rates; this will increase entropy export and result in lower *t_{crStart}* values. How does this fit with the concept of the optimal *t_{crStart}*? What phenomenon or process requires a so called minimum *t_{crStart}*? Can we check with the [one dish prüfstand](#) if the gradient of DCC and additive develop in another way (stronger or broader) depending on the *t_{crStart}*? Or are we dealing with a “ripening time” as stated by

von Hahn, or an “inner arrangement” as Bessenich stated?

P9.3: a stronger evaporation will reduce the diffusion of DCC and additive in the dish.

P10: malic acid D+ / L- influences

Vester’s [11] malic acid experiments were repeated ([50], p. 11, pictures shown in Appendix 2.2.1 Mandelic acid), and show a “breakdown” of the overall crystallization behavior at the racemate (50 / 50) mixture. The unmixed (D + or L - malic acid) pictures showed a “normal” picture at the edge of dewetting. The 50 / 50 D + / L - malic acid mixture showed a breakdown of the needle properties and perhaps offers some insight into the otherwise long distance (4.5 cm to 9 cm) directed growth of the DCC needle structures.

P11: additive included in crystal

This topic is covered in chapter [2.9 Additive built into CuCl₂ 2H₂O?](#)

P12: phase separation

A phase separation was first observed in mixtures of DCC with carrot juice, standing in the fridge at 4 °C (see master thesis Benny 2024 [51]). If this happens during evaporation and the DCC is in the upper phase of the solution, then the DCC crystal is growing on a “layer” of carrot juice.

Chemical level

C1: complex building

Complex building between DCC and the additive can be followed by the viscosity changes of the solution. DCC itself is not a Newtonian fluid (see chapter [1.7 Evaporation issues](#)). For the crystallization process the viscosity behavior at the solubility border is important, which is different for e.g. glycogen at low and high DCC amounts (see chapter [1.7 Evaporation issues](#)). See additional research Viscosity measurements.

Biological level

Assuming the existence of a biological level in the evaporation / crystallization process, the first verification concerns the entropy export of the system. The entropy export question is handled in the [physical level P9](#) and in Busscher 2014 [12]. The entropy export value has the magnitude of a plant leaf, as calculated by Aoki [52]. More details can be found in the chapter [2.16 Complex physical versus simple biological](#). Here we give an overview of how to deal with the DCC image results from a more biological perspective, taking some system variations as a degree of freedom for the system. See for a discussion of degrees of freedom chapter [2.17 Lowering disturbances](#).

Training for observation

When dealing with the physical or chemical level, the usual role of the experimenter is that of an observer. In most cases there is a clear distinction between the phenomenon and the observer. This can be maintained when approaching the biological level, but then the biological system is regarded as a complicated physical chemical system. Addressing the Gestalt phenomenon of the DCC picture requires looking first at the whole and then at the parts, e.g., in terms of criteria. Weight and significance of the perceived parts is assigned in the context of the recognized Gestalt (Doesburg 2014 [25]). It can be compared to first recognizing a five star as a shape, as an entity, and later seeing that it is made up of five lines. See also chapter [2.15 Formation integrated pattern](#). It is through this order of perception that the evaluation process enters the observer. The experimenter becomes the measurement instrument, which needs schooling and training to become a tool for evaluation. This can be done by training on DCC pictures in the same way as it is done in sensory analysis. This is a critical step because the training is not easy and can best be done in a group with recurrent feedback, as is common in sensory analysis, described in ISO norm 11035 and applied to DCC pictures by Huber (2010 [53]), Fritz [54] and Doesburg [25]. The following working points are based on the described training.

B1 Sorting pictures by tcrStart

When the replicates of DCC pictures from a sample with the same DCC and additive amounts are sorted according to the tcrStart, a transformation “flow” can be seen in the pictures. Here we take the tcrStart as a degree of freedom (see chapter [2.17 Lowering disturbances](#)) and try to see how the sample deals with the different conditions like a “Blattreihe” (leave series) as described by Bockemühl (1980 [55], p. 14). Usually 1 out of 5 - 10 pictures forms an outlier in this flow.

B2 Sorting pictures by additive amount

The same principle of a development flow, as described in B1 for tcrStart, can be used when looking at DCC pictures of different additive amounts, sorting them both by additive amount and by tcrStart. In this way, two degrees of freedom can be evaluated for each sample. The generation of the sheets for this evaluation is described in the [Appendix 3.5.1 Sheets4GestaltEvaluation](#). The evaluation results of this procedure are published in Fritz (2011 [56]), Doesburg (2014 [25]), Fritz (2018 [54]), and conceptually described in Doesburg (2021 [54]) and Fritz (2022).

B3 Compare aging stages

Another dimension is created when the samples in question are aged e.g. by storing the juices or extracts in the fridge by 6 °C. This has been used by Graf (1994 [57]), Fritz (2011 [56]) and Athmann (2011 [58]) to determine how the different sample qualities deal with the aging process.

Resume

Various hypotheses that may underlie the arrangement of the DCC needles are listed and discussed. The hypotheses were grouped according to the increasing complexity of interacting with the sample, into physical, chemical and biological interactions. Experiments were designed to research the different hypotheses, which are listed in Additional research.

Additional research

Overview experiments and hypotheses

Table 2.1 List of experiments to check the hypotheses.

Nr	Experiment
P1.1	Gathering of DCC around the geometrical center should be visible by the absorbance of the DCC.
P1.2	Different ring heights gave differences in the strength of the <i>Wachstumsfeld (growth field)</i> . The radius of the crystal should be closer to the rim when the ring height increases.
P2	Surface movement (of particles) during evaporation.
P3	Dependency on the viscosity or the molecular weight (PVP).
P4	Modulating inner chamber regulator. Does this reduce the warmth structures? See also chapter 2.7 Substance spirals .
P5.1	Visualize the warmth structure and DCC distribution at different wall temperatures in a dish during evaporation by means of an infra red camera (see one-dish-prüfstand).
P5.2	Asymmetric warmth check? Is the pictures asymmetry correlated to the wall temperatures? Orientation of the pictures with the CrystEval tool.
P5.3	Test the homogeneity of evaporation with a pH indicator in the Petri-dishes.
P6.1	Different crystals for different amounts (e.g. transition border split <-> dendrites).
P7	No experiments planned.
P8	X-ray verification of the crystal structures.
P9.1	Samples with different entropies (aging or molecular weight). How to handle the ternary question? Find or measure missing ternary data.
P9.2	Does a higher evaporation rate result in a higher entropy export and consequently earlier pictures (with less complexity? How to define complexity?) do we have a “ripening time”?
P9.3	Does a stronger evaporation reduce the diffusion of DCC? Will we get a more spiky DCC distribution like the one from Hollemann?
P10	Malic acid D+ / L- experiments with other concentrations, making a full concentration matrix.
P11	Additive included in the crystal (see Additional research in chapter 2.9 Additive included in CuCl₂).
P12	Phase separation; test DCC / carrot juice mixtures in the chamber, photograph the dishes with a 45 ° mirror from the side.
C1	Complex building, viscosity at the solubility border.
B1	Sorting pictures according to the tcrStart. How can the transformation flow be described?
B2	Sorting pictures according to additive amount and tcrStart. How can the transformation flow be described? As described in Fritz 2018 [54].
B3	Sorting pictures according to the degree of aging of the additive. How can the transformation flow be described? As described in Doesburg 2014 [25] and Fritz 2011 [56] and 2018 [54].

Appendix 2.2.1 Mandelic acid

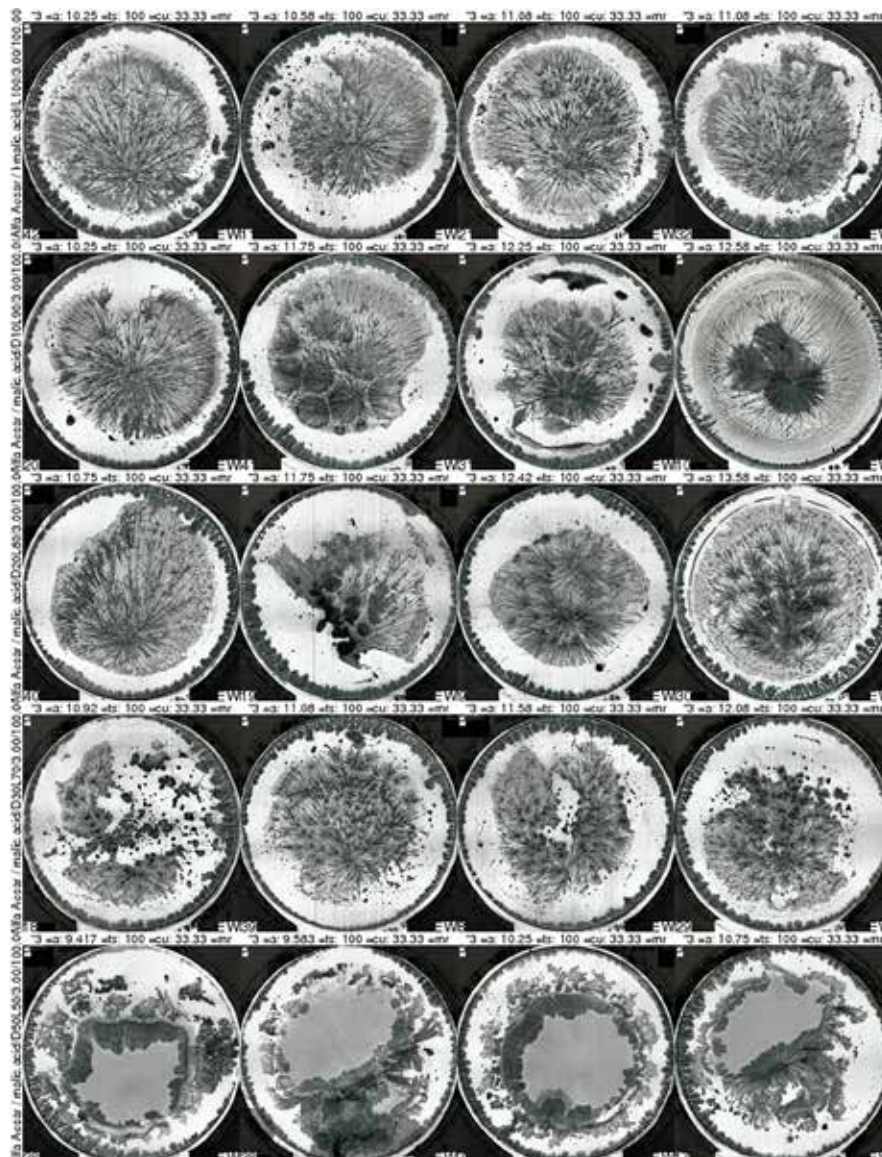


Fig. 2.2.3 X-axis replicates, sorted according to the tcrStart (lowest left). Y-axis different mixtures of D+ / L-. Upper row (1) D = 0, L = 100, second row (2) D = 10, L = 90, third row (3) D = 20, L = 80, fourth row (4) D = 70, L = 30, lowest row (5) D = 50, L = 50. Data from ProPar project report nr 5 (2017 [50]).

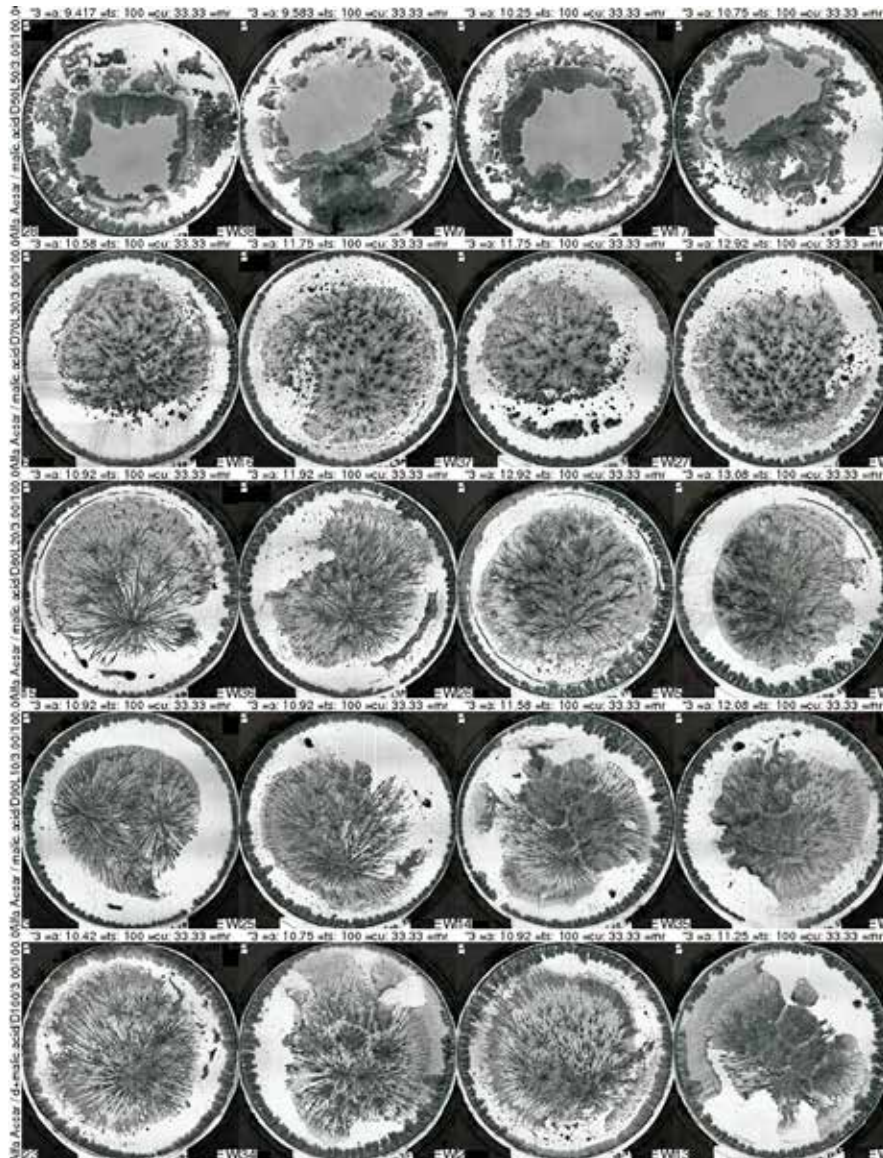


Fig. 2.2.4 X-axis replicates, sorted according to the $t_{crStart}$ (lowest left). Y-axis different mixtures of D+ / L-. Upper row (1) D = 50, L = 50, second row (2) D = 70, L = 30, third row (3) D = 80, L = 20, fourth row (4) D = 90, L = 10, lowest row (5) D = 100, L = 0. Data from ProPar project report nr 5 (2017 [50]).

References

- [1] Holleman LWJ. Ein Beitrag zum Verständnis der empfindlichen Kristallisation. *Elemente der Naturwissenschaft* 1966; 4: 24-33 <https://doi.org/10.18756/edn.4.24>.
- [2] Nickel E. Die Reproduzierbarkeit der sogenannten empfindlichen Kupferchloridkristallisation. PhD Thesis, Universitätsverlag, Freiburg (Schweiz). 1968.
- [3] Leray J. Profile de la surface libre d'un film liquide heterogene. *Journal de chimie physique* 1973; 10: 1428-1432.
- [4] Nitschmann G. Gedanken zur empfindlichen Kristallisation mit Kupferchlorid. Im Anschluss an die Arbeit von R. E. Hummel: Liefert die Kupferchlorid Kristallisations-Methode einen Nachweis für die Gestaltkräfte des Lebendigen? *Elemente der Naturwissenschaft* 1993; 58: 14-19 <https://doi.org/10.18756/edn.58.14>.
- [5] Hummel RE. Liefert die Kupferchlorid-Kristallisations-Methode einen Nachweis für die Gestaltkräfte des Lebendigen? *Elemente der Naturwissenschaft* 1992; 57: 112-121 <https://doi.org/10.18756/edn.57.112>.
- [6] Saylor JR, Smith GB, Flack KA. An experimental investigation of the surface temperature field during evaporative convection. *Physics of Fluids* 2001; 13: 428-439 <https://doi.org/10.1063/1.1337064>.
- [7] Kolwankar K, Prakash P, Radhakrishnan S et al. Effect of heat source on the growth of dendritic drying patterns. *Pramana - J Phys* 2015; 84: 387 <https://doi.org/https://doi.org/10.1007/s12043-015-0939-2>.
- [8] Pettersson BD. Beiträge zur Entwicklung der Kristallisationsmethode mit Kupferchlorid nach Pfeiffer IV. Wie verschiedene Kristallbilder bei der Pflanzenkristallisation entstehen. *Lebendige Erde* 1969; 3: 112-126.
- [9] Bessenich F. Zur Methode der empfindlichen Kristallisation (Naturwissenschaftliche Sektion am Goetheanum Dornach, 1960).
- [10] Cölfen H and Antonietti Markus Wiley 2008S1-6 Mesocrystals and nonclassical crystallization (Wiley, 2008).
- [11] Vester F. Zur Indikation biochemischer Vorgänge durch kristallisierendes Kupferchlorid. *Cellular and Molecular Life Sciences* 1960; 16: 279-281 <https://doi.org/doi:10.1007/BF02157670>.
- [12] Busscher N, Kahl J, Ploeger A. From needles to pattern in food quality determination. *Journal of the Science of Food and Agriculture* 2014; 94: 2578-2581 <https://doi.org/doi:10.1002/jsfa.6498>.
- [13] Busscher N, Kahl J, Doesburg P, Mergardt G, Ploeger A. Evaporation influences on the crystallization of an aqueous dihydrate cupric chloride solution with additives. *Journal of Colloid and Interface Science* 2010; 344: 556–562 <https://doi.org/doi:10.1016/j.jcis.2009.12.045>.
- [14] Busscher N, Doesburg P, Mergardt G, Sokol A, Kahl J, Ploeger A. Influence of dewetting on the crystallization behavior of CuCl₂ in the presence of BSA during evaporation in a Petri dish. *Heliyon* 2019; 5: e01102 <https://doi.org/10.1016/j.heliyon.2018.e01102>.
- [15] Kumar R and Singh R. Coordination chemistry of copper(II) complexes with N₄, N₄S₂, and N₄O₂ donor macrocyclic ligands: Biological aspects—antifungal, synthesis, spectral studies, and magnetic moments. *Russian Journal of Coordination Chemistry* 2006; 32: 192-198 <https://doi.org/DOI: 10.1134/S1070328406030055>.
- [16] Fritz JJ. Chloride complexes of copper(I) chloride in aqueous solution. *The Journal of Physical Chemistry* 1980; 84: 2241-2246.
- [17] Khan M, Meullemeestre J, Schwing M, Vierling F. Stability, spectra and structure of the copper(II) chloride complexes in acetic acid. *Polyhedron* 1983; 2: 459 - 463 [https://doi.org/DOI: 10.1016/S0277-5387\(00\)87093-X](https://doi.org/DOI: 10.1016/S0277-5387(00)87093-X).
- [18] Wang M, Zhang Y, Muhammed M. Critical evaluation of thermodynamics of complex formation of metal ions in aqueous solutions III. The system Cu(I,II) -Cl⁻ -e at 298.15 K. *Hydrometallurgy* 1997; 45: 53 - 72 [https://doi.org/DOI: 10.1016/S0304-386X\(96\)00074-6](https://doi.org/DOI: 10.1016/S0304-386X(96)00074-6).
- [19] Mergardt G. Simulation des Entstehungsvorganges von Kristallbildern zur Messung der physikalischen Parameter pH-Wert, Dichte und Viskosität am Beispiel von PVP, Glykogen und Bovine Serum Albumin. Technical Report, University of Kassel. 2012.
- [20] HarperCollins Publishers Limited. Collins English Dictionary – Complete and unabridged 10th edition, 2019.
- [21] Bortoft H. The Wholeness of Nature: Goethe's way toward a science of conscious participation in nature (Floris Books, 1996).
- [22] Parnas J. The core Gestalt of schizophrenia. *World Psychiatry* 2012; 11: 67-69 <https://doi.org/10.1016/j.wpsyc.2012.05.002>.
- [23] van der Bie G Wholeness in Science: A methodology for pattern recognition and clinical intuition (Louis Bolk Instituut, Driebergen, 2012).
- [24] Galotti K Cognitive Psychology In and Out of the Laboratory (SAGE Publications, 2017).
- [25] Doesburg P, Huber M, Andersen J-O, Athmann M, van der Bie G, Fritz J et al. Standardization and performance of a visual Gestalt evaluation of biocrystallization patterns reflecting ripening and decomposition processes in food samples. *Biological Agriculture & Horticulture* 2014; 31: 128-145.
- [26] Meyer T Ein Leben für den Geist: Ehrenfried Pfeiffer (1899-1916) (Perseus Verlag, 2000).
- [27] Von Hahn F-V Thesigraphie. (Franz Steiner Verlag, 1962).
- [28] Schweizer F. Störungs- und Regenerationserscheinungen bei der Biokristallisation. *Elemente der Naturwissenschaft* 2013; 99: 5-20 <https://doi.org/10.18756/edn.99.5>.

- [29] Anand JN, Karam HJ. Surface deformation of thin coatings caused by evaporative convection : III. Theoretical and experimental observations. *Journal of Colloid and Interface Science* 1969; 31: 208-215.
- [30] Gallinet JP, Gauthier-Manuel B. Wetting of a glass surface by protein adsorption induces the crystallization of an aqueous cupric chloride solution. *Journal of Colloid and Interface Science* 1992; 148: 155-159 [https://doi.org/doi:10.1016/0021-9797\(92\)90123-4](https://doi.org/doi:10.1016/0021-9797(92)90123-4).
- [31] Lindsay SM, Yin J. Temperature gradients drive radial fluid flow in petri dishes and multiwell plates. *AIChE J.* 2016; 62: 2227-2233.
- [32] Zhang N, Chao DF. Mechanisms of convection instability in thin liquid layers induced by evaporation. *International Communications in Heat and Mass Transfer* 1999; 26: 1069 - 1080 [https://doi.org/https://doi.org/10.1016/S0735-1933\(99\)00098-6](https://doi.org/https://doi.org/10.1016/S0735-1933(99)00098-6).
- [33] Schatz MF, VanHook SJ, McCormick WD, Swift JB, Swinney HL. Onset of Surface-Tension-Driven Benard Convection. *Phys. Rev. Lett.* 1995; 75: 1938-.
- [34] Flack KA, Saylor JR, Smith GB. Near-surface turbulence for evaporative convection at an air/water interface. *Physics of Fluids* 2001; 13: 3338-3345 <https://doi.org/10.1063/1.1410126>.
- [35] Conover, T. and Saylor, J. Statistics of the surface temperature field of an air/water interface under airflow, *Experiments in Fluids* 2007-10-01 43: 509-524.
- [36] Misyura S. Evaporation and heat transfer of aqueous salt solutions during crystallization. *Applied Thermal Engineering* 2018; 139: 203 - 212 <https://doi.org/https://doi.org/10.1016/j.applthermaleng.2018.04.068>.
- [37] Kumar N, Arakeri JH. Natural Convection Driven Evaporation from a Water Surface. *Procedia IUTAM* 2015; 15: 108 - 115 <https://doi.org/https://doi.org/10.1016/j.piutam.2015.04.016>.
- [38] Busscher N. Checking Influences: Untersuchung der Einflussgrößen bei der Biokristallisation als Voraussetzung für die Übertragbarkeit der Kammern und Prozeduren in andere Laboratorien und zur Reduzierung der Variationen durch die Kammer und die Orte. Technical Report, University of Kassel. 2009.
- [39] Basu H, Kolwankar KM, Dharmadhikari AK, Dharmadhikari JA, Bambardekar K, Sharma S et al. Laser-Driven Accelerated Growth of Dendritic Patterns in Liquids. *J. Phys. Chem. C* 2012; 116: 11480-11485 <https://doi.org/10.1021/jp3031573>.
- [40] Kurz W. Solidification Microstructure-Processing Maps: Theory and Application. *Advanced engineering materials* 2001; 3: 443-452 [https://doi.org/https://doi.org/10.1016/0956-7151\(94\)90044-2](https://doi.org/https://doi.org/10.1016/0956-7151(94)90044-2).
- [41] Busscher N. Absorbance Project Report. Technical Report, University of Kassel. 2017.
- [42] Schweizer F, Andersen J-O, Jens-Laursen. Beobachtungen bei der Kupferchloridkristallisation: vom Eiweiß-Vorbild zum Kupferchlorid-Nachbild. *Elemente der Naturwissenschaft* 2010; 92: 62-93 <https://doi.org/DOI:10.18756/edn.92.62>.
- [43] Gawande MB, Goswami A, Felpin F-X, Asefa T, Huang X, Silva R et al. Cu and Cu-Based Nanoparticles: Synthesis and Applications in Catalysis. *Chem. Rev.* 2016; 116: 3722-3811 <https://doi.org/10.1021/acs.chemrev.5b00482>.
- [44] Granasy L, Pusztai T, Borzsonyi T, Warren JA, Douglas JF. A general mechanism of polycrystalline growth. *Nat Mater* 2004; 3: 645-650 <https://doi.org/10.1038/nmat1190>.
- [45] Driessche V, Alexander E. S, Van Gerven N, Bomans PHH, Joosten RRM, Friedrich H et al. Molecular nucleation mechanisms and control strategies for crystal polymorph selection. *Nature* 2018; 556: 89-94 <https://doi.org/10.1038/nature25971>.
- [46] Zhou J, Yang Y, Yang Y, Kim DS, Yuan A, Tian X et al. Observing crystal nucleation in four dimensions using atomic electron tomography. *Nature* 2019; 570: 500-503.
- [47] Pfeiffer E Empfindliche Kristallisationsvorgänge als Nachweis von Formkräften im Blut (Emil Weises Buchhandlung Dresden, 1935).
- [48] Koopmans A. Zeitabhängigkeiten bei empfindlichen Kristallisationen. *Elemente der Naturwissenschaft* 1965; 2: 1-7 <https://doi.org/10.18756/edn.2.1>.
- [49] Baumgartner S, Doesburg P, Scherr C, Andersen J-O. Development of a Biocrystallisation Assay for Examining Effects of Homeopathic Preparations Using Cress Seedlings. *Evidence-Based Complementary and Alternative Medicine* 2012; 2012: 14 <https://doi.org/10.1155/2012/125945>.
- [50] Busscher N, Doesburg P. ProPar Project Report nr 5 2017. Technical Report, CuCl₂ Research. 2017.
- [51] Benny C. Influence of Viscosity on pictorial properties of Polyvinylpyrrolidone (PVP) with different K-value in Dihydrate Cupric Chloride (DCC) method. MSc Thesis, University of Kassel. 2024.
- [52] Aoki I. Entropy budget of conifer branches. *Journal of Plant Research* 1989; 102: 133-141.
- [53] Huber M, Andersen J-O, Kahl J, Busscher N, Doesburg P, Mergardt G et al. Standardization and Validation of the Visual Evaluation of Biocrystallizations. *Biological Agriculture and Horticulture* 2010; 27: 25-40.
- [54] Fritz J, Athmann M, Andersen J-O, Doesburg P, Geier U, Mergardt G. Advanced panel training on visual Gestalt evaluation of biocrystallization images: ranking wheat samples from different extract decomposition stages and different production systems. *Biological Agriculture & Horticulture* 2018; 35: 1-12 <https://doi.org/doi:10.1080/01448765.2018.1492457>.
- [55] Bockemühl J Lebenszusammenhänge, erkennen, erleben, gestalten (Naturwissenschaftliche Sektion am Goetheanum (CH), 1980).

- [56] Fritz J, Athmann M, Kautz T, Köpke U. Grouping and classification of wheat from organic and conventional production systems by combining three image forming methods. *Biological Agriculture & Horticulture* 2011; 27: 320-336.
- [57] Balzer-Graf U. Qualitätsforschung mit bildschaffenden Methoden. *Beiträge SH Forschung* 1994; 42 : 411-442.
- [58] Athmann M. Produktqualität von Salatrauke (*Eruca sativa* L.) und Weizen (*Triticum aestivum* L.): Einfluss von Einstrahlungsintensität, Stickstoffangebot, Düngungsart und Hornkieselapplikation auf Wachstum und Differenzierung. PhD Thesis, University of Bonn. 2011.

2.3 Crystal growth and Branching

How can we understand the growth and the branching? How is the dependency on the amounts of $\text{CuCl}_2 \cdot 2\text{H}_2\text{O}$ and additive?

Abstract

The salt $\text{CuCl}_2 \cdot 2\text{H}_2\text{O}$ (cupric chloride di-hydrate, further named [DCC](#)), without additives, crystallizes on a glass plate in needles, which end in star-like formations, which in turn are the beginning of new needles. Branching depends on the additional presence of an additive. Using Bovine Serum Albumin (BSA) as an example, the dependency of the branching on the additive amount is discussed. The current state of knowledge about DCC crystal growth and branching with and without additives is reported and the most promising concepts are mentioned. DCC can grow as a single crystal or be formed from substructures as in the case of a meso-crystal. The DCC picture with its properties can be viewed as the result of a combination of a (bottom-up) building block process and a (top-down) structuring process.

Introduction

The growth and branching of $\text{CuCl}_2 \cdot 2\text{H}_2\text{O}$ (cupric chloride di-hydrate, further named DCC) with and without additives is preceded by evaporation (see chapter [1.7 Evaporation issues](#)) and nucleation (see [chapter 2.11 Nucleation](#)). These points are handled in detail in their own chapters. The results of these processes of course influence the growth and the branching, so this chapter cannot be written without repeating some of the results from those chapters. This also applies to the so called substance spirals (see chapter [2.7 Substance spirals](#)), where also chiral properties are discussed.

Historical overview

Many studies exist about crystal growth and branching. Here we focus on those studies which have a direct connection to DCC or where a connection to general laws, which are possibly also valid for DCC, can be presumed. As an example of such a general law, the main measures of crystal growth are growth velocity and, in the case of branching, the crystal tip diameter (see for dendrites Kurz 2001 [1]), Langer 1977 [2], Langer 1980 [3], Sekerka 1993 [4]).

In his PhD thesis in 1959 [5] Beckmann reported results on the nucleation and growth of DCC. He found that ultra-fine filtered DCC solutions (p. 61) had a lower undercooling temperature than unfiltered DCC. Furthermore, in experiments in which he added DCC crystal seeds to the crystallization solution, he found in 1961 [6] that freshly prepared DCC solutions had a lower growth velocity, while if they had been "aged" (i.e. allowed to stand for 6-8 days) they showed a higher growth velocity. He concluded that substructures were formed in the DCC stock solution, that the substructures were inhomogeneous, and that not all of the substructures could be used for crystal growth.

A review about Cu nano particles by Desiraru in 2013 [7] showed that DCC is able to build nano particles. So, the idea that the solution is filled with substructures may be possible. From the work of Cölfen 2008 [8] on calcite as a meso-crystal it was shown that the single nanometer substructures failed to grow any further by themselves. The process of crystal growth could only be continued by combining the nano meter substructures. This has been researched by Desiraju [7] and recently supported by Driesche in 2018 [9] (short introduction into this article by Alberstein 2018 [10]). Lee and Ahn 2018 [11] described the creation of nanometer gold particles with chiral optical properties (i.e. the ability to turn polarized light) that involves the use of amino acids and peptides to control the optical activity. Mukherjee and Sharma 2015 [12] (p. 2) made a distinction between self-organization structures (top-down) and those from self-assembly or building blocks (bottom-up) in the following quote:

"We refer to the shaping of an initially featureless film due to such instabilities, which can be spontaneous or can be mediated by an externally imposed force field as self-organization. This is clearly distinct from self-assembly, where a large number of molecules/small building blocks come together and assemble in an ordered fashion to form a larger supra-molecular assembly. In contrast, self-organization involves a spontaneous change of shape from a simple to a more complex organization. For example, a thin film spontaneously fragmenting into an array of holes or droplets due to instability is opposite of the self-assembly, though minimization of the free energy remains the key driving force in both the cases."

Schweizer [13] studied the branching angle of dendrites from DCC in the presence of glycogen, and found that the distribution of the angles between the branches and the needles showed a dependency on the mixing ratio of DCC and additive. At a defined mixing ratio the distribution of the angles became very narrow, which means that the needle structures look quite uniform. Nickel 1968 [14] and Waldburger 2013 [15] observed that for blood as additive the DCC needles started at the surface of the solution. Misyura 2018 [16] observed the same for the salts CaCl_2 , BaCl and LiCl evaporating from a dish. This seems to be a general effect, due to the lower temperature at the surface of the solution (Busscher 2010 [17]). Vester 1960 [18] researched the influence of mixtures of D+ and L- (left and right turning capability of polarized light) mandelic acid on DCC crystallization. For a 50/50 mixture, the entire structure disintegrated.

First Resume historical overview

So far it looks as if a needle can grow as a single crystal needle or that it can be built from different building blocks, or pre-structures (e.g. like a meso-crystal). The underlying processes can build the crystal needle depending on the boundary conditions. Crystallization seems to start at the surface of the solution in the Petri-dish. There is a general process difference between a final crystal form resulting from a building block scheme or self-assembly (bottom-up) and a crystal form resulting from a self-organization structure (top-down). Blasco and Spiegel (2024 [19]) see for technical systems an advance of top-down methods versus bottom-up methods in the possibility of top-down methods by “*providing pathways to improved shape control*”.

Growth and branching

DCC shows a special behavior, e.g. compared to frozen water structures. The morphology map of ice (Librecht 2005) [20] (p. 840 Fig. 2) showed besides needles and plates and columns mainly hexagonal structures in the case of dendrites. These structures are always made up of six arms starting from the center. In the case of DCC there is a “*broader*” behavior. In the case of split-growth, there are two directions, increasing to four in the case of the formation of a so called Maltese cross, while more than four directions form a star-like formation. The center already seems to define the overall structure of the picture, as if the start already defines the rest, or the structure to appear defines the starting form, respectively. The question of how the type of the center and the type of the crystals correlate, needs to be researched further, which is described in chapter [2.11 Nucleation](#).

The DCC system provides the conditions that needles require to manifest. In the case of no or little additive the DCC in the DCC system crystallizes as needles. Sometimes in the case of DCC only crystallization occurs at the rim of the Petri-dish (dewetting before crystallization), resulting not only in the formation of needles, but also of branches. This effect has to be investigated further.

The crystal needle growth is different from the planar growth of a crystal. As described by Kurz [1] (p. 445 Fig. 2) the needle is a special case. A simple introduction can be found in Nature’s Pattern/Branching (p. 18) by Ball 2008 [21]. The needle is a [self-organization](#) system. On the molecular level it is chaotic, like an explosion (positive feedback increases the effect) and on a macroscopic level it is limited by diffusion of the DCC to the needle and by the heat dissipation away from the needle (transfer). Branching can be viewed as a needle starting at an angle from a previous needle. The same process is “*applied*” again and again. The conditions for branching are described in Trivedi 1990 [22], Kurz 2001 [1], Asta 2009 [23] and Haxhimali 2006 [24].

Crystallization starts at the surface

Nickel [14] and Waldburger [15] observed for blood as additive that the start of the crystallization occurs at the surface of the solution. Nakoryakov 2016 [25] confirmed this observation for NaCl and Misyura 2018 [16] for LiBr , CaCl_2 and LiCl . Nickel describes how the crystallization develops with what he called a surface skin “*Oberflächenhaut*” ([14] p.107). He also made observations of adding a surfactant to reduce the surface tension ([14] p. 108). As a result, the needles started to grow not only in a plane on the surface of the solution (parallel to the glass plate) but in 3 dimensions.

When one assumes that for additives of chemical or agricultural origin the crystallization starts at the surface of the solution (maybe depending on the surface tension of the mixture), then the results of Schweizer [26] who observed water-soluble and water-insoluble crystals from the DCC solution, can probably be understood. This is discussed in Fig. 2.3.1 below.

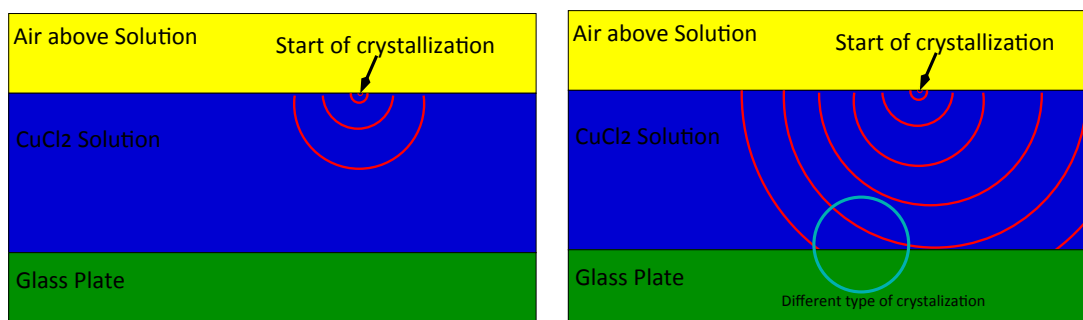


Fig. 2.3.1 Growth of the DCC crystal from the surface towards the glass plate. Left: Situation after start, crystal growing into the solution. Right: situation when the growing crystal touches the glass plate.

When the crystallization starts at the surface of the solution, as in Fig. 2.3.1 left part, then the crystal grows into the solution. Finally, the growing crystal touches the glass plate (Fig. 2.3.1 right). Then the crystal growth continues, but the growth near the glass plate has different conditions than the growth within the solution. Can this explain why the crystals at the intersection between the needle and the glass plate (magenta circle in Fig. 2.3.1. Right) are different as Schweizer found? It is assumed that the crystal grows faster than the evaporation effect reduces the height of the solution.

Needle building process

Needles can be built by an ongoing process as a single crystal or based on a gathering of nano-particles like pearls on a string (Driesche [9], Cölfen [8]). The gathering of nano-particles can be identified with x-ray measurement, see Cölfen [8] p. 39 (see also in additional research and in chapter [2.2 Arrangement](#)-> meso-crystals).

Second Resume Historical

The relationship between the visual form of the DCC crystals at the beginning of the crystallization and the type of crystal (long needles, split-growth, dendrites,...) requires further study. The needle and the branches are built according to the same needle principle. The needle is a special type of crystallization. As a self-organization system it is chaotic on an atomic level (positive feedback like an explosion) and stabilized by diffusion and heat dissipation on a macroscopic level (negative feedback). It needs to be verified whether the crystal starts at the surface or at the glass plate (one-dish-Prüfstand). Does this have consequences for the form of the needles? Whether the needles are built from de novo or from a lining up of nano structures can be checked by x-ray. Experiments with a mixture of enantiomers of mandelic acid show a breakdown of the needles for a 50/50 mixture.

Authors measurements

The evaluation of the research with DCC and BSA is laid down in a publication (Busscher 2019) [27]. In the following a short summary is given:

2019 article about DCC and BSA

The pdf and the supplementary pdf from the 2019 article [27] are added to the references and can be read there. Here only the abstract and the highlights are presented.

Title: Crystallization patterns of an aqueous dihydrate cupric chloride solution in the presence of different amounts of Bovine Serum Albumin

Abstract

The crystallization patterns of DCC, crystallized with Bovine Serum Albumine (BSA) as an additive in a Petri-dish, depend strongly on the amount combinations of the salt and the protein. These patterns were studied over a wide range of amounts of the salt and the protein. Different combinations of the two substances yielded distinct patterns, which could be visually described and analytically verified. The influence of the protein was researched over a 0.1 to 10^4 monolayer range (e.g. till the inhibition of the crystallization) and the salt over a $10^{2.5}$ mg range. The following sequence of phenomena could be described. Dewetting, deposit formation, split-growth, dendrites and inhibition of crystallization (amorphous phase). The transitions between the dewetting, deposit formation and split-growth areas are delimited by specific BSA values. The other areas, with higher BSA amounts, are delimited by defined mixture ratios of salt to protein.

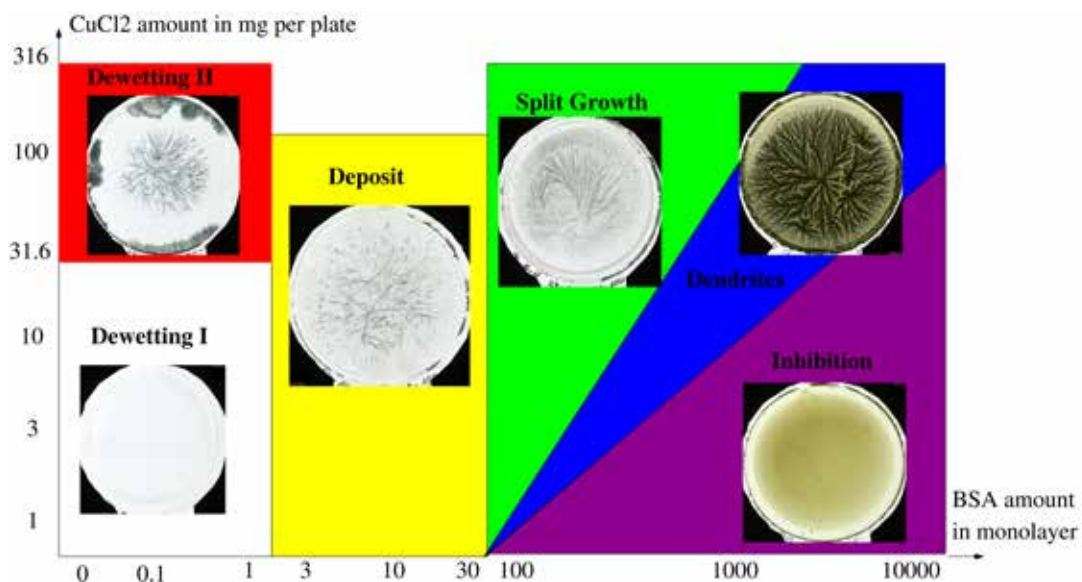
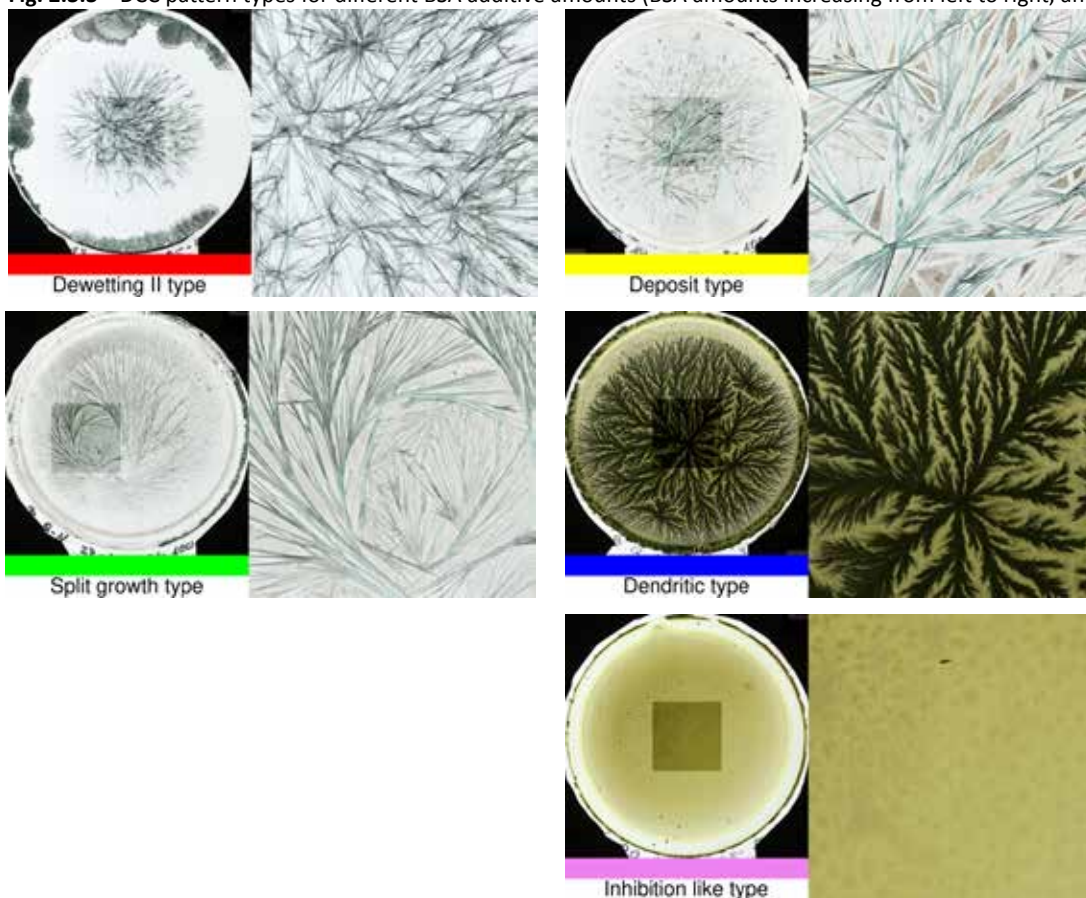


Fig. 2.3.2 Overview of the [Concentration Matrix](#) with colored areas with comparable patterns and thumbnails of representative patterns. The DCC amount in mg per plate is plotted on the Y-axis. The X-axis represents the BSA amount in calculated monolayer per plate. The red area represents the dewetting II type, the yellow area the deposit type, the green area the split-growth type, the blue area the dendritic type, and the violet area the inhibition-like type. The plates in the white area, called dewetting I area have been discussed earlier [28].

Fig. 2.3.3 DCC pattern types for different BSA additive amounts (BSA amounts increasing from left to right, and



from top to bottom) for DCC = 100 mg per plate. The colored bars, above the text describing the crystal type, relate to the similarly colored [CMX](#) areas in Fig. 2.3.2.

Highlights

- BSA was researched over a 0.1-10000 monolayer range and DCC over a 3.1-316 mg range.
- The resulting patterns could be divided into six distinct groups.
- These exhibit dewetting, deposits, split-growth, dendrites and nucleation inhibition.
- Between split-growth and dendrites the light absorbance and growth velocity changed.
- The 1-centered split-growth showed the viscosity negating the nucleation probability.
- The dendrite and nucleation inhibition area were delimited by the DCC - BSA ratio.

Other samples than BSA

Similar studies are needed for other samples besides BSA to determine if this order and type of crystallization is a common phenomenon in the DCC crystallization matrix with additives.

Measurements with mandelic acid

The measurements of Vester 1960 [18] were repeated. The effect that a racemate mixture of the two mandelic acid enantiomers (50/50) disrupts longer needles crystallization (like in Fig. 2.3.3 for the type split-growth or dendrite), could be confirmed. This effect needs to be researched with more concentrations, to see if this effect occurs in the complete crystallization matrix or only for a small area in the CMX. It would be interesting to see if this effect also exist e.g. for carotenes, because the relation of cis and trans carotenes is affected due to the processing of carrots (Lemmens 2009 [29], Lemmens 2010 [30], Knockaert 2011 [31]).

Resume authors measurements

For BSA as additive the dendritic growth depends on the amounts of DCC and additive in the CMX. Different areas in the concentration matrix could be found, which can be separated by different criteria. The observation that in the split-growth area in most cases one-centered pictures were found, is a special phenomenon and seems to be a consequence of the increasing viscosity of the solution due to the increasing additive amount, outweighing the higher nucleation probability according to the increase in heterogeneous crystallization start centers. This has already been observed by von Hahn [32] (p. 23). The angles between the dendrite stems and the needles were in most cases higher than the angles in the split-growth area.

Additional research

Do we see comparable patterns for the concentration matrix of freeze dried wheat and carrot juice and black currant juice? This is under evaluation, will be added to the chapter [1.8 Concentration matrix](#).

Does the crystallization start at the surface?: (tests with [one dish Prüfstand](#))

Does this depend on the surface tension of the DCC/additive mixture?

Wheat has a high and carrot has a low surface tension (Busscher 2010) [17] (in mixtures with DCC)

Question nano particles → [meso-crystals](#) (check with X-ray as described by Cölfen [8], p. 39.) See also in chapter [2.2 Arrangement](#):

Question fresh DCC solutions? Does the growth rate of DCC without additives depend on the age of the DCC solution. Age in terms below 6-8 days (hours 1, 2, 4, 8, 16,..). Pfeiffer states he made the DCC solution fresh prior to each experiment (ref from PD).

Question on growth velocity: Is the growth velocity constant for the same mixing ratio?

- Evaluation of the BSA matrix
- Evaluation of the freeze dried wheat matrix
- Evaluation of the black currant matrix

Question growth velocity: How does the growth velocity depend on the tcrStart value?

- Check for interaction with the mixture ratio.
- Evaluation of the BSA matrix (small pretest: it looks like the correlation is positive for low additive amounts, is it negative for higher additive amounts ?)
- Evaluation of the freeze dried wheat matrix
- Evaluation of the black currant matrix

Check the behavior of DCC only at the acrylic ring: It is showing a dendritic pattern. Is this from an influence of the meniscus or from the gluing substance (Vaseline)?

The quotation from Mukherjee and Sharma [12] is very important. It opens a door to a non Lego-like perception of the formation of the crystal form. The form is now shaped from something “outside” the building blocks. How to connect and to continue with this?

The crystallization process is expected to expel the additive (cleaning of a substance by ongoing crystallization). Do we see an increase in additive in the direction of the rim of the Petri-dish? (Glycogen pictures and carrot substance spirals start at the rim, not at the center?)

Can we see the influence of the type of viscosity (BSA and glycogen are shear thinning, PVP is Newtonian)?

- Where do we expect to see this influence?

How did the width of the needle depend on the sample and the amounts?

- Evaluate with the structure image analysis.

How can we come to an hypothesis what happens in the area with the surface tension- and temperature-gradient (Busscher 2019) [28] and how does it influence the crystal growth?

- Is this connected to the visual evaluation criterion *Durchstrahlung* (Huber 2010 [33])?
- See for the most sensitive area with the highest sample differentiation also chapter [1.6 Sensitive area](#).
- Is this an interaction of top-down and/or bottom-up processes?

References

- [1] Kurz W. Solidification Microstructure-Processing Maps: Theory and Application. *Advanced engineering materials* 2001; 3: 443-452 [https://doi.org/https://doi.org/10.1016/0956-7151\(94\)90044-2](https://doi.org/https://doi.org/10.1016/0956-7151(94)90044-2).
- [2] Langer JS, Müller-Krumbhaar J. Stability effects in dendritic crystal growth. *Journal of Crystal Growth* 1977; 42: 11 - 14 [https://doi.org/DOI: 10.1016/0022-0248\(77\)90171-3](https://doi.org/DOI: 10.1016/0022-0248(77)90171-3).
- [3] Langer JS. Instabilities and pattern formation in crystal growth. *Rev. Mod. Phys.* 1980; 52: 1-28 <https://doi.org/10.1103/RevModPhys.52.1>.
- [4] Sekerka RF. Role of instabilities in determination of the shapes of growing crystals. *Journal of Crystal Growth* 1993; 128: 1-12.
- [5] Beckmann H. Über Keimbildung, Einkristallwachstum und Auffächerungswachstum von $\text{CuCl}_2 \cdot 2\text{H}_2\text{O}$ in reinwässrigen und Eiweiß-haltigen Lösungen. PhD Thesis, Universität Bonn. 1959.
- [6] Beckmann H. Strukturzustand der Lösung und Kinetik des Kristallwachstums im System Kupferchlorid. *Fortschritte der Mineralogie* 1961; 39: 33-36.
- [7] Desiraju GR. Crystal Engineering: From Molecule to Crystal. *J. Am. Chem. Soc.* 2013; 135: 9952-9967 <https://doi.org/10.1021/ja403264c>.
- [8] Cölfen H and Antonietti Markus Wiley 2008S1-6. Mesocrystals and nonclassical crystallization (Wiley, 2008).
- [9] Driessche V, Alexander E. S, Van Gerven N, Bomans PHH, Joosten RRM, Friedrich H et al. Molecular nucleation mechanisms and control strategies for crystal polymorph selection. *Nature* 2018; 556: 89-94 <https://doi.org/10.1038/nature25971>.
- [10] Alberstein RG, Tezcan FA. Observations of the birth of crystals. *Nature* 2018; 556: 41-42.
- [11] Lee H-E, Ahn H-Y, Mun J, Lee YY, Kim M, Cho NH et al. Amino-acid- and peptide-directed synthesis of chiral plasmonic gold nanoparticles. *Nature* 2018; 556: 360-365.
- [12] Mukherjee R, Sharma A. Instability, self-organization and pattern formation in thin soft films. *Soft Matter* 2015; 11: 8717-8740 <https://doi.org/10.1039/C5SM01724F>.
- [13] Schweizer F. Beobachtungen bei der Biokristallisation von Glykogen. *Elemente der Naturwissenschaft* 2007; 87: 76-89.
- [14] Nickel E. Die Reproduzierbarkeit der sogenannten empfindlichen Kupferchloridkristallisation. PhD Thesis, Universitätsverlag, Freiburg (Schweiz). 1968.
- [15] Waldburger B. Die Blutkristallisation als Schulungsmethode. *Merkurstab* 2013; 5: 402-414.
- [16] Misyura S. Evaporation and heat transfer of aqueous salt solutions during crystallization. *Applied Thermal Engineering* 2018; 139: 203 - 212 <https://doi.org/https://doi.org/10.1016/j.applthermaleng.2018.04.068>.
- [17] Busscher N, Kahl J, Doesburg P, Mergardt G, Ploeger A. Evaporation influences on the crystallization of an aqueous dihydrate cupric chloride solution with additives. *Journal of Colloid and Interface Science* 2010; 344: 556-562 <https://doi.org/doi:10.1016/j.jcis.2009.12.045>.
- [18] Vester F. Zur Indikation biochemischer Vorgänge durch kristallisierendes Kupferchlorid. *Cellular and Molecular*

- Life Sciences* 1960; 16: 279-281 <https://doi.org/doi:10.1007/BF02157670>.
- [19] Blasco CAS&E. Mass production of 3D microcomponents. *Nature* 2024; 627: 276-277.
- [20] Libbrecht KG. The physics of snow crystals. *Reports on Progress in Physics* 2005; 68: 855.
- [21] Ball P. *Nature's Patterns* (Oxford University Press, 2008).
- [22] Trivedi R, Kurz W. Modeling of solidification microstructures in concentrated solutions and intermetallic systems. *Metallurgical Transactions A* 1990; 21: 1311–1318 <https://doi.org/10.1007/BF02698258>.
- [23] Asta M, Beckermann C, Karma A, Kurz W, Napolitano R, Plapp M et al. Solidification microstructures and solid-state parallels: Recent developments, future directions. *Acta Materialia* 2009; 57: 941-971 <https://doi.org/10.1016/j.actamat.2008.10.020>.
- [24] Haxhimali T, Karma A, Gonzales F, Rappaz M. Orientation selection in dendritic evolution. *Nat Mater* 2006; 5: 660-664 <https://doi.org/doi:10.1038/nmat1693>.
- [25] Nakoryakov, Vladimir, Misyura, Sergei, Morozov, Vladimir. Surface Crystallization of Aqueous Salt Solution Under Overheating and Overcooling. *MATEC Web Conf.* 2016; 72: 01072 <https://doi.org/10.1051/mateconf/20167201072>.
- [26] Schweizer F, Andersen J-O, Jens-Laursen. Beobachtungen bei der Kupferchloridkristallisation: vom Eiweiß-Vorbild zum Kupferchlorid-Nachbild. *Elemente der Naturwissenschaft* 2010; 92: 62-93 <https://doi.org/DOI:10.18756/edn.92.62>.
- [27] Busscher N, Doesburg P, Mergardt G, Sokol A, Kahl J, Ploeger A. Crystallization patterns of an aqueous dihydrate cupric chloride solution in the presence of different amounts of Bovine Serum Albumin. *Journal of Crystal Growth* 2019; <https://doi.org/doi:10.1016/j.jcrysgro.2019.125272>.
- [28] Busscher N, Doesburg P, Mergardt G, Sokol A, Kahl J, Ploeger A. Influence of dewetting on the crystallization behavior of CuCl₂ in the presence of BSA during evaporation in a Petri dish. *Heliyon* 2019; 5: e01102 <https://doi.org/10.1016/j.heliyon.2018.e01102>.
- [29] Lemmens L, Van Buggenhout S, Oey I, Van Loey A, Hendrickx M. Towards a better understanding of the relationship between the β-carotene in vitro bio-accessibility and pectin structural changes: A case study on carrots. *Food Research International* 2009; 42: 1323-1330 <https://doi.org/https://doi.org/10.1016/j.foodres.2009.04.006>.
- [30] Lemmens L, De Vleeschouwer K, Moelants KRN, Colle IJP, Van Loey AM, Hendrickx ME. β-Carotene Isomerization Kinetics during Thermal Treatments of Carrot Puree. *J. Agric. Food Chem.* 2010; 58: 6816-6824 <https://doi.org/10.1021/jf100449t>.
- [31] Knockaert G, Roeck AD, Lemmens L, Buggenhout SV, Hendrickx M, Loey AV. Effect of thermal and high pressure processes on structural and health-related properties of carrots (*Daucus carota*). *Food Chemistry* 2011; 125: 903 - 912 <https://doi.org/http://dx.doi.org/10.1016/j.foodchem.2010.09.066>.
- [32] Von Hahn F-V. Thesigraphie. (Franz Steiner Verlag, 1962).
- [33] Huber M, Andersen J-O, Kahl J, Busscher N, Doesburg P, Mergardt G et al. Standardization and Validation of the Visual Evaluation of Biocrystallizations. *Biological Agriculture and Horticulture* 2010; 27: 25–40.

2.4 Concentration gradient in the dish

How can we understand it, how does it depend on the $\text{CuCl}_2 \cdot 2\text{H}_2\text{O}$ Chamber system in Witzenhausen, Bonn and Darmstadt?

Abstract

The evaporation measurements from Hollemann [1] and Busscher [2] are described and compared. The $\text{CuCl}_2 \cdot 2\text{H}_2\text{O}$ (cupric chloride di-hydrate, further named [DCC](#)) concentration profiles during the evaporation are depending on time. In the beginning, the evaporation in the middle of the Petri-dish is stronger than at the rim. Therefore, in the beginning of the evaporation, the DCC concentration is higher in the middle of the Petri-dish than at the rim. Strong differences in the measured DCC concentration profiles over the Petri-dish at the beginning of the evaporation became visible. Holleman [1] measured a spiky mountain DCC concentration profile, while Busscher [2] measured a DCC concentration profile with a broad plateau. The question is if the differences in the DCC concentration profiles vanish at the end of the evaporation, just when the crystallization starts. Additional research for the comparison is described.

Introduction

In the Petri-dish with an evaporating $\text{CuCl}_2 \cdot 2\text{H}_2\text{O}$ (cupric chloride di-hydrate, further named [DCC](#)) solution, a DCC concentration and temperature profile can be measured [1] [2]. The highest concentration and the lowest temperature are in the middle of the Petri-dish, while the lowest concentration and the highest temperature are at the rim. The hypothesis is that the evaporation in the middle of the Petri-dish is stronger than at the rim due to the shielding of the passing air flowing by the rim of the Petri-dish [1] [2]. This is consistent with the concentrations and the temperatures, because a high evaporation gives a higher concentration and lower temperature and vice versa. The difference in concentration and temperature from the middle to the rim of the Petri-dish creates a concentration and temperature gradient in the Petri-dish. The form of the gradient depends on the height of the rim of the Petri-dish (see chapter [1.4 Surface tension cleaning ring height](#)) and the strength and direction of the air-flow. The concentration and temperature gradients cause gradients in the surface tension [3] [4]. Gradient forces are significant and can lead to dewetting [5] [6]. One difference between the so called [Triangle chamber system](#) (Witzenhausen, D; Roepaen, NL; BRAD, DK) and the chamber system in Bonn is the directionality of the airflow, which is from above (Bonn), from below (Triangle), and undetermined (Darmstadt).

Historical overview

The DCC concentration gradient was measured by Hollemann [1] for a top-down airflow. The measurements were repeated by Busscher [2] for the so called Triangle system, where the airflow from bottom to top, which confirmed the existence of a concentration and a temperature gradient in the Petri-dish. Petterson [7] discussed the question of whether the gradient also exists for the additive. This should be the reason for the zonal distribution (see chapter [1.13 Picture zones](#)), because the DCC-additive ratio is different throughout the dish, as can be confirmed visually in the final crystal. Nickel [8] and Leray [9] expected that the gradient creates a so called "*Wachstumsfeld*" which should guide the crystallization.

Holleman's results

Holleman measured the concentration in the Petri-dish during the evaporation. For the description of the used Petri-dish he referred to Bessenich 1960 [10], but she gave no data about the height of the ring. Pfeiffer ([11], p. 14) used rings with 10 mm height. Selawry ([12], p. 8) used 15 mm as ring height.

In Fig. 2.4.1 shown below (Fig. 1 from Hollemann's article [1]), after reading the description, it was assumed that the top left plot is referred to as 1.a, the upper right as 1.b, the lower left as 1.c and bottom right as 1.d. The figure was additionally labeled in this way.

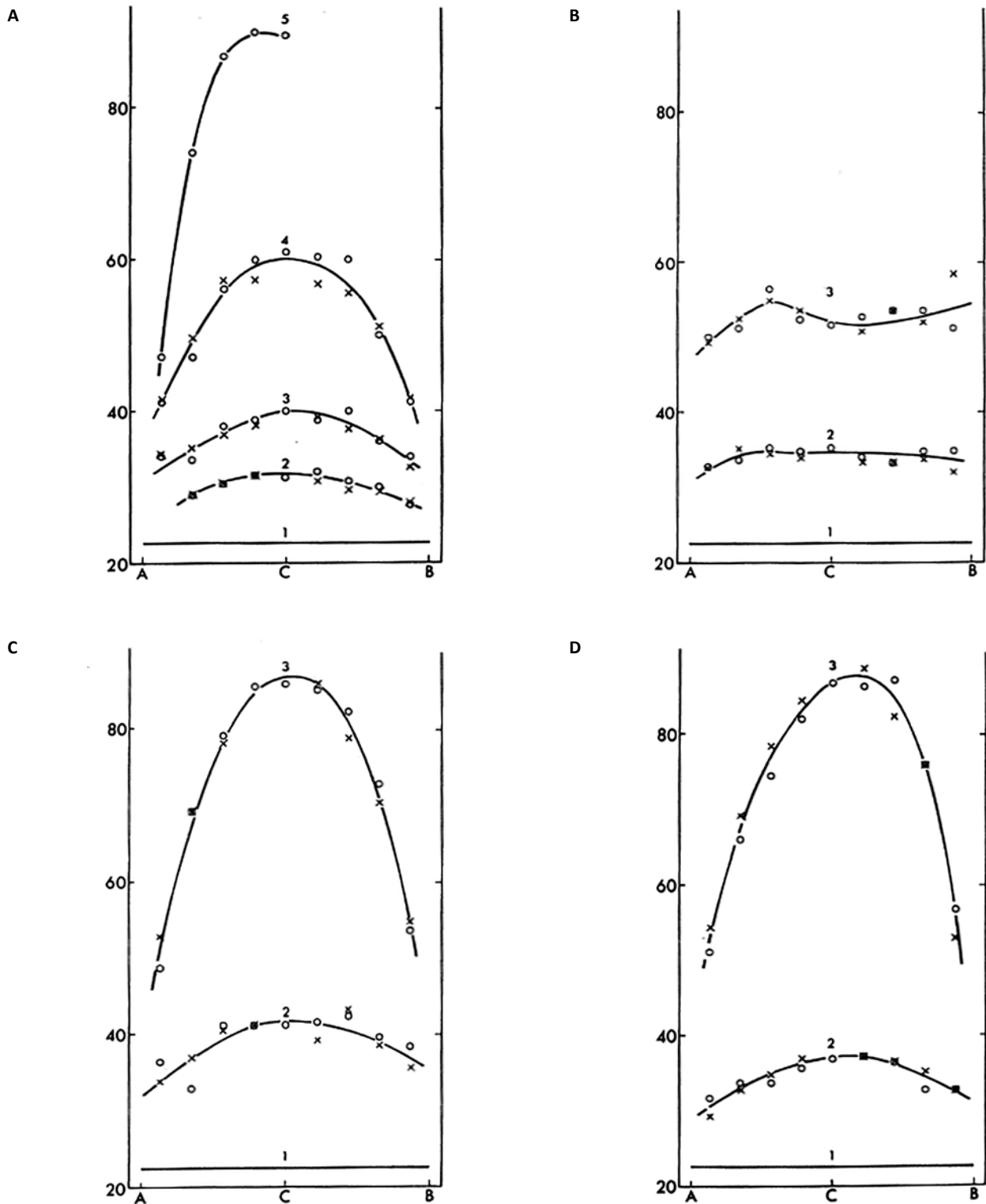


Fig. 2.4.1 DCC concentration versus location in the Petri-dish. The curves are according to the following experiments: Fig. 2.4.1 A is measured in an open dish, Fig. 2.4.1 B dish covered with a fine-meshed wire netting and a layer of desiccant, such as anhydrous silica gel, as in Fig. 2.4.2.1 C dish covered with a fine-meshed wire netting and a layer of desiccant, bent as closely as possible to the shape in Fig. 2.4.1 D dish covered with a flat perforated plate as in Fig. 2.4.4. (Fig. nr 1 from Hollemann 1966 [1]).

Hollemann tried to find the curve of how the passing air bends into the dish. This is where the airflow passing the dish meets the diffusion from the surface of the solution. According to Stefan [13] [14] the diffusion part is proportional to $1/L$, where L is the height between the surface of the solution and the point where the airflows. The shorter the distance, the stronger the diffusion, as can be seen in the curved shape in Fig. 2.4.3 (see also in [1.2 Water transport](#)).

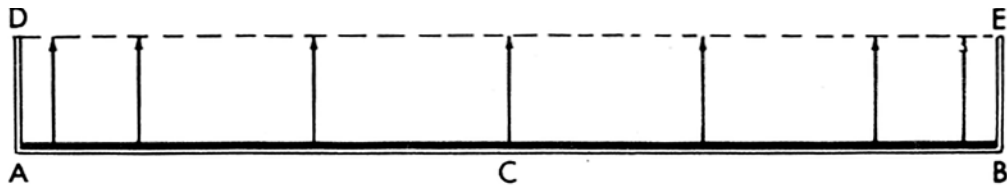


Fig. 2.4.2 Evaporation of a dish, where the air is not “bending” into the dish (Ideal Stefan problem). Fig. no. 3 from Hollemann 1966 [1].

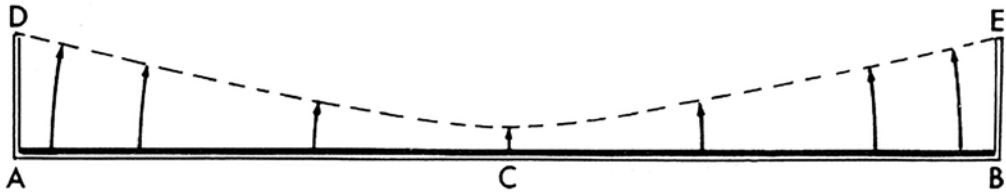


Fig. 2.4.3 Evaporation in a dish where the airflow is “bending” into the dish. The curved surface indicates where the diffusion from the solution surface (Stefan problem) meets the airflow. Fig. no. 4 from Hollemann 1966 [1].

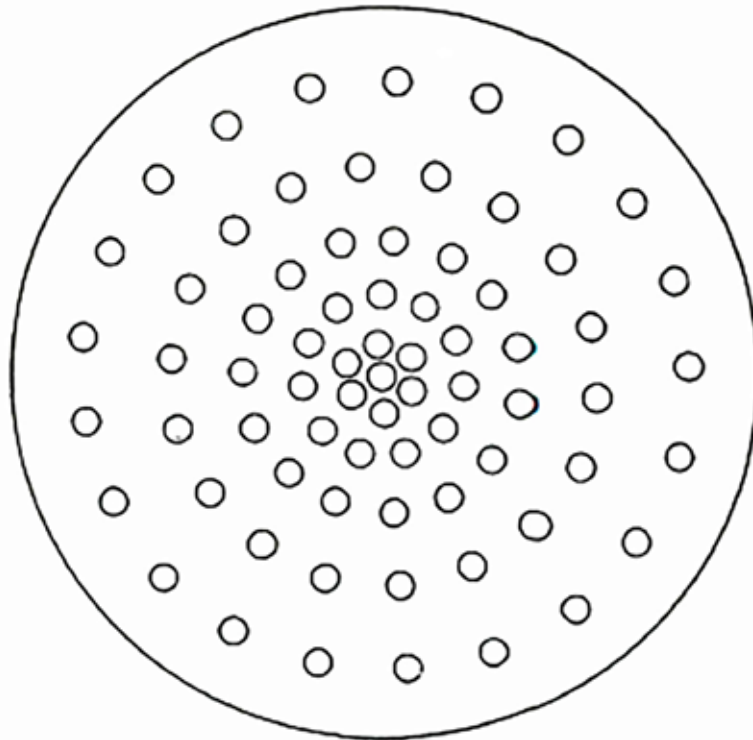


Fig. 2.4.4 Mask with specially distributed holes to be placed on the Petri-dish. This was used by Hollemann to create the same gradient in the Petri-dish as in the chamber, without a airflow bending into the dish. Fig. no. 5 from Hollemann 1966 [1].

Resume article Hollemann

The result in Fig. 2.4.3 means that already at a ring height of 10 mm, if the air is coming from above (as we assume), there is still a 2 mm diffusion distance between the airflow and the surface of the solution. The air bends 8 mm into the dish.

Authors Measurements

Distribution of the DCC concentration in the dish (Triangle system)

During evaporation (see chapter [1.2 Water transport](#)), a DCC concentration gradient is built in the dish. This is due to the wind shielding effect of the acrylic ring [1]. The highest concentration of DCC is found in the area around the geometric center. In the case of the Triangle chambers (Andersen 1998 [15]) with 35 mm high acrylic rings forming the rim of the Petri-dish, this is constant in an area between 0 % and 40 % of the dish radius (see below for details). In Fig. 2.4.5 the situation is plotted for three measurement points during evaporation (and one estimated time point for $t = 12$ h) according to the data published in [2].

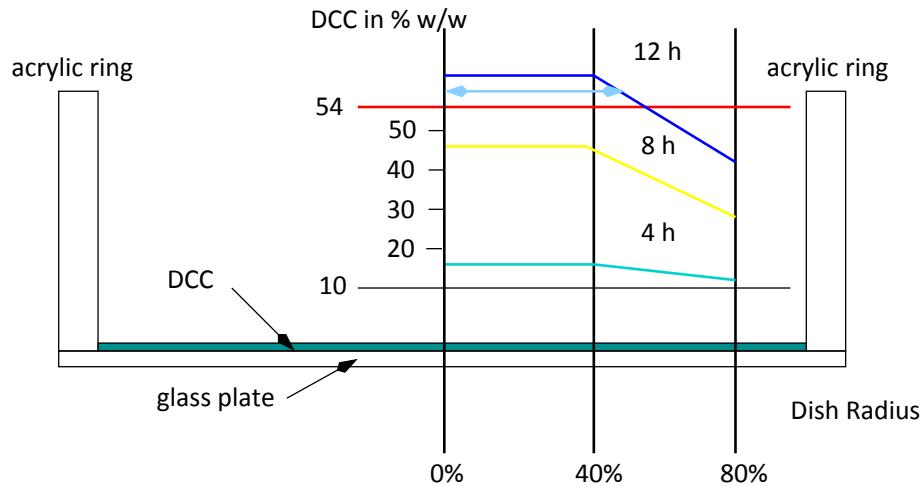


Fig. 2.4.5 Y-axis DCC concentration in % w/w in the dish during evaporation versus the percentage of the dish radius around the geometric center (X-axis in percentage of total dish radius). Measured DCC concentrations: at start 10 % w/w (grey line), after 4 hours (green) and after 8 hours (yellow) evaporation. Estimated values for 12 hours (blue). Saturation concentration 54 % w/w (red line).

For a 600 mg DCC [amount per plate](#) the evaporation starts at a 10 % w/w concentration, which is shown as a horizontal grey line in Fig. 2.4.5. The airflowing from below passes the dish and transports the humidity, which is evaporating from the solution [16]. During the evaporation the area around the geometric center has a higher evaporation rate than the areas close to the acrylic ring due to the shielding of the acrylic ring. The (back) diffusion through the DCC gradient seems to be of equal or lower order compared to the influence of the evaporation rate, because it does not counterbalance the DCC gradient. Hollemann [1] described that if the evaporation is stopped at the moment when the first crystals appear, the crystals disappear again. Leray [9] measured the diffusion coefficient of DCC and calculated the length of diffusion for 4 hours to 0.34 cm. This explains why the concentration gradient can exist and is not compensated by the (back) diffusion of the DCC.

When the DCC concentration reaches the saturation concentration (the red line) of the solution, usually no crystallization takes place. When the concentration exceeds the saturation concentration, a so called supersaturation occurs. The supersaturation is defined as the difference between the DCC concentration and the saturation concentration, normalized by the saturation concentration. The probability of nucleation grows exponentially with the level of supersaturation. It reaches a maximum when it is balanced by the increase in viscosity of the DCC solution [17] [18] [19] (see also chapter [2.11 Nucleation](#)).

Comparison with Holleman's results

The concentration distributions in the Petri-dish for the different chamber systems are quite different. The Hollemann measurements show a spiky mountain form, while Busscher's measurements show a plateau at least to 40 % of the dish radius. The question is whether the Hollemann distribution becomes more plateau-like at the end of the evaporation as the evaporation rate decreases due to the increasing concentration gradient (see chapter [1.2 Water transport](#)).

- How to test the difference between the chamber systems:
 - A first guess would be to check for the distribution of the radius of the centers (see chapter [2.11 Nucleation](#)). This should give smaller values for the radii, when the concentration profile

maintains its spiky mountain character.

- A second possibility is to check during the evaporation, using a pH indicator as additive for the spreading of the pH (the DCC concentration), if they are still different when the crystallization starts.

Resume

The comparison of the Holleman and the Busscher measurements raises the question whether the differences at the beginning of evaporation are still present when the crystallization starts?

Additional research

- Build a [one dish Prüfstand](#) with one dish on a scale with pH indicators
 - Check the homogeneity of the concentration (pH) distribution during evaporation
 - Check how fast the evaporation “grows” to the rim of the Petri-dish? (difference of the systems)
- Compare the distributions of the radii (and the tcrStart if possible).
 - Preparation for the Radii evaluation: read the photos of the pictures into [LabDoc](#) and evaluate them in that context.
- Measure the temperature profile during the evaporation.
 - The evaporation rate depends on the DCC concentration. At the end of the evaporation the temperature distribution can be homogeneous when the concentration becomes homogeneous.

References

- [1] Holleman LWJ. Ein Beitrag zum Verständnis der empfindlichen Kristallisation. *Elemente der Naturwissenschaft* 1966; 4: 24-33 <https://doi.org/10.18756/edn.4.24>.
- [2] Busscher N, Kahl J, Doesburg P, Mergardt G, Ploeger A. Evaporation influences on the crystallization of an aqueous dihydrate cupric chloride solution with additives. *Journal of Colloid and Interface Science* 2010; 344: 556–562 <https://doi.org/doi:10.1016/j.jcis.2009.12.045>.
- [3] Leray J. Profile de la surface libre d'un film liquide heterogene. *Journal de chimie physique* 1973; 10: 1428-1432.
- [4] Nitschmann G. Gedanken zur empfindlichen Kristallisation mit Kupferchlorid. Im Anschluß an die Arbeit von R. E. Hummel: Liefert die Kupferchlorid-Kristallisations-Methode einen Nachweis für die Gestaltkräfte des Lebendigen? *Elemente der Naturwissenschaft* 1993; 58: 14-19 <https://doi.org/10.18756/edn.58.14>.
- [5] Habibi M, Rahimzadeh A, Eslamian M. On dewetting of thin films due to crystallization (crystallization dewetting). *Eur. Phys. J. E* 2016; 39: 30 <https://doi.org/doi:10.1140/epje/i2016-16030-9>.
- [6] Busscher N, Doesburg P, Mergardt G, Sokol A, Kahl J, Ploeger A. Influence of dewetting on the crystallization behavior of CuCl₂ in the presence of BSA during evaporation in a Petri dish. *Heliyon* 2019; 5: e01102 <https://doi.org/10.1016/j.heliyon.2018.e01102>.
- [7] Pettersson BD. Beiträge zur Entwicklung der CuCl₂ Methode nach Pfeiffer. *Elemente der Naturwissenschaft* 1966; 5: 29-39.
- [8] Nickel E. Die Reproduzierbarkeit der sogenannten empfindlichen Kupferchloridkristallisation. PhD Thesis, Universitätsverlag, Freiburg (Schweiz). 1968.
- [9] Leray J. Profile de la surface libre d'un film liquide heterogene. *Journal de chimie physique* 1973; 10: 1428-1432.
- [10] Bessenich F. Zur Methode der empfindlichen Kristallisation (Naturwissenschaftliche Sektion am Goetheanum Dornach, 1960).
- [11] Pfeiffer E. Studium von Formkräften an Kristallisationen (Naturwissenschaftliche Sektion am Goetheanum, 1931).
- [12] Selawry A and Selawry O. Die Kupferchlorid-Kristallisation in Naturwissenschaft und Medizin (Gustav-Fischer-Verlag, 1957).
- [13] Stefan J. Ueber die Verdampfung aus einem kreisförmig oder elliptisch begrenzten Becken. *Annalen der Physik* 1882; 253: 550-560.
- [14] Suehrcke, H. and Harris, J. A. Enhancement of water evaporation from a cylindrical container due to concentration induced free convection. Proceedings of the Twelfth Australasian Fluid Mechanics Conference, The University of Sydney, Sydney, Australia. 1995.

- [15] Andersen JO, Laursen J, Koelster P. A Refined Biocrystallization Method applied in a Pictomorphological Investigation of a Polymer. *Elemente der Naturwissenschaft* 1998; 68: 1-20 <https://doi.org/DOI: 10.18756/edn.68.1>.
- [16] Busscher N, Kahl J, Ploeger A. From needles to pattern in food quality determination. *Journal of the Science of Food and Agriculture* 2014; 94: 2578-2581 <https://doi.org/doi:10.1002/jsfa.6498>.
- [17] Beckmann H. Über Keimbildung, Einkristallwachstum und Auffächerungswachstum von $\text{CuCl}_2 \cdot 2\text{H}_2\text{O}$ in reinwässrigen und Eiweiß-haltigen Lösungen. PhD Thesis, Universität Bonn. 1959.
- [18] Leray JL. Growth kinetics of hydrated cupric chloride. *Journal of Crystal Growth* 1968; 3-4: 344-349 [https://doi.org/DOI: 10.1016/0022-0248\(68\)90172-3](https://doi.org/DOI: 10.1016/0022-0248(68)90172-3).
- [19] Reiter G, Barth J-G. Some general remarks on crystallization in the presence of additives. *Elemente der Naturwissenschaft* 2010; 92: 39-61 <https://doi.org/10.18756/edn.92.39>.

2.5 Warmth of process

Cooling by evaporation and heating by crystallization, how is this affected by the chamber design?

Abstract

The heat fluxes (the flow of heat per unit area per unit time) through the Petri-dish during evaporation and crystallization depend on the heat fluxes from the environment (e.g. heating). The various crystallization systems, such as used by the Triangle members [1], the one used in Darmstadt, Bonn, the chamber from Barth [2], and the [one dish Prüfstand](#), differ in their heat fluxes running through the Petri-dishes and their thermal connection to the inner chamber walls. For the Triangle system, the influence of ambient heat was listed and discussed.

Introduction

Starting points for the discussion on process warmth

The evaporation process decreases the temperature of the solution, while the crystallization process increases the temperature of the crystals and the solution. The different crystallization systems, like the one used by the Triangle members, or the one in Darmstadt, in Bonn, Barth's chamber, or the one dish Prüfstand, have different heat fluxes running through the Petri-dish. The Triangle system [1] has a temperature regulation below the dishes and a warmth shielding around the Petri-dishes, while the Darmstadt system heats the inner chamber only by heating the outer chamber, and the Bonn system heats the air before it enters the chamber. Barth [2] uses a temperature regulated metal ring, on which the dishes are placed. The [one dish Prüfstand](#) has no temperature regulation of itself. A more detailed description is found in chapter [3.1 Chamber systems](#).

The question is, how the heat flow from the Petri-dish to the environment affects the crystallization pattern and how the heat flow is affected by the temperature distribution of e.g. the inner chamber walls, or the metal parts of the crystallization apparatus below the Petri-dishes.

Historical overview

The evaporation from a Petri-dish is called the Stefan problem [3] (see for details Chapter [2.13 Evaporation model](#)). The question discussed here is how to deal with the heat flow through the dish. Sparrow [4] reported the difference in isothermal (an isothermal process is a change of a system, in which the temperature remains constant) and non-isothermal evaporation from open tubes. DCC with additives is based on a non-isothermal evaporation process, for which Sparrow states: *"in addition to natural convection in the gas vapor space, account must be taken of thermal radiation at the bounding surfaces of the gas-vapor space and of natural convection in liquid pool"*. Saylor [5] discussed the heating from below. Kumar [6] discussed the heating from below and from above. Flack [7] discussed the cooling from above. Misyura [8] reported about crystallization in a Petri-dish for different metal chlorides solutions (not DCC). Barth [2] built a new type of chamber in 2011, which has 1: a carefully designed and tested airflow and 2: a massive metal ring, where the dishes are placed on, to reduce the temperature variation between the Petri-dishes.

Authors research

Heating (the air) from below the dishes

In the Triangle chambers, the air passing the dishes is heated from below the dishes. See the geometry in [Appendix 2.5.2 Heating](#) below. During evaporation, the heating counterbalances the cooling from the evaporation process in the dish. The evaporation reduces the surface temperature of the solution by 2 °C [9], see also in [Appendix 2.5.1 Temperature](#).

The used power is around 70 Watt for 43 dishes without evaporation. If the light inside the chamber is left on for a longer period of time (> 1 hour, power = 2 * 15 Watt = 30 Watt for the former light system), then due to the excess heat from the lights, the heating regulation is reduced and is insufficient to reach an average crystallization starting time (tcrStart) of 12 - 14 h. The newer light system is made up of 4 * 4 Watt LED light bulbs, reducing the heating from above.

During the winter the heating below the dishes increases. Perhaps the chamber floor is cooling down in response to the outside temperature, or the outer room regulator is in need of improvement.

From 2017 to 2018 the chamber handling in Roepaen (Crystal Lab, chamber P) was changed. When no experiments were being performed, the positions of the dishes in the chamber were covered with glass plates (Petri-dishes without the acrylic ring). In case of an experiment, the glass plates were removed and the Petri-dishes were placed. This should result in a more stable temperature behavior of the chamber, because the airflow is unchanged before and after an experiment (see chapter [1.1 Crystallization starting time](#)).

Warmth shielding of the crystallization apparatus

The dishes positioned on the double steel ring showed an inhomogeneous evaporation rate between the inner and outer ring prior to the application of a warmth shield around the acrylic tubes (data from 20.08.2007 chamber P, NL). To have a more homogeneous warmth distribution the evaporation apparatus was shielded (~ 2003) and the heating of the inner and outer ring was adjusted to reduce the difference between their mean $t_{crStart}$ values (see also Checking Influences project report [10] and HOM II SubReport [11]).

Evaporation effects

The temperature changes in the dish during the evaporation inside the dish were measured (a lower temperature around the center, a higher temperature at the rim of the Petri-dish) and published in Busscher 2010 [9]. As described by Holleman [12] due to a stronger evaporation around the geometrical center of the Petri-dish, the decrease of the temperature due to evaporation was up to 2 °C ([9] Fig. 5) in the center of the Petri-dish and around 1 °C close to the rim. The temperature situations were documented in 2014 with an IR camera in Roepaen, NL (Crystal Lab, chamber P) and the results could be repeated. For details of the IR photos see [Appendix 2.5.1 Temperature](#).

Checking Influences project

The Checking Influences project revealed differences in the chamber wall temperatures. There was no simple correlation between the influence of wall temperatures and crystallization start times. The variation of the $t_{crStart}$ values due to the variation of the acrylic tube geometry ([10] p. 89 ff.) was in most cases larger.

Absorbance Project asymmetry of DCC in the pictures

The symmetry evaluation (left to right, top to bottom) of the spatial distribution of DCC in the Petri-dish in the Absorbance project [13] was performed to find a quantitative approach to:

- 1: the possible warmth influence from the chamber walls on the DCC distribution in dish during the crystallization
- 2: the influence of the asymmetry of the airflow during evaporation on the distribution of the DCC in the dish.

The absorbance, as the logarithm of the light transmission of the image, is first order proportional to the amount of DCC on the glass plate (Lambert Beer's law). Quadrants of the pictures were evaluated (see [13] Fig. 1 p. 2).

To verify or calibrate the measurements, experiments were performed in which the dishes were tilted (6 mm over 1 m). Usually the dishes are positioned with the center facing "downwards" during scanning. In order to preserve the information as to how they lay on the double ring, the dishes were scanned as they were oriented on the double ring. The experiments were performed with PVP, freeze dried wheat and carrot as additive. Only the freeze dried wheat pictures showed the expected effect, with more DCC on the tilted side. There was no left / right imbalance towards the tilted side.

For the tilted experiments the pictures were oriented on the scanner the same way as they were oriented in the chamber. The results were compared with leveled dish experiments, using the default scan procedure, in which the pictures are oriented "center down" on the scanner. The experiments with wheat, DOK 2003 samples [14] and Geel 2007 samples [15] were evaluated. The center area showed more DCC than the other areas, in both experiments. One hypothesis would point to the assumption that the crystallization process would attract more DCC, or that during the evaporation process the DCC has a higher amount (not only concentration) around the center position. In addition, a left / right unbalance in the leveled wheat pictures became visible, which could not be understood, because the tilted dish experiment did not show this phenomenon.

Resume

The evaluation of the asymmetric coverage of the Petri-dishes with DCC did not provide an approach to evaluate the influence of the temperature of the chamber walls on the picture, because the asymmetry of the DCC coverage has additional factors of influence. These include the sample, or the asymmetry of the airflow, passing

the dish. The difference between the inner and outer ring was reduced by mounting a warmth shield, which shows that the warmth has an influence on the tcrStart. Perhaps this evaluation should be repeated using the [CrystEval](#) tool, which can determine the orientation of the dish in the chamber and can determine the crystallization growth rate, which may depend on the temperature of the chamber walls.

Additional research

The influence of the warmth was first recognized by the missing shielding of the inner and outer acrylic tube. The IR photos in Appendix 2.5.1 Temperature show that the variation of the temperature in the dish during the evaporation (relative to the ambient air: -1 °C towards the rim, -2 °C in the center area) is in the range of the direct measurements from Busscher [9]. There is no temperature asymmetry visible in Appendix 2.5.1 Temperature in the range of 1 °C - 2 °C. From this, it can be deduced that the evaporation phase is not disturbed by the heating. The warmth from the dish environment could interact with the crystal growth process, in addition to possibly affecting nucleation.

- Is the left / right DCC imbalance in the evaluated wheat pictures also visible when the wheat pictures are “turned” to their original orientation in the chamber on the double steel ring? A reevaluation with the CrystEval tool should be done, measuring the crystallization growth rate, and the location of the center, which can show a dependency on the temperature of the chamber walls.
- Study the differences between Triangle (heating) and Darmstadt (no direct heating in the chamber, but heating of the outer chamber room). Check if the article from Sparrow [4] about isothermal and non-isothermal processes gives insights to understand the differences in humidity. Sparrow [4] reported the difference in isothermal and non isothermal processes from open tubes (check if the airflow velocity is comparable to ours).
- Maybe the asymmetry effect can be checked with the [turbidity effect](#) on mixtures of DCC with BSA or PVP in a comparison between the [Triangle System](#) and the system in Darmstadt.
- In the tilted dish experiment only freeze dried wheat shows DCC centralization while PVP and carrot as additive do not. What is the reason for this? Is this depending on the DCC amount → separation from the rim? Or is the composition of the sample determining this effect? Check as a basis the orientation of the dish in the chamber with the CrystEval tool (see chapter [3.3 CrystEval tool](#)).
- Check the homogeneity of the image analysis data inside an ROI. Maybe the asymmetry is due to data inhomogeneity in an ROI. Maybe we need other ROI's to deal with the symmetry question.
- Direct access of the (warmth) environment of one dish in the one-dish Prüfstand to study the asymmetry. Check whether the cause of the asymmetry is due to the thermal symmetry around the Petri-dish or to the asymmetry of the air passing by the dish. See for more information the chapter one dish prüfstand.

Appendix 2.5.1 Temperature

Observation of the temperature of the Petri-dishes in the Triangle type chamber.

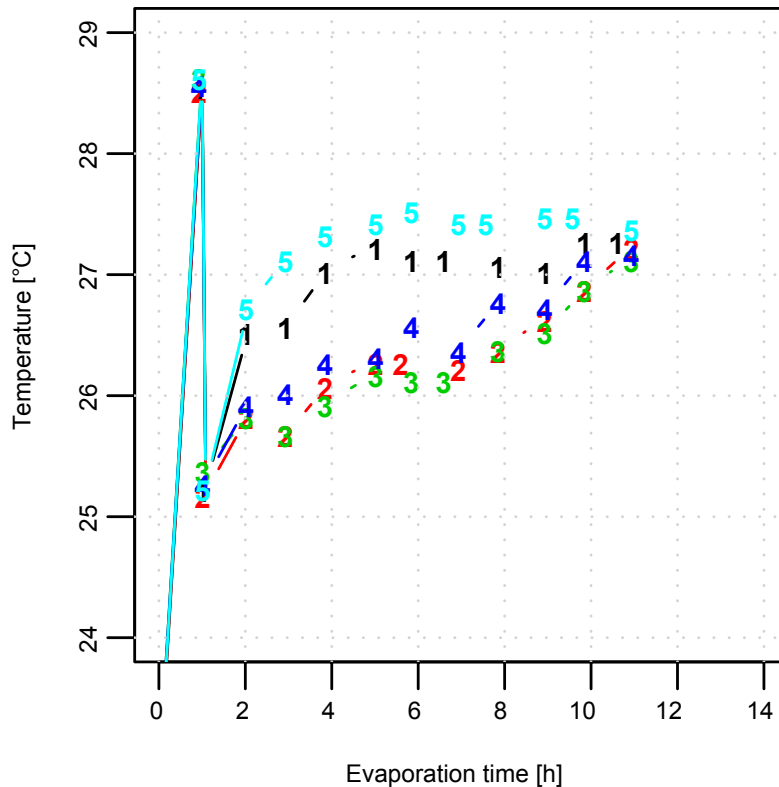


Fig. 2.5.1 Dependency of the surface temperature of the DCC-only solution on position and evaporation time. Data shown from one experiment, which was repeated two times with similar results. Data from Busscher 2010 [8], Fig. 5.

In Fig. 2.5.1 the dishes were placed at $t = 0$ in the chamber. The dishes have a temperature of around 25 °C. Compared to the ambient temperature, they appear as cool, see Fig. 2.5.2 and 2.5.3. Then they warm up, reaching 30 °C after approximately 45 min (as in Fig. 2.5.4). When the solution is pipetted after ~ 1 hour, the temperature decreases to 25.5 °C. Then the solution warms up again and simultaneously cools down due to the evaporation. The numbers 1 - 5 relate to spatial locations in the dishes; 1 and 5 are closer to the geometrical center of the dish (high evaporation rate), whereas 2, 3, 4 are located more peripherally.

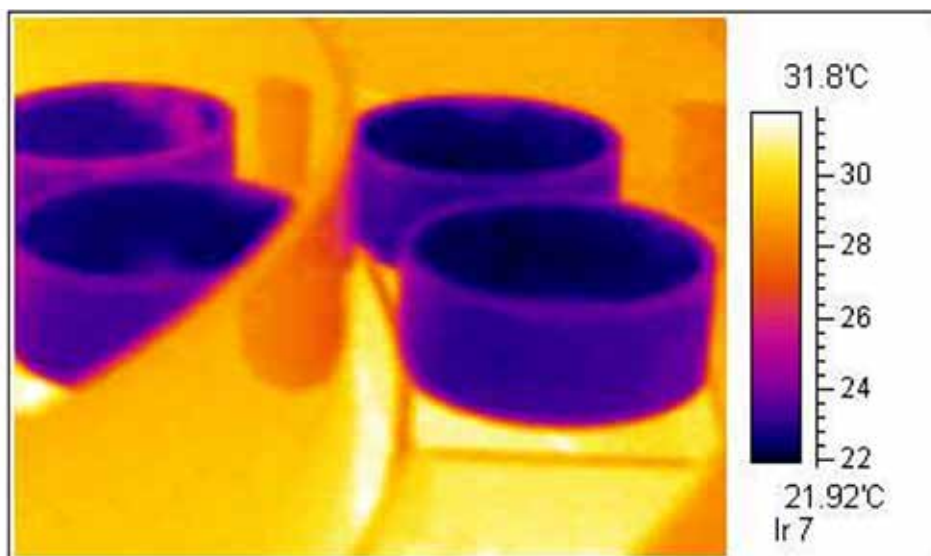


Fig. 2.5.2 Infra red measurements of room temperature Petri-dishes placed in the 30 °C chamber (sideview).

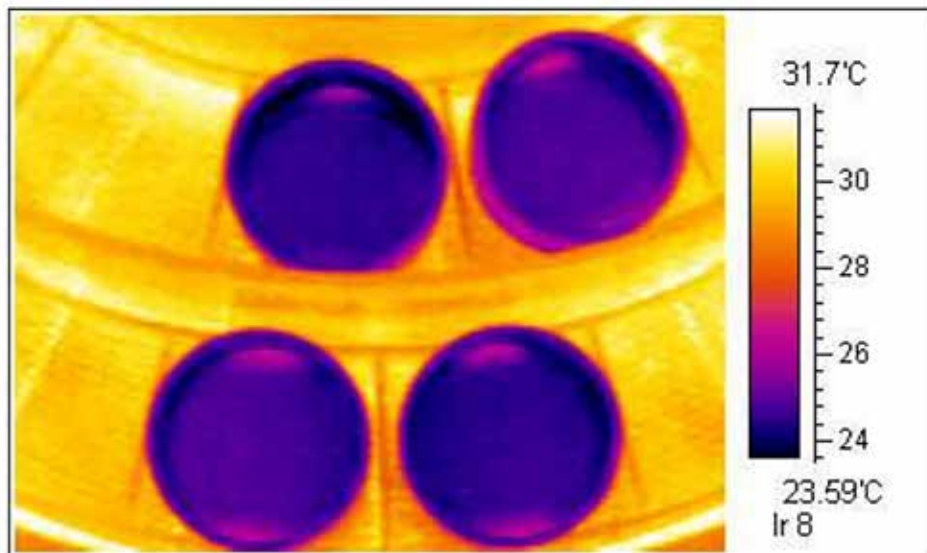


Fig. 2.5.3 Thermal image of room temperature Petri-dishes placed in the 30 °C chamber (top view).

In Fig. 2.5.3 the Petri-dish glass plates warm up (violet) where they are in contact with the steel ring. The rest of the glass plate is colder (blue).

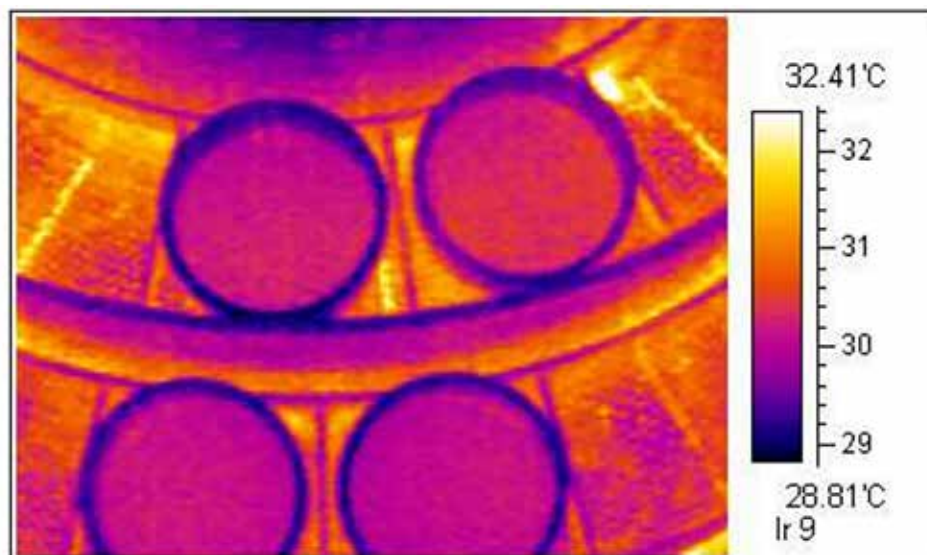


Fig. 2.5.4 Thermal image of Petri-dishes heating up to the ambient chamber temperature of 30 °C (top view).

In Fig. 2.5.4 the Petri-dish glass plates now have a homogeneous and higher temperature (violet) than in Fig. 2.5.3 when they were just placed in the chamber.

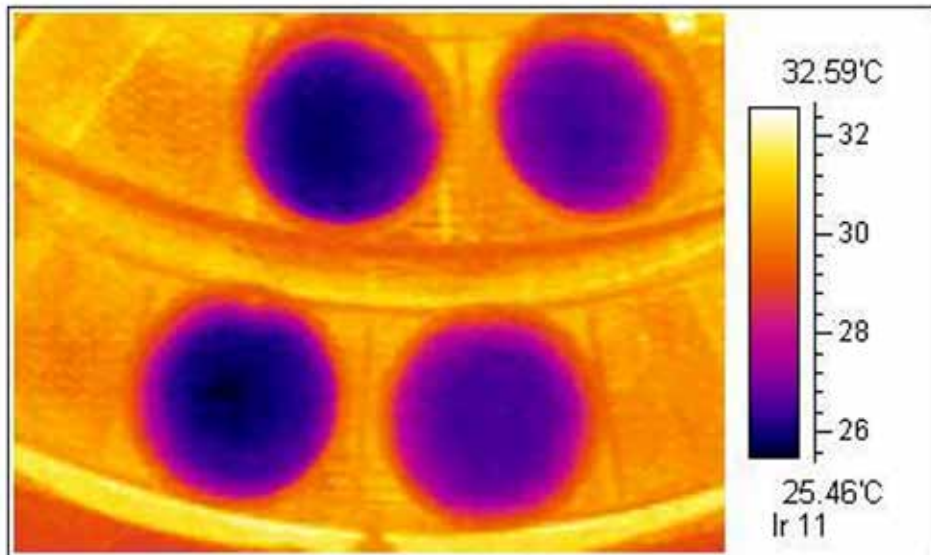


Fig. 2.5.5 Thermal image of the Petri-dishes after pipetting the (~ 20 °C) chamber solution.

In Fig. 2.5.5 the solution in the Petri-dish has a cooler temperature (blue) around the middle of the Petri-dish. The temperature at the rim is higher (violet).

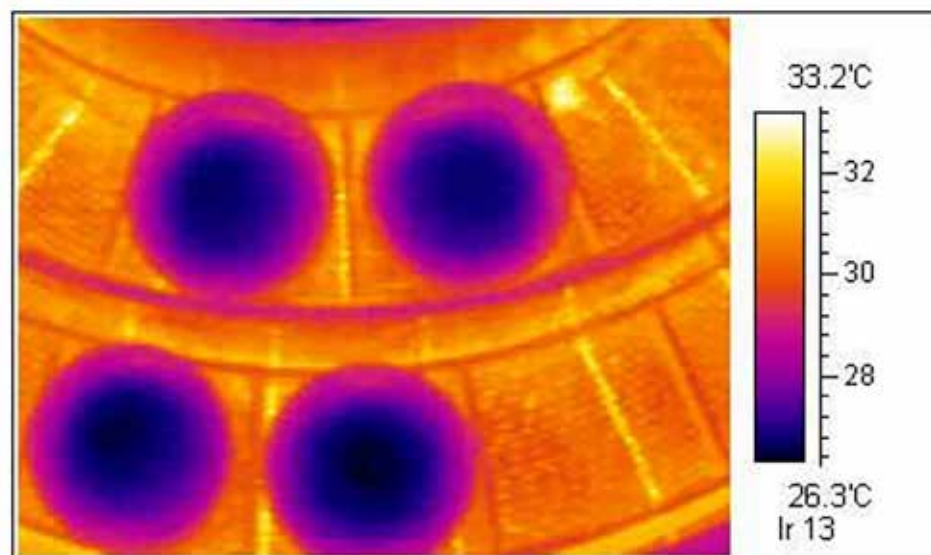


Fig. 2.5.6 Thermal image of the temperature distribution of the solution in the Petri-dishes during evaporation. The solution evaporates and the lowest temperature is in the center of the dish (black), while the temperature increases toward the rim of the Petri-dish (blue, violet).

Appendix 2.5.2 Heating

Heating principle in the Triangle chambers.

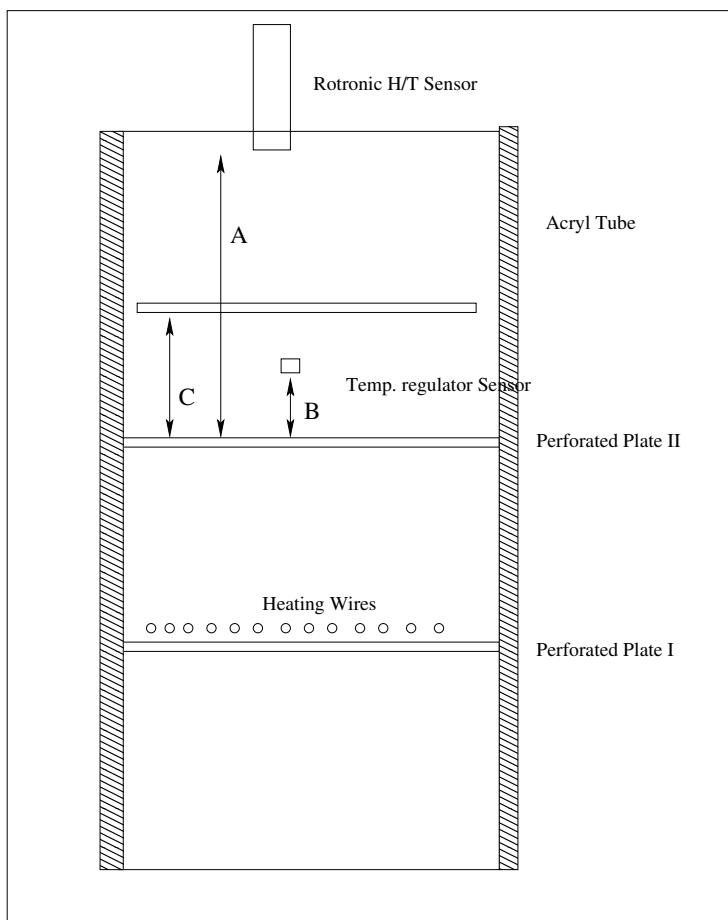


Fig. 2.5.7 Heating principle of the Triangle type chambers.

In Fig. 2.5.7, the heating principle of the Triangle type chambers is shown. The dish (at the upper tip of arrow C) is placed above two perforated plates in an acrylic tube.

The constantan heating wires are mounted on perforated plate I. Heated air passes through perforated plate I, around the dish, and finally to the sensor (at the top of arrow A).

References

- [1] Kahl J. Entwicklung, in-house Validierung und Anwendung des ganzheitlichen Verfahrens Biokristallisation für die Unterscheidung von Weizen-, Möhren- und Apfelproben aus unterschiedlichem Anbau und Verarbeitungsschritten. PhD Thesis, University of Kassel. 2007.
- [2] Barth J-G, Roussau J, Suppan K, dos Santo SR. Crystallisation of a film of copper chloride in the presence of additives. *Elemente der Naturwissenschaft* 2011; 94: 69-99 <https://doi.org/DOI: 10.18756/edn.94.69>.
- [3] Stefan J. Versuche über die Verdampfung. *Sitzungsberichte / Akademie der Wissenschaften in Wien, Philosophisch-Historische Klasse* 1873; 2: 385-423.
- [4] Sparrow E, Nunez G. Experiments on isothermal and non-isothermal evaporation from partially filled, open-topped vertical tubes. *International Journal of Heat and Mass Transfer* 1988; 31: 1345 - 1355 [https://doi.org/https://doi.org/10.1016/0017-9310\(88\)90244-X](https://doi.org/https://doi.org/10.1016/0017-9310(88)90244-X).
- [5] Saylor JR, Smith GB, Flack KA. An experimental investigation of the surface temperature field during evaporative convection. *Physics of Fluids* 2001; 13: 428-439 <https://doi.org/10.1063/1.1337064>.
- [6] Kumar N, Arakeri JH. Natural Convection Driven Evaporation from a Water Surface. *Procedia IUTAM* 2015; 15: 108 - 115 <https://doi.org/https://doi.org/10.1016/j.piutam.2015.04.016>.
- [7] Flack KA, Saylor JR, Smith GB. Near-surface turbulence for evaporative convection at an air/water interface. *Physics of Fluids* 2001; 13: 3338-3345 <https://doi.org/10.1063/1.1410126>.
- [8] Misyura S. Evaporation and heat transfer of aqueous salt solutions during crystallization. *Applied Thermal Engineering* 2018; 139: 203 - 212 <https://doi.org/https://doi.org/10.1016/j.applthermaleng.2018.04.068>.
- [9] Busscher N, Kahl J, Doesburg P, Mergardt G, Ploeger A. Evaporation influences on the crystallization of an aqueous dihydrate cupric chloride solution with additives. *Journal of Colloid and Interface Science* 2010; 344: 556–562 <https://doi.org/doi:10.1016/j.jcis.2009.12.045>.
- [10] Busscher, N. Checking Influences: Untersuchung der Einflussgrößen bei der Biokristallisation als Voraussetzung für die Übertragbarkeit der Kammern und Prozeduren in andere Laboratorien und zur Reduzierung der Variationen durch die Kammer und die Orte, 2009.
- [11] Doesburg, P. Characterizing the crystallization chamber positions for use in a randomisation procedure, HOMII subreport 2012.
- [12] Holleman LWJ. Ein Beitrag zum Verständnis der empfindlichen Kristallisation *Elemente der Naturwissenschaft* 1966; 4: 24-33 <https://doi.org/10.18756/edn.4.24>.
- [13] Busscher, N. Absorbance Project Report, 2017.
- [14] Kahl J, Busscher N, Mergardt G, Maeder P, Torp T, Ploeger A. Differentiation of organic and non-organic winter wheat cultivars from a controlled field trial by crystallization patterns. *J. Sci. Food Agric.* 2014; 95: 53-58 <https://doi.org/doi:10.1002/jsfa.6818>.
- [15] Szulc M, Kahl J, Busscher N, Mergardt G, Doesburg P, Ploeger A. Discrimination between organically and conventionally grown winter wheat farm pair samples using the copper chloride crystallisation method in combination with computerised image analysis *Computers and Electronics in Agriculture* 2010; 74: 218-222 <https://doi.org/doi:10.1016/j.compag.2010.08.001>.

2.6 Molecular weight and branching

Is there a correlation between the molecular weight of a sample and the degree of branching?

Abstract

There is a strong correlation between the molecular weight of a sample and the branching intensity of the $\text{CuCl}_2 \cdot 2\text{H}_2\text{O}$ (cupric chloride di-hydrate, further called [DCC](#)) crystallization pictures. The first one who researched this question was Hummel (1992 [1]). He tested PolyVinyPyrolidon ([PVP](#)) [2] [3] of different mean molecular weights with DCC crystallization and compared the pictures with those obtained from aged carrot juice. For the comparison, the molecular weight profile of the aged juice was measured using gel permeation chromatography. He pointed out that the DCC pictures from PVP with different molecular weights and those from the aged carrot juice with different molecular weights were comparable. The general correlation was visible, but the pictures differed morphologically as Ballivet [4] pointed out.

Before Hummel, O. Selawry [5] had done a lot of work with defined substances. But Hummel's work opened the door to experiments with a defined substance (PVP) with a broad range of mean molecular weights available, while maintaining chemical and biological parameters. The research on PVP was continued by Andersen [6], [7], Busscher [8] and Kahl [9]. In this regard, it is worth mentioning that Andersen also performed computerized texture analysis on DCC pictures of aged carrot juices [10]. In summary, the aforementioned work provided the opportunity to relate the branching conditions of DCC crystals (not the entire macroscopic pattern) to the viscosity (molecular weight) of the sample (Busscher 2014 [11]). The viscosity influences the branching conditions through the heat conductivity (Bearman 1958 [12], cited in Dakroury 1990 [13]).

Introduction

In order to study the influence of different additive molecular weights on the branching properties of DCC needles, PVP was chosen as a sample. Hummel (1992 [1]) suggested that these branching properties are related to phenomena observed in DCC pictures of aged solutions of organic origin, which also have differing (lower) molecular weights. Data from publications that considered aged solutions, such as Andersen (1999 [10]) for carrots and Fritz (2018 [14]) for wheat, however lacked molecular weight information.

PVP was used as additive, because it is a physically and chemically well defined sample, is stable in high saline solutions, pH resistant, and is available in different mean molecular weights (from 2 kDa to 2.5 MDa) [3]. It can simply be ordered by the usual chemical suppliers (CAS # 9003-39-8). DCC pictures from experiments with PVP were made by Andersen (1998 [6]), Busscher (2010 [8]), Kahl (2014 [9]) and Mergardt (2012 [15]) and the scans are accessible. In the following, first PVP is described and then the DCC experiments with PVP, milk fractions and carrot juice as additive from different authors.

Sample PVP

PVP was invented by Reppe (1939 [3]). It is a polymerization product and available in different mean molecular weights from approximately 2 kDa to 2.5 MDa. It was used as a blood volume expander during world war II until ~ 1950. Due to the deposit building in the human body its application in blood was abandoned. Nowadays it is widely used in chemistry, food, pharmaceutical and steel technology [3] [16]. PVP is a real Newtonian fluid (i.e. a fluid whose viscosity does not change with the rate of flow). The Newtonian behavior of PVP was reproduced by Mergardt (2012 [15]) for a watery solution but also in the presence of different amounts of DCC up to the saturation border of DCC. The molecular weights of the samples are measured by their intrinsic viscosity (for a 1 % solution at 25 °C [16], see Table II) or K value according to [Fikentscher](#) (DIN EN ISO 1628-1, [17]). The K value is used as the ordering information. PVP is available from 2 kDa (2 kg / mol) to 2.5 MDa (2.5 Mg / mol), or K12 to K115 [3]. A high amount of experimental data of watery solutions of PVP are available. To list some of the latest ones: the thermal properties were measured by Dakroury [13]. Surface tension, density and viscosity of watery solutions of PVP were measured by Bolten [18]. PVP is known for its ability to influence the nucleation and crystal growth properties [19]. It builds complexes with metal chlorides [20], [19] (DCC was not tested). The watery mixture of PVP K90 and DCC shows an anomaly in the viscosity at low DCC (~ 2 % w / w) concentrations [21] (see also in chapter [1.7 Evaporation issues](#)), which was reproduced by Mergardt [15]. PVP is known to support the building of micelles of other substances ([22] [23] [24] [25]).

Existing Work (Publications)

The following is a description of the work that has been published on the subject of molecular weight and branching in DCC pictures.

Table 2.6.1 List of articles about molecular weight influences on DCC pictures. If the Pic column contains an X, then the pictures are available (at least as scans) for further evaluation in the [LabDoc](#) system.

Author	Ref	Year	Pic	Remark
Hummel	[1]	1992		Aged carrot juice and different molecular weights of PVP.
Ballivet	[4]	1993		Differences between the carrot and PVP pictures from Hummel.
Andersen	[6]	1998	X	PVP pictures for different molecular weights; visual and texture evaluation.
Andersen	[10]	1999		Aging of carrot juice evaluated by computer texture analysis.
Andersen	[7]	2001	X	PVP and texture image analysis (manuscript in PhD thesis).
Busscher	[8]	2010	X	Coverage of the plate for different DCC amounts.
Kahl	[9]	2014	X	Different PVP K values and different milk fractions.
Busscher	[11]	2014	X	Entropy argumentation and picture properties.
Fritz	[14]	2018		Visual and Gestalt evaluation of aged extracts (wheat).

Article Hummel [1] (EdN 1992)

Title: Does the copper chloride crystallization method provide evidence for the formative forces of the living? Original title: *“Liefert die Kupferchlorid Kristallisations Methode einen Nachweis für die Gestaltkräfte des Lebendigen?”*.

Hummel compared DCC pictures of PVP of different molecular weights (K15, K30, K90) with photos of DCC pictures of several aged carrot juices from Engquist’s book (1970 [26]). He measured the molecular weight of different carrot juice samples and found a correlation between a decrease in molecular weight (from fresh to aged samples) and a decrease in branching. He concluded that the DCC pictures are not showing the *“Gestaltkräfte des Lebendigen”* (Formative forces of the living), as formulated by Engquist [26]. This article received a lot of attention. Ballivet [4] responded that the pictures were different in their expression. Knijpenga [27] replied that it is not an absolute method but a comparative method. Nitschman [28] compared it to the effect of a thermometer, which can determine temperatures but can not decide between sickness or health. Hummel [29] responded to this by pointing out the differences between synthetic substances and those derived from life processes, both of which are capable of building structures of higher molecular weights.

The research on PVP as additive for DCC crystallization was followed up by Andersen [6] [7], Busscher [11] and Kahl [9].

Article Andersen [6] (EdN 1998)

Title: A Refined Biocrystallization Method applied in a Pictomorphological Investigation of a Polymer.

The article describes a new type of evaporation and crystallization chamber for 18 Petri-dishes, a prototype of the current [Triangle Chamber](#). The discriminating ability was examined by the visual evaluation of textural features of PVP pictures with different molecular weights (10 kDa, 40 kDa, 160 kDa, 360 kDa, 700 kDa) at varying amounts (0.18, 0.36 [mainly], and 0.54 mg per plate, with 45 mg DCC per plate). For reference purposes it is informative to know that mature BSA protein has a mass of approximate 66 kDa. Branching increased most between 160 and 360 kDa. Some of the pictures are shown in the [Appendix 2.6.1 JOA-1998](#) (see below).

Chapter from Andersen’s [7] PhD thesis (2001), p. 108 ff.

Title: Computerized image analysis of PVP-biocrystallograms (manuscript).

Some of the image analysis parameters reacted in a monotonic manner to the increasing molecular weight of the different PVP samples. See the results on p. 113 of his thesis.

Appendix 4. Andersen et al. (2001b). Computerized image analysis of PVP-biocrystallograms.

ROI	Total set		Subset 3-low		Subset 3-middle		Subset 3-high		Aver. subset rates
	Ord.	Jack.	Ord.	Jack.	Ord.	Jack.	Ord.	Jack.	
C-50	79	71	67	47	100	80	100	93	81
C-55	74	67	73	40	93	87	100	73	73
C-60	86	64	87	67	100	80	100	87	87
C-65	81	72	87	53	80	60	93	53	71
C-70	83	80	100	60	80	60	80	60	73
C-75	64	62	100	80	100	100	100	87	95
C-80	93	88	100	100	100	100	100	80	97
C-85	81	79	87	60	100	100	87	80	86
C-90	83	76	87	60	100	100	87	80	86
C-95	88	81	87	73	93	87	87	60	81
C-100	83	71	87	67	87	73	100	73	81
Aver.	81	74	87	65	94	84	94	75	

Table 1. Classification rates concerning PVP-biocrystallogram images, for each combination of ROI (region-of-interest), including the total set of 42 images, and three subsets of 15 images (3-low, 3-middle, 3-high); type of classification (ordinary, jackknifed), and average rates relative to the set, and to the ROIs for the subsets for each combination of ROI and sets, as well as average rates.

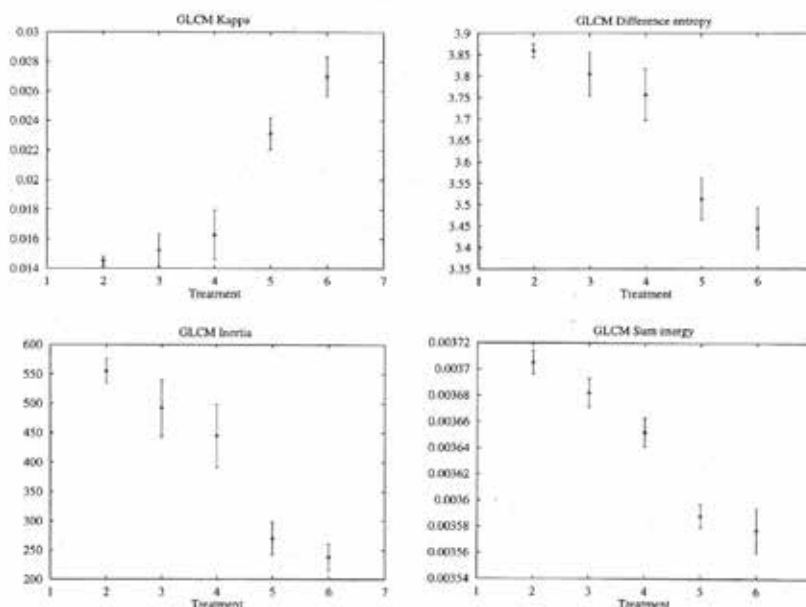


Figure 2. The second-order parameters Kappa (upper left), Difference entropy (upper right), Inertia (lower left) and Sum Energy (lower right) plotted against the polymerization level, with 2 corresponding to PVP-10, 3 to PVP-40 etc.

Fig. 2.6.1 Image analysis results of increasing PVP polymerization levels (Andersen [7], p. 113) with the statistical results (Table 1) and four graphs corresponding to four GLCM image analysis parameters (top left, Kappa; top right, Difference entropy; bottom left, Inertia; bottom right, Sum energy). The X-axis represents 6 increasing PVP polymerization levels. 2 = 10 kDa, 3 = 40 kDa, 4 = 160 kDa, 5 = 360 kDa, 6 = 700 kDa. The analyzed region of interest (ROI) is CircleCircle 0 – 80 %. Additive amount = 0.36 mg per plate, DCC amount = 45 mg per plate (1998 [6], Table 1). The 4 different image analysis parameters increase or decrease monotonically with the degree of polymerization.

Article Kahl [9] (2014)

Title: A novel approach for differentiation of milk fractions and polyvinylpyrrolidone with different molecular weight by patterns derived from cupric chloride crystallization with additives.

A comparison was performed between the branching of DCC crystals obtained from PVP of different molecular weights (40 kDa and 700 kDa) and different milk fractions, which also had different molecular weights. In both cases the higher molecular weight resulted in a higher degree of branching. See Fig. 2.6.2 below (Fig. 1 from article [9]).



Fig. 2.6.2 Patterns from DCC crystallization with PVP K90 (top left, higher molecular weight), PVP K40 (top right, higher molecular weight), milk protein concentrate (bottom left, higher molecular weight) and whey protein concentrate (bottom right, higher molecular weight) as additives. From Kahl 2014 [9], Fig. 1).

Article Busscher [11] (2014)

Title: From needles to pattern in food quality determination.

As mentioned above, the difference in the photos of the DCC pictures of fresh and aged carrot juice from Engquist 1970 [26] was connected by Hummel [1] to his measurements of the decrease in molecular weight from fresh to aged carrot juices. The differences in molecular weight of the aged juices were connected to possible differences in the viscosity. The viscosity is equivalent to the heat transfer coefficient (Bearman 1958 [12], cited in Dakroury 1990 [13]), which, along with the diffusion coefficient, is the second basic parameter determining the onset of branching [30] [31] [32].

Article Andersen: [10] COMPAG (1999)

Title: Computerized image analysis of biocrystallograms originating from agricultural products.

A correlation between the aging of carrot extracts and the image analysis of the DCC pictures was demonstrated. The correlation had the same direction as the PVP molecular weight experiments from Andersen's PhD thesis [7]. See Fig. 2.6.3 (Fig. 4 from [7] p. 74) and Fig. 2.6.4 (from [7] p.81) below.

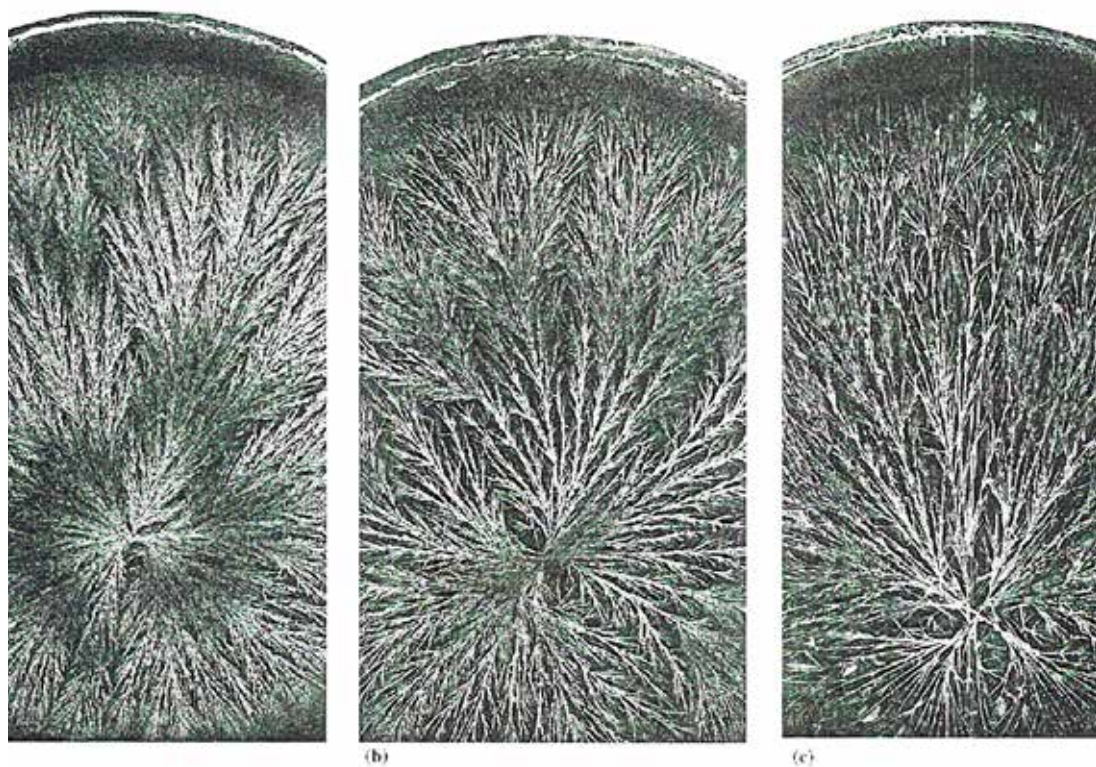


Fig. 2.6.3 Enlarged photographic sections from DCC pictures with degraded carrot as additive (from Andersen 2001 [7], p. 74). From left to right, the increase in degradation is shown: (a) after 1 day of storage at 6 °C , (b) after 4 days of storage, (c) after 7 days of storage. The branching intensity also decreases from left to right.

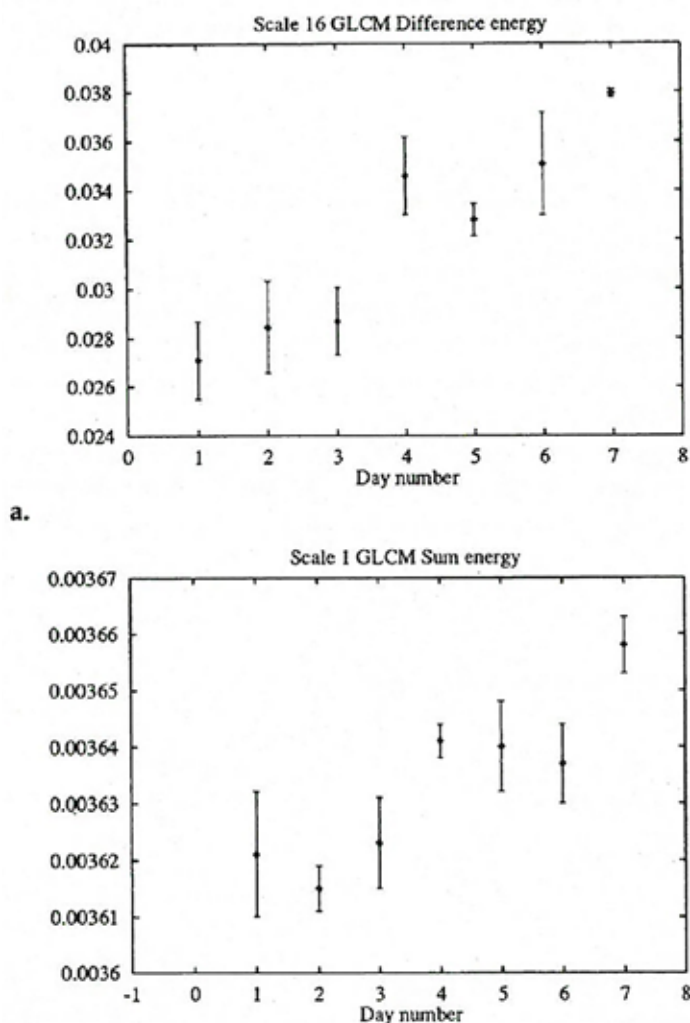


Fig. 2.6.4 Image analysis results of DCC pictures of degrading carrot juice (Andersen 2001 [7], p. 81). The two graphs correspond to two GLCM image analysis parameters (top, Difference entropy; bottom, Sum energy). The X-axis represents the degradation intensity in days due to non-specific autolytic and microbial degradation at 6 0 C. The analyzed ROI is CircleCircle 0 – 70 % for Difference energy, and CircleCircle 0 – 80 % for Sum energy. Additive amount = 200 mg per plate, DCC amount = 80 mg per plate.

When comparing the plots in Fig. 2.6.4 for the image analysis variables “Difference Energy” and “Sum Energy” with those in Fig. 2.6.1 we see the following: the variables are increasing with the day number (the degree of degradation) in Fig. 2.6.4, while in Fig. 2.6.1 the variables are decreasing in response to an increasing polymerization level. When the degree of degradation is expressed as a reduction in molecular weight, both plots (Fig. 2.6.1 and Fig. 2.6.4) show the same correlation.

Existing Work (pictures available but results not published)

Experiment Uni Kassel / Witzenhausen (2006)

PVP matrices were made with three DCC amounts (25, 45 and 65 mg per plate) and three PVP amounts (0.18, 0.36 and 0.54 mg per plate) for PVP K15, K30, K60, K90. The DCC / PVP values were chosen according to Andersen [6]. Pictures were made on six days in two so called Triangle chambers [33] producing 43 pictures per run. In every experiment two K values were combined, which gave 2 pictures per chamber and combination per experiment. This experiment yielded in total 432 pictures with PVP and 85 freeze dried wheat reference pictures. Each combination of DCC / PVP – Kx yielded 12 replicas. See some of the pictures in the Appendix 2.6.2 PVP-Matrix below.

The ring3 (the radius of the DCC covered area in the Petri-dish) and the dewetting (if any) evaluation was only partly done in [LabDoc](#) (Additional Research). For the ring3 definition see Supplementary Information of Busscher 2019 [34]. The ring3 evaluation was performed by hand, using a scale on the scanned picture on the computer screen. The statistical evaluation of the ring3 radius implied, as reported in [34] a stronger dependency on the DCC amount than on the additive amount. This ring3 evaluation should be repeated using the [CrystEval](#) tool, so

the results will be well documented and the evaluation can also take the molecular weight into account.

Resume

The results from Hummel [1], Andersen [6] [7] and Kahl [9] describe three samples (carrot juice, PVP, and milk fractions) which all indicate a positive correlation between the molecular weight and the degree of branching. For carrot juice (Hummel [1]) and milk fractions (Kahl [9]) the molecular weight was measured. In the study by Andersen [10] the molecular weight of the aging carrot juice was not determined. The pictures from Fritz [14] did not show a simple decrease in the branching for aged wheat extracts. An overview of the data is listed in Table 2.6.2 below.

Table 2.6.2 Overview of the different samples examined regarding the presence of a correlation between the molecular weight of the sample and the degree of branching of the DCC crystal. The "Mol weight" column indicates whether or not the mean molecular weight was documented. The "Process" column indicates the process applied to the sample. The "Corr." column indicates whether or not (Y / N) a correlation was found between the mean molecular weight of the sample and the degree of branching of the DCC crystal.

Author	Sample	Mol weight	Process	Corr
Hummel	PVP	Yes		Y
Hummel	Carrot juice	Yes	Aging	Y
Andersen	PVP	Yes		Y
Andersen	Carrot extract	No	Aging	Y
Kahl	PVP	Yes		Y
Kahl	Milk fractions	Yes	Fractionation	Y
Fritz	Wheat extract	No	Aging	N?

In connection with Busscher [11] the influence of the molecular weight (or viscosity) on the branching conditions can be understood and, with the correlation described above, extended to the aging of a sample's juice.

Additional research

Ring3 evaluation of PVP pictures

DCC pictures with PVP (see Appendix PVP Matrix) show a clear separation from the rim of the Petri-dish. As stated before, a first rough evaluation showed a difference in dependency of the ring3 (radius of the DCC coverage) on DCC (strong dependency) in comparison to the additive amount (weak dependency). This would perhaps support the hypothesis of Busscher [34] that the amount of DCC is too low for the PVP experiments performed so far. Repeating the ring3 evaluation using the [CrystEval](#) tool would give a better documentation and will allow an extension of the ring3 diameter to a molecular weight dependency.

Extended matrix comparison of PVP with different molecular weights

In a extended concentration matrix of PVP with different molecular weights of PVP the following questions could be handled:

- Q1 At first glance the molecular weight effect looks like an additive amount effect. In terms of viscosity this would fit. The test would be to compare DCC pictures from the same (calculated) viscosity amount but with different PVP molecular weights. This could provide information about the crystallization process, whether it depends only on the molecular weight or the viscosity, or a combination of both. The viscosity of the PVP sample needs to be measured, because it is not the same as the info supplied by the producer (see Bolton [18] Table 1). Measurements can be done according to ISO norm 1628 [17].
- Q2 Also the DCC amount where the coverage of the plate (ring3) reaches 100 % could be tested.
- Q3 What are the minimum (dewetting) and maximum (inhibition) PVP additive concentrations for different molecular weights? If these effects only depend on the viscosity then the amounts should differ for different PVP molecular weights.

- Q4 Why was the strongest difference in the DCC / PVP pictures of Andersen found between 160 and 360 kDa? This showed up in the visual and the texture image analysis. See also [Appendix 2.6.1 JOA-1998](#).
- Q5 The DCC pictures from Hummel ([1] Fig. 3) showed “*Hohlforms*”, which means that there should be split-growth [35] in the PVP matrix. Maybe this was because he used 2.2 mg PVP per plate which is a quite “high” amount, relative to the 0.54 mg per plate used in the research by Andersen and Kahl.
- Q6 The PVP matrix is interesting, because also substance spirals (see chapter [2.7 Substance spirals](#)) were observed, which did not show up for BSA. Maybe this is due to the superior abilities of BSA to cover a glass plate?

Appendix 2.6.1 JOA-1998

Pictures from Article Andersen [6] (EdN 1998)

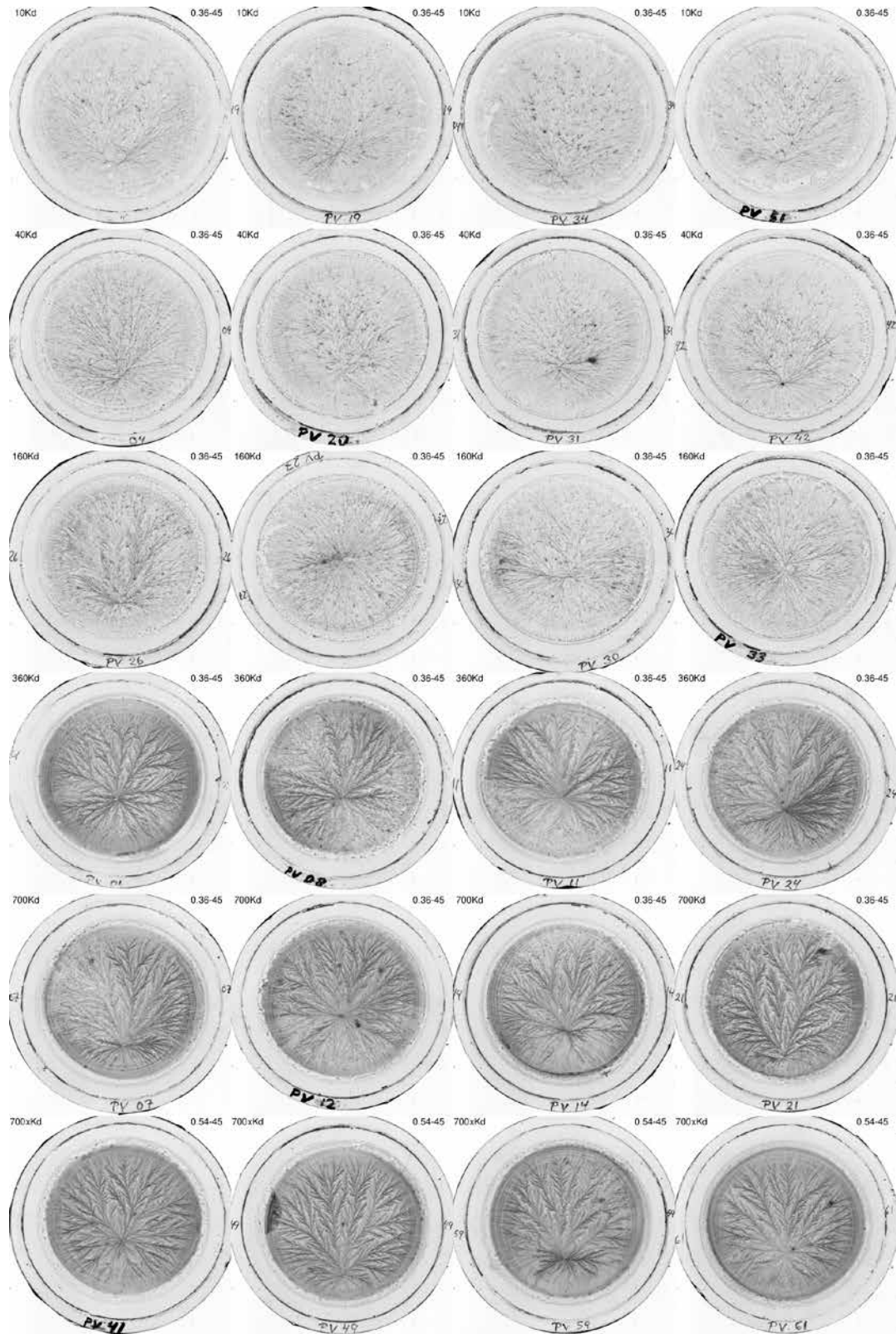


Fig. 2.6.5 DCC pictures of PVP with different molecular weights. Per row 4 replicates of each PVP sample are shown. Upper row 10 kDa, next row 40 kDa, then 160 kDa, then 360 kDa, then 700 kDa and last is 700 kDa with a higher additive amount.

In Fig. 2.6.5 the branching increased with increasing molecular weight of PVP. The strongest increase is from 160 kDa to 360 kDa.

Appendix 2.6.2 PVP-Matrix

The following PVP concentration matrices were made in 2006 at the University of Kassel, Witzenhausen (D). The PVP matrices were made with 3 DCC amounts (25, 45 and 65 mg per plate) and 3 PVP amounts (0.18, 0.36, 0.54 mg per plate) for K15, K30, K60, K90. (PVP and DCC amounts according to [6]).

The concentration matrix has the following form for each molecular weight.

Table 2.6.3 Schematic representation of the PVP concentration matrix, with on the Y-axis the amounts of DCC in mg per plate, and on the X-axis the amounts of each PVP-Kx.

65			
45			
25			
DCC/PVP	0.18	0.16	0.54

Only one of the 12 replicates is shown in the following figures Fig. 2.6.6 – Fig. 2.6.9. The pictures were selected based on their median crystallization starting time. Because the crystallization starting time increases with the additive amount, the pictures shown do not have the same crystallization starting time.

Each picture has a line with information printed above it. As can be seen from the upper left picture on the next page for K90.

0.18 = a: 10.97 = ts: 65 = cu: 361.1 = mr

a is the amount of additive in mg per plate, here 0.18.

ts is the crystallization starting time in hours with a decimal minute format, here 10.97.

cu is the amount of DCC in mg per plate, here 65.

mr is the mixture ratio (DCC / Additive), here $361.1 = (65 / 0.18)$.

In the upper left corner of the picture the chamber name is denoted, here C (University of Kassel / Witzenhausen).

In the lower left corner of the picture the position nr in the chamber is denoted, here 14.

In the lower right corner of the picture the LabDoc series name is denoted, here series KD.

The following matrices show that the branching increases with the additive amount and that all pictures have a crystal free area between the rim of the Petri-dish and the picture. For K60 a banding in the picture was visible, which is not so strong as for K90 and non existing for K30 and K15. Noteworthy is that the relation between the K values and the kDa values from the Supplier (Fluka) have a strong variation. See Bolton ([18] Table 1). The supplier info for K90 states 360 kDa.

Molecular weight K90



Fig. 2.6.6 PVP concentration matrix for K90 molecular weight. On the Y-axis is the DCC amount in mg per plate, on the X-axis the additive amount in mg per plate. Pictures University Kassel (D).

Molecular weight K60



Fig. 2.6.7 PVP concentration matrix for K60 molecular weight. On the Y-axis is the DCC amount in mg per plate, on the X-axis the additive amount in mg per plate. Pictures University Kassel (D).

Molecular weight K30



Fig. 2.6.8 PVP concentration matrix for K30 molecular weight. On the Y-axis is the DCC amount in mg per plate, on the X-axis the additive amount in mg per plate. Pictures University Kassel (D).

Molecular weight K15



Fig. 2.6.9 PVP concentration matrix for K15 molecular weight. On the Y-axis is the DCC amount in mg per plate, on the X-axis the additive amount in mg per plate. Pictures University Kassel (D).

References

- [1] Hummel RE. Liefert die Kupferchlorid-Kristallisations-Methode einen Nachweis für die Gestaltkräfte des Lebendigen? *Elemente der Naturwissenschaft* 1992; 57: 112-121 <https://doi.org/10.18756/edn.57.112>.
- [2] Reppe W Polyvinylpyrrolidon (Verlag Chemie, GmbH, 1954.).
- [3] Fischer F, Bauer S. Polyvinylpyrrolidon. Ein Tausendsassa in der Chemie. *Chemie in unserer Zeit* 2009; 43: 376-383.
- [4] Ballivet C. Empfindliche Kristalle zwischen unorganischer und organische Natur. *Elemente der Naturwissenschaft* 1993; 58: 76-82.
- [5] Selawry A and Selawry O Die Kupferchlorid-Kristallisation in Naturwissenschaft und Medizin (Gustav-Fischer-Verlag, 1957).
- [6] Andersen JO, Laursen J, Koelster P. A Refined Biocrystallization Method applied in a Pictomorphological Investigation of a Polymer. *Elemente der Naturwissenschaft* 1998; 68: 1-20 <https://doi.org/DOI: 10.18756/edn.68.1>.
- [7] Andersen J-O. Development and application of the biocrystallization method. PhD Thesis, Department of Agricultural Sciences/Organic Farming Unit The Royal Veterinary and Agricultural University Copenhagen. 2001.
- [8] Busscher N, Kahl J, Doesburg P, Mergardt G, Ploeger A. Evaporation influences on the crystallization of an aqueous dihydrate cupric chloride solution with additives. *Journal of Colloid and Interface Science* 2010; 344: 556–562 <https://doi.org/doi:10.1016/j.jcis.2009.12.045>.
- [9] Kahl J, Busscher N, Hoffmann W, Mergardt G, Clawin-Raedecker I, Ploeger A. A novel approach for differentiation of milk fractions and polyvinylpyrrolidone with different molecular weight by patterns derived from cupric chloride crystallization with additives. *Anal. Methods* 2014; 6: 3173-3176 <https://doi.org/doi:10.1039/C3AY41568F>.
- [10] Andersen JO, Henriksen CB, Laursen J, Nielsen AA. Computerised image analysis of biocrystallograms originating from agricultural products. *Computers and Electronics in Agriculture* 1999; 22: 51-69 [https://doi.org/doi:10.1016/S0168-1699\(98\)00043-X](https://doi.org/doi:10.1016/S0168-1699(98)00043-X).
- [11] Busscher N, Kahl J, Ploeger A. From needles to pattern in food quality determination. *Journal of the Science of Food and Agriculture* 2014; 94: 2578-2581 <https://doi.org/doi:10.1002/jsfa.6498>.
- [12] Bearman RJ. Statistical Mechanical Theory of the Thermal Conductivity of Binary Liquid Solutions. *The Journal of Chemical Physics* 1958; 29: 1278-1286 <https://doi.org/http://dx.doi.org/10.1063/1.1744710>.
- [13] Dakrouy A, Osman M, El-Sharkawy A. Thermal properties of aqueous solutions of polyvinylpyrrolidone in the temperature range 20-80°C. *International Journal of Thermophysics* 1990; 11: 515-523.
- [14] Fritz J, Athmann M, Andersen J-O, Doesburg P, Geier U, Mergardt G. Advanced panel training on visual Gestalt evaluation of biocrystallization images: ranking wheat samples from different extract decomposition stages and different production systems. *Biological Agriculture & Horticulture* 2018; 35: 1-12 <https://doi.org/doi:10.1080/01448765.2018.1492457>.
- [15] Mergardt G. Simulation des Entstehungsvorganges von Kristallbildern zur Messung der physikalischen Parameter pH-Wert, Dichte und Viskosität am Beispiel von PVP, Glykogen und Bovine Serum Albumin. Technical Report, University of Kassel. 2012.
- [16] Ashland. PVP Polyvinylpyrrolidone polymers, 2013.
- [17] CEN. DIN EN ISO 1628-2 --:2020-12, 2020.
- [18] Bolten D, Türk M. Experimental Study on the Surface Tension, Density, and Viscosity of Aqueous Poly(vinylpyrrolidone) Solutions. *J. Chem. Eng. Data* 2011; 56: 582-588.
- [19] Trasi NS, Abbou Oucherif K, Litster JD, Taylor LS. Evaluating the influence of polymers on nucleation and growth in supersaturated solutions of acetaminophen. *CrystEngComm* 2015; 17: 1242-1248.
- [20] Patel DD, Anderson BD. Adsorption of Polyvinylpyrrolidone and its Impact on Maintenance of Aqueous Supersaturation of Indomethacin via Crystal Growth Inhibition. *J. Pharm. Sci.* 2015; 104: 2923-2933.
- [21] Hao C, Zhao Y, Dong X, Zhou Y, Xu Y, Wang D et al. Anomalous rheological behavior of poly(1-vinyl-2-pyrrolidone) and CuCl₂ in solution and their interactions in solid composites. *Polym. Int.* 2009; 58: 906-911.
- [22] Hu Y, Jiang Z, Chen R, Wu W, Jiang X. Degradation and Degradation-Induced Re-Assembly of PVP-PCL Micelles. *Biomacromolecules* 2010; 11 (2): 481–488 <https://doi.org/10.1021/bm901211r>.
- [23] Benahmed A, Ranger M, Leroux J-C. Novel Polymeric Micelles Based on the Amphiphilic Diblock Copolymer Poly(N-vinyl-2-pyrrolidone)-block-poly(D,L-lactide). *Pharmaceutical Research* 2001; 18: 323-328 <https://doi.org/DOI: 10.1023/A:1011054930439>.
- [24] Guettari M, Aferni AE, Tajouri T. Effect of micellar collisions and polyvinylpyrrolidone confinement on the electrical conductivity percolation parameters of water/AOT/isooctane reverse micelles. *Journal of Molecular Structure* 2017; 1149: 712-719 <https://doi.org/https://doi.org/10.1016/j.molstruc.2017.08.026>.
- [25] Zhao L, Wang J. Biomimetic synthesis of hollow microspheres of calcium carbonate crystals in the presence of polymer and surfactant. *Colloids and Surfaces A: Physicochemical and Engineering Aspects* 2012; 393: 139-143

- <https://doi.org/https://doi.org/10.1016/j.colsurfa.2011.11.012>.
- [26] Engquist M Die Gestaltkräfte des Lebendigen (Vittorio Klostermann, 1970).
- [27] Knijpenga H. Kristallisationsbilder und vergleichende Methode. *Elemente der Naturwissenschaft* 1993; 58: 83-84.
- [28] Nitschmann G. Gedanken zur empfindlichen Kristallisation mit Kupferchlorid. Im Anschluss an die Arbeit von R. E. Hummel: Liefert die Kupferchlorid Kristallisations-Methode einen Nachweis für die Gestaltkräfte des Lebendigen? *Elemente der Naturwissenschaft* 1993; 58: 14-19 <https://doi.org/10.18756/edn.58.14>.
- [29] Hummel RE. Weitere Gedanken zur Interpretation von Kupferchloridkristallisaten von lebendigen und synthetischen Substanzen. *Elemente der Naturwissenschaft* 1993; 59: 81-84 <https://doi.org/10.18756/edn.59.81>.
- [30] Haxhimali T, Karma A, Gonzales F, Rappaz M. Orientation selection in dendritic evolution. *Nat Mater* 2006; 5: 660-664 <https://doi.org/doi:10.1038/nmat1693>.
- [31] Asta M, Beckermann C, Karma A, Kurz W, Napolitano R, Plapp M et al. Solidification microstructures and solid-state parallels: Recent developments, future directions. *Acta Materialia* 2009; 57: 941-971 <https://doi.org/10.1016/j.actamat.2008.10.020>.
- [32] Kurz W. Solidification Microstructure-Processing Maps: Theory and Application. *Advanced engineering materials* 2001; 3: 443-452 [https://doi.org/https://doi.org/10.1016/0956-7151\(94\)90044-2](https://doi.org/https://doi.org/10.1016/0956-7151(94)90044-2).
- [33] Kahl J, Busscher N, Meier-Ploeger A. Ganzheitliche Untersuchungsmethoden zur Erfassung und Prüfung der Qualität ökologischer Lebensmittel: Stand der Entwicklung und Validierung, Abschlußbericht Projekt 02OE170,. Technical Report, Bundesprogramm Ökolandbau.. 2003.
- [34] Busscher N, Doesburg P, Mergardt G, Sokol A, Kahl J, Ploeger A. Influence of dewetting on the crystallization behavior of CuCl₂ in the presence of BSA during evaporation in a Petri dish. *Heliyon* 2019; 5: e01102 <https://doi.org/10.1016/j.heliyon.2018.e01102>.
- [35] Busscher N, Doesburg P, Mergardt G, Sokol A, Kahl J, Ploeger A. Crystallization patterns of an aqueous dihydrate cupric chloride solution in the presence of different amounts of Bovine Serum Albumin. *Journal of Crystal Growth* 2019; <https://doi.org/doi:10.1016/j.jcrysro.2019.125272>.

2.7 Substance spirals, banding, spherulite

Abstract

The phenomenon described in this chapter is called “*substance spirals*” (see Fig. 2.7.1). The name is derived from the visual evaluation criterion defined in Huber 2010([1], Table 2) for DCC pictures (the name of the salt $\text{CuCl}_2 \cdot 2\text{H}_2\text{O}$ = cupric chloride di-hydrate is shortened to [DCC](#)). In a crystallographic context the term spherulite (Popoff 1904 [2]) or banding (Keith 1996 [3]) is commonly used to indicate such formations. In the DCC-additive [concentration matrix](#) substance spirals appear at increasing additive amounts below the inhibition of the crystallization (Andersen 2003 [4]). In Andersen 2003 [4] one can observe that the number of substance spirals per cm not only increases with the additive amount, but also decreases with the DCC amount. As can be seen in Fig. 2.7.1 (right, at 4 o’clock) the darker areas also include some red needles.

There are different possible hypotheses to explain the effect. One hypothesis is that the crystal needles are turned (mechanically and optically) according to Bernauer 1929 [5]. Another one is that the crystallization process expels the additive and colors the solution outside of the needle. This can also be described as a “*Liesegang Ring*” [6] [7] [8] effect. A third hypothesis is that the depletion of the DCC around the growing crystal is the reason for the effect (Wang 1991 [9]). Additional work is necessary to sort the hypotheses, starting with the most promising one. This effect is very important for the DCC method, because the appearance of the substance spirals, indicates that the sample is beginning to “*over-concentrate*”.

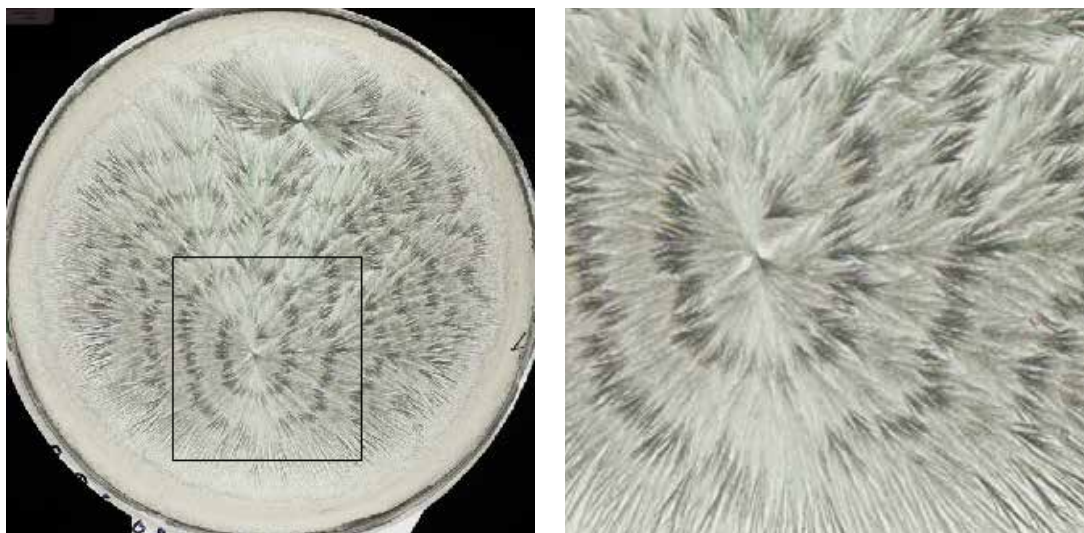


Fig. 2.7.1. DCC picture with wheat as additive, demonstrating substance spirals. Left total view, right enlargement of middle section. (Data from University of Kassel (D) [LabDoc](#) series 2003.11.06.D-S, no. 8, from chamber B). The substance spiral has a darker apparent color in the picture and starts in the lower middle of Fig. 2.7.1 left and in the middle of Fig. 2.7.1 right. In the right enlarged section also colored needles (e.g. red) are visible in the darker areas.

Introduction:

The first time rhythmic crystallizations with the salt $\text{CuCl}_2 \cdot 2\text{H}_2\text{O}$ = cupric chloride di-hydrate in short [DCC](#), were mentioned by Selawry (1957 [10], p. 60, Fig. 24) for Ephedrin as additive. She called them “*rhythmische Kristallanordnung gedrillter Kristalle*”. In the Triangle group the so called substance spirals were recognized in connection with DCC was in pictures with [Polyvinyl Pyrollidon](#) (PVP) as additive during a meeting of the [Triangle group](#) in the Louis Bolk Institute (NL) in 2002. Afterwards, they were also observed in DCC pictures with other additives like carrot (Fig. 2.7.2 left) and wheat (Fig. 2.7.2 right and Fig. 2.7.1). This effect was -as a side effect- documented by Andersen [4] (see also [Appendix 2.7.1 Matrices](#) below). The substance spiral pattern, which looks like an oscillation of the brightness of the color within the DCC picture, is especially visible for higher amounts of additive.

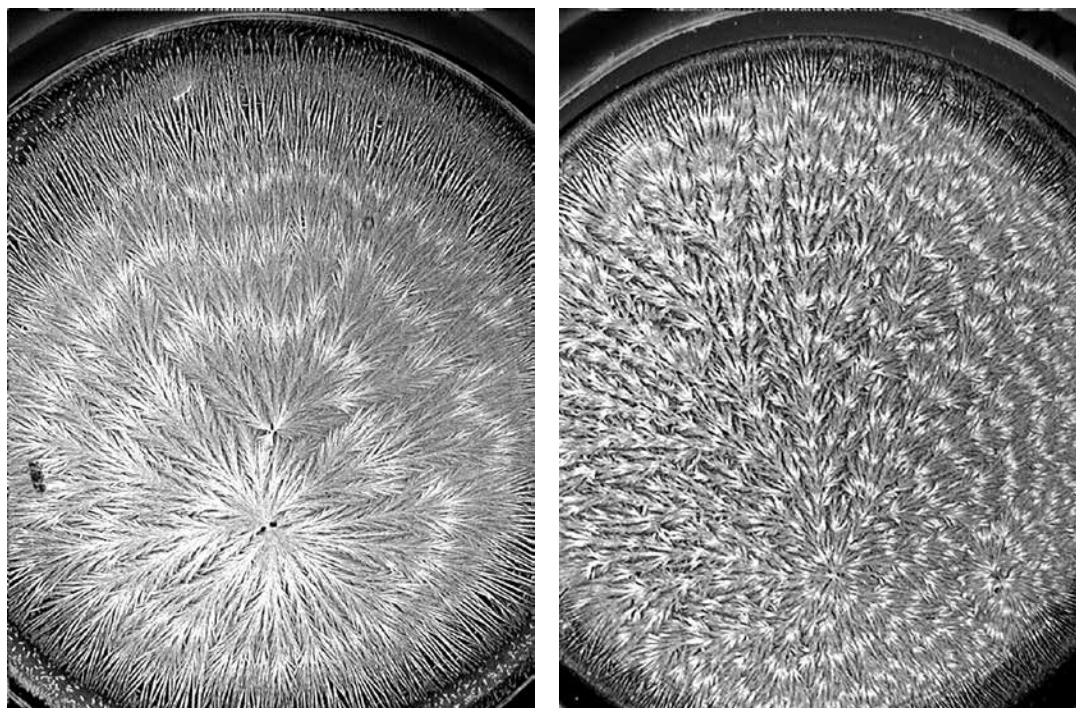


Fig. 2.7.2 Examples of substance spirals for DCC pictures with carrot (left) and wheat (right) as additive (from Andersen 2003 [4]).

In the visual morphological evaluation of the DCC pictures from Huber 2010 [1] the term “*substance spirals*” was defined as the 10th criterion out of 14 morphological criteria which were finally chosen to characterize the DCC pictures. The frequency of the spirals per cm seemed to increase with the additive amount and decrease with the DCC amount (see [Appendix 2.7.1 Matrices](#), below). So far this phenomenon has not been observed for DCC pictures with Bovine Serum Albumin (BSA) and milk as additive [11]. A list of samples that showed substance spirals in their DCC pictures can be found in [Appendix 2.7.2 Samples](#).

Historical overview

The so called spherulites were first described by Popoff (1904) [2] and the twisted and rhythmic crystals were described by Bernauer [5] in 1929 in his book “*Gedrißte Kristalle*”. Rhythmic crystallizations of different salts and additives were described by Solé in 1954 [12] and in 1956 [13] [14]. He referred in [12] to Liesegang (1924), Küster (1913) and Kägi (1923). The effect of “*Liesegang rings*” was studied by different authors and is generally described as the phenomenon connected to a process depending on precipitation and diffusion [6] [7] [8]. The Liesegang rings are also considered as a self-organization process [15]. Oscillations during crystallization were observed by Wang [9], which were caused by dewetting due to depletion of the salt at the tip of the growing crystal needle. Keath and Padden [3] connected the banding phenomenon with the twisting of crystals, observed for polyethylene and other polymers. The work of Bernauer [5] [16] has been taken up by the group around [Kahr](#). The twisted crystallization is an ongoing topic (2024.03.08) at the [Kahr lab](#) [17] [18] [19] [20]. There Stukenberg [18] and Ye [20] showed how to sort between the optical and crystallographic effects on hippuric acid [18] as example. Recently the transfer of protein chirality to the light rotating properties of gold nano particles was reported by Lee [21]. Banding as a type of crystallization is also mentioned by Kurz [22] in his [morphology map](#). Andersen used additive concentrations, which were chosen in such a way, that resulted in the appearance of just two to three substance spirals [23] [24] as shown in Fig. 2.7.3.

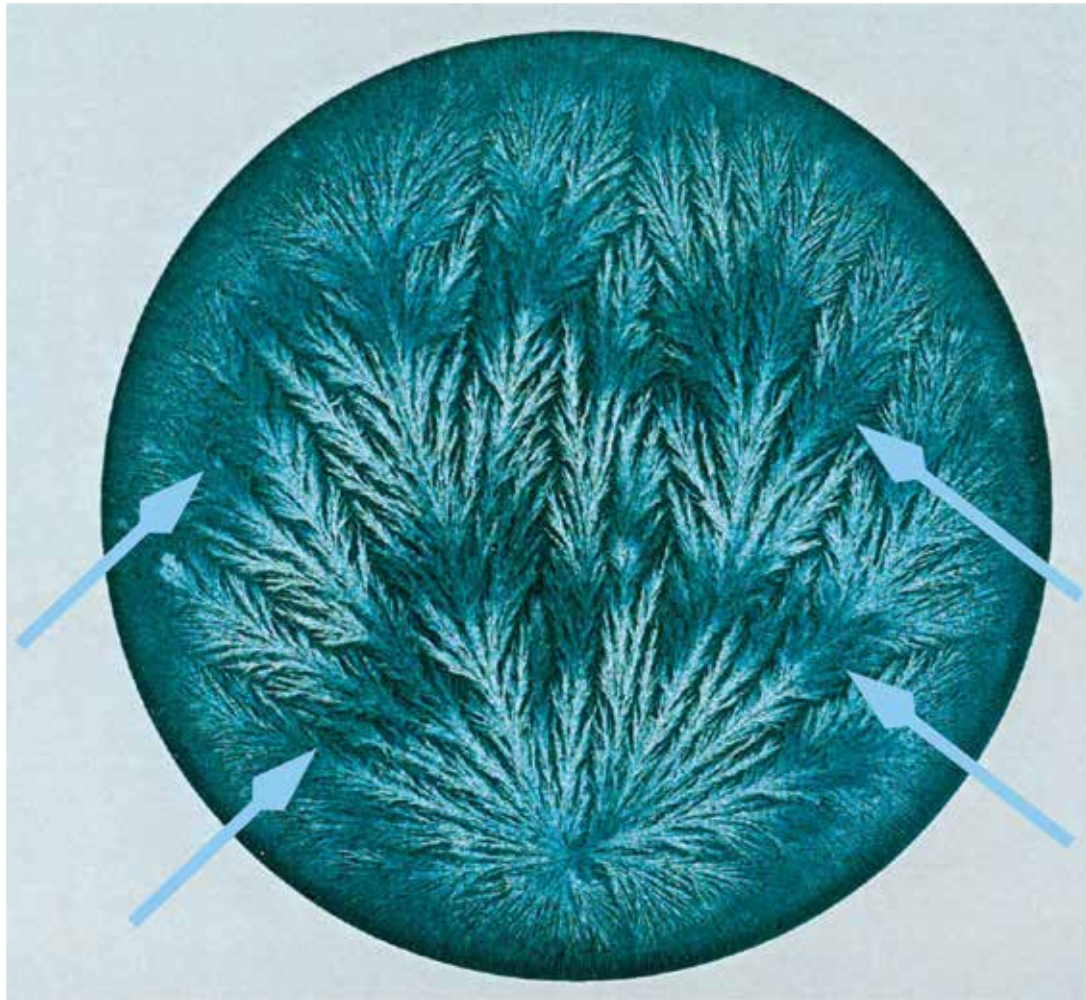


Fig. 2.7.3 DCC picture from carrot juice with two substance spirals. The substance spirals are the dark areas, to which the light blue arrows point. From Andersen [23], front page.

Resume historical overview:

So far the following hypotheses exist for the observed substance spirals in the DCC pictures:

- Depletion of DCC and maybe dewetting at the crystallization tip (Wang [9])
- Accumulation of the additive around the crystallization tip (Pettersen [25])
- Precipitation and diffusion around the crystallization tip (Liesegang effect)
- Twisted crystal: physical and optical turning of the crystal (Bernauer, Keith, Kahr, Lee)

Authors Observations

Observations received during ongoing projects, that could not be followed up, are listed here.

The first observation was, that in the DCC pictures the substance spirals appeared only at higher amounts of the additive.

The second one was that the frequency of substance spirals per cm increase with an increasing additive amount, and decrease with increasing DCC amount (see [Appendix 2.7.1 Matrices](#)).

The third one was: The effect appeared for freeze dried wheat and for black currant juice as additive between the dendritic growth-area and the inhibition area of the crystal growth (see article [26] in preparation). The localization of the substance spirals within the “*morphological map*” for PVP , carrot and wheat as additive is not clear until now (see as comparison the morphology map or concentration matrix for BSA in chapter [2.3 Crystal growth and branching](#)).

The fourth observation was that the DCC pictures are optical active in most cases. When scanned between two crossed polarization filters, some areas became visible while others remained dark. Also the appearance of colorful needles in the substance spirals, as can be seen in Fig. 2.7.1 pointed into this direction. The polarization effect has been observed and used for photography of the DCC pictures by Manthei [27]. He used circular polarized light.

Additional research

Questions about substance spirals:

- Amounts: localization of the phenomenon of substance spirals within the morphological “map” for different additives: (see as comparison the morphology map or concentration matrix for BSA in chapter [2.3 Crystal growth and branching](#)).
- Is it always located between the dendritic and inhibition crystal types?
- Concentration effect:
 - Is the number of substance spirals constant for the mixing ratio $m_x = \text{DCC}/\text{Additive}$?
 - Is the number of substance spirals constant throughout the whole DCC picture?
- Twisted crystals:
 - Are the substance spirals (and maybe also other crystal types) optically active (scan with crossed polarization filters)
 - See chapter [2.12 Light polarization effect](#)
- [One Dish Prüfstand](#): Is the growth “halted” at the start of each substance spiral? This would point to the depletion effect from Wang [9].
- If the substance spirals are optical active (as we expect, see Fig. 2.7.1):
 - Is it possible to sort between the optical and crystallographic parts as in Sthukenberg [18] or Ye [20]. Read more from [kahrlab publications](#).
 - How to contact Kahrlab? (www.kahrlab.com)
 - What kind of cooperation is needed for this research?
- Is there any correlation to quality questions known?
 - E.g. the concentrations used by Andersen.
 - Do different qualities of e.g. wheat or carrot show a difference in the optical activity?

Appendix 2.7.1 Matrices

Pictures from Andersen 2003 [4]: In Fig. 2.7.4 and Fig. 2.7.5 (see below) the matrices from Andersen for wheat (Fig. 2.7.4) and carrot (Fig. 2.7.5) are shown.

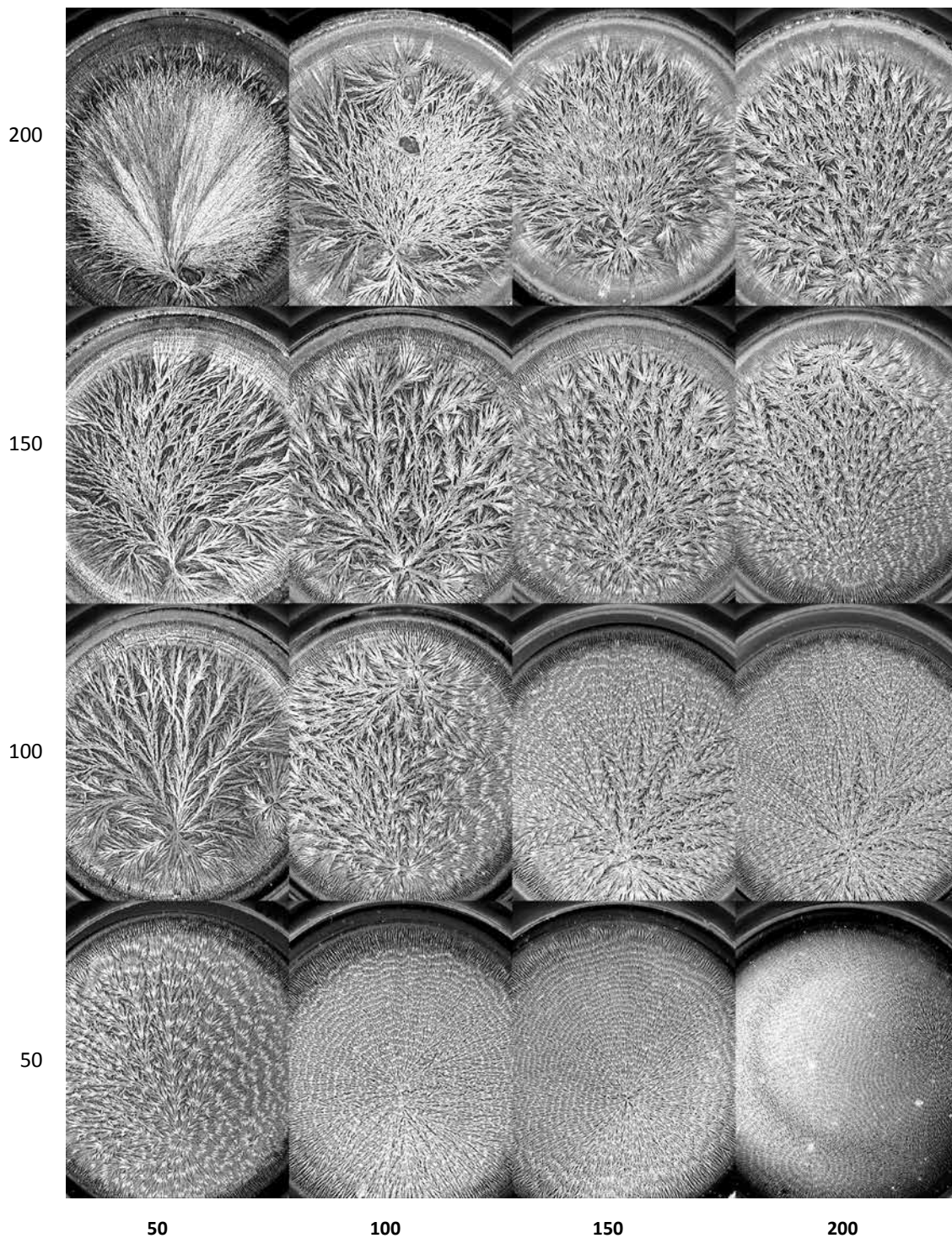


Fig. 2.7.4 Wheat matrix. Y-axis: DCC amount in mg per plate. X-axis: additive in mg per plate (From Andersen [4]).

One observation was that the frequency of the substance spirals increased with the additive amount. This is clearly visible in Fig. 2.7.4 (wheat) in the lowest row (DCC = 50 mg). From left to right, the additive amount increased, as did the frequency per cm of the substance spirals. Comparing the bottom row (DCC = 50 mg) with the row above (DCC = 100 mg), it can be seen that the number of substance spirals in row no. 3 (DCC = 100 mg) is lower than in row no. 4 (DCC = 50 mg) for the same additive amount. This means that the number of substance spirals decreased with an increasing DCC amount.

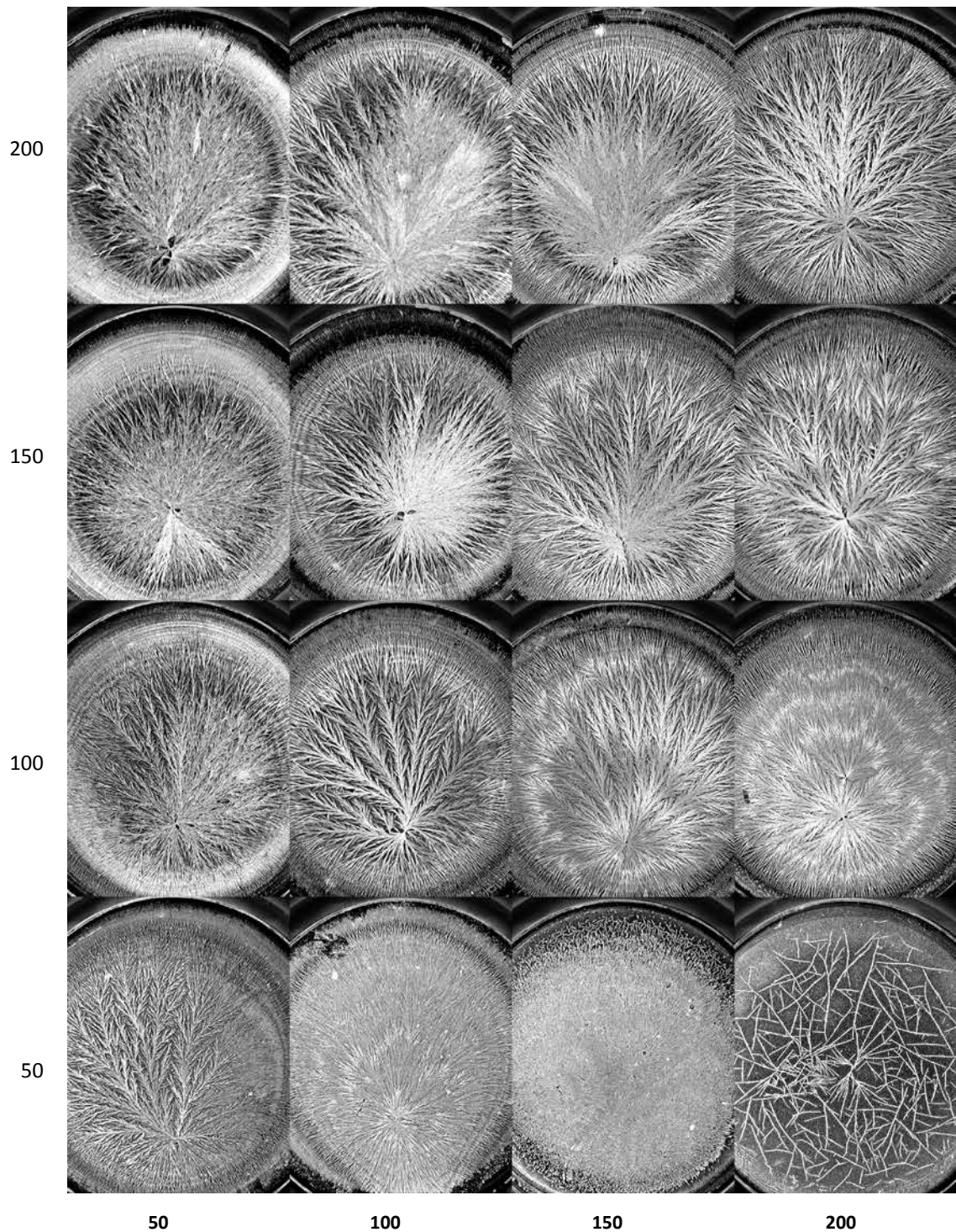


Fig. 2.7.5 Carrot Matrix. Y-axis: DCC amount in mg per plate. X-axis: additive in mg per plate (From Andersen [4]).

In Fig. 2.7.5 (carrot) the increase of the number of substance spirals can be seen in row no. 3 (DCC = 100 mg) in the two most right pictures, where the additive is 150 and 200 mg.

Appendix 2.7.2 Samples

Table of samples which show substance spirals in their DCC pictures

Sample	Substance Spirals Visible	Reference
Wheat	Yes	Andersen 2003 [4]
Carrot	Yes	Andersen 2003 [4]
Freeze dried wheat	Yes	Busscher 2020-2 (to be published)
Black currant Juice	Yes	Busscher 2020-2 (to be published)
PVP K60	Yes	See 2.6 Molecular weight and branching
BSA	No	Busscher 2020-1 [11]
Apple juice	No	Kahl 2016 [28]

Table 2.7.1 Appearance of substance spirals (yes/no) in DCC pictures for different samples.

References

- [1] Huber M, Andersen J-O, Kahl J, Busscher N, Doesburg P, Mergardt G et al. Standardization and Validation of the Visual Evaluation of Biocrystallizations. *Biological Agriculture and Horticulture* 2010; 27: 25–40.
- [2] Popoff B. Eine neue Untersuchungsweise sphärolithischer Bildungen. *Tscherm. Min. Petr. Mittl.* 1904; 23: 153-179 <https://doi.org/10.1007/BF02993455>.
- [3] Keith HD, Padden FJ. Banding in Polyethylene and Other Spherulites. *Macromolecules* 1996; 29: 7776-7786.
- [4] Andersen JO, Huber M, Kahl J, Busscher N, MeierPloeger A. A concentration matrix procedure for determining optimal combinations of concentrations in biocrystallization. *Elemente der Naturwissenschaft* 2003; 79: 97-114.
- [5] Bernauer FJohnson, A. editors. Gedrillte Kristalle (Gebrüder Borntraeger, 1929).
- [6] Cartwright JHE, García-Ruiz JM, Villacampa AI. Pattern formation in crystal growth: Liesegang rings. *Proceedings of the Europhysics Conference on Computational Physics CCP* 1998 1999; 121-122: 411-413.
- [7] Krug HJ, Brandstädter H, Jacob KH. Morphological instabilities in pattern formation by precipitation and crystallization processes. *Geologische Rundschau* 1996; 85: 19-28.
- [8] Krug H-J, Brandstädter H. Morphological Characteristics of Liesegang Rings and Their Simulations. *J. Phys. Chem. A* 1999; 103: 7811-7820 <https://doi.org/10.1021/jp991092l>.
- [9] Wang M, Ming N-b. In situ observation of surface-tension-induced oscillation of aqueous solution film in needlelike crystal growth. *Phys. Rev. A* 1991; 44: R7898-R7901 <https://doi.org/10.1103/PhysRevA.44.R7898>.
- [10] Selawry A and Selawry O. Die Kupferchlorid-Kristallisation in Naturwissenschaft und Medizin (Gustav-Fischer-Verlag, 1957).
- [11] Busscher N, Doesburg P, Mergardt G, Sokol A, Kahl J, Ploeger A. Crystallization patterns of an aqueous dihydrate cupric chloride solution in the presence of different amounts of Bovine Serum Albumin. *Journal of Crystal Growth* 2019; <https://doi.org/doi:10.1016/j.jcrysgro.2019.125272>.
- [12] Solé A. Die rhythmischen Kristallisationen im Influenzstagogramm. *Colloid & Polymer Science* 1954; 137: 15-19.
- [13] Solé A. Untersuchung über die Bewegung der Teilchen im Stagogramm und Influenzstagogramm. *Colloid & Polymer Science* 1957; 151: 55-62.
- [14] Solé A. Stagoskopische Untersuchungen über die Rhythmik einiger Aminosäuren sowie anderer organischer Verbindungen. *Colloid & Polymer Science* 1957; 151: 126-136.
- [15] Nakouzi E, Steinbock O. Self-organization in precipitation reactions far from the equilibrium. *Science Advances* 2016; 2 <https://doi.org/10.1126/sciadv.1601144>.
- [16] Bernauer F. Über die sogenannte rhythmische Kristallisation. *Neues Jahrbuch für Geologie und Paläontologie, Beilagenbände A* 1927; 56: 342-356.
- [17] Asaf Haddad Hillel Aharoni ESAGSBK, Efrati E. Twist renormalization in molecular crystals driven by geometric frustration. *Soft Matter* 2019; 15: 116 <https://doi.org/10.1039/c8sm01290c>.
- [18] Alexander G. Shtukenberg Ankit Gujral ERXC, Kahr B. Mechanics of twisted hippuric acid crystals untwisting as they grow. *CrystEngComm* 2015; 17: 8817 <https://doi.org/10.1039/c5ce00195a>.
- [19] Gunn E, Sours R, Benedict JB, Kaminsky W, Kahr B. Mesoscale Chiroptics of Rhythmic Precipitates. *J. Am. Chem. Soc.* 2006; 128: 14234-14235 <https://doi.org/DOI:10.1021/ja065139+>.
- [20] Ye H-M, Freudenthal JH, Tan M, Yang J, Kahr B. Chiroptical Differentiation of Twisted Chiral and Achiral Polymer Crystals. *Macromolecules* 2019; 52: 8514-8520 <https://doi.org/10.1021/acs.macromol.9b01526>.
- [21] Lee H-E, Ahn H-Y, Mun J, Lee YY, Kim M, Cho NH et al. Amino-acid- and peptide-directed synthesis of chiral plasmonic gold nanoparticles. *Nature* 2018; 556: 360-365.
- [22] Kurz W. Solidification Microstructure-Processing Maps: Theory and Application. *Advanced engineering materials* 2001; 3: 443-452 [https://doi.org/https://doi.org/10.1016/0956-7151\(94\)90044-2](https://doi.org/https://doi.org/10.1016/0956-7151(94)90044-2).
- [23] Andersen J-O. Development and application of the biocrystallization method. PhD Thesis, Department of Agricultural Sciences/Organic Farming Unit The Royal Veterinary and Agricultural University Copenhagen. 2001.
- [24] Andersen JO, Henriksen CB, Laursen J, Nielsen AA. Computerised image analysis of biocrystallograms originating from agricultural products. *Computers and Electronics in Agriculture* 1999; 22: 51-69 [https://doi.org/doi:10.1016/S0168-1699\(98\)00043-X](https://doi.org/doi:10.1016/S0168-1699(98)00043-X).
- [25] Pettersson BD. Beiträge zur Entwicklung der Kristallisationsmethode mit Kupferchlorid nach Pfeiffer IV. Wie verschiedene Kristallbilder bei der Pflanzenkristallisation entstehen. *Lebendige Erde* 1969; 3: 112-126.
- [26] Busscher N, Doesburg P, Mergardt G, Kahl J, Ploeger A. Defining ratios of CuCl₂ · 2H₂O and organic additives exhibiting minimal disturbances in the crystallization patterns when crystallized in a Petri-dish. In preparation.
- [27] Manthei C. Zur Darstellung von Kupferchloridkristallisationsbildern mit Mitteln der klassischen Schwarz-Weiß-Fotografie. *Elemente der Naturwissenschaft* 2004; 80: 121-124.
- [28] Kahl J, Busscher N, Doesburg P, Mergardt G, Will F, Schulzova V et al. Application of Crystallization with Additives to Cloudy and Clear Apple Juice. *Food Analytical Methods* 2016; 10: 1-9 <https://doi.org/doi:10.1007/s12161-016-0575-6>.

2.8 Dewetting by crystallization

Abstract

Crystallization induced dewetting is described. The implications for the $\text{CuCl}_2 \cdot 2\text{H}_2\text{O}$ (cupric chloride di-hydrate, further called DCC) evaporation are discussed. The increase in surface tension caused by the crystallization growth front leads to dewetting after crystallization in the region where the temperature and DCC concentration gradient are highest.

Introduction

Crystallization induced dewetting was described by Okerberg (2009 [1]) for Polycaprolactone and by Habibi (2016 [2]) for PbI_2 . It was also observed for the salt $\text{CuCl}_2 \cdot 2\text{H}_2\text{O}$ (cupric chloride di-hydrate, further called DCC) by Busscher (2019 [3]). Dewetting caused the liquid film to retract, resulting in a separation of the final picture into a small DCC portion at the rim and a DCC picture around the geometric center of the Petri-dish. The coverage of the plate with DCC is therefore below 100 %. The dependency of the crystallization induced dewetting on the temperature was researched by Okerberg (2009 [1]). His study of the dewetting phenomena of Polycaprolactone showed that there is a threshold temperature below which crystallization growth is faster than the growth of dewetting holes, and above which the growth of the dewetting holes is faster than crystal growth. The influence of ultrasound vibration on nucleation and crystallization was researched by Zabihi (2018 [4]) for PbI_2 . For a power of 5 W during 1 minute the crystals transformed from a 2D structure to a 3D columnar structure, resulting in the suppression of crystallization dewetting.

Authors Measurements

During the review process of the 2019 dewetting article (Busscher 2019 [3]) the articles from Habibi (2016 [2]) and Okerberg (2009 [1]) were brought to our attention. They described how the advancing crystallization front promotes dewetting of the solution. With this insight we could explain most of our dewetting phenomena in terms of overstressing of the crystallization front. The dependency of the DCC coverage of the plate on different cleaning procedures and different ring heights could be explained from this point of view (see chapter [1.4 Surface tension, cleaning, ring height](#)). The main conclusion from this is that there is an area between the geometric center and the rim where the DCC concentration and temperature gradients are highest (see chapter [2.4 Concentration gradient](#)) and where the surface tension forces are increased by the growing crystal front (see also in chapter [1.6 Sensitive area](#)).

Resume

The crystallization induced-dewetting effect, as termed by Okerberg [1], increases the surface tension in front of the DCC crystal growth boundary. When the crystallization front enters the area where the gradients of the DCC concentration and the temperature are highest, the increase in surface tension due to the crystal growth front can induce dewetting if a threshold is exceeded.

Additional research

- Quantify the coverage of the plate with CrystEval (see chapter [3.3 CrystEval](#) tool) in connection to the zonal approach of Engquist (already in Additional research of chapter [1.13 Picture zones](#)).
- The sensitive zone is the transition between inner and outer zone.
 - How to make this transition zone stronger or weaker? By cleaning? With which samples?
- Perform a literature study on how the surface tension interacts with the growing crystal (see articles of Langer 1980 [5], Langer and Müller Krumbhaar 1977 [6], Sekerka, 1993 [7], Kurz 2001 [8]).
- The temperature effect of Okerberg (2009 [1]). Would an increase of the temperature of the Petri-dish increase the dewetting effect, and a reduction reduce it? How sensitive (0.1, 1 or 10 °C) is this effect in changing the value of the coverage of the plate by 1 %?
- Is there a dependency on the growth velocity of the crystal front? Higher additive amounts have lower growth velocities.

References

- [1] Okerberg BC, Berry BC, Garvey TR, Douglas JF, Karim A, Soles CL. Competition between crystallization and dewetting fronts in thin polymer films. *Soft Matter* 2009; 5: 562-567.
- [2] Habibi M, Rahimzadeh A, Eslamian M. On dewetting of thin films due to crystallization (crystallization dewetting). *Eur. Phys. J. E* 2016; 39: 30 <https://doi.org/doi:10.1140/epje/i2016-16030-9>.
- [3] Busscher N, Doesburg P, Mergardt G, Sokol A, Kahl J, Ploeger A. Influence of dewetting on the crystallization behavior of CuCl₂ in the presence of BSA during evaporation in a Petri dish. *Heliyon* 2019; 5: e01102 <https://doi.org/10.1016/j.heliyon.2018.e01102>.
- [4] Zabihi F, Eslamian M. Effect of the Ultrasonic Substrate Vibration on Nucleation and Crystallization of PbI₂ Crystals and Thin Films. *Crystals* 2018; 8 <https://doi.org/doi:10.3390/cryst8020060>.
- [5] Langer JS. Instabilities and pattern formation in crystal growth. *Rev. Mod. Phys.* 1980; 52: 1-28 <https://doi.org/10.1103/RevModPhys.52.1>.
- [6] Langer JS, Müller-Krumbhaar J. Stability effects in dendritic crystal growth. *Journal of Crystal Growth* 1977; 42: 11 - 14 [https://doi.org/DOI: 10.1016/0022-0248\(77\)90171-3](https://doi.org/DOI:10.1016/0022-0248(77)90171-3).
- [7] Sekerka RF. Role of instabilities in determination of the shapes of growing crystals. *Journal of Crystal Growth* 1993; 128: 1-12.
- [8] Kurz W. Solidification Microstructure-Processing Maps: Theory and Application. *Advanced engineering materials* 2001; 3: 443-452 [https://doi.org/https://doi.org/10.1016/0956-7151\(94\)90044-2](https://doi.org/https://doi.org/10.1016/0956-7151(94)90044-2).

2.9 Additive built into $\text{CuCl}_2 \cdot 2\text{H}_2\text{O}$?

Abstract

Depending on the additive, the $\text{CuCl}_2 \cdot 2\text{H}_2\text{O}$ (cupric chloride di-hydrate, further named DCC) pictures display different colors and needle types. The question arose if the additive is incorporated in the crystal (lattice). The results of different research approaches are listed, as well as ways to test whether the additive is contained in the DCC crystal (lattice).

Introduction

The starting observation was that the $\text{CuCl}_2 \cdot 2\text{H}_2\text{O}$ (cupric chloride di-hydrate, further named DCC) pictures had different colors, depending on the additive. The question arose whether the additive was included in the DCC crystal. An inclusion of the additive would make the crystal system much more complex. The DCC - water system is already a binary system. If the additive were to be incorporated into the crystal a ternary system would have to be discussed. Different approaches and possibilities are listed in the historical overview.

Historical overview

Bessenich (1951 [1], p. 33) reported on X-ray studies on DCC crystals, in the presence of different additives, *“dass die Zugehörigkeit zum rhomboedrischen Kristallsystem, dem das DCC angehört, nicht geändert wird”* (“that the affiliation to the rhombohedral crystal system, to which the DCC belongs, will not be changed”). Kleber (1959 [2]) and Steinike-Hartung (1958 [3]) tested different additives like NaCl, NH_4 , KCl, proteins and citric acid and observed, depending on the concentrations, that additives like proteins, citric acid and aminocaproic acid, *“ins Gitter eingebaut werden können”* (1958 [3], p. 93). The minerals form chemical structures which form crystals. Gallinet (1991 [4]) tested the question if Bovine Serum Albumin (BSA) as additive is incorporated in the DCC crystal. He used for this radioactive BSA. At the additive levels tested, there was no radioactivity in the DCC that he washed off the plate for testing. The plate, without the DCC, but with the radioactive BSA showed no structure. Shibata (1998) compared DCC crystals without and with blood as additive. He did not find differences in the crystal structure, but the differential scanning calorimetry (DSC) measurements showed differences that he attributed to additional water in the DCC crystal grown in the presence of blood as additive. This would be consistent with the results of Sokol (2013 [5]) who found a change in color and weight in the first 24 hours after crystallization. Schweizer (2010 [6], p. 82, Fig. 11) found two types of DCC on the glass plate. The differences between the two types were in the ratio of Cl to Cu. The normal DCC has a ratio of 2, while the other, which was not water soluble, had a ratio around 0.6. Schweizer compared the X-Ray structure and identified it as Atacamit ($2\text{CuCl}_2 \cdot 5\text{Cu}(\text{OH})_2 \cdot 2\text{H}_2\text{O}$). For DCC as a precursor it is mentioned by Gawande (2016), that DCC builds Cu nano-particles (ref. 107 or for DCC in ref. 170 in Table I). Perhaps DCC can generate building blocks and build complex structures from them, as described in Cölfen's concept of meso-crystals (2008 [7]) for Calcite, or Driesche (2018 [8]) for the polymorphic behavior of DCC.

Authors Contributions

In the DCC pictures from different cereals a big variety in the crystals became visible. As an example the DCC pictures from barley and from wheat as additive (see Fig. 2.9.1 left and right) are shown. Also the other cereals like oat show different patterns (not shown here). One guess is that the mineral composition of the cereals can build different types of crystals, as Kleber [2] and Steinike-Hartung [3] stated. Potassium in particular is contained in grain at 400 mg / 100 gram.



Fig. 2.9.1. DCC pictures with (upper picture) barley as additive (DCC = 240 mg per plate, additive = 80 mg per plate) and (lower picture) wheat: DCC = 90 mg per plate, additive = 90 mg per plate. Pictures from University of Kassel (D) barley: LabDoc series C.2006.07.17.KW no. 11, wheat: DOK wheat, bio-dyn, LabDoc series C.2006.02.22.JP, no. 38.

The differences in the pictures can be described as follows: the picture from barley as additive (upper picture) shows thick rope-like stems with very few side needles. The picture from wheat as additive (lower picture) have thinner stems with heavy branching and many side needles.

Resume

Two cases have to be separated. Case 1 is when the additive is a part of the crystal lattice and (case 2) when the additive is incorporated in the crystal. Steinike-Hartung [2] [3] states that minerals like K or Mg can build a new crystal with DCC. This can be checked with X-ray techniques. Shibata [9] stated that water was incorporated into the lattice. This can be tested with DSC or as Sokol [5] showed by simply weighing the DCC picture. Gallinet found no BSA in the DCC crystal when used as an additive.

As an additional case, it is possible that the crystal is built from basic blocks as a meso-crystal. This can be checked by an X-ray technique.

It might be possible that all cases appear at different locations in the concentration matrix.

Additional research

- X-ray examination of needles from BSA pictures from the DCC – BSA concentration matrix, to check for meso-crystals as described by Cölfen (2008 [7], p. 39).
- Check DCC pictures with additions of minerals such as present in cereals (K ~ 400 mg / 100 g Mg ~ 80 mg / 100 g) with and without PVP or BSA as additive. Look at the minerals Selawry (1957 [10], Part B, p. 28-33) found as interesting being closest to the sensitivity of DCC.

References

- [1] Bessenich F. Beiträge zur Erforschung der Bildekräfte durch empfindliche Kristallisation (Goethenaum (Dornach), 1951).
- [2] Kleber W, Steinike-Hartung U. Ein Beitrag zur Kristallisation von Kupfer(II)-chlorid-Dihydrat aus Lösungen. *Zeitschrift für Kristallographie* 1959; 111: 213-234 <https://doi.org/DOI:10.1524/zkri.1959.111.1-6.213>.
- [3] Steinike-Hartung. Die Kristallisation des Kupfer II Chlorid dihydrates in Gegenwart von Lösungsgenossen, Diplomarbeit Humboldt Universität Berlin, 1958 .
- [4] Gallinet JP, Gauthier-Manuel B. Wetting of a glass surface by protein adsorption induces the crystallization of an aqueous cupric chloride solution. *Journal of Colloid and Interface Science* 1992; 148: 155-159 [https://doi.org/doi:10.1016/0021-9797\(92\)90123-4](https://doi.org/doi:10.1016/0021-9797(92)90123-4).
- [5] Sokol A. Digital Color Analysis of Copper (II) Chloride Crystallograms. MSc Thesis, University of Aalborg. 2013.
- [6] Schweizer F, Andersen J-O, Jens-Laursen. Beobachtungen bei der Kupferchloridkristallisation: vom Eiweiß-Vorbild zum Kupferchlorid-Nachbild. *Elemente der Naturwissenschaft* 2010; 92: 62-93 <https://doi.org/DOI:10.18756/edn.92.62>.
- [7] Cölfen H and Antonietti Markus Wiley 2008S1-6. Mesocrystals and nonclassical crystallization (Wiley, 2008).
- [8] Driessche V, Alexander E. S, Van Gerven N, Bomans PHH, Joosten RRM, Friedrich H et al. Molecular nucleation mechanisms and control strategies for crystal polymorph selection. *Nature* 2018; 556: 89-94 <https://doi.org/10.1038/nature25971>.
- [9] Shibata T, Takakuwa Y, Tanaka A, Kogure M, Iguchi T, Obata H et al. Crystal structures of blue and green hydrated cupric chloride grown from aqueous solutions with and without human blood addition: single crystal X-ray diffraction analysis and differential scanning calorimetry(DSC). *Journal of Tokyo Women's Medical College* 1998; 68: 358-369.
- [10] Selawry A and Selawry O. Die Kupferchlorid-Kristallisation in Naturwissenschaft und Medizin (Gustav-Fischer-Verlag, 1957).

2.10 Evaporation prefiguration (Vorbild)

Are there observations of a creation of a prefiguration during the evaporation?

Abstract

The evaporation prefiguration is one of the hypotheses (P4) listed in the chapter [arrangement](#). Crystallization probably starts at the surface of the solution, because this is the coldest layer due to the evaporation. If there is a spatial temperature structure on the surface, then the crystallization would grow along the lower temperature of this structure. A temperature structure has been expected by the observation of the vapor from a tea cup (Pollack [1], p. 265) or in a Petri-dish (Flack [2]), or in a Petri-dish when the heating from below is switched from on to off (Kumar [3]). Measurements of the surface temperature of a [DCC / PVP](#) solution evaporating in a Petri-dish (Busscher [4]) showed a gradient from the center of the Petri-dish to the rim, which implied circular isothermal zones.

Introduction

The idea of a prefiguration, was first uttered by Pfeiffer (in Bessenich [5] p. 84) in connection with a possible protein prefiguration (Pfeiffer called it "Vorbild"). Alternatively, a possible prefiguration could also be thought of as a thermal structure, which may define the growth path of the crystal. When the crystallization starts at the surface of the solution, which was observed by Nickel [6] and by Waldburger [7] for blood as additive and by Misyura [8] for the salts CaCl_2 , LiBr and LiCl , then a spatial (lower) temperature structure at the surface of the solution can have an influence on the crystallization form. This would be called an evaporation prefiguration. This is one of the hypotheses (P4) listed in the chapter [arrangement](#). The height of the solution is $\sim 1\text{mm}$ at the start of the evaporation.

Historical overview

Nickel [6] and Waldburger [7] observed that the CuCl_2 crystallization in the presence of blood as additive started at the surface and grew from there. Von Hahn [9], p.12, had the hypothesis that the most important processes for the development of the forms of the [DCC](#) pictures occur during the evaporation.

Observations from Flack [2] and Saylor [10] showed a structure of the evaporating surface for 15 cm deep solutions in a quadratic ($16 * 16\text{ cm}^2$) tank and the influence of a surfactant on the pattern. Kumar [3] reported that temperature structures became visible on the surface of the solution during a cooling phase. The solution was heated from below, and then cooled down (height of the solution 1 to 10 cm), which resulted in the appearance of structures. Flack [10] reported structures formed when the solution was cooling by a passing airflow. Chevalier [11] reported that the surface tension drove the orientation of the crystals on the surface. Pollack [1] (p.265) reported photographs of water damp on the surface of coffee in a mug, which showed a non-homogeneous distribution. That would mean that the evaporation process itself can have a temperature structure at the surface of the solution.

Authors Measurements

The surface temperature of a [DCC / PVP](#) solution in the Petri-dish was measured during the evaporation process by Busscher in 2010 [4] in a so called [Triangle Chamber](#). In the middle of the Petri-dish, where evaporation was strongest, cooling up to $2\text{ }^\circ\text{C}$ was measured. At the Petri-dish rim, a decrease of only $1\text{ }^\circ\text{C}$ was measured because evaporation was lower close to the rim due to shielding of the ring (for details see Holleman [12] and chapter [2.4 Concentration gradient](#)). The temperature distribution in the Petri-dish during evaporation (close to the ring and close to the center), was monitored with an IR camera. Initially, the evaporation had a radial structure, i.e. there are circular isothermal zones in the Petri dish, as shown in the IR photos in the [2.5 Warmth of process](#) chapter. Later in the evaporation process, the temperature gradient decreases as the evaporation rate decreases due to an increasing DCC concentration (Busscher 2010 [4]).

Additional research

Doesburg observed that when the vaseline used in the laboratory to glue the Petri-dishes cools down, the structures observed by Kumar [3] appear. In the future this could be photographically documented and researched.

According to Kumar [3], if the evaporation is modulated by the airflow, due to the On/Off switching of

the [inner chamber](#) temperature heating ([two point regulator](#)), which is situated below the Petri-dishes (see chapter [3.1 Chamber systems](#)), structures like his Fig. 9.d should appear.

Sometime so called heat rings were observed (private communication Amons) , which were possible connected to the On/Off cycles of the inner chamber heating system. If this is the case, then this would imply that the additive concentration in the solution is close to the solubility border. (see also chapter [2.7 Substance spirals](#)).

If the surface temperature structure of the solution and possibly the substance spirals are due to the On/Off switching of the inner chamber temperature regulator, then changing to a different power actor (e.g. a so called [PID](#) regulator), which allows control without On/Off phases, should influence the picture properties. Consequently, a change in the substance spirals and the variation of the crystallization starting time is expected.

It should also be checked if the start of the crystallization is correlated to the onset of heating or cooling of the current two-point regulator heating system.

References

- [1] Pollack GH. Wasser – viel mehr als H₂O (VAK Verlag Freiburg, 2012).
- [2] Flack KA, Saylor JR, Smith GB. Near-surface turbulence for evaporative convection at an air/water interface. *Physics of Fluids* 2001; 13: 3338-3345 <https://doi.org/10.1063/1.1410126>.
- [3] Kumar N, Arakeri JH. Natural Convection Driven Evaporation from a Water Surface. *Procedia IUTAM* 2015; 15: 108 - 115 <https://doi.org/https://doi.org/10.1016/j.piutam.2015.04.016>.
- [4] Busscher N, Kahl J, Doesburg P, Mergardt G, Ploeger A. Evaporation influences on the crystallization of an aqueous dihydrate cupric chloride solution with additives. *Journal of Colloid and Interface Science* 2010; 344: 556–562 <https://doi.org/doi:10.1016/j.jcis.2009.12.045>.
- [5] Bessenich F. Zur Methode der empfindlichen Kristallsation (Naturwissenschaftliche Sektion am Goetheanum Dornach, 1960).
- [6] Nickel E. Die Reproduzierbarkeit der sogenannten empfindlichen Kupferchloridkristallisation. PhD Thesis, Universitätsverlag, Freiburg (Schweiz). 1968.
- [7] Waldburger B. Die Blutkristallisation als Schulungsmethode. *Mercurstab* 2013; 5: 402-414.
- [8] Misyura S. Evaporation and heat transfer of aqueous salt solutions during crystallization. *Applied Thermal Engineering* 2018; 139: 203 - 212 <https://doi.org/https://doi.org/10.1016/j.applthermaleng.2018.04.068>.
- [9] Von Hahn F-V. Thesigraphie. (Franz Steiner Verlag, 1962).
- [10] Saylor JR, Smith GB, Flack KA. An experimental investigation of the surface temperature field during evaporative convection. *Physics of Fluids* 2001; 13: 428-439 <https://doi.org/10.1063/1.1337064>.
- [11] Chevalier NR, Guenoun P. Surface Tension Drives the Orientation of Crystals at the Air-Water Interface. *J. Phys. Chem. Lett.* 2016; 7: 2809-2813 <https://doi.org/10.1021/acs.jpcllett.6b01312>.
- [12] Holleman LWJ. Ein Beitrag zum Verständnis der empfindlichen Kristallisation. *Elemente der Naturwissenschaft* 1966; 4: 24-33 <https://doi.org/10.18756/edn.4.24>.

2.11 Nucleation

**How can we understand the statistical distribution of the crystallization starting times and the statistical distribution of the distance of the crystallization center from the geometrical center?
How is the nucleation depending on the amounts of $\text{CuCl}_2 \cdot 2\text{H}_2\text{O}$ and additive?**

Abstract

The start of the crystallization in the $\text{CuCl}_2 \cdot 2\text{H}_2\text{O}$ system (further called [DCC system](#)) is preceded by a nucleation. Not all nucleations in the Petri-dish will proceed as a visible crystallization start. Location and the time of the crystallization start follow different distributions. The Crystallization starting time follows a Gaussian distribution, pointing to the expected random process. The distribution of the location of the starting point is in a defined area reflecting the constant supersaturation in this defined area. The crystallization starting time increases with the additive amount, by preventing the clustering of DCC molecules to the minimum of 20-50 atoms for growth initiation [1]. With increasing amounts of DCC, the crystallization starting time is expected to decrease. However, empirical data points suggests that the crystallization starting time initially increases with increasing DCC amount, reaching a maximum at ~ 2000 mg DCC per plate and then decreases as the amount of DCC increases. This effect was observed for -so far- all additives. This is unexpected, but can be understood from the dependency of the evaporation rate on the DCC concentration, which influences the partial pressure above the DCC solution during the evaporation [2] [3]. The dependency of the location of the crystallization start on the additive and DCC amounts is not equal for all samples and has to be studied in future.

Introduction

The start of the crystallization is a phenomenon that is simple to observe, but not simple to understand. The phase transition from the solubilized DCC to solid DCC in a crystal is initiated by a so called nucleation which is not simply adding DCC molecules together in a Lego brick-like way [1] [4]. The nucleus *in statu nascendi* does not always show the later atomic crystal lattice structure, but can also be amorphous [1] (see intro to [1] by Vekilov [5]). The question is, if the nucleus can continue to grow further, or if the nucleus ends in a building block, which does not grow any further as described by Driesche [6] and Cölfen [7]. If the nucleus cannot grow any further, a crystal can only be built by combining these building blocks. This is described by Driesche [6] for glucose isomerase (an enzyme for glucose \rightarrow fructose) and by Cölfen [7] for calcite building sea urchin spines. The way the building blocks are combined depends on the conditions (e.g. the concentrations of the involved compounds) in the solution. This is called Crystal Polymorph Selection. The further growth of the crystal for DCC is described in [2.3 Crystal growth and branching](#). The observed crystallization start is not the moment of nucleation, because several DCC nucleations can be present in the solution simultaneously before crystallization starts, but it is the moment when crystallization continues and becomes visible, perhaps by accumulating nucleation building blocks. Crystals which were built from building blocks are called meso-crystals. They can be identified by their X-ray pattern (see Cölfen [7] p. 38). This is the way to distinguish the meso-crystals from the usual single-crystal type.

To better understand the processes behind the crystallization start, the moment and the location of the crystallization start is studied. Understanding their dependencies on the amounts of DCC and the additive can provide access to understanding the nucleation processes. In the following, the start time and the start location are first defined. Their statistical distributions are studied to relate them to the possible processes. Then the dependencies of the crystallization starting time and location on the DCC and additive amount are discussed.

The crystallization start studied here is a spontaneous process. There is always the question of why in the used DCC system the crystallization is not started by adding a small crystal to the solution? It is simply left to the system itself. This kind of nucleation is called a heterogeneous crystallization due to the existence of additives in the solution. Nevertheless it can also start without additives [8]. This question of [heterogeneous](#) or [homogeneous crystallization](#) is further discussed below.

Historical overview

Gmelin [9] reported basic data of DCC like solubility, surface tension, viscosity, diffusion, light absorbance (and more). In his PhD thesis Beckmann [8] reported about his studies on the nucleation of DCC. He determined the supersaturation when the crystallization starts by cooling the solution until the crystallization started. The so called undercooling temperature and the supersaturation at which the crystallization starts are equivalent (see [Appendix 2.11.2 Supersaturation](#)). He found that ultra - fine filtered DCC solutions (p. 61) had a lower undercooling temperature than unfiltered ones. In a later research [10] he found that freshly prepared

supersaturated DCC solutions had a lower growth velocity than “aged” ones (e.g. prepared > 72 hours in advance). The “aged” supersaturated DCC-only solutions showed a higher growth velocity on a DCC crystal that had been added to the solution. He concluded that in the supersaturated DCC-only solution different DCC substructures were built, but the one which can be used for the crystal growth needed some time to be created. He considered a two-step model [10] , where the first nucleus is built by a very fast process, from which a second structure is built in a second, slower step, which could be used for the growth of a crystal. It took some time (days) until enough second structures were built to crystallize at a higher growth rate.

A review about Cu nano particles [11] showed that DCC was able to build Cu nano particles. Therefore a possible hypothesis is that the DCC solution might be filled with substructures. From the meso-crystal work of Cölfen [7] on calcite it was shown that the substructures, which had been built, did not grow further themselves, they had to be combined as complete structures on a higher level. The question on the relation between the structure of a molecule in the solution and the structure of a crystal from this molecule, which has building steps in between, was researched by Desiraju [4] and recently supported by Driesche [6] for the building of glucose isomerase crystals (see Alberstein [12] for a simple introduction into the work of Driesche). The classical nucleation theory (CNT) is that a certain number of molecules (e.g. 50) must be in close proximity to each other [13] to initiate a self-organization process that allows the nucleus to continue growing and not dissolve again. Recently it was observed by Zhou [1] (simple introduction to the work of Zhou by Vekilov [5]) for iron-platinum alloy (FePt) that the process for the nucleation can be different from the CNT and that the structure of the nucleus can be amorphous, so that the later structure is not defined at the beginning [5].

Resume historical overview

So far, it seems as if the nucleation is a state that can grow in different directions depending on the boundary conditions in the solution. It can be assumed that different building blocks or “substructures” are present in the solution as pre-structures that can build the crystal depending on the boundary conditions. Heterogeneous nucleation seems to be an inherent property of the pure DCC solution without additive [10].

Authors Measurements

In experiments with Bovine Serum Albumin (hereafter [BSA](#)) it was observed that the crystal types changed with increasing amounts of BSA. At first, with no BSA (only DCC), there were long linear needles branching in to star-like structures , then with increasing amounts of BSA, broader single needles, then [hole-forms \(Hohlformen\)](#) and finally needles with branching appeared [14] (see also in [2.3 Crystal growth and branching](#) and [1.8 Concentration matrix](#)).

Dependencies of crystallization starting time and location

Definition starting time, radius

The starting of a picture is defined by the observation of the beginning of the crystallization. The beginning of the crystallization is preceded by a nucleation. The so called starting time [tcrStart](#) is calculated as the time difference between the start of pipetting the solution into the dish in the chamber and the visual observation of the start of the crystallization in the Petri-dish. The location where the crystallization starts is called the [center](#) and is characterized by its [radius](#). This is the distance between the crystallization center and the geometric center of the dish. The [radius](#) is expressed in % of the radius of the entire dish. In the [Triangle](#) chambers the diameter of the dish is 9 cm (100 %).

Why check the statistical distribution?

Generally the type of a statistical distribution of a parameter gives access to the processes behind the parameter. For the DCC system the hypothesis is that the crystallization starting time [tcrStart](#) is a random effect, which usually has a Gaussian distribution. The statistical distribution of the location of the start of the crystallization should be for the simplest case (a homogeneously saturated dish) a constant distribution over the dish. The so called cumulative statistical distribution would then be proportional to the area in question in the dish. The cumulative probability is 1 for the whole dish. When expressing it in terms of the [radius](#) (the distance from the geometric center of the dish to the location of the crystallization starting point) it is proportional to $\text{radius} * \text{radius}$.

So, checking for the statistical distributions, one would expect for the distribution of the [tcrStart](#) time a Gaussian distribution, if it is the hypothesized random process. For the location, the cumulative distribution has a quadratic increase with the radius.

Passing the solubility border by evaporation

In the following, the conditions for the nucleation of a crystal and for the growth of an existing crystal are described. This is needed to understand the used concepts and the connection to the processes in the dish which can modify the statistical distributions.

DCC salt can be added to a watery DCC solution until the concentration C_x reaches the so called solubility border or saturation concentration (C_s). Then all additionally added DCC will not solubilize but form a deposit. This means that the solubility border cannot be “exceeded” by adding more DCC salt to the solution. The solubility border C_s increases with the temperature of the solution in an exponential way as shown in Fig. 2.11.1 Supersaturation below.

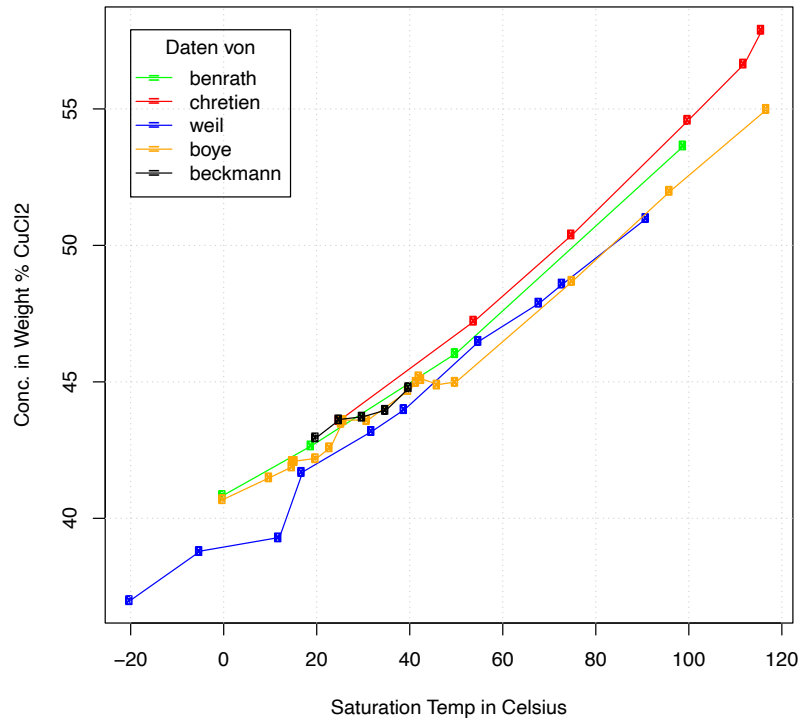


Fig. 2.11.1 The solubility in % (w/w) of anhydrous CuCl_2 (Y-axis) versus the temperature (X-axis) of the solution from different sources. Data from Benrath, Chretien, Boye and Weil are from Gmelin1958 [9] and Beckmann from Beckmann [8], p. 11.

The graph in Fig. 2.11.1 shows that for 20 °C the solubility border is at ~ 42.5 % (w/w) for CuCl_2 which is equivalent to 53.55 % (w/w) for $\text{CuCl}_2 \cdot 2\text{H}_2\text{O}$ (i.e. DCC). This value fits to the amount according to Handbook of Chemistry and Physics [15], which is 83,2 gr/100 mL or 54.59 % (w/w) at 20 °C. Wikipedia stated at 20 °C 75,7 gr/100 mL for DCC. The value from Koglin [16] is 77.5 gr/100 mL at 17.5 °C for DCC. So far the differences for the DCC solubility border have not been understood. Benrath 1934 [17] suggested that for data from Boye 1933 [18] the equilibrium was not achieved. From the experiments of G. Mergardt [19] the solubility border for DCC was determined to be 55 % (w / w) at 25 °C.

To increase the concentration of the DCC solution C_x above the solubility border concentration C_s , either the temperature of the solution must be decreased (in Fig. 2.11.1 moving to the left on the X-axis, while keeping the concentration constant) or the solvent (in our case the water) must be evaporated (in Fig. 2.11.1 moving upwards on the Y-axis while keeping a constant temperature). See also in Appendix 2.11.2 Supersaturation below.

The concentration difference $dC = C_x - C_s$ is the concentration above the solubility border (or below if negative). It is normalized with the solubility border and called supersaturation $\sigma = (C_x - C_s)/C_s$.

When a crystal is added to a solution where the concentration of the solution C_x is lower than the solubility border C_s , the crystal will dissolve. (supersaturation $\sigma < 0$). When the concentration of the solution is above the solubility border ($\sigma > 0$) the crystal will grow. It will grow faster when σ increases [20]. The relation between the growth velocity of the crystal versus the supersaturation was measured by Leray 1986 [21] and Beckmann [8] for “small ($< 1\%$)” supersaturations by adding a DCC crystal into a supersaturated DCC solution with and without additives. The data are shown here in Fig. 2.11.2 below.

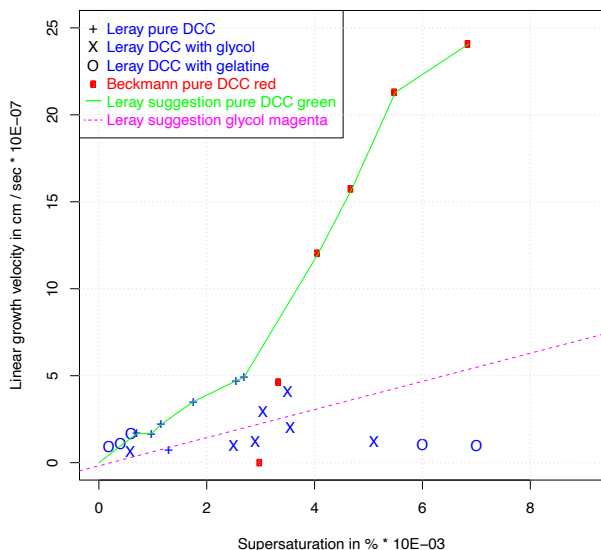


Fig. 2.11.2 Growth rate (Y-axis) versus supersaturation (X-axis). Own plot, data from Beckmann [8] and Leray 1968 [21].

In Fig. 2.11.2 Beckmann’s data (marked with ■ in Fig. 2.11.2) started at 0.3 % supersaturation (supersaturation on the X-axis is in 1/1000, so 3 on the X-axis is equivalent to 0.3 %). Leray’s data for the pure DCC solution (in Fig. 2.11.2 indicated with +) are similar to Beckmann’s at ~0.4 % (data not shown). For values below 0.4 % Leray attributed the differences in the growth velocity to imperfect stirring of the solution by Beckmann. Leray’s data showed that for glycol as additive (indicated by an x in Fig. 2.11.2), the growth rate seemed to be lower than that of the pure DCC solution (+), with outliers at $\sigma = 0.5$ and 0.6 %, while gelatin (in Fig. 2.11.2 indicated with o) (σ between 0 and 0.1 %) as additive seemed not to hinder the growth of the crystal.

Besides the growth velocity, the nucleation probability also depends on the supersaturation. This is described by Reiter and Barth (see Fig. 5 in [20]) for the simple nucleation theory. The nucleation probability is 0 for supersaturation $\sigma = 0$. It increases with increasing supersaturation, because there are more molecules in the solution, giving a higher probability of reaching the required number of molecular participants (e.g 50) [13] [22] to initiate nucleation. However, the viscosity of the solution also increases as the solution becomes more concentrated. This viscosity effect will then finally outweigh the supersaturation and will decrease the nucleation probability with increasing supersaturation. Therefore, the nucleation probability has a maximum at a specific supersaturation value (see Fig. 2.11.3 below from Sangwal [23] p. 29, Fig. 2.5).

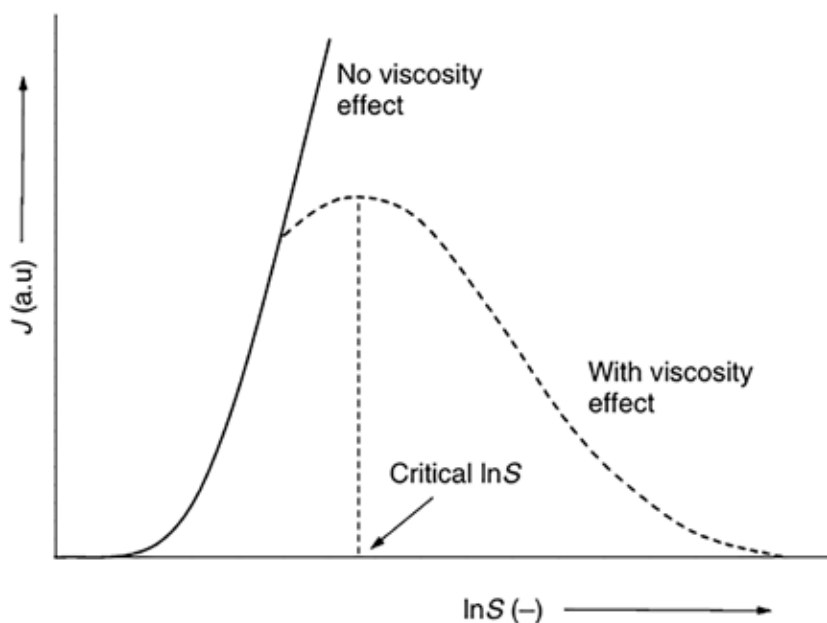


Fig. 2.11.3 General dependency of the 3-Dimensional nucleation rate of a salt (Y-axis) on the supersaturation (X-axis) including the influence of the increasing viscosity at higher salt concentrations (from Sangwal [23] p. 29 Fig. 2.5).

To find out, which part of the curve in Fig. 2.11.3 corresponds to the usual conditions for DCC evaporation and crystallization, the $t_{crStart}$ distribution of the concentration ratio where multiple centers appear is examined (see chapter [1.12 Multiple centers](#)).

If there are no evaporation differences between the positions of the different Petri-dishes in the chamber (see chapter [2.17 Lowering disturbances](#)), a later start of the crystallization would be accompanied by a higher supersaturation. This would connect a later [crystallization starting time](#) to a higher supersaturation in the Petri-dish.

Separation of water and DCC at nucleation

When the nucleation takes place, the DCC and an amount of water has to be separated. At the solubility border, the concentration of DCC is 55 % w/w at 25 °C (data from Mergardt [19]). The solution then contains ~ 7.4 mol water and 1 mol DCC. After nucleation, a crystal is formed in the same volume (specific to DCC, see below for details.) with a ratio of 1 mol DCC and 7.4 mol water outside the crystal. When crystallization takes place, first green crystals appear [24]. They continue to dry -over several minutes or hours- and turn blue. The blue crystals are DCC. Sokol [25] estimated that the DCC in the green crystals can contain up to 2 additional molecules of H₂O. See for details in [Appendix 2.11.2 Supersaturation](#).

Volume before and after crystallization

The concentration of DCC at 20 °C at the solubility border is 5.0 mol/L according to Beckmann [8] p. 9. Therefore, 1 mol CuCl₂·2H₂O is contained in 200 cm³. After crystallization the volume of the water is 133.92 cm³ and the volume of the crystals is 67.9 cm³ in total 67.9 + 133.92 = 201.82 cm³. So the volume hardly changes (details see [Appendix 2.11.10 Volume](#)).

Measured statistical distributions of the starting locations and times

Starting locations

The location of the primary crystallization center in DCC pictures is between the geometric center ([radius](#) = 0 %) and the rim of the Petri-dish (radius 100 %). To get a first look at the data for all the different samples measured so far, boxplots of the radius versus the different samples are plotted. The mean of the histogram distribution of the [radius](#) lays between 35 % and 50 %, depending on the sample in question (see Fig. 2.11.4 below).

The reading of a boxplot is explained in detail in [Appendix 2.11.1 Boxplot](#). Here in short: The box contains 50 % of the data. The line inside the box is the median (50 % of the data). The ends of the box indicate the higher (Q3) or the lower (Q1) quantile of the data. The length of the lines with the whiskers is 1.5 times the height of the box. Outliers from this area are marked with circles.

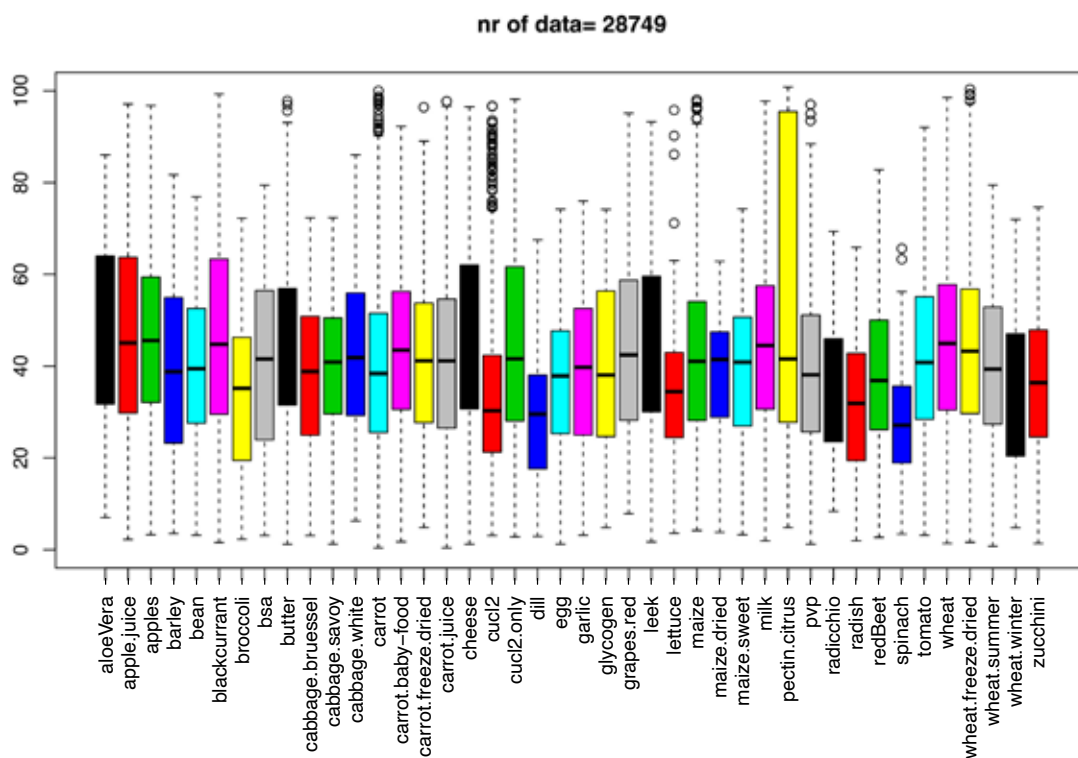


Fig. 2.11.4 Boxplot (see [Appendix 2.11.1 Boxplot](#) for a general boxplot description) of the radius (Y-axis) of the location of the primary crystallization center, in percentage of the total Petri-dish (set at 100 %) versus the sample (X-axis). Data were generated at the University of Kassel Witzenhausen (Germany) (chamber C data from 2002 to 2024). Each sample is represented by 72 pictures at least. In total ~ 30.000 pictures are included in the graph. Colors have no meaning, just to improve the readability.

In Fig. 2.11.4, the lowest values were observed for the radii of dill (median radius ~ 30) and spinach (median radius ~ 25). This might be sample-specific radii. However, it may also be a result of the amount of DCC and additive selected for each sample. The outlier for pectin (yellow) is due to the large number of pictures with dewetting. The dependence of the radius on the DCC and the additive amount needs to be investigated further.

Looking at the boxplots in Fig. 2.11.4, for most samples the median line is in the center of the box. This means that the statistical distribution of the radius is a symmetric one, like e.g the Gaussian distribution.

Distribution of the radius

As discussed above, the simplest approach to understanding the distribution of the radius is the case of a constant DCC supersaturated area throughout the Petri-dish. Each location in this area has the same probability of nucleation. This means that the cumulative probability (sum) of the nucleation is proportional to the area in question. When this area in question is calculated in terms of the radius from the geometric center, then the dependency of the cumulative probability of the nucleation on the radius would increase proportionally to the area = $2 * \pi * \text{radius} * \text{radius}$.

This simple approach already explains why there is a limited number of pictures that start to crystallize from the exact geometric center, because for radius = 0 the cumulative nucleation probability is zero. The cumulative nucleation probability should increase quadratically with the radius. This only holds true assuming the entire plate is uniformly saturated. From the measurements in the dish [26] (see also chapter [2.4 Concentration gradient](#)) it can be assumed that a constant concentration of DCC exists only in the area from the geometric center to a radius between 40 % and 80 % of the Petri-dish. Beyond this radius the concentration is lower.

If we expect the cumulative nucleation probability (see also in [Appendix 2.11.8 Distribution](#)) to be proportional to radius * radius, then a plot of the square root of the cumulative nucleation probability should show a linear relationship with the radius. As long as a linear relation is fulfilled the assumption of the constant concentration is fulfilled. The data shown in Fig. 2.11.4 are plotted in this way in Fig. 2.11.5 below.

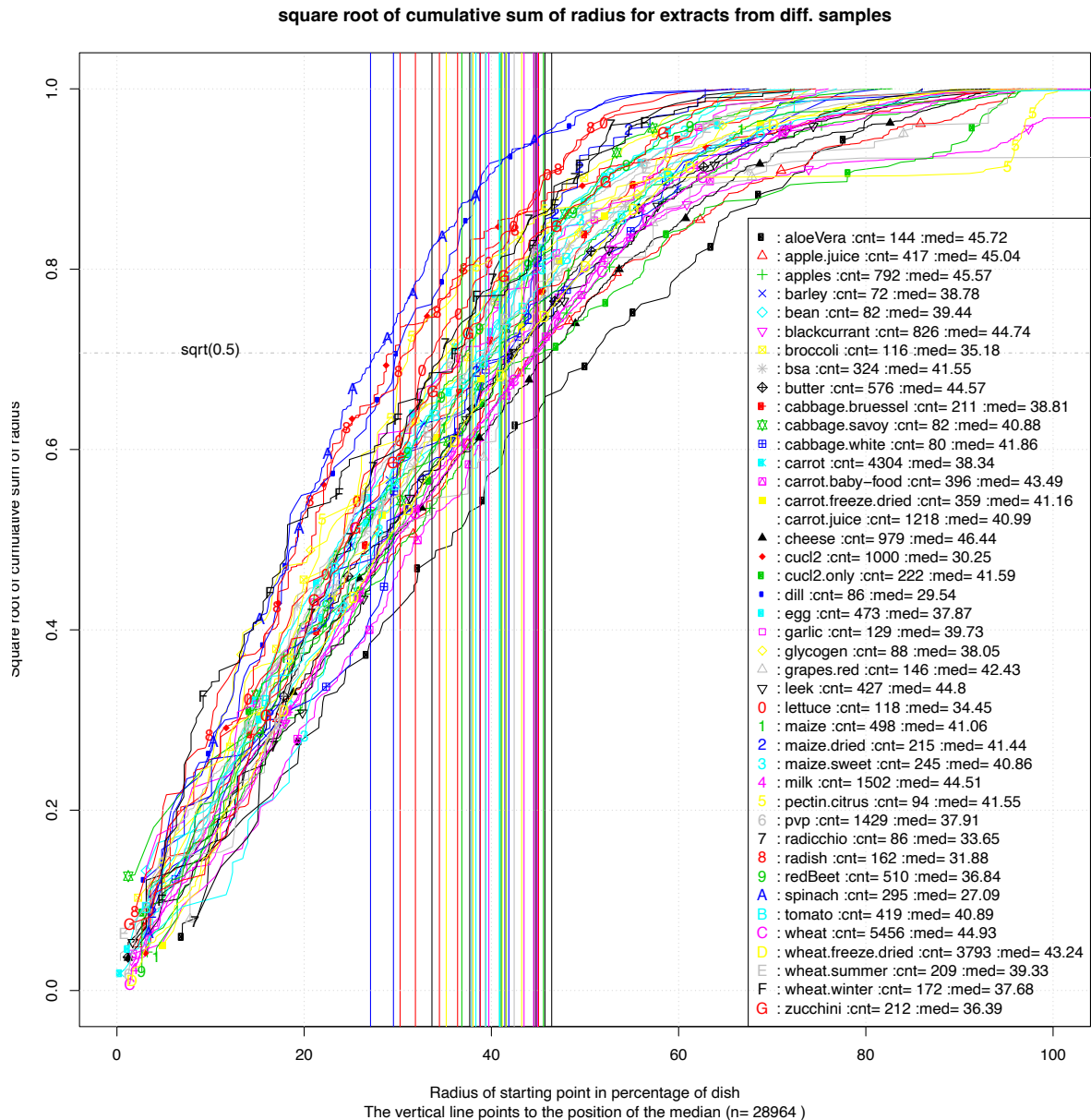


Fig. 2.11.5. Square root of cumulative sum of radius (Y-axis) versus (on the X-axis) the radius of the location of the primary crystallization center, in % of the dish radius. The colors show different samples as noted in the legend. The name is followed by the number of used pictures (cnt) and the median radius (med) of the Petri-dish where crystallization initiates. For each sample the median radius is plotted (vertical lines). The $\sqrt{0.5}$ horizontal line indicates where the $\sqrt{\text{median}(\text{cumulative sum})}$ of crystallization occurs. Data were generated at the University of Kassel Witzenhausen Germany (chamber C), data between 2012 and 2024. Only samples are shown, for which more than 72 DCC pictures exist. In total ~ 29.000 DCC pictures are shown.

In Fig. 2.11.5 the linear relation is best fulfilled for smaller radii below 40 %. At first sight, the curves are comparable for the different samples, nevertheless they have different medians. The reason for the different median values is an open question, which cannot simply be answered by the shielding of the rim of the Petri-dish, because then the median value should be the same for all samples.

Examples from samples with minimal and maximal median radii of the location of the primary crystallization center are shown in Fig. 2.11.6 below. Minimum median radius is for pictures from spinach and maximum medium radius is for pictures from apple. List of regression data is in [Appendix 2.11.7 Regression data](#).

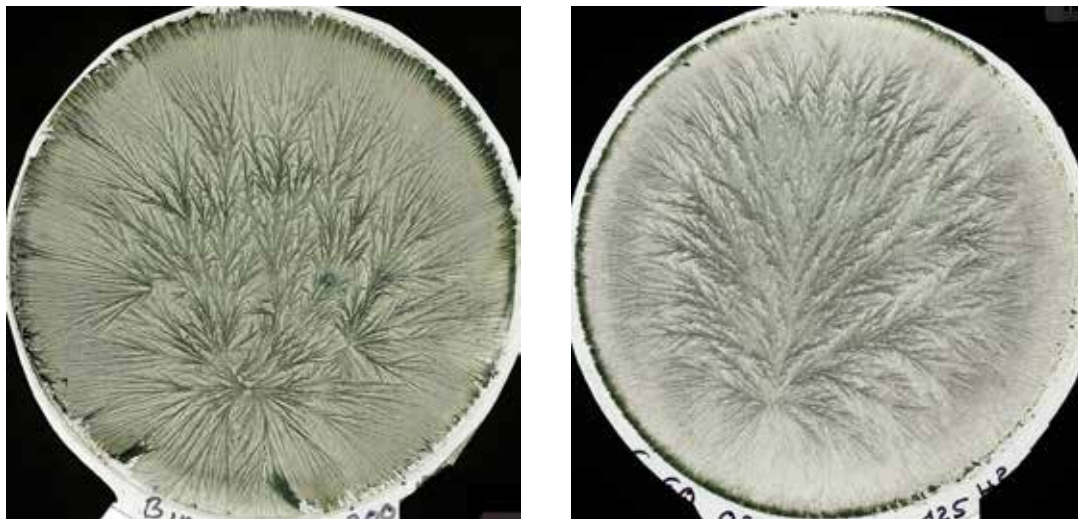


Fig. 2.11.6 Left: scanned picture of spinach (DCC = 150 mg per plate, additive = 200 mg per plate, radius median = 27.09 %). Right: scanned picture of apple (DCC = 125 mg per plate, additive = 180 mg per plate, radius median = 45.57 %).

In Fig. 2.11.6 the area covered with needle branches (view from the center) is smaller for spinach (left) than for apple (right). See for more info the chapter [1.13 Picture zones](#).

Of course, a visual evaluation of the correlation between the cumulative nucleation probability and the radius of the crystallization center is not enough to check for a statistical distribution. The exponent of the cumulative sum (cumsum abbreviated) of the radius has to be determined by a [nonlinear least squares](#) (NLS) evaluation. (for details see [Appendix 2.11.6 NLS](#)). To check also for an Gaussian distribution as an indication for a more random origin of the radius data the mean, median and the standard deviation (sd) is calculated by a [nonlinear least squares](#) (NLS) fit.

The results are shown in Fig. 2.11.7 for the radius data. In Fig. 2.11.7 the cumsum radius data for carrots from the 2004 Fleck-carrot trial are plotted on the Y-axis (data normalized; 100% radius set to 1), versus the radius on the X-axis. The data are shown for all experimental days. The Information per day is shown in [Appendix 2.11.3 Fleck data](#).

The following first describes how the measured data, the square root of the measurement data, and the regression lines through the square root of the data are displayed in the plot. Second, the results of two fits (Gaussian and exponential) of the data are described.

First: The blue circles represent the cumsum of the radius data. The median value of the measurement data is marked with a steel blue vertical line (42 %). The red curve represents the sqrt of the cumsum radius data, which is linear in the case of quadratic increase of the cumsum data. The orange line is the regression over the full range of the sqrt cumsum data, while the green line is for the data limited to those below $0.8 * \text{median} = 33\%$. This value is marked by the magenta vertical line.

Second: The pink curve is calculated based on the assumption of a Gaussian distribution (fit with tanh, see [Appendix 2.11.4 Tanh](#)). The parameters for the Gaussian distribution, mean and sd, are calculated from the radius measurement data. The magenta curve is calculated with the parameters from the NLS exponent evaluation of the data below the median. The exponent is shown in the legend.

The r_{adj} value is a measure of the amount of data explained by the regression (see [Appendix 2.11.5 \$r_{\text{adj}}\$](#) for details), where 1 represents a perfect fit, and 0 no fit. This helps determine which fit best matches the measured data.

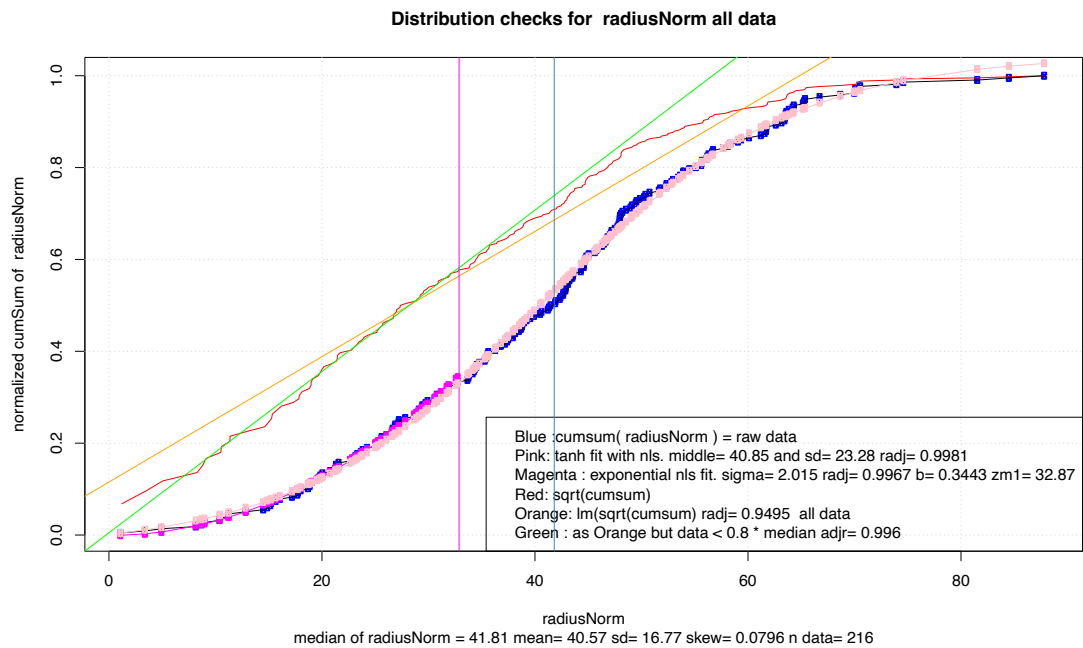


Fig. 2.11.7 Y-axis: normalized cumsum (from 0 to 1) of the radius data (blue, pink, magenta) and sqrt(cumsum) for (green, red, orange) versus the radius data (X-axis). Blue circles are the measurement data for carrot samples. Steelblue vertical line represents the median(radius). Red curve is sqrt(cumsum) data. Orange curve is the regression of the sqrt(cumsum) over all data. Green curve is the regression of the sqrt(cumsum) data below $0.8 * \text{median}$. Pink curve represents the Gaussian distribution NLS fit (tanh). Magenta curve represents an NLS exponential regression fit (data below $0.8 * \text{median}$). Data from Fleck-Carrots 2004, University of Kassel Witzenhausen (Germany) chamber B and C.

For the radius data the NLS exponential evaluation (magenta curve) for the data below the median, gave an exponent of 2.01 which is close to the exponent of 2.0 for quadratic behavior. The $r.\text{adj}$ value was 0.9967, indicating a near perfect fit. The Gaussian fit gave an $r.\text{adj}$ of 0.998 and is a better fit than the quadratic behavior. The red curve as the sqrt(cumsum) was not an ideal line, having points above and below the line. The green line as a fit for the sqrt(data) below $0.8 * \text{median}$ gave a $r.\text{adj}$ of 0.996 which is the same as the [NLS](#) fit for the exponent.

The radius of the crystallization start is an indirect measure of the supersaturated area, because crystallization can only start within the supersaturated area. The radius of the crystallization start location is always smaller than the radius of the supersaturated area. The later area is defined in [2.4 Concentration gradient](#), Fig. 2.11.15. Holleman [27] had a parabolic concentration gradient in his system, while Busscher's [26] data, as shown in [2.4 Concentration gradient](#) show a constant concentration in the Petri-dish for a radius from 0 % to 40 % to 80 % around the geometric center.

Resume

The cumulative distribution of the location of the crystallization starting process is quadratic with the radius for an area below $0.8 * \text{median} = 33 \%$. This fits with the measurements of a homogeneous supersaturated area in the Petri-dish.

Crystallization starting time

From the carrot data of the 2004 Fleck-carrot trial the same calculations were performed for the [crystallization starting time](#) as for the radius, to check for the statistical distribution type.

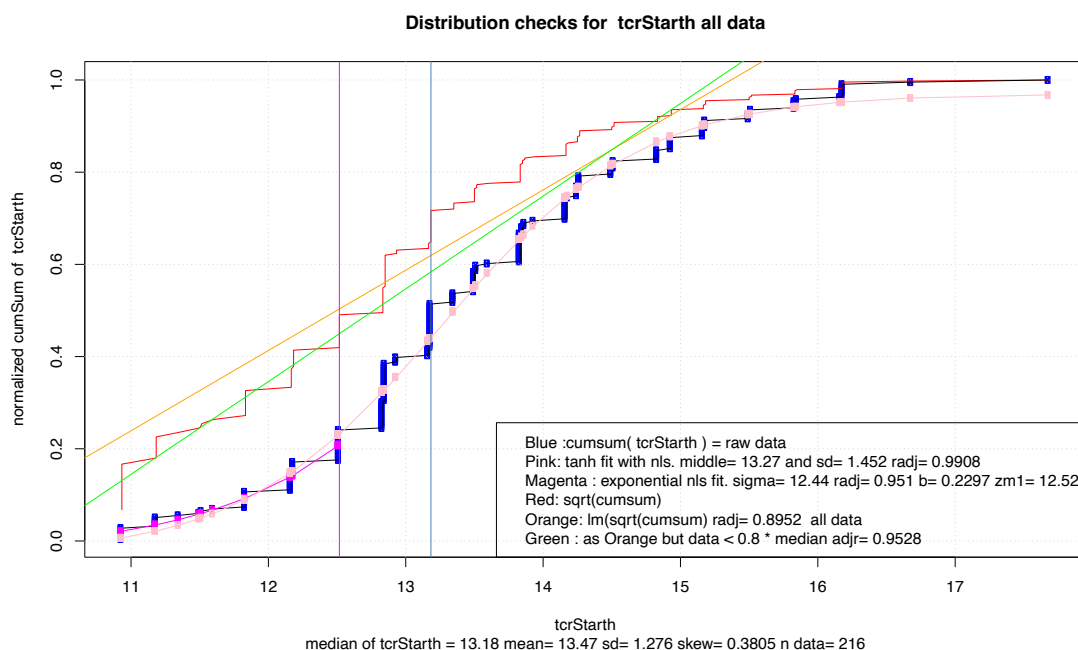


Fig. 2.11.8 Y-axis: normalized cumsum (from 0 to 1) of the TCT Start data (blue, pink, magenta) and sqrt(cumsum) for (green, red, orange) versus the tcrStart (X-axis in hours). Blue circles are measurement data. Steelblue vertical line is the median(tcrStart). Red curve sqrt(cumsum) data. Orange curve is the regression of the sqrt(cumsum) over all data. Green curve is the regression of the sqrt(cumsum) data below $0.8 * \text{median}$. Pink curve represents the Gaussian distribution NLS fit (tanh). Magenta curve represents an NLS exponential regression fit (data below $0.8 * \text{median}$). (data from Fleck-Carrots 2004 University of Kassel (Germany) Witzenhausen Chamber B and C).

As shown in Fig. 2.11.8 for the crystallization starting time, the NLS evaluation (magenta curve) gives an exponent of 12.4 (being far away from the 2.0 for the radius data) and the calculated data fits quite well to the measurement data (blue circles). This is for the data below the median, with an $r.\text{adj}$ of 0.95. The Gaussian fit (pink curve) has an $r.\text{adj}$ of 0.990 which is close to the one from in Fig. 2.11.7. It is calculated for all data, which can be seen as it also follows the bow of the cum sum data for tcrStart values higher than the median. (The $r.\text{adj}$ for the regression lines are 0.95 (green) and $r.\text{adj}$ = 0.89 (orange).

Resume

This is just a start, and of course much more testing needs to be done on other data, but looking at the radius and start time results in Fig. 2.11.7 and 2.11.8, it became apparent that in both cases the best fit is a Gaussian distribution. Which supports the random behavior of the nucleation probability. The radius for data below the median is modeled by a distribution with an exponent approaching two (2.01). This seems to indicate the presence of a region of constant supersaturation, resulting in a quadratic behavior of the radius for the cumulative probability.

Dependency of the crystallization starting time on the DCC and additive amount

The dependency of the crystallization starting time (further called tcrStart) on the DCC and additive amount is surprising and gave some insights into the evaporation and nucleation process. For tcrStart to be dependent on the amount of DCC, one would expect tcrStart to decrease as the amount of DCC increases because in the 6 mL volume pipetted into the dish, the amount of water decreases as the amount of DCC increases. The less water has to evaporate in order to reach the solubility border, the earlier the crystallization can start. This hypothesis was already falsified in Busscher [26], Fig. 7 in 2010 for DCC amounts from 60 to 600 mg. To verify this, experiments were conducted with DCC amounts ranging from 60 mg to close to the solubility border at 30 °C (5600 mg DCC per plate), with and without the additives carrot juice, freeze dried wheat and Polyvinylpyrrolidone (PVP).

The results are presented in Fig. 2.11.9 left. In Fig. 2.11.9 left, the crystallization starting time is about 11 hours for 60 mg DCC for the DCC-only experiment (red line) and decreases slightly with additives. As the amount of DCC increases, the curve reaches a maximum at ~ 2000 mg DCC per plate and then decreases to 5 to 7 hours at 4800 mg DCC per plate.

The dependency on the additive amount is quite different as shown in Fig. 2.11.9, right. The data are from an experiment with Bovine Serum albumin (BSA). The expectation is that the additive will eventually inhibit

crystallization due to the increase in viscosity with increasing additive amounts. In general this is fulfilled in Fig. 2.11.9 right for BSA.

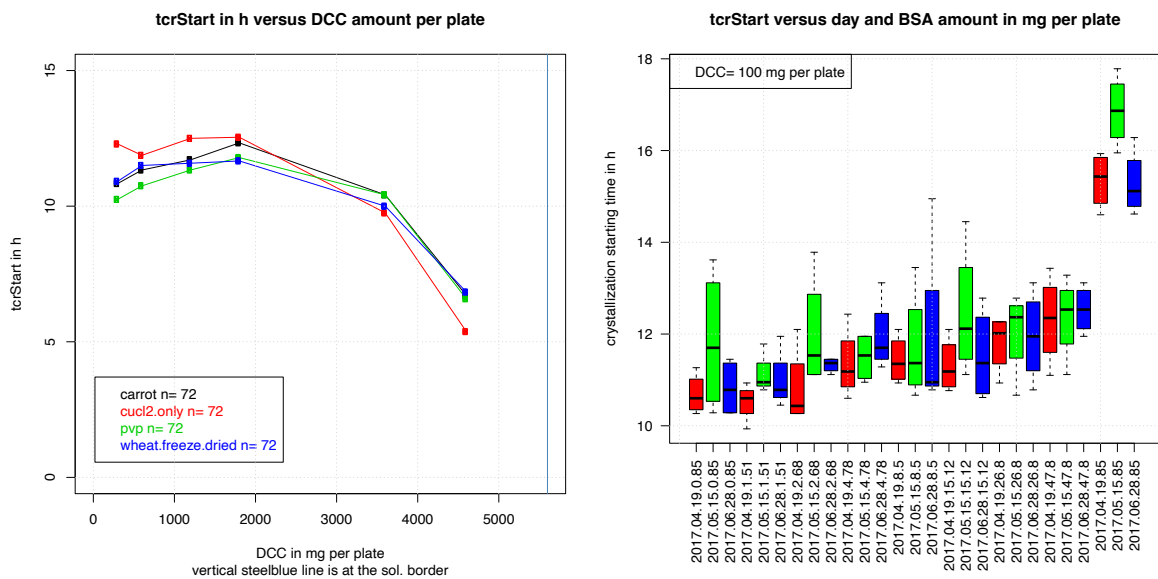


Fig. 2.11.9 Dependency of the crystallization starting time ($t_{crStart}$) (Y-axis) on the amount of DCC (left) and additive (BSA in mg per plate, right). In 2.11.9 left, different additives are shown (red : DCC only, black : carrot, blue : freeze dried wheat and green : PVP). The additive amounts are for carrot 11.5 mg per plate, freeze dried wheat 90 mg per plate and PVP 0.2 mg per plate. In Fig. 2.11.9 right the data of three experimental days are shown. Colors: red : day1, green: day2, blue : day3. The DCC amount for the BSA experiment is 100 mg per plate. Data from 2017 Roepaen (NL), chamber P.

Looking at Fig. 2.11.9 left, one might get the impression that the dependence of the $t_{crStart}$ value is independent of the sample. However, there seems to be a shift for some samples at DCC = 3000 mg per plate. The DCC only-sample (red curve) has higher $t_{crStart}$ values at lower DCC concentrations and lower $t_{crStart}$ values at higher DCC concentrations. For the PVP samples (green curve) it was the other way around.

In Fig. 2.11.9 right, the dependence of the $t_{crStart}$ value on the increasing amount of additive is evident up to 10 mg BSA per plate, then flattens out up to ~ 20 mg BSA per plate and then increases again.

Dependency on the DCC amount

As stated above, the simple assumption that the $t_{crStart}$ should decrease with increasing DCC amount, is not true. However, simulations (see chapter [2.13 Evaporation model](#)) showed that the evaporation rate was not constant, but decreased with increasing DCC concentration. This is due to the decrease of the partial pressure of the water vapor above the solution at higher DCC concentrations (from 100 % in the absence of DCC to 67 % at the DCC solubility border at 25 °C [28]). Also, the transport rate of the humidity from the Petri-dish, which depends on the difference of the partial pressure above the solution and the relative humidity in the chamber (problem of Stefan [29]) slowed down because of an increase of the [chamber](#) humidity (see chapter [1.2 Water transport](#) for details). Here the volume of the [chamber](#) finally limited the evaporation. This can explain the behavior seen in Fig. 2.11.9 left. See also chapter [2.13 Evaporation model](#).

Below 3000 mg DCC, the highest $t_{crStart}$ values are found for the case of DCC without additives (red curve in Fig. 2.11.9), suggesting that the additives support heterogeneous nucleation. For DCC values above 3000 mg per plate, the $t_{crStart}$ of DCC without additives (red curve in Fig. 2.11.9) precedes that of DCC with additives. This can be understood by the hindrance of nucleation by the additives, that increase viscosity at higher DCC amounts, illustrated on the right side of [Fig. 2.11.3](#) (dependency of nucleation rate on supersaturation).

Resume

The dependency of the $t_{crStart}$ on the DCC amount seems to be related to the partial pressure of the humidity above the Petri-dish (which depends on the DCC concentration of the solution), and the chamber volume limitations. The sample is not of great importance for the $t_{crStart}$ dependency on the DCC amount. Since most pictures are usually made with DCC concentrations between 100 and 200 mg per plate, which is far below 3000 mg per plate, $t_{crStart}$ will increase with increasing DCC amount.

Dependency on the additive amount (BSA and Apple Juice)

In both graphs of Fig. 2.11.10 (left BSA and right apple juice) the $t_{crStart}$ value increased with increasing amount of additive. This is generally observed not only for BSA ([14], Fig. 11) and for apple juice [30], Fig. 2.11.10 but also for other samples (publication in preparation).

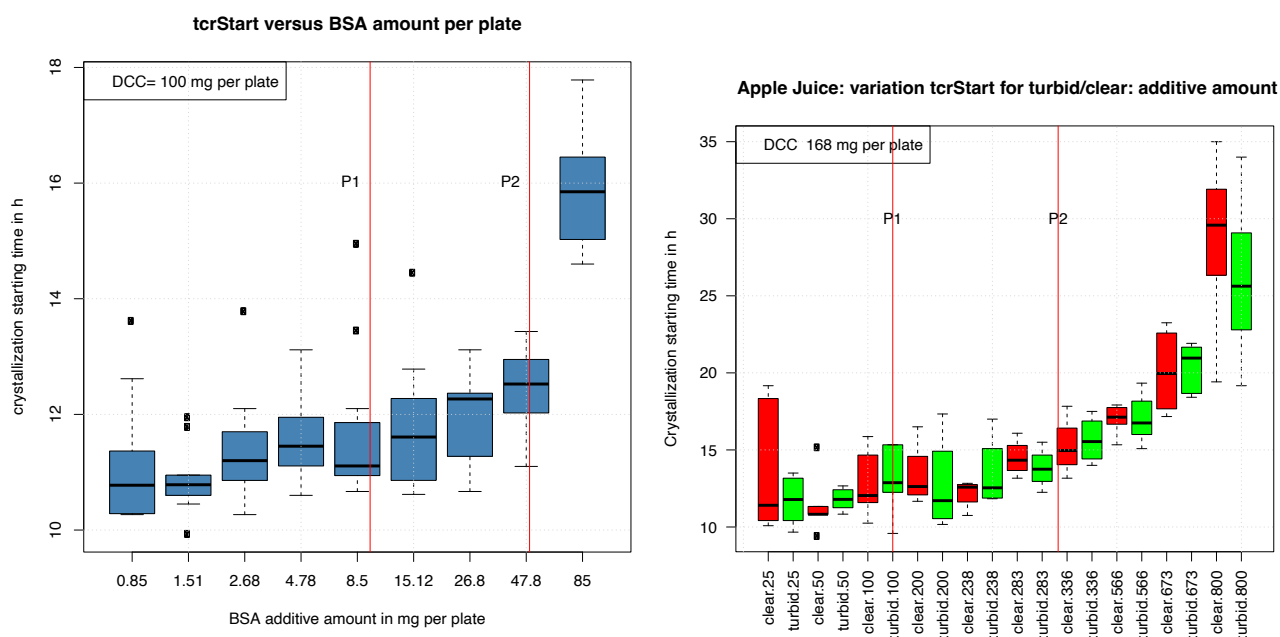


Fig. 2.11.10 Dependency of $t_{crStart}$ (Y-axis) on the additive amount (X-axis, in mg per plate). Left: additive is BSA (mean of the three days shown in Fig. 2.11.9), DCC =100 mg per plate. Right: additive is apple juice (process: red = Clear apple juice, green = Turbid apple juice), X-axis is combination of process and additive-amount, DCC = 168 mg per plate. For the variation of the data with the chamber or the day repetition see Appendix 2.11.9 Variation.

For BSA in Fig. 2.11.10 left, the graph can be divided in three parts. First an increase in $t_{crStart}$ for the additive amount from 0 to 10 mg per plate (P1), followed by a second increase from 10 to 50 mg per plate (P2), followed by a sharp increase above 50 mg per plate (P2), which appears more than linear.

The graph of the apple juice data in Fig. 2.11.10 right shows a similar behavior for P2.

The measurements for P1 at low additive amounts have an outlier for clear juice at 25 mg additive per plate. This is due to the dewetting effect of clear juice at lower additive amounts. As expected the increasing amount of additive hinders the nucleation and results in a later $t_{crStart}$ value.

In Fig. 2.11.9 left, for low DCC amounts (below 2000 mg per plate) the starting times for solutions with additives are earlier than for the DCC only case (red curve in Fig. 2.11.9 left). When combining the results from the DCC dependency with the additive dependency, one would expect the $t_{crStart}$ to decrease upon the addition of a limited amount of additive. This was neither visible in Fig. 2.11.9 right, nor in 2.11.10 left. The lowest BSA amounts in Fig. 2.11.9.left left were 0.85 mg per plate or 100 calculated monolayers. The results for lower BSA values (0.1, 1, 3, 10, 30 calc. monolayers) are shown in Fig. 2.11.23 left (see below) and showed a tendency for a decrease of the $t_{crStart}$ values when the BSA additive amount were between 0.1 and 100 calculated monolayer, while the results shown in Fig. 2.11.11 right show the decrease of the $t_{crStart}$ for the BSA values (0, 0.1, 1) calculated monolayer.

The apple juice data (Fig. 2.11.10 right) include a comparison of clear and turbid apple juice. One difference between these samples was the amount of pectin particles (Apple Juice report 2015 [30], additional report about the $t_{crStart}$ times [31] and Kahl 2016 [32]). The pectin particles are in the size of 1 μm [33] and might have formed additional centers for heterogeneous crystallization. However in Fig. 2.11.9 right no difference in $t_{crStart}$ could be found between clear and turbid apple juice. Does this mean that the heterogeneous nucleation centers are smaller than 1 μm or are there not enough additional centers added with the turbid apple juice, or does the DCC already have enough heterogeneous centers as proposed by Beckmann [10], or is the nucleation or the visible crystallization start different from the heterogeneous (nucleation) process? The question of heterogeneous crystallization is connected with the question whether the DCC system is vulnerable for dust particles. So far this seems not to be the problem.

Resume

The dependency of the $t_{crStart}$ on the additive amount can be understood by the inhibition of the nucleation process at “higher” additive amounts (Fig. 2.11.10, region P2). For lower additive amounts (from 0 to region P1, see Fig. 2.11.10) a decrease in $t_{crStart}$ with increasing additive amount would be expected assuming a heterogeneous process. Also a decrease would be expected for additives which include particles of 1 μm . The decrease of $t_{crStart}$ by the addition of a limited amount of additive can be seen in Fig. 2.11.11 right, but this experiment needs to be repeated for a clearer result. The dust question could maybe be researched in connection with the influence of the summer versus winter, because the amount of dust particles increases in winter time, but the cleaning of the air by the dehumidifier may compensate the dust influence.

Heterogeneous crystallization of DCC with BSA?

From Busscher 2019 ([14], Fig. 11) the following graphs are available: In Fig. 2.11.11 right, the $t_{crStart}$ is plotted versus the BSA additive amount in calculated monolayers. The background colors mark the different crystallization types. The expected decrease in $t_{crStart}$ by the addition of a limited amount of BSA is clearly visible. At 10 monolayers (yellow background) the $t_{crStart}$ was lowest. The variation in the data (data based on 4-6 replicates per DCC/additive combination) could be limited by repeating the experiment over three days. When comparing these results with those shown in Fig. 2.11.10 left (100 monolayer BSA corresponds to 0.85 mg per plate, being the minimum value in Fig. 2.11.10 Left), the decrease in $t_{crStart}$ for BSA values between >0 to 10 monolayers (0,085 mg per plate), is clearly visible. For BSA it is well known, that it covers glass already with 1 monolayer. This is inhibiting the dewetting phenomenon (Busscher 2019 [38]). For other additives, this ability to prevent dewetting occurs at higher amounts, where the nucleation is already hindered by the increasing additive concentration.

The crystal growth, which is a criterion to distinguish crystal types in the so called morphology map from Kurz [34], is different for different crystallization types. For BSA the main differences were between the needle types (red and yellow background), the split-growth type (green background) and the dendritic growth type (blue background) used in Fig. 2.11.11, defined in [14] and described below in Fig. 2.11.13.

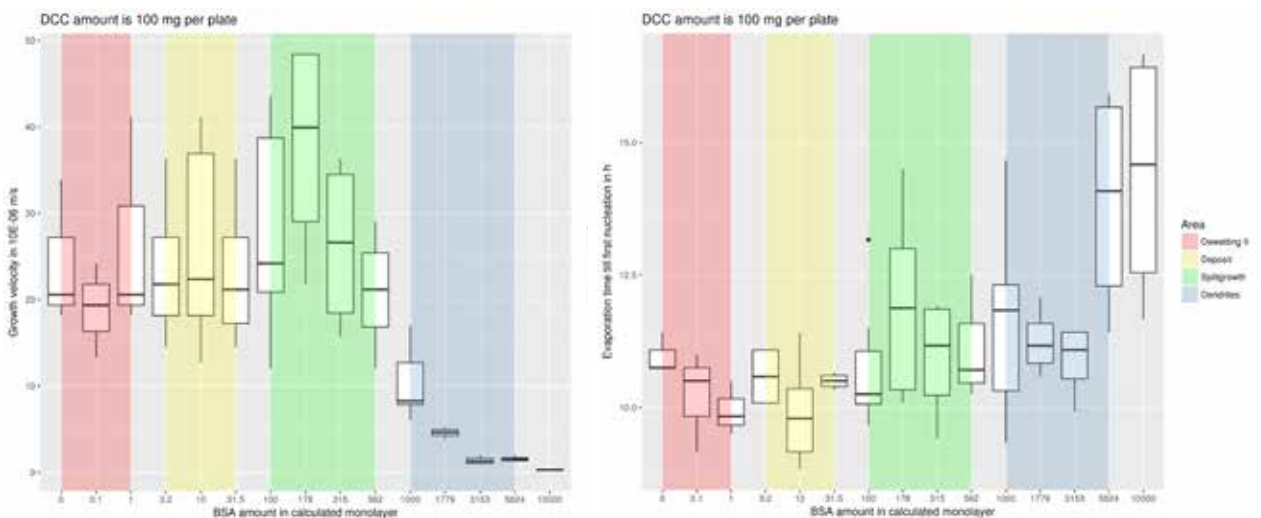


Fig. 2.11.11 (from [14], Fig. 11) Left: Linear growth rate of the crystals in $10\text{E}-06$ m/s versus the BSA amount in calculated monolayers. Right: evaporation time in hours versus the BSA amount in calculated monolayers. Crystallization pattern areas are highlighted with colors: red: dewetting II area, yellow: deposit area, green: split-growth area and blue: dendritic area.

Considering that the number of centers (see chapter 1.12 Multiple centers) has a minimum in the split-growth area (most BSA pictures had only one center in the split-growth area, see [14]), the supersaturation for BSA in the split-growth area would be expected to be in Fig. 2.11.3 on the right side of the maximum. (see also chapter 4.2 about the number of centers in [14]). The minimum of the $t_{crStart}$ (maximum nucleation probability?) at 10 monolayer BSA would point to the maximum of the nucleation probability in Fig. 2.11.3.

Resume

Considering the decrease in $t_{crStart}$ upon addition of a limited amount of additive in Fig. 2.11.11 (right), as well as the number of centers, and assuming that we are on the viscosity dominated side of the nucleation

probability plot 2.11.3, then the BSA results support a heterogeneous nucleation process for DCC. Maybe this is only visible (and verifiable) for BSA as additive due to the glass-plate covering abilities of BSA at low concentrations.

Possible connection between the picture type and nucleation type?

For water, the crystals are known to be hexagonal in all cases, nevertheless the shapes are different (see Fig. 2.11.12 and Librecht [35], [36], [37]).

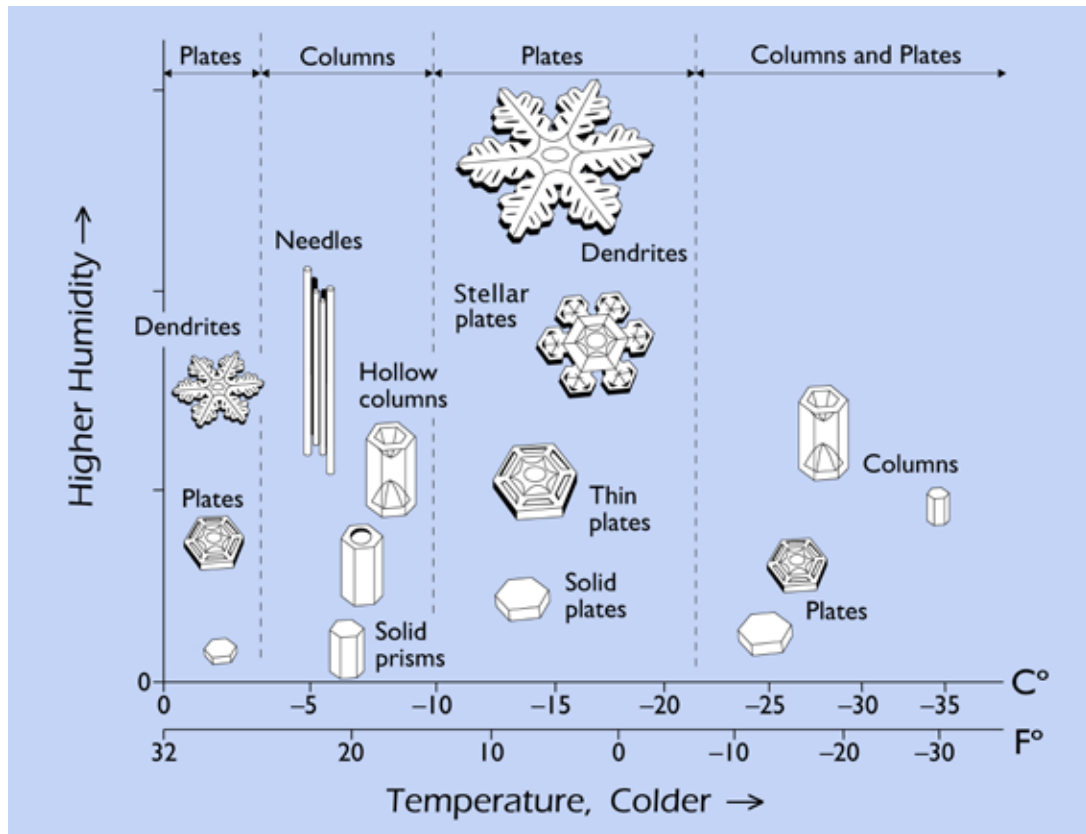


Fig. 2.11.12 Morphology diagram of ice (from Librecht [35]).

For DCC the structures are not following a strict geometrical pattern like observed for ice.

From the BSA experiments we observed, that there were different types of crystals located in different areas in the Concentration Matrix (CMX). The number of branches from the DCC crystal center varies, differing from ice, which always has 6 branches.

For DCC and BSA, a simple morphology map (see Fig. 2.11.13) from [14] also showed different types of crystals, although they do not always have the same n-folded symmetry as water, which has a 6 folded symmetry.

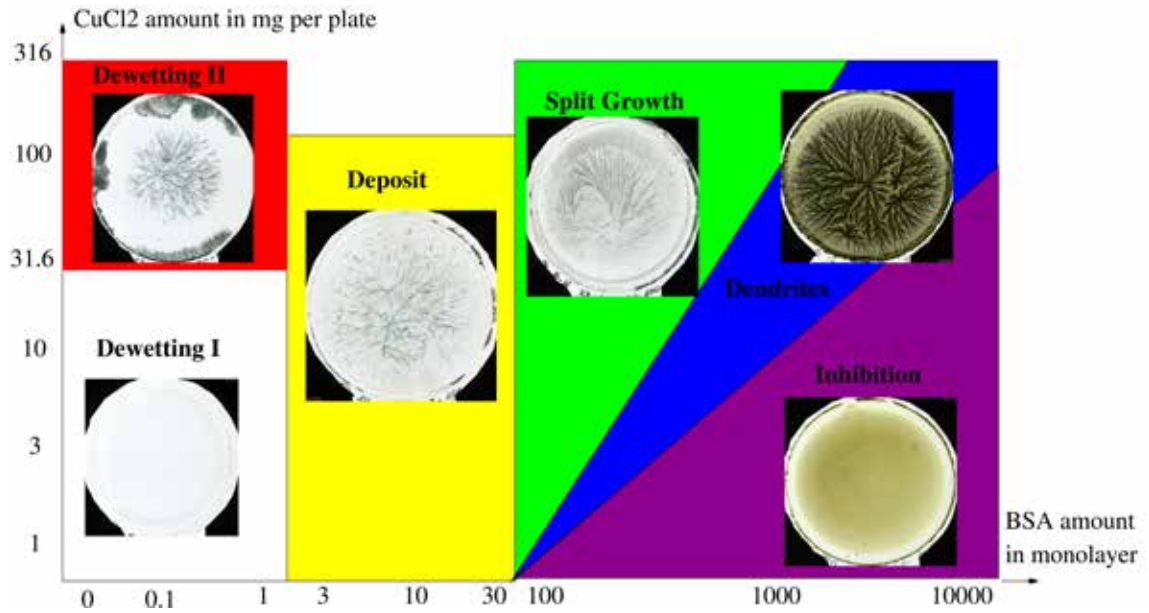


Fig. 2.11.13 Morphology map from Busscher 2019 ([14], Fig. 1). Overview of the CMX with colored areas with comparable patterns and thumbnails of representative patterns. The DCC amount in mg per plate is plotted on the Y-axis. The X-axis represents the BSA amount in calculated monolayer per plate. The red area represents the dewetting II type, the yellow area the deposit type, the green area the split-growth type, the blue area the dendritic type, and the violet area the inhibition-like type. The plates in the white area, called dewetting I area have been discussed earlier [38].

For the split-growth area (*hohlformen*) the number of branches or needles starting in the center are in most cases 2 or 4. In the dewetting II area they start in star-like formations with numbers > 4 , also the dendrites have no specific number of branches arising from the center, which is unlike the always 6 folded form for water.

One could hypothesize that the nucleus determines the growth of the crystals.

From the current understanding of nucleation, the first step is not necessarily a small version of the final crystal as stated by Zhou [1]. Also Reiter [20] stated that the conditions of the solution can have a different influence on the growing crystal than on the nucleation. A study is required to determine if and how there is a relationship between the type of center and the type of crystals.

Additional research

Types of centers

To be able to recognize the different types of centers, they need to be categorized. This could start with the types in the BSA CMX (Busscher 2019 [14]) and then be extended to the types showing up in the CMX of other samples, like freeze dried wheat, carrots, black currant juice,....

The dependency on the basic conditions (additive, DCC, additive amount, tcrStart) should be determined for an evaluation of the following questions: When does which type of center appear and whether it is connected to the type of crystals that appear?

The needles grow beyond the nucleation “area” in different “forms”. Roughly 20 %, 1 out of 5 pictures, when sorted by tcrStart, does not fit in the morphological “flow”. Maybe this has to do with the connection between the nucleus and the needles growing beyond the nucleus, The research should check if the growth velocity is different, which define thy crystal type.

Heterogeneous crystallization

The basic hypothesis is that the crystallization starts on a “foreign particle” (impurity).

The apple juice experiments with size particles $> 1 \mu\text{m}$ (e.g. turbid juice) did not show this effect.

- Make experiments with different concentrations of pectin.
- Maybe there are already clusters of DCC in the solution ([8]) $< 1 \mu\text{m}$
- Crystallization of filtered DCC solutions.
- Crystallization of fresh (1-2 hours) made solutions ([10]) and aged solution.
- Influence on tcrStart, growth rate?
- Crystallization of warmed DCC solution (higher solubility)
- Beckmann reported a lower growth rate, when using “freshly” prepared DCC solutions.

Repeat tcrStart experiments of Fig. 2.11.9 at low additive and DCC amounts for BSA and PVP. PVP showed the lowest crystallization starting time in Fig. 2.11.9 for lower DCC amounts.

Radius model

Calculate, in the Petri-dish, the time dependency of the concentration border of the supersaturated area (where the DCC concentration is equal to the solubility border) as a function of the spreading of the crystal covered area as described in the chapter [1.13 Picture zones](#). Does this dependency fit with the assumption that the crystallization is following this border.

Why is the radius median dependent on the sample? ([Fig. 2.11.5](#)).

Radius exponent fit for data below the median as in Fig. 2.11.7

Take the data from [Fig. 2.11.5](#) and make per sample an NLS regression. How is the variation of the parameters? Are they close enough to see a general feature of the DCC pictures. Do the parameters vary by chamber for the same sample?

Position in the nucleation probability(supersaturation) graph ([Fig. 2.11.3](#)).

- Is for BSA the split-growth located on the right side of the maximum?
- How is this for other samples? Does the split-growth area have the same properties for all additives?

Radius versus DCC and additive

The dependency of the radius on the DCC and additive amount has to be verified.

Radius versus radius of the crystal coverage of the Petri-dish (ring3)

Why are some of the radii so small (samples dill or spinach)? Do the radius and the ring3 correlate? (For the definition of the crystal coverage parameter of the Petri-dish “ring3” see Busscher 2019 [38], supplement, chapter 2, Coverage of the dish)

tcrStart distribution

In [Fig. 2.11.8](#) there is a deviation to the Gaussian curve. It should be checked if the inclusion of the skewness of the tcrStart data as a parameter improves the fit.

tcrStart distribution

The tcrStart mean varies per experiment (day effect) much more than the radius. This makes handling all tcrStart data from a sample more complicated than handling radius data from the same sample. How to include or exclude the day effect? It could be normalized on mean and sd, like so:

- $\text{normed}(\text{data}) = (\text{data} - \text{mean}(\text{data})) / \text{sd}(\text{data})$
- $\text{normed}(\text{data})$ has the mean = 0 and the sd = 1

It could also be checked how the sd and the mean/median of the tcrStart for one chamber (a so called [LabDoc series](#)) correlate. The correlation between this sd and the mean/median could show a connection to the sample as the radius did.

Correlation tcrStart versus radius

The correlation shows the different distributions and their origin. For early crystallization starting times the radius does not correlate with the tcrStart (data not shown). All radii in the supersaturated area are possible. For later tcrStart values, later than the radius quadratic dependency of the nucleation probability, there is a correlation. What is the reason for this? Is this for all samples in the same way?

Correlation of mean(tcrStart) versus sd(tcrStart) and mean(radius) versus sd(radius)

The data for DOK wheat from the years 2005, 2006, 2007 (University of Kassel) showed that the correlation of mean and sd are different for tcrStart and radius. This needs to be checked.

Starting of the crystallization on the surface

The starting of the crystallization on the surface of the solution would give a 2 dimensional nucleation which is different from the 3 dimensional nucleation model, on which [Fig. 2.11.3](#) is based. The literature for this question has to be studied and checked for the differences and described how it will show up in which kind of measurements. (e.g. on the one dish Prüfstand).

Different CuCl₂ n H₂O stages

The remarks from Benrath [17] points to unstable intermediate CuCl₂ crystals with more than 2 molecules of H₂O. The weight and wetting experiment from Sokol [25] p. 49, could be repeated under better controlled conditions. The color of the pictures could be followed during the crystallization and the drying in the chamber.

Appendix 2.11.1 Boxplot

Boxplot description (from <https://www.data-to-viz.com/caveat/boxplot.html>)

The boxplot in R-cran has the following description:

A boxplot gives a nice summary of one or more numeric variables. A boxplot is composed of several elements:

- The line that divides the box into 2 parts represents the [median](#) of the data. If the median is 10, it means that there are the same number of data points below and above 10.
- The ends of the box shows the upper (Q3) and lower (Q1) [quartiles](#). If the third quartile is 15, it means that 75% of the observation are lower than 15.
- The difference between Quartiles 1 and 3 is called the [interquartile range](#) (IQR)
- The extreme line shows $Q3+1.5 \times IQR$ to $Q1-1.5 \times IQR$ (the highest and lowest value excluding outliers).
- Dots (or other markers) beyond the extreme line shows potential outliers.

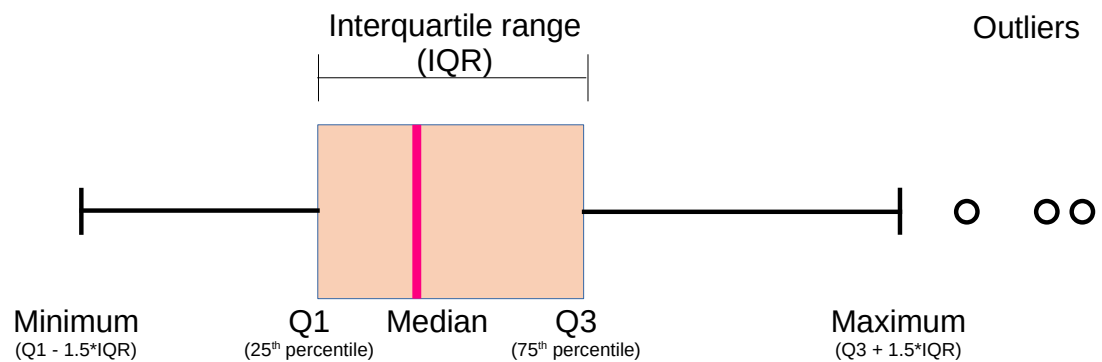


Fig. 2.11.14 Details of Boxplot (quantile, median, whiskers and outliers). The whiskers (the lines extending from the box on both sides) typically extend to 1.5x the Interquartile Range (the box) to set a boundary beyond which would be considered outliers. Hence the name, box, and whisker plot.

Appendix 2.11.2 Supersaturation

The following is a discussion of the path from solution to supersaturation (due to evaporation) and crystallization (due to nucleation) to the final crystal. To include the crystal in the graph, the concentration is calculated as a percentage of the DCC amount. The final crystal will be plotted at 100 %.

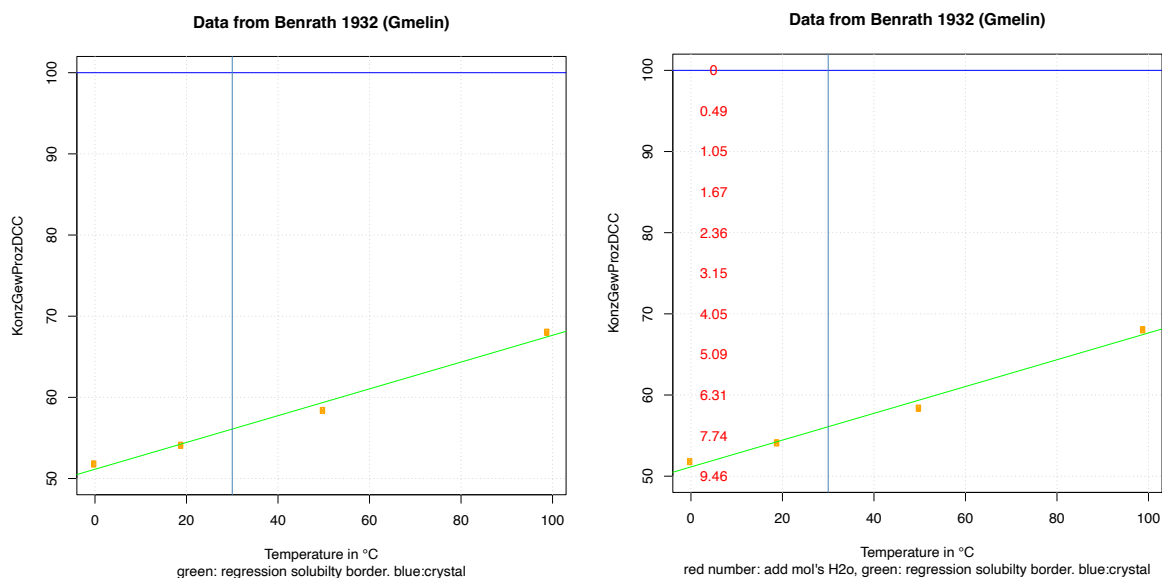


Fig. 2.11.15 Left: DCC concentration in % DCC from solution to crystal (Y-axis) versus the temperature on the X-axis. Right: Y-axis as in Fig. 2.11.15, left, but adding the number of moles of water above the 2H₂O from DCC.

In Fig. 2.11.15 during the evaporation at 30 °C the concentration is following the path along the blue vertical line. The concentration starts below the green line as a watery solution and is ending at the blue horizontal line at the top as a DCC crystal. During the evaporation, moles of water evaporate, which can be followed by the reduction of the red number in Fig. 2.11.15 right.

When the DCC concentration reaches the solubility border (the green line) during evaporation, the crystallization very rarely starts immediately. Evaporation can increase the DCC concentration above the solubility border (which can not be achieved by adding more DCC). Above the solubility border is an area in which the crystallization can start. This is called the Ostwald-Miers area and is shown in Fig. 2.11.16 left as green dotted parallel lines to the solubility border.

In between these lines the crystallization starts. The resulting crystal contains not only 2 H₂O like the DCC crystal, but many more moles of water. Shibata 1998 found 0.5 mole more water for the green CuCl₂ · n H₂O with and without blood as additive [39]. He identified that the green CuCl₂ · n H₂O had n = 2.5 H₂O molecules, while the blue colored DCC crystal had the usual n = 2 H₂O incorporated. This is reflected by the dotted blue line in Fig. 2.11.16 right at 1 additional mol at the (red numbered) Y-axis. Maybe there is also a n = 4 H₂O possible, which is shown at the blue dotted line at 2 mol. Benrath stated in 1933 [17] that unstable CuCl₂ could exist with 2, 4 or 6 mol H₂O (according to the ones existing for cobalt, nickel and manganese chloride). The time required to reach stable DCC is set to days and weeks by Benrath [17]. A simple wetting and weighing experiment, where the CuCl₂ crystals turn from blue to green during atmospheric wetting, was done by Sokol [25] p. 49. The result was that the additional weight for the color change from blue to green was between 1.7 and 2 mol H₂O. The main information of this plot is that there is a gap between the highest dotted green line of the Ostwald-Miers area and the lowest dotted blue line at the crystal. This is the number of moles of water that must leave the volume in which the crystal separates from the solution.

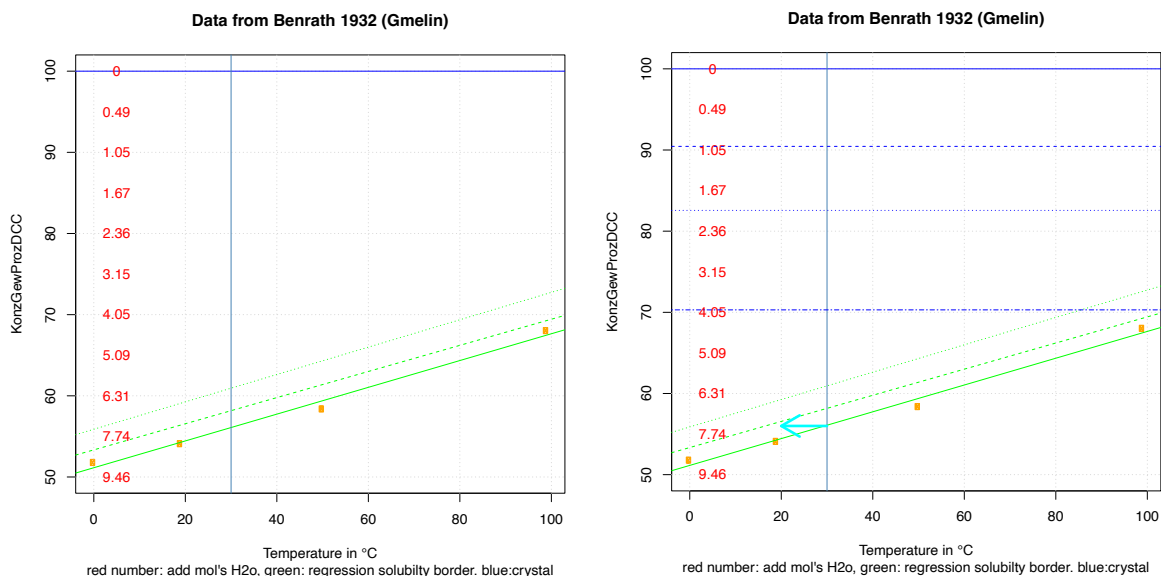


Fig. 2.11.16 Left: Y-axis: black numbers: concentration of DCC in % DCC from solution to crystal and (red numbered) the number of moles of water above the 2H₂O from DCC versus the temperature in °C (X-axis). Green dotted lines indicated the supersaturated Miersch area. Blue dotted lines are for the cases CuCl₂ 2+n H₂O, where n can be 0 (blue crystals) or 1 (green crystals).

If we consider, following Benrath [17], that besides the green colored version of DCC with an additional 2 H₂O, there may also exist an unstable (short lived) version with 4 additional H₂O (double dashed blue line in Fig. 2.11.16 left and right), then the gap between the supersaturated solution and the stable (blue) DCC is smaller than at first sight.

Maybe this can connect to the observation of the crystallization start. When we follow the crystallization we can see that directly after the crystallization starts, the crystals are “unsharp” and it takes some time until the final crystals appear.

Appendix 2.11.3 Fleck data

Evaluation of all Fleck data

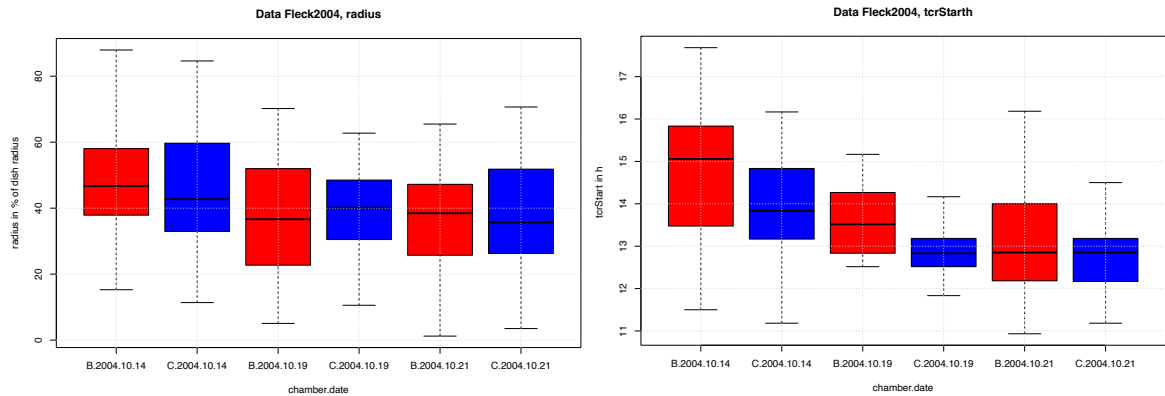


Fig. 2.11.17 Left: Radius data (Y-axis) in % from the Fleck 2004 data versus the chamber and day (X-axis). Right: tcrStart data (Y-axis) in h of the Fleck2004 data versus the chamber and day (X-axis).

The day variation in Fig. 2.11.17 is higher in terms of significance for the tcrStart data (right) than for the radius data (left).

radiusNorm

Coefficients:

	Estimate	Std. Error	t value	Pr(> t)
(Intercept)	46.5472	2.2213	20.955	< 2e-16 ***
chamberC	0.1215	2.2213	0.055	0.956426
day_date2004.10.19	-8.6492	2.7205	-3.179	0.001697 **
day_date2004.10.21	-9.4726	2.7205	-3.482	0.000604 ***

tcrStart:

Coefficients:

	Estimate	Std. Error	t value	Pr(> t)
(Intercept)	14.5986	0.1471	99.268	< 2e-16 ***
chamberC	-0.5315	0.1471	-3.614	0.000377 ***
day_date2004.10.19	-1.0891	0.1801	-6.047	6.58e-09 ***
day_date2004.10.21	-1.5053	0.1801	-8.358	8.41e-15 ***

Day variation radiusNorm

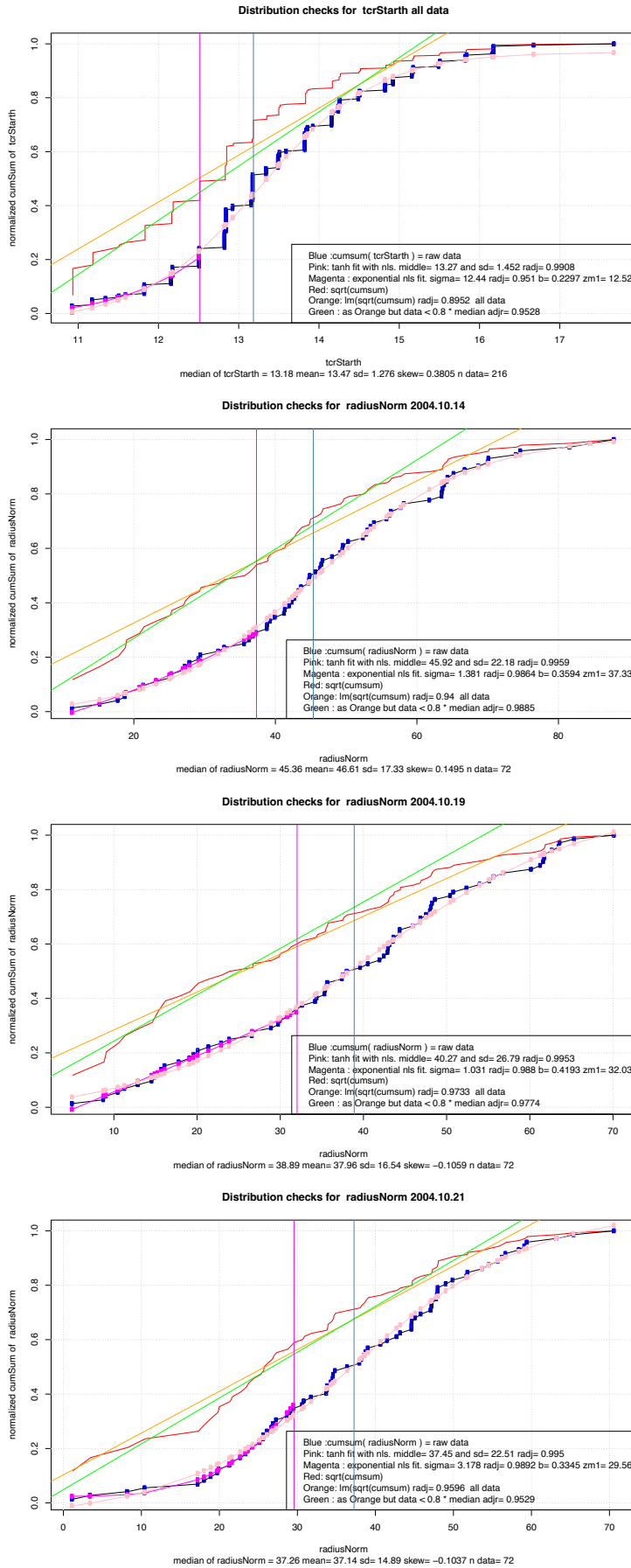


Fig. 2.11.18 Cumsum plots for radiusNorm for (from top to bottom): all data, day 2004.10.14, day 2004.10.19, day 2004.10.21. Description see Fig.2.11.8.

Day Variation tcrStart

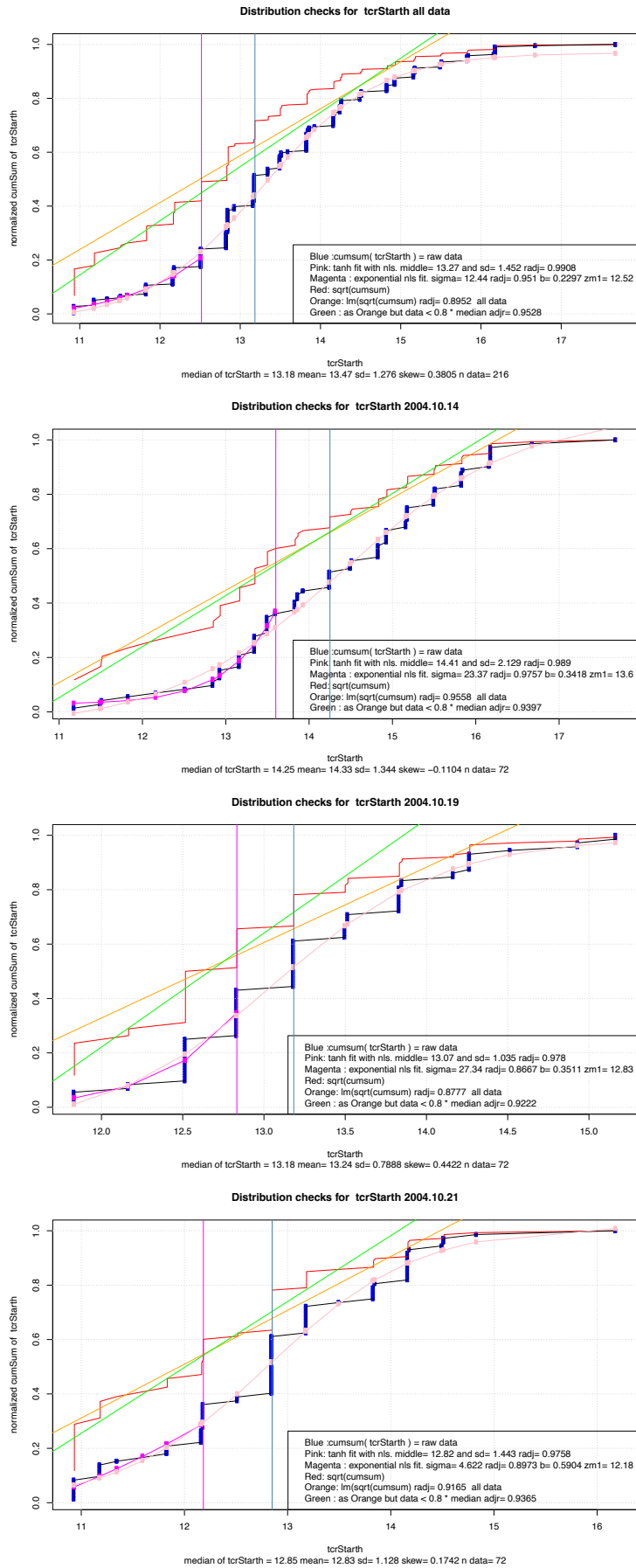


Fig. 2.11.19 Cumsum plots for tcrStart for (from top to bottom): all data, day 2004.10.14, day 2004.10.19, day 2004.10.21. Description see Fig. 2.11.8.

Appendix 2.11.4 Tanh

The fit with the cumsum of the Gaussian distribution (1-erfc) is very close to the fit with a tanh (tangens hyperbolicus) [40]. The differences between these two functions would become only visible for a higher number of data which is not the case in our evaluations, shown in Fig. 2.11.7 and Fig. 2.11.8.

Appendix 2.11.5 r.adj

The statistical measure r.adj is a number between 0 and 1. It is calculated by comparing the regressions fit result with the measured data. The result of this is showing how much of the variation of the measurement data is explained by the regression fit. When r.adj is 1 then all variation is explained by the fit, if r.adj is zero, nothing is explained. Usually r.adj has a value in between 0 and 1. See also at wikipedia [R²](#)

Appendix 2.11.6 NLS

The log/log plot is a way to determine the exponent of relationship.

If the relation is $Y^2 = X^3$

then $Y = X^{3/2}$.

Then $\log(Y) = \log(X^{3/2})$

which gives $= 3/2 * \log(X)$

The log transformation converts the exponent of a relation to a slope in the log/log plot.

For the evaluation of a slope, simple linear regression tools can be used to evaluate the relation.

For the NLS evaluation the formula with parameter and some meaningful starting values are given. The NLS algorithm will optimize the parameters according to the data. The NLS routine from r-cran [41] is used.

Appendix 2.11.7 Regression data

Regression data for Fig. 2.11.5

"sample"	"npictures"	"mean"	"median"	"slope"	"intercept"	"r.adj.squared"
"spinach"	295	"27.26"	"27.09"	0.0253855293199939	0.0217735895814673	0.996577358043483
"dill"	86	"28.77"	"29.54"	0.0217988653210944	0.0606980258125289	0.976563166314458
"cucl2"	1000	"33.91"	"30.25"	0.0240104323713125	0.0119336908450567	0.989795247756375
"radish"	162	"31.38"	"31.88"	0.020654673415409	0.087598794130968	0.986862912433975
"radicchio"	86	"34.8"	"33.65"	0.0251214484928695	-0.132679469303946	0.979706294727482
"lettuce"	118	"34.88"	"34.45"	0.0190100695618793	0.0520903878302251	0.993407051587297
"broccoli"	116	"34.21"	"35.18"	0.0176503874463	0.0709217160648756	0.983354063710353
"zucchini"	212	"36.24"	"36.39"	0.0200968645005691	-0.00876062472537167	0.989395050918249
"redBeet"	510	"37.98"	"36.84"	0.019070219736453	0.000343347637825295	0.997958661600211
"wheat.winter"	172	"35.37"	"37.68"	0.0161943754772306	0.152423349930007	0.956135342986995
"egg"	473	"37.06"	"37.87"	0.0182158804536796	0.0275884873943871	0.997576544399258
"glycogen"	88	"39.46"	"38.05"	0.017059380793956	0.11180393258502	0.969393168316029
"pvp"	1378	"39.17"	"38.11"	0.0187863129146294	0.0250952824278899	0.996400825008294
"carrot"	4261	"39.25"	"38.36"	0.0190982282814947	0.0306403070129852	0.99569593512169
"barley"	72	"39.54"	"38.78"	0.0178026659586534	0.033471165763203	0.972651759701542
"cabbage.brussels"	211	"38.3"	"38.81"	0.0173647247860908	0.0340152407511354	0.995576485447264
"wheat.summer"	209	"39.84"	"39.33"	0.0183216002743568	0.00477795357214486	0.985497086360312
"bean"	82	"40.27"	"39.44"	0.0169419188419857	0.0275130022839109	0.984985595210791
"garlic"	129	"38.74"	"39.73"	0.0178833290134939	0.0603971399235018	0.98514485240182
"tomato"	376	"42.31"	"40.8"	0.0173151610758046	0.0386855096847135	0.994051360899249
"maize.sweet"	245	"38.83"	"40.86"	0.0228885840336644	-0.135369386317841	0.97057552388157
"cabbage.savoy"	82	"38.93"	"40.88"	0.0141782771859346	0.104405552408242	0.987422725949901
"maize"	498	"42.52"	"41.06"	0.016317826401358	0.0682857872356442	0.977023322215606
"carrot.juice"	1140	"41.3"	"41.13"	0.0164095145038587	0.0626008497269735	0.992022209800402

"carrot.freeze.dried"	359	"41.59"	"41.16"	0.0171829211525321	0.0279838297578076	0.983151921002693
"maize.dried"	215	"38.01"	"41.44"	0.0155955994479282	0.0654478452566472	0.991030854613441
"bsa"	324	"49.76"	"41.55"	0.0163905262821947	0.0628148469547397	0.973060199834152
"pectin.citrus"	94	"52.17"	"41.55"	0.0204733346950162	0.0335807822614418	0.976774112504378
"cucl2.only"	222	"47.11"	"41.59"	0.0149774256785641	0.0689096010428837	0.995581896376135
"cabbage.white"	80	"42.61"	"41.86"	0.0170891080352312	0.00391583300266632	0.945253999235062
"grapes.red"	146	"45.49"	"42.43"	0.0141885372718827	0.0653414866468207	0.966311497286303
"wheat.freeze.dried"	3793	"43.69"	"43.24"	0.016714686844686	0.0076512319571961	0.99706182449174
"carrot.baby-food"	396	"44.71"	"43.49"	0.01683171759852	-0.0481006929830276	0.996652818033775
"milk"	1502	"44.85"	"44.51"	0.015477316938219	0.0315290079201208	0.996839152459059
"butter"	576	"44.72"	"44.57"	0.0159977172286358	0.0377453930839823	0.993921390699788
"blackcurrant"	826	"51.14"	"44.74"	0.0172796870752313	-0.0112652685535411	0.996068596038521
"leek"	427	"45.29"	"44.8"	0.0166678926701261	0.0057284745786713	0.991980929829375
"wheat"	5456	"44.73"	"44.93"	0.015692209428656	0.0200257204628197	0.997096664342406
"apple.juice"	417	"47.79"	"45.04"	0.0153565057899983	0.0332071014827043	0.995185249694034
"apples"	792	"46.53"	"45.57"	0.0157429643865475	0.00961838044625586	0.998939601471426
"aloeVera"	144	"47.5"	"45.72"	0.0147625598427662	-0.0192197322461816	0.995977450278091
"cheese"	979	"47.48"	"46.44"	0.0145132704573612	0.0556231646933083	0.989527845446346

Appendix 2.11.8 Distribution

Distribution and cumulative distribution.

The Fig. 2.11.20 left shows the normal Gaussian distributions. The distribution is defined by two parameters. The mean is called μ and the broadness $\sigma^2 = \text{sd}$. In Fig. 2.11.20 most curves have as mean 0, only the green curve has as mean -2. The curves are normalized in the way that the sum (the integral) of the whole curve is one. Therefore the broader curves, e.g. the orange one with $\sigma^2 = 5$ have a smaller amplitude at $x = 0$.

The cumulative distribution is generated by simply counting (integral) all existing x -values. This gives a distribution similar to the one shown in Fig. 2.11.20 right. This means that the cumulative probability gives the overall probability for the x values in question. The probability over all x -values should of course be 1. Based on this cumulative distribution, it is simpler to create a hypothesis for the radius .

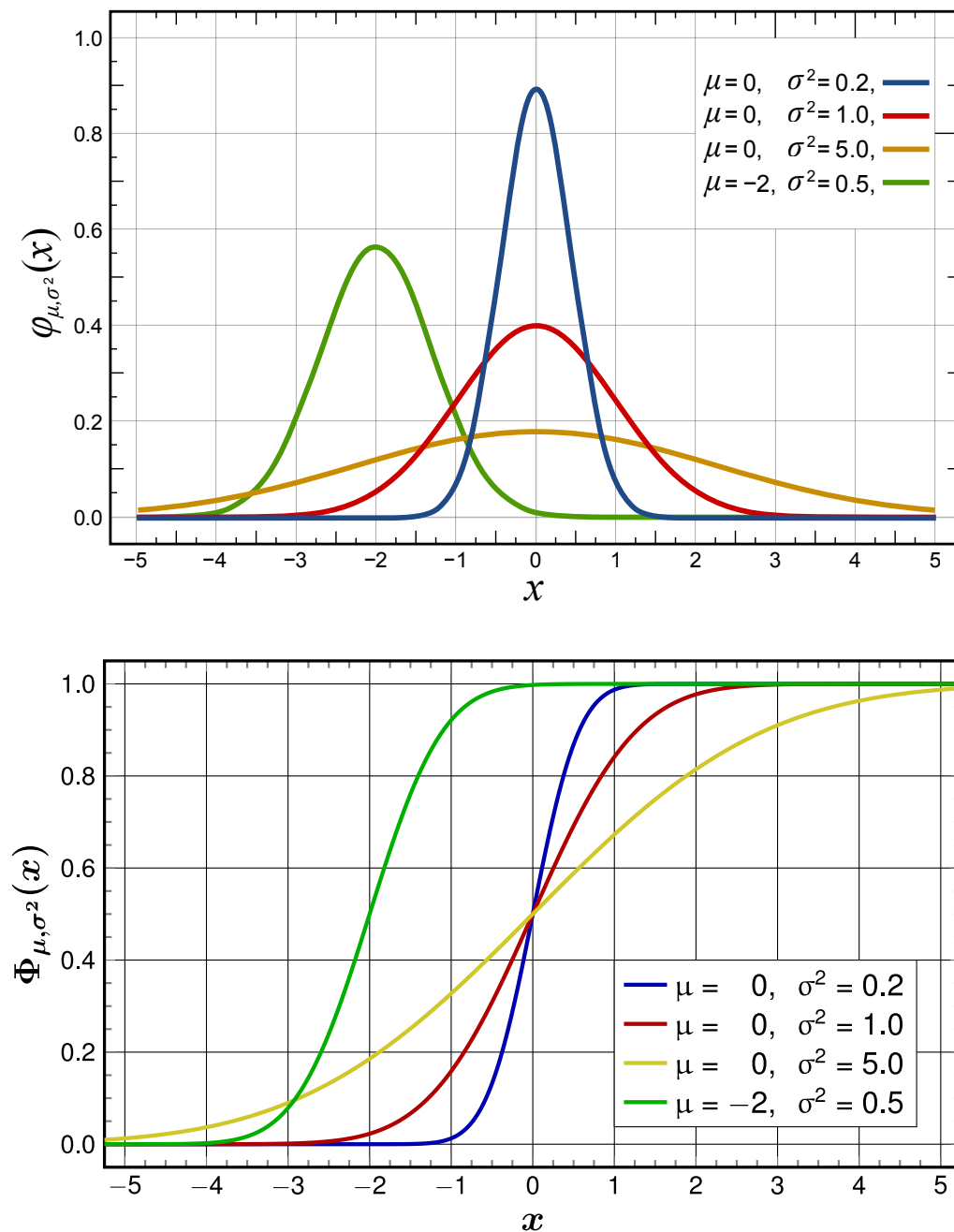
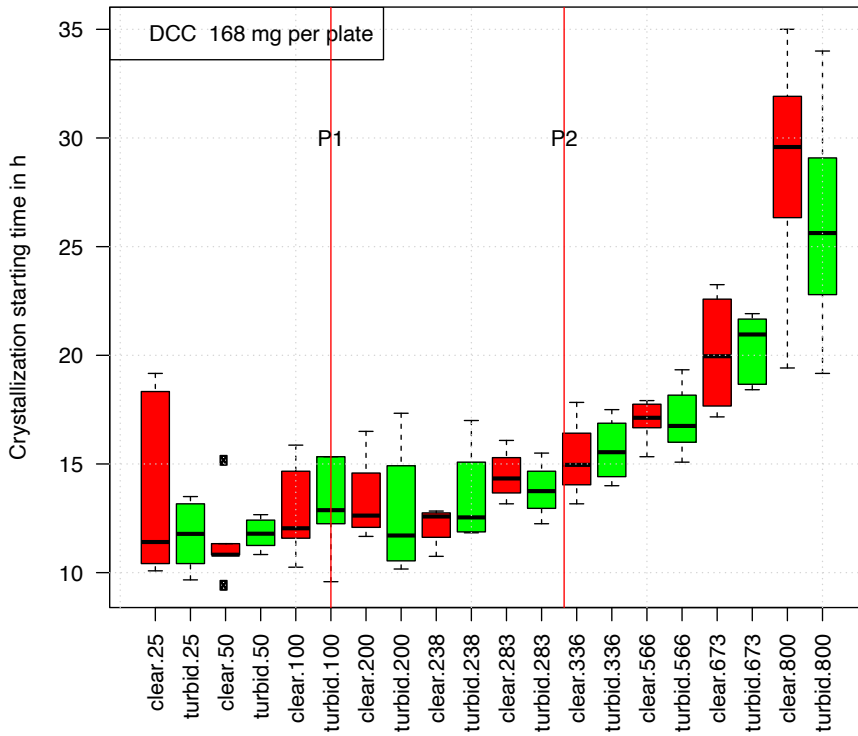


Fig. 2.11.20 Histogram (density function $\sim \exp(-((x-\mu)/\sigma)^2)$) (top) and cumulative distribution function $\text{erfc}(-((x-\mu)/\sigma)^2)$ (bottom). x are normalized values by σ .

Appendix 2.11.9 Variation

In the following the variation in the tcrStart data per chamber and day is shown:

Apple Juice: variation tcrStart for turbid/clear:additive amount



Apple Juice: variation tcrStart for chamber:turbid/clear:additive amount

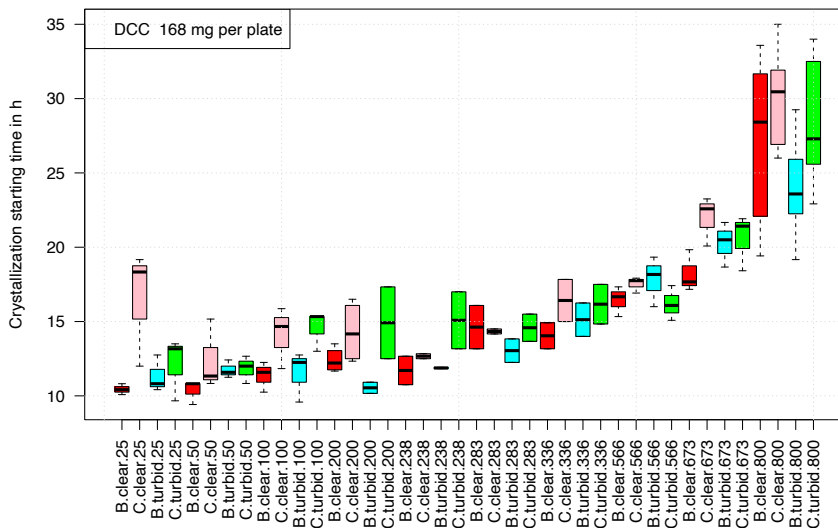


Fig. 2.11.21 Top: tcrStart versus process per additive concentration. Colors: red, clear apple juice; green, turbid apple juice. Lines P1 and P2 show the increase of tcrStart (left from P1), constant tcrStart (between P1 and P2), and another increase of tcrStart (right from P2). Additive concentrations range from 25 - 800 mg juice per plate (indicated below the boxes).

Bottom: tcrStart versus chamber per process per additive concentration. Colors: red, chamber B.clear apple juice; pink, chamber C.clear apple juice; cyan, chamber B.turbid apple juice; green, chamber C.turbid apple juice. Additive concentrations range from 25 - 800 mg juice per plate (indicated below the boxes).

The variation of tcrStart between the chambers is quite visible. The measurements have been performed on different days, so the day variation cannot be shown, but is inherent to the chamber difference.

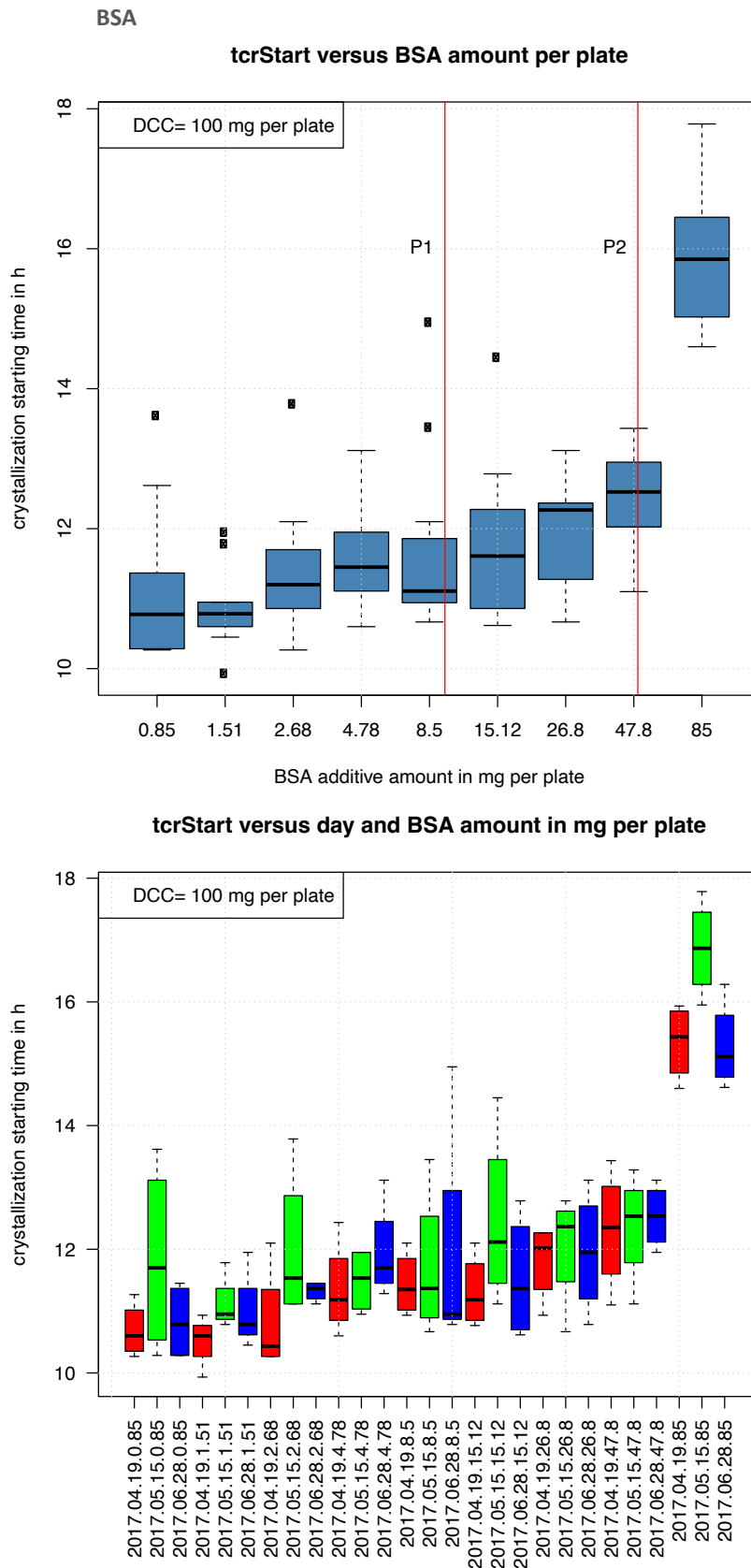


Fig. 2.11.22 Top: tcrStart versus additive amount for BSA. Lines at P1 and P2 show: increase of tcrStart (left side from P1), constant tcrStart (between P1 and P2), again increase of tcrStart (right side from P2). Bottom: tcrStart versus day per additive amount. Colors: red :day1, green : day2, blue : day3. Data from 2017 Roepaen (NL), chamber P.

The differences between the days became quite visible. In this case day2 (green) is sticking out for some amounts.

Quantitative plots for BSA and Apple Juice

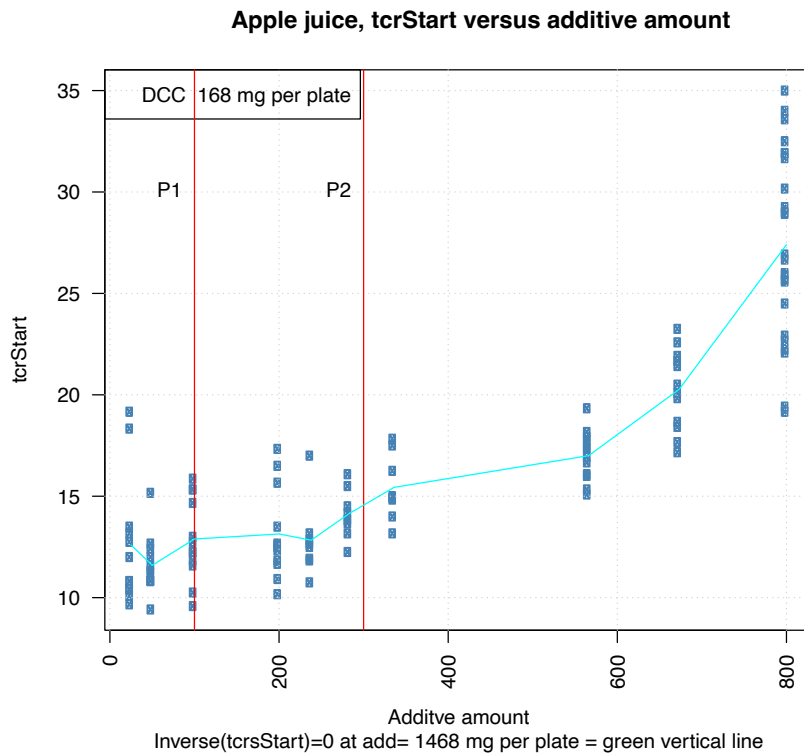
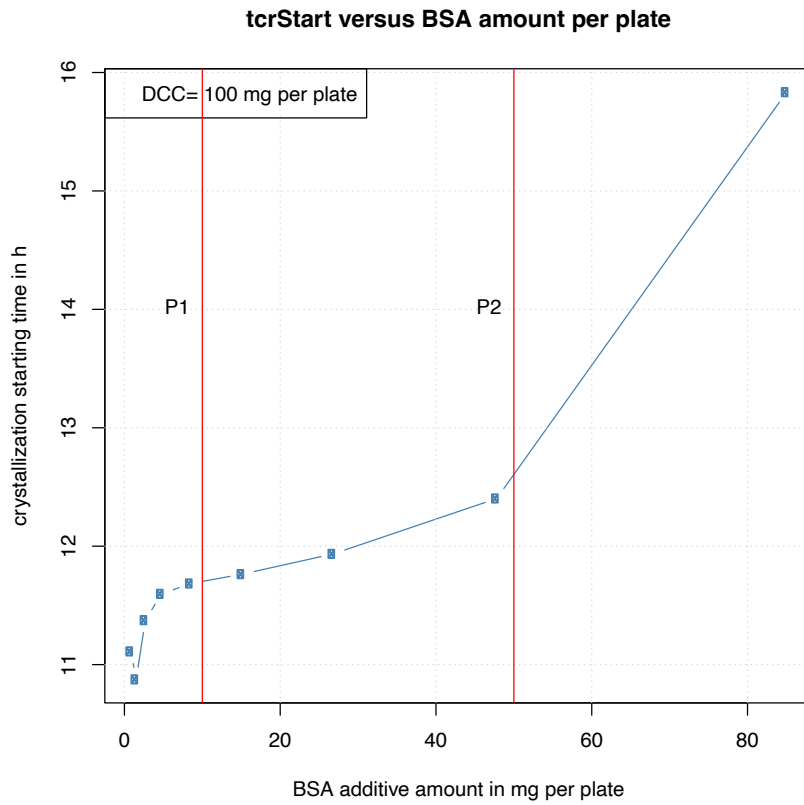


Fig. 2.11.23 Plot of tcrStart (Y-axis) versus the additive amount in mg per plate. Top plot for BSA, bottom plot for turbid and clear apple juice. Lines at P1 and P2 show: increase of tcrStart (left from P1), constant tcrStart (between P1 and P2), followed by a second increase of tcrStart (right from P2).

The strong increase of tcrStart with the additive amount for data on the left side of the vertical line P1 is for the mean values of tcrStart clearly visible for BSA (left) and not so clear for apple juice (right).

Appendix 2.11.10 Volume

Prior to crystallization, the DCC is dissolved in water. After the crystallization, the crystal and some water are divided. Here we are calculating the change of the total volume of each stage (before and after the crystallization).

The density of DCC at the solubility border is 1.524 g / cm^3 . The density of the DCC crystal is 2.51 g / cm^3 . The amount of water to leave the volume is 7.43 mol.

1 mol DCC amounts to 170.46 g

At the solubility border the concentration is (5.0 mol / L)

At the solubility border there is: 1 mol DCC in 200 mL (5.0 mol / L)

1 mol DCC as crystal has a volume of $170.46 \text{ g} / 2.51 \text{ g / cm}^3 = 67.9 \text{ cm}^3$

7.43 mol water $\rightarrow 133.92 \text{ cm}^3$

The overall volume of DCC and water is before crystallization = 200 mL

after crystallization: $67.9 + 133.92 = 201.82 \text{ cm}^3$

is - at first sight - not changed!

References

- [1] Zhou J, Yang Y, Yang Y, Kim DS, Yuan A, Tian X et al. Observing crystal nucleation in four dimensions using atomic electron tomography. *Nature* 2019; 570: 500-503.
- [2] Lilich LS, Timofeev VI. Dampfdruck in den Systemen: MeCl₂ - HCl - H₂O (ZnCl₂-HCl-H₂O und CuCl₂-HCl-H₂O). *Vestn.Leningr.Univ.Fiz.Khim* 1956; 10: 68-74.
- [3] Lilich LS, Sapozhnikova OV. Dampfdruck in den Systemen CuCl₂ - HCl - H₂O und Cu(ClO₄)₂ - HClO₄ - H₂O. *Izv. Vyssh.Uchebn.Zaved.Khim.Khim.Tekhnol.* 1963; : 572-577.
- [4] Desiraju GR. Crystal Engineering: From Molecule to Crystal. *J. Am. Chem. Soc.* 2013; 135: 9952-9967 <https://doi.org/10.1021/ja403264c>.
- [5] Vekilov PG. Crystallization tracked atom by atom. *Nature* 2019; 570: 450-452.
- [6] Driessche V, Alexander E. S, Van Gerven N, Bomans PHH, Joosten RRM, Friedrich H et al. Molecular nucleation mechanisms and control strategies for crystal polymorph selection. *Nature* 2018; 556: 89-94 <https://doi.org/10.1038/nature25971>.
- [7] Cölfen H and Antonietti Markus Wiley 2008S1-6. Mesocrystals and nonclassical crystallization (Wiley, 2008).
- [8] Beckmann H. Über Keimbildung, Einkristallwachstum und Auffächerungswachstum von CuCl₂ * 2H₂O in reinwässrigen und Eiweiß-haltigen Lösungen. PhD Thesis, Universität Bonn. 1959.
- [9] Gmelin. Gmelin Handbuch der anorganischen Chemie (Gmelin-Institut, Frankfurt am Main, 1958).
- [10] Beckmann H. Strukturzustand der Lösung und Kinetik des Kristallwachstums im System Kupferchlorid. *Fortschritte der Mineralogie* 1961; 39: 33-36.
- [11] Gawande MB, Goswami A, Felpin F-X, Asefa T, Huang X, Silva R et al. Cu and Cu-Based Nanoparticles: Synthesis and Applications in Catalysis. *Chem. Rev.* 2016; 116: 3722-3811 <https://doi.org/10.1021/acs.chemrev.5b00482>.
- [12] Alberstein RG, Tezcan FA. Observations of the birth of crystals. *Nature* 2018; 556: 41-42.
- [13] Oxtoby DW. Phase transitions: Catching crystals at birth. *Nature* 2000; 406: 464-497.
- [14] Busscher N, Doesburg P, Mergardt G, Sokol A, Kahl J, Ploeger A. Crystallization patterns of an aqueous dihydrate cupric chloride solution in the presence of different amounts of Bovine Serum Albumin. *Journal of Crystal Growth* 2019; <https://doi.org/doi:10.1016/j.jcrysgro.2019.125272>.
- [15] Haynes W. Crc Handbook of Chemistry and Physics, 91st Edition (CRC Press, 2010).
- [16] Koglin W. Koglin, W. editors. Kurzes Handbuch der Chemie (Koglin, W., 1952).
- [17] Benrath H. Über die Löslichkeit des Kupfer-2-chlorids in Wasser und die Umwandlungspunkte seiner Hydrate. Bemerkungen zu der gleichnamigen Arbeit von Erich Boye. *Z. anorg. Chem* 1934; 216: 207-208 <https://doi.org/https://doi.org/10.1002/zaac.19332160215>.
- [18] Boye E. Über die Löslichkeiten des Kupfer-2-chlorids in Wasser und die Umwandlungspunkte seiner Hydrate. Über das Tetrahydrat. *Zeitschrift für anorganische und allgemeine Chemie* 1933; 215: 75-80 <https://doi.org/https://doi.org/10.1002/zaac.19332150109>.
- [19] Mergardt, G. Simulation des Entstehungsvorganges von Kristallbildern zur Messung der physikalischen Parameter pH-Wert, Dichte und Viskosität am Beispiel von PVP, Glykogen und Bovine Serum Albumin, 2012 .
- [20] Reiter G, Barth J-G. Some general remarks on crystallization in the presence of additives. *Elemente der Naturwissenschaft* 2010; 92: 39-61 <https://doi.org/10.18756/edn.92.39>.
- [21] Leray JL. Growth kinetics of hydrated cupric chloride. *Journal of Crystal Growth* 1968; 3-4: 344-349 [https://doi.org/DOI: 10.1016/0022-0248\(68\)90172-3](https://doi.org/DOI: 10.1016/0022-0248(68)90172-3).
- [22] Yau S-T, Vekilov PG. Quasi-planar nucleus structure in apoferritin crystallization. *Nature* 2000; 406: 494-497.
- [23] Sangwal K. Additives and Crystallization Processes - From Fundamentals to Applications (John Wiley & Sons, 2007).
- [24] Shibata T, Shirasaka R, Ogawa T, Takakuwa Y, Furiya K, Tanaka A et al. Effect of human blood addition on dendritic growth of cupric chloride crystals in aqueous solutions. *Journal of Crystal Growth* 1994; 142: 147 - 155 [https://doi.org/DOI: 10.1016/0022-0248\(94\)90282-8](https://doi.org/DOI: 10.1016/0022-0248(94)90282-8).
- [25] Sokol A. Digital Color Analysis of Copper (II) Chloride Crystallograms. MSc Thesis, University of Aalborg. 2013.
- [26] Busscher N, Kahl J, Doesburg P, Mergardt G, Ploeger A. Evaporation influences on the crystallization of an aqueous dihydrate cupric chloride solution with additives. *Journal of Colloid and Interface Science* 2010; 344: 556-562 <https://doi.org/doi:10.1016/j.jcis.2009.12.045>.
- [27] Holleman LWJ. Ein Beitrag zum Verständnis der empfindlichen Kristallisation. *Elemente der Naturwissenschaft* 1966; 4: 24-33 <https://doi.org/10.18756/edn.4.24>.
- [28] Rockland LB. Saturated Salt Solutions for Static Control of Relative Humidity between 5 and 40 C. *Analytical Chemistry* 1960; 32: 1375-1376.
- [29] Stefan J. Versuche über die Verdampfung. *Sitzungsberichte / Akademie der Wissenschaften in Wien, Philosophisch-Historische Klasse* 1873; 2: 385-423.
- [30] Busscher N. Additional Apple Juice Report. Technical Report, University of Kassel. 2015.
- [31] Busscher N. Apple juice Project. Technical Report, University of Kassel. 2015.
- [32] Kahl J, Busscher N, Doesburg P, Mergardt G, Will F, Schulzova V et al. Application of Crystallization with Additives

- to Cloudy and Clear Apple Juice. *Food Analytical Methods* 2016; 10: 1-9 <https://doi.org/doi:10.1007/s12161-016-0575-6>.
- [33] Zhu D, Shen Y, Wei L, Xu L, Cao X, Liu H et al. Effect of particle size on the stability and flavor of cloudy apple juice. *Food Chemistry* 2020; 328: 126967 <https://doi.org/https://doi.org/10.1016/j.foodchem.2020.126967>.
- [34] Kurz W. Solidification Microstructure-Processing Maps: Theory and Application. *Advanced engineering materials* 2001; 3: 443-452 [https://doi.org/https://doi.org/10.1016/0956-7151\(94\)90044-2](https://doi.org/https://doi.org/10.1016/0956-7151(94)90044-2).
- [35] Libbrecht KG. Morphogenesis on ice: the physics of snow crystals. *Engineering & Science* 2001; 1: 10-19.
- [36] Libbrecht KG. The physics of snow crystals. *Reports on Progress in Physics* 2005; 68: 855.
- [37] Libbrecht KG. Physical Dynamics of Ice Crystal Growth. *Annual Review of Materials Research* 2017; 47: 271-295 <https://doi.org/10.1146/annurev-matsci-070616-124135>.
- [38] Busscher N, Doesburg P, Mergardt G, Sokol A, Kahl J, Ploeger A. Influence of dewetting on the crystallization behavior of CuCl₂ in the presence of BSA during evaporation in a Petri dish. *Heliyon* 2019; 5: e01102 <https://doi.org/10.1016/j.heliyon.2018.e01102>.
- [39] Shibata T, Takakuwa Y, Tanaka A, Kogure M, Iguchi T, Obata H et al. Crystal structures of blue and green hydrated cupric chloride grown from aqueous solutions with and without human blood addition: single crystal X-ray diffraction analysis and differential scanning calorimetry(DSC). *Journal of Tokyo Women's Medical College* 1998; 68: 358-369.
- [40] Leibovici, C. Why the error function is so similar to the hyperbolic tangent?, 2016 .
- [41] R Core Team. R: A Language and Environment for Statistical Computing, 2017.

2.12 Light polarization effect

How can we understand the light polarization effect in the pictures?

Abstract

The pictures from $\text{CuCl}_2 \cdot 2\text{H}_2\text{O}$ (cupric chloride di-hydrate, further called DCC) with additive can be viewed in three different modes by changing the illumination. Either in transparency mode, reflection mode, or by observing the dark-field scatter. Since the crystals are sometimes optically active, there is a fourth possibility, photographing the pictures between crossed polarization filters.

Historical Overview

The first who worked with the polarization phenomenon of DCC pictures was Manthei (2004 [1]). He distinguished between different ways of photographing the DCC pictures. Beside using the illumination for transparency or for reflection he also used dark-field illumination (scattered light). Dark field illumination is the most frequently used technique for photographing the DCC pictures. In addition, he photographed the pictures in between crossed linear polarization filters. This resulted in different colored phenomena depending on the position of the DCC pictures between the crossed filters. He realized that if he used circular polarizing filters, he would capture all positions of the DCC pictures in the linear polarization filters in one photograph.

Authors work

A first test was made by hand for DCC pictures from freeze dried wheat and DCC only. See Fig. 2.12.1 and [Appendix 2.12.1. Polfilter](#).

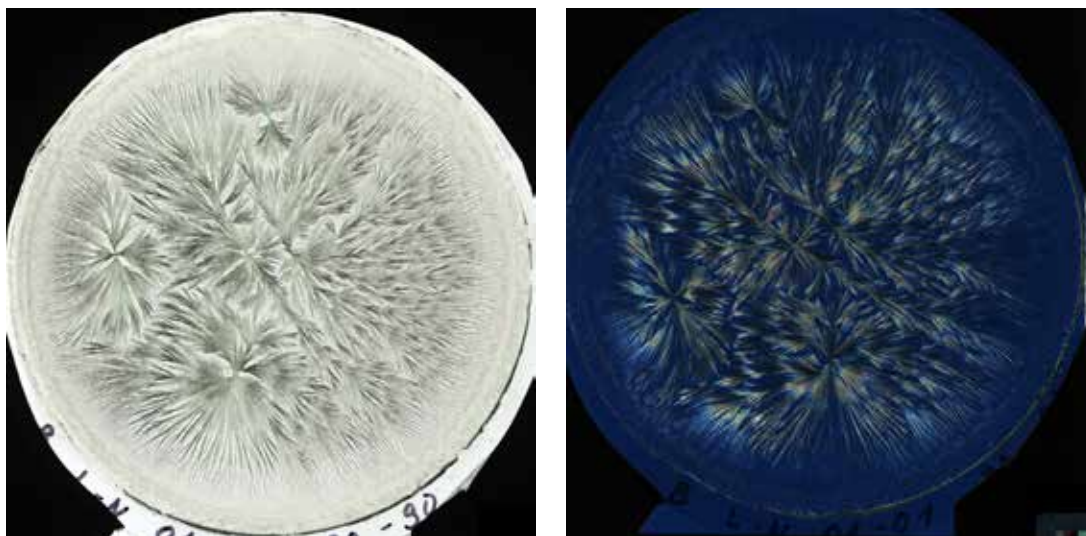


Fig. 2.12.1 Left: transparency scan of a DCC picture of 90 mg DCC and 90 mg freeze dried wheat per plate, right: transparency scan of the same picture between two crossed linear polarization filters. Pictures from University of Kassel (D), LabDoc series 2006.11.17.L-N no. 01 (chamber B).

The colors are quite impressive, but so far we don't know how we can connect the colors to a physical phenomenon or to the quality of the sample. The color phenomenon is also visible for DCC only pictures (see in Appendix 2.12.1 Polfilter Fig. 2.12.3 and Fig. 2.12.4). This may be an indication of the phenomenon of twisted crystals as described by Bernauer (1929 [2]), which would be related to chiral chemical systems. This type of crystallization is still researched by the [Kahr group](#). They wrote an overview article about the Bernauer Bands (Shtukenberg 2011 [3], see also chapter [2.7 Substance spirals](#)). The main question is whether the polarization color effect can be used for quality analysis. For this, DCC pictures from series need to be re-scanned between (circular) polarization filters and evaluated. Since 2016 the [LabDoc system](#) and the database have been prepared for scanning DCC pictures between polarization filters.

Resume

DCC images between polarized filters look beautiful. The effect appears with and without additive. It remains to be tested whether it could improve the discrimination of different sample qualities with computer image analysis (at present based on non-polarized light transparency scanning) or human Gestalt evaluation (at present based on dark field photography).

Additional research

- Check for which samples the DCC pictures are optical active.
- Check at which additive amount the polarization effect increases.
- The crystallization at the meniscus in Fig. 2.12.3 and 2.12.4 needs special attention, because it is not a planar 2D crystallization, but a 3D volume crystallization.
- Does the optical activity allow differentiating qualities?
- Re-evaluate series, that are optical active (DOK 2005).
- Re-evaluate substance spirals (matrix carrot, freeze dried wheat).
- Discuss the findings with experts, e.g. the Kahr group.

Appendix 2.12.1 Polfilter

Four pictures were scanned as a test. Two pictures were from LabDoc series B.2006.11.17.L-N (no. 1 and 2, sample is freeze dried wheat). Two pictures were from LabDoc series B.2007.05.10.Cu-IX no 1 and 2, sample = DCC only. The pictures that were rescanned between crossed polarization filters (type Kodak) were assigned to the LabDoc series C.TEST-SCAN-2006.11.17.LN. as pictures no. 1, 2, 5, 6.

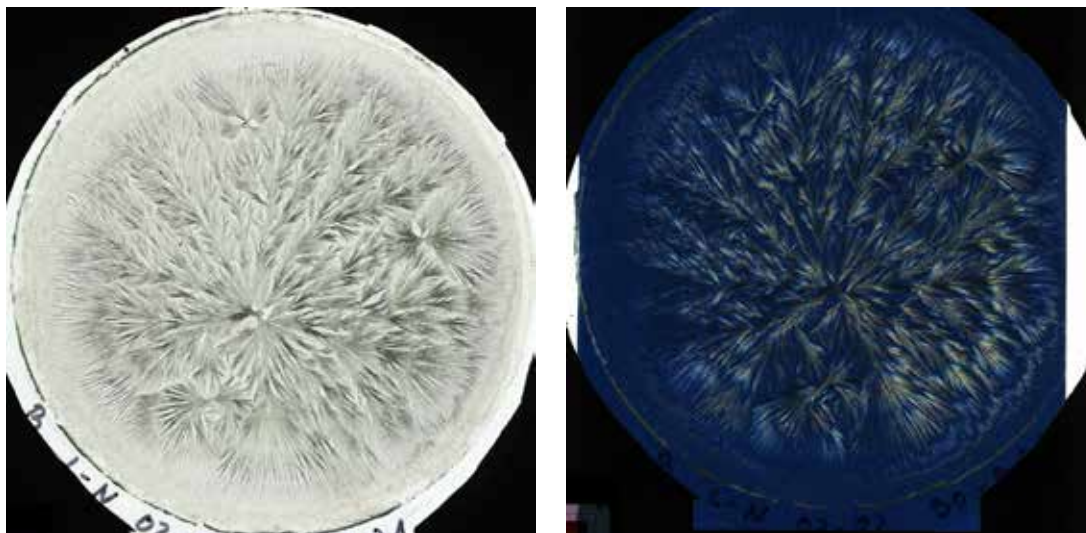


Fig. 2.12.2 left: transparency scan of a DCC picture of 90 mg DCC and 90 mg freeze dried wheat per plate, right: transparency scan of the same DCC picture between two crossed linear polarization filters. Pictures from University of Kassel (D), LabDoc series 2006.11.17.L-N no. 02 (chamber B).

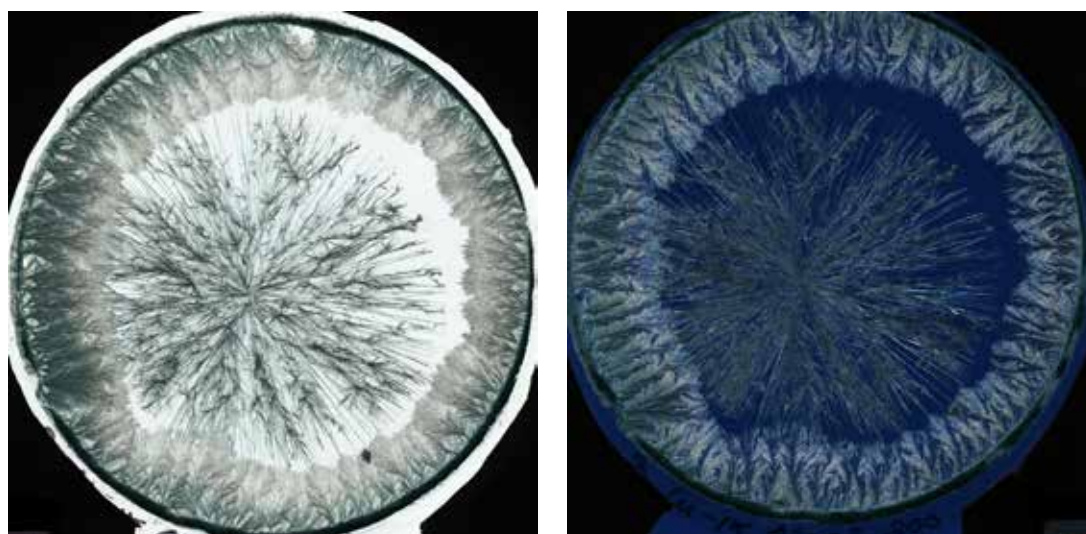


Fig. 2.12.3 left: transparency scan of a DCC picture of 600 mg DCC per plate, (no additive) right: transparency scan of the same DCC picture between two crossed linear polarization filters. Pictures from University of Kassel (D), LabDoc series 2007.05.10.Cu-IX no. 02 (chamber B).

In Fig. 2.12.3 the needles around the geometric center are not as colorful (optically active) as the crystals at the rim, which show more of a dendritic behavior.

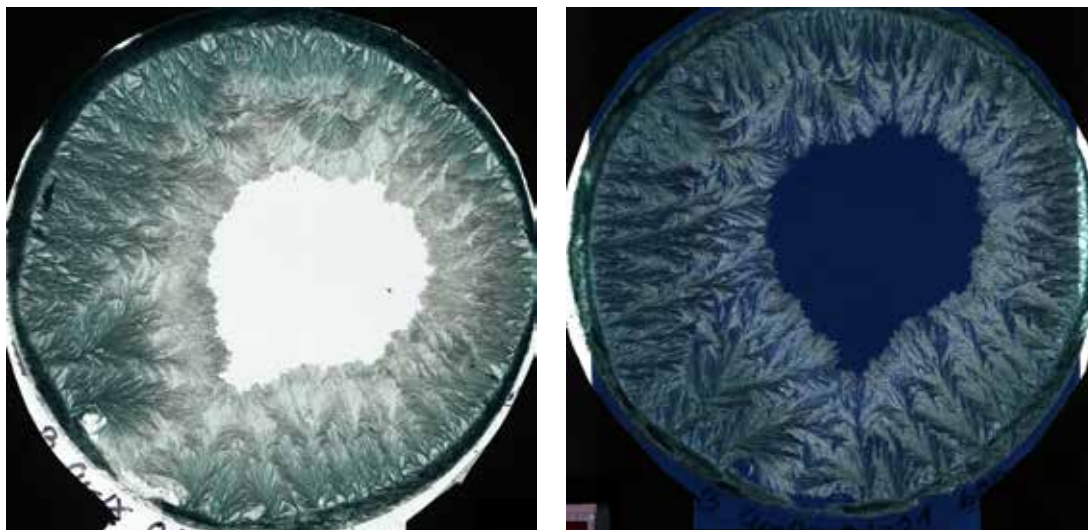


Fig. 2.12.4 left: transparency scan of the DCC picture of 600 mg DCC per plate, (no additive) right: transparency scan of the same DCC picture between two crossed linear polarization filters. Pictures from University of Kassel (D), LabDoc series 2007.05.10.Cu-IX no. 01 (chamber B).

References

- [1] Manthei C. Zur Darstellung von Kupferchloridkristallisationsbildern mit Mitteln der klassischen Schwarz-Weiß-Fotografie. *Elemente der Naturwissenschaft* 2004; 80: 121-124.
- [2] Bernauer F Johnson, A. editors. *Gedrißte Kristalle* (Gebrüder Borntraeger, 1929).
- [3] Shtukenberg A, Gunn E, Gazzano M, Freudenthal J, Camp E, Sours R et al. Bernauer's Bands. *ChemPhysChem* 2011; 12: 1558-1571 <https://doi.org/10.1002/cphc.201000963>.

2.13 Evaporation model

Abstract

A simplified model for the evaporation of a watery solution of the salt $\text{CuCl}_2 \cdot 2\text{H}_2\text{O}$ (cupric chloride di-hydrate, further called DCC) until the onset of crystallization is described. It takes into account the evaporation from a Petri-dish, the evaporation from a water reservoir and the absorbance of the humidity into the wooden wall of the inner chamber and the transfer through the humidity-permeable wall into to outer chamber. In addition, the dependence of the partial pressure above the DCC solution on the DCC concentration is taken into account. With this model the dependency of the crystallization starting time on the starting humidity can be explained as well as the dependency of the crystallization starting time on the DCC amount. The observed threshold of 67 % relative humidity in the chamber during the evaporation seems to be a dynamic effect of the system and not due to the relative humidity of 67 % above the saturated DCC solution. This needs to be checked because it contradicts our previous expectations. The limitations of the model due to the adaptation of the solution of the Stefan tube problem to an airflow system, the (incorrect) assumption that all dishes start at the same time and the fact that the change in partial pressure above the Petri-dish when the crystallization starts is not considered, are discussed.

Introduction

Some non-intuitive relations appeared during the work on the crystallization of the aqueous solution of the salt $\text{CuCl}_2 \cdot 2\text{H}_2\text{O}$ (cupric chloride di-hydrate, further named DCC) evaporating from a Petri-dish. Like the non-dependence (Busscher 2010 [1]) or increase of the crystallization starting time ([tcrStart](#)) with the increase of the DCC amount, the sensitive dependency of the tcrStart on the starting humidity (1 hour increase in tcrStart for 1 % rel. humidity increase, Kahl 2004 [2]) and lastly, the relative humidity in the Triangle type chamber during evaporation always being below 67 %. To gain a deeper understanding of these relationships, a computerized simulation was performed. The simulation setup included not only the Petri-dish but also the evaporation chamber. In the following the ongoing work is described in the chapter Historical Overview and the actual work in the chapter Authors Results. The Petri-dish described in this chapter consists of an acrylic ring and a glass plate (Triangle DCC system). In the description of the “Problem of Stefan” the ring is called a tube. To be consistent, in this chapter we will use the word “tube” in all places where a ring would normally be expected.

Historical Overview

The first step in understanding the conditions of a DCC solution evaporating in a Petri-dish was taken by Holleman 1966 [3]. Starting from the open tube evaporating problem of Stefan 1886 [4] (see also McBain 2000 [5] and Suehrcke 1995 [6]) he measured the DCC concentration gradient from the center of the Petri-dish until the rim. The aim was finding the form of the interface where the diffusion controlled evaporation from the solution surface in the Petri-dish met the airflow passing around the Petri-dish. He found a convex indentation into the tube ([3] p. 30, Fig. 4, or Fig. 2.13.5 below). The simulation of the evaporation of a DCC solution in a Petri-dish was done by Leray 1973 [7]. Leray calculated how the spatial profile of the surface of the solution develops during the evaporation, taking into account the concentration gradient in the Petri-dish as measured by Holleman 1966 [3] and the changes in the surface tension due to the increasing DCC concentration. The dependency of the tcrStart from the starting humidity (the humidity in the chamber before the solution was pipetted into the Petri-dish) was roughly estimated by Kahl 2004 [2] as a 1 hour increase of tcrStart for each 1 % increase of the starting humidity (which was around 50 %). The variation of the tcrStart, i.e. the standard deviation (in the following abbreviated as sd) also increased as the tcrStart increased [2]. This was confirmed in the Checking Influences project (2009 [8], p. 61, 62). The dependence of the tcrStart on the DCC amount was measured by Busscher 2010 ([1] Fig. 7). This was not consistent with a simple model predicting a decrease in tcrStart as the DCC increases ([1], Fig. 12).

Authors Results

The model is described in [Appendix 2.13.1 Model](#) and the determination of the parameters in [Appendix 2.13.2 Parameter](#).

Despite the limitations of the model, the results of the evaporation simulation agree with the measurement data. The parameters will need to be improved in further optimization runs, but so far we have found a set of parameters that agree with the measurement data.

Here, the answers to four questions obtained by simulating the model with the actual parameters found are presented and discussed:

1. dependency of the tcrStart and sd(tcrStart) from the starting humidity
2. dependency of the tcrStart from the amount of DCC
3. dependency of the tcrStart from the height of the tube
4. why is the relative humidity is always below 67 %

Question-1. Dependency of the tcrStart and sd(tcrStart) from the starting humidity

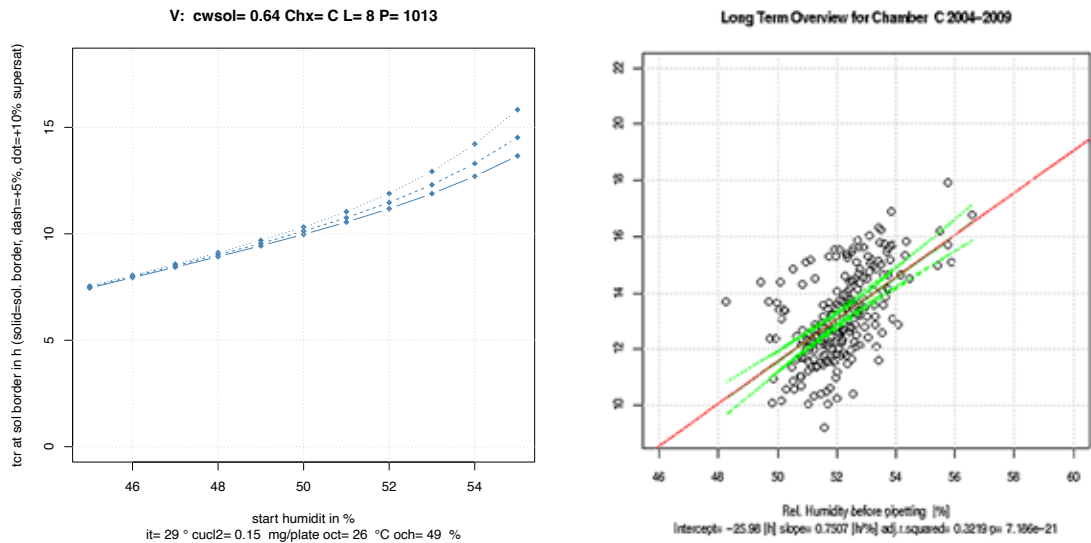


Fig. 2.13.1 Dependency of tcrStart (Y-axis) on the starting (relative) humidity (X-axis) in %. Left simulation result, right measurement data. Left: points on the solid line represent the evaporation time until the DCC concentration reaches the solubility border. Points on the dashed line represent the evaporation time until the DCC concentration reaches 5 % supersaturation, dotted line is the evaporation time until the DCC concentration reaches 10 % supersaturation. Right: measurements from the Checking Influences project 2009 [8], p. 61. The red linear regression line has a slope of 0.75 hour / %. Data from University of Kassel, Witzenhausen (D) from 2004 to 2009, Chamber C.

In Fig. 2.13.1 left the dependency of the simulated tcrStart from the starting (relative) humidity is shown. The crystallization can start when the DCC concentration, due to the evaporation, reaches the solubility border (solid line). Usually a supersaturation is needed for a crystallization to start, therefore the 5 % supersaturation (dashed line) and the 10 % supersaturation (dotted line) are shown too. The difference between the solubility border (solid line) and the 10 % supersaturation (dotted line) is low (5.5 minutes) for a starting humidity in the chamber of 45 % (left side of the X-axis). Whereas at 55 % starting humidity (right side of the X-axis) this difference increases to 2.2 hours. This fits with the observation that the variation of the sd of the tcrStart increases with the (relative) starting humidity. The change in tcrStart between 50 % and 55 % starting humidity for the solid line (solubility border; 0 % supersaturation) goes from 10 to 13.6 hours (a difference of 3.68 hours) and for the dotted line (10 % supersaturation) from 10.3 to 15.8 hours (difference = 5.5 hours). These predictions $3.68 \text{ h} / 5 \% = 0.73 \text{ h} / \%$ and $5.5 \text{ h} / 5 \% = 1.1 \text{ h} / \%$, are in agreement with the observations from Kahl 2004 [2] and the measurements of the Checking Influences project [8] (see also the slope in Fig. 2.13.1 right).

Question-2. dependency of the tcrStart from the DCC amount

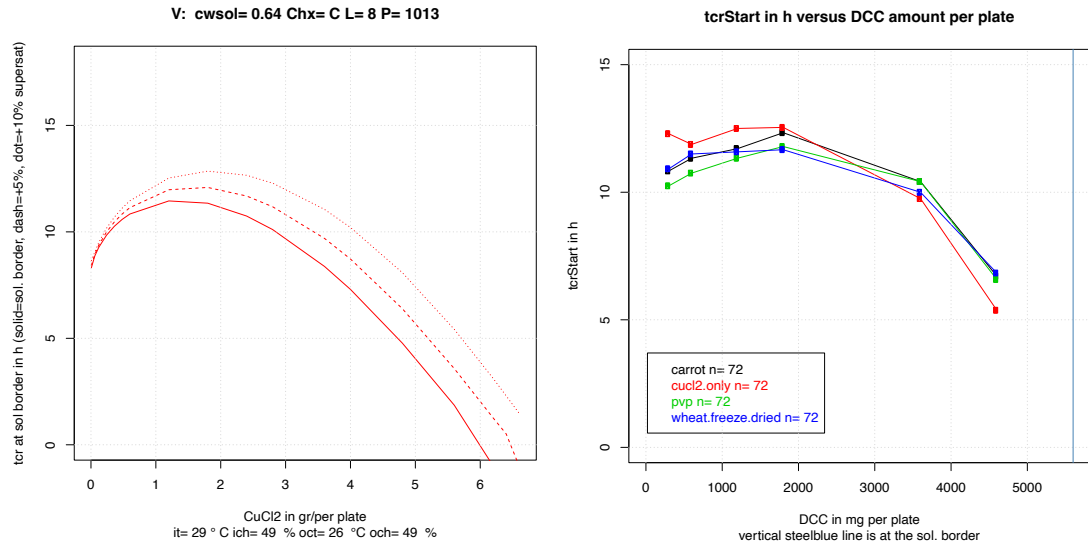


Fig. 2.13.2 Dependency of tcrStart (Y-axis) on the DCC amount. Left simulation result, right measurement data. Left: points on the solid line represent the evaporation time until the DCC concentration reaches the solubility border. Points on the dashed line represent the evaporation time until the DCC concentration reaches 5 % supersaturation, dotted line is the evaporation time until the DCC concentration reaches 10 % supersaturation. Right: mean tcrStart value from three additives and for DCC only.

In Fig. 2.13.2 left (simulation results) the tcrStart increases for DCC amounts of 0 to 2000 mg per plate. Beyond 2000 mg per plate DCC the tcrStart decreases. This is quite comparable to the measurement data shown in the right plot of Fig. 2.13.2.

Resume of Question-1 and Question-2.

Looking at the results from question 1 and 2, the evaporation can be described as follows:

The evaporation rate from the dish depends, according to Stefan (see formula in Appendix 2.13.1 Model), on the difference of the humidity in the chamber and the partial pressure or the humidity just (< 1 mm) above the solution. The relative humidity above the solution is 100 % when there is no DCC in the solution.

Immediately after pipetting, evaporation from the dishes is at its highest and flows into the chamber volume and the inner wall of the chamber. Evaporation into the chamber volume increases the humidity in the chamber. Simultaneously, the DCC concentration in the dish increases which reduces the humidity above the solution. This difference between the humidity in the chamber (increasing from 50 % starting humidity onward) and the humidity above the dish (decreasing from 100 %) is reduced from both sides. The increasing humidity in the chamber increases the humidity flow through the permeable chamber wall to the outer chamber. When (simplifying) that these two flows, from the dish into the chamber and from the chamber into the outer room are the same, then the maximum relative humidity is reached see also Fig. 2.13.7. After this maximum, the DCC concentration in the dish will increase further and the humidity in the chamber will start to decrease. The difference between the humidity above the dish and in the chamber are approaching each other, which reduces the evaporation rate from the dish to almost a hold (the so called “hold-on” phase). Finally, crystallization starts, because the DCC concentration in the Petri-dish exceeds the solubility border.

The effect observed in response to question 1 (1 hour increase in tcrStart for a 1 % higher starting humidity) is caused by the earlier reduction of evaporation due to the already humid chamber. This results in an extension of the “hold-on” phase because relatively more water is still present in the dishes.

The effect observed in response to question 2 (tcrStart increases for DCC amounts from 0 to 2000 mg per plate) is caused by an earlier onset of the partial pressure effect due to the higher DCC starting concentration, which reduces the evaporation rate. This overcompensates the lower amount of water in the 6 mL pipetted volume, due to the increasing DCC amount.

The effect observed in response to question 4 (the maximum humidity is 67 %) points to a dynamic effect of the system rather than a direct connection to the saturation humidity above the DCC solution at the solubility border. The simulation data shows that with the above parameters, the solubility border is reached later than the maximum humidity in the chamber. This means that the humidity above the solution at the solubility border is not reflected in the maximum value of 67 % relative humidity.

A graph from the simulation will help to illustrate the above description. The graph below in Fig. 2.13.3 shows the humidity transport over time during evaporation.

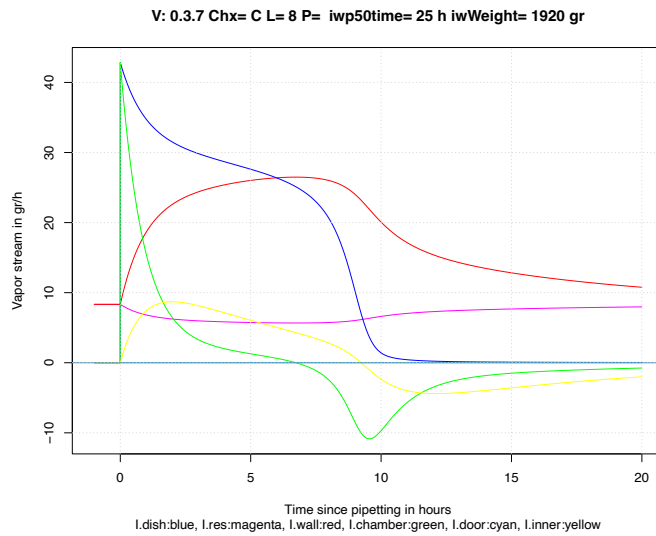


Fig. 2.13.3 Simulation results of the humidity flow (Y-axis) per model element in g / h versus the evaporation time in hours (X-axis). Colors represent the different humidity flows: blue from the Petri-dish, magenta from the reservoir, red through the chamber wall, yellow into the chamber wall, green into the chamber volume.

In Fig. 2.13.3 the humidity flow per simulation model element is shown. Pipetting takes place at the zero time point. Before the zero time point, there is only a red curve visible, which is the humidity flow through the permeable wall into the outer chamber. Before the zero time point, this humidity comes exclusively from the reservoir (magenta color, covered by the red line until $t = 0$). Immediately after pipetting, the red line (humidity flow through the chamber wall) increases as the humidity in the chamber increases. The magenta line (reservoir) decreases because less humidity is coming from the reservoir. The blue line is the evaporated humidity from the Peri-dish. Initially, the flow is very high, but it is progressively reduced as the humidity in the chamber increases (between 0 to 5 h). The green line is the humidity filling the chamber (if positive) and emptying the chamber (if negative). The humidity flow into the chamber wall is yellow. Between $t = 5$ and $t = 10$ hours the evaporation from the dish (blue line) decreases because it is increasingly hindered by the increased DCC concentration in the dish. The humidity flow from the dish approaches the humidity level in the chamber (see Fig. 2.13.7), which reduces the evaporation of water from the solution in the Petri-dish. This is the so called “hold-on” phase at around $t = 10$ hours.

Question-3 dependency of the tcrStart from the height of the tube

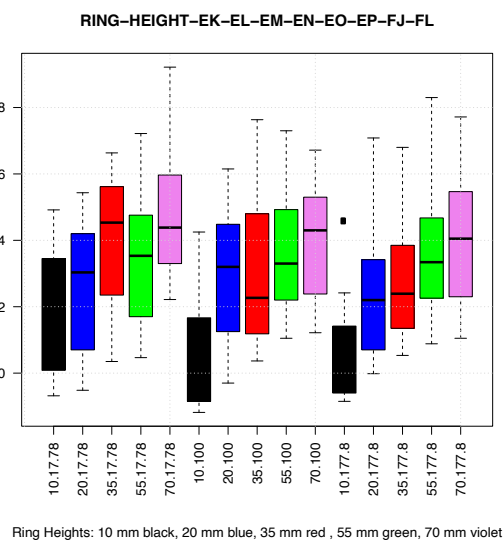
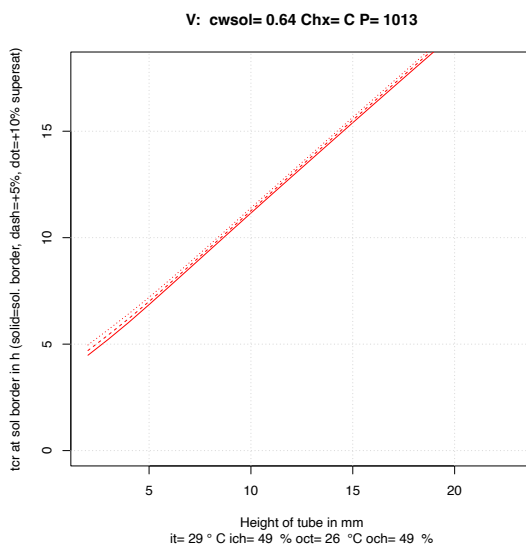


Fig. 2.13.4 Dependency of tcrStart (Y-axis) from the height of the tube in mm (X-axis). Left simulation result, right measurement data. Left: points on the solid line represent the evaporation time until the DCC concentration reaches the solubility border. Points on the (partly overlapping) dashed line represent the evaporation time until

the DCC concentration reaches 5 % supersaturation, dotted line is the evaporation time until the DCC concentration reaches 10 % supersaturation. Right plot: mean tcrStart values from BSA as additive for five tube heights (black = 10 mm, blue = 20 mm, red = 35 mm, green = 55 mm and violet = 70 mm) at three DCC amounts (17.78 (left group), 100 (middle group) and 177 (right group)) in mg per plate. BSA amount was 2.68 mg per plate. See also chapter [1.4 Surface tension, cleaning, ring height](#).

The slope in Fig. 2.13.4 right, for the group on the right, ranges from a mean of 11 h (10 mm tube height, black box) to 14 h (70 mm tube height, violet box). Which results in: $14 \text{ h} - 11 \text{ h} / (70 \text{ mm} - 10 \text{ mm}) = 3 \text{ h} / 60 \text{ mm} = 0.05 \text{ h} / \text{mm}$ increase in tcrStart. The slope of the simulated data (left graph) ranges from 7 h at 5 mm height to 15 h at 15 mm. Which results in: $15 \text{ h} - 7 \text{ h} / (15 \text{ mm} - 5 \text{ mm}) = 8 \text{ h} / 10 \text{ mm} = 0.8 \text{ h} / \text{mm}$. This is a difference of a factor of 16. The mean tcrStart for the 35 mm tube height (right group, red box, Fig. 2.13.4 right) is 12 h, which compares to a simulated tube height of 11 mm; i.e. a difference of factor 3. The mean tcrStart for the 70 mm tube height ($t = 14 \text{ h}$, right group, violet box, Fig. 2.13.4 right) compares to a simulated tube height of 14 mm. Building on the idea of an interface between the airflow and the diffusion area in the dish, the above data point to the question of how far the airflow “bends” into the tube, and how this affects the effective height of the tube and the effective diffusion area in the dish. A literature study is needed to see if there are other solutions to calculate the evaporation rate from a Petri-dish.

Resume

The three non intuitive effects, like the non dependency (Busscher 2010 [1]) or increase of the tcrStart with an increasing DCC amount and the sensitive dependency of the tcrStart on the starting humidity (1 hour tcrStart increase for 1 % relative humidity increase, Kahl 2004) and the fact that the relative humidity in the chamber during the evaporation is always below 67 % could be understood from the simple model of the evaporation of a DCC solution from a Petri-dish. Two effects were important. The first was the inhibition of evaporation by the increasing humidity in the chamber, and the second was the “hold-on” of evaporation from the Petri-dish by the humidity in the chamber reaching the partial pressure above the Petri-dish, and simultaneously, the decrease of the partial pressure above the solution in the Petri-dish. The 67 % humidity limit during evaporation was not caused by the saturation humidity of the DCC solution of 67 %, but by a dynamic effect. The dependency of tcrStart on the height of the tube needs more attention and maybe needs a redesign for the part of the airflow around the tube.

Additional research

- Adapting parameters e.g. iwWeight = the amount of water the inner wall can take up (is there more information about the dynamics of wood absorption like Thybring 2019 [9]). Is there a simple measurement for this? (changing the temperature in the inner chamber?).
- Adapting the handling of the reservoir (following the work of Assouline 2010 [10] on covered water surfaces or like Stefan’s pond).
- Add the crystallization effect to the model, the DCC concentration in water expelled by crystallization is lowered → partial pressure rises again, this water evaporates faster.
- The DCC concentration can be higher near the surface than in the bulk of the solution (Style 2007 [11] [12]) This can change the conditions for the start of the crystallization to an earlier moment.
- Understand the tcrStart results for different tube heights.
- Change the number of dishes and pipetting volume. What is the influence on the tcrStart?
- Add a chamber reset (door opening for a defined time) to check for the humidity overswing phenomenon for short periods (see chapter [1.4 chamber reset](#)). This could be influenced by the inner wall.
- Measure tcrStart ve starting humidity (Fig. 2.13.1) for more data and other chambers.
- Measure tcrStart for lower DCC amounts (Fig. 2.13.2).
- Include the simulation of the temperature. So far the temperature is constant in the simulation. Should the double ring of the Triangle System be covered with glass plates when no experiments are

running, or is it sufficient to place the dishes 45 minutes before an experiment?

- Measure the linearity of the permeability of the chamber wall. Reduce the outer chamber temperature stepwise, and check if the resulting humidity in the chamber fits to a linear approach.
- Simulate a step-response challenge of the outer chamber to check the accessibility of the inner wall. Compare with measurement data.
- Calculate the mean of the inverse length parameter for Stefan's formula, assuming a quadratic or other form of the indentation (see Fig. 2.13.5). Does this give the results in Fig. 2.13.3?
- Does the maximum relative humidity in the Darmstadt chamber differ from the 67 % measured in the Triangle chambers?

Appendix 2.13.1 Model

Modeling the flow

The model has been developed to cover the process until the start of the crystallization. This is because the aim is to see the dependency of the $t_{crStart}$ on the DCC amount and on the starting humidity in the chamber. It mimics the water flow of evaporation from the dishes and the reservoir to respectively, the chamber volume, the chamber walls and through the humidity permeable walls to the outer chamber. The climate in the outer chamber is regulated and therefore, in this model, it is considered constant. Moreover the 43 Petri-dishes ([Triangle System](#)), are considered as one dish. This assumes that all dishes have the same $t_{crStart}$. In the model, unlike the reality, the onset of the crystallization does not change the evaporation behavior. In particular, it does not take into account that the water is expelled from the crystals and that the partial pressure and the evaporation rate increase again as result.

1. Modeling the permeability of the chamber walls

The permeability of the wooden walls is considered as a flow resistance. The flow through the wall is the resistance multiplied by the difference of the absolute humidity between the inner and outer chamber.

2. Evaporation from the dish

The evaporation from the dish is considered as the problem of Stefan (diffusion in a tube). The Petri-dish is regarded as a virtual tube with a lower actual height, following the idea of Hollemann 1966 ([3] p. 30, Fig. 4, or Fig. 2.13.5 in this text) that the airflow “bends” into the tube, creating a concave indentation into the tube, that can be viewed as a smaller distance to the surface of the solution than the tube actually would have.

Looking at the flow from the surface of the solution to the rim of the Petri-dish ([Triangle System](#)):

The diffusion in a open cylindrical tube is described as the problem of Stefan (1873 [13]). Actual measurements from Prata [14] show how precise the formula is, as long as the diffusion case is valid. A good introduction to this can be found in Suehrcke [6]. The first measurements of the evaporation and concentration gradient in a DCC Petri-dish were done by Hollemann [3]. The system that he was researching was, as he stated, distant from this Stefan problem. Maybe the [Triangle System](#) with the 3.5 cm high tubes is closer to this, because the transport from the surface of the solution is limited by diffusion. The difference between isothermal and non-isothermal is discussed by Sparrow [15] (with heating, and without heating below the dish).

Case diffusion: (Stefan’s formula as in Suehrcke [6])

$$dm/dt / A = D * P / (R * S * T * L) * \ln ((P - P_{s,L}) / (P - P_{s,i})) \quad (1)$$

dm change of mass in time dt

A area in question

D binary diffusion constant water humidity into air

P total pressure

R gas constant for water vapor

T absolute temperature

$P_{s,L}$ partial pressure at the mouth of the container

$P_{s,i}$ partial pressure at the liquid surface interface

L length between water surface and mouth of container

$D = 0.239 \text{ cm}^2 / \text{sec}$ (at $8 \text{ }^\circ\text{C}$) from the CRC Handbook of Chemistry and Physics 1983 p. F-46 [16]. $D = 0.24 \text{ cm}^2 / \text{sec}$ at $20 \text{ }^\circ\text{C}$ from Massman 1998 ([17] p. 1118, Fig. 1).

The idea from Holleman was to find the interface between the diffusion area from the surface of the solution in the dish and the airflow, which makes a concave indentation into the tube. As an illustration the drawing from Holleman (1966, p. 30, Fig. 4) is shown below.

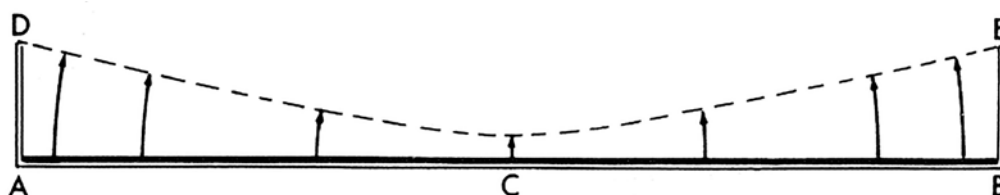


Fig. 2.13.5 Illustration from Holleman (1966 [3] p. 30, Fig. 4).

The idea is, that at point C the solution in the Petri-dish will be at its minimum level. The effective mean height of a virtual tube would be a bit above this value. The simplest approach would be to leave the dish area as it is and adjust the height of a virtual tube with the constraint that the DCC concentration in the dish should be at the DCC solubility border after ~ 10 hours (\sim first possible crystallization start in Fig. 2.13.4 right).

3. Inner wall effect

This parameter was set as a question of whether a part of the evaporated humidity would be stored in the inner wall of the chamber. From the article from Thybring 2019 [9] we had the impression that there should be such an effect. The parameters were defined as

- 1 the time for 50 % of the humidity change in the wood to occur (iw50time). For this 25 minutes were estimated.
- 2 the amount of humidity that could be stored into the wall (iwWeight).

The calculation of iwWeight is shown in [Appendix 2.13.3 Weight](#).

4. partial pressure above the DCC solution

According to the measurements of Lilich 1956 [18] and Lilich 1963 [19] the partial pressure above a DCC solution has an ideal gas behavior. The temperature dependency of the saturated solution between 20 and 40 °C is low (Rockland 1960 [20]).

5. Density of DCC solution

The density of the DCC solution has been measured by Beckmann 1959 [21] and Mergardt 2012 [22]. See chapter [1.7 Evaporation issues](#) - Density for graphs.

6. Temperature dependency of the solubility border

The temperature dependency measurements of the DCC solubility border are from Beckmann 1959 [21], Gmelin 1958 [23] and Benrath 1934 [24]. See chapter [2.11 Nucleation](#) - Solubility for graphs.

7. modeling of the reservoir

The reservoir was simply modeled. At the defined conditions of a chamber, the flow is equal to the refill amount. As the humidity increases, the flow decreases.

Appendix 2.13.2 Parameter

Setting the parameters:

- Permeability of the chamber wall was derived from the amount of water required to refill the reservoir.
- Height of the dish was based on the mean evaporation rate.
- Time constant and size of the wall effect was based on step response data.
- Partial pressure above the DCC solution was obtained from Lillich, and from Rockland for 100 %).
- Density of the DCC solution was based on own measurements and Beckmann.
- Temperature dependency of DCC solubility border was obtained from Gmelin and Benrath.

1. Permeability of chamber walls (from refilling the reservoir)

The humidity permeability of the chamber wall can be calculated from the refill amount per week of the reservoir and the difference in the absolute humidity between the inner and outer chamber. The refill amount is ~ 1400 mL water per week, 200 g / day or 8.33 g / hour. The absolute humidity is calculated from the temperature and the relative humidity when there are no experiments and the values are constant. This can differ for each chamber.

2. Adapt the height of the tube

The height of the tube in the [Triangle System](#) is usually 35 mm. Since the airflow passing the Petri-dish affects the effective tube height, the height of the tube was adjusted according to the idea of Holleman, so that a volume of ~ 5.8 g water (up to the solubility border) evaporates in 10 hours. This results in a tube height of 8 mm.

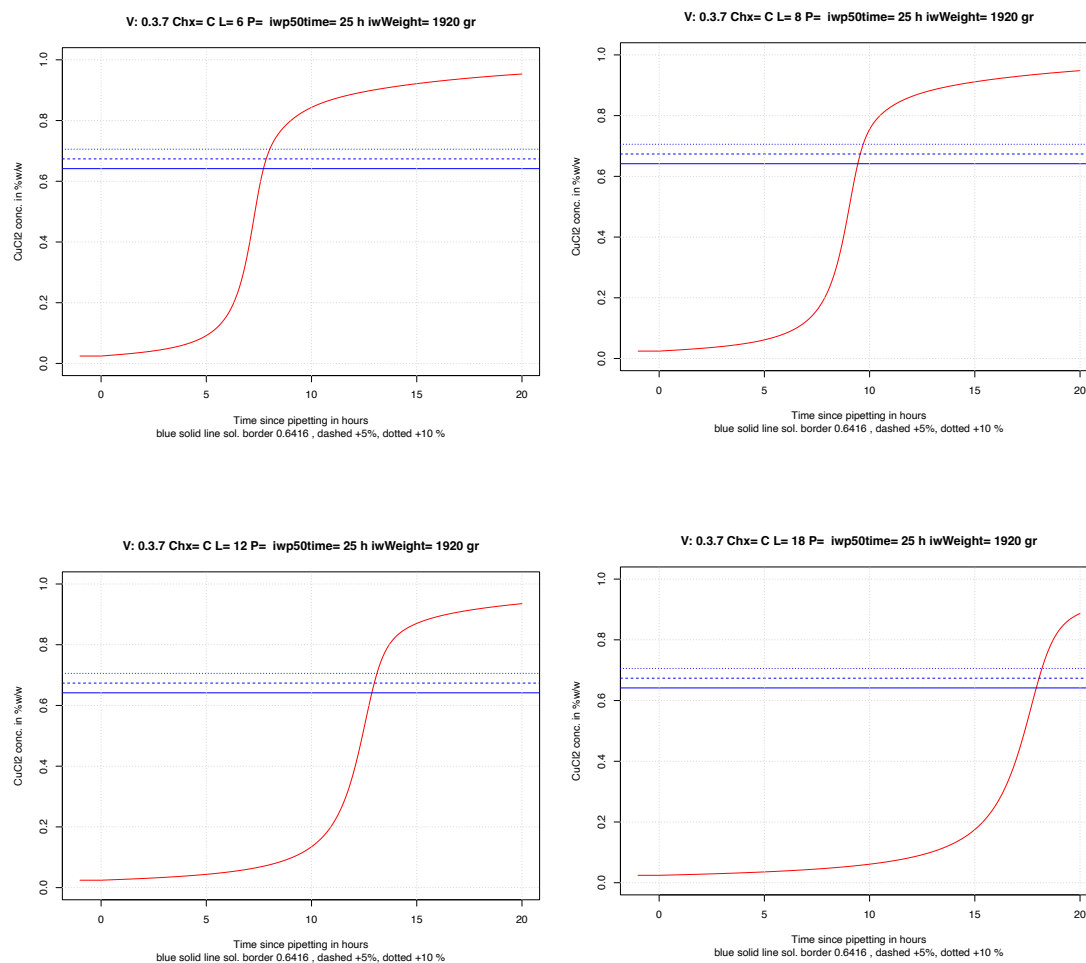


Fig. 2.13.6 The red curve represents the DCC concentration in a dish in % (w/w) Y-axis plotted against the evaporation time for tube height L. Upper left plot, L = 6 mm; upper right plot, L = 8 mm; lower left plot, L = 12 mm; lower right plot, L = 18 mm. the horizontal continuous line represents the solubility border at 29 °C, the dashed line represents the concentration at 5 % supersaturation, the dotted line at 10 % supersaturation.

In Fig. 2.13.6 upper left plot ($L = 6$ mm) the solubility border is reached at 7.5 hours evaporation time, in the upper right plot ($L = 8$ mm) at 10 hours, in the lower left plot ($L = 12$ mm) at 12.5 hours and in the lower right plot ($L = 18$ mm) at 17.5 hours. Based on Fig. 2.13.6 the adapted length of the tube was set to 8 mm in the simulation model.

3. Time constant and impact of the wall effect

The effect of water absorption by the wall is reflected in the steepness of the humidity increase in the chamber volume after pipetting, and limits the height of the humidity signal in the chamber. Without the wall effect (Fig. 2.13.7, left), the humidity increases above the observed threshold of 67 %. The wall effect lowers the maximum humidity in the chamber. The importance of the wall effect has been considered with respect to the so called “hold-on” phase. The parameters for the wall effect are the amount of water that can be absorbed (parameter $iwWeight$) and how fast this occurs (parameter $iwp50time$, giving the time for 50 % change). The parameters are calculated from experimental data in [Appendix 2.13.3 Weight](#) and can be different per Triangle chamber, depending on local differences of the wood characteristics.

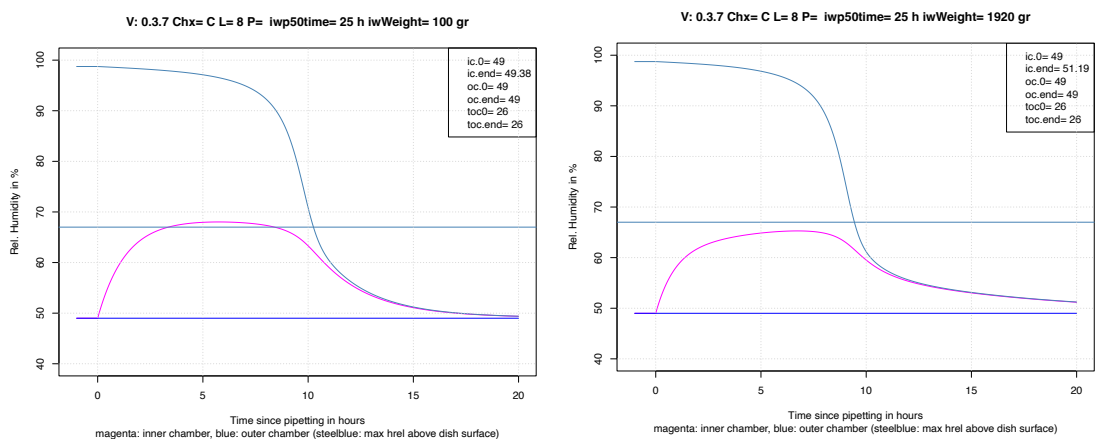


Fig. 2.13.7 Relative humidity changes in % in a Triangle chamber during the evaporation of DCC from a Petri-dish. Colors: magenta curve, inner chamber relative humidity, blue: outer chamber relative humidity, steelblue curve: relative humidity (partial pressure) above the solution. Steelblue horizontal line, 67 % saturation humidity above DCC solution at solubility border (Rockland 1960 [20]). Left : parameter $iwWeight = 100$ g (simulating more or less the absence of water absorbance by the chamber walls), right parameter $iwWeight = 1920$ g.

In Fig. 2.13.7 the so called “hold-on” effect can be seen. The humidity diffusion from the surface of the solution in the Petri-dish depends, according to Stefan (see formula 1 in [Appendix 2.13.1 Model, Evaporation from the dish](#)), on the difference between the partial pressure of the humidity in the inner chamber and the partial pressure above the dish, which depends on the DCC concentration in the dish. The higher the DCC concentration in the Petri-dish, the lower the partial pressure above the solution, the lower the evaporation rate. The partial-pressure of the DCC solution can be understood as the ability of the water to leave the solution.

The partial pressure above the Petri-dish is indicated by the steelblue curve in Fig. 2.13.7. At the beginning of the evaporation ($t = 0$ in Fig. 2.13.7) the partial pressure, expressed in relative humidity, is close to 100 %. This is the situation when no salt is in the solution. During the evaporation the DCC concentration in the dish increases and the partial pressure/relative humidity above the dish decreases.

At the same time the relative humidity in the chamber (magenta curve) increases due to the evaporating humidity from the dishes. After 8 hours the humidity in the chamber, magenta line in Fig. 2.13.7 right, reaches a maximum and the humidity starts to decrease again. The relative humidity above the surface of the dish decreases due to the increase of the DCC concentration in the Petri-dish. At $t = 10$ hours these two curves become very close to each other, which means that the evaporation nearly stops. This is the so called “hold-on” moment. The first crystallization can start at $t = 10$ hour.

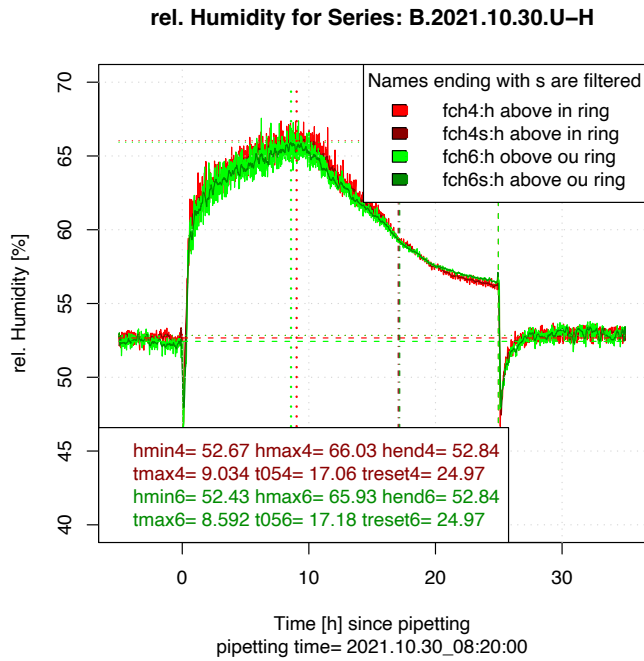


Fig. 2.13.8 Relative humidity (Y-axis) versus the evaporation time in hours (X-axis) for the experiment U-H from 2021.10.30 chamber B in Uni Kassel (D). Colors: red / green represent data obtained from sensors 14 cm above the reference Petri-dishes (raw data). The dark red / green lines are Savitzky-Golay (1964 [25]) filtered data (with an “s” in the legend name).

In Fig. 2.13.8 the pipetting starts at $t = 0$. The relative humidity above the dishes increases very strongly ($0 < t < 1$ hour), then slows down and increases slowly until the maximum value is reached ($1 < t < 10$ h). The relative humidity then decreases until $t = 25$, when the chamber door is opened and the humidity is exchanged with the outer chamber humidity. The maximum relative humidity is just below 67%.

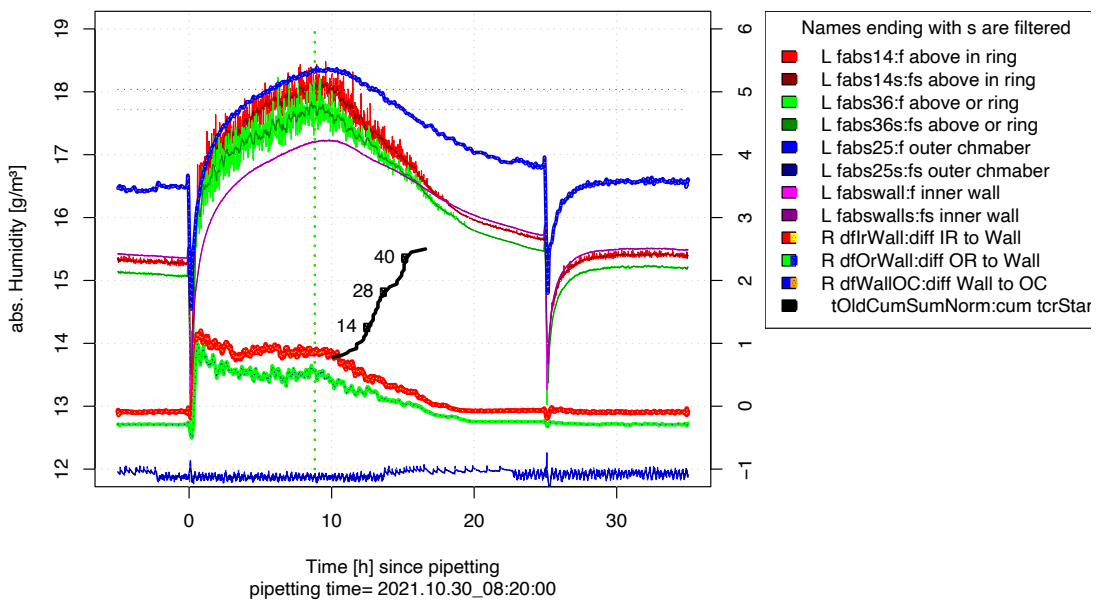


Fig. 2.13.9 Absolute humidity (left Y-axis) versus the evaporation time in hours (X-axis) for the experiment U-H from 2021.10.30 chamber B in Uni Kassel (D). Colors: red / green represent data obtained from sensors 14 cm above the reference Petri-dishes. The dark red / green lines are Savitzky-Golay (1964 [25]) filtered data (with an “s” in the legend name). Magenta: sensor at the inner wall of the chamber. Red-yellow and green-blue (lower lines) are the differences between the sensors above the dishes and the sensor at the inner wall, which is proportional to the humidity flow from the dishes (right Y-axis). Blue line at the bottom is the humidity at the outer wall in the outer chamber. Blue-orange line (top line) is the difference between the inner and the outer wall (right Y-axis). The black line is the cumulative number of dishes that have begun to crystallize.

Fig. 2.13.9 is from the same experiment as Fig. 2.13.8. The additional information is the black line with the cumulative numbers of dishes that have begun to crystallize. The line begins roughly one hour after the maximum of the humidity curve is reached. At the moment the evaporation from the dishes starts to decrease.

The parameter iwWeight (the amount of humidity that can be stored in the chamber walls) has a negative correlation with tcrStart. For the comparison of different iwWeight parameter values (100, 1920, 3840 g), the absolute humidity (1st row), the humidity flows (2nd row) and the DCC concentration (3rd row) are plotted Fig. 2.13.10.

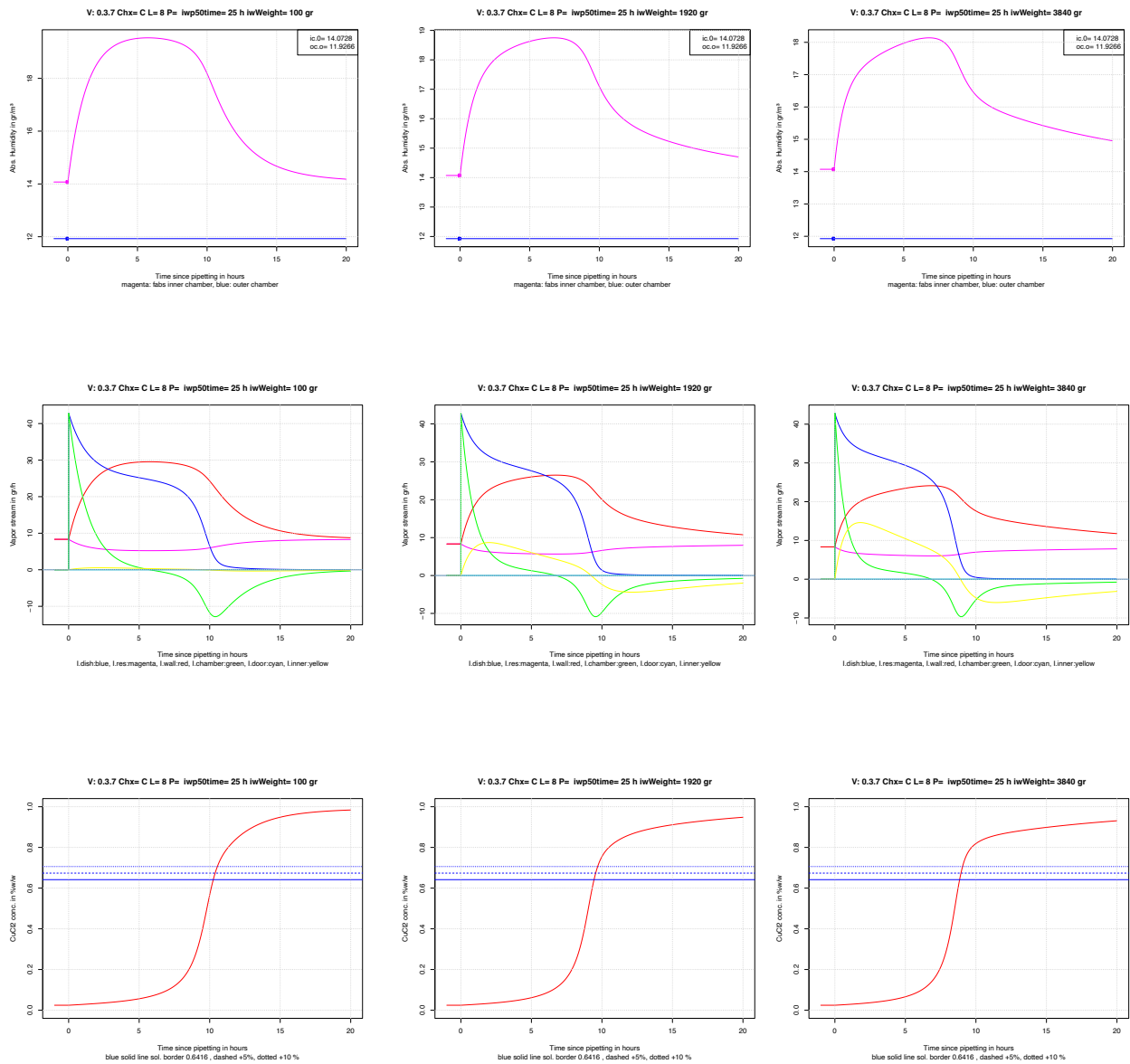


Fig. 2.13.10 Upper row: absolute humidity (Y-axis) in g / m³ versus time in hours (X-axis). Middle row: humidity flow in g / hours versus time in hours (X-axis). Lower row: DCC concentration in % (w / w) versus time in hours (X-axis). Left column parameter iwWeight = 100 g, middle column parameter iwWeight = 1920 g, right column parameter iwWeight = 3840 g. All other parameters are the same. Colors represent the different humidity flows: blue from the Petri-dish, magenta from the reservoir, red through the chamber wall, yellow into the chamber wall, green into the chamber volume.

In the top row of Fig. 2.13.10, the different absolute humidity curves during the evaporation are shown for the three iwWeight values. The curve in the right column has the slowest increase to the maximum humidity and is the closest to the measurement curves in Fig. 2.13.9. The tcrStart values decrease as the ability of the inner wall to absorb humidity from the chamber increases (left: 10 - 10.5 hours for 100 g, middle: 9 - 9.5 hours for 1920 g and right: 8 - 9 hours for 3840 g). This makes sense, because more water can leave the dish without having

to pass through the permeable wall to the outer chamber.

In the middle row of Fig. 2.13.10 the humidity flow per location is shown. At time point zero the pipetting takes place. Before pipetting only a red curve is visible, which is the color of the flow through the permeable wall to the outer chamber. Before the zero time point, this humidity originates from the reservoir only (magenta color, covered by the red line). Immediately after pipetting, the red line (humidity flow through the chamber wall) increases because more humidity is passing through the permeable wall, and the magenta colored line decreases because there is less humidity evaporating from the reservoir. The blue line is the evaporated humidity from the Peri-dish. Immediately after pipetting the flow is very high, but is increasingly impeded by the increasing humidity in the chamber. The green line represents the humidity filling the chamber (if positive) and leaving the chamber (if negative). The humidity flow into the chamber wall is yellow, which increases from left to right in Fig. 2.13.10, because the parameter *iwWeight* for the wall increased, so it can take more humidity in at the same time.

4. Partial pressure above DCC solution

The dependence of the partial pressure over the DCC solution on the DCC concentration in the solution is given by Lillich 1956 [19] and Lillich 1963 [18]. The temperature dependency of the relative humidity above a saturated DCC solution are from Rockland 1960 [20].

5. Density from own measurements and Beckmann

The dependency of the density of a DCC solution on the DCC concentration is from Beckmann 1959 [21] and Mergardt [22] 2012.

6. Temperature dependency of DCC solubility border

The temperature dependency of the DCC solubility border is from Beckmann 1959 [21], Gmelin 1958 [23] and Benrath 1934 [24].

Appendix 2.13.3 Weight

From the Checking Influences project the relation between air humidity and wood humidity has been determined. See report Checking Influences 2009 [8] p. 68. To estimate the amount that can be stored during evaporation (10 - 20 hours) the surface of the inner chamber is needed.

- The wall surface is 8 times $2 * 1 = 16 \text{ m}^2$
- The floor and the ceiling surfaces are each $= 1 * 2.4 + 2 * 1 * 0.7 * 2 + 0.7 * 0.7 / 2 * 4$
 $= 2.4 + 0.98 + 1.4 = 4.8 \text{ m}^2$

Total surface = $16 + 9.6 = 25.6 \text{ m}^2$

The data from the Checking Influences project over the project time (2 years) gave:

- 8.5 % wood humidity at 42 % air humidity
- 10.5 % wood humidity at 52 % air humidity

A 10 % change in air humidity resulted in a 2 % change in wood humidity.

The density of pine / spruce is 0.3 - 0.7 (Wood Handbook 1999 [26]), or 300 - 700 kg/m^3

When we assume a fast humidity access to 1 mm of the wood we get:

- $25.6 \text{ m}^2 * 1\text{E-}03 \text{ m} = 25.6 \text{ E-}03 \text{ m}^3$
- with $500 \text{ kg}/\text{m}^3 * 25.6 \text{ E-}03 \text{ m}^3 = 12.8 \text{ kg wood}$
- 10 % of 12.8 kg gives 1.28 kg of wood accessible to water, assuming 1 mm of wood is accessible.

The choice of the time constant and the weight amount are not independent from each other. In the simulation they are divided by each other.

References

- [1] Busscher N, Kahl J, Doesburg P, Mergardt G, Ploeger A. Evaporation influences on the crystallization of an aqueous dihydrate cupric chloride solution with additives. *Journal of Colloid and Interface Science* 2010; 344: 556–562 <https://doi.org/doi:10.1016/j.jcis.2009.12.045>.
- [2] Kahl J. NBGMJ-OAMH, Meier-Ploeger A. Bestimmung der Zeitabhängigkeit der Kristallisationsvorgänge bei der Kupferchloridkristallisation als eine Voraussetzung zur Validierung der Methode. *Elemente der Naturwissenschaft* 2004; 80: 90-100.
- [3] Holleman LWJ. Ein Beitrag zum Verständnis der empfindlichen Kristallisation. *Elemente der Naturwissenschaft* 1966; 4: 24-33 <https://doi.org/10.18756/edn.4.24>.
- [4] Stefan J. Ueber die Beziehung zwischen den Theorien der Capillarität und der Verdampfung. *Annalen der Physik* 1886; 265: 0655 - 0665.
- [5] McBain GD, Suehrcke H, Harris JA. Evaporation from an open cylinder. *International Journal of Heat and Mass Transfer* 2000; 43: 2117-2128.
- [6] Suehrcke H and Harris JA Enhancement of water evaporation from a cylindrical container due to concentration induced free convection (Twelfth Australasian Fluid Mechanics Conference, 1995).
- [7] Leray J. Profile de la surface libre d'un film liquide heterogene. *Journal de chimie physique* 1973; 10: 1428-1432.
- [8] Busscher N. Checking Influences: Untersuchung der Einflussgrößen bei der Biokristallisation als Voraussetzung für die Übertragbarkeit der Kammern und Prozeduren in andere Laboratorien und zur Reduzierung der Variationen durch die Kammer und die Orte. Technical Report, University of Kassel. 2009.
- [9] Thybring EE, Glass SV, Zelinka SL. Kinetics of Water Vapor Sorption in Wood Cell Walls: State of the Art and Research Needs. *Forests* 2019; 10 <https://doi.org/10.3390/f10080704>.
- [10] Assouline S, Narkis K, Or D. Evaporation from partially covered water surfaces. *Water Resources Research* 2010; 46: n/a-n/a <https://doi.org/10.1029/2010WR009121>.
- [11] Style, B. The evaporation of a salty film, 2007.
- [12] Style RW, Wettlaufer JS. Evaporatively driven morphological instability. *Physical review. E, Statistical, nonlinear, and soft matter physics* 2007; 76: 1-6.
- [13] Stefan J. Versuche über die Verdampfung. *Sitzungsberichte / Akademie der Wissenschaften in Wien, Philosophisch-Historische Klasse* 1873; 2: 385-423.
- [14] Prata AT, Sparrow EM. Diffusion-Driven Nonisothermal Evaporation. *Journal of Heat Transfer* 1985; 107: 239-242 <https://doi.org/10.1115/1.3247384>.
- [15] Sparrow E, Nunez G. Experiments on isothermal and non-isothermal evaporation from partially filled, open-

- topped vertical tubes. *International Journal of Heat and Mass Transfer* 1988; 31: 1345 - 1355 [https://doi.org/https://doi.org/10.1016/0017-9310\(88\)90244-X](https://doi.org/https://doi.org/10.1016/0017-9310(88)90244-X).
- [16] Weast RC CRC Handbook of Chemistry and Physics (CRC Press, 1984).
- [17] Massman W. A review of the molecular diffusivities of H₂O, CO₂, CH₄, CO, O₃, SO₂, NH₃, N₂O, NO, and NO₂ in air, O₂ and N₂ near STP. *Atmospheric Environment* 1998; 32: 1111-1127 [https://doi.org/https://doi.org/10.1016/S1352-2310\(97\)00391-9](https://doi.org/https://doi.org/10.1016/S1352-2310(97)00391-9).
- [18] Lilich LS, Timofeev VI. Dampfdruck in den Systemen: MeCl₂ - HCl - H₂O (ZnCl₂-HCl-H₂O und CuCl₂-HCl-H₂O). *Vestn.Leningr.Univ.Fiz.Khim* 1956; 10: 68-74.
- [19] Lilich LS, Sapozhnikova OV. Dampfdruck in den Systemen CuCl₂ - HCl - H₂O und Cu(ClO₄)₂ - HClO₄ - H₂O. *Izv. Vyssh.Uchebn.Zaved.Khim.Khim.Tekhnol.* 1963; X: 572-577.
- [20] Rockland LB. Saturated Salt Solutions for Static Control of Relative Humidity between 5 and 40 C. *Analytical Chemistry* 1960; 32: 1375-1376.
- [21] Beckmann H. Über Keimbildung, Einkristallwachstum und Auffächerungswachstum von CuCl₂ * 2H₂O in reinwässrigen und Eiweiß-haltigen Lösungen. PhD Thesis, Universität Bonn. 1959.
- [22] Mergardt G. Simulation des Entstehungsvorganges von Kristallbildern zur Messung der physikalischen Parameter pH-Wert, Dichte und Viskosität am Beispiel von PVP, Glykogen und Bovine Serum Albumin. Technical Report, University of Kassel. 2012.
- [23] Gmelin Gmelin Handbuch der anorganischen Chemie (Gmelin-Institut, Frankfurt am Main, 1958).
- [24] Benrath H. Über die Löslichkeit des Kupfer-2-chlorids in Wasser und die Umwandlungspunkte seiner Hydrate. Bemerkungen zu der gleichnamigen Arbeit von ERICHBOYE. *Z. anorg. Chem* 1934; 216: 207-208 <https://doi.org/https://doi.org/10.1002/zaac.19332160215>.
- [25] Savitzky A, Golay MJE. Smoothing and Differentiation of Data by Simplified Least Squares Procedures. *Anal. Chem.* 1964; 36: 1627-1639.
- [26] Forest Products L Wood handbook: Wood as an engineering material. (Forest Products Laboratory, 1999).

2.14 Self-organisation and $\text{CuCl}_2 \cdot 2\text{H}_2\text{O}$

Is the concept of self-organization applicable to the pattern formation in $\text{CuCl}_2 \cdot 2\text{H}_2\text{O}$ crystallization?

Abstract

The Rayleigh-Benard (RB) instability is used as an example to illustrate the concept of self-organization. The RB system is characterized and stabilized by the circular flow of oil, due to buoyancy and surface tension effects, creating regular pattern of convection cells called Benard cells. Crystal needles, including the $\text{CuCl}_2 \cdot 2\text{H}_2\text{O}$ (di-hydrate cupric chloride, further called [DCC](#)) needles, are also built by a so called self-organization process. While the building principle is the same as for the RB system, the underlying processes (local instability on atomic level and stabilization by diffusion and heat flow) are different. The applicability of the RB concept in understanding the pattern formation of the DCC crystallization with additives is considered. The DCC needle is formed by a self-organization process. The additive modifies this process, which can result in branching of the needle. However, the process by which the needles are arranged to create a pattern remains unclear. Because the nature of the process is unknown, it is not clear whether the pattern formation as such can be called a self-organization process.

Introduction

One of the main questions in connection with the $\text{CuCl}_2 \cdot 2\text{H}_2\text{O}$ (di-hydrate cupric chloride, further called [DCC](#)) crystallization with additives is the perception of a whole in the picture. The question that precedes the perception is to comprehend how a whole can be built. Are there concepts that describe the formation of a whole as it is perceived? (see chapter [2.15 Formation integrated pattern](#) and chapter [2.2 Arrangement](#)). One concept that appears on the border between physics and biology is the concept of self-organization. In its simplest form, it describes systems, where processes run in a logical order as the Rayleigh-Benard (RB) instability in a spatial cycle. The start and end point for an analytical input–output process can not be identified. Therefore, it is regarded as a self-organization system. Inside the cycle the system provides feedback for the stabilization.

The needle formation process of the DCC pattern is also called a self-organization system. The processes underlying the system are local instability and stabilization by diffusion and heat flow. DCC needles branching is based on the same process as the needle formation. This means that the parts (the needles) that make up the whole pattern are formed by a self-organization process. The additive modifies this self-organization process.

Until now, the process by which the needles are arranged as the parts into a whole remains unclear. This is discussed more deeply in the chapter [2.2 Arrangement](#).

Historical overview:

The first self-organization system was described by Benard 1900 [1], who observed structures while heating a pan with whale oil. The first part of the explanation (buoyancy) was from Benard [2] and Rayleigh [3]. The second part and final explanation (adding the surface tension effect) was done by Pearson 1959 [4]. Since the Rayleigh-Benard system is quite simple to understand, it gave the possibility to understand the principles of a self-organization system. The logical idea of a cycle is built here in the form of a spatial cycle.

The observations which Benard made were very simple. At one point, as he heated the whale oil, hexagonal structures of several cm in size appeared in the pan (see Fig. 2.14.1). They disappeared, when he removed the heat source and reappeared when he turned it back on again. When the heating was increased the structures became smaller and finally the whale oil started boiling. The physics behind the effect is simple. It is the transfer of heat from the bottom of the pan to the surface changing from conduction to convection. Heat conduction is when you burn your finger on the hot pan or when you sit still and wait until your hair dries. Heat convection is when the water is boiling or when a hot wind is drying your wet hair. The conduction in the pan is increased Brownian motion, but the solution does not move/flow. The convection is when the solutions moves/flows. This can be seen as an emergent property of whale oil, or as a special process that transforms increasing Brownian movement into a shape.

Rayleigh Benard effect

The following chapter describes the basic physical processes of how structures emerge -by self-organization- and that the driving “force” is the negative entropy flow.

As an example of a self-organization system the Rayleigh Benard [3] effect is discussed. The effect is an example of so called spontaneous building of a structure facilitated by a negative entropy flow in an open system. The experimental design is the following. An oil film is heated from below with heat amount (power) dQ . This creates a temperature gradient between the temperature at the bottom T_b and the temperature at the surface T_s .

For the open system is $dQ/T_b - dQ/T_s < 0$ because $T_b > T_s$. Normally one would expect the Brownian motion to increase with heating. The heat moves from the bottom to the surface. When the temperature gradient

increases to a threshold, heat transfer changes from conduction to convection, forming e. g. hexagonal structures (see Fig. 2.14.1 left), in which the oil circulates.

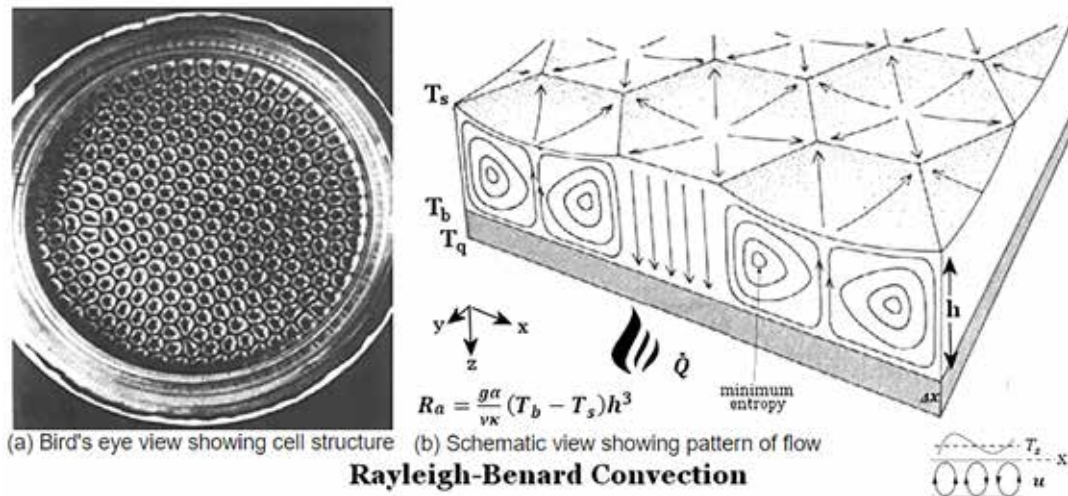


Fig. 2.14.1 Benard cell from above (left) and schematic from the side (right). From: <https://universe-review.ca/R13-09-thermodynamics08.htm>

When the gradient drops below the threshold the structures disappear. The oil circulation is done in a geometrical form (Fig. 2.14.1 right), defined by the process. If you think of the Benard Cell as a cooling pump, it creates and maintains the necessary pump-walls itself. This self-organization process is not like the self-maintenance of a biological system to keep itself in shape (like homeostasis for physiological processes), but the form and function of the “pump” is constantly maintained.

Another interesting detail is to study the transition from conduction to convection (see Fig. 2.14.1 right). It starts at the bottom with very small volumes of hotter oil, which is lifted by buoyancy. When this volumes reaches the surface, a small area of the surface has a higher temperature. This lowers the surface tension in this small area (Pearson 1958) [4] and (Anand 1969) [5] and the resulting forces move the oil on the surface toward the cooler side. From below the surface more hotter oil rises, and at the cooler part of the surface, cooler oil flows downwards. The effect is amplified by the positive feedback, as more volumes of “hot” oil flows upwards from below. The process stabilizes by circular flow and the formation of structures. This is a characteristic principle of a self-organization system. It starts with a positive feedback, which could grow “endlessly”. On a “higher” level the system is stabilized by building a structure. The driving forces are linked to each other, so that no “outer” forces have a direct causal influence. Therefore, the process is called self-organization.

Prigogine [6] quantifies the transition from the Brownian motion (conduction) to self-organization (convection) by the so called coherence length. This length was defined by Einstein in 1905 [7] when discussing the temperature-driven total atomic movement of one atom in a solution. In the case of conduction Einstein estimated the coherence length for Brownian motion to be below 10^{-05} cm [7]. Convection involves billions of atoms moving in the same direction. The coherence length in the case of convection is the diameter of the Benard cells, which is in the order of cm. In the case of the DCC picture it can be as large as the diameter of the dish, if the crystal needle branches extend from the center to the rim of the Petri-dish.

Resume Rayley-Bernard

This self-organization effect is driven by a temperature gradient. When the gradient increases and passes a threshold the heating transport changes from conduction to convection. This is a transition from an intensified atomic Brownian motion to a coherent movement of billions of atoms. The movement builds structures, whereby the form of the structure is maintained by the process. The process within the structures has a cyclic form. No starting and end point can be assigned. Therefore it is called a self-organization system.

Here we see three levels: First, a heated oil in a pan, where the coherence length is defined by the Brownian motion [7] (1^{-05} cm), which increases by conduction as the temperature increases. The second level is the switch to convection, where the coherence length jumps to 1 cm and billions of atoms are moving in the same direction. The third level is the Petri-dish with the DCC crystals in the dish. The crystals are not aligned in the same direction but rather towards the rim of the Petri-dish AND towards each other in such a way that they form a picture(see Chapter [2.2 Arrangement](#) , sub chapter *Wachstums-feld*).

Self-organization and the DCC system

The first who connected the concept of self-organization with the DCC system was Nitschmann [8] who considered the DCC system to have a “self” that controls the process. Then, as an answer to Hummel [9] (See also Chapter [2.3 Crystal growth and branching](#)) Nitschmann [10] described the processes in the Petri-dish (see also in Chapter [2.16 Complex physical versus simple biological](#)), such as evaporation, nucleation, growth, and compared them to the seven live processes described by Steiner [11]. Busscher [12] showed that one of the driving forces of the DCC system is a temperature gradient. There is a higher temperature at the bottom of the dish and a lower temperature at the evaporating surface of the solution (see Chapter [2.16 Complex physical versus simple biological Appendix 2.16.1](#)). This temperature gradient is similar to the condition in the RB system. A continuous flow of warmth passes through the Petri-dish. As in biological systems, this allows structures to be generated, e.g. by a self-organization process.

Usually crystals including DCC crystals, grow in layers at “low” supersaturation and “low” growth rates as described by Reiter [13], Leray [14] and Beckmann [15]. Conversely the DCC needles in the context of the DCC system exhibit higher growth rates [16] (Fig. 11 left). It does not grow as a planar (2-dimensional) structure, but rather as a 1-dimensional structure (with a volume around it), because the DCC crystal has a preferential growth direction (an anisotropic c axis).

The DCC needle process is a self-organization process: This statement is based on a so called structural undercooling [17] (see in [Appendix 2.14.1 Structural undercooling](#) below), which results in instability at the molecular level. The instability amplifies itself and therefore behaves like an explosion. The instability is captured by a macroscopic process (diffusion of DCC to the needle and crystallization heat transfer away from the needle) and forms a needle due to the anisotropic behavior of the crystallization. The branching of the needle is the same process. Again an instability starts the needle formation [17]. In the metallurgic science the described process is a well-known phenomenon and dendritic growth is used e.g. for building turbo blades for aircraft engines. The type of dendrite depends on the mixture ratio of the involved compounds in question and the growth velocity of the structures. This dependency is shown in a so called morphology map [18], where the properties (e.g. type of crystal) of a mixture depend on the mixing ratio and the growth velocity.

Resume

The concept of self-organization process seems applicable to needle formation and DCC needles branching. The process behind the formation of the pictures is unknown, which is essential to the understanding of the perception of wholeness and the connection to the sample. Therefore, it cannot be decided whether the picture formation is a self-organization process or not.

Also, the common understanding of the self in self-organization is seen as an emergent effect and not as a “self” that “steers” the process as Nitschmann [10] pointed out. The “Lego” way of thinking expects the wholeness to emerge from the parts (bottom-up), rather than the parts being organized by a self (top-down), which can be perceived as a whole by a human being. There is an interesting way of looking at this problem, discussed by Mukherjee and Sharma [19], who distinguish between bottom-up (self-assembly, block building, e.g. crystal growth) and top-down (self-organization, e.g. surface-tension dewetting) processes. See also Chapter [2.2 Arrangement, Hypothesis meso-crystals](#)

Additional research

The additional research is described in the Chapter [2.2 Arrangement](#).

Appendix 2.14.1 Structural undercooling

The appearance of needles is in general a special case of crystal growth. The formation of a needle is due to anisotropy of the material and instability of the growth process. In the following the instability, which is called structural undercooling, is explained. The explanation is based on Billia Trivedi [17] (Handbook of crystallization) Fig. 4 (p. 909 and Fig. 6 (p. 911) and S.Langer [20] Fig. 5 (p. 6) and Fig. 6 (p. 7).

Short description: The structural undercooling is a dynamic effect. When the growth velocity of the crystal passes a threshold the conditions in an area of the solution directly in front of the growing crystal change from a pure liquid solution phase to a state where both liquid and solid phases can exist. This is explained in the following by using Fig. 2.14.2 (a) and (b) and Fig. 2.14.3.

In Fig. 2.14.2 (a) the dependency of the solute concentration (Y-axis) on the distance z (X-axis) is shown. The X-axis includes the interface between the solid (left) and the liquid (right) where the growth occurs. The concentration is higher close to the solid than in the bulk area of the liquid. The gradient of the concentration in the liquid depends on the growth velocity. The higher the growth velocity, the steeper the concentration curve (not shown in Fig. 2.14.2 a, but in Fig. 2.14.3).

Fig. 2.14.2 (b) shows the so called phase diagram of a mixture of e.g. a salt and water. The concentration of the mixture is plotted on the X-axis and the temperature of the mixture is plotted on the Y-axis. It simply shows at which temperature and which concentration the phase is liquid or liquid + solid or solid. The three phases in Fig. 2.14.2 b are separated by two bold lines which are marked with the distance ΔT_0 at C_0 . Above the lines the phase is liquid. Between the lines the phase is liquid + solid and below the lines the phase is solid. This means that the temperature at which the solution "freezes" is lower for higher concentrations of the solute. This effect is used when salt is spread on roads during snowfall to turn ice into water. The lower the temperature the more salt has to be added, to change the snow into water.

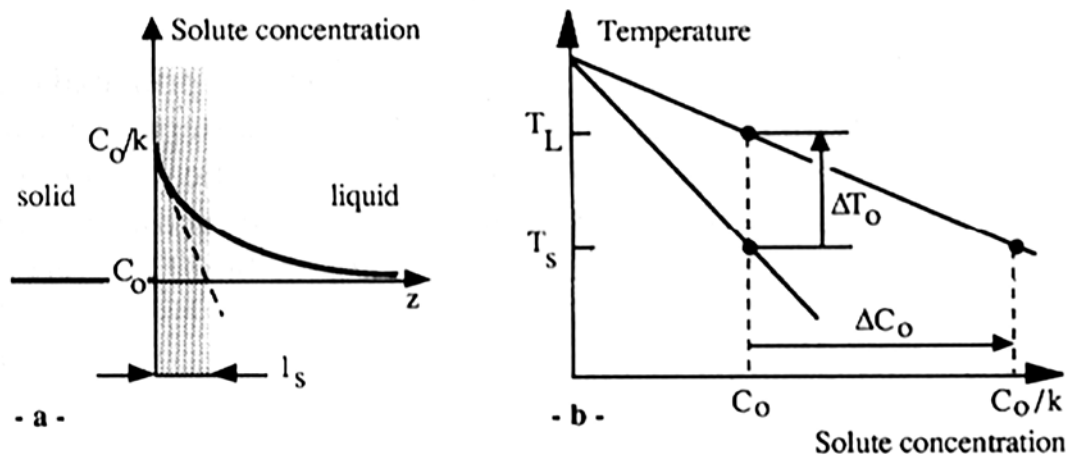


Fig. 2.14.2 (a) Solute profile in the liquid phase ahead of a planar solidification front, illustrating the solutal length scale l_s . (b) Phase diagram of a binary alloy, showing the the solute miscibility gap ΔC_0 and the freezing range ΔT_0 , which give, respectively, the concentration and temperature scales.

How to combine the two plots into one? This is described in detail by Langer [20], p. 7, Fig. 6). The basic idea is, that from the experimental conditions the Z-axis in Fig. 2.14.2 (a) can be converted by a simple calculation into a temperature axis as the Y-axis in Fig. 2.14.2 (b). The Y-axis of Fig. 2.14.2 (a) is already the concentration and is now plotted in Fig. 2.14.2 (b) on the X-axis. The concentration dependency is calculated for different velocities. The higher the growth velocity the steeper the curve in Fig. 2.14.2 (a) and in Fig. 2.14.3 is. Placing the information from 4 (a) in 4 (b) in this way produces Fig. 2.14.3.

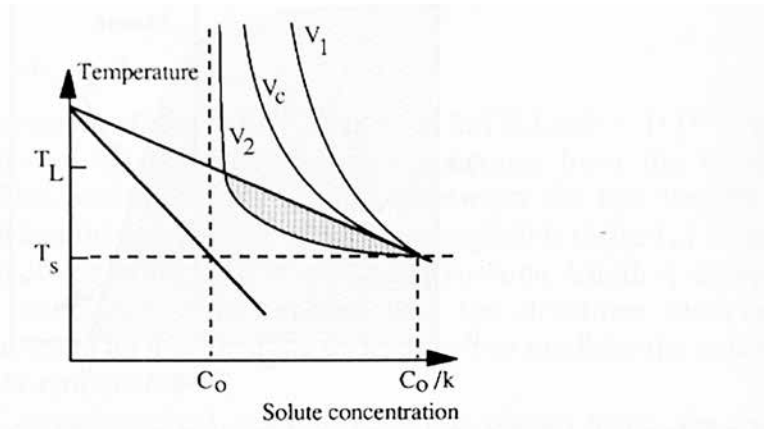


Fig. 2.14.3 Representation on the phase diagram of the building of constitutional supercooling in the liquid (grey area) as the growth velocity is increased above the critical velocity V_c ($V_2 > V_c > V_1$).

In Fig. 2.14.3, the conditions for three growth velocities V_1 , V_c and V_2 are shown. At the lower growth rate, V_1 , the phase in front of the growing crystal is made up only of liquid. (above the upper curve). When the growth velocity increases to V_c , a critical limit is reached. When the growth velocity exceeds this threshold up to V_2 , the phase in an area in front of the growing crystal below the upper line (shaded in Fig. 2.14.3), becomes liquid + solid. This implies a local “undercooling” of the solution, resulting in an instability in front of the growing crystal.

References

- [1] Benard H. *Les-tourbillons cellulaires dans une nappe liquide. Revue générale des sciences pures et appliquées* 1900; 1261-1271.
- [2] Benard H. Les tourbillons cellulaires dans une nappe liquide. - Méthodes optiques d'observation et d'enregistrement. *J. Phys. Theor. Appl.* 1901; 10:254-266 <https://doi.org/10.1051/jphystap:0190100100025400>.
- [3] Rayleigh L. On convection currents in a horizontal layer of fluid, when the higher temperature is on the under side. *Philosophical Magazine Series 6* 1916; 32: 529-546.
- [4] Pearson JRA. On convection cells induced by surface tension. *Journal of Fluid Mechanics Digital Archive* 1958; 4: 489-500 <https://doi.org/10.1017/S0022112058000616>.
- [5] Anand JN, Karam HJ. Surface deformation of thin coatings caused by evaporative convection : III. Theoretical and experimental observations. *Journal of Colloid and Interface Science* 1969; 31: 208-215.
- [6] Prigogine I. *Die Gesetze des Chaos* (Insel Verlag, 1998).
- [7] Einstein A. Über die von der molekularkinetischen Theorie der Wärme geforderte Bewegung von in ruhenden Flüssigkeiten suspendierten Teilchen. *Annalen der Physik* 1905; 322: 549-560.
- [8] Nitschmann G. Welches Selbst organisiert die Kristallisation? *Goetheanum* 1990; 429-430.
- [9] Hummel RE. Liefert die Kupferchlorid-Kristallisations-Methode einen Nachweis für die Gestaltkräfte des Lebendigen?. *Elemente der Naturwissenschaft* 1992; 57: 112-121 <https://doi.org/10.18756/edn.57.112>.
- [10] Nitschmann G. Gedanken zur empfindlichen Kristallisation mit Kupferchlorid . Im Anschluß an die Arbeit von R. E. Hummel: Liefert die KupferchloridwKristallisations-Methode einen Nachweis für die Gestaltkräfte des Lebendigen? *Elemente der Naturwissenschaft* 1993; 58: 14-19 <https://doi.org/10.18756/edn.58.14>.
- [11] Steiner R. GA 170, Kosmische und menschliche Geschichte Band I (Rudolf Steiner Verlag, 1992).
- [12] Busscher N, Kahl J, Ploeger A. From needles to pattern in food quality determination. *Journal of the Science of Food and Agriculture* 2014; 94: 2578-2581 <https://doi.org/doi:10.1002/jsfa.6498>.
- [13] Reiter G, Barth J-G. Some general remarks on crystallization in the presence of additives. *Elemente der Naturwissenschaft* 2010; 92: 39-61 <https://doi.org/10.18756/edn.92.39>.
- [14] Leray JL. Growth kinetics of hydrated cupric chloride. *Journal of Crystal Growth* 1968; 3-4: 344-349 [https://doi.org/DOI:10.1016/0022-0248\(68\)90172-3](https://doi.org/DOI:10.1016/0022-0248(68)90172-3).
- [15] Beckmann H. Über Keimbildung, Einkristallwachstum und Auffächerungswachstum von $\text{CuCl}_2 \cdot 2\text{H}_2\text{O}$ in reinwässerigen und Eiweiß-haltigen Lösungen. PhD Thesis, Universität Bonn. 1959.
- [16] Busscher N, Doesburg P, Mergardt G, Sokol A, Kahl J, Ploeger A. Crystallization patterns of an aqueous dihydrate cupric chloride solution in the presence of different amounts of Bovine Serum Albumin. *Journal of Crystal Growth* 2019; <https://doi.org/doi:10.1016/j.jcrysgro.2019.125272>.
- [17] Billia R, Trivedi R. Pattern Formation in Crystal growth, In: Hurle D editors, Handbook of crystal growth Elsevier; 1993.
- [18] Kurz W. Solidification Microstructure-Processing Maps: Theory and Application. *Advanced engineering materials* 2001; 3: 443-452 [https://doi.org/https://doi.org/10.1016/0956-7151\(94\)90044-2](https://doi.org/https://doi.org/10.1016/0956-7151(94)90044-2).
- [19] Mukherjee R, Sharma A. Instability, self-organization and pattern formation in thin soft films. *Soft Matter* 2015; 11: 8717-8740 <https://doi.org/10.1039/C5SM01724F>.
- [20] Langer JS. Instabilities and pattern formation in crystal growth. *Rev. Mod. Phys.* 1980; 52: 1-28 <https://doi.org/10.1103/RevModPhys.52.1>.

2.15 Formation integrated pattern

What can we learn from the laws and limits of a Gestalt perception to understand the process of the formation of an integrated pattern.

Abstract

The tree-like perception of a $\text{CuCl}_2 \cdot 2\text{H}_2\text{O}$ (cupric chloride di-hydrate, further called DCC) pattern with additives can be understood from the building conditions in the Petri-dish. What can additionally be learned about the building process by considering the laws and limits of a Gestalt perception? Is it possible to arrive at an approach as exists for color perception? Or does the approach of sensory analysis, as it is used today, fit better?

The possible combinations of stimuli to be taken into account are calculated for color, odor and Gestalt perception. Nevertheless this is only the start of an exploratory study, the numerical values for the possible combinations are quite different. While the combinations for colors are in the range of 6 to 7 digits, for odor they reach at least 120 digits, and for Gestalt evaluation they exceed a million digits. The approach for color evaluation can not be applied for Gestalt evaluation, as the number of possible combinations is simply too high, and color perception lacks a physical representation. The approach for odor, according to sensory analysis, is more appropriate. Metamerism, which is known for color and odor perception, has an equivalent in the size independent recognition of a Gestalt. This is an important consideration for us and raises some additional research questions.

Introduction

So far the other chapters have dealt with the building process from the physical, chemical or biological point of view. This chapter look at the building process from a Gestalt perspective. What are the laws behind this perception, what are the limits? This provides a different way of looking at the building process and a different way of acquiring an understanding of the building process. To understand Gestalt perception, it is compared to the human perception of color and odor. There are references and norms for color and odor perception, and the norm for sensory evaluation is already applied to Gestalt evaluation of DCC pictures. How does Gestalt perception relate to these other two, and what are the common laws, concepts and limitations? This introduction ends with a description of the tree-like Gestalt and its background and starts looking at the picture as an array of pixels to compare this to the perception of color and odor.

How can we understand the plant or tree-like Gestalt of a DCC picture from the building process and how can we approach it from the side of the perception? The difference between a crystal and a plant can best be described by comparing the development of a crystal and a plant. A plant or tree starts from a seed. It grows in opposite directions, into the earth (darkness) and towards the sun (light). The plant changes its appearance during growth. From stem to branches to leaves, growing to flower and fruit to seed, while the rest of the plant decays. The plant grows to a defined size, in accordance with the conditions (Heitler 1964 [1], p. 41 ff.). The crystal also starts from something called a seed, and grows continuously by adding more of the same as long as there is enough salt in the solution. The needle has branches as an additional feature, so it can be considered one step closer to the plant, although there is no flowering, no fruit and no seed, and it can grow indefinitely. How can we perceive a plant-like impression from the DCC pictures, when the origins of plant and crystal needle are so different? Due to the concentration gradient (and DCC depletion) in the Petri-dish, the DCC needles grow through different mixing ratios of DCC and additive from start to finish (see chapter [2.4 Concentration gradient](#)). This results in different types of needles from the beginning to the end of crystallization, giving the impression of different stages of a plant or a tree. At the beginning of the growth the stems are broader whilst during branching, in most cases the branches become thinner and finally fade out as they reach the rim.



Fig. 2.15.1 Left: scanned DCC picture with apple juice as additive. Right: scanned DCC picture with cress extract as additive, showing the tree or plant-like structure from the crystallization start to the rim.

As can be seen in the picture from Waldburger in the chapter [2.2 Arrangement](#), the tree-like structure of the DCC crystallization is a consequence of the rim of the Petri-dish. The sample in question “modulates” this basic pattern, e.g. into different zones around the crystallization center (see chapter [1.13 Picture zones](#)) or to a complete breakdown of the crystallization gesture from center to rim, as occurs with the racemate mixture of mandelic acid (see DCC pictures in Mandelic acid in chapter [2.2 Arrangement](#)). The system of DCC and additive can produce DCC pictures that range between randomness and an ordered structure, depending on the additive.

In the following the number of possible patterns is calculated in relation to the perception of color or taste / odor. What is the “dimension” of visual perception compared to e.g. colors and RGB recognition or taste / odor perception?

How to count the “dimension” of the Gestalt perception?

We can define the “dimension” of a perception by determining the possible combinations which can be stimulated. The color perception and the taste / odor perception, which are well researched, are used as examples.

The simplest visual perception is connected to the visual recognition of a color (if the intensity of the light is high enough). Research on this question started more than 100 years ago and resulted in the CIE standards and norms (see [CIE \(International Commission on Illumination\)](#)). The CIE defined the smallest difference between two colors that a human can perceive as the value dE . On a normal screen, an 8 bit resolution is already possible for each basic Red, Green and Blue color. This allows $256^3 = 16.777.216$ color combinations. The human eye can distinguish even more combinations.

The CIE approach is that any color perceived by a human can be generated by superimposing the three primary colors (and receptors) red, green and blue, the so called XYZ representation. Color perception is based on the sensitivities to red, green and blue. Depending on the intensity of each of the three primary colors, the spectral colors can also be represented. The spectral colors are composed of a single wavelength and are located at the edges of the so called [CIE Color Space Diagram](#) which has a horseshoe-like form, see Appendix 2.15.3 CIE. In the middle of the horseshoe humans perceive white ($X = Y = Z$). The white point and the colors between the spectral border are perceptions which do not have a representation in physics (like the spectral colors do). Human perception constructs this by itself. The perception of color is based on three sensors, where the possible combinations are limited by the minimum sensitivity of a human being to distinguish between two colors. The perception of a color, besides the spectral colors, is something that can be stimulated by the external setting of the RGB combination. But it remains a human perception that doesn't have a physical representation like the spectral colors. Especially white is a special case that is innate to humans. There are also so called metamers (Wandel 1996 [2], p. 80) that stimulate the same human perception for different stimuli values.

The olfactory sense contains 400 so called odorant receptors (Billesbølle 2023 [3]). Following the above reasoning, if we were to consider these receptors as either being on or off, this would result in a system with 2^{400} combinations, which is a 120 digit number. It contains, like the visual system, so called metamers,

where different values at the sensors result in the same perception (Ravia 2020 [4]). Due to the vast number of combinations, this perception is not as easy to define and study as RGB color perception. The fact that metamers exist would indicate a common structure of human perception for both odor and color.

To estimate the number of possible combinations in Gestalt perception, the resolution in gray levels and in dots per inch needed to recognize e.g. a person in a picture can be tested (see Appendix 2.15.1 Resolution). From this the possible states of a system can be counted. The result of Appendix 2.15.1 Resolution is that at least 100 dpi * 100 dpi at 2 bit grayscale resolution are required for a reasonable Gestalt recognition. This values seem rather low. We will nevertheless maintain these numbers to make the calculations “easier” to follow. A normal picture has 256 gray levels and a resolution of 1000 dpi * 1000 dpi, which results in $256^{1.000.000}$ combinations, i.e. a number with more than 2.4 million digits.

To give an impression of how high the numbers are, they are calculated for a $10 * 10$ resolution. This is the case in Appendix 2.15.1 Resolution, where the photo of Einstein can hardly be recognized. A 10 dpi * 10 dpi at 2 bit grayscale resolution image results in $2^{100} = 1.26^{30}$ combinations, i.e. a 30 digit number. A picture with all white dots or all black dots has 1 possible combination of dot order in this $10 * 10$ area. A picture with one white dot has 100 combinations, a picture with 2 white dots has 4950 combinations, and a picture with three white dots has 161.699 combinations. While 50 dots offers 1^{29} possibilities. This means that if half of the picture is filled with white dots, there are 1^{29} possibilities to arrange the dots in a $10 * 10$ array. See Fig. 2.15.2 below for the number of dots set as the X-variable and $\log_{10}(\text{possibilities})$ as the Y-variable. The maximum combination size is reached when half of the dots are freely positioned. In our case, 50 out of 100. See Fig. 2.15.3 below for an example of a combination of 50 out of 100 squares.

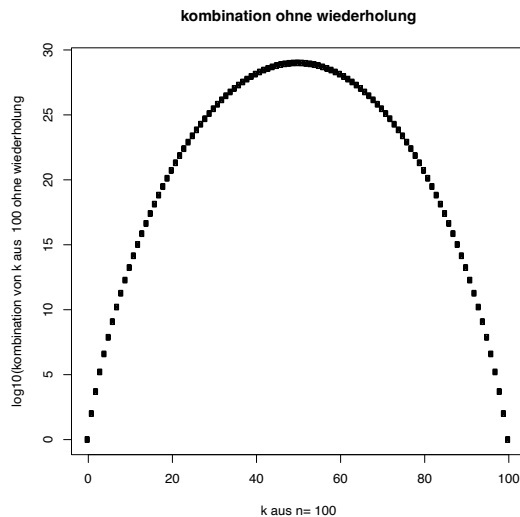


Fig. 2.15.2 Possible combinations (Y-axis) of k elements (X-axis) in an $n = 10 * 10$ array.

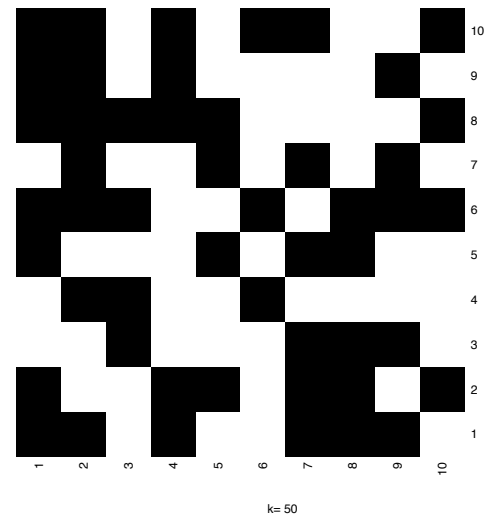


Fig. 2.15.3 $10 * 10$ array with a random combination of 50 white squares.

In Fig. 2.15.3 no Gestalt nor meaningful form is visible, and a Gestalt is expected to be seen seldom, as can be seen in Appendix 2.15.1 Resolution. Fig. 2.15.3 shows an interconnected structure that can only be experienced in the two dimensional representation. For the calculation of the combinations, the array could also be treated as a vector, building the vector by adding the lines of the picture one by one, creating a vector of 100 digits, and the calculations would still be valid. The connectedness of a structure in a picture requires a two dimensional representation. This is e.g. used by computer texture analysis. For the building process, all possible combinations can be created. For a Gestalt perception a minimum of a $100 * 100$ array may be necessary (see Appendix 2.15.1 Resolution). An array of $100 * 100$ would have $2^{10.000} = 10^{3010}$ possibilities (a 3010 digit number), and yet it is only a black and white picture. The brute force approach of calculating all combinations and subsequently calculating a GLCM or the structure analysis parameters and comparing them to those combinations that have a Gestalt determined by a human will simply take too long. This reflects the ability of humans to discern meaningful wholes in complex visual stimuli.

The question of how many combinations can be recognized as a Gestalt, cannot be answered. We can calculate, for example, how many combinations can be regarded as a geometric shape, like a circle or a square or a triangle. Since humans can recognize a shape regardless of its size (Galotti 2017 [5], p. 40) the geometric combinations can have different sizes, and the smaller they are, the more can exist.

In the Appendix 2.15.2 Rectangle it is demonstrated that the highest number of combinations for a $10 * 10$ array that can be obtained by reducing the size of the form to one pixel would of course be 100 combinations. Obviously, this size is too small to recognize any geometry, but it is sufficient to determine the magnitude. Compared to the above number of 1.26^{30} possible combinations at a 2 bit grayscale resolution, it can be estimated that the random combinations will largely predominate. As a side effect of these calculations, we can conclude that in visual perception size independent metamers occur. Also, in the visual context we can understand the metamer concept, while in the sensory and the color perception the conceptual background remains unclear. In addition, the visual system has something that is the “inverse” of a metamer, which can be seen in Fig. 2.15.4.



Fig. 2.15.4 The young-old-woman illusion (also known as the My Wife and My Mother-In-Law illusion), already popular in Germany in the 19th century when having been frequently depicted on postcards. Boring (1930 [6]) was the first who presented this illusion in a scientific context.

As Walcher (1994 [7], p. 21) remarks in the Introduction of Physics for Medics the image information that reaches the retina is mathematically exact. The subsequent perceptual process transcends the realm of physics. The picture shows an old or a young woman, depending on your point of view. The picture is given a meaning that goes beyond physics. There are several of these pictures, they constitute two meanings, no more. Maybe it depends on one's perspective. But it also works if you look with only one eye.

Resume

Where are we now, after calculating all these numbers, recognizing metamers and images with “double meanings” for the visual system? How can we get closer to a Gestalt? A brute force approach, as realized for color perception, would mean computing features from all possible combinations in an array to see if we can identify combinations that represent a Gestalt based on known Gestalts. The number of possible combinations of a $1000 * 1000$ pixel picture with 256 gray levels is a 2.4 million digit number (remember, a million has 6 digits), making this approach impossible. For color perception, where the brute force approach works, there are CIE standards and norms. For sensory analysis, with the same combination number problem as Gestalt perception, there are ISO norms (ISO 11035 and connected norms) to train panelists to evaluate food. The training is done with samples, that are close to or from the group of samples to be evaluated. It is well known, that there are well trained panels for wine quality evaluation. As we saw above, the combination for all possible sensory stimuli is at least a number with 240 digits. For the Gestalt evaluation, the number of possible stimuli is much higher. We saw that the system of DCC with additives in a Petri-dish generates tree-like structures whose Gestalt is modified by the sample in question. So far the only approach to deal with the Gestalt of the pictures is to adapt the ISO norms for sensory analysis (which has been done by Huber 2010 [8], Doesburg 2014 [9], Fritz 2018 [10]) and develop criteria that are derived from defined reference pictures, that are in the range of the different possible Gestalt variations to be evaluated.

What can we learn from the above for the building process. The Gestalt evaluation needs a minimum array resolution to perceive the Gestalt. The question of the gray level resolution could not be estimated because Einstein's photo could still be recognized, even though it was only a black and white photo. Interestingly, the computer texture analysis is based on the characterization of co-occurring grayscale values. The Gestalt perception has a metamer in the size independency of the Gestalt perception. There are also DCC pictures with smaller diameters

(e.g. von Hahn, 50 mm diameter, 1962 [11], and Manthei, 62 mm diameter, 2022 [12]). The question is whether the Gestalt formation is also independent from the size of the Petri-dish. There is an effect known from trees, that they adapt e.g. to the climate at different altitudes. Close to the tree line, the pines, for example, are quite small, but the species is still recognizable by its Gestalt.

Additional research

- Evaluate the image analysis results (e.g. texture analysis) for decreasing resolutions, and determine if and when the F-values for the differentiation starts to decrease.
- Can we test the necessary geometrical and gray level values required for human Gestalt evaluation by incrementally reducing them?
- Can we see the same Gestalt, when using different sizes of the Petri-dish? Is there a limit?

Appendix 2.15.1 Resolution

In the following the famous Einstein photo is used to show the influence of the array dimensions or granularity (the geometrical resolution, e.g in blocks).

Upper Left 10 * 10 blocks, upper right 20 * 20 blocks, lower left 40 * 40, lower right 100 * 100.



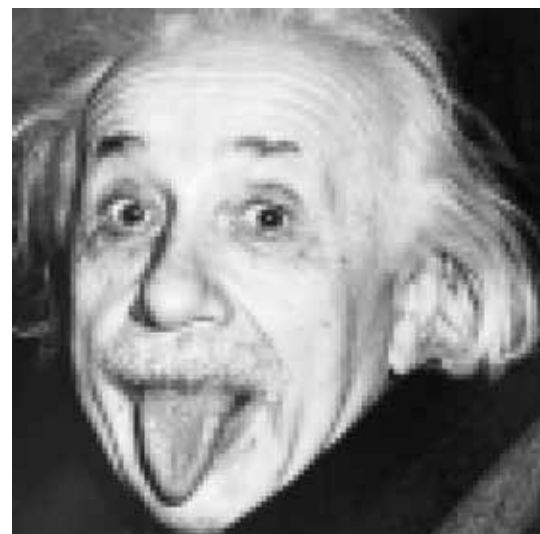
Array 10 * 10



Array 20 * 20



Array 40 * 40

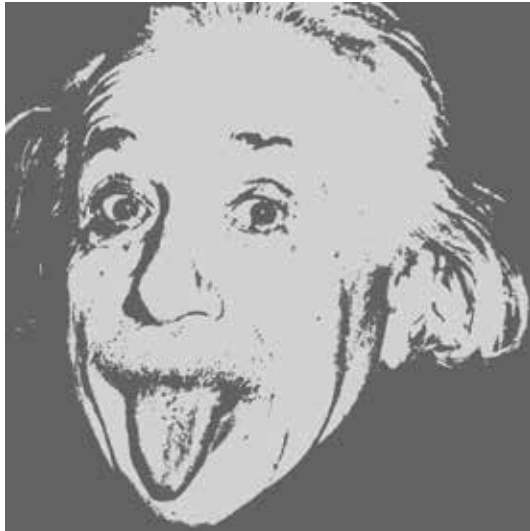


Array 100 * 100

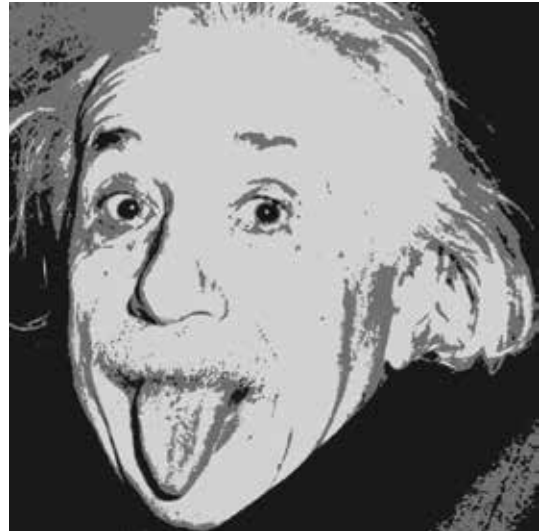
Fig. 2.15.5 Variations of the number of pixels in geometric resolution (dpi) of Einstein's photo required to recognize Einstein.

Interestingly, if one narrows the eyes to a slit, Einstein becomes more easily recognizable in the photos in Fig. 2.15.5. The resolution of 100 * 100 gave a reasonable perception.

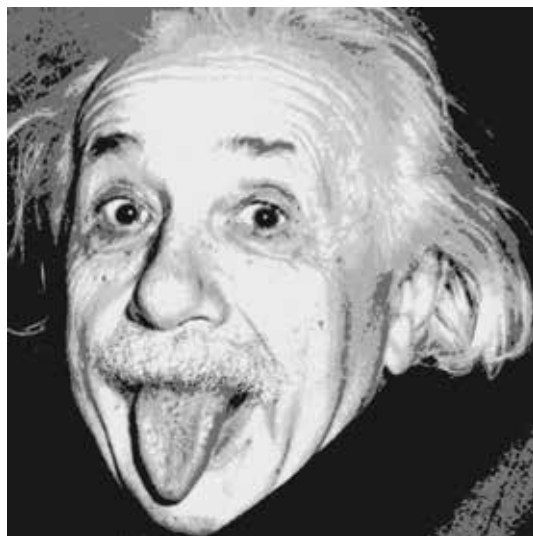
Reduction of the gray level resolution from 256 to 2 (black and white), see Fig. 2.15.6.



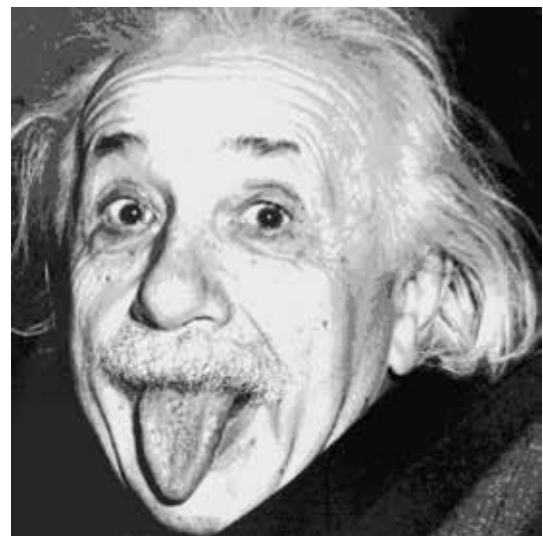
2 bit gray level



3 bit gray level



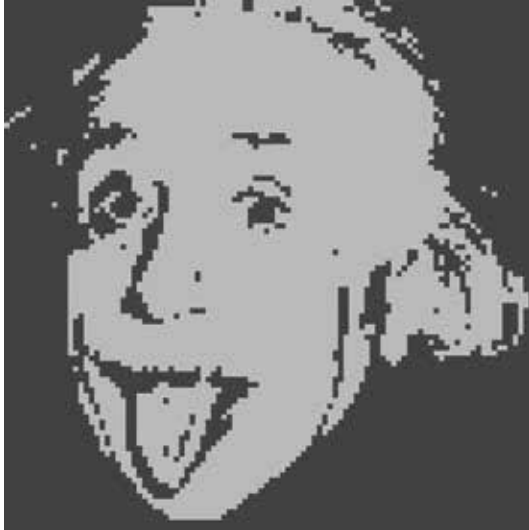
5 bit gray level



7 bit gray level

Fig. 2.15.6 Influence of the gray level resolution on the photo. (resolution granularity 1793 * 1793 dpi). The lower right picture is the original picture.

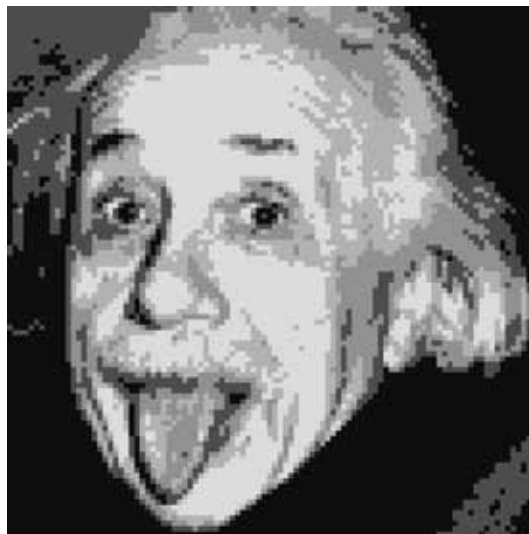
In the case of a granularity of $100 * 100$ pixels we get the following (see Fig. 2.15.7).



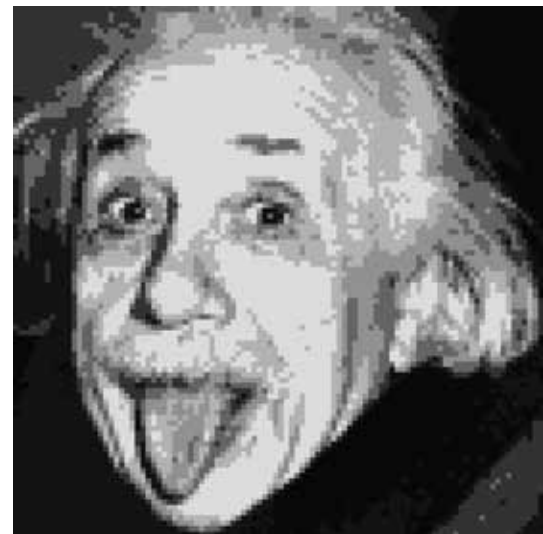
2 bit gray level



3 bit gray level



5 bit gray level



7 bit gray level

Fig. 2.15.7 Different gray level resolutions for a granularity of $100 * 100$ pixels.

Appendix 2.15.2 Rectangle

If the size of an image is $10 * 10$ ($np = 10$), the combinations of a rectangle with a size nr smaller or equal to the size of the array are calculated and listed in Table R.1.

Table 2.15.1 Combinations of adding a rectangle with nr line length in a $10 * 10$ pixel picture.

nr	$np - nr$	Combinations
$10 * 10$	0	1
$9 * 9$	1	4
$8 * 8$	2	9
$7 * 7$	3	16

The above results in Table 2.15.1 would point to $(np - nr + 1)^2$. So for $nr = 1$ we get 100, which is the possibility to arrange one pixel in 100 possible positions.

Appendix 2.15.3 CIE

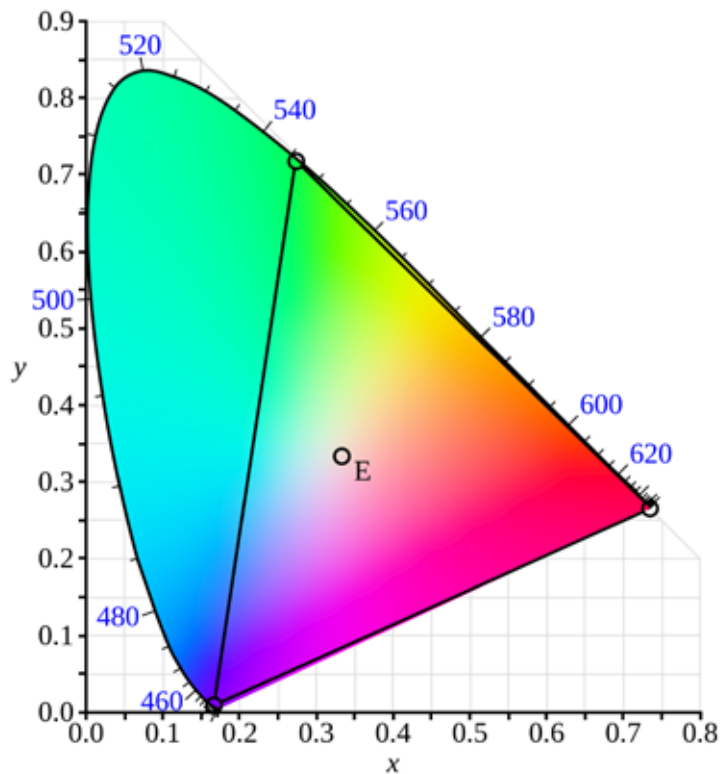


Fig. 2.15.8 The so called “horseshoe” from the CIE 1931 color space. The circle E denotes $X = Y = Z$, which is perceived by humans as white (see CIE Color space (Wikipedia) for more information). (Picture from BenRG, Public Domain).

The CIE color space in Fig. 2.15.8 shows the perceived colors by a human being, according to the RGB light stimulus. The border of perception, the outer curve of the “horseshoe”, where the wavelengths from 620 (red) to 460 (blue) are plotted, is the location of the spectral colors.

References

- [1] Heitler W Der Mensch und die naturwissenschaftliche Erkenntnis (Vieweg, 1970).
- [2] Wandell BA Foundations of Vision (Sinauer Associates, 1996).
- [3] Billesbølle CB, de March CA, van der Velden WJC, Ma N, Tewari J, del Torrent CL et al. Structural basis of odorant recognition by a human odorant receptor. *Nature* 2023; 615: 742-749.
- [4] Ravia A, Snitz K, Honigstein D, Finkel M, Zirler R, Perl O et al. A measure of smell enables the creation of olfactory metamers. *Nature* 2020; 588: 118-123.
- [5] Galotti K Cognitive Psychology In and Out of the Laboratory (SAGE Publications, 2017).
- [6] Boring EG. A new ambiguous figure. *The American Journal of Psychology* 1930; 42: 444–445 <https://doi.org/https://doi.org/10.2307/1415447>.
- [7] Kamke D and Walcher W Physik für Mediziner (B. G. Teubner Stuttgart, 1994).
- [8] Huber M, Andersen J-O, Kahl J, Busscher N, Doesburg P, Mergardt G et al. Standardization and Validation of the Visual Evaluation of Biocrystallizations. *Biological Agriculture and Horticulture* 2010; 27: 25–40.
- [9] Doesburg P, Huber M, Andersen J-O, Athmann M, van der Bie G, Fritz J et al. Standardization and performance of a visual Gestalt evaluation of biocrystallization patterns reflecting ripening and decomposition processes in food samples. *Biological Agriculture & Horticulture* 2014; 31: 128-145.
- [10] Fritz J, Athmann M, Andersen J-O, Doesburg P, Geier U, Mergardt G. Advanced panel training on visual Gestalt evaluation of biocrystallization images: ranking wheat samples from different extract decomposition stages and different production systems. *Biological Agriculture & Horticulture* 2018; 35: 1-12 <https://doi.org/doi:10.1080/01448765.2018.1492457>.
- [11] Von Hahn F-V Thesigraphie. (Franz Steiner Verlag, 1962).
- [12] Manthei, C.. Script Kupferchloridkristallisationen mit einfachen Mitteln, 2023.

2.16 Complex physical versus simple biological

Abstract

The gap between the view of the DCC system as a physicochemical system and a biological system is discussed. Some of the existing criteria for a biological system and the so far known physicochemical processes are compared. The gap cannot be closed, but a condensed description of the process has been formulated.

Introduction

When describing the building process of the $\text{CuCl}_2 \cdot 2\text{H}_2\text{O}$ (cupric chloride di-hydrate, further called DCC) picture, we think in terms of a complex physicochemical process (see physical level in chapter [2.2 Arrangement](#)). When we look at the DCC picture from the human evaluation side, following the Goetheanistic phenomenological approach (Bockemühl 1980 [1]), we treat the DCC picture as an image, as a biological structure (see biological level in chapter [2.2 Arrangement](#)). This fundamental gap between the physicochemical description of the process and its evaluation as a biological process has not been bridged to date. One possible solution is to hypothesize that during the process of evaporation until the end of crystallization, the DCC system passes through a phase in which the needle arrangement is biologically determined. This is expressed in the statement: *Is the DCC system a complex physicochemical system or a simple biological system?* The basic approach followed in this chapter, is to take the definitions of a biological system and check in which stages the DCC system fits to this. This poses the problems that we do not fully understand the DCC system in terms of physicochemical concepts, there are different definitions and criteria defining what a biological system (life) is, and the existing concepts are not suitable to differentiate living from non-living as Rosslénbroich stated [2]. Some concepts of a biological system and their criteria are listed below and compared to a Benard system (see chapter [2.14 Self-organization and \$\text{CuCl}_2 \cdot 2\text{H}_2\text{O}\$](#)) and DCC processes with and without additives. The additive amount is defined by the criteria of having one center and remaining below the beginning of the substance spiral area in the concentration matrix. The preferred area is the area of the split-growth or dendrite crystal type in the concentration matrix (see chapter [1.9 Optimal amounts](#)). The additive is the initial element in the DCC system that generates the Gestalt.

Historical overview

Describing the problem

The first who addressed the problem whether the DCC system can be considered a complex physical or a simple biological system was Koopmans in 1971 [3] p. 21, “...We believe that the phenomena of the crystallization method can only be mastered conceptually if we dare to include biology and the concepts demanded by the objects here”. He cited Wieser [4] (indetermination of a biological system) and Heitler [5] [6] “It’s becoming clear that biological behavior can ‘override’ the laws of physics” (1967, p. 179), when dealing with the evaluation problems of DCC pictures with blood as additive. Next was Nitschmann (1989 [7]) who described crystallization in general as a self-organization process and asked which self is organizing the process. In 1993 [8] he connected the DCC system to the seven live processes of Steiner 1992 [9].

Definition of biological systems (internet)

The criteria for a biological system or life are defined in different ways. One way is the reductionistic way consisting of five basic criteria:

Table 2.16.1 Five basic criteria for life (from the internet 2024.05.20).

Nr	Criterion	Description
1	Growth and development	Increase in size, while changing shape (most obvious for a plant: from seed through stem (and root) and leaves to blossom fruit and seed again).
2	Metabolism (material and energy exchange)	Assimilation, breathing, nutrition, excretion, warmth flow (open system), keeping the form while dynamically changing the parts.
3	Response to environment	React on outer influences (touch, humidity, temperature, air pressure).
4	Reproduction	As described in growth and development from seed to seed.
5	Agency	The ability to fulfill a purpose or to reach a goal.

The Brockhaus Encyclopedia (1970) also includes "Individuality" as a criterion for a biological system. Various sources consider cells as the basic unit (i.e. "unicellular").

The following is a review of the above listed criteria as they apply to the DCC system with additives.

Growth and development

The rim of the Petri-dish generates DCC and additive gradients from the geometrical center to the rim. These gradients result in different mixture ratios of DCC / additive throughout the dish. During growth, the different crystal types emerge, creating an overall tree-like structure (see also chapter [2.15 Formation integrated pattern](#)). According to Nüsslein-Volhard, the concentration gradient in dividing cells and the combination of different gradients [10] [11] [12] was at the beginning of life (cell division and form generating).

Metabolism (material and energy exchange)

The Petri-dish is an open system. In addition to the evaporation of water, a heat flux flows through the Petri-dish (see Appendix 2.16.1 Warmth). Busscher in 2014 [13], following Aoki [14], calculated the entropy export capability of the DCC Petri-dish system, which has the size of a tree leaf. Aoki 2012 [14] studied the biological behavior of various biological systems from leaves, to animals to humans to lakes. He follows Schrödinger's initial thoughts 1944 [15], who considered food as having a negative entropy. Aoki's main point is that a biological system (of plants, animals, humans, lakes, and the earth) can only function if the entropy it produces is exported. Also inside the Petri-dish, due to the DCC and additive gradients, there are flows of DCC and additive. Due to the reduction of the pH during evaporation (see chapter [1.7 Evaporation issues](#)) the additive is affected (entropy increase).

Response to environment

The dendritic and split-growth crystal types respond differently to the climate parameters. In the case of dendritic growth (see chapter [1.8 Concentration matrix](#)), the growth of one dendrite would look like a pine tree (Kahlweit 1970 [16], Fig. 5 and 7), a triangular shape with the apex pointing in the growth direction. In the DCC picture, there are several dendrites that would overlap if they would not interact with each other during growth (see Fig. 2.16.1 right).

The split-growth crystal type starts with a 0.5 to 1 cm linear needle, which grows in both directions and starts branching. The branches grow into an open space and almost form a circle (a hole) until both directions of growth meet (see Fig. 2.16.1 left).



Fig. 2.16.1 Left: DCC with BSA displaying the split-growth crystal type. Right: DCC with BSA displaying the dendritic growth crystal type. Data from Busscher 2019 [17] Fig. 6, Fig. 7.

The DCC system is sensitive to the climate parameters as relative humidity and temperature (see chapter 1 [Practical considerations](#)).

Reproduction

The formation of a seed as the beginning of the crystallization is considered by Nitschmann 1993 [8] as a reproductive step. This is of course much simpler than the biological process, where e.g. for a plant the seed is the start and end of life, or where male and female cells unite. Maybe it is comparable to the level of vegetative reproduction.

Agency

The concept of agency, which means that something is organizing to fulfill a purpose (Watson 2024 [18]), or reach a goal, is a concept which fits for different reasons. From the human Gestalt evaluation the criterion Center coordination (Huber 2010 [19]) was defined and is still used as an important criterion, perceiving to what extent the primary crystallization center is able to coordinate the picture elements like a conductor. This also implies that the three zones are connected (see chapter [1.13 Picture zones](#)). The other reason why this concept seems applicable to the DCC system is that the variations of the system can be seen as an disturbance or a degree of freedom, which are used by the agency to reach its goal. See chapter [2.17 Lowering disturbances](#) for details.

Table 2.16.2 Attributes of Benard and DCC systems with and without additive.

System	Growth and development	Material and energy exchange	Response to environment	Reproduction	Agency
DCC Bulk growth	Yes	Yes	Yes	(Yes)	No
Benard System	Increasing cell numbers	Yes	Yes	No	No
DCC Needle growth	Yes	Yes	Yes	(Yes)	No
DCC Needle growth with additive	Yes	Yes	Yes	(Yes)	Yes

Living systems definition

There is also the definition of living-systems (Miller 1978) [20], which is based on open self-organizing systems, which are maintained by a flow of information, energy and matter. From Wikipedia: ([Living Systems](#)) *“Instead of examining phenomena by attempting to break things down into components, a general living systems theory explores phenomena in terms of dynamic patterns of the relationships of organisms with their environment.”* For the DCC system, the flow of matter is represented by the evaporation of the water and the flow of DCC and

additive through the gradients in the Petri-dish. The energy part is described by the entropy export (see subject heading Metabolism above), while the information is defined by the additive.

Other Criteria

In addition to the general criteria that characterize the context of life, several criteria were found that are related to the known conditions of the DCC system.

Individuality (Brockhaus 1970) - Agency

This term was first introduced by Nickel in his 1968 thesis [21], and discussed by Koopmans 1971 [3]. Our observations showed that no identical pictures are formed, although the solutions in the Petri-dishes are pipetted from the same solution. In the Checking Influences project (2009 [22]) we could see that the variation is not only due to the different crystallization starting times (tcrStart), but that the tcrStart correlates to the different locations on the evaporation unit. If we consider the variation in the tcrStart as a degree of freedom (see chapter [2.17 Lowering disturbances](#)), then in each Petri-dish the agency tries to deal with the conditions and attempts to generate THE individuality. The question is how this differs for samples from chemical sources such as BSA or PVP versus fresh juice or extract.

Limitation of form (Heitler [6])

The form of the DCC picture is limited by the glass plate to 2 dimensions. What e.g. a leaf does by itself, depends on the ring and the defined volume of the solution for the DCC system. The shielding of the ring creates a concentration and temperature gradient (like Benard) which is the reason for the tree-like structure (see chapter [2.15 Formation integrated pattern](#)).

Concentration Gradient (Wachstumsfeld)

Nickel (1986 [21]) showed in his thesis the concept of the *Wachstumsfeld*, created by the concentration gradient in the dish as a consequence of the shielding by the acrylic ring (see P1 in chapter [2.2 Arrangement](#)). The acrylic ring, which causes the concentration gradient, in combination with a DCC / additive mixture ratio that results in one-centered [pictures](#), forms the boundary condition for the appearance of a picture or an image. In this context it is interesting that Nüsslein-Vollhardt in 2004 [10] p. 34 describes the basic conditions for the start of the spatial organization of a fertilized *Drosophila* egg, before the start of further cell division, as “*concentration gradient and combination*”. In our case, we have the DCC concentration gradient and combined with it the additive concentration gradient, both of which change during the whole process (evaporation and crystallization). This was first pointed out as important by Petterson in 1969 [23]. As we know from the matrix experiments, the mixture ratio has a clear influence on the crystal types. When the mixture ratio changes from the geometric center to the rim, the crystallization types will change too, which is reflected in the appearance of a sensitive area in the dish. The ring of the Petri-dish, which creates the concentration gradient, is an important part of the DCC system.

Resume criteria

The DCC system has properties such as entropy export of the evaporating solution in the Petri-dish, responsiveness to the environment, and growth and development and agency, that also exist in living systems. The most interesting one is the agency, which is directly recognized as a criterion in the human Gestalt evaluation. The needles are built by self-organization systems.

Additional forces?

To discuss the idea of additional forces and how it is possible to research them, the following is written, starting from the limitations of the mathematical reductionistic approach.

The mathematical-materialistic approach is the one to choose if you want to build a machine that is supposed to run stable for years. It does not matter if the machine is an airplane or a car or a television or a computer or a washing machine. The building procedure is the same. It is a step by step process of building larger units from carefully built and tested smaller units or parts. If you do not do it in this way, you run into the problem of the 1986 NASA Challenger disaster described by Feynman [24]. The variation of the whole system - over its life time - is the sum of the variation of the parts over time. It works very well, as we can see in our world. But it is limited to the machine world as discussed by Heitler [6] and Wieser [4].

The parts of the organic world can also be constructed, e.g. proteins from atoms→amino-acids→peptides. But then the problem arises of how to arrange the parts, as a carrot seed does during its growth process. The building blocks can be understood from a bottom-up assembly perspective (as the proteins or meso-crystals [25]), but the arrangement of the blocks is more of a top-down concept (e.g. the wide range of CaCO₃ spine forms in sea-urchins [25] p. 51), or as discussed by Mukherjee and Sharma on thin films [26] and as Blasco 2024 [27]

formulates “*Top-down approaches can overcome the shortcomings of bottom-up techniques, providing pathways towards improved shape control,...*”. In animals and humans, the building blocks are replaced on the fly, so that the variation of the parts is kept constant over time. When we are dealing with living creatures, we can take into account additional forces that can, for example, create and maintain a Gestalt (Kiene 2023 [28]). Grohmann points out in his diploma thesis [29] that these forces (he discussed vitalism with Driesche as his mentor) cannot be the ones we know so far, otherwise they would have already been discovered in our technical world. This would mean that these forces cannot be used to build the usual mechanical machines. Steiner describes that these forces are not radial forces, as used to build a machine, but circumferential forces. This concept was applied to DCC pictures by Selawry 1955 [30] and Engquist 1975 [31]. They identified the split-growth needles as the ones affected by these additional forces (split-growth needles appear in the additive range where one-centered pictures exist). The forces act in a circumferential manner, while the DCC needles grow radially. The scientific question is how to study these forces, when they are not accessible by the usual technical measures?

Condensation

Looking at the physicochemical process, after reviewing the criteria of biological processes, the following can be formulated:

The DCC system is an open system and has (1) a heat flux through the system (entropy export, due to evaporation). It has a DCC concentration gradient (2) and an additive gradient (3) from the geometric center to the rim (due to the shielding by the rim) which generates the tree-like patterns. There is in addition a temperature gradient (3b). All gradients induce a surface tension effect (4) which is increased by the crystallization wave (5) (dewetting by crystallization) and is strongest in the middle zone. As the needles grow, initially in the central zone, they strongly interact with each other during their development due to the limited space available per needle. (6) When the needles enter the middle zone, the needles have more space to spread and the interactions between the needles decrease. In the middle zone, the effects (4) and (5) meet as either a top-down effect (surface tension, 4) or a bottom-up effect (needle crystallization, 5). In the peripheral zone, the crystallization wave has to deal with the depletion of the DCC and the increase of the additive and fades out toward the rim. The effects 4 and 5 are modulated / influenced by the additive and determine (7 agency) in the middle zone whether the central and peripheral zones appear as connected or whether they fall apart.

Resume

So far the question (simple biological system or complex physicochemical system) cannot be answered. One problem is the lacking definition of what a biological system is. From the living system definition, the dish with DCC and additive would fulfill these criteria. Also the entropy export of the system, according to Aoki, is fulfilled. The agency concept corresponds to the Gestalt criterion Coordination. The question of additional forces cannot be researched so far, because these forces are not detectable by technical equipment. From the definition of an organism the DCC system is not fulfilling the criteria, because the end product is a static crystal. The problem is that the possible behavior as a biological system is limited to the period between the pipetting of the solution into the Petri-dish and the end of the crystallization, the final dry crystal. The arrangement of the crystals is only an intermediate result of the process. The additive concentration at which the phenomenon occurs, can be determined by the criteria: one center, no substance spirals (see chapter [1.9 Optimal concentration](#)), but it is not clear why the system meets the criteria for a biological system in this additive range.

Additional research

Is the DCC picture variation of a solution from a fresh sample higher than from an aged sample?

Is there an “optimum” at a special DCC / additive amount?

- define DCC amount by contact to the ring
- diffusion and warmth transport. How is the dependency from the additive amount?
 - How does the warmth transport change with the additive amount?
 - is there a balance between diffusion and warmth transport for higher additive amounts?
 - (Stokes-Einstein relation between diffusion coefficient $diff$ and viscosity η : $diff \sim 1 / \eta$)
- What is special at the optimum mixture ratio, is this optimum different for image analysis and Gestalt evaluation?
- Which life processes are there?

Appendix 2.16.1 Warmth

In an open system the heat flux is the basis for entropy export, which is the basis for structure building.

Aoki [32] [33] [14]: the biological system (earth, plant, animal, human) is considered an open system from a physical point of view. The entropy for biological systems is defined in terms of entropy flow and entropy production. For biological systems, the total entropy flow is negative, exporting the entropy production of the system. The main entropy export is carried by the thermal flow.

The entropy flow in the dish: is comparable with the degree of entropy export from a leaf (Busscher 2014 [13]).

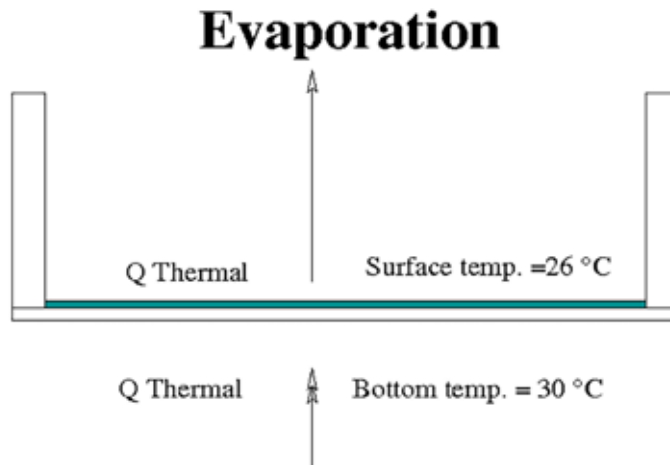


Fig. 2.16.2 Warmth flow through a Petri-dish with DCC.

References

- [1] Bockemühl J Lebenszusammenhänge, erkennen, erleben, gestalten (Naturwissenschaftliche Sektion am Goetheanum (CH), 1980).
- [2] Rosslenbroich B. Properties of Life: Toward a Coherent Understanding of the Organism. *Acta Biotheoretica* 2016; 64: 277-307 <https://doi.org/10.1007/s10441-016-9284-1>.
- [3] Koopmans A. Die Frage der Lokalisation im Kupferchlorid-Kristallisationsbild. *Elemente der Naturwissenschaft* 1971; 14: 19-30 <https://doi.org/10.18756/edn.14.19>.
- [4] Wieser W Organismen, Strukturen, Maschinen (Fischer Bücherei KG, 1959).
- [5] Heitler. Leben = Physik + Chemie ?. *Chimia* 1967; 21: 176-179.
- [6] Heitler W Der Mensch und die naturwissenschaftliche Erkenntnis (Vieweg, 1970).
- [7] Nitschmann, G. Die Kristallisation- ein System mit Selbstorganosation, 1989.
- [8] Nitschmann G. Gedanken zur empfindlichen Kristallisation mit Kupferchlorid. Im Anschluss an die Arbeit von R. E. Hummel: Liefert die Kupferchlorid Kristallisations-Methode einen Nachweis für die Gestaltkräfte des Lebendigen?. *Elemente der Naturwissenschaft* 1993; 58: 14-19 <https://doi.org/10.18756/edn.58.14>.
- [9] Steiner R GA 170, Kosmische und menschliche Geschichte Band I (Rudolf Steiner Verlag, 1992).
- [10] Nüsslein-Volhard C Von Genen und Embryonen (Reclam, Philipp, 2004).
- [11] Driever W, Nüsslein-Volhard C. The bicoid protein determines position in the Drosophila embryo in a concentration-dependent manner. *Cell* 1988; 54: 95-104.
- [12] Johnston DS, Nüsslein-Volhard C. The origin of pattern and polarity in the Drosophila embryo. *Cell* 1992; 68: 201-219 [https://doi.org/https://doi.org/10.1016/0092-8674\(92\)90466-P](https://doi.org/https://doi.org/10.1016/0092-8674(92)90466-P).
- [13] Busscher N, Kahl J, Ploeger A. From needles to pattern in food quality determination. *Journal of the Science of Food and Agriculture* 2014; 94: 2578-2581 <https://doi.org/doi:10.1002/jsfa.6498>.
- [14] Aoki I Entropy Principle for the Development of Complex Biotic Systems: Organisms, Ecosystems, the Earth (Elsevier Insights) (Elsevier, 2012).
- [15] Schroedinger E What is life? (Cambridge University Press, 1944).
- [16] Kahlweit M. On the dendritic growth of NH₄Cl crystals from aqueous solutions. II. *Journal of Crystal Growth* 1970; 7: 74-78.
- [17] Busscher N, Doesburg P, Mergardt G, Sokol A, Kahl J, Ploeger A. Crystallization patterns of an aqueous dihydrate cupric chloride solution in the presence of different amounts of Bovine Serum Albumin. *Journal of Crystal*

- Growth* 2019; <https://doi.org/doi:10.1016/j.jcrysgro.2019.125272>.
- [18] Watson R. Agency, Goal-Directed Behavior, and Part-Whole Relationships in Biological Systems. *Biological Theory* 2024; 19: 22-36.
- [19] Huber M, Andersen J-O, Kahl J, Busscher N, Doesburg P, Mergardt G et al. Standardization and Validation of the Visual Evaluation of Biocrystallizations. *Biological Agriculture and Horticulture* 2010; 27: 25–40.
- [20] Miller JG Living Systems, the Basic Concepts (, 1978).
- [21] Nickel E. Die Reproduzierbarkeit der sogenannten empfindlichen Kupferchloridkristallisation. PhD Thesis, Universitätsverlag, Freiburg (Schweiz). 1968.
- [22] Busscher N. Checking Influences: Untersuchung der Einflussgrößen bei der Biokristallisation als Voraussetzung für die Übertragbarkeit der Kammern und Prozeduren in andere Laboratorien und zur Reduzierung der Variationen durch die Kammer und die Orte. Technical Report, University of Kassel. 2009.
- [23] Pettersson BD. Beiträge zur Entwicklung der Kristallisationsmethode mit Kupferchlorid nach Pfeiffer IV. Wie verschiedene Kristallbilder bei der Pflanzenkristallisation entstehen. *Lebendige Erde* 1969; 3: 112-126.
- [24] Feynman RP Leighton, R. editors. What do you care what other people think? (WW Norton, 2001).
- [25] Cölfen H and Antonietti Markus Wiley 2008S1-6 Mesocrystals and nonclassical crystallization (Wiley, 2008).
- [26] Mukherjee R, Sharma A. Instability, self-organization and pattern formation in thin soft films. *Soft Matter* 2015; 11: 8717-8740 <https://doi.org/10.1039/C5SM01724F>.
- [27] Blasco CAS&E. Mass production of 3D microcomponents. *Nature* 2024; 627: 276-277.
- [28] Kiene H, Hamre HJ. A Fundamental Question for Complementary Medicine: Are There Other Forces in the Natural World Besides the Physical Forces?. *Complementary Medicine Research* 2023; : 1-7 <https://doi.org/10.1159/000534592>.
- [29] Grohmann G. Der Kausalitätsbrieff in seinem Verhältnis zum Vitalismus. *Tycho de Brahe Jahrbuch für Goetheanismus* 2003; : 7-18.
- [30] Selawry A. Studium von Zentralkräften und Universalkräften an Kupferchlorid-Kristallisationen. *Goetheanum* 1955; 43: 346-347.
- [31] Engquist M Physische und lebensbildende Kräfte in der Pflanze (Vitorio Klostermann, 1975).
- [32] Aoki I. Entropy and Exergy Principles in Living Systems, In: Joergensen SE editors, CRC Press; 2001.
- [33] Aoki I. Entropy production in living systems: from organisms to ecosystems. *Thermochimica Acta* 1995; 250: 359 - 370 [https://doi.org/DOI: 10.1016/0040-6031\(94\)02143-C](https://doi.org/DOI: 10.1016/0040-6031(94)02143-C).

2.17 Lowering disturbances

How to keep the evaporation, and the crystallization undisturbed from external influences?

Abstract

The term perturbation is discussed in the context of the $\text{CuCl}_2 \cdot 2\text{H}_2\text{O}$ (cupric chloride di-hydrate, further named DCC) system which can be seen as a complex technical system or a simple biological system (see also chapter [2.16 Complex physical versus simple biological](#)). The crystallization starting time is used as an example representative for the first degree of freedom. The second degree of freedom is represented by the multiple additive concentrations used in the same experiments. The third degree of freedom is represented by the “latency period” at the end of the evaporation before the start of the crystallization (see also chapter [2.13 Evaporation model](#)). As a fourth degree of freedom the concentration gradient between the geometric center and the rim of the Petri-dish is considered. From the historical development of the DCC system, factors of influence are described and classified as a perturbation or degree of freedom. These factors are then discussed according to the existing knowledge. In the section Additional Research further work is proposed.

Introduction

The definition of perturbations for the $\text{CuCl}_2 \cdot 2\text{H}_2\text{O}$ (cupric chloride di-hydrate, further named DCC) system is a matter of perspective. When we approach it from a physical-chemical (technical) point of view a perturbation is something different than if we look from a biological perspective (see also chapter [2.16 Complex physical versus simple biological](#)). For example the crystallization starting time ($t_{crStart}$) variation is a perturbation for a technical system, whereas it is a feature for a biological system. A technical system is defined by its boundary conditions, whereas a biological system deals with its boundary conditions to express itself. Therefore, factors which can be considered as perturbations in a technical context, can be degrees of freedom in a biological context. The DCC system has characteristics of both contexts, and to maintain both possibilities, the crystallization start is not initiated by seeding with a DCC crystal, but is allowed to self-initiate. Some samples deal with the $t_{crStart}$ in a different way than other samples. The question is whether there are more differences between a technical and a biological view of the DCC system, and what are the perturbations for both (like external vibrations or air pressure changes through the weather or lightning)? The conclusion of what is a perturbation and what is a feature is discussed according to the different chamber systems researches work with (see for different chamber system chapter [3.1 Chamber systems](#)).

Historical

Pfeiffer

The first description of the parameters and their variation came from Pfeiffer 1930 [1], 1931 [2] (p. 13 ff.) and 1935 [3] (p. 56 ff.). He took special care of the cleaning of the plates (Chrome sulphuric acid) and claimed that the $t_{crStart}$ should be between 14 and 16 hours. The temperature should be between 26 and 30 °C and the relative humidity between 40 and 50 %. If heating is required, it is best to use a heater in another room. He kept out electrical and magnetic radiation. According to him, the Petri-dishes should be placed on a table whose position in the chamber should be determined experimentally for the best homogeneity of the pictures. The volume of the room (in our terminology the inner and the outer chamber were one room) in which the evaporation apparatus stood should be $4 * 2.5 * 2.5 = 25 \text{ m}^3$ (1935 [3], p. 63). A smaller volume would disturb the evaporation. He emphasized the importance of the renewal of the air after each experiment. He observed a difference in the pictures between summer and winter. He also mentioned a possible influence from the weather (storm, lightning, sudden weather changes ([3] p. 62).

In the updated 1975 English version [4] (p. 46 ff.) he emphasized the importance of keeping the starting humidity, close to the Petri-dishes, between 35 and 55 % (best is 45 %) and the starting temperature between 28 and 32 °C (best is 30 °C). Otherwise the $t_{crStart}$ would exceed the specified range of 14 to 16 hours. The chamber should be air tight (dimension $1.65 * 2.15 * 1.65 = 5.8 \text{ m}^3$). He described checking for possible vibrations by observing Lycopodium seeds on the surface of water in a Petri-dish.

Andersen, Triangle chamber

Andersen 1998 [5] followed the description of Pfeiffer [4] (p. 46 ff.) and not only adjusted the temperature but also acclimatized the [outer chamber](#), to reduce the influences between summer and winter. The [inner part of the wooden chamber](#) was heated by electrical heating below the dishes. The warm air was allowed to flow through perforated steel plates to homogenize the airflow. He designed a chamber type to reduce the $t_{crStart}$ variation of the different Petri-dish positions in the chamber. The dishes were placed in between two large

tubes so that the airflow passed each dish in the same way. The height of the rim of the Petri-dishes, to shield the solution, was determined during his master thesis [6] by measuring the temperature variation on the glass plate (10 cm outer-, 9 cm inner diameter) of the Petri-dish. The shielding showed a minimum variation at a height of 3.5 cm from the surface of the solution. When he designed a second chamber version with two evaporation rings, the crystallization apparatus had to be thermally shielded to minimize differences between the inner and the outer ring, see Fig. 2.17.1.

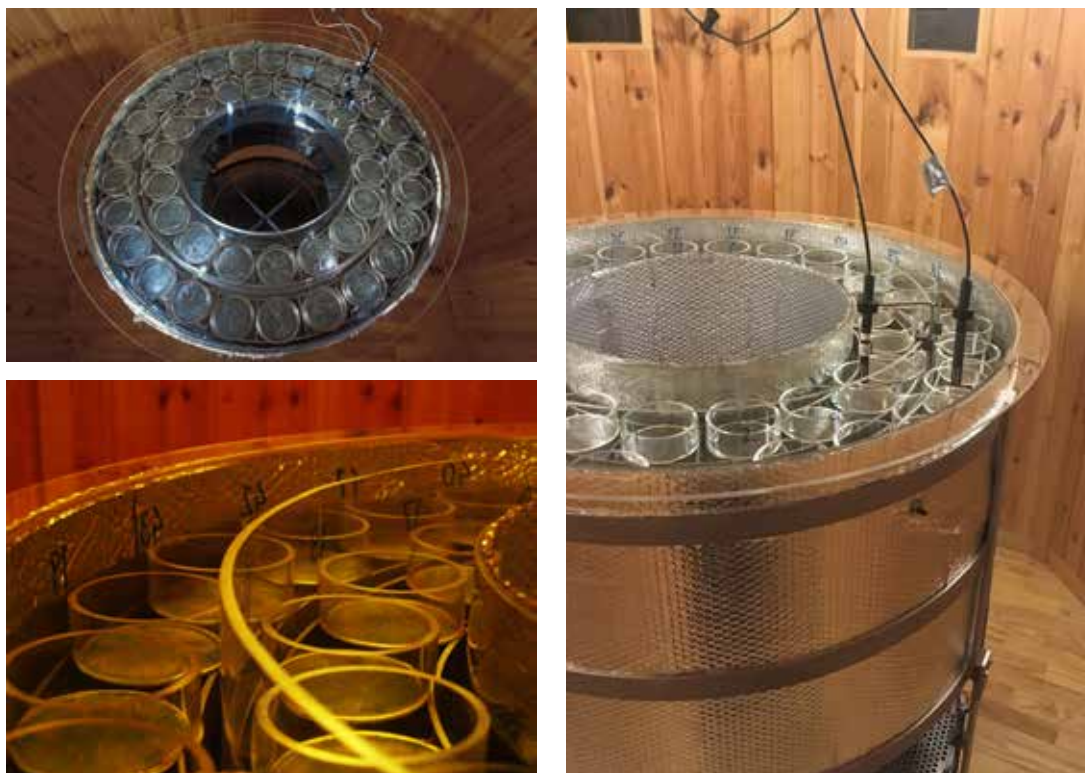


Fig. 2.17.1 Views on the Triangle evaporation apparatus with Petri-dishes. Upper left photo is taken from the ceiling of the chamber towards the crystallization apparatus holding 43 crystallization plates. Chamber of University of Kassel (D). Bottom left: view inside the inner and outer tubes with the Petri-dishes. Chamber in Roepaen (NL). Right: Side view of the apparatus with Petri-dishes. Chamber in Roepaen (NL).

This is the so called [Triangle Chamber](#). Status in 2018: 1 chamber located in the Biodynamic Research Association Denmark (BRAD, DK), 2 at the University of Kassel (D), 1 in Crystal Lab, Roepaen (NL). Despite the addition of a water reservoir in the [inner chamber](#), the starting humidity variation remained a problem (Andersen opened the door after pipetting until the desired starting humidity was reached).

Other authors and chambers

Nickel [7] and Ballivet [8] also experimented with ring heights and so called “Chimneys”. Koopmans (1971 [9] p. 25) observed that when evaporation is too strong, the center of the picture is close to the geometric center of the Petri-dish. He linked this to the hypothesis that the concentration gradient from the center of the Petri-dish to the rim was very high due to the strong evaporation. In 2006 Graf was the first to look at the variation of the $t_{crStart}$ as a degree of freedom and not as an perturbation (private communication).

In the Forschungsring Darmstadt (Bornhütter and Geier) the dishes stand on a circular table, and the chamber itself is not heated. The system is started up 3 days before a crystallization is planned. Three additive concentrations are used. The outer chamber is acclimatized with respect to temperature and humidity. During the 3 day startup phase, the door of the chamber is left open to achieve similar temperature and humidity conditions as in the outer chamber. The chamber door is closed directly after pipetting the chamber solutions into the dishes. Info from Kahl 2015 [10].

In the University of Bonn (Fritz) the dishes were positioned on glass strips and the air was forced through the chamber (from ceiling to floor) homogeneously. Three additive concentrations were used. The outer chamber was acclimatized. The starting humidity was achieved by opening the chamber door until the relative humidity in the chamber reached the desired value.

In Crystal Lab (Roepaen, NL) (2010 - 2020, Doesburg), in order to improve the consistency of the positioning of the dishes in the Triangle chamber system, the positions on the crystallization apparatus were marked, so that the dish could be placed in exactly the same position as before. The evaporation rate per location was checked [11] during a project by weighing the solution before and after 5 hours of evaporation. The variation of the results was large, but could be reduced by further tuning the interaction between inner and outer ring heating.

The Triangle chamber system at the University of Kassel showed a summer / winter difference in heating that affected the $t_{crStart}$ value, indicating a climate influence from the outer chamber floor. Nevertheless, placing the chamber in the cellar is a good option, as it acts like a buffer against excessive outside temperature fluctuations (see Checking Influences report 2009 [12] p. 22 ff.). Data from the other chambers types (see chapter [3.1 Chamber systems](#)) have to be measured for comparison.

The measurements in the Triangle chamber system showed that the relative humidity during evaporation was limited to 67 %. This is the saturation value of the concentrated DCC solution at the solubility border [13]. When this value is reached, the evaporation of the solution in the Petri-dish slows down or ceases (see also chapter [2.13 Evaporation model](#)).

In the ProPar Project (2017 [14]) a test was performed in the Triangle chamber in Roepaen on the effect of covering the positions of the crystallization apparatus with glass plates when no experiment was running, in order to reduce the temperature variation at the beginning of an experiment. To have a better definition of the starting humidity, the humidity inside the chamber was regulated with a dehumidifier in the chamber.

Barth [15] designed a chamber with a strong reduction of the variation of the $t_{crStart}$. He considered the $t_{crStart}$ as a perturbation and not as a degree of freedom.

Defining Influences: perturbation and / or degrees of freedom

From the above we get the following list of factors of influence and how to assess the type of influence, and if the topic is already taken up in a chapter of the handbook.

Table 2.17.1 Defining the types of influence. If the topic is covered by a chapter, its shortcut is listed in the chapter name.

Topic	Type of Influence	Chapter
Crystallization starting time	Degree of freedom	1.3 Crystallization start and starting humidity
Three additive concentrations	Degree of freedom	1.9 Optimal amounts
Filling of the chamber with humidity up to the saturation value	Degree of freedom	1.2 Water transport
Cleaning of the glass plate	Degree of freedom/ perturbation	1.4 Surface tension, cleaning, ring height
Height of the ring (concentration gradient)	Degree of freedom	1.4 Surface tension, cleaning, ring height
Starting humidity of experiment	Perturbation	1.3 Crystallization start and starting humidity
The water leaving the chamber (stability of humidity flow)	Perturbation	1.2 Water transport
Location in the chamber	Perturbation/Degree of freedom	
Precision of positioning the dishes on the apparatus	Perturbation	
Seasonal influences (Summer/ Winter)	Perturbation	
Particles	Perturbation?	2.11 Nucleation
Vibration	Perturbation	
Air Pressure	Perturbation	
Lightning	Perturbation	

Crystallization starting time

In general the tcrStart is considered a degree of freedom. But if we can't keep the median or mean tcrStart of the experiments constant over a year (e.g. due to seasonal influences), then this effect (the variation over a year) should be considered more as a perturbation, because it points to a technical problem. What could be the threshold value for the year variation? Looking at the yearly overviews in Fig. 2.17.2 and 2.17.3, 50 % of the tcrStart values are inside the range of ± 1 hour. To test for seasonal variations, experiments should be performed in which all samples in the experiment are reference samples. When the change of the mean (tcrStart) per experiment is above ± 30 min then there is a technical problem in the system, which needs attention.

On the other hand, if the tcrStart per chamber position has a constant deviation from the mean value, then this can be considered a degree of freedom. To illustrate this, the tcrStart values of the 43 positions in the Triangle type chambers are shown (see Fig. 2.17.2 and 2.17.3). The chambers are coded in the database by the letters A, B, C and D. At 2007 / 2008 the status was: BRAD (DK) letter A, Uni Kassel (D) letter B and C and Louis Bolk Institute (NL) letter D. Data over the years 2007, 2008 are shown from the Checking Influences report 2009 [12] (p. 104 - 107, see the graphs in [Appendix 2.17.1 Variation](#)). Fig. 2.17.2 and 2.17.3 show a large variation in the tcrStart between the 43 positions and, dependent on the chamber, also between the inner (red boxes) and outer (green boxes) rings. These effects simply cannot be due to imprecise positioning of the dishes or the overall difference in initial humidity, as these random effects should sum to zero over two years. If the effect is caused by differences between the inner and outer ring of the evaporation apparatus (see Fig. 2.17.2 left for chamber A; inner ring red, outer ring green), then the temperature regulation of the two rings and also the homogeneity of the 43 positions must be considered. Concerning the latter, the Checking Influences report 2009 [12] p. 89) showed some correlations between the inhomogeneity of the 43 positions and the tcrStart variation. Another source of variation resulted from temperature differences between the inner wall panels of the chamber due to incorrect positioning of the acclimatization apparatus in the outer chamber. According to Table 2.17.1 these inconsistencies can be considered a feature, because they allow different tcrStart values to occur. The question is whether the deviation per dish from the chamber mean is stable (this can be tested with an pH indicator as additive, which is calibrated on the [single dish Prüfstand](#)). The conditions in chamber A (and for the other chambers) were adapted, so that differences between the inner ring (red) and the outer ring (green) were no longer significant.

Three concentrations

Three concentrations give a degree of freedom for the sample to express itself, which is limited if only one concentration is available. The question is how to choose the three concentrations also in relation to the influence of the tcrStart on the picture. See chapter [1.9 Optimal amounts](#).

Water filling the chamber (latency period)

During the evaporation of the solution in the Petri-dish the relative humidity in the chamber increases. The limit of this increase is around 67 %. This is exactly the saturation humidity above a DCC solution at the solubility border. When the humidity in the chamber is at this level, the evaporation is reduced, perhaps down to zero. This means that at the end of the evaporation, before the crystallization starts, there is a "latency period" of little or no evaporation. This can also be seen as a degree of freedom. It is assumed that the latency period depends on the pipetted volume in the Petri-dish. The higher the volume, the longer the latency period. See for details in chapter [1.2 Water transport](#) and chapter [2.13 Evaporation model](#).

Water leaving the chamber

The evaporated water has to leave the chamber. This either penetrates the wooden walls or passes through small openings into the outer chamber. Evaluation of a so called [step response test](#) should help to clarify this distinction. Small openings are physically not very stable because they are dependent on the degree of wood expansion and therefore on the humidity of the wood. See for details in chapter [1.2 Water transport](#).

Starting Humidity

This is a tricky issue, and everyone is trying to find a solution. Some people keep the chamber door open after pipetting and close it at a defined relative humidity (Fritz Uni Bonn, Andersen BRAD, Bornhütter Forschungsring Darmstadt). The Triangle systems open the door after an experiment for a defined length of time (e.g. 20 minutes) and let the chamber reset by closing the door. See also the chapter [1.14 Chamber reset](#).

If no experiment is performed, the humidity is kept constant by means of a dehumidifier in the inner chamber (tests in Roepaen NL for the Triangle Chamber). See for details in chapter [1.3 Crystallization start and starting humidity](#).

Cleaning of the glass plate

The cleaning of the glass plate influences the surface tension between the solution and the glass plate

in the Petri-dish (ProPar report nr 5 from 2017 [14]). This can have a strong effect if the concentration of the sample used is close to the dewetting range of the sample. See Apple Juice report [16] and the article about dewetting [17] and chapter [1.4 surface tension, cleaning, right height](#).

Particles in the air

The influence of dust particles in the air is not clear. The experiments with turbid and clear apple juice showed no differences in tcrStart (extra report Apple Juice [18]). A difference in tcrStart was expected, because the turbid juice has 20 times more weight in pectin (Kahl 2016 [19], Table 1) and should have particles in the size of 1 ~ 10 micrometer [20] which should have an influence.

In the winter there should be more particles in the air than in the summer due to heating and dust particle production, as can be seen in the PM2.5 and PM10 measurement of particles. This is usual available in the measurement data of the federal climate stations (see data on our local wiki server). Measurements of filtered DCC solutions showed that the tcrStart decreased when the solution was filtered (ProPar report nr 5 2017 [14]). The additives and the structures in the unfiltered DCC solution seem to hinder the crystallization start. The humidity regulation of the outer chamber is facilitated by a water based air cleaner which is only active during the winter period. Maybe this catches away most of the dust particles, so we cannot consider this as a factor of influence.

Resume

For the DCC system the factors of influence are listed. They are divided into factors that are needed as a degree of freedom and those that are considered perturbations. As the degrees of freedom the tcrStart, the latency period (the time between the evaporation slowing down when the chamber is filled with humidity and the tcrStart) and the application of more than one concentration can be named. As perturbations the starting humidity, the stability of the water leaving the chamber (starting humidity) and the summer / winter influence are considered. Most of the interesting factors have already been described in detail in a chapter of its own in this handbook.

Additional Research

Starting humidity

- The relation between the tcrStart and the starting humidity of an experiment should be checked (again).
- How to adapt the starting humidity in a reproducible manner.

Seasonal (summer / winter) dependency of tcrStart

- The actual dependency should be checked (data from University of Bonn and Forschungsring Darmstadt?).
- For the Triangle chambers a sensor is placed above the reservoir. If the influence is due to insufficient floor insulation, this sensor should indicate this. Also the heating should show a difference. The dust amount can be higher in the winter. The data from the local weather stations and the measurements in the outer chamber should be compared.

Water filling the chamber (latency period)

- For the Triangle chamber an additional sensor below the dish was applied. This gave us the possibility to check if the absolute humidity below and above the dish are the same, allowing to check whether evaporation stops. The latency period can be shortened / prolonged by applying a lower / higher pipetting volume than the 6 mL actually used to check the evaporation model.

Water leaving the chamber

- Step response experiments can be performed to determine whether water enters the inner chamber wall or whether it leaves the chamber through small openings.

Stability of the dish positions in the chamber

- Check the stability of the dish positions in the chamber with the calibrated pH indicator from the [one dish Prüfstand](#).
- Check the precision of placing the Petri-dish on a dish position (with pH indicator as above)
- Do we have a constant (per dish position) asymmetry in the picture? (evaluate with tool in chapter [3.3 CrystEval tool](#))

Using three concentrations

- What are the statistics behind this?
- How to compare the influence from the concentrations versus those from the starting time?

Air pressure

- Is there an influence (so far not seen)? Maybe there is an influence when the pressure changes. Check that the pressure change outside the building is the same as inside the building and inside the chamber.

Particles

- So far no effect could be seen... What does this mean? Didn't the particles from outside the building reach the inner chamber? Is the air cleaner so effective?

Vibrations

- Measure the vibration influence with a sensor to see whether there are any vibrations. Check for a correlation between the tcrStart and possible vibrations.

Concentration gradient

- If the concentration gradient changes with the height of the acrylic ring, then this should affect not only the tcrStart (as was seen) but also the distance between the crystallization start location and the geometric center of the Petri-dish. But this was not confirmed in chapter [1.4 surface tension , cleaning ,righ height](#).

Appendix 2.17.1 Variation

Boxplots of the crystallization starting times versus the location in the four Triangle type chambers. Data for the years 2007 and 2008. Red boxes represent the 18 inner ring positions, green boxes represent the 25 outer ring positions.

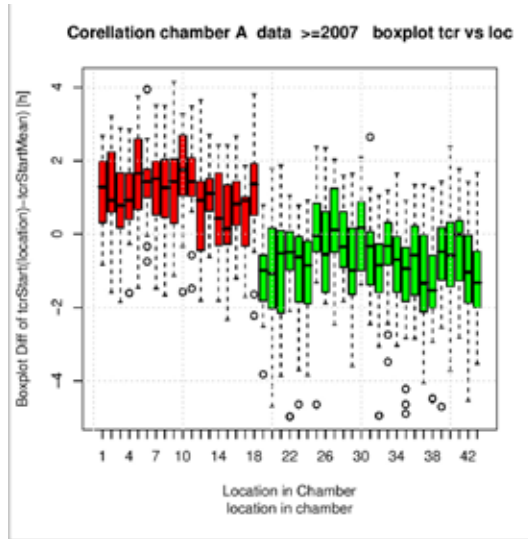


Fig. 3.5.8.1 Chamber A. Strong difference between the inner (red) and outer (green) double ring.

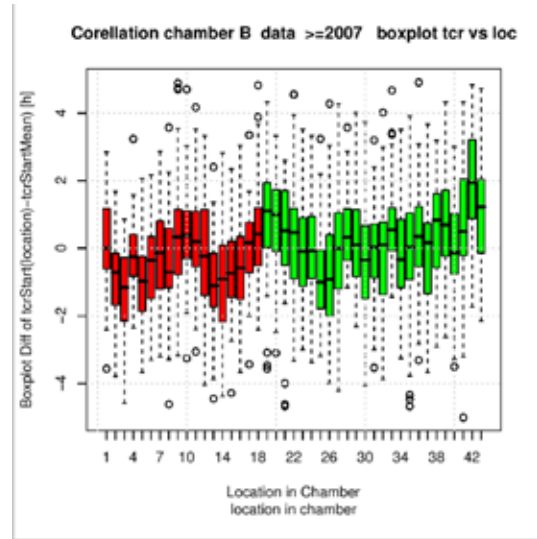


Fig. 3.5.8.2 Chamber B. Difference of tcrStart to day mean over the location in the chamber for data > 2007. Inner ring is red, outer ring is green.

Fig. 2.17.2 Left: chamber A, BRAD; right chamber B, Uni Kassel.

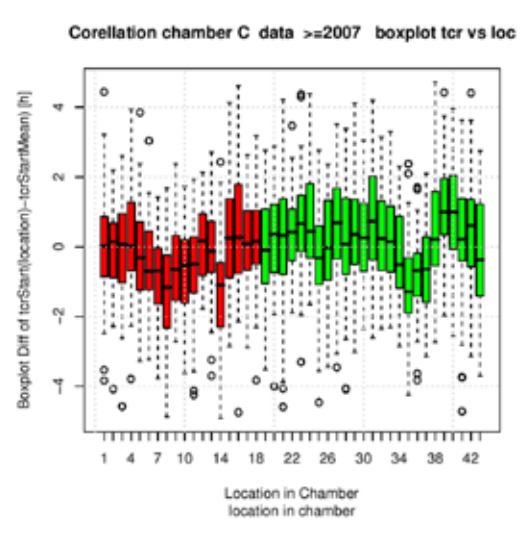


Fig. 3.5.8.3 Chamber C. Difference of tcrStart to day mean over the location in the chamber for data > 2007. Inner ring is red, outer ring is green.

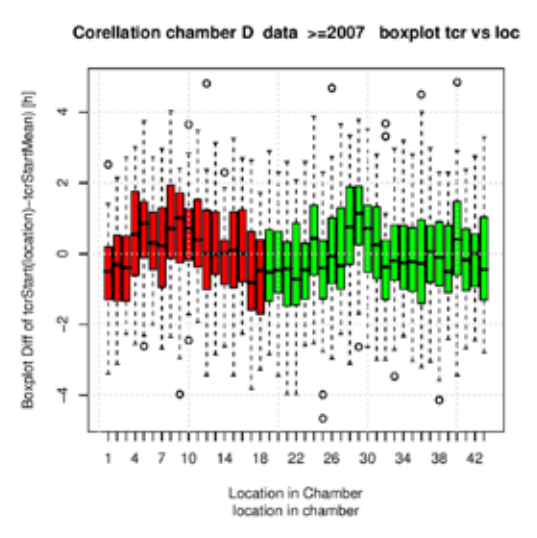


Fig. 3.5.8.4 Chamber D. Difference of tcrStart to day mean over the location in the chamber for data > 2007. Inner ring is red, outer ring is green.

Fig. 2.17.3 Left: chamber C, Uni Kassel; right: Chamber D, LBI.

References

- [1] Pfeiffer E Kristalle (Orient Occident Verlag, 1930).
- [2] Pfeiffer E Studium von Formkräften an Kristallisationen (Naturwissenschaftliche Sektion am Goetheanum, 1931).
- [3] Pfeiffer E Empfindliche Kristallisationsvorgänge als Nachweis von Formkräften im Blut (Emil Weises Buchhandlung Dresden, 1935).
- [4] Pfeiffer E Sensitive Crystallization Processes: A Demonstration of Formative Forces in the Blood (Anthroposophic Press, 1975).
- [5] Andersen JO, Laursen J, Koelster P. A Refined Biocrystallization Method applied in a Pictomorphological Investigation of a Polymer. *Elemente der Naturwissenschaft* 1998; 68: 1-20 <https://doi.org/DOI: 10.18756/edn.68.1>.
- [6] Andersen J-O. Kobberklorid—krystallisationsmetoden kvalitativt og kvantitativt. MSC Thesis, University of Copenhagen. 1992.
- [7] Nickel E. Die Reproduzierbarkeit der sogenannten empfindlichen Kupferchloridkristallisation.. PhD Thesis, Universitätsverlag, Freiburg (Schweiz). 1968.
- [8] Ballivet C, Knijpenga H, Barth J-G, Clad R. Zur Empfindlichkeit der Methode der Kupferchloridkristallisation. *Elemente der Naturwissenschaft* 1999; 70: 1-32 <https://doi.org/10.18756/edn.70.1>.
- [9] Koopmans A. Die Frage der Lokalisation im Kupferchlorid-Kristallisationsbild. *Elemente der Naturwissenschaft* 1971; 14: 19-30 <https://doi.org/10.18756/edn.14.19>.
- [10] Kahl J, Andersen J-O, an Nicolaas Busscher MA, Doesburg P, Fritz J, Geier U et al. Laboratory Intercomparison for biocrystallization applied to different wheat varieties. *Elemente der Naturwissenschaft* 2015; 102.
- [11] Doesburg P. Characterizing the crystallization chamber positions for use in a randomisation procedure. Technical Report, Crystallab. 2012.
- [12] Busscher N. Checking Influences: Untersuchung der Einflussgrößen bei der Biokristallisation als Voraussetzung für die Übertragbarkeit der Kammern und Prozeduren in andere Laboratorien und zur Reduzierung der Variationen durch die Kammer und die Orte. Technical Report, University of Kassel. 2009.
- [13] Rockland LB. Saturated Salt Solutions for Static Control of Relative Humidity between 5 and 40 C. *Analytical Chemistry* 1960; 32: 1375-1376.
- [14] Busscher N, Doesburg P. ProPar Project Report 2017. Technical Report, CuCl₂ Research. 2017.
- [15] Barth J-G, Roussau J, Suppan K, dos Santo SR. Crystallisation of a film of copper chloride in the presence of additives. *Elemente der Naturwissenschaft* 2011; 94: 69-99 <https://doi.org/DOI: 10.18756/edn.94.69>.
- [16] Busscher N. Apple juice Project. Technical Report, University of Kassel. 2015.
- [17] Busscher N, Doesburg P, Mergardt G, Sokol A, Kahl J, Ploeger A. Influence of dewetting on the crystallization behavior of CuCl₂ in the presence of BSA during evaporation in a Petri dish. *Heliyon* 2019; 5: e01102 <https://doi.org/10.1016/j.heliyon.2018.e01102>.
- [18] Busscher N. Additional Apple Juice Report. Technical Report, University of Kassel. 2015.
- [19] Kahl J, Busscher N, Doesburg P, Mergardt G, Will F, Schulzova V et al. Application of Crystallization with Additives to Cloudy and Clear Apple Juice. *Food Analytical Methods* 2016; 10: 1-9 <https://doi.org/doi:10.1007/s12161-016-0575-6>.
- [20] Zhu D, Shen Y, Wei L, Xu L, Cao X, Liu H et al. Effect of particle size on the stability and flavor of cloudy apple juice. *Food Chemistry* 2020; 328: 126967 <https://doi.org/https://doi.org/10.1016/j.foodchem.2020.126967>.

2.18 What is special for CuCl₂ 2H₂O?

Abstract

One of the recurring questions is what is so special about the salt CuCl₂ 2H₂O (cupric chloride di-hydrate, further named DCC) as it is the only salt used for crystallization with additives. So far we don't know. Pfeiffer checked 200 other salts and Selawry tested ~ 40 of them again, but DCC was the salt that fitted the purposes best. Vester (1960) showed that the DCC crystallization breaks down for the racemate (50 / 50 mixture) of mandelic acid, which was repeated by us with the same result.

Introduction

Since Pfeiffer (1920) began working with the salt CuCl₂ 2H₂O (cupric chloride di-hydrate, further named DCC) in the presence of additives, the ongoing question was, why DCC was used. Pfeiffer himself tested ~ 200 different salts (quote from von Hahn 1957[1], p. 9, 10) and based on this as a follow up Selawry (1957 [2], p. 28 - 33) tested ~ 40 out of the 200 salts from Pfeiffer. When using blood as additive, they always returned to DCC as the salt that showed the most sensitive differences according to their research questions. To date, no property of DCC has been found to explain Pfeiffer and Selawry's observations. However, the plant-like forms of DCC crystals are not limited to DCC. Around 1820 the first publications appeared e.g. by Vogelsang. (see section Historical below). The Historical section lists some other salts with DCC like properties and documents the DCC specifications that were used. One important aspect was shown by Vester (1960 [3]). When DCC crystallizes in the presence of a racemate of mandelic acid, the crystallization disintegrates. This observation was repeated by us (ProPar report 2017 [4], p. 40 ,41). It is not clear whether this is a special feature of DCC or a general salt crystallization feature.

Historical

DCC supply

Pfeiffer mentioned (1975 [5], p. 50) that since 1950 he used CuCl₂ 2H₂O (cupric chloride di-hydrate, further named DCC) from Merck Darmstadt as a special brand for crystallization, accessible through Th. Geyer Stuttgart. Selawry (1957 [2], Part B, p. 1) used DCC from Merck, Darmstadt reinst (99% min) pro analysi. DCC rein (97 %) instead of reinst (99 %) was not suitable for blood as additive (no special observations were shared). Also von Hahn (1962 [1], p. 11, 12) used DCC from Merck, Darmstadt purissimum (= reinst) pro analysi. Bessenich (1960 [6], p. 13) described that they also obtained their DCC from Merck, Darmstadt. They observed fine differences with different batches for blood as additive. They conducted suitability tests for every new batch of DCC.

Other Salts

Pfeiffer apparently tested 200 different salts (quote from von Hahn (1962 [1], p. 9, 10). Selawry (1957 [2], Part B, p. 28 - 33) reexamined some of these salts and reported the results. The salts MgSO₄, Zn₂.2H₂O, and CuSO₄, produced crystals that most closely resembled DCC. But DCC was more stable (in the sense of maintaining the form best) and more suitable for the research questions with blood as additive.

Plant-like forms not only appeared with salts. Kohlschütter (1925 [7] [8] [9] [10] and 1930 [11]), cited in Bessenich (1951 [12], p. 29), used Ca(HCO₃)₂ (calcium bicarbonate) and produced with various additives -what he called - "*somatoide Formen*" (somatoid or body-like forms), which he described in some cases as "*organismische Bildungen*" (organismic formations) (1925 [10], p. 21). He referred to Vogelsang [13], who had published on these phenomena as early as 1875. Scheuchzer, as cited in Ball (2009 [14], p. 29) found mineral dendrites in 1709, that showed plant-like forms.

Authors Thoughts

The phenomenon that the crystallization requires a preparation time of at least 10 hours before it starts is mentioned by Pfeiffer from the beginning (1923) and is emphasized by von Hahn (1957 [1], p. 12). During this time there seems to be some "*inner arrangement*" as Bessenich (1951 [12], p. 31) put it. From the [concentration matrix](#) with BSA (Busscher 2019 [15]) and other samples, it was seen that for some mixing ratios of additive and DCC, only one-centered pictures appear. This can be explained by the dynamic coincidence of the decrease in nucleation probability with the increasing additive amount, while the crystallization growth is still high enough to cover the 9 cm diameter Petri-dish, before the next crystallization can start.

So far there is no simple explanation for the special suitability of DCC. Several special features are

listed here:

- There is little change in the total volume as crystallization begins and the volume is transformed from a solution to a crystal with solution.
- The pH value at the crystallization start is very low (pH 0.5).
- The ability of DCC to build complexes is important.
- DCC can maybe build Cu nano crystals.
- The DCC crystallization breaks down with a racemic mixture of mandelic acid of 3 % as additive (Vester 1960 [3]).

Resume

The appearance of plant-like forms in crystallizations of mixtures with salts or calcium bicarbonate was recognized before Pfeiffer started with DCC in 1921. There is no simple explanation for the suitability of DCC.

Additional research

- Most interesting for a test are those salts mentioned by Selawry (1957 [2] Part B, p. 31)
- Did these salts show the same concentration dependency with BSA as DCC?
- Do all concentrations of the racemic mixture of mandelic acid show the breakdown of the crystallization?
- Does mandelic acid crystallize without DCC? And if yes, does the racemate disintegrate the crystallization?
- Is the breakdown visible for all racemic mixtures e.g. for mixtures of carotenoids?
- Ephedrine with DCC showed substance spirals very clear (Selawry 1957 [2], p. 60). But Ephedrine is banned, purchasing is currently limited and monitored, as it's a basic element of the synthetic drug Crystal meth.

References

- [1] Von Hahn F-V Thesigraphie. (Franz Steiner Verlag, 1962).
- [2] Selawry A and Selawry O Die Kupferchlorid-Kristallisation in Naturwissenschaft und Medizin (Gustav-Fischer-Verlag, 1957).
- [3] Vester F. Zur Indikation biochemischer Vorgänge durch kristallisierendes Kupferchlorid. *Cellular and Molecular Life Sciences* 1960; 16: 279-281 <https://doi.org/doi:10.1007/BF02157670>.
- [4] Busscher N, Doesburg P. ProPar Project Report 2017. Technical Report, CuCl₂ Research. 2017.
- [5] Pfeiffer E Sensitive Crystallization Processes: A Demonstration of Formative Forces in the Blood (Anthroposophic Press, 1975).
- [6] Bessenich F Zur Methode der empfindlichen Kristallisation (Naturwissenschaftliche Sektion am Goetheanum Dornach, 1960).
- [7] Kohlschütter V, Egg C. Über somatoide Bildungsformen. *Helvetica Chimica Acta* 1925; 8: 457-469 <https://doi.org/10.1002/hlca.19250080172>.
- [8] Kohlschütter V, Egg C. Über Änderungen des Habitus und der Modifikation von Calciumcarbonat durch Lösungsgenossen. *Helvetica Chimica Acta* 1925; 8: 470-490 <https://doi.org/10.1002/hlca.19250080173>.
- [9] Kohlschütter V, Egg C. Über Wirkungen von Farbstoffzusätzen auf die Krystallisation des Calciumcarbonats. *Helvetica Chimica Acta* 1925; 8: 697-703.
- [10] Kohlschütter V, Bobtelsky M, Egg C. Über Bedingungen und Grundlagen der Bildung somatoider Formen. *Helvetica Chimica Acta* 1925; 8: 703-723.
- [11] Kohlschütter V, Luethi M. Untersuchungen über Prinzipien der genetischen Stoffbildung II Zur Kenntnis des Verlaufs chemischer Reaktionen in Krystallen I. Versuche an Kupferverbindungen. *Helvetica Chimica Acta* 1930; 13: 978-1006.
- [12] Bessenich F Beiträge zur Erforschung der Bildekräfte durch empfindliche Kristallisation (Goetheanum (Dornach), 1951).
- [13] Vogelsang H Die Krystalliten. (F. Zirkel, 1875).
- [14] Ball P Nature's Patterns (Oxford University Press, 2008).
- [15] Busscher N, Doesburg P, Mergardt G, Sokol A, Kahl J, Ploeger A. Crystallization patterns of an aqueous dihydrate cupric chloride solution in the presence of different amounts of Bovine Serum Albumin. *Journal of Crystal Growth* 2019; <https://doi.org/doi:10.1016/j.jcrysgro.2019.125272>.

2.19 How to name the $\text{CuCl}_2 \cdot 2\text{H}_2\text{O}$ system, especially in publications

Usually in all chapters the term $\text{CuCl}_2 \cdot 2\text{H}_2\text{O}$ is replaced by DCC. In this chapter we are talking about the name of the method. So far in the name the text copper chloride is used. This will not be changed to DCC in this chapter.

Abstract

In publications a simple and neutral name should be used. Since it has been used for a long time, the most desirable term to describe the method would be *biocrystallization* [1] (as introduced by Engquist). However, this term is also used, at least since 1999 [2], for crystallization processes occurring within living organisms when stressed. It is assumed that a discussion with e.g. the maintainers of the Wikipedia page [Biocrystallization](#) will not be fruitful. The next most likely name, *CuCl₂ method*, is not suitable, because, as von Hahn stated [3], it is putting the emphasis on the indicator CuCl_2 and not on the change of the crystal forms by an additive. Hitherto the name *CuCl₂ crystallization with additives* seems to be the most neutral one to be used in publications.

Status Internet search biocrystallization

A search for different terms gave the following results (all on 2023.10.08).

When typing biocrystallization into DuckDuckGo, as first the Wikipedia [Biocrystallization](#) page shows up. In Google it is the same, but the “Image” photos are showing CuCl_2 crystallization pictures (see [Appendix 2.19.1 Screenshots](#)). In the Wikipedia [Biocrystallization](#) page the first line says: Biocrystallization is the formation of [crystals](#) from organic [macromolecules](#) by living [organisms](#).

In the second line is the German term *Kupferchloridkristallisation*. For the German term [Kupferchloridkristallisation](#) there is a only German Wikipedia page. In the first line there is standing: *Die Kupferchloridkristallisation oder Biokristallisation (engl. copper chloride biocrystallization) ist ein anthroposophisches Verfahren.*

Historical names

Pfeiffer originally called the method Kristallisationen [4]. Later he talked about „*die Methode der empfindlichen Kristallisation*“ [5], which was translated to English as “*sensitive crystallization*” in 1975 [6]. Selawry called it *Kupferchlorid Kristallisation* [7].

Bessenich wrote about *empfindliche Kristallisation* [8]. Petterson used *CuCl₂ Methode nach Pfeiffer* [9] or *Kristallisationmethode mit Kupferchlorid nach Pfeiffer* [10]. Engquist talked at first about *Kupferchlorid Kristallisation* [11], then about *Kupferchlorid Kristallisations Methode* [12] and finally about *Biokristallisation* [13].

Von Hahn created the term Thesigraphie [3] (from thesis = *Lagerung, Anordnung*) because he wanted to emphasize on the position or arrangement of the crystals, not on the indicator (*Kupferchlorid*) nor on the process (*Kristallisation*). Koopmans talked about *empfindliche Kristallisation* [13] and *Blutkristallisation* [14].

Barth used the terms *crystallization of copper chloride in the presence of additives* [15] or *copper chloride crystallization with additives* [16]. Balzer-Graf used the term *Kupferchlorid Kristallisation* [17]. Knijpenga used the term *empfindliche Kristallisation* [18], [19]. Andersen used the term *biocrystallization* [20]. In connection with the Triangle Consortium the term “*food pictures*” was registered as a trademark, but never really used. Kahl used the term *Biokristallisation* in his habilitation thesis [21]. Capuano used the term *Copper chloride crystallisation* [22]. Most of the Triangle Consortium publications used the term *biocrystallization*. Fritz and colleagues also used the term *biocrystallization* [23]. Doesburg et al [24] used the term *fingerprint analysis* in addition to *CuCl₂ crystallization*. Scherr suggested *CuCl₂-biocrystallization* or *CuCl₂ crystallization with biological additives*.

Discussion

Both Engquist [1] and versus von Hahn [3] searched for another name than “*Kupferchlorid Kristallisation*” because they placed the CuCl_2 phenomenon in the kingdom of biology rather than of pure physics. Indeed one can have the same hypothesis (see also chapter [2.16 Complex physical versus simple pattern](#)), even though the toxicity of CuCl_2 makes it difficult to connect the CuCl_2 phenomenon to biology.

The above definition of [Biocrystallization](#) from Wikipedia as “*the formation of [crystals](#) from organic [macromolecules](#) by living [organisms](#)*” cannot be used due to the above-mentioned toxicity of CuCl_2 .

The term *CuCl₂ crystallization with biological additives* prompts a discussion about the question of what is a biological system in terms of a juice or an extract. In the case of milk as an additive the reasoning would be clearer, but it is not in the environment of an abiological system any more.

The name given by Petterson *Kristallisationmethode mit Kupferchlorid nach Pfeiffer* is interesting, because it connects to the original discoverer of the phenomenon.

The name which Barth chose is *copper chloride crystallization with additives*. This describes the phenomenon, the indicator and the process, in the most neutral way.

Resume

The name *copper chloride crystallization with additives* seems to be the most promising one to be used for publications. It describes the phenomenon (with additives), the indicator (CuCl₂) and the process (crystallization), in the most neutral way. We expect that this could be the most accepted name in future publications.

Appendix 2.19.1 Screenshots

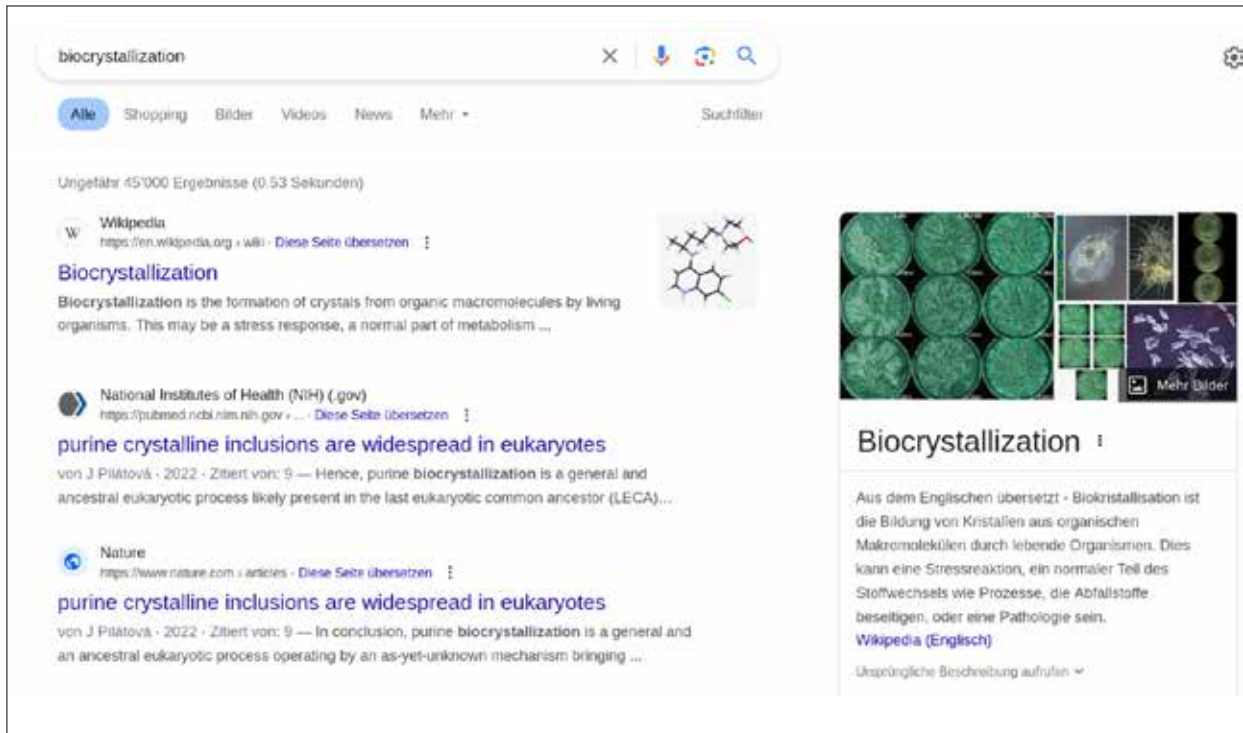


Fig. 2.19.1 Screenshot for Google search about the term biocrystallization at 2023.10.08

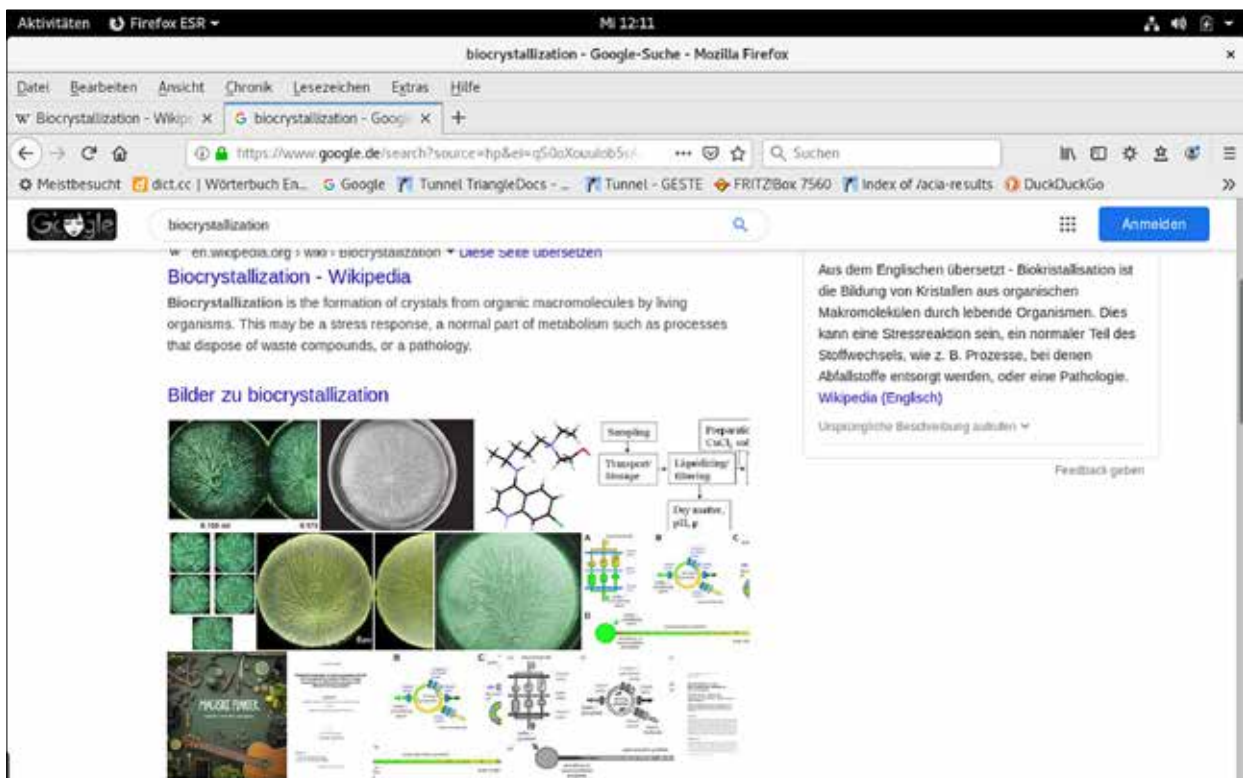


Fig. 2.19.2 Screenshot for Google search about the term biocrystallization at 2020.01.22

References

- [1] Engquist M. Physische und lebensbildende Kräfte in der Pflanze (Vitorio Klostermann, 1975).
- [2] Wolf SG, Frenkiel D, Arad T, Finkel SE, Kolter R, Minsky A. DNA protection by stress-induced biocrystallization. *Nature* 1999; 400: 83-85.
- [3] Von Hahn F-V. Thesigraphie. (Franz Steiner Verlag, 1962).
- [4] Pfeiffer E. Kristalle (Orient Occident Verlag, 1930).
- [5] Pfeiffer E. Empfindliche Kristallisationsvorgänge als Nachweis von Formkräften im Blut (Emil Weises Buchhandlung Dresden, 1935).
- [6] Pfeiffer E. Sensitive Crystallization Processes: A Demonstration of Formative Forces in the Blood (Anthroposophic Press, 1975).
- [7] Selawry A and Selawry O. Die Kupferchlorid-Kristallisation in Naturwissenschaft und Medizin (Gustav-Fischer-Verlag, 1957).
- [8] Bessenich F. Zur Methode der empfindlichen Kristallisation (Naturwissenschaftliche Sektion am Goetheanum Dornach, 1960).
- [9] Pettersson BD. Beiträge zur Entwicklung der CuCl₂ Methode nach Pfeiffer. *Elemente der Naturwissenschaft* 1966; 5: 29-39.
- [10] Pettersson BD. Beiträge zur Entwicklung der Kristallisationsmethode mit Kupferchlorid nach Pfeiffer IV. Wie verschiedene Kristallbilder bei der Pflanzenkristallisation entstehen. *Lebendige Erde* 1969; 3: 112-126.
- [11] Engquist M. Die Gestaltkräfte des Lebendigen (Vittorio Klostermann, 1970).
- [12] Engquist M. Qualitätsprüfung an Gemüse durch die Kupferchlorid-Kristallisationsmethode (Järna Tryckeri AB, Schweden, 1989).
- [13] Koopmans A. Zeitabhängigkeiten bei empfindlichen Kristallisationen. *Elemente der Naturwissenschaft* 1965; 2: 1-7 <https://doi.org/10.18756/edn.2.1>.
- [14] Koopmans A. Zum Begriff der Malignomdisposition im Hinblick auf die Blutkristallisations—Methode. *Elemente der Naturwissenschaft* 1990; 52: 36-41 <https://doi.org/10.18756/edn.52.36>.
- [15] Barth J-G, Roussau J, Suppan K, dos Santo SR. Crystallisation of a film of copper chloride in the presence of additives. *Elemente der Naturwissenschaft* 2011; 94: 69-99 <https://doi.org/DOI: 10.18756/edn.94.69>.
- [16] Barth J-G, Roussaux J, Wilkens A, Jacobi M. Techniques for washing the supports used for copper chloride crystallization with additive. *Elemente der Naturwissenschaft* 2013; 98: 5-19 <https://doi.org/DOI: 10.18756/edn.98.5>.
- [17] Balzer-Graf U, Balzer F. Milchqualität im Spiegel bildschaffender Methoden. *Lebendige Erde* 1991; 5: 236-255.
- [18] Mandera R, Ballivet C, Knijpenga H. Untersuchungen mit der Methode der Empfindlichen Kristallisation an Bilsenkraut (*Hyoscyamus niger*). *Elemente der Naturwissenschaft* 1990; 52: 1-32 <https://doi.org/10.18756/edn.52.1>.
- [19] Knijpenga H. Einflüsse unterschiedlicher Behandlungen auf die biologische Wertigkeit von Kuhmilch. Untersuchungen mit der Methode der Empfindlichen Kristallisation. *Elemente der Naturwissenschaft* 2001; 75: 48-60 <https://doi.org/10.18756/edn.75.48>.
- [20] Andersen J-O. Development and application of the biocrystallization method. PhD Thesis, Department of Agricultural Sciences/Organic Farming Unit The Royal Veterinary and Agricultural University Copenhagen. 2001.
- [21] Kahl J. Entwicklung, in-house Validierung und Anwendung des ganzheitlichen Verfahrens Biokristallisation für die Unterscheidung von Weizen-, Möhren- und Apfelproben aus unterschiedlichem Anbau und Verarbeitungsschritten. Habil Thesis, University of Kassel. 2007.
- [22] Capuano E, Boerrigter-Eenling R, van der Veer G, van Ruth SM. Analytical authentication of organic products: an overview of markers. *J. Sci. Food Agric* 2013; 93: 12-28 <https://doi.org/doi:10.1002/jsfa.5914>.
- [23] Fritz J, Athmann M, Andersen J-O, Doesburg P, Geier U, Mergardt G. Advanced panel training on visual Gestalt evaluation of biocrystallization images: ranking wheat samples from different extract decomposition stages and different production systems. *Biological Agriculture & Horticulture* 2018; 35: 1-12 <https://doi.org/doi:10.1080/01448765.2018.1492457>.
- [24] Doesburg P, Andersen J-O, Scherr C, Baumgartner S. Empirical investigation of preparations produced according to the European Pharmacopoeia monograph 1038. *European Journal of Pharmaceutical Sciences* 2019; 137: 104987 <https://doi.org/https://doi.org/10.1016/j.ejps.2019.104987>.

CHAPTER 3

EVALUATION AND DOCUMENTATION TOOLS

**Tools to document the DCC system, Image analysis,
Image features evaluation**

3.0 Tools to document the DCC system, Image analysis, Image features evaluation

Abstract

For the documentation of experiments of $\text{CuCl}_2 \cdot 2\text{H}_2\text{O}$ (cupric chloride di-hydrate, further called DCC) with additives different tools exist. The tools are developed with the idea that 1. the data should be entered only once and 2. the software should support the researcher and not be a burden. For the evaluation of the DCC pictures there is an image analysis tool with different algorithms and a possibility to evaluate the DCC pictures according to specific criteria. For quality control of the system the stored climate measurement data are evaluated over days, weeks, months and years. The scanned and photographed pictures can be organized to create working sheets for the Gestalt evaluation.

Introduction

Initially, the work with the DCC pictures was documented using a paper-based system. In 1999, the idea of a close collaboration between different laboratories ([Triangle group](#)) was born, based on harmonizing procedures in term of the experimental tools (such as the evaporation chamber, the lab equipment and the laboratory and evaluation procedures). This included the exchange of the experimental designs and the experimental results, therefore an easier accessible and standardized way of documenting became necessary. The choice fell on a computer based system. The software was developed based on the idea that 1. the data should be entered only once and 2. the software should support the researcher and not be a burden. In the beginning, the system simply calculated the required volumes of DCC and additive based on user-defined concentrations and volumes per plate. It also supported and documented the specific positioning of the different chamber solutions in the evaporation chamber (based on random positioning, or a defined design) and connected the data with the scanned picture. This documentation system, called LabDoc, documents the laboratory data and links them to the locations of the Petri-dishes in the evaporation chamber and to the scanned pictures, so that the data per dish are defined.

A first version was written by the author, but after a short time, project money was available, so a professional software developer could step in (Degert, papyrus-gmbh.de). He has been involved in the planning, discussion, and structuring of the system from the beginning. The scanning of the DCC pictures was integrated from the beginning, with an IT8 reference target, to check and maintain the color stability of the pictures.

The LabDoc information made it possible to create a computer based connection to the existing image analysis software, Applied Crystal Texture Analysis (ACTA), which provided texture analysis (Hendriksen 1998 [1]). The ACTA system was restructured to use LabDoc data as the basis for image analysis and to allow future integration of image analysis routines other than texture analysis. This was called Applied Crystal Image Analysis (ACIA). The structure analysis designed by Doesburg and Nierop was added in 2013 [2]. An absorbance evaluation in 2017 [3] and a polar structure evaluation in 2016. Approaches for a tree-based evaluation (Rommerskirchen 2022 [4]), a neural network analysis and a fractal dimension analysis were planned and structured, but not started yet.

In the LabDoc program a simple technical evaluation was added, to count the number of centers and measure the coverage of the plate. As more and more picture properties appeared, like the crystal types or the growth velocity of the needles, the evaluation part was redesigned and for development reasons placed in a new tool called CrystEval (see chapter [3.3 CrystEval](#)). This tool made it possible to define new properties that have only a geometrical representation in the picture, like a point, a line or an ellipse. The point is for example a center, while a line represents for example the orientation of the picture, and an ellipse is used for the coverage of the plate or an area with a specific crystal property. All these properties are connected to the time they occur during the evaporation, so that e.g. the growth rate of the DCC image can be determined by a vector of points, where the points represent the growth of the needle tip over time.

In different projects the software was extended. The integration of time-lapse images from a camera mounted on the ceiling of the evaporation chamber allowed the growth of the crystals to be followed. The evaluation of the LabDoc data by R-scripts (r-cran [5]) allowed a visualization of e.g. the mean crystallization starting time of the different chamber solutions. For ACIA a statistical evaluation of the image analysis results was added (Meelursarn 2007 [6]).

The documentation system was extended to other types of DCC systems with different geometries for

the placement of the Petri-dishes in the inner chamber and in most cases also different numbers of Petri-dishes per experiment.

The Gestalt evaluation is so far not included in the system. The Gestalt evaluation uses sheets of 6 pictures (e.g. 3 concentrations and 2 crystallization starting times) per product quality. The generation of the (pdf) sheets for the Gestalt evaluation is based on a script and on data from the database, which also includes the photos or the scans of the DCC pictures (see [Appendix 3.5.1 Sheets4GestaltEvaluation](#)).

Overview

For some of the tools a chapter of its own is available:

1. LabDoc: see chapter [3.2 LabDoc tool](#) (laboratory documentation)
2. ACIA: see chapter [3.4 Image analysis](#) (image analysis)
3. CrystEval: see chapter [3.3 CrystEval](#) (image features evaluation)

The following are in the chapter [3.5 Additional tools](#):

4. Labselect: (overall data request of the data base, see Appendix Labselect)
5. Sheets4GestaltEvaluation (see Appendix 3.5.1 Sheets4GestaltEvaluation)
6. Overall evaluation (see Appendix Overall Evaluation)
7. View Climate Measurement Data (see Appendix View Climate Measurement)

The tools run on LINUX® containers, so they are stable and do not need to be adapted when software updates are released or new computer hardware is bought.

Resume

Tools for documentation and image analysis by computer algorithms or visual evaluation criteria of DCC pictures exist and are stable. New algorithms can be added to the image analysis tool and all pictures can be reevaluated. Due to the database, all results can be evaluated from an overall context and sheets for the Gestalt evaluation can be generated from the different experiments. The climate measurement data can be viewed over days, weeks, months, years to secure the system quality.

References

- [1] Andersen JO, Henriksen CB, Laursen J, Nielsen AA. Computerised image analysis of biocrystallograms originating from agricultural products. *Computers and Electronics in Agriculture* 1999; 22: 51-69 [https://doi.org/doi:10.1016/S0168-1699\(98\)00043-X](https://doi.org/doi:10.1016/S0168-1699(98)00043-X).
- [2] Doesburg P, Nierop AF. Development of a structure analysis algorithm on structures from CuCl₂·2H₂O crystallization with agricultural products. *Computers and Electronics in Agriculture* 2013; 90: 63-67 <https://doi.org/doi:10.1016/j.compag.2012.11.003>.
- [3] Busscher N. Absorbance Project Report. Technical Report, University of Kassel. 2017.
- [4] Rommerskirchen EM. Rule-based simulation of dendritic Structures from Cupric Chloride Di-hydrat. MSc Thesis, Uni Göttingen. 2022.
- [5] Core-Team, R.-D.. R: A Language and Environment for Statistical Computing, <http://www.R-project.org> 2009.
- [6] Meelursarn A. Effect of image parameters to differentiate samples from different farming systems. PhD Thesis, University of Kassel. 2007.

3.1 Chamber Systems

Abstract

Different chamber systems are described. The size of the evaporation chambers and the way in which the climatic conditions for the evaporation are dealt with are listed.

Introduction

One of the basic requirements for creating a repeatable process from sample to DCC image is the control of the evaporation process. On one side the evaporation process has to be shielded from disturbances (of the airflow and from mechanical vibrations), on the other side the humidity must leave the environment of the Petri-dish, otherwise the evaporation stops (see chapter [1.2 Water transport](#)). To fulfill these conditions of shielding and water transport different chambers systems have been used since the beginning of DCC crystallization in 1924. The systems used so far consist of a support (e.g. a glass table), on which the Petri-dishes are placed inside a wooden or acrylic chamber (size from 0.39 m³ to 10 m³). Inside the chamber the climate (temperature and humidity) is controlled in different ways. The water (and the volatile elements of the solution in the dish) evaporates in a defined manner and after 10 - 16 hours of evaporation in the chamber, crystallization starts. We deliberately restrict ourselves here not only to DCC systems for which results have been published, but for which we also know the researchers involved and can judge them on their merits. For some chamber systems, it is not possible to add much more than the geometric information. If available, floor plans have been added in [Appendix 3.1.3 Chambers](#).

Historical overview

The historical overview is limited to the actual used chambers with published research.

Resume chamber types:

Table 3.1.1 Chamber types, sizes and climate parameter handling.

Name	Volume	Temp.	Humid. reg. in/outside	Control tcrStart	Vibr	Nr. picture
Barth	0.77 m ³	Yes	Air supply with defined humidity	Flow of warm, dry air	No	18
Bonn	1,8 * 1,8 * 1,8 = 5.83 m ³	Yes	Air supply with defined humidity	Flow of warm, dry air	No	30
Darmstadt	10 m ³	Outer chamber	Outer chamber	Gradient absolute humidity (fabs) over the chamber wall	No	52
Dornach Topf	Pi * 0.50 * 0.5 * 0.5 = 0.39 m ³	Yes	Air supply with defined humidity	Flow of dry air, internal heating	No	12
Triangle	10 m ³	Yes	Outside. More or less defined start humidity	Gradient fabs over the chamber wall, internal heating	Yes	43
One dish Prüfstand		No	Passive; ambient conditions	Passive; ambient conditions	No	1
Schweizer	0.16 m ³	Yes	Salt to limit humidity	Internal heating, limiting humidity	No	12

Barth System

Chamber

The system of Barth is characterized by a very low variation of the crystallization starting time (tcrStart), with an exceptionally high tcrStart of ~ 25 h. The low variation in tcrStart is achieved by placing the Petri-dishes on a metal ring and by controlling the air movement in a very defined way. It is documented in Barth 2011 [1] and Barth 2019 [1].

Volume

Tube of 0.75 height and 1.15 m diameter. $V = \pi * r^2 * h = 0.77 \text{ m}^3$.

Climate Control

Air from an air-conditioned room in which the tube is located is forced through the tube at a slow speed.

Vibration Control

No vibration control.

Publications

Barth 2011 [2], Barth 2013 [3], Barth 2019 [1].

University of Bonn System**Chamber**

Dimensions are estimated. Volume: height 1.8 m * width 1.8 m * depth = 1.8 m = 5.8 m³

Climate Control

Air is forced through the chamber. The air intake and outlet is through two tubes. The tubes are mounted on the sides of the chamber. The inlet is located on the bottom of the chamber and the outlet is located on the opposite roof side, so the air passes through the whole chamber. The suspended glass strips on which the Petri-dishes are standing are positioned transverse to this airflow (see Fig. 3.1.2). The tubes have increasing hole diameters toward the outer ends to ensure a uniform air in and outlet. The chamber door is left open after pipetting and is closed when a threshold humidity is reached.

Vibration Control

No vibration control.

Publications

Fritz 2009 [4], Fritz 2011 [5], Athmann 2011, Fritz 2017 [6], Fritz 2018 [7], Fritz 2020 [8].

Forschungsring Darmstadt System**Chamber**

The climate chamber is a variation on the Triangle chamber type (10.09 m³). It is located in an insulated outer room (3.985 m x 2.64 m x 2.50 m = 26.3 m³) that is kept at a constant temperature and humidity (20 °C, 40 % rh).

Climate Control

The inner chamber has no temperature and/or humidity control, but depends on the outer chamber climate. 2 - 3 days before an experiment, the outer chamber climate is regulated (30 °C, 50 % rh) and the door remains open to allow the humidity in the inner and outer chambers to equalize. When the dishes are filled with solutions, the door is closed and the initial humidity of 50 % is reached. This type of climate control results in very little air movement in the chamber, but similar to the Barth chamber in an exceptionally high tcrStart value of ~ 28 h.

Vibration Control

No vibration control.

Publications

Geier 2005 [9], 2005 [10], Geier 2016 [11], Kahl 2015 [12].

DornachTopf System

Documented in Koopmans 1971 [13].

Chamber

0.39 m³ insulated aluminum pan.

Climate Control

Silica gel dried air is blown through a perforated horizontal positioned tube rotating above the plates at a speed of ~ 5 rpm. The perforations increase in diameter toward both ends of the tube to ensure an equal outflow of dried air along the entire length of the tube. A heating element in the bottom of the pan ensures even heating of the plates.

Vibration Control

No vibration control.

Publications

Koopmans 1971 [13], Hotho 2010 [14], Knijpenga 2001 [15], Microwave Project 2004 [16].

Schweizer System**Chamber**

Chamber according to Blot (see reference in Schweizer 2007 [17] p. 8) or Bloch (Schweizer 2013 [18] p. 6). The chamber volume is $0.66 \text{ m} \times 0.485 \text{ m} \times 0.51 \text{ m}$ (width * height * depth) = 0.16 m^3 .

Climate Control

The chamber temperature is controlled at $30 \text{ }^\circ\text{C} \pm 1 - 2 \text{ }^\circ\text{C}$. Heating is provided by small light bulbs under a thick glass plate on which the Petri-dishes are placed. The humidity is not regulated and depends on the humidity of the room in which the chamber is placed.

Vibration Control

No vibration control.

Publications

Schweizer 2007[17], 2010 [19], 2013 [18].

Triangle System**Chamber**

Volume inner chamber 10 m^3 .

Climate Control

The chamber temperature is controlled and the humidity is supported by a water reservoir located below the evaporation apparatus in the chamber. The resulting humidity depends on the temperature and relative humidity in the outer chamber and the water permeability of the wooden chamber walls. The climate in the outer chamber (temperature and relative humidity) is regulated.

Vibration Control

Vibration control is achieved by using an IPK vibration isolation package to isolate the crystallization unit from external vibration.

Publications

Andersen 1998 [20], 1999 [21], 2001 [22], 2003 [23], 2004 [16], Kahl 2004 [24], 2007 [25], 2007 [26], 2009 [27], 2010 [28], 2013 [29], 2014 [30] [31] [32], 2015 [12], 2016 [33].
Doesburg 2010 [34], 2014 [35], 2019 [36], 2020 [37].
Busscher 2006 [38], 2010 [39] [40], 2014 [41], 2019 [42] [43].

One dish Prüfstand**Chamber**

Documented in ProPar project report nr. 7 (2019 [43]) and nr. 8 (2020 [44]).

A dish is placed on a balance with a rH sensor directly above the dish, and a camera positioned about 25 cm above the dish. The evaporation rate can directly be determined from the weight loss on the balance.

The camera is able to follow the evaporation effects from closeup in a higher resolution than in any crystallization chamber.

Climate Control

The Prüfstand is placed in the acclimatized outer room (Triangle situation; 26 °C, ~ 47 % rH), the climate conditions in the Prüfstand are passively controlled by the ambient conditions.

Vibration Control

None

Publications

ProPar project report nr. 7 (2019 [43]) and nr. 8 (2020 [44]).

Resume

Among the present types of working chambers, there seem to be two principles for regulating the climate during evaporation in the inner chamber.

1. An acclimatized airflow actively forced into the inner chamber (Bonn, Topf, Barth).
2. The climate in the chamber depends on the humidity permeability of the walls between the inner and outer chambers and the temperature and rH conditions in the outer chamber (Triangle, Darmstadt).

So far it is not clear which principle has which advantages in relation to which research question.

Appendix 3.1.1 Chambers

Schemes / plans of chambers at different locations

Crystallization setup Forschungsring Darmstadt



Fig. 3.1.1 Circular glass table with 52 dishes in the chamber at the Forschungsring Darmstadt.

Crystallization setup University Bonn



Fig. 3.1.2 Glass strokes with 30 dishes in the chamber at the University of Bonn.

Schematic representation of the Dornach Topf

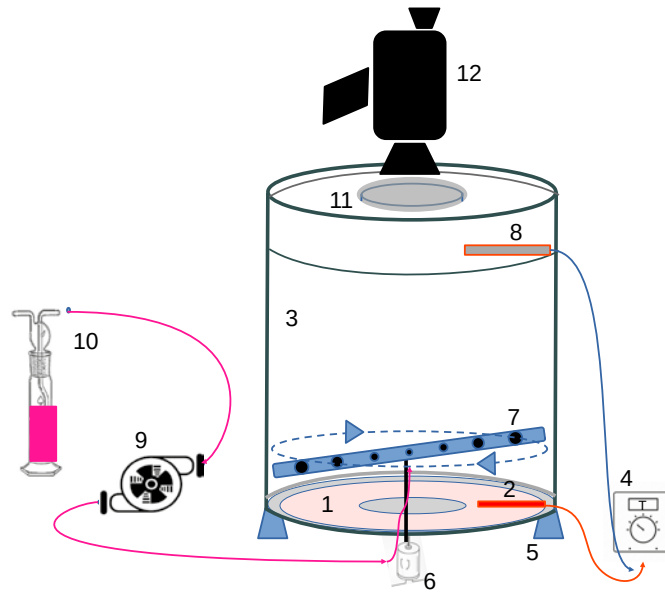


Fig. 3.1.3 Schematic setup of the Dornach Topf system. Petri-dishes (12 in total) are placed on the bottom of an aluminum pan that is heated from below (1). A regulator (4) with a temperature sensor (2) keeps the temperature at a constant value. To dry the evaporated air from the dishes, silica-gel dried air (10) is pumped into the pan (9) above the dishes via an air rod (7) rotating at 5 rpm. The input of dried air is regulated (4) with a second sensor (8). The crystallization process is monitored by a camera (12).

Schematic representation of the one dish Prüfstand, chamber W

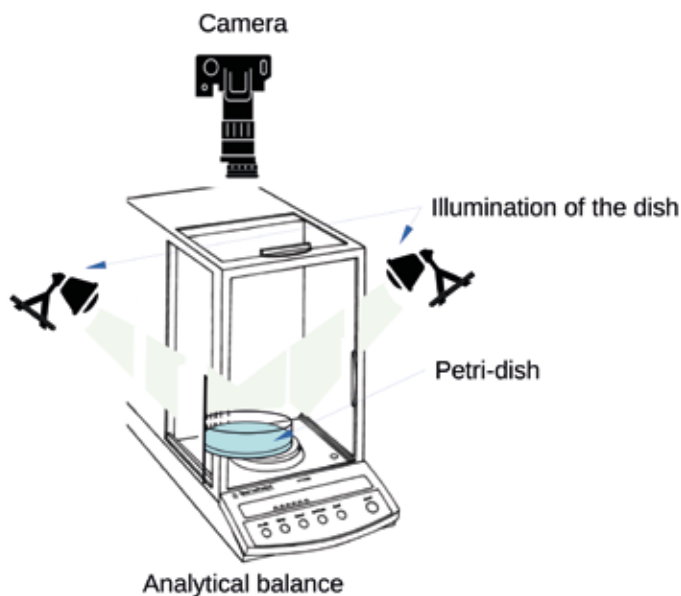


Fig. 3.1.4 Schematic representation of the one dish Prüfstand. The Petri-dish is positioned on an analytical balance. The evaporation can be followed by the decreasing weight. The climatic conditions are the ambient conditions (in principle the outer room of the Triangle DCC system; 26 °C, 50 % rH). The process is monitored from above by a camera.

Triangle DCC system BRAD (Galten DK), chamber A (from 2000 to 2018)

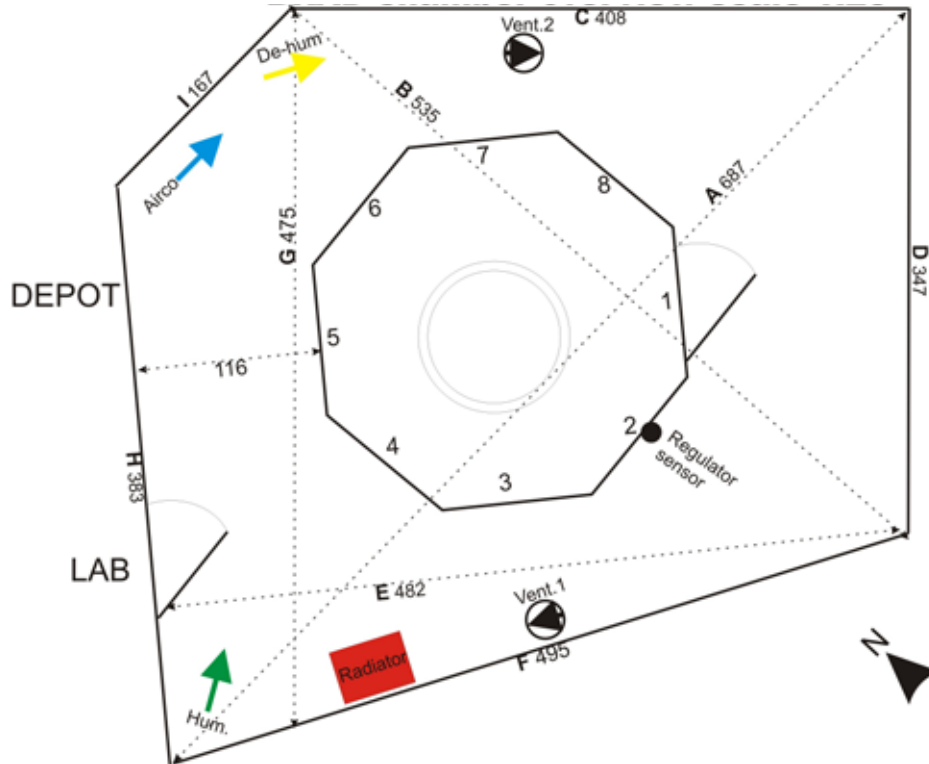


Fig. 3.1.5 Setup of the Triangle chamber in BRAD (DK), scale 1:25.

Triangle DCC system Uni. Kassel chamber B

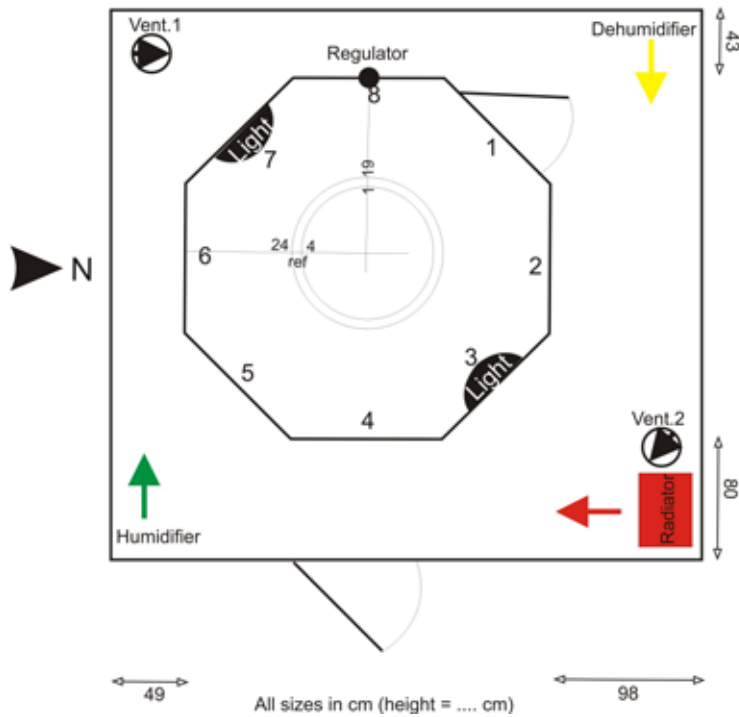


Fig. 3.1.6 Setup of the Triangle chamber in University of Kassel (chamber B), scale 1:25.

Triangle DCC system Uni. Kassel chamber C

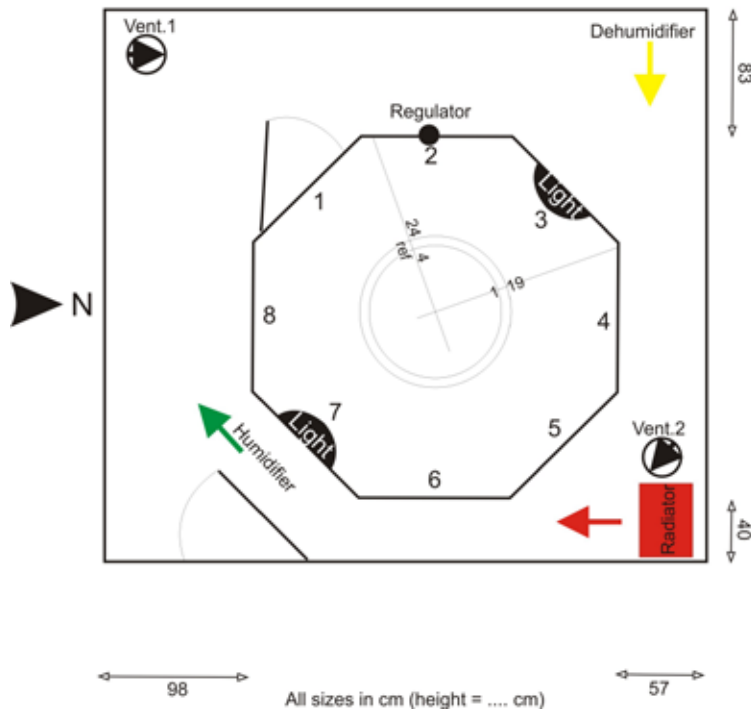


Fig. 3.1.7 Setup of the Triangle chamber in University of Kassel (chamber C), scale 1:25.

Triangle DCC system Louis Bolk Institute (Driebergen NL from 2002 to 2010), Crystal Lab (Roepaen, Ottersum NL from 2010 to 2019)

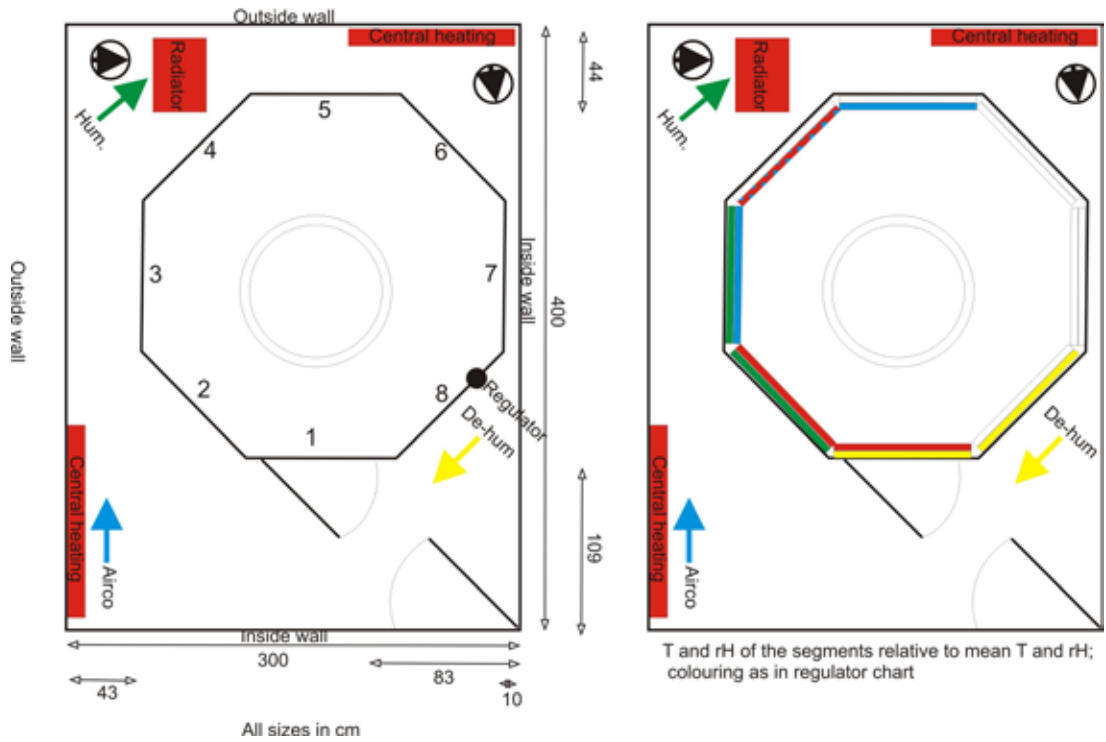


Fig. 3.1.8 Setup of the Triangle chamber in Louis Bolk Institute (NL) (chamber D), scale 1:25.

References

- [1] Barth J-G. Cupric Chloride Crystallisation in the Presence of Additive: Experimental Conditions and Developmental Perspectives. *Elemente der Naturwissenschaft* 2019; 111: 46-55 <https://doi.org/10.18756/edn.111.46>.
- [2] Barth J-G, Roussau J, Suppan K, dos Santo SR. Crystallisation of a film of copper chloride in the presence of additives. *Elemente der Naturwissenschaft* 2011; 94: 69-99 <https://doi.org/DOI: 10.18756/edn.94.69>.
- [3] Barth J-G, Roussau J, Wilkens A, Jacobi M. Techniques for washing the supports used for copper chloride crystallization with additive. *Elemente der Naturwissenschaft* 2013; 98: 5-19 <https://doi.org/DOI: 10.18756/edn.98.5>.
- [4] Fritz JGM, M Athmann UK. Untersuchung von Traubensaft mit den drei Bildschaffenden Methoden. *Wiss Tagung Zürich* 2009.
- [5] Fritz J, Athmann M, Kautz T, Köpke U. Grouping and classification of wheat from organic and conventional production systems by combining three image forming methods. *Biological Agriculture & Horticulture* 2011; 27: 320-336.
- [6] Fritz J, Athmann M, Meissner G, Kauer R, Köpke U. Quality characterisation via image forming methods differentiates grape juice produced from integrated, organic or biodynamic vineyards in the first year after conversion. *Biological Agriculture & Horticulture* 2017; 33: 1-19.
- [7] Fritz J, Athmann M, Andersen J-O, Doesburg P, Geier U, Mergardt G. Advanced panel training on visual Gestalt evaluation of biocrystallization images: ranking wheat samples from different extract decomposition stages and different production systems. *Biological Agriculture & Horticulture* 2018; 35: 1-12 <https://doi.org/doi:10.1080/01448765.2018.1492457>.
- [8] Fritz J, Athmann M, Meissner G, Kauer R, Geier U, Bornhütter R et al. Quality assessment of grape juice from integrated, organic and biodynamic viticulture using image forming methods. *OENO One* 2020; 54 <https://doi.org/10.20870/oeno-one.2020.54.2.2548>.
- [9] Geier U. Pflanzenorganbildtypen in Kupfer-chloridkristallisation und Steigbild. *Lebendige Erde* 2005; 5: 42-45.
- [10] Geier U. Grundlagen der Bildauswertung in den Bildschaffenden Methoden Kupferchloridkristallisation, Steigbild und Rundfilterchromatogramm. Technical Report, Forschungsinstitut am Goetheanum. 2005.
- [11] Geier U. Untersuchung der Auswirkungen verschiedener Leuchtmittel unterschiedlicher Herkunft auf Lebensmittel (Möhre, Apfel, Honig). Technical Report, Forschungsring Darmstadt. 2016.
- [12] Kahl J, Andersen J-O, an Nicolaas Busscher MA, Doesburg P, Fritz J, Geier U et al. Laboratory Intercomparison for biocrystallization applied to different wheat varieties. *Elemente der Naturwissenschaft* 2015; 102.
- [13] Koopmans A. Die Frage der Lokalisation im Kupferchlorid-Kristallisationsbild. *Elemente der Naturwissenschaft* 1971; 14: 19-30 <https://doi.org/10.18756/edn.14.19>.
- [14] Hotho G, Waldburger B. Investigation of olive oil quality using the sensitive crystallisation method. *Elemente der Naturwissenschaft* 2010; 93: 73-95 <https://doi.org/10.18756/edn.93.73>.
- [15] Knijpenga H. Einflüsse unterschiedlicher Behandlungen auf die biologische Wertigkeit von Kuhmilch. Untersuchungen mit der Methode der Empfindlichen Kristallisation. *Elemente der Naturwissenschaft* 2001; 75: 48-60 <https://doi.org/10.18756/edn.75.48>.
- [16] Andersen J-O. Microwave heating project. Technical Report, Biodynamic Research Association Danmark. 2004.
- [17] Schweizer F. Beobachtungen bei der Biokristallisation von Glykogen. *Elemente der Naturwissenschaft* 2007; 87: 76-89.
- [18] Schweizer F. Störungs- und Regenerationserscheinungen bei der Biokristallisation. *Elemente der Naturwissenschaft* 2013; 99: 5-20 <https://doi.org/10.18756/edn.99.5>.
- [19] Schweizer F, Andersen J-O, Jens-Laursen. Beobachtungen bei der Kupferchloridkristallisation: vom Eiweiß-Vorbild zum Kupferchlorid-Nachbild. *Elemente der Naturwissenschaft* 2010; 92: 62-93 <https://doi.org/DOI: 10.18756/edn.92.62>.
- [20] Andersen JO, Laursen J, Koelster P. A Refined Biocrystallization Method applied in a Pictomorphological Investigation of a Polymer. *Elemente der Naturwissenschaft* 1998; 68: 1-20 <https://doi.org/DOI: 10.18756/edn.68.1>.
- [21] Andersen JO, Henriksen CB, Laursen J, Nielsen AA. Computerised image analysis of biocrystallograms originating from agricultural products. *Computers and Electronics in Agriculture* 1999; 22: 51-69 [https://doi.org/doi:10.1016/S0168-1699\(98\)00043-X](https://doi.org/doi:10.1016/S0168-1699(98)00043-X).
- [22] Andersen J-O. Development and application of the biocrystallization method. PhD Thesis, Department of Agricultural Sciences/Organic Farming Unit The Royal Veterinary and Agricultural University Copenhagen. 2001.
- [23] Andersen JO, Huber M, Kahl J, Busscher N, Meier-Ploeger A. A concentration matrix procedure for determining optimal combinations of concentrations in biocrystallization. *Elemente der Naturwissenschaft* 2003; 79: 97-114.
- [24] Kahl Johannes NBGMJ-OAMH, Meier-Ploeger A. Bestimmung der Zeitabhängigkeit der Kristallisationsvorgänge

- bei der Kupferchloridkristallisation als eine Voraussetzung zur Validierung der Methode. *Elemente der Naturwissenschaft* 2004; 80: 90-100.
- [25] Kahl J, Busscher N, Meier-Ploeger A. Differenzierung und Klassifizierung von Öko-Produkten mittels validierter analytischer und ganzheitlicher Methoden, Abschlussbericht zum Projekt Nr. 02OE170/F2. Technical Report, Bundesprogramm Ökologischer Landbau. 2007.
- [26] Kahl J. Entwicklung, in-house Validierung und Anwendung des ganzheitlichen Verfahrens Biokristallisation für die Unterscheidung von Weizen-, Möhren- und Apfelproben aus unterschiedlichem Anbau und Verarbeitungsschritten. Habil Thesis, University of Kassel. 2007.
- [27] Kahl J, Busscher N, Doesburg P, Mergardt G, Huber M, Ploeger A. First tests of standardized biocrystallization on milk and milk products. *European Food Research and Technology* 2009; 229: 175-178 <https://doi.org/doi:10.1007/s00217-009-1039-7>.
- [28] Kahl J, Busscher N, Ploeger A. Validation of holistic methods testing organic food quality. *Biological Agriculture and Horticulture* 2010; 27: 81-94.
- [29] Kahl J, Busscher N, Hoffmann W, Mergardt G, Clawin-Raedecker I, Kiesner C et al. Development and Performance of Crystallization with Additives Applied on Different Milk Samples. *Food Analytical Methods* 2013; : 1-8 <https://doi.org/doi:10.1007/s12161-013-9759-5>.
- [30] Kahl J, Busscher N, Mergardt G, Maeder P, Torp T, Ploeger A. Differentiation of organic and non-organic winter wheat cultivars from a controlled field trial by crystallization patterns. *J. Sci. Food Agric.* 2014; 95: 53-58 <https://doi.org/doi:10.1002/jsfa.6818>.
- [31] Kahl J, Busscher N, Mergardt G, Ploeger A. Standardization and performance test of crystallization with additives applied to wheat samples. *Food Analytical Methods* 2014; 8: 2533-2543 <https://doi.org/doi:10.1007/s12161-015-0142-6>.
- [32] Kahl J, Busscher N, Hoffmann W, Mergardt G, Clawin-Raedecker I, Ploeger A. A novel approach for differentiation of milk fractions and polyvinylpyrrolidone with different molecular weight by patterns derived from cupric chloride crystallization with additives. *Anal. Methods* 2014; 6: 3173-3176 <https://doi.org/doi:10.1039/C3AY41568F>.
- [33] Kahl J, Busscher N, Doesburg P, Mergardt G, Will F, Schulzova V et al. Application of Crystallization with Additives to Cloudy and Clear Apple Juice. *Food Analytical Methods* 2016; 10: 1-9 <https://doi.org/doi:10.1007/s12161-016-0575-6>.
- [34] Doesburg P, Nierop AF. Development of a structure analysis algorithm on structures from CuCl₂·2H₂O crystallization with agricultural products. *Computers and Electronics in Agriculture* 2013; 90: 63-67 <https://doi.org/doi:10.1016/j.compag.2012.11.003>.
- [35] Doesburg P, Huber M, Andersen J-O, Athmann M, van der Bie G, Fritz J et al. Standardization and performance of a visual Gestalt evaluation of biocrystallization patterns reflecting ripening and decomposition processes in food samples. *Biological Agriculture & Horticulture* 2014; 31: 128-145.
- [36] Doesburg P, Andersen J-O, Scherr C, Baumgartner S. Empirical investigation of preparations produced according to the European Pharmacopoeia monograph 1038. *European Journal of Pharmaceutical Sciences* 2019; 137: 104987 <https://doi.org/https://doi.org/10.1016/j.ejps.2019.104987>.
- [37] Doesburg P, Fritz J, Athmann M, Bornhütter R, Busscher N, Geier U et al. Kinesthetic engagement in Gestalt evaluation outscores analytical 'atomic feature' evaluation in perceiving aging in crystallization images of agricultural products. *PLOS* 2021; 16 <https://doi.org/https://doi.org/10.1371/journal.pone.0248124>.
- [38] Busscher N, Kahl J, Andersen J-O, Huber M, Mergardt G, Ploeger A. Das Verfahren der Biokristallisation und das Konzept der Selbstorganisation. *Elemente der Naturwissenschaft* 2006; 85: 93-102.
- [39] Busscher N, Kahl J, Doesburg P, Mergardt G, Ploeger A. Evaporation influences on the crystallization of an aqueous dihydrate cupric chloride solution with additives. *Journal of Colloid and Interface Science* 2010; 344: 556-562 <https://doi.org/doi:10.1016/j.jcis.2009.12.045>.
- [40] Busscher N, Kahl J, Andersen J-O, Huber M, Mergardt G, Doesburg P et al. Standardization of the Biocrystallization Method for Carrot Samples. *Biological Agriculture and Horticulture* 2010; 27: 1-23 <https://doi.org/10.1080/01448765.2010.10510427>.
- [41] Busscher N, Kahl J, Ploeger A. From needles to pattern in food quality determination. *Journal of the Science of Food and Agriculture* 2014; 94: 2578-2581 <https://doi.org/doi:10.1002/jsfa.6498>.
- [42] Busscher N, Doesburg P, Mergardt G, Sokol A, Kahl J, Ploeger A. Crystallization patterns of an aqueous dihydrate cupric chloride solution in the presence of different amounts of Bovine Serum Albumin. *Journal of Crystal Growth* 2019; <https://doi.org/doi:10.1016/j.jcrysgro.2019.125272>.
- [43] Busscher N, Doesburg P, Mergardt G, Sokol A, Kahl J, Ploeger A. Influence of dewetting on the crystallization behavior of CuCl₂ in the presence of BSA during evaporation in a Petri dish. *Heliyon* 2019; 5: e01102 <https://doi.org/10.1016/j.heliyon.2018.e01102>.
- [44] Busscher N, Doesburg P. ProPar Project Report nr 8 2020. Technical Report, CuCl₂ Research. 2020.

3.2 LabDoc tool

Tool for documenting experiments with $\text{CuCl}_2 \cdot 2\text{H}_2\text{O}$ and additives.

Abstract

The Laboratory Documentation tool (LabDoc) is described in how it serves the researcher along the workflow in the laboratory from sample arrival to the scanning of the $\text{CuCl}_2 \cdot 2\text{H}_2\text{O}$ (cupric chloride di-hydrate, further called DCC) picture. The LabDoc system was adapted to other DCC systems which have either another geometry (Forschungring Darmstadt, Topf Dornach, One dish Prüfstand) and/or number of dishes.

Introduction

The LabDoc tool was designed to document the parameters of experiments of an additive and the salt $\text{CuCl}_2 \cdot 2\text{H}_2\text{O}$ (cupric chloride di-hydrate, further called DCC). The design goal was to support the researcher in the laboratory work and that the data should be entered in the system only once. Therefore, the structure of the tabs of the program follows the steps in the laboratory from the sample arriving in the laboratory to the scanning of the picture.

Follow the workflow

When LabDoc is started, an overview of the existing experiments for the selected chamber is displayed. When an existing series (experiment) is selected, or a new one is created, LabDoc opens and the tabs for the selected series appear, as shown in Fig. 3.2.1. As mentioned before, the tabs represent the laboratory workflow, from left the right.

LabDoc Series: 2017.05.23.E1, Chamber P

General Info | Plate Data | Substances | Basic Solutions | Chamber Solutions | Chamber Work | Time Observ. | Scripts

Description: POD 3x3 MEX
Who in charge: PD free space: 2.1 TB Version 6f37e3/master/2024-05-06

Remarks:
POD 1500 monolayers: 1. 3xUntreated 2. 3xhigh pressure carbon dioxide 3. 3xHPP 100mg CuCl_2 /plate. 4.4 Chamber solution repetitions!!! adequate for 4 plate repetitions. The acquired Volume of water to obtain a 2.5mg/ml stock for each enzyme was pipetted in the glass petri dishes in which the enzymes were transported (32mg POD in 12.6ml H_2O). Because no deadvolume is integrated into this LabDoc version the pipetting scheme was calculated manually: POD 1500 monolayers/ 2.5mg/ml stock/ 4.4Chamber solutions 12.3ml Stock 4.4ml 10% CuCl_2 9.7ml H_2O

Sensor Nr.	Type	Sensor Placement	par. x	centr. y	height z
01	Inner Ring, Plate No.	4	/ 0.0	0.0	14.5
02	Outer Wall, Segm. No.	3	/ 0.0	0.0	129.8
03	Outer Ring, Plate No.	24	/ 0.0	0.0	14.5
04	Inner Wall, Segm. No.	3	/ 0.0	0.0	127.0

Project: /
Year: /
Sample: /
Processing: /
Organisation: /

transmissive Scan Make Docu Save Cancel OK

Fig. 3.2.1 LabDoc main screen, starting with the General Info of the selected experiment (2017.03.23.ET for chamber P, Roepaen, NL).

Preparation

Usually, the experiment is copied from an existing experiment that is to be repeated, or from an experiment that is very “close” to the actual experiment (e.g. samples with different codes from a project that are measured in different experiments). The series name follows for most experiments a two-letter alphabetical order, which, together with the date and the chamber name, provides a unique series identifier. The laboratory workflow usually starts with the preparation of the experiment.

General Info

The experiment is described with a short (freehand) description in the Description field and the responsible person is indicated. Further relevant info and observations during the experiment are added to the Remarks field.

Plate Cleaning

For each dish the cleaning procedure of the glass plates and the acrylic rings is set. The cleaning procedure can be selected from a pull-down menu of several previously saved cleaning procedures. The height of the ring is also set here. Normally the default procedure is used, so this tab is not changed.

Substances

The codes for the experimental samples are set in the Group field, the supplier in the Supplier field and the type of sample (carrot, wheat or zucchini, ...) can be selected from a pull-down menu. So far 109 different samples (from alcohol to zucchini) are listed. See Fig. 3.2.2 on the next page. For some of the samples a detailed laboratory procedure from sample to DCC picture is accessible by right-clicking on the sample.

From Fig. 3.2.2 it can be seen that DCC pictures are most often made from samples as carrots, milk and wheat (~ 1200 each).

Basic Solutions

The basic solutions are generated from the samples. For carrots this is a juicing process, while for wheat this is an extraction process. PVP and BSA, which are provided in powder form, are simply dissolved. The procedure to be used can be selected from a drop-down menu for the additive in question. Right clicking on the selected procedure will open a pdf file to review some procedural details.

Chamber Solutions

From the basic solutions the so called chamber solutions are generated. This is done by mixing a DCC stock solution with the basic solution and water to achieve the desired amount of additive and DCC per plate.

Chamber Work

Here the positioning of the solutions at the numbered locations in the inner chamber is set. After the solutions are pipetted, the camera at the ceiling is started and the crystallization process can be followed in real time. See Fig. 3.2.3.

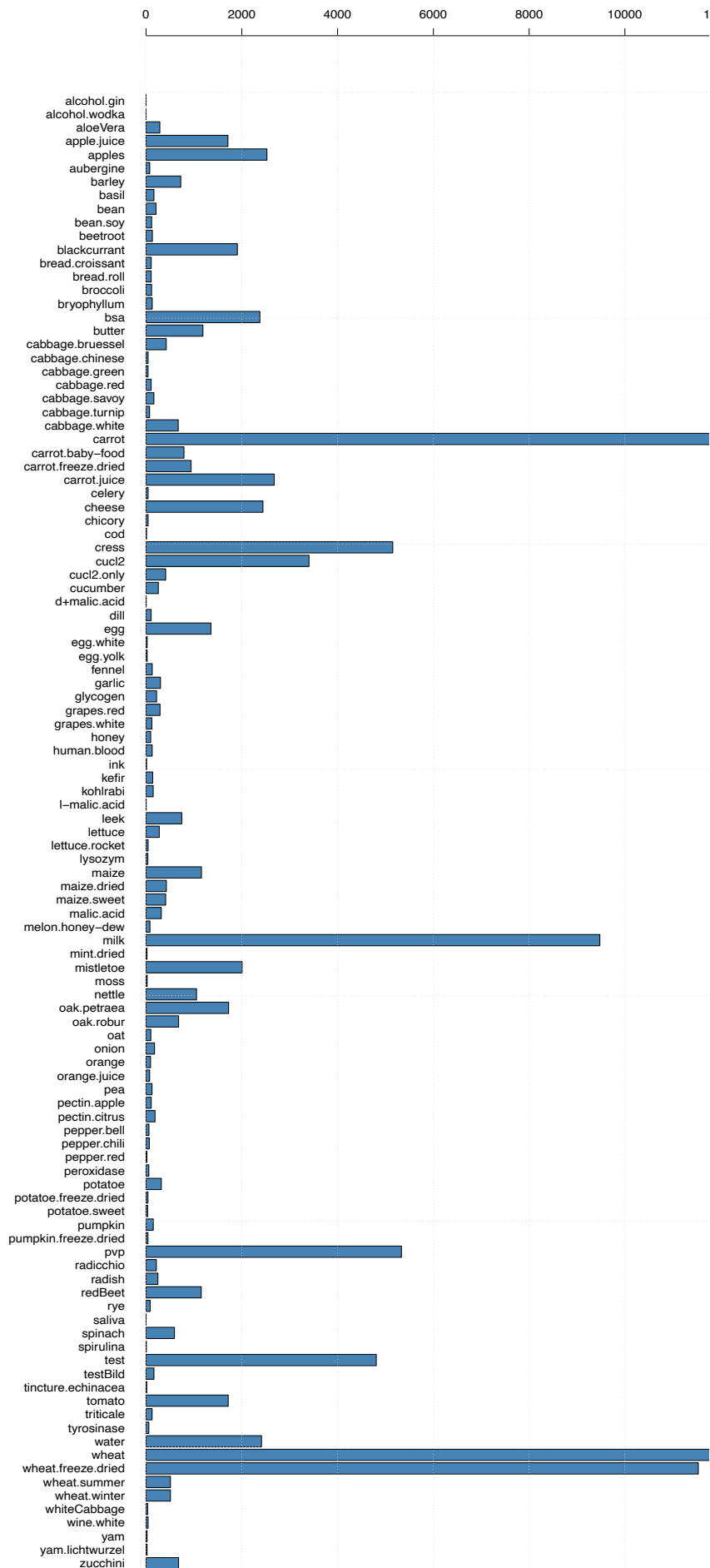


Fig. 3.2.2 Histogram of DCC pictures for different additives stored in the LabDoc database (status 2024.04.30).

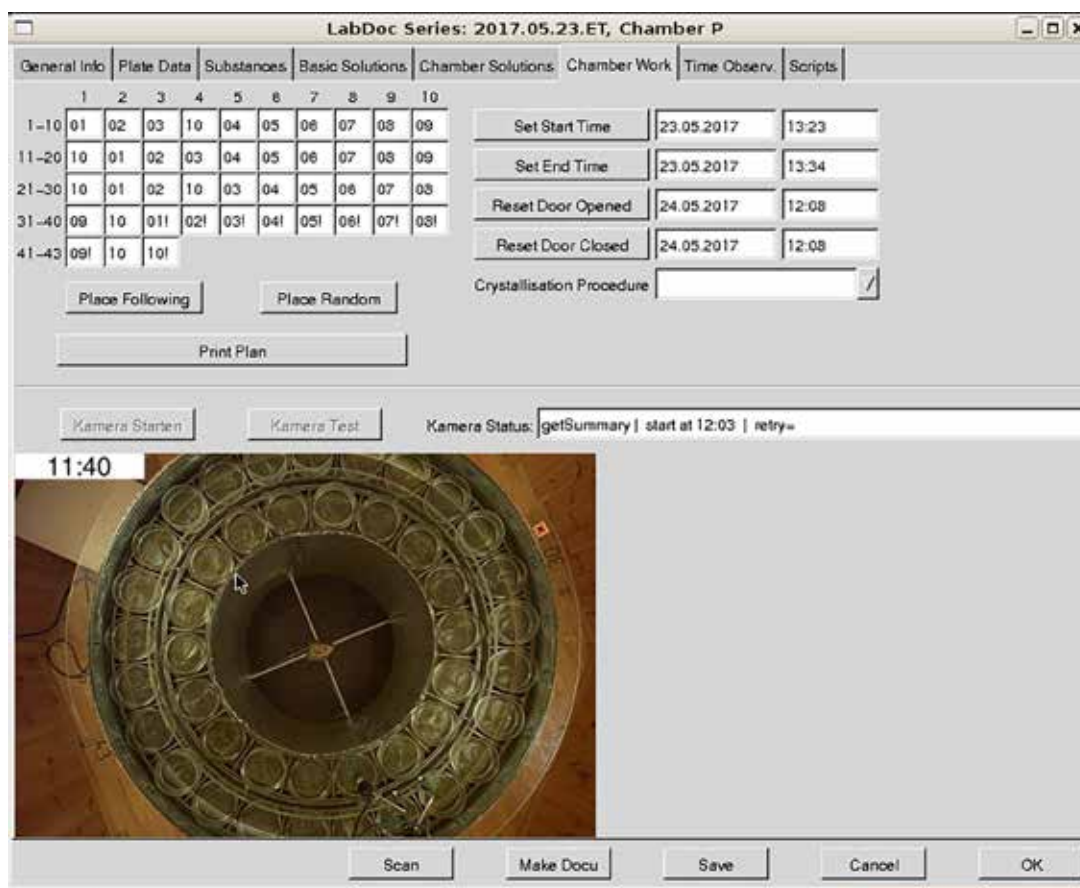


Fig. 3.2.3 LabDoc tab for Chamber Work. Upper left matrix shows the location of the different chamber solutions (numbered 1 to 10) on the evaporation apparatus. The photo is taken from the ceiling of the chamber towards the Petri dishes on the evaporation apparatus.

The process ends with the printing of the laboratory plan which contains the quantities of water, DCC stock solution and additive required to prepare the chamber solutions, and the plan with the location of the chamber solutions on the evaporation apparatus.

Scanning the picture

After the pictures are crystallized, they are removed from the chamber and labeled. After two days of drying in the outer chamber, the pictures are scanned for documentation purposes and as input for computer image analysis. So far, this is done at 600 dpi with a UMAX Powerlook III type scanner, although a Heidelberg Linoscan 1400s (seems to be an OEM product) also works well. The color stability of the scanner is controlled by an [it8 reference dia](#) (see below). After two days drying the color of the DCC pictures stabilizes (Sokol 2013 [1]). Additionally the pictures can be photographed against a dark-field illuminated background (lightbox). These photos can be used for the CrystEval picture properties evaluation tool, described in chapter [3.3 CrystEval](#), and for the Gestalt evaluation (see in chapter [3.5 Appendix 3.5.1 pdf2sheet](#)), for which usually six pictures are combined on one sheet.

IT8-reference-dia

The IT8 reference dia is an industry standard to check the color consistency of a photo or scan. The color resolution of the dia is the same as that perceived by the human eye. The units are so called CE units. 1 CE unit is the lowest difference between two colors a human being can perceive. This is defined by the [International Commission on Illumination \(CIE\)](#), see Wandell 1996 [2]. We are using the littlecms software (www.littlecms.com) to check the IT8 reference dia.

Tab Scripts

The tab Scripts contains R-CRAN scripts which allow a simple evaluation of the results (to check e.g. for unexpected deviations) like the crystallization starting time (`tcrStart`) for the different samples used (Fig. 3.2.4 left) or for the chamber solutions (Fig. 3.2.4 right) or the climate conditions in the chamber during the evaporation (Fig. 3.2.5).

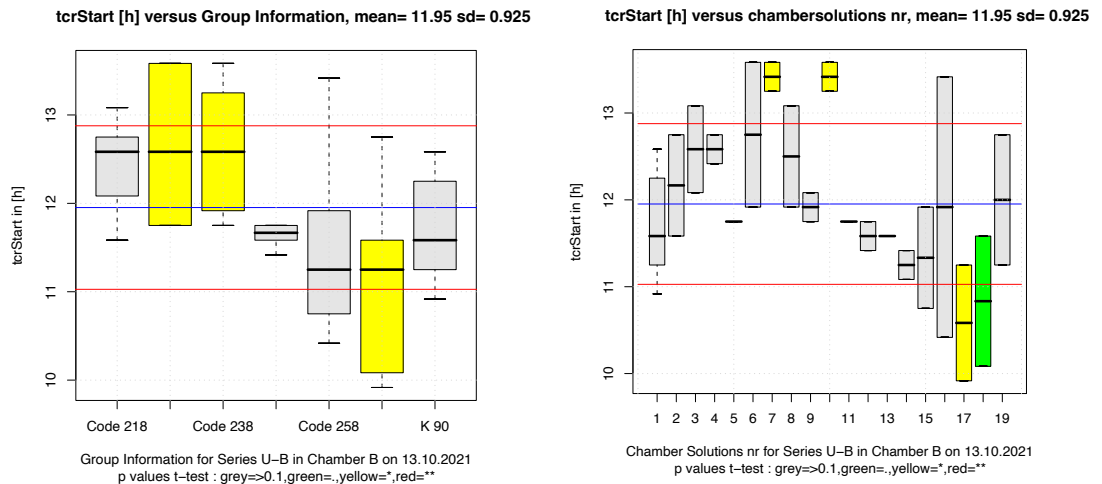


Fig. 3.2.4 Left: tcrStart versus the group info (samples). K90 is the reference sample. Right: tcrStart versus the number of chamber solutions. Three additive concentrations per sample were used. Solution nr 1 is the reference. The colors indicate the T-test significance levels: grey for $p > 0.1$, green for $p < 0.1$, yellow for $p \leq 0.05$.

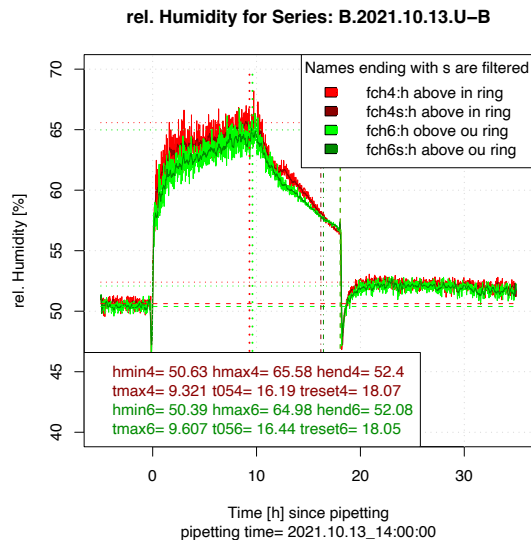


Fig. 3.2.5 Relative humidity above the Petri-dishes in the inner ring (red), and outer ring (green) for series B.2021.10.13.U-B, chamber B, university Kassel (D). Pipetting at $t = 0$ h, resetting the chamber conditions at $t = 18$ h.

General issues

The LabDoc tool can be adapted to different chamber geometries and no. of Petri-dishes. For example, the One-dish Prüfstand (one dish test bench) is also organized by LabDoc, as is the chamber in Darmstadt with 52 Petri-dishes arranged on a table, while the Triangle chamber has 43 Petri-dishes positioned on two rings. The LabDoc software is virtualized in a so called LINUX[®] container, which makes it independent of software updates due to operation system updates or new hardware. The development of the crystallization can be followed in real time on a pocket computer (smartphone) due to the virtualization of the screen on the LINUX[®] container.

Resume

The LabDoc tool is subservient to the researcher in the laboratory. All parameters are entered and can be used for other purposes too (like visual evaluation and image analysis). The LabDoc system was adapted to other DCC systems which have either another geometry (Forschungring Darmstadt, Topf Dornach, One dish Prüfstand) and/or number of dishes.

Additional research

The system is stable. The ceiling cameras are increased in resolution. The current maximum resolution is achieved with a NIKON 800e with 36 MB. Recently, the technical evaluation was improved by using CrystEval as an external tool. the next step would be to integrate CrystEval into the LabDoc workflow.

References

- [1] Sokol A. Digital Color Analysis of Copper (II) Chloride Crystallograms. MSC Thesis, University of Aalborg. 2013.
- [2] Wandell BA Foundations of Vision (Sinauer Associates, 1996).

3.3 CrystEval tool

Abstract

The CrystEval program is a further development of the technical evaluation of $\text{CuCl}_2 \cdot 2\text{H}_2\text{O}$ (cupric chloride di-hydrate, further called [DCC](#)) pictures in [LabDoc](#). The advantage of CrystEval is its configurability. Every criterion, that can be defined geometrically as a point, a line or an ellipse, can be configured and analyzed. Simple search conditions help to narrow down the LabDoc series of interest.

Introduction

The main idea behind the CrystEval tool is that it should be easy to adapt the evaluation of new picture properties without reprogramming the application. Each picture property, which can be defined geometrically as a point, a line or an ellipse, can be represented and stored in a configuration file. It is also possible to define properties that appear at different moments in the development of the picture. For example, if there is more than one crystallization center, the time at which they appear can be set by the user by marking the crystallization center in the corresponding time-lapse still. For more details see below.

When the program is started, a list of LabDoc series per chamber appears, as in LabDoc. The CrystEval program has some search options at the top of the interface to select series based on: Series Name, Samples / Description, Year and Who (in charge of the experiment), in order to reduce the number of series and find the series in question very fast.

Ch	Date	Name	Cnt	who	Samples	Description
B	2009-05-05	N-M	0	gm	carrot.baby-food, cucl	Moehrenbrei-Matrix Core
B	2009-04-29	N-L	0	gm	cucl2, wheat.freeze.dr	Standard -Intercomparison
B	2009-03-17	N-K	0	gm	cucl2, wheat, wheat.fr	Weizensorten Ringversuch 2
B	2009-03-10	N-J	0	gm	cucl2, wheat, wheat.fr	Weizensorten Ringversuch 1
B	2009-02-24	N-I	0	gm	cucl2, wheat, wheat.fr	Weizen DOK 2007 4. Feldwdh.
B	2009-02-17	N-H	0	gm	cucl2, wheat, wheat.fr	Weizen DOK 2007 3. Feldwdh.
B	2009-02-03	N-G	0	gm	cucl2, wheat, wheat.fr	Weizen DOK 2007 2. Feldwdh.
B	2009-01-27	N-F	0	gm	cucl2, wheat, wheat.fr	Weizen DOK 2007 1. Feldwdh.
B	2009-01-13	N-E	0	gm	carrot.freeze.dried, cu	Standard -Intercomparison
B	2008-12-09	N-D	0	gm	carrot.freeze.dried, cu	Standard -Intercomparison
B	2008-12-04	H2O	0	gm	water	H2O
B	2008-09-30	N-C	0	gm	cucl2, cucl2.only, whe	High CuCl2 Weizen und CuCl2
B	2008-09-21	N-B	0	gm	carrot, cucl2, wheat.fr	High CuCl2 Moehre und Weizen gefrier trocken
B	2008-09-09	N-A	0	gm	carrot, cucl2, pvp, whe	High CuCl2 PVP und Moehre gefrier trocken
B	2008-09-02	M-Z	0	gm	cucl2, cucl2.only, pvp,	High CuCl2 CuCl2 und PVP
B	2008-08-27	M-Y	0	gm	carrot.freeze.dried, cu	Standard -Intercomparison
B	2008-07-14	M-X	0	gm	carrot.freeze.dried, cu	Standard - Weizen - Moehre neu
B	2008-07-08	M-W	0	gm	carrot.baby-food, cucl	Moehrenbrei Core-Organic III
B	2008-07-01	M-V	0	gm	carrot.baby-food, cucl	Moehrenbrei Core-Organic II
B	2008-06-24	M-U	0	gm	carrot.baby-food, cucl	Moehrenbrei Core-Organic I
B	2008-06-17	M-T	0	gm	carrot.baby-food, cucl	Moehrenbrei Core-Organic I
B	2008-06-03	M-S	0	gm	carrot.baby-food, cucl	Moehrenbrei-Matrix Core II
B	2008-05-27	M-R	0	gm	carrot.baby-food, cucl	Moehrenbrei-Matrix Core
B	2008-04-07	M-Q	0	gm	cucl2, wheat, wheat.fr	Weizensorten Ringversuch Alterung
B	2008-03-31	M-P	0	gm	cucl2, wheat, wheat.fr	Weizensortenversuch Ringversuch

Fig. 3.3.1 Start screen from CrystEval with chamber B selected.

When a LabDoc series is selected and opened, the following screen appears:



Fig. 3.3.2 Working level of CrystEval program for LabDoc series 2019.08.21.GD from chamber P for the dish at location no. 5 in the chamber (left), and the corresponding scanned picture (right).

These two pictures represent different views of the same DCC picture. On the left side are the time-lapse stills of the Petri-dish during evaporation in the inner chamber. The photos were taken from the ceiling. The red striped column on the left is the time line at which the photos were taken. The red pointer points to the time of the time-lapse still shown.

To the right is the scan of the finalized DCC picture. it may also be a photo, or a scan between polarization filters, or a reflection scan (see chapter 3.2 LabDoc tool).

Scrolling through the time-lapse stills allows users to observe and track the onset and growth of crystallization and other phenomena occurring in the dish over time.

Working with the tool

As an example: the tool was used in connection with a student project in the years 2021/2022 at the University of Kassel [1]. There were 5 participants involved in the evaluation. Each participant had their own VNC account. The results of each participant (the topic was crystal types and crystal growth velocities of a carrot crystallization matrix) were compared and visualized. The differences in the evaluations were noted, visualized, and discussed to improve the definition of the crystal types. Each participant also could see how many DCC pictures had been evaluated and how many remained to be evaluated (see Fig. 3.3.3 at the beginning of the project and Fig. 3.3.4 at the end of the project). Additional criteria were added on the fly during the evaluation as a result of a discussion.

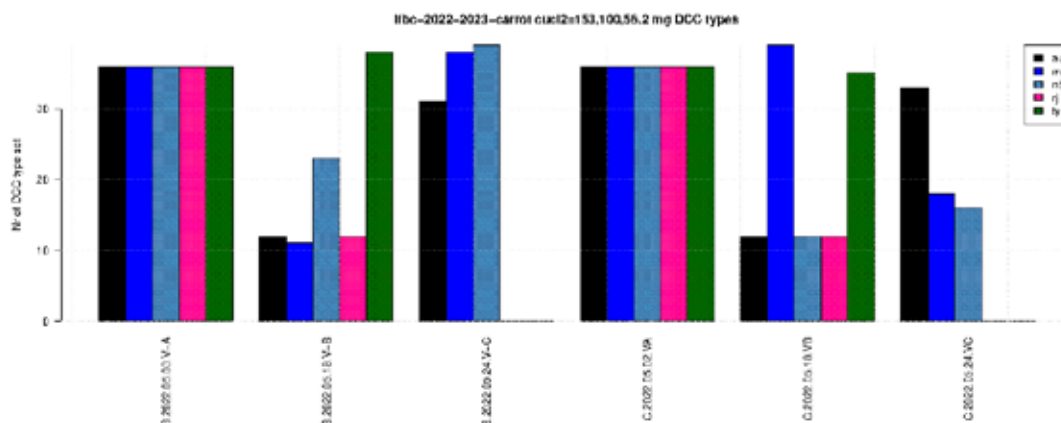


Fig. 3.3.3 Y-axis: nr. of pictures evaluated per LabDoc series (defined by the six block repetitions) and user (defined by the different colors), X-axis: the 6 LabDoc series evaluated for the DCC type criterion at the start of the project.

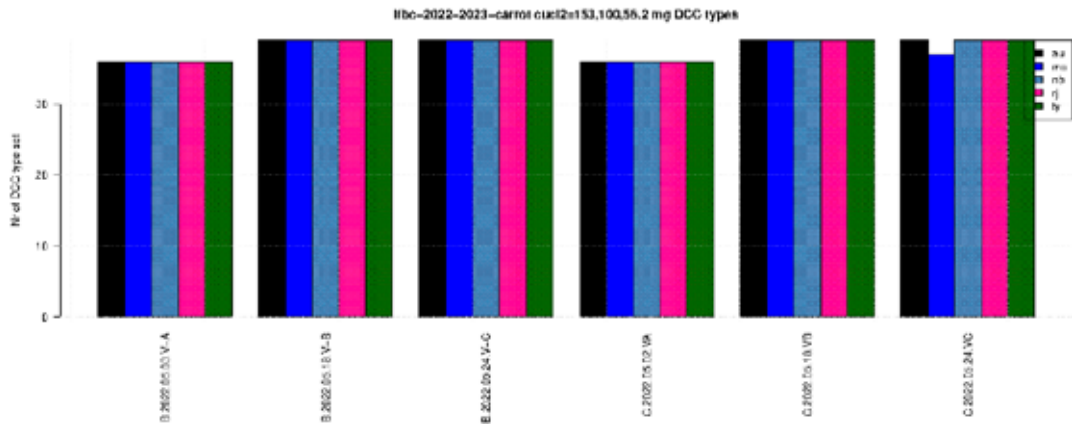


Fig. 3.3.4 Y-axis: nr of pictures evaluated per LabDoc series (defined by the six block repetitions) and user (defined by the different colors), X-axis: the 6 LabDoc series evaluated for the DCC type criterion at the end of the project. Only one evaluation is missing, for the blue participant for series C.2022.05.24.VC.

A second example is the dependency of the growth velocity of DCC / carrot crystallizations on the amount of additive for different carrot varieties (bachelor thesis, Herzer 2022 [2]). The result was that the growth velocity (measured with the CrystEval tool) showed a different behavior over time depending on the additive amounts (see Fig. 3.3.5 for 100 mg additive, and Fig. 3.3.6 for 475 mg additive per plate). There was no clear significant difference from the carrot varieties used in this experiment.

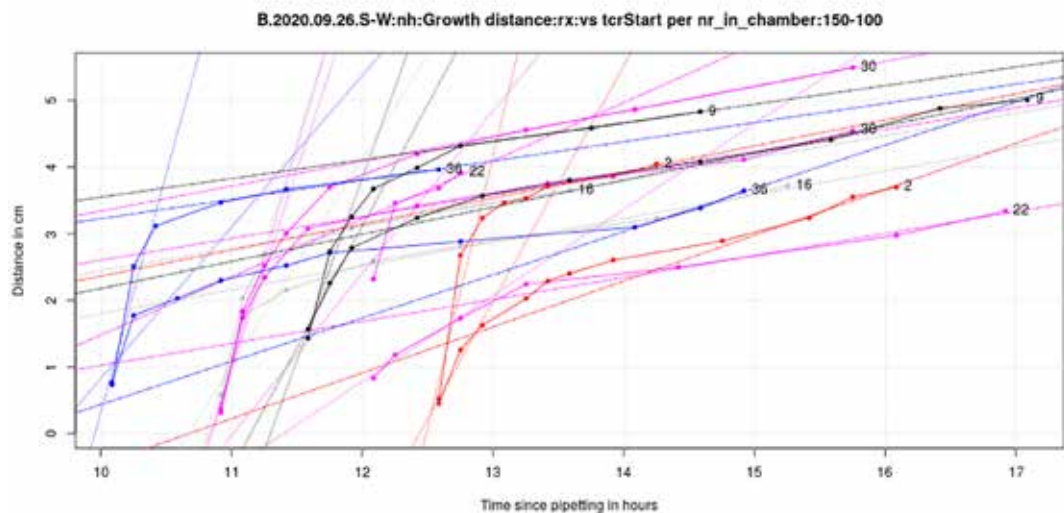


Fig. 3.3.5 Y-axis: distance from the crystallization center to the tip of the growing crystal versus the time since pipetting in hours (X-axis). The colored lines represent the growth velocity for different dishes (indicated by the numbers) in the chamber. Dotted lines are regression lines through the first 3 and the last 3 measurement points. DCC amount = 150 mg, additive amount = 100 mg per plate. Sample is carrot juice. Data from University of Kassel, LabDoc series B.202.09.26.S-W, from Herzer (2022 [2]).

For lower additive amounts (100 mg per plate, see Fig. 3.3.5), the velocity was very high at the start of crystallization and then decreased to a constant value. For higher additive amounts (475 mg per plate, see Fig. 3.3.6) the velocity was constant throughout the growth process from the crystallization start to the end.

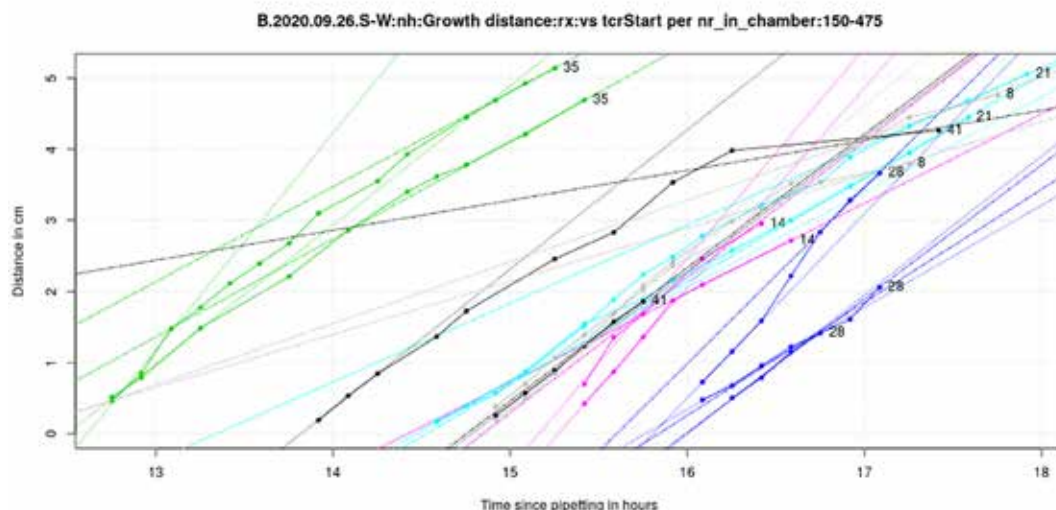


Fig. 3.3.6 Y-axis: distance from the crystallization center to the tip of the growing crystal versus the time since pipetting in hours (X-axis). The colored lines represent the growth velocity for different dishes (indicated by the numbers) in the chamber. Dotted lines are regression lines through the first 3 and the last 3 measurement points. DCC amount = 150 mg, additive amount = 475 mg per plate. Sample is carrot juice. Data from University of Kassel, LabDoc series B.202.09.26.S-W, from Herzer (2022 [2]).

When different growth rates occur, one would expect to see different crystal types, or a transition between two crystal types in the pictures, whereas a constant growth velocity would indicate a homogeneous crystal type (to be checked).

The work of Herzer (2022 [2], p. 36 ff.) contains a short documentation on how to work with the CrystEval program.

Resume

The CrystEval tool offers a criteria based evaluation of picture properties of DCC pictures. The criteria can be defined very easily and also on the fly during a project. The learning curve of the participants can be easily visualized and the need for further discussion in case of discrepancies in the scoring of the criteria can be easily identified. In most cases thus far, the criteria needed to be described more clearly.

Additional research

The next step would be the integration of CrystEval into the LabDoc tool, replacing the technical evaluation and the setting of the crystallization start time.

The data from Herzer should be re-evaluated, e.g. by comparing the type of growth versus the crystallization starting time (are there different start and end velocities?) and how homogeneous the crystal type in the pictures is. The development of the start and end velocity as a function of the additive amount should also be plotted in one plot.

References

- [1] Mansi Antil RJ, TanuYadav UA. Report: IFBC project 2022/2023. Technical Report, University of Kassel. 2023.
- [2] Herzer N. Bestimmung von Bildeigenschaften der Kupferchlorid-Bilder von Möhrensorten (EATMORE-Projekt) mittels computergestützter Auswertung. BSC Thesis, University of Kassel. 2022.

3.4 Image analysis tool

Abstract

The image analysis tool ACIA (Applied Crystal Image Analysis) is described. The input are the LabDoc series files, from which the series information is read. For the evaluation of an experiment the necessary number of series can be combined and evaluated. The results can be exported or a statistical evaluation can be performed within ACIA.

Introduction

The ACIA tool allows users to perform image analysis on $\text{CuCl}_2 \cdot 2\text{H}_2\text{O}$ (cupric chloride di-hydrate, further called DCC) pictures. Usually several experiments (LabDoc series) have to be combined in one evaluation. For example, for the publication of Kahl 2014 [1] on DOK wheat, the data from 40 LabDoc series ~ 1440 pictures had to be combined. This is done in the ACIA program. The first step is to press the button “Create Series” in the upper right button block in Fig. 3.4.1. This opens a screen (not shown) where the names of the LabDoc series belonging to this evaluation can be combined. All LabDoc series are shown in a dropdown menu and the series are added by highlighting the series name and pressing the Add button.

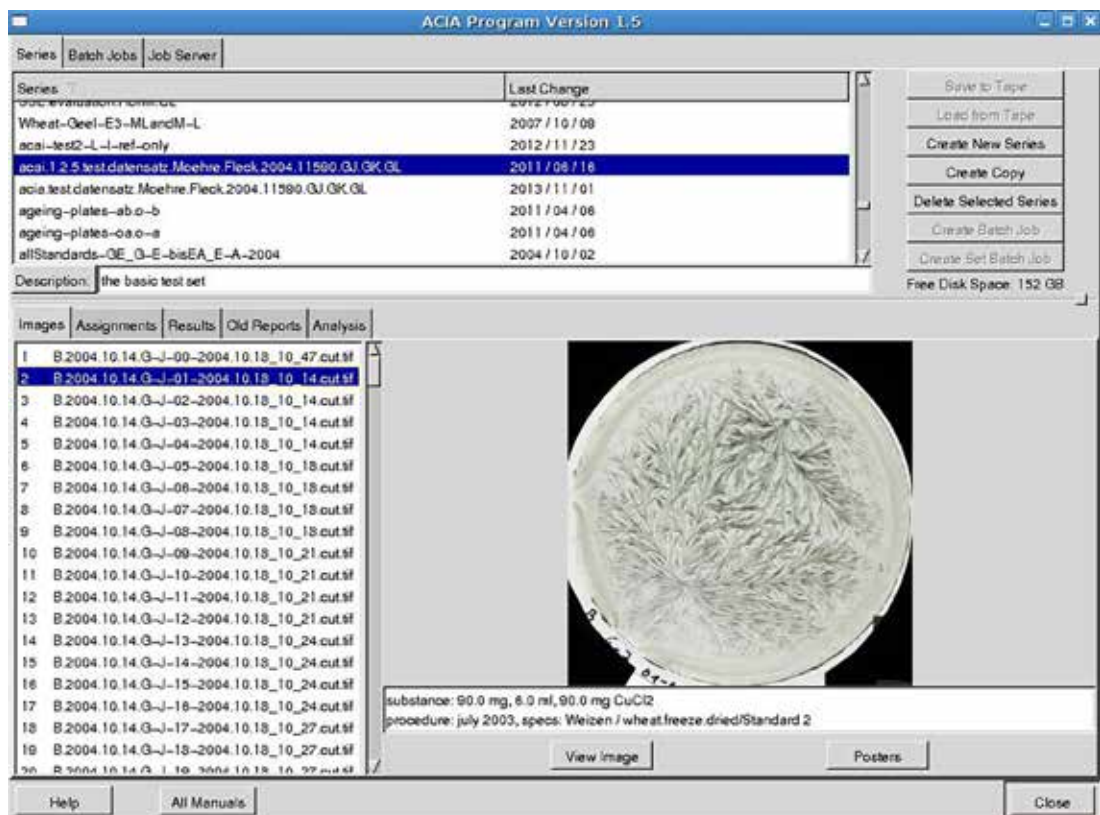


Fig. 3.4.1 Main screen of the ACIA program.

Create new Series

The LabDoc series are chosen from a pull down menu (Fig. 3.4.1 lower left). Each scan is checked for the presence of the accompanying IT8 reference scan. The IT8 reference slide is used to check that the scanner operates within its normal range. After the ACIA series has been created, the so called assignment for the statistical grouping has to be defined. In an assignment, the pictures of an experiment are selected that should be evaluated together, e.g. the reference pictures are excluded or only some concentrations or treatments are selected to form a group for the statistical evaluation.

Create a Batch Job

To start the image analysis calculation, the parameters need to be set. The parameters are the color transformation (from RGB color to gray (default), or from RGB to only R or G or B, or from RGB to L or C or h), the Region of Interest (abbreviated as ROI), and the scripts for the image analysis algorithm (see Appendix 3.4.1

Algorithm). See for the concept of the ROI the Appendix 3.4.2 ROI. The color transformation is necessary because all image analysis algorithms only work on 1 dimensional “gray level” pictures.

The statistical model for the evaluation (lme model with repeated measurements via crossed effects) was developed in a PhD thesis (Meelursarn PhD 2007 [2]) The statistical model separates the influences of the sample (the quality) from the chamber and from the day variation. For examples of this statistical evaluation, see chapter [1.13 Picture zones](#).

View the Results

The evaluation scripts produce html pages of results that can be viewed with a Web browser. The results can also be exported for further statistical evaluation. All data, LabDoc series and algorithm results can also be exported by the LabSelect tool. This is a very powerful generation of SQL queries for the generation of one data table, while the user only has to list the variables in question (see [Appendix 3.5.4 LabSelect](#) in [chapter 3.5 Additional tools](#)).

Final remarks

The ACIA program and the LabDoc program are virtualized and running inside a LINUX container. This makes it stable and independent from operating system updates or new computers.

Resume

The image analysis tool ACIA allows the evaluation of projects consisting of several LabDoc series (experiments). The selected dataset can be limited to a certain parameter by the assignment feature in ACIA, which allows an inclusion or exclusion of pictures according to the research question (e.g. a certain concentration ratio or a subset of the pictures). The algorithms are calculated on the basis of one-dimensional “gray scale” images, limited by the previously defined ROI. Results can be exported or directly statistically evaluated.

Additional research

Add more algorithms for the image analysis.

- Neural networks
- Fractal analysis
- Tree-like based simulations (master thesis Rommerskirchen 2022 [3])
- Add a compression routine instead of texture analysis to the output of the polar sampling
- Check if and how it is possible to recognize samples and treatments with the existing image analysis results.

Appendix 3.4.1 Algorithm

The following algorithms are calculated (status 2024.04.29).

Table 3.4.1 List of implemented algorithms in ACIA with a short description.

Name	Short description
Texture (4 scales)	Texture analysis according to Carstensen 1992 [4])
Structure analysis (length and width of a needle)	Doesburg and Nierop 2013 [5]
Structure Analysis of the crystal free areas. (length and width)	Doesburg and Nierop 2013 [5]
Structure Analysis: Combinations of length and width of a needle	
CF Structure Analysis: Combination of length and width of crystal free areas	
Absorbance evaluation (LCh)	Absorbance Projekt Report 2017 [6]
Polar sampling: implementation of a crystallization-start based ROI	Polar sampling report 2016 [7]

Appendix 3.4.2 ROI

The concept of Region of Interest (ROI) is also discussed in Andersen 1999 [8], Fig. 5. Here are some examples of ROIs used in publications.

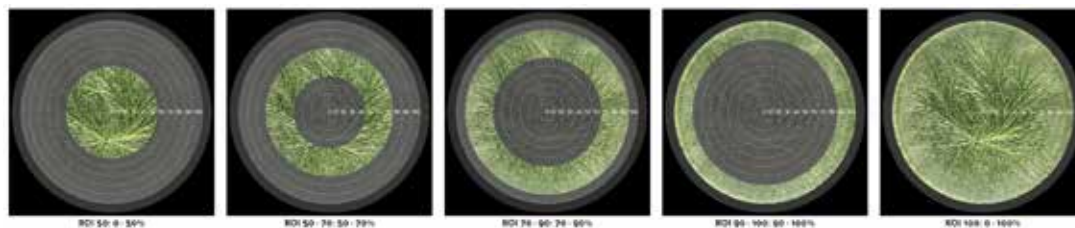


Fig. 3.4.2 Examples of circle – circle ROIs (from Doesburg 2019 [9], Fig. 6).

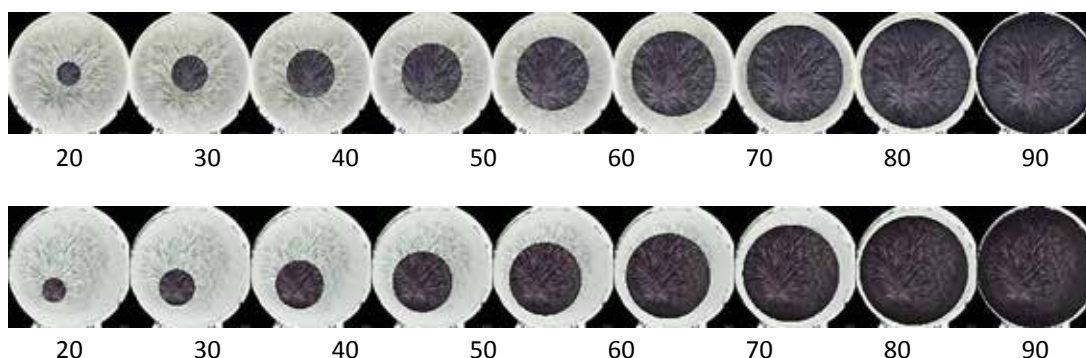


Fig. 3.4.3 The darkened area shows the geometric center based ROI (top row) or the crystallization start based ROI (bottom row). The radius of the circle is given as a percentage of the total dish radius.(from Polar Sampling report 2016 [7]).

References

- [1] Kahl J, Busscher N, Mergardt G, Maeder P, Torp T, Ploeger A. Differentiation of organic and non-organic winter wheat cultivars from a controlled field trial by crystallization patterns. *J. Sci. Food Agric.* 2014; 95: 53-58 <https://doi.org/doi:10.1002/jsfa.6818>.
- [2] Meelursarn A. Effect of image parameters to differentiate samples from different farming systems. PhD Thesis, University of Kassel. 2007.
- [3] Rommerskirchen EM. Rule-based simulation of dendritic Structures from Cupric Chloride Di-hydrat. MSC Thesis, Uni Göttingen. 2022.
- [4] Carstensen. JM. Description and Simulation of Visual Texture. PhD Thesis, Institute of Mathematical Statistics and Operations Research, Technical University of Denmark, Lyngby. 1992.
- [5] Doesburg P, Nierop AF. Development of a structure analysis algorithm on structures from $\text{CuCl}_2 \cdot 2\text{H}_2\text{O}$ crystallization with agricultural products. *Computers and Electronics in Agriculture* 2013; 90: 63-67 <https://doi.org/doi:10.1016/j.compag.2012.11.003>.
- [6] Busscher N. Absorbance Project Report. Technical Report, University of Kassel. 2017.
- [7] Busscher N, Doesburg P. Polar Sampling. Technical Report, CuCl_2 Research. 2016.
- [8] Andersen JO, Henriksen CB, Laursen J, Nielsen AA. Computerised image analysis of biocrystallograms originating from agricultural products. *Computers and Electronics in Agriculture* 1999; 22: 51-69 [https://doi.org/doi:10.1016/S0168-1699\(98\)00043-X](https://doi.org/doi:10.1016/S0168-1699(98)00043-X).
- [9] Doesburg P, Andersen J-O, Scherr C, Baumgartner S. Empirical investigation of preparations produced according to the European Pharmacopoeia monograph 1038. *European Journal of Pharmaceutical Sciences* 2019; 137: 104987 <https://doi.org/https://doi.org/10.1016/j.ejps.2019.104987>.

3.5 Additional tools

Here the additional tools are listed in Appendices

Sheets4GestaltEvaluation (see Appendix 3.5.1 Sheets4GestaltEvaluation)

Overall evaluation (see Appendix 3.5.3 Overall Evaluation)

View Climate Measurement Data (see Appendix 3.5.2 Overview Climate Measurement)

Labselect: (overall data request of the data base, see 3.5.4 Appendix Labselect)

Appendix 3.5.1 Sheets4GestaltEvaluation

At first glance, generating sheets for Gestalt evaluation seems like a simple task. Doing this manually is time-consuming and prone to errors, e.g. the pictures in the sheets are sorted by the crystallization starting time. A script was designed which generates the sheets, depending on the experimental design (nr. of samples, nr. of concentrations, nr. of replicates, nr. of day repetitions, different chambers, etc.). The pictures and sheets can be randomly coded to create a blind design in a simple and defined way. Depending on the experiment, 2 or more sheets are generated in one pdf. See the example of one sheet in Fig. 3.5.1.

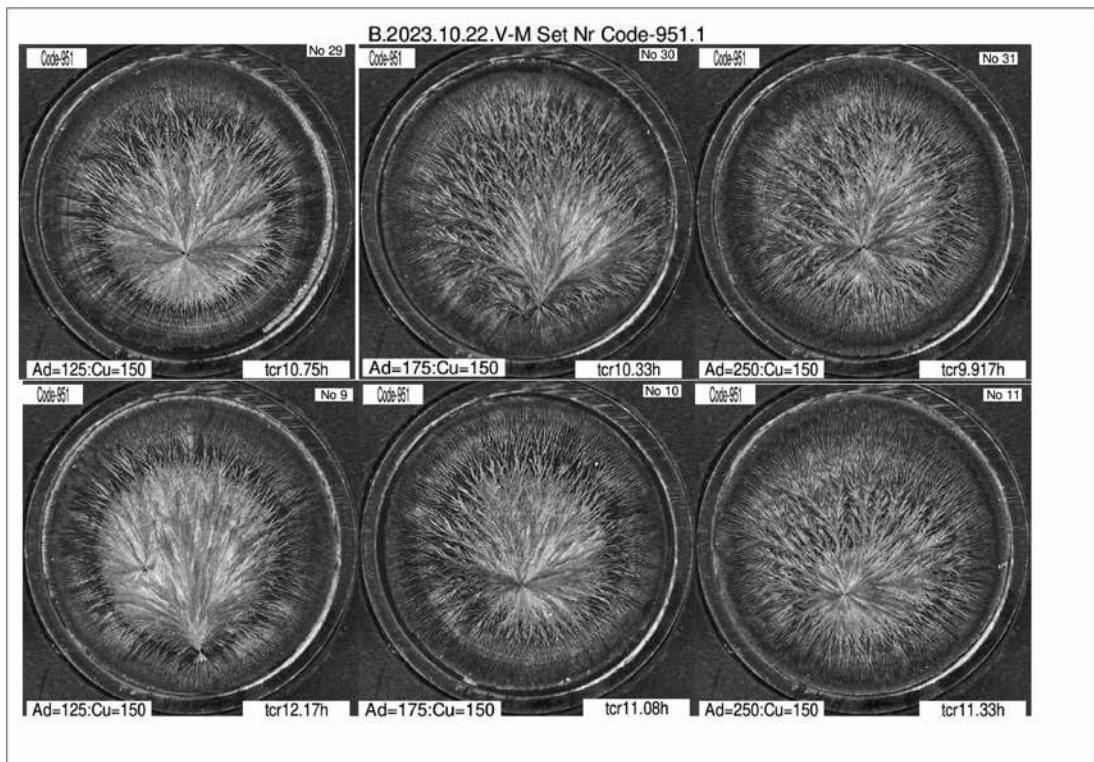


Fig. 3.5.1 Evaluation sheet for carrot samples. The Y-axis represents the crystallization starting time (lower time in the upper row), the X-axis represents the additive amounts (125, 175 and 250 mg per plate). DCC amount is 150 mg per plate for all. This sheet shows one sample (same codes). Data from University of Kassel, LabDoc series B.2023.10.22.V-M.

Appendix 3.5.2 Overview Climate Measurements

Climate and control data are stored for system quality control. They can be viewed online over hours for system troubleshooting, over 3 days (for LabDoc experiment conditions, see chapter [1.14 Chamber reset](#) for an example) and over weeks, months and years.

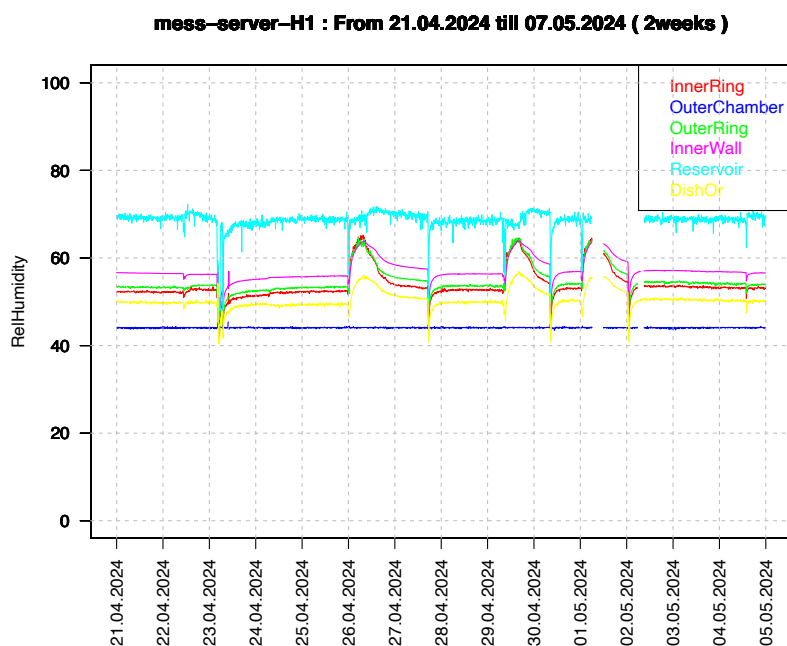


Fig. 3.5.2 Relative humidity (Y-axis) over a 2-week period (X-axis) from 21.04.2024 - 07.05.2024 for the Triangle chamber H1 in Hiscia (CH). In cyan, sensor data directly above the reservoir; in pink, at the inner wall; in red, above the inner ring; in green, above the outer ring; in yellow, below the reference dish on the inner ring; in blue, in the outer room. crystallization experiments are recognizable by the sudden and synchronous increase of the inner ring, outer ring, under dish and inner wall relative humidity (e.g. 26.04.2024, 29.04.2024, 01.05.2024). Missing sensor data (e.g. 01 - 02.05.2024) is due to either cable, computer or network problems.

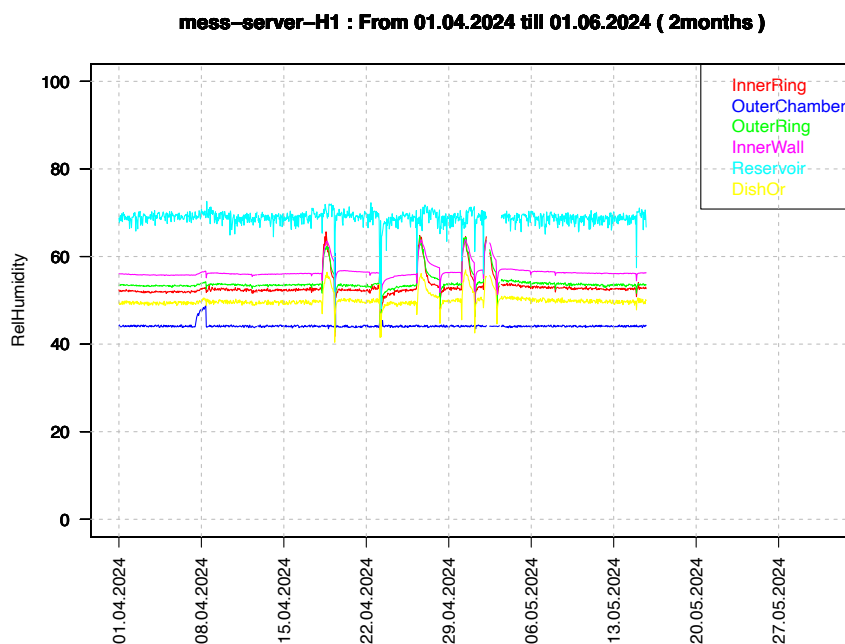


Fig. 3.5.3 Relative humidity (Y-axis) over a 2-month period (X-axis) from 01.04.2024 - 01.06.2024 for the Triangle chamber H1 in Hiscia (CH). In cyan, sensor data directly above the reservoir; in pink, at the inner wall; in red, above the inner ring; in green, above the outer ring; in yellow, below the reference dish on the inner ring; in blue, in the outer room. crystallization experiments are recognizable by the four sudden and synchronous increase of the four inner ring, outer ring, under dish and inner wall relative humidity. Missing sensor data (is due to either cable, computer or network problems).

Appendix 3.5.3 Overall-Evaluation

For quality control of the DCC system the data like `tcrStart`, `radius` (the distance between the location of the first crystallization center and the geometric center of the dish in % of the dish radius) are monitored to check for deviations and unexpected behavior.

A short-term check (over one day) is to see if a sample in an experiment deviates from the other samples (see example in [3.2 LabDoc tool “Tab scripts”](#))

A Long-term check (over one year) is e.g. the variation of `tcrStart` versus the location in the chamber (see Appendix in chapter [2.17 Lowering disturbances](#)).

Every week an overall evaluation of the database is done. As example the number of picture data sets in the database is calculated (see Fig. 3.5.4 left and right).

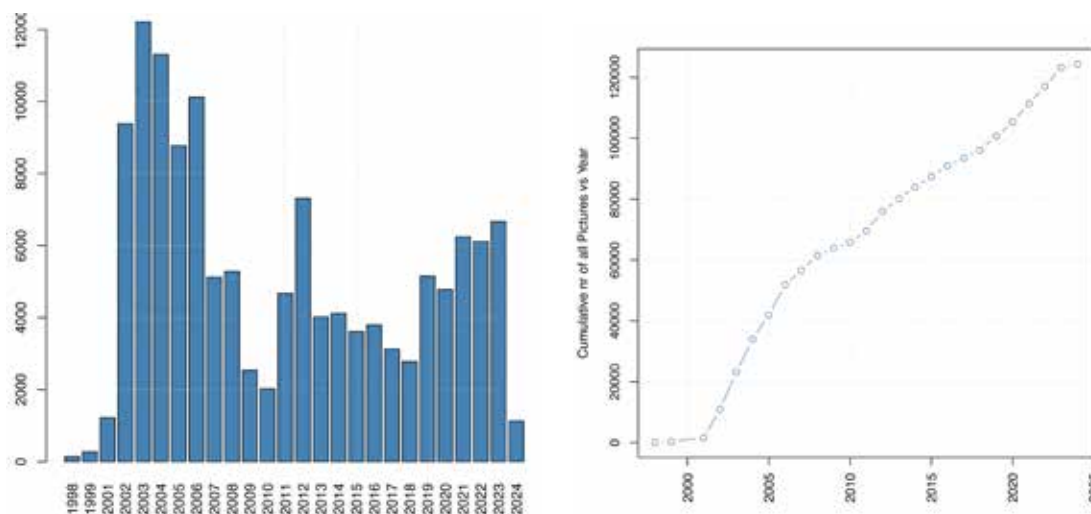


Fig. 3.5.4 Left: number of DCC Pictures per year. Right: cumulative number of DCC pictures in the database.

An overview is generated of the number of DCC images per sample (see [3.2 LabDoc tool](#) substances) for all documented samples, in which chamber which sample was researched, and in which year.

The `tcrStart` and the `radius` are evaluated per chamber. An example is the graph of the distribution of the `radius` for all samples in the database in chapter [2.11 Nucleation](#). The unexpected result was that the `radius` depends on the sample.

For older experiments (before 2004) sometimes the used samples were not documented. These missing data are listed in a table for correction.

- B) If no further member can be found and “tabs” is not empty, a cluster graph is built based on the table graph. Cluster nodes are built from the tables in “joined”, in “tabs”, and all other tables are kept as nodes. The tables on the shortest path from “tabs” to “joined” are added to “joined”. The continue with step A until “tabs” is empty.

Steps A and B are done on the graph Fig. 3.5.5 with only black edges; if this fails those steps are repeated on the graph with black and blue edges. Black edges represent “preferred connections”.

An example: if tables experiment, dish and substance are referenced in the query, the algorithm adds chamber_solution and basic_solution to have a path between substance and dish, and the connection to experiment is found via one of the blue edges.

Some “database tables” in the graph are based on SQL select constructs and SQL functions and introduce dependencies on other tables and lateral joins. This resolved with a topological sort of the tables before constructing the SQL joins.

The algorithm doesn’t rest on a profound theory but seems to deliver the expected table joins for the labselect queries on the existing set of tables.

Fig. 3.5.5 (below) presents an overview over the database. In the upper left corner the LabDoc data describing the experiment (L:experiment, L:dish, L:substance, L:basic_solution, L:chamber_solution) is presented. In the middle the results of the image analysis are displayed, starting from L:image_file and connecting to the different algorithms and calculation parameters (all beginning with A:). On the far right side are the databases that begin with Q:. They are intended for extended documentation of projects, where the structure of experiments and the results of additional methods on the same samples can be organized. See project report CORE-Organic EU Project 2009 [1]. This is not further explained.

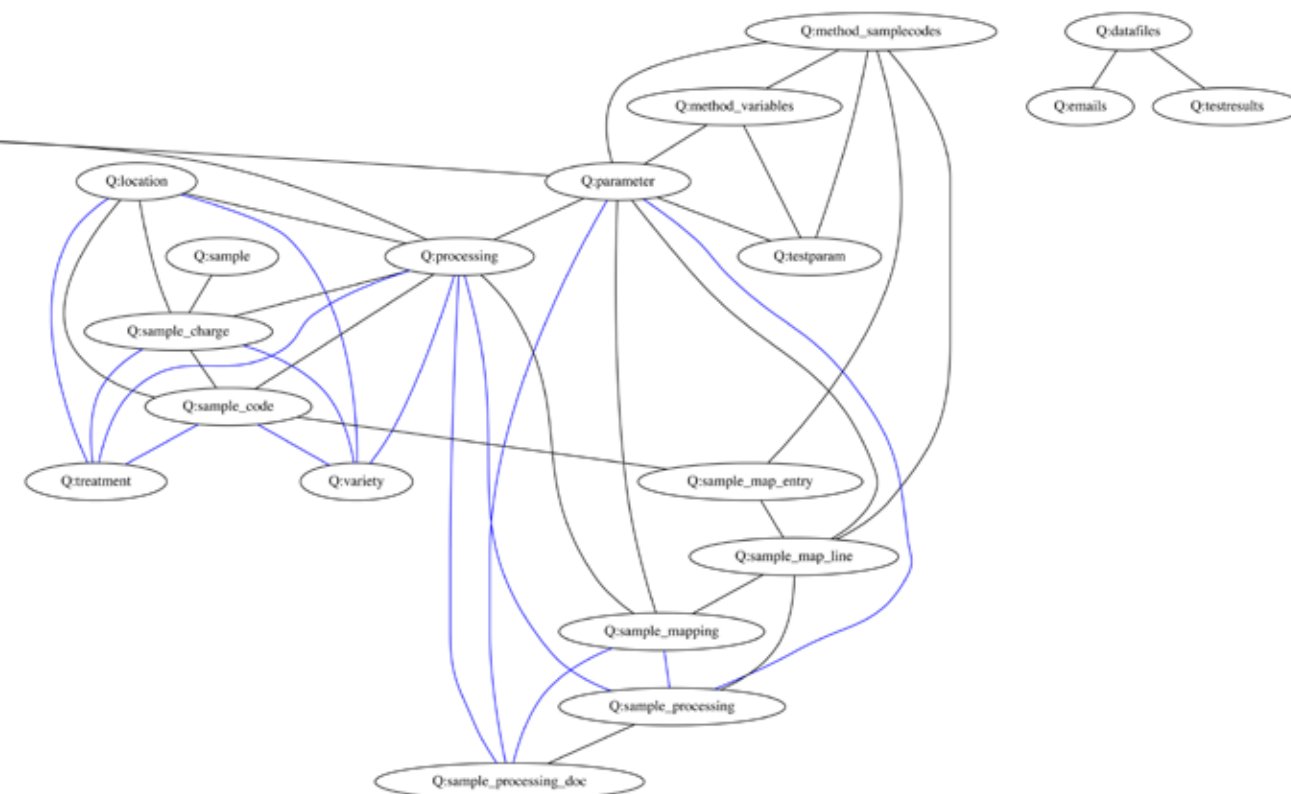


Fig. 3.5.5 The relations between the LabDoc data base tables are graphically presented. The black lines are the direct and preferred paths to connect data tables and resolve relations. When the resolving through the black lines fails then the resolving through the direct blue lines is attempted.

References

- [1] Busscher, N.; Kahl, J.; Degert, A. and Ploeger, A. Organisation und Zusammenfassung quantitativer und qualitativer Messdaten im Rahmen des CORE-Organic QACCP Projektes, 2009.

CHAPTER

4

GLOSSARY

CuCl₂ · 2H₂O System

Glossary

The glossary for the $\text{CuCl}_2 \cdot 2\text{H}_2\text{O}$ system is in alphabetical order.
Lower and uppercase letters are not used for ordering.

Additive

The additive is the aqueous solution of the researched sample, to which the solution of the salt $\text{CuCl}_2 \cdot 2\text{H}_2\text{O}$ (cupric chloride di-hydrate, further named [DCC](#)) is added. In most cases the additives are a result from an extraction or a solubilization (like [BSA](#) or [PVP](#) powder) or -juicing process of a [sample](#). In simple cases e.g. milk or juices from a shop there is no process.

Additive Vector

A concentration series, for a constant DCC amount and different additive amounts, which includes the two extreme points of a crystallization matrix. The extremes are the lower boundary where the dewetting before crystallization changes to dewetting after crystallization and the upper boundary, where the inhibition of the crystallization begins. The number of concentrations should be high enough to include all crystallization types.

Absolute humidity

The amount of humidity (water vapor) in the air (density) is usually measured in g/m^3 . The maximum amount of humidity that air can hold depends on the temperature and is $30 \text{ g}/\text{m}^3$ at $30 \text{ }^\circ\text{C}$ and 1 Bar [1]. The maximum amount increases exponentially with the temperature, doubling roughly every $12 \text{ }^\circ\text{C}$. If the amount of water in the air is constant, the absolute humidity will not change as the temperature increases. In contrast, the [relative humidity](#) will then decrease. See also in chapter [1.2 Water transport](#).

Amount in mg per plate

For practical reasons the amount of a [sample](#) that is used in the laboratory process of dissolving (BSA), extracting (wheat) or juicing (carrot), is reported. These amounts are the highest possible amounts that can be on the plate after the water has evaporated. This can have some pitfalls. For the [DCC](#) this can be quite accurate, because little is lost during dissolving, but during the mixing process with the additive and during the evaporation, there can be losses due to complex formation with the additive, which reduces the amount available for crystallization. This can reduce both the DCC as well as the additive amount. The amount of the additive may be lower, because some loss can be expected during laboratory (e.g. BSA on glass ware) and filtration steps. GLP (Good Laboratory Practice) should at least ensure that the amounts should be comparable when replicating an experiment. In some cases, the dry matter of the sample solution was determined before the mixing with DCC (the last laboratory step).

BSA

Bovine Serum albumin (CAS # 9048-46-8) is one of the best researched proteins. It is also called the Drosophila of the protein chemist. The first who used BSA in connection with DCC pictures was Gallinet in 1992 [2], because of its well known ability to cover a glass plate, to study wetting phenomena.

Buoyancy

Buoyancy forces are driven by density differences of e.g. an air filled ball under water. It can also occur when density differences are caused by temperature differences.

Ceiling photos

The entire evaporation process is monitored by means of time-lapse stills at 5 or 10-minute intervals from a digital camera mounted on the ceiling of the crystallization chamber. Based on the photographs obtained, the tcrStart can be determined for each crystallization plate, i.e. the time in hours/minutes from the onset of the experiment until initial nucleation.

Chamber

In most cases the so called inner chamber is meant.

Computer Image Analysis

The scanned images can be evaluated by a computer by applying different algorithms which are applied for a chosen [ROI](#). So far texture [3] [4], structure [5], fractal dimension, transmission (absorbance), and polar sampling analysis are used. See for more details in chapter [3.4 Image analysis](#).

Concentration Matrix

The concentration matrix (Selawry [6], Petterson [7], Andersen [8], Busscher [9]) shows the dependency of the DCC pattern on the amount combinations of DCC and additive. The patterns are placed in a matrix representation where the DCC amounts are positioned on the Y-axis and the additive amounts on the X-axis. For more details see chapter [1.9 Optimal amounts](#) and chapter [1.8 Concentration matrix](#).

CMX

Shorthand for Concentration Matrix

Crystallization Center

The (primary) center of a DCC crystallization picture is the visible starting location of the crystallization. Usually there is only one center. It differs from a nucleation point. There can be a lot of nucleations in a dish, which are so small that they are invisible. Multi-centered pictures are also possible. For examples of centers see [1.12 Multiple centers](#).

Crystallization Chamber

The evaporation of the additive/DCC mixture in a Petri-dish takes place in a so called Crystallization Chamber. The purpose of the crystallization chamber is to allow evaporation to take place under defined climatic conditions and an undisturbed airflow.

Crystallization starting time

The moment at which the [crystallization center](#) becomes visible. See also [tcrStart](#).

CrystEval tool

The CrystEval tool is an improvement of the so called Technical Evaluation of a DCC picture, which was included in the LabDoc tool until 2020. It started with the evaluation of onset and position of the crystallization center(s) See [3.3 CrystEval tool](#).

CuCl₂ 2H₂O

The salt which is usually used for the so called CuCl₂ pictures is called Di-hydrate Cupric Chloride (DCC). The 2H₂O is usually not mentioned. Chemically without the 2H₂O, the salt is very hygroscopic (yellow colored) and will change to CuCl₂ 2H₂O [10] (blue) by attracting water from the air. The CuCl₂ 2H₂O is stable below 70 % relative air humidity. The color is blue in this state [6] [10] [11]. If it is more humid (~ 3H₂O) it turns to blue-green [12]. The partial pressure or saturation humidity above the solution in the Petri-dish decreases with the increasing CuCl₂ 2H₂O concentration. At the solubility border, it is 67 % [13] [14].

DCC

Short form for CuCl₂ 2H₂O (cupric chloride di-hydrate). Usually only the term CuCl₂ is used for CuCl₂ 2H₂O, but this can conflict with CuCl₂ without H₂O. Because CCD was already booked by Charge Coupled Devices we chose DCC for di-hydrate cupric chloride.

DCC System

The DCC system consists of the procedures for laboratory work and the procedures for the evaluation of the DCC pictures and all the equipment needed to complete a research question for a sample. In addition to a laboratory with equipment for the preparation of petri dishes and aqueous solutions, there is a so called inner and outer chamber. For documentation purposes, the process is monitored by sensors and a computer based project documentation. Image analysis is done on a computer, the human visual evaluation in a "Sensory Lab" according to ISO Norms 11035 and 8587 for sensory analysis of food products, adapted for use in the visual evaluation by Huber 2010 [15].

Dewetting

Dewetting is the process of retraction of the DCC solution (usually during crystallization in the absence of an additive) in the Petri-dish during evaporation, leaving a dewetted area. This can start when the height of the solution falls below a threshold [16] [17] [18]. The threshold depends on the surface tension of the solution and the height of the solution. It shows the balance between surface tension and the gravitational forces. Because the height of the solution decreases with decreasing DCC amount [18], the dewetting has a higher probability for lower DCC amounts. Above 600 mg DCC per plate the situation is usually stable.

Dish

The dish is usually built from two parts. A circular glass plate and a ring. The glass plate is 2 mm thick and 10

cm in diameter. The most commonly used acrylic ring has an outer diameter of 10 cm and an inner diameter of 9 cm. The height of the ring varies between 3.5 cm (Triangle chambers) and 1.0 cm. The ring is molded onto the glass plates by means of heated vaseline or paraffin. The ring shields the evaporating solution from air turbulence.

Double Steel Ring

In the [Triangle](#) system the Petri-dishes are placed on a so called double steel ring inside the evaporation apparatus [19]. The double steel ring consists of two rings. Each ring is made up of two metal rings, like two circular train tracks. On these tracks the Petri-dishes are placed allowing the air to pass by from below. The double steel ring is positioned on three eccentric screws inside the evaporation apparatus and is balanced horizontal ≤ 1 mm over 1 m.

Heterogeneous Nucleation

When the DCC nucleation depends on an additive like dust or a molecule, not belonging to the crystal.

Hole-forms

For a special range of additive and DCC amounts (the so called split-growth area in the concentration matrix) pictures appear which have hole-like forms around the crystallization center. See Fig. 6 for an example of a hole and split-growth area in Busscher 2019 [9].

Homogeneous Nucleation

When the nucleation only depends on the crystal solution, not on e.g. dust particles.

Image

See Pattern/picture/image

Inner Chamber

The Triangle DCC system consists of an acclimatized room (the so called outer chamber) in which the wooden evaporation chamber, the so called inner chamber, is located. See for more details the chapter [3.1 Chamber systems](#).

iso pH

The iso pH is the isoelectric point of a protein. This is the pH at which the protein has a neutral charge, and can precipitate.

LabDoc

LabDoc is the shorthand for the Laboratory Documentation system. It was developed since 1999 in connection with the Triangle consortium for the documentation of the experiments. The data for the documentation of an experiment (samples, suppliers, concentrations, locations in the chamber) are added into this system only one time. The data is stored in a database, which can also be used by the image analysis system. The user is provided with a work sheet for preparing the solutions in the lab and pipetting the solutions in the chamber. The scanning of the pictures is controlled from here, as well as the start of the ceiling camera run and the evaluation of the crystallization starting time (tcrStart). Simple statistical evaluations can be made and compared to the climate measurements during the experiment. Different lists of the results can be generated. See also chapter [3.2 LabDoc tool](#).

Meso-crystal

From [wikipedia](#): A meso-crystal is a material structure composed of numerous small crystals of similar size and shape, which are arranged in a regular periodic pattern. It is a form of oriented aggregation, where the small crystals have [parallel crystallographic](#) alignment but are spatially separated.

Morphology map

The term morphology map was introduced by Kurz [20] in 2001. It is a two-dimensional plot with the growth rate of the crystal on the Y-axis and the mole fraction on the X-axis. Areas with the same crystal morphology can be identified in this plot.

Nonlinear Least Square (NLS)

Determine the nonlinear (weighted) least-squares estimates of the parameters of a nonlinear model. This function allows the fitting of a data curve with a non-linear function. This function is implemented in R-cran [21].

One Dish test bench or Prüfstand

Equipment for observing the DCC and additive in one Petri-dish during evaporation and crystallization. The weight of the dish is monitored (the Petri-dish is placed on a balance), the crystallization is monitored by a digital camera, the climate by a sensor. When the additive is a pH indicator, the situation can hopefully be compared to the situation in the chamber during evaporation/crystallization. See for more details in chapter [3.1 Chambers systems](#).

Optimal concentration

See [Picture Optimum](#)

Pattern/Picture/Image

These three concepts are sometimes used as replacements of each other. Maybe the following helps. The term DCC pattern is used, when a texture or a structure or a fractal dimension is described. The term DCC picture is used when the picture properties are addressed, like looking at a painting. The term DCC image is used when referring to what the DCC picture triggers (*auslösen*, resonates with) in ourselves.

Picture Optimum

The image optimum describes the concentration range in which images do not show any characteristics of substance over- or under concentrations.

Picture Properties

The properties of a DCC picture can be determined by morphological or Gestalt evaluation by a human being [15] [22] [23] or by image-analysis by a computer [3] [4] [5].

PID Regulator

Proportional, Integral, Differential regulator. With this regulator a precise control value can be reached. It depends on a linear actor and cannot work with a simple On/Off actor. (See also [PID Wikipedia](#))

ProPar Project

Project running from 2016 to 2024. It dealt with the processes and the parameters of the [DCC system](#).

PVP

Shorthand of Polyvinylpyrrolidone. PVP is a polymerization product available in different molecular weights. PVP can be simply ordered by its CAS # 9003-39-8. It is a water-soluble polymer made from the monomer N-vinylpyrrolidone. It was used first as an additive by Hummel [24] to falsify the hypothesis that the DCC system is 'an indicator for the living'.

See for more details in chapter [2.6 Molecular weight and branching](#).

ROI

ROI is the shorthand of Region Of Interest. This describes the area in a picture which is evaluated by image analysis or visually. It can have different geometric forms [4] p. 9, Fig. 5.

Radius of the crystallization center

The distance between the geometrical center of the plate and the crystallization center is called the radius of the center. It is usually expressed in percentage of the radius of the Petri-dish 0-100 % (radius dish = 4.5 cm). The geometric center of the Petri-dish is by definition 0 %, the rim 100 %.

Radj.square

The radj.square value gives information in % about how much of the variation is explained by a statistical model. This informs about hidden parameters or a strong random effect.

Relative humidity

The [absolute humidity](#) has a maximum value which increases exponentially (doubling roughly every 12 °C) with the temperature. The relative humidity is the percentage ratio of the current absolute humidity to the maximum absolute humidity at the given temperature. The values range from 0 - 100 %. When the value is 100 % then condensation can start. When the water amount is constant and the temperature increases, the relative humidity will decrease, while the absolute humidity will remain constant.

Sample

A sample is something, taken from a larger amount by a statistical procedure. A sample can be e.g. wheat

kernels from a growth system trial or carrots from a variety comparison or carrot mash from different pasteurization temperature procedures or milk from different cows. It is defined by a process and by a statistical definition (e.g. field replicate, or a growth system or procedure replicate, or a variety). In the laboratory it is converted by a laboratory process (e.g. extraction for wheat or juicing for carrots) to a so called additive.

Self-organization

A self-organized system is a stable system consisting of systems connected in a loop. No part can be addressed as the main one. It is organized as a self. See also chapter [2.14 Self-organization and \$\text{CuCl}_2 \cdot 2\text{H}_2\text{O}\$](#) .

Solubility Border

The solubility border defines the maximum amount of a salt that can be dissolved in a solvent. For instance DCC in water has a solubility border at 56 % (w/w) at 30 °C. This border cannot be exceeded by adding more salt. During the evaporation of a solution this border can be exceeded. See chapter [2.11 Nucleation](#).

Starting humidity

This is the humidity in the chamber at the start of the experiment. It can be the value before entering the chamber for an experiment to place the dishes and pipette the solutions, or it can be the humidity at which the chamber door is closed after the solutions are pipetted.

Step Response Test

The step response test is used to characterize a chamber system based on the dynamic climate coupling (temperature and humidity) between the inner and the outer chamber. In a step response test the temperature/humidity of the outer chamber is changed from one value to another, like a step. The response of the temperature/humidity inside the chamber provides information about the parameters and possible models of the process by which the water passes through the chamber walls.

Supersaturation

The DCC supersaturation is the difference between the actual DCC concentration and the DCC concentration at the solubility border, divided by the value of the solubility border. When the supersaturation is positive, nucleation can occur.

tcrStart

The time difference between the time of the first appearance of a crystal in a dish, the [crystallization starting time](#), and the pipetting of the solution is called tcrStart. The later the crystallization starts the higher the supersaturation should be. A higher supersaturation has an influence on the crystallization pattern in the dish.

Triangle Chamber

Chamber system (outer and [inner chamber](#)) used by the Triangle Consortium. Several characterization and validation steps were performed to define the crystallization system. See chapter [3.1 Chamber systems](#) and Andersen 1998 [19] and Andersen 2001 [25] and Kahl 2007 [26] for more details.

Triangle Consortium

Cooperation of Jens-Otto Andersen, Marianne Paulsen (BRAD DK), Machteld Huber, Paul Doesburg (Louis Bolk Institute NL) and Angelika Ploeger, Nicolaas Busscher, Johannes Kahl, Gaby Mergardt (Uni Kassel Witzenhausen D) from 2001 to 2008. Goal of the cooperation was the standardization of the DCC phenomenon by a validated procedure (Habilitation Kahl [26] BLE Project [27]) which resulted in common and shared working and documentation procedures how to produce the DCC pictures (see also LabDoc) and a list of publications (see in chapter [Introduction](#) > Historical overview)

Two Point Regulator

Simple regulation principle. It has a upper and a lower limit. For example, a heating controller. If the temperature falls below the lower limit, the heater will turn on, and if the temperature rises above the upper limit, the heater will turn off. This regulator keeps the temperature between the lower and the upper limit. See also [Zwei Punkt Regler Wikipedia](#).

Visual Evaluation

The human evaluation of a DCC picture is called visual evaluation. It takes into account the geometric properties of the pictures [15] as well as the impression the DCC picture makes on a human being when it is handled as an image [28] [22].

Vorbild

The protein “*Vorbild*” or prefiguration was uttered by Pfeiffer in Bessenich (196 [29], p. 84 ff.). The idea is that before the crystallization starts some of the protein of the additive precipitates on the glass plate and the crystals grow along this protein pattern. After washing off the DCC, Pfeiffer recognized the same pattern on the glass plate. The *Vorbild* question was studied by Francois Schweizer for plant extracts as additive [30]. He found that there were two types of DCC on the glass plate. One water soluble and one water insoluble where the crystal needle touched the glass plate. See also [1.7 Evaporation issues](#).

(w / w) %

The weight percentage (w/w) % is simple measure of, e.g. the solubility of DCC in water. If you add 100 mg of DCC to 900 mg of water, you have a solution of 100 mg/1000 mg = 10 (w / w) %.

The (w / w) % is a simple and practical measure that doesn't depend on the temperature in the laboratory.

References

- [1] Baehr HD. Mollier-i, x-Diagramme für feuchte Luft: in den Einheiten des Internationalen Einheitensystems (German Edition) (Springer, 1961).
- [2] Gallinet JP, Gauthier-Manuel B. Wetting of a glass surface by protein adsorption induces the crystallization of an aqueous cupric chloride solution. *Journal of Colloid and Interface Science* 1992; 148: 155-159 [https://doi.org/doi:10.1016/0021-9797\(92\)90123-4](https://doi.org/doi:10.1016/0021-9797(92)90123-4).
- [3] Carstensen. JM. Description and Simulation of Visual Texture. PhD Thesis, Institute of Mathematical Statistics and Operations Research, Technical University of Denmark, Lyngby. 1992.
- [4] Andersen JO, Henriksen CB, Laursen J, Nielsen AA. Computerised image analysis of biocrystallograms originating from agricultural products. *Computers and Electronics in Agriculture* 1999; 22: 51-69 [https://doi.org/doi:10.1016/S0168-1699\(98\)00043-X](https://doi.org/doi:10.1016/S0168-1699(98)00043-X).
- [5] Doesburg P, Nierop AF. Development of a structure analysis algorithm on structures from CuCl₂·2H₂O crystallization with agricultural products. *Computers and Electronics in Agriculture* 2013; 90: 63-67 <https://doi.org/doi:10.1016/j.compag.2012.11.003>.
- [6] Selawry A and Selawry O. Die Kupferchlorid-Kristallisation in Naturwissenschaft und Medizin (Gustav-Fischer-Verlag, 1957).
- [7] Pettersson BD. Beiträge zur Entwicklung der CuCl₂ Methode nach Pfeiffer. *Elemente der Naturwissenschaft* 1966; 5: 29-39.
- [8] Andersen JO, Huber M, Kahl J, Busscher N, MeierPloeger A. A concentration matrix procedure for determining optimal combinations of concentrations in biocrystallization. *Elemente der Naturwissenschaft* 2003; 79: 97-114.
- [9] Busscher N, Doesburg P, Mergardt G, Sokol A, Kahl J, Ploeger A. Crystallization patterns of an aqueous dihydrate cupric chloride solution in the presence of different amounts of Bovine Serum Albumin. *Journal of Crystal Growth* 2019; <https://doi.org/doi:10.1016/j.jcrysgr.2019.125272>.
- [10] Gmelin. Gmelin Handbuch der anorganischen Chemie (Gmelin-Institut, Frankfurt am Main, 1958).
- [11] Beckmann H. Über Keimbildung, Einkristallwachstum und Auffächerungswachstum von CuCl₂ * 2H₂O in reinwässrigen und Eiweiß-haltigen Lösungen. PhD Thesis, Universität Bonn. 1959.
- [12] Shibata T, Takakuwa Y, Tanaka A, Kogure M, Iguchi T, Obata H et al. Crystal structures of blue and green hydrated cupric chloride grown from aqueous solutions with and without human blood addition: single crystal X-ray diffraction analysis and differential scanning calorimetry(DSC). *Journal of Tokyo Women's Medical College* 1998; 68: 358-369.
- [13] Rockland LB. Saturated Salt Solutions for Static Control of Relative Humidity between 5 and 40 C. *Analytical Chemistry* 1960; 32: 1375-1376.
- [14] Haynes W. Crc Handbook of Chemistry and Physics, 91st Edition (CRC Press, 2010).
- [15] Huber M, Andersen J-O, Kahl J, Busscher N, Doesburg P, Mergardt G et al. Standardization and Validation of the Visual Evaluation of Biocrystallizations. *Biological Agriculture and Horticulture* 2010; 27: 25–40.
- [16] Sharma A, Ruckenstein E. Energetic criteria for the breakup of liquid films on nonwetting solid surfaces. *Journal of Colloid and Interface Science* 1990; 137: 433 - 445 [https://doi.org/DOI: 10.1016/0021-9797\(90\)90418-N](https://doi.org/DOI: 10.1016/0021-9797(90)90418-N).
- [17] de Gennes P-G, Brochard-Wyart F and Quéré D. Capillarity and Wetting Phenomena Drops, Bubbles, Pearls, Waves (Springer New York, 2004).
- [18] Busscher N, Kahl J, Doesburg P, Mergardt G, Ploeger A. Evaporation influences on the crystallization of an aqueous dihydrate cupric chloride solution with additives. *Journal of Colloid and Interface Science* 2010; 344: 556–562 <https://doi.org/doi:10.1016/j.jcis.2009.12.045>.
- [19] Andersen JO, Laursen J, Koelster P. A Refined Biocrystallization Method applied in a Pictomorphological

- Investigation of a Polymer. *Elemente der Naturwissenschaft* 1998; 68: 1-20 <https://doi.org/DOI: 10.18756/edn.68.1>.
- [20] Kurz W. Solidification Microstructure-Processing Maps: Theory and Application. *Advanced engineering materials* 2001; 3: 443-452 [https://doi.org/https://doi.org/10.1016/0956-7151\(94\)90044-2](https://doi.org/https://doi.org/10.1016/0956-7151(94)90044-2).
- [21] R Core Team. R: A Language and Environment for Statistical Computing, 2017.
- [22] Fritz J, Athmann M, Andersen J-O, Doesburg P, Geier U, Mergardt G. Advanced panel training on visual Gestalt evaluation of biocrystallization images: ranking wheat samples from different extract decomposition stages and different production systems. *Biological Agriculture & Horticulture* 2018; 35: 1-12 <https://doi.org/doi:10.1080/01448765.2018.1492457>.
- [23] Doesburg P, Fritz J, Athmann M, Bornhütter R, Busscher N, Geier U et al. Kinesthetic engagement in Gestalt evaluation outscores analytical 'atomic feature' evaluation in perceiving aging in crystallization images of agricultural products. *PLOS* 2021; <https://doi.org/https://doi.org/10.1371/journal.pone.0248124>.
- [24] Hummel RE. Liefert die Kupferchlorid-Kristallisations-Methode einen Nachweis für die Gestaltkräfte des Lebendigen? *Elemente der Naturwissenschaft* 1992; 57: 112-121 <https://doi.org/10.18756/edn.57.112>.
- [25] Andersen J-O. Development and application of the biocrystallization method. PhD Thesis, Department of Agricultural Sciences/Organic Farming Unit The Royal Veterinary and Agricultural University Copenhagen. 2001.
- [26] Kahl J. Entwicklung, in-house Validierung und Anwendung des ganzheitlichen Verfahrens Biokristallisation für die Unterscheidung von Weizen-, Möhren- und Apfelproben aus unterschiedlichem Anbau und Verarbeitungsschritten. Habil Thesis, University of Kassel. 2007.
- [27] Kahl, J.; Busscher, N. and Meier-Ploeger, A. Differenzierung und Klassifizierung von Öko-Produkten mittels validierter analytischer und ganzheitlicher Methoden, Abschlussbericht zum Projekt Nr. 02OE170/F2, 2007.
- [28] Doesburg P, Huber M, Andersen J-O, Athmann M, van der Bie G, Fritz J et al. Standardization and performance of a visual Gestalt evaluation of biocrystallization patterns reflecting ripening and decomposition processes in food samples. *Biological Agriculture & Horticulture* 2014; 31: 128-145.
- [29] Bessenich F. Zur Methode der empfindlichen Kristallsation (Naturwissenschaftliche Sektion am Goetheanum Dornach, 1960).
- [30] Schweizer F, Andersen J-O, Jens-Laursen. Beobachtungen bei der Kupferchloridkristallisation: vom Eiweiß-Vorbild zum Kupferchlorid-Nachbild. *Elemente der Naturwissenschaft* 2010; 92: 62-93 <https://doi.org/DOI: 10.18756/edn.92.62>.



The CuCl_2 crystallisation method was developed in the 1920'ies, and since then numerous persons have worked with the method. However, only a few have managed to build up a long-term experience with the method. The method may appear simple, yet its complexity is most challenging. To produce pictures based on scientifically optimised equipment, as well as to visually evaluate the pictures based on well-described criteria, represents a major personal, scientific, and financial challenge.

At the start of the new millennium, a transdisciplinary group of researchers came together with the aim of facing these challenges, including a physicist, a biochemist, an agronomist, a medical doctor, as well as lab technicians. By good fortune, a fruitful cooperation was started with the visionary German foundation Software AG-Stiftung, a cooperation which is still ongoing, including this groundbreaking handbook.

The handbook represents a milestone, emphasising the need to include and understand both the biological and physical aspects of the CuCl_2 method. Thus, all pictures emerge from a complex interaction between the biological sample and the inorganic CuCl_2 salt, including minute changes in air temperature, humidity, and movements in the crystallisation chamber, as well as subtle influences from the solution surface tension, changes in pH, and viscosity phenomena.

Over the last decade a new and larger group of researchers, including the authors of this handbook, have worked in parallel to establish a more holistic approach to the visual evaluation of the pictures. As such, future research will have solid ground to stand on, keeping in mind both the biological 'agens', as well as the inorganic CuCl_2 'reagens'. Last, but not least, the handbook represents a first step towards a discussion in a broader scientific context, bridging the present gap to the 'conventional' crystallisation research.

PhD Jens-Otto Andersen
Biodynamic Research Association Denmark

